

ARMY MATERIEL COMMAND  
U.S. ARMY  
FOREIGN SCIENCE AND TECHNOLOGY CENTER

AD 741037



FERROELECTRICS AND ANTIFERROELECTRICS

By

G. A. SMOLENSKIY

Reproduced by  
NATIONAL TECHNICAL  
INFORMATION SERVICE  
Springfield, Va 22151

SUBJECT COUNTRY: USSR

DDC  
RECEIVED  
MAY 8 1982  
B

*This document is a rendition of the original foreign text without any analytical or editorial comment.*

Approved for public release; distribution unlimited.

633

R

# TECHNICAL TRANSLATION

FSTC-HT-23- 456-72

ENGLISH TITLE: FERROELECTRICS AND ANTIFERROELECTRICS

FOREIGN TITLE: SEGNETOELEKTRIKI I ANTISEGNETOELEKTRIKI

AUTHOR: G. A. SMOLENSKIY

SOURCE: NOT APPLICABLE

Translated for FSTC by ACSI

## NOTICE

The contents of this publication have been translated as presented in the original text. No attempt has been made to verify the accuracy of any statement contained herein. This translation is published with a minimum of copy editing and graphics preparation in order to expedite the dissemination of information. Requests for additional copies of this document should be addressed to Department 4, National Technical Information Service, Springfield, Virginia 22151. Approved for public release; distribution unlimited.

### Translator's Note

The authors use the terms "seignetteoelectric" and "seignetteoelectricity" [by analogy with the properties of Seignette's salt] instead of "ferroelectric" and "ferroelectricity", and explain their reason for doing so in the third paragraph of chapter 1. However, because Seignette's salt is only one of dielectric materials (the others being Rochelle salt, potassium dihydrogen phosphate, barium titanate, etc.) exhibiting spontaneous polarization and hysteresis between polarization and field and to conform to the usage in English-language sources the translator has used the terms "ferroelectric" and "ferroelectricity."

ERRATA

Страница	Строчка или формула	Напечатано	Должно быть
34	Формула (3.28)	$\zeta P(r)$	$\delta P$
40	Формула (3.42)	$f_n^{(n)}$	$f_n^{(n)}$
45	Формула (3.48)	$P_{2n}^2 B_{2n}^2$	$P_{2n}^2 P_{2n}^2$
55	Формула (3.57)	$\cos^2 \alpha_{xy}$	$\frac{1}{2} \cos^2 \alpha_{xy}$
63	5 сверху 3	$\frac{\partial \Phi_P}{\partial \sigma_P} = 0$	$\left(\frac{\partial \Phi_P}{\partial \sigma_P}\right)_{\sigma_P=0} = -u_{2k}$
77	Формула (3.130)	$\frac{\partial A_P}{\partial u_P} = -c_P$	$\frac{\partial A_P}{\partial u_P} = c_P$
95	Формула (4.44)	$N_{r,0}$	$N_{r,0}$
95	Формула (4.45)	$\eta_j$	$\eta_j$
95	Формула (4.47)	$\text{ch } A \eta_1$	$\text{sh } A \eta_1$
108	10 сверху 4	$\Delta x^2$	$\frac{\Delta x^2}{2}$
159	Формула (5.81)	$\Phi_L - R +$	$\Phi_L - R +$
159	Формула (5.83)	$R_0$	$R$
160	15 и 23 сверху 5	$R_0$	$R$
182	25 сверху 6	$R \sim (T-0)$	$R = R_0 (1 + \epsilon T)$
174	Формула (5.118)	$\omega_T$	$\omega_T^2$

Key: (1) Page (5) 15 and 23 from the top  
 (2) Line or formula (6) 25 from the bottom  
 (3) 5 from the bottom (7) Printed  
 (4) 10 from the bottom (8) Should be

Translator's note: Correct expressions were used where errors occurred in the Russian text rather than in numbered formulas.

UNCLASSIFIED

Security Classification

DOCUMENT CONTROL DATA - R & D

(Security classification of title, location, abstract, and index information must be entered when the overall report is classified)

1. ORIGINATING ACTIVITY (Corporate author) Foreign Science and Technology Center US Army Materiel Command Department of the Army	2a. REPORT SECURITY CLASSIFICATION Unclassified
	2b. GROUP

3. REPORT TITLE  
FERROELECTRICS AND ANTIFERROELECTRICS

4. DESRIPTIVE NOTES (Type of report and inclusive dates)  
Final Report

5. AUTHOR (Last name, middle initial, first name)  
G. A. SMOLENSKI

6. REPORT DATE 27 January 1971	7a. TOTAL NO OF PAGES 125	7b. NO OF REFS N/A
-----------------------------------	------------------------------	-----------------------

8a. CONTRACT OR GRANT NO.	9a. ORIGINATOR'S REPORT NUMBER(S) F 10-411-2-1-1-71
b. PROJECT NO. c. 17-23-1-2-11	9b. OTHER REPORT NUMBER(S) (Any other numbers that may be assigned this report)
d. Requester SMOLENSKI, G. A.	

10. DISTRIBUTION STATEMENT  
Approved for public release; distribution unlimited.

11. SUPPLEMENTARY NOTES	12. SPONSORING MILITARY ACTIVITY US Army Electronics Research and Development Center
-------------------------	---

13. ABSTRACT  
The book is devoted to a systematic description of the properties of ferroelectric and antiferroelectric materials. Special attention is given to model theories of ferroelectricity, dielectric, piezoelectric, and other properties of a wide range of materials. Results of experimental studies, theoretical models, and applications of ferroelectric materials are also discussed. Ferroelectricity is defined as a property of materials which exhibit a spontaneous polarization. The book is intended for scientists and engineers working in the field of solid state physics and materials science.

DD FORM 1473 1 NOV 66

REPLACES DD FORM 1473, 1 JAN 64, WHICH IS OBSOLETE FOR ARMY USE.

UNCLASSIFIED Security Classification

UNCLASSIFIED

Security Classification

14. KEY WORDS	LINK A		LINK B		LINK C	
	ROLE	WT	ROLE	WT	ROLE	WT
Ferroelectricity Ferroelectric Material Mussbauer effect Solid State Physics Diagnostic Methods Electrooptic Effect Magnetic Domain Structure  SUBJECT CODE: 20, 14 COUNTRY CODE: UR						

UNCLASSIFIED

Security Classification

UDC 537.226.23

FERROELECTRICS AND ANTIFERROELECTRICS (Book by G. A. Smolenskiy et al.); Nauka Publishing House, Leningrad Branch, Leningrad, 1971, pp 1-476

Abstract

The book is devoted to a systematic description of physical phenomena in ferroelectrics and antiferroelectrics. Serious attention is given to thermodynamic, dynamic and model theories of ferroelectricity, which are set forth in a form understandable to a wide range of readers. Results of experimental studies and their correspondence to theoretical representations are discussed in detail using several of the most typical ferroelectrics as an example. Considerable space is set aside for the study of ferroelectrics with the aid of new methods: radiospectroscopy, Messbauer effect, scattering of slow neutrons, electrooptics, etc. A review of ferroelectric and antiferroelectric materials is given including ferroelectrics with magnetic orderliness and with a blurred phase transition. The book is intended for engineers, scientific workers, for graduate and upper-class undergraduate students studying problems of solid state physics, problems of radio electronics, electroacoustics, etc.

Bibliography of 1,988 titles, 189 figures, 33 tables.

## FOREWORD

Ferroelectricity is a young section of solid state physics which, however, has already gained a firm foothold. The interest in it is very great. This is explained on one hand by the importance of physical problems in the field of ferroelectricity and on the other -- by the ever increasing practical application of ferroelectrics.

Ferroelectrics are characterized by a high specific inductive capacitance, a high piezomodulus, by the presence of dielectric hysteresis loop, by interesting electrooptical properties, and are, therefore, widely used in many fields of present-day engineering: radio engineering, electroacoustics, quantum electronics and measuring technique. Ferroelectronics are used for making small-sized capacitors, piezoelements, pyroelectric radiant-energy receivers, nonlinear capacitive elements, oscillators, laser-radiation modulators, parametric generators, etc.

The flow of works on ferroelectricity physics increases every every year and the processing of information contained in them is an important task. Under these conditions, periodic generalization and evaluation of results achieved in this area of physics are very desirable.

A number of books on ferroelectricity physics have been published at the present time: Kentzig's survey (1957), a book small in volume by Megaw (1957), a fundamental monograph by Jona and Shirane (1962), a book by Martin with a stress on application (1965), a book by Boerfut (1967), a small monograph by Fatuzzo and Merz (1967), a book by Zheludev (1968), a popular-science book by Smolenskiy and Kraynik (1969), etc. The monograph by Jona and Shirane and Kentzig's survey have been translated into Russian.

The works of the Soviet scientists are insufficiently illuminated in these publications but their role in the development of ferroelectricity physics is great. The most important stages of development of this field of science are connected

with the names of I. V. Kurchatov, B. M. Vul and V. L. Ginzburg. I. V. Kurchatov investigated in detail for the first time the properties of Seignette's salt and laid down the fundamentals of ferroelectricity physics. B. M. Vul discovered and investigated ferroelectric properties of barium titanate -- representative of a new class of ferroelectrics. This discovery played a decisive role in the development of ferroelectricity physics and in the application of ferroelectrics in engineering. V. L. Ginzburg developed thermodynamic theory and laid down the fundamentals of dynamic theory of ferroelectricity. A large number of ferroelectrics and antiferroelectrics with different crystal-line structures have been discovered in the Soviet Union. The Soviet scientists investigated in detail the physical properties of many ferroelectrics, they applied symmetry theory to the prediction of characteristics of ferroelectric state, and successfully utilized the latest methods of physical experiments for investigation of ferroelectric phenomena.

The aim of this book is setting forth the fundamentals of ferroelectricity physics and discussion of its present-day state. Overcoming in advance the entire complexity of this task the authors accomplished it using a large group. Nevertheless, apparently the number of authors is as yet not so large as to have a negative effect on the quality of the book. In any case, everything possible was done during its writing in order that the authors' individuality would not interfere with the integrity of the presentation.

In essence the book is an assemblage of thematically interconnected survey (in some cases quite detailed) chapters which throw light on different sections of ferroelectric and antiferroelectric physics.

Chapter 1 is devoted to a description of basic phenomena in ferroelectrics. An idea of special features of ferroelectric phase transitions of the 1st and 2nd kind is given. Breaking up of crystals into domains and also behavior of ferroelectrics in strong fields are examined. Classification of ferroelectrics according to the type of chemical bond is given. Concept of antiferroelectrics is also given. A semiempirical criterion of the appearance of ferroelectricity is examined in conclusion.

Chapter 2 gives information on crystalline structure of the most important ferroelectrics. Using them as an example ferroelectric phenomena are discussed in later chapters. Conditions for the existence of perovskite-type structure in which barium titanate and many other ferroelectrics crystallize are examined. Phase transitions in  $\text{BaTiO}_3$  and displacements of ions in these transitions are described. Crystalline structure of potassium dihydrophosphate, triglycine phosphate, Seignette's salt and sodium nitrite are discussed.

Chapters 3-6 set forth theory of ferroelectric phenomena. The authors strove to illuminate it sufficiently completely and in a form understandable to a wide range of readers. Chapter 3 sets forth thermodynamic theory based on Landau and Ginzburg general theory of phase transitions. In addition to this, a new and fruitful direction of theory connected with the use of concepts of critical indices and with similarity relationships is examined. Theoretical description of a number of properties of ferroelectrics, including nonlinear effects, is also given.

Chapter 4 is devoted to microscopic model theories. Both comparatively early model representations (model of local minima, model of anharmonic oscillators, Janes electron theory, etc.) which have not lost their significance are set forth, and recently published works in which problems of ferroelectricity are analyzed with the aid of Ising model, Bogolyubov method, within the framework of pseudo-Yang-Teller effect, with the aid of isospin method, etc. In doing so, the authors endeavored to trace historical lines of development of model theories, connection between them, to compare model theories with dynamic approach to the problem of ferroelectricity and to draw attention to the similarity of some of their most important propositions.

Chapter 5 sets forth dynamic theory of ferroelectricity based on Ginzburg's ideas developed later by Anderson, Cochrane and others. It examines dynamic theory of Born-Karman crystal lattices, sets forth the fundamentals of theoretical group analysis of vibration spectra necessary for interpretation of experimental data, and gives results of calculations of vibration spectra of actual ferroelectric crystals. The main attention is devoted to the connection of ferroelectric transition with the loss of stability of crystal lattice relative to one of its vibrations ("soft mode"), and some of the effects caused by the presence of "soft mode" are also examined.

Chapter 6 is in essence a theoretical group supplement. Its aim is to make understandable to a wider range of readers the problems connected with the application of symmetry theory and set forth in chapters 3-5, 15, etc.

Chapter 7 is devoted to a description of domain structure of ferroelectrics. Causes of the formation of domains are analyzed. Representations of domain walls are briefly examined. A description of domain structure of some of ferroelectrics is given and also a description of methods of detecting the domain structure.

Chapter 8 examines temperature dependences of spontaneous polarization of several of the most typical ferroelectrics and also repolarization processes. Nonlinear electric properties brought about by repolarization are also described here.

Chapter 9 is devoted to polarization of ferroelectrics in a weak electric field. It discusses temperature dependences of specific inductive capacitance and losses, nonlinearity in paraelectric phase, reversible characteristics, and dispersion of specific inductive capacitance.

Electromechanical properties of ferroelectrics are examined in chapter 10. General relationships connecting piezoelectric coefficients with electrostrictive coefficients, spontaneous polarization and dielectric susceptibilities are derived for ferroelectrics not having piezoelectric effect in paraelectric phase. A description of electromechanical properties of barium titanate and triglycine sulfate is given. Electromechanical properties of ferroelectrics having piezoelectric effect in paraelectric phase are discussed using potassium dihydrophosphate and Seignette's salt as an example. Experimental data on internal friction and absorption of ultrasound in ferroelectrics are briefly cited at the end of the chapter.

Chapter 11 is devoted to electrooptical and certain other nonlinear optical phenomena in ferroelectrics. General concepts of such nonlinear optical effects as electrooptical effect, generation of harmonics, and of their characteristics in ferroelectrics are given in this chapter. Data on nonlinear optical properties of the principal ferroelectric materials are cited.

Thermal properties of ferroelectrics are described in chapter 12. Thermal anomalies at the Curie point are examined using several compounds as an example, and a few -- for the time being -- experimental data on thermal conduction and electrocalorific effect are cited.

The effect of external actions (of electric field and hydrostatic pressure) on ferroelectric phase transition is discussed in chapter 13.

Chapter 14 describes studies of ferroelectrics using the methods of electronic paramagnetic, nuclear magnetic and nuclear quadrupole resonances, and with the aid of Messbauer effect. An idea of physical parameters determined by these methods is given. Results of investigation of a number of ferroelectrics are cited.

Chapter 15 is devoted to the studies of vibrations of the crystal lattice of ferroelectrics near Curie temperature

using the infrared spectroscopy, Raman effect, inelastic neutron scattering and thermal diffusion scattering of x-rays and electrons. In doing so, the main attention is devoted to investigations in which data on ferroactive low-frequency vibrations of the lattice were obtained.

Chapter 16 describes the features of ferroelectrics with a blurred phase transition. Transitions of this kind were found in many ferroelectric substances, in particular in a number of ferroelectric materials used in practice.

Chapter 17 examines the properties of antiferroelectric compounds and solid solutions. Much attention is devoted to antiferroelectrics with a structure of perovskite type. The concept of antiferroelectricity is discussed.

Chapter 18 is devoted to a comparatively new class of substances -- ferroelectrics with magnetic order. The main results of phenomenological theory of ferroelectrics-ferromagnetics are given and three groups of ferroelectrics with magnetic order are examined -- perovskites, hexagonal manganites and boracites.

Chapter 19 gives a survey of properties of ferroelectric oxides, halides, and chalcogenohalides. Crystalline and domain structures, characteristics of phase transitions, dielectric polarization, piezoelectric, elastic, thermophysical, optical and electrooptical properties are described.

Foreword and chapter 1 were written by G. A. Smolenskiy, chapter 2 -- by G. A. Smolenskiy and V. A. Isupov, chapters 3-6 -- by R. Ye. Pasynkov and M. S. Shur, chapters 7-10, 12 and 13 -- by V. A. Bokov, chapters 11 and 15 -- by G. A. Smolenskiy and N. N. Kraynik, chapters 14 and 17 -- by N. N. Kraynik, chapter 18 -- by G. A. Smolenskiy and V. A. Bokov, and chapters 16 and 19 -- by V. A. Isupov.

## CHAPTER 1. BASIC CONCEPTS OF FERROELECTRICITY PHYSICS

Seignettelectrics [called so by analogy with the properties of Seignette's salt; see Translator's Note in front] is the term used to call crystalline substances in which spontaneous polarization occurs in a certain temperature range in the absence of an external electric field and mechanical stresses. The direction of this polarization can be changed by an electric field and in a number of cases by mechanical stresses. As a rule, seignettelectric crystals are divided into separate regions (domains) characterized by the direction of spontaneous polarization.

With a rise of temperature, seignettelectrics undergo a phase transition accompanied by the disappearance of spontaneous polarization and by a change in the symmetry of the crystal lattice. Temperature at which a phase transition takes place is called Curie temperature ( $T_c$ ) regardless of whether this transition is of the first or second kind. This transition may be brought about by a change in mechanical stresses and electric field. A high susceptibility of a seignettelectric in regard to various physical influences (temperature  $T$ , mechanical stresses  $\sigma_{ik}$ , electric field  $E$ ) is usually observed near a phase transition. For the same reason the dependence of seignettelectrics' polarization on  $T$ ,  $\sigma_{ik}$  and  $E$  may have a non-linear character. In classical pyroelectrics (tourmaline, etc.) no such phase transition exists and the respective dependences are practically linear.

Seignettelectric properties were discovered for the first time in Seignette's salt from which this name originated. The term "ferroelectricity" which underscores analogy with ferromagnetism is used in foreign literature more often [1, 2]. However, this analogy exists only in the purely phenomenological scheme. The microscopic nature of these phenomena is completely dissimilar. [Except to draw the distinction as above, the translator has been and will be using the terms "ferroelectricity" and "ferroelectric" to conform to the English-language sources].

Spontaneous polarization ( $P_s$ ) occurs in classical pyroelectrics and in ferroelectrics owing to a displacement of ion sublattices or ordering of atomic groups having a dipole moment. In doing so, ions responsible for the appearance of  $P_s$  in ferroelectrics are displaced comparatively easily (dipole groups change the direction of electric moment). It is precisely owing to this that ferroelectric phase transition proves to be possible. In classical pyroelectrics such ions or dipole groups are rigidly fixed in the entire temperature range of existence of solid state. In this case, external electric fields and mechanical stresses are unable to reorient spontaneous polarization. It is helpful to note that ferroelectric substances with very high Curie temperature approaching the melting points are known at the present time, for example  $\text{LiNbO}_3$ , etc. Thus, the "hardness" of some ferroelectrics is also very great and in properties they approach classical pyroelectrics.

Phase (including ferroelectric) transitions are subdivided into transitions of the first and second kind <sup>\*)</sup>. Second derivatives of the thermodynamic potential: specific inductive capacitance, thermal capacity, coefficient of linear expansion, moduli of elasticity, piezomodulus, etc. sharply change in phase transition of the second kind. In addition to a sharp change in these quantities, first derivatives of the thermodynamic potential such as spontaneous polarization and entropy undergo a jump in phase transition of the first kind, and latent heat of the transition is released.

Temperature dependence of the specific inductive capacitance, more exactly of susceptibility above ferroelectric transition, is described by Curie-Weiss law:

$$\epsilon \approx \frac{C}{T - \theta} \quad (1.1)$$

Here  $C$  is Curie constant and  $\theta$  -- Curie-Weiss temperature. Hence, by analogy with magnetism the nonpolar phase is often called paraelectric. In some cases it is necessary to take into account the additional term  $\epsilon_0$  which actually does not depend on temperature, and then

$$\epsilon = \epsilon_0 + \frac{C}{T - \theta} \quad (1.2)$$

In phase transitions of the first kind the temperature of transition  $T_c > \theta$ ;  $(T_c - \theta)$  is usually of the order of  $10^2$ , and in phase transitions of the second kind  $T_c = \theta$  (Figure 1.1)

The behavior of ferroelectrics below Curie point is determined to a considerable degree by their domain structure.

<sup>\*)</sup> Translator's note: English-language sources use the term "first and second order transitions".

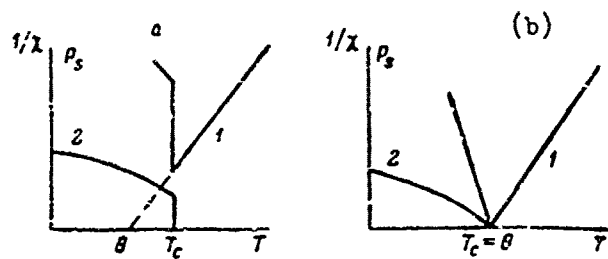


Figure 1.1. Temperature dependence of inverse dielectric susceptibility  $1/\chi$  (the curves 1) and of spontaneous polarization  $P_s$  (the curves 2) in the case of transitions of the first kind (a) and of the second kind (b).

The causes of the formation of domains may be qualitatively explained in the following manner. If a homogeneous crystal is spontaneously polarized, then the charges appearing on its surface create an electric field (this field is called a depolarizing field). Breaking up of a crystal into domains, i.e. into regions with different directions of spontaneous polarization, decreases the depolarizing field and, consequently, the energy connected with it, and is, therefore, advantageous from the standpoint of energy. However, with the breaking up of a crystal into domains energy necessary for the formation of domain walls increases and, thus, the domain structure is determined by "energy compromise" between these two factors. In a more rigid examination the effect of mechanical stresses has to be taken into account.

In ferroelectrics the thickness of the boundary between antiparallel domains is small; it does not exceed a few interatomic distances while the boundary energy is high (energy density of the boundary layer is of the order of  $10 \text{ ergs/cm}^2$ ). In particular, ferroelectrics differ in this respect from ferromagnetics in which the thickness of the boundary layers between the domains reaches tens and hundreds of interatomic distances.

A rearrangement of domain structure takes place in a multidomain crystal under the effect of external field. In this process, spontaneous polarization changes its direction in a certain volume of the crystal. The process of reorientation of spontaneous polarization is accomplished by means of motion of domain walls and also by means of formation and intergrowth of nuclei of new domains with a direction of spontaneous polarization approaching the direction of electric field.

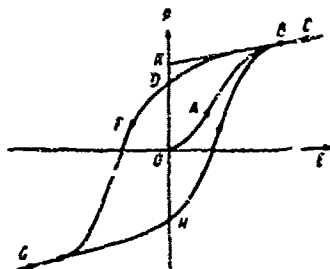


Figure 1.2. Schematic representation of dielectric hysteresis loop in a ferroelectric.

In sufficiently weak fields, polarization linearly depends on the field (Figure 1.2). Processes of reversible displacement of domain walls predominate on this section. With an increase of the field, the formation of nuclei of new domains begins and displacement of domain walls becomes irreversible. In doing so, polarization increases faster than in accordance with linear law.

At a certain field strength corresponding to the point B the crystal becomes a single-domain crystal and the so-called saturation is reached. With a further increase of the field the total polarization of the crystal continues to increase only owing to an increase in induced polarization (the section BC) which is especially high near the phase-transition point. The curve OABC is often called the initial or fundamental branch of hysteresis loop. If after reaching the saturation the field strength is decreased, the polarization of the crystal will change not in accordance with the initial curve but in accordance with the curve CBD and in the case of a field equal to zero the crystal remains polarized. The magnitude of polarization defined by the line segment OL is called residual polarization. Extrapolation of the section CB onto the Y-axis cuts off the line segment OK which is approximately equal to spontaneous polarization. If the direction of the field is changed, then polarization will decrease, it will change sign and with a certain field will again reach saturation (the section DFG). Field strength defined by the line segment OF, at which polarization is equal to zero is called coercive field ( $E_c$ ). Thus, relationship of polarization to electric field strength is described by the curve CBDFGHBC called hysteresis loop.

At the present time, a considerable number of ferroelectrics are known which represent different types of chemical compounds: oxides, sulfates, tartrates and other compounds having different crystal structure. With respect to chemical bond and type of the phase transition ferroelectrics may be divided into two large groups.

1. Ferroelectrics which are mainly crystals with a considerable degree of ionicity of the bond and which do not contain atomic groups having a permanent dipole moment. In these crystals spontaneous polarization is brought about by a displacement of equilibrium position of anharmonically vibrating sublattices of the ions. Inasmuch as in this case the phase transition from paraelectric state into ferroelectric state occurs as a result of displacement of ions it is called phase transition of the displacement type and the crystal -- ferroelectric of the displacement type. A classical example of a ferroelectric of this type is barium titanate. Curie-Weiss constant  $C$  for specific inductive capacitance in displacement-type transitions proves to be large and amounts, for example, for barium titanate to about  $1.5 \cdot 10^5$  °K.

2. Ferroelectrics containing dipole groups formed by atoms bound with each other chiefly by covalent forces. These dipole groups may have a charge. In this case, their bonds with ions not contained in these groups have chiefly an ionic character. In crystals of this type there are several possible equilibrium positions of dipole groups with these positions corresponding to different orientations of the dipoles. In the paraelectric region the long-range order is absent in the arrangement of the dipoles but it appears in the ferroelectric region.

Thus, here the phase transition and appearance of spontaneous polarization are connected with the orderedness of the dipoles. Hence the names: phase transition of the order-disorder type and ferroelectrics of the order-disorder type. In this case the value of Curie-Weiss constant amounts approximately to  $10^3$  °K, i.e. two orders less than in ferroelectrics of displacement type. Examples of ferroelectrics of the order-disorder type are potassium dihydrophosphate, sodium nitrite, etc. It should be noted that the division examined is approximate and ferroelectric transitions of mixed type are possible.

This is not the only method of classifying the ferroelectrics [1-3]. They may also be grouped according to the character of phase transition from nonpolar into polar phase (of the first or second kind), according to the presence or absence of piezoeffect in paraelectric phase, according to the number of possible directions of spontaneous polarization (uniaxial and multiaxial), and according to the type of crystal structure.

Phase transition with a change in lattice symmetry takes place in some crystals at certain temperatures. In doing so, ions of the same kind are displaced not parallel to each other as in ferroelectrics but antiparallel to each other. This

leads to an antiparallel orientation of dipole moments. Such an orderedness of moments also exists in some crystals having dipole groups. Crystals with dipole moments ordered in antiparallel are called antiferroelectrics. Crystals whose free energy approaches the free energy of isomorphous ferroelectrics have been assigned of late to antiferroelectrics. It should be noted that a noncollinear arrangement of dipole moments which produces a zero resultant polarization is possible.

Antiferroelectrics may be regarded as an assemblage of two or more sublattices with one being inserted into the other and with the dipole moments in each sublattice being oriented parallel to each other. Spontaneous polarization in each sublattice is not equal to zero but the aggregate spontaneous polarization in the crystal proves to be equal to zero. In the simplest cases the crystal lattice in an antiferroelectric has a center of symmetry and the piezoeffect is absent. A maximum of specific inductive capacitance the magnitude of which is smaller than in ferroelectrics with the same crystal structure is observed at the point of transition. A multiple increase of dimensions of unit cell is usually observed in a phase transition from paraelectric state into antiferroelectric state. In Figure 1.3, in paraelectric region the unit cell is represented by the squares  $abcd$  whereas in antiferroelectric phase the unit cell is represented by the rectangle  $abef$ .

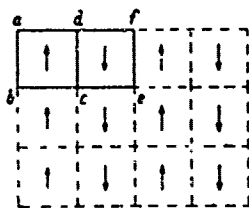


Figure 1.3. Schematic representation of dipole moments in an antiferroelectric.

When a sufficiently strong electric field is superimposed the antiferroelectric may change into ferroelectric state. The fact is that parallel orientation of dipole moments in the presence of an external field may prove to be more advantageous from the standpoint of energy than an antiparallel orientation. With such a "forced" phase transition, "double" hysteresis loops are observed in a strong variable field (Figure 1.4). In the case of a small field strength, polarization vs. field dependence is practically linear. Transition into ferroelectric state occurs when field strength reaches a critical magnitude  $E_{cr 1}$ . With a decrease of the field strength the crystal returns into ferroelectric state but with an  $E_{cr 2}$  which is smaller than  $E_{cr 1}$ .

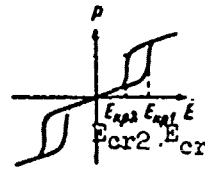


Figure 1.4. Double hysteresis loop.

Incomplete compensation of dipole moments of the sublattices may occur in more complex cases. By analogy with ferromagnetics these substances are called ferroelectrics.

According to the present-day concepts which are based on Ginzburg's ideas [4] developed later by Anderson [5], Cochran [6] and others, ferroelectric transition of the displacement type takes place owing to the compensation of effective force constants corresponding to the long-range dipole-dipole forces and short-range repulsive forces. With such a compensation the frequency of optical oscillation of the lattice reaches anomalously small values, the crystal loses stability relative to this oscillation and a ferroelectric transition takes place. On the basis of these theoretical concepts and also on the basis of an earlier model of an anharmonic oscillator [7-9] it was possible to formulate certain qualitative considerations which were used for finding new ferroelectric crystals, chiefly of the oxyoctahedral type. It is obvious that dipole-dipole interaction will be the stronger the larger the internal field in a crystal, and also the higher the electronic and ionic polarizability.

Calculations have shown that in crystals containing oxygen octahedrons arranged in a certain manner the internal fields are large [8, 10, 11]. Thus for example, connection of octahedrons with their apexes, the way this occurs in structures of the perovskite type, lithium niobate and potassium-tungsten bronze is opportune. Oxygen octahedrons containing ions of transition elements which have a noble-gas shell after yielding the s- and d-electrons are characterized by a high electronic polarizability. It is assumed that a large number of electronic states with like energies [12, 13] and a relatively small size of the slit between the filled p-region of oxygen and d-region of conductance [14-16] are characteristic of these octahedrons. Upon superimposition of electric field the small size of the slit between p-region and d-region ensures a high probability of transition of electrons to an excited state and a high electronic polarizability of the octahedron.

An important role is played not only by electronic polarizability of an oxygen octahedron in perovskites and in crystals of some of the other structural types but also by the polarizability of ions located between the octahedrons. The  $Pb^{3+}$  and  $Bi^{3+}$  and apparently the  $Tl^{1+}$  ions are characterized by high electronic polarizability [17]. Accordingly, many compounds containing  $Pb^{2+}$  and  $Bi^{3+}$  ions are ferroelectrics with high Curie temperatures.

A number of authors have voiced a supposition that loose packing of ions in crystals contributes to the appearance of spontaneous polarizability. An excessively great significance was ascribed to this factor in early works.

The semiempirical crystallophysical considerations examined above which are useful in the search for new oxyoctahedral ferroelectrics were formulated in the works [18, 19]. They played an important part in the discovery of new ferro- and antiferroelectrics and also of substances with a high specific inductive capacitance.

A number of ferroelectrics have been discovered recently, for example,  $YMnO_3$  in which minor cations have no electron shell characteristic of noble-gas atoms. In addition to this, cations do not always have the coordination number six, for example in  $Mn^{3+}$  and  $YMnO_3$  the coordination number is equal to five. Thus, the criteria in question for the appearance of spontaneous polarization in crystals of oxyoctahedral type cannot be considered as general criteria. Therefore, an important problem is the further clarification and more exact determination of conditions for the appearance of spontaneous polarization for this broad class of substances. In searching for ferroelectrics the guide used is first of all considerations of the existence of hydrogen bonds in crystals and of groups having a large dipole moment in crystals ( $NO_2^-$ ,  $NO_3^-$ ,  $SO_4^{2-}$ ,  $SeO_4^{2-}$ , etc.).

#### BIBLIOGRAPHY

1. V. Kentzig. Segnetoelektriki i Antisegetoelektriki [Ferroelectrics and Antiferroelectrics]. IL [Foreign Literature Press], Moscow (1960).
2. F. Jona, D. Snirane. Segnetoelektricheskiye Kristally [Ferroelectric Crystals]. Mir Publishing House, Moscow (1965).

3. G. A. Smoleskiy, N. N. Kraynik. Segnetoelektriki i Antisegetelektriki [Ferroelectrics and Antiferroelectrics]. Nauka Publishing House, Moscow, (1968).

4. V. L. Ginzburg, FTT, Vol 2, p 2031 (1960).

5. P. Anderson. Fizika Dielektrikov [Physics of Dielectrics]. Published by Academy of Sciences USSR, Moscow, p 290 (1960).

6. W. Cochran, Adv. Phys., Vol 9, p 387 (1960); Vol 10, p 401 (1961).

7. V. L. Ginzburg, ZhETF [Journal of Experimental and Theoretical Physics], Vol 15, p 729 (1945); Vol 19, p 36 (1949); UFN [Achievements of Physical Sciences], Vol 38, p 490 (1949).

8. J. C. Slater, Phys. Rev., Vol 78, p 748 (1950).

9. A/ F/ Devonshire, Phil. Mag., Vol 40, p 1040 (1949); Vol 42, p 1065 (1961).

10. G. I. Skanavi. Fizika Dielektrikov [Physics of Dielectrics]. GITFL [State Publishing House for Technical and Theoretical Literature], Moscow--Leningrad (1948).

11. V. Kh. Kozlovskiy, ZhTF [Journal of Technical Physics], Vol 21, p 1388 (1951).

12. W. Shockley, Phys. Rev., Vol 73, p 1273 (1948).

13. J. Tessen, A. Kann, W. Shockley, Phys. Rev., Vol 92, p 890 (1953).

14. J.H. van Santen, F. de Boer. Nature, Vol 163, p 957 (1949).

15. J. H. van Santen, J. N. Jonker, Philips Res. Rep., Vol 3, p 371 (1948).

16. A. H. Kahn, A. J. Leyendecker, Phys. Rev., Vol 135, A13 21 (1964).

17. L. E. Orgel, J. Chem. Soc., Vol 12, p 3815 (1959).

18. G. A. Smolenskiy, N. V. Kozhevnikova, DAN SSSR [Proceedings of USSR Academy of Sciences], Vol 76, p 519 (1951).

19. B. T. Matthias, Science, Vol 113, p 591 (1951).

## CHAPTER 2. CRYSTAL STRUCTURE OF THE MOST IMPORTANT FERROELECTRICS

This chapter gives a brief description of crystal structure of those ferroelectrics which will be chiefly used as an example in the discussion of ferroelectric phenomena in the subsequent chapters. Among these ferroelectrics are barium titanate, Seignette's salt, potassium dihydrophosphate, triglycine sulfate and sodium nitrite. Crystal structure of the other ferroelectrics is discussed in a survey of properties of ferroelectric crystals. Crystal structures of antiferroelectrics are discussed in chapter 17.

### Par. 1. Barium Titanate

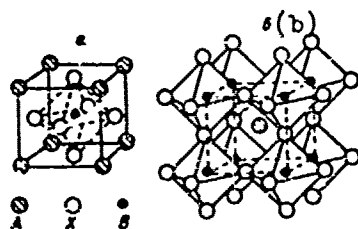


Figure 2. . Crystal structure of perovskite type.

a -- unit cell; b -- framework of octahedrons.

Many ferroelectrics crystallize in a structure of perovskite type characteristic of  $ABX_3$  compounds with a general chemical formula  $ABX_3$  where A and B are cations and X -- anions.

A structure of perovskite type is constructed of  $BX_6$  octahedrons connected with each other by vertices (Figure 2.1). Connection of octahedrons takes place in such a manner that rectilinear chains of octahedrons parallel to each other can be differentiated by all of the three mutually perpendicular axes. Octahedrons of the neighboring chains are connected by their vertices. As a result of this, a three-dimensional framework of octahedrons is obtained (Figure 2.1b). A cation is located in the spaces between the octahedrons. Thus, if B cations are surrounded by six X anions, then occupying the center of the cubo-octahedron the A ions are surrounded by 12 anions. X anions are surrounded by six cations: four cations A lying at a distance  $a/\sqrt{2}$  (where a is lattice parameter) in the vertices of the square whose center is an anion, and two B cations lying at a distance  $a/2$  in a direction perpendicular to the square made up of A ions.

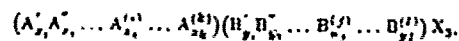
The crystal lattice of compounds with a structure of perovskite type: of ferroelectric compounds in paraelectric state and of nonferroelectric compounds has in many cases a cubic symmetry and belongs to the space group  $O_h^1$ --Pm3m. In this case the unit cell contains one formulaic unit.

Satisfaction of the following two geometric conditions ensuring a close packing of atoms and determining the permissible dimensions of A and B cations and of anions is mandatory for the existence of the compound  $ABX_3$  with a structure of perovskite type [1]:

$$R_B > 0.41R_X; \quad t_1 < t = \frac{R_A + R_X}{\sqrt{2}(R_B + R_X)} < t_2$$

$R_B$  and  $R_X$  are here the tabular ionic radii assigned to ions with the coordination number (c.n.) 6, and  $R_A$  is tabular radius for coordination number 12 ( $R_{(c.n.12)} = 1.12 R_{(c.n.6)}$ ). The value of t approaches unity but, as a rule, differs from it and lies in a range from  $t_1 = 0.76$  to  $t_2 = 1.03$ . Satisfaction of the condition  $t_1 < t < t_2$  alone is insufficient to form perovskite structure. For example, for  $AlBO_3$  (ferromagnetic structure)  $t = 0.91$  and lies within permissible limits but perovskite structure does not form owing to a small radius of boron ion.

In the case of complex perovskite compounds the general chemical formula may have the following form [2]:



where  $\sum_{i=1}^k x_i = 1$  and  $\sum_{j=1}^l y_j = 1$  ( $x_i > 0$ ;  $y_j > 0$ ). In addition to this, the following requirement of electric neutrality of the crystal must be observed:

$$\sum_{i=1}^k x_i n_{A(i)} + \sum_{j=1}^l y_j n_{B(j)} + 3n_X = 0$$

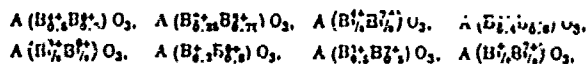
(where  $n_{A(i)}$ ,  $n_{B(j)}$  and  $n_X$  are the valences of the respective ions), and also the requirement of the condition:

$$t_1 < t_2 = \frac{R_A + R_X}{\sqrt{2}(R_B + R_X)} < t_3; \quad a_1 < \frac{R_{A(i)}}{R_X} < a_2; \quad b_1 < \frac{R_{B(j)}}{R_X} < b_2$$

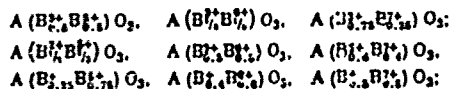
where  $\bar{R}_A = \sum_{i=1}^k x_i R_{A(i)}$  and  $\bar{R}_B = \sum_{j=1}^l y_j R_{B(j)}$ . These conditions limit the dimensions of the  $A^{(i)}$  and  $B^{(j)}$  ions and the mean radii  $\bar{R}_A$  and  $\bar{R}_B$ . As already mentioned,  $b_1 = 0.41$ ; the values of  $a_1$ ,  $a_2$  and  $b_2$  have not as yet been determined exactly but apparently  $a_2$  is not less than 0.74;  $a_1 \approx 0.73$  and  $a_2$  is not less than 1.13 ( $R_A$  were corrected to c. n. 12).

If X is an oxygen ion  $O^{2-}$ , then by combining in octahedrons the ions with different valences the following groups of complex perovskite compounds may be obtained.

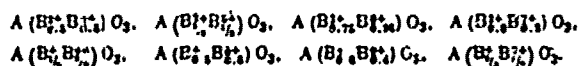
With  $n_A = 1$ :



with  $n_A = 2$ :



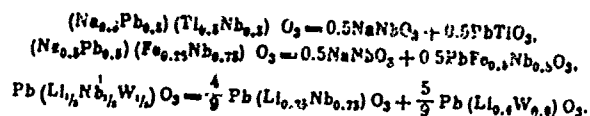
with  $n_A = 3$ :



Only the  $A_{0.5}^+ A_{0.5}^3 B^{4+} O_3$  group of compounds can be obtained with  $n_B = 4$ . (Owing to the small size and, probably, too high a charge, ions with a valence of 4, 5, etc. cannot be taken as

ions with c.u. 12). Apparently the compounds  $A_{0.5}^+ A_{0.5}^{3+} B_{0.4}^+ B_{0.6}^{6+} O_3$ ,  $A_{0.5}^+ A_{0.5}^{3+} B_{0.5}^{2+} B_{0.5}^{6+} O_3$ ,  $A_{0.5}^+ A_{0.5}^{3+} B_{0.5}^+ B_{0.5}^{7+} O_3$  and  $A_{0.5}^+ A_{0.5}^{3+} B_{0.6}^{2+} B_{0.4}^{7+} O_3$  can also be obtained. These groups exhaust all of the possible types of complex perovskite compounds. Apparently not all of the types can be realized. In any case, for many of them the representatives have not been found up to the present time.

It is necessary to underscore that, as a rule, complex formulas, for example  $(A_x^+ A_{1-x}^{3+}) (B_y^+ B_{1-y}^{6+}) O_3$  and  $A (B_x^+ B_{1-x-y}^{6+} B_y^{7+}) O_3$ , describe solid solutions. The following may be cited as an example:



In the case of the last equality, compounds corresponding to the formulas on the right apparently do not exist. However, solid solutions may exist even in this case and a phase with perovskite may be observed in a more or less wide range of values of the concentrations. Whether the compound  $Pb1/3(Li1/3 \times Nb1/3W1/3)O_3$  exists in this case can only be determined from the form of the phase diagram of the system formed by two combinations of oxides that are on the right in the last equality (for example, from the presence of a maximum on the liquidus curve). A compound of perovskite type cannot, by far, form with any combinations of ions satisfying the formulas cited above. The tendency of the ions to the formation of these or other hybrid bonds leads to this or other oxygen encirclement. It may turn out that the preferable oxygen encirclement will not correspond to the encirclement of atoms in a structure of perovskite type.

Barium titanate  $BaTiO_3$  is the most investigated ferroelectric with a structure of perovskite type. Above Curie temperature ( $120^\circ C$ ) this compound has a cubic lattice with a lattice parameter of  $\sim 4 \text{ \AA}$ . In this case the coordinates of the atoms of Ba are:  $(0, 0, 0)$ , of Ti:  $(\frac{1}{2}, \frac{1}{2}, \frac{1}{2})$ , of O:  $(\frac{1}{2}, \frac{1}{2}, 0)$ ,  $(\frac{1}{2}, 0, \frac{1}{2})$ ,  $(0, \frac{1}{2}, \frac{1}{2})$ . Below  $120^\circ C$  barium titanate becomes tetragonal with the lattice parameters  $a=3.992 \text{ \AA}$  and  $c=4.036 \text{ \AA}$  at room temperature [4] and belongs to the space group  $C_{4v}^1 - P4mm$ . The lengthening of the cell's edges takes place in the direction in which spontaneous polarization occurs (along the c axis) (Figure 2.2b). Coordinates of the

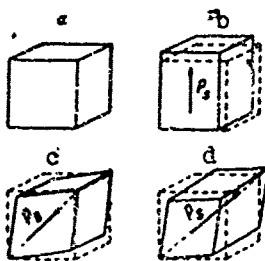


Figure 2.2. Unit cell of  $\text{BaTiO}_3$  in different phases.

a -- cubic; b -- tetragonal; c -- rhombic; d -- rhombohedral. Broken lines show the initial cubic cell. Arrowhead indicates the direction of spontaneous polarization.

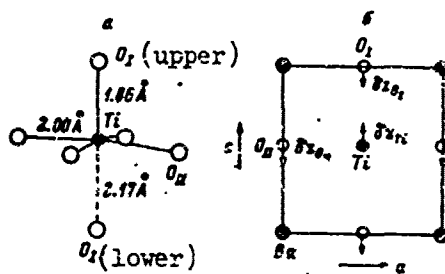


Figure 2.3. Displacement of ions in a tetragonal  $\text{BaTiO}_3$ .  
 a -- distortion of  $\text{TiO}_3$  octahedron;  
 b -- directions of the displacements of ions in a unit cell.

atoms may be described in the following manner:

$$\text{Ba}: (0, 0, 0), \text{Ti}: \left(\frac{1}{2}, \frac{1}{2}, \frac{1}{2} + \delta z_{\text{Ti}}\right), \text{O}_I: \left(\frac{1}{2}, \frac{1}{2}, \delta z_{\text{O}_I}\right),$$

$$2\text{O}_{II}: \left(\frac{1}{2}, 0, \frac{1}{2} + \delta z_{\text{O}_{II}}\right), \left(0, \frac{1}{2}, \frac{1}{2} + \delta z_{\text{O}_{II}}\right).$$

The quantities  $\delta z$  represent here the displacements of atoms from the center of parallelepiped formed by barium ions (Figure 2.3).

An exact determination of the displacements of ions is difficult owing to a strong connection between the magnitudes of displacements and parameters of thermal vibrations of the ions [4]. However, as Megaw [5] points out, the average magnitudes of the displacements of ions and of the parameters of thermal vibrations determined in various works satisfactorily agree with each other both in the signs and in the order of magnitude. Thus for example, the average magnitude of  $\delta z_{O_I} = 0.014_2$  (expressed in fractions of lattice parameter), and the average deviation from this magnitude in the works of different investigators amounts to  $0.000_7$ . The average  $\delta z_{O_I} = -0.025_5$  and the average deviation is equal to  $0.002_3$ , the average  $\delta z_{O_{II}} = -0.012_3$  and the average deviation amounts to  $0.008_2$ . It may be seen from these figures that the values of  $\delta z_{Ti}$  and  $\delta z_{O_I}$  obtained in different works agree well, and there is no satisfactory agreement only for  $\delta z_{O_{II}}$ .

A phase transition from ferroelectric tetragonal to ferroelectric rhombic phase takes place near  $0^\circ\text{C}$ . In doing so, spontaneous polarization sets in in the direction of  $ca$  diagonal of the face of the cubic unit cell and the lengthening of the lattice takes place in this same direction. The cell acquires a monoclinic distortion (Figure 2.2c). The rhombic cell a transition to which from the monoclinic cell is possible has the parameters  $a \approx a_M \sqrt{2}$ ,  $b \approx a_M \sqrt{2}$ ,  $c = c_M$  where  $a_M$ ,  $b_M$  and  $c_M$  are parameters of the monoclinic cell, and no longer contains only one but two formulaic units. The lattice symmetry is described by the space group  $C_{2v}^{11} - C2mm$ .

At  $-10^\circ\text{C}$  the parameters of  $\text{BaTiO}_3$  are equal to:  $a = 5.682$ ,  $b = 5.669$  and  $c = 3.990 \text{ \AA}$ . The positions of ions are determined by the displacements  $\delta x_{Ti}$ ,  $\delta x_{O_I}$ ,  $\delta y_{O_{II}}$  (Figure 2.4a). According to the data of neutron diffraction study [6]  $\delta x_{Ti} = +0.010$ ,  $\delta x_{O_I} = -0.010$ ,  $\delta x_{O_{II}} = -0.013$ ,  $\delta y_{O_{II}} = +0.03$  or expressed in angstroms:  $\delta x_{Ti} = 0.06$ ,  $\delta x_{O_I} = -0.06$ ,  $\delta x_{O_{II}} = -0.07$ ,  $\delta y_{O_{II}} = 0.017 \text{ \AA}$ . The ions of Ti and Ba are displaced relative to the oxygen octahedron by  $0.13$  and  $0.07 \text{ \AA}$  respectively along the positive direction of the  $x$ -axis. Distortion of the octahedron may be seen from Figure 2.4b. Spontaneous polarization calculated on the basis of ion displacements is equal to  $16 \cdot 10^{-6} \text{ coulombs/cm}^2$  (experimental value is  $\sim 30 \cdot 10^{-6} \text{ c/cm}^2$ ).

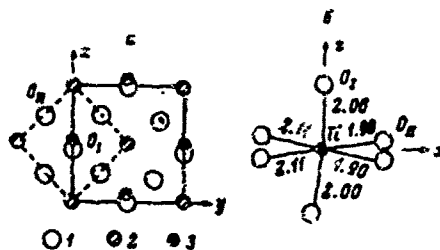


Figure 2.4. Displacements of ions in rhombic  $\text{BaTiO}_3$ .

a -- directions and magnitudes of displacements; b -- distortion of  $\text{TiO}_6$  octahedron (after Shirane et al. [6]).  
 1 -- oxygen; 2 -- barium; 3 -- titanium.

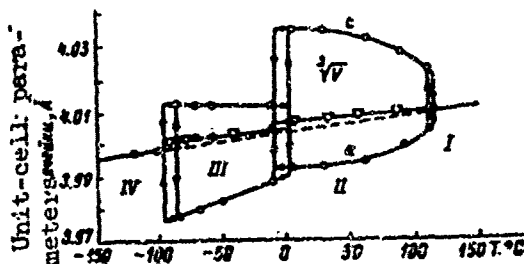


Figure 2.5. Temperature dependence of lattice parameters and of the volume  $V$  of unit cell of  $\text{BaTiO}_3$ . (After Kay and Vousden [7]).

I -- cubic phase; II -- tetragonal phase;  
 III -- rhombic phase; IV -- rhombohedral phase.

Transition into ferroelectric rhombohedral phase takes place at about  $-90^\circ\text{C}$ . In this phase, spontaneous polarization is oriented along the volume diagonal of the cubic cell and the cell is elongated in this direction (Figure 2.2d). The rhombohedral phase of barium titanate is described by the space group  $C_{3v}^5$  --  $R3M$ . At  $-100^\circ\text{C}$  the lattice parameter  $a = 3.998 \text{ \AA}$  [3].

Temperature dependence of lattice parameters (of the length of unit-cell edges) is shown in a wide temperature range in Figure 2.5.

## Par. 2. Seignette's Salt

Seignette's salt is a double sodium-potassium tartrate  $\text{NaKC}_4\text{H}_4\text{O}_6 \cdot 4\text{H}_2\text{O}$ . In nonferroelectric state (above  $23\text{--}24^\circ\text{C}$ ) this salt has rhombic structure. At  $+35^\circ\text{C}$  the lattice parameters are equal to  $a=11.878$ ,  $b=14.246$  and  $c=6.218 \text{ \AA}$  [3]. The unit cell contains 4 formulaic units. In doing so, the lattice is described by the space group  $D_2^3\text{--}P2_12_12_1$ . According to [3] the atoms in the unit cell occupy positions shown in Table 1.

Table 1  
Positions of Atoms in a Unit Cell of  
Seignette's Salt

Atom	x	y	z	Atom	x	y	z
K (a)	0.00	0.00	0.05	H <sub>2</sub> O (7)	0.40	0.08	0.50
K (4b)	0.00	0.50	0.15	H <sub>2</sub> C (8)	0.25	0.03	0.87
Na	0.23	0.99	0.52	H <sub>2</sub> O (9)	0.44	0.30	0.05
O (1)	0.12	0.10	0.37	H <sub>2</sub> O (10)	0.42	0.40	0.45
O (2)	0.22	0.20	0.12	C (1)	0.15	0.18	0.28
O (3)	0.23	0.40	0.82	C (2)	0.22	0.28	0.42
O (4)	0.08	0.37	0.85	C (3)	0.17	0.27	0.85
OH (5)	0.18	0.28	0.32	C (4)	0.15	0.35	0.80
OH (6)	0.29	0.24	0.83				

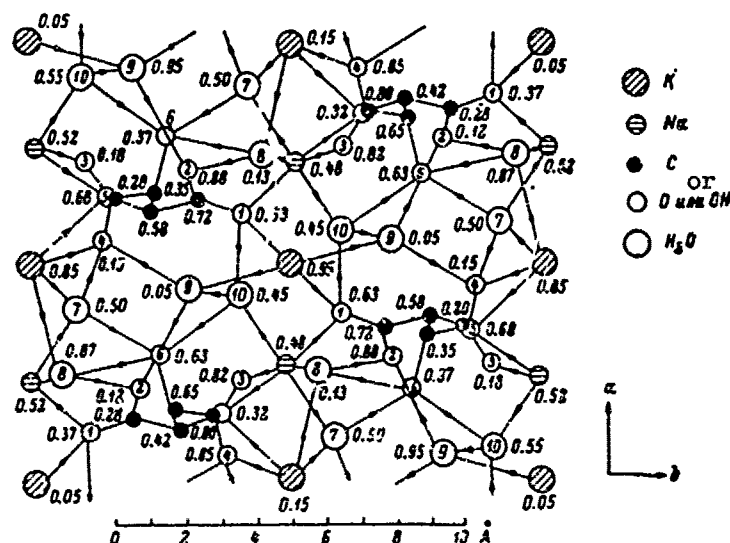


Figure 2.6 Projection of the structure of Seignette's salt onto the plane (001).

Figures in circles are the numbers of the atoms; figures near the atoms indicate the z coordinates (after Beevers and Hughes [8]).

Projection of the structure onto the plane (100) is shown in Figure 2.6. Each atom of sodium is surrounded by a group of six atoms of oxygen with an average distance of 2.39 Å (2.39, 2.34, 2.29, 2.31, 2.49 and 2.52 Å). Out of them, three atoms of oxygen belong to the tartrate group and three -- to the water molecules. An atom of potassium in (0, 0, 0.05) has a coordination number 4 with two atoms of oxygen from the tartrate group and two -- belonging to the water molecules. The other potassium atoms have a coordination number 8 with four oxygens from the tartrate group and with four water molecules. The distances lie in a range of from 2.75 to 3.07 Å. Carbon atoms in the tartrate molecule lie in nearly one plane. The groups  $-C(OH) \cdot COOH$  are nearly coplanar and are inclined  $60 \pm 2^\circ$  to the plane of the carbon atoms.

Ferroelectric phase existing in a temperature range of from  $-18$  to  $+24^\circ C$  is monoclinic and belongs to the space group  $C_2^2-P2_1$  [9] with the polar axis being parallel to the direction of the rhombic axis of [100]. Spontaneous deformation consists of a displacement of  $y_z$  in the plane (100). Owing to this, the angle between the b- and c-axes differs somewhat from  $90^\circ C$  (by a quantity of from  $1'48''$  to  $3'$  [3]).

The low-temperature phase of Seignette's salt, stable below  $-18^\circ C$ , as well as the high-temperature phase, is described by the space group  $D_2^3-P2_12_12$  [10]. Some of the atoms in this phase are displaced somewhat from positions characteristic of the high-temperature phase. Anisotropy of the oscillations of the oxygen  $O_3$  and  $O_8$  atoms was noted (Figure 2.6) with the direction of maximum oscillation being parallel to the rhombic a-axis. At the same time, oscillations of the O ion are most intensive along the b-axis. Very strong thermal vibrations were found in potassium atoms.

The most important problem in the study of crystal structure of Seignette's salt is determination of the position of hydrogen bonds in a crystal. As the neutron diffraction study [11] showed, orientation of hydroxyl group, indicated by numeral 5 in Figure 2.6, is of great significance for the emergence of ferroelectric state. According to [3] a change in the orientation of this hydroxyl group leading to a change in the direction of its electric moment brings about a displacement of protons along the a-axis and makes the main contribution to the development of spontaneous polarization. Displacements of the other ions apparently also make a contribution to spontaneous polarization.

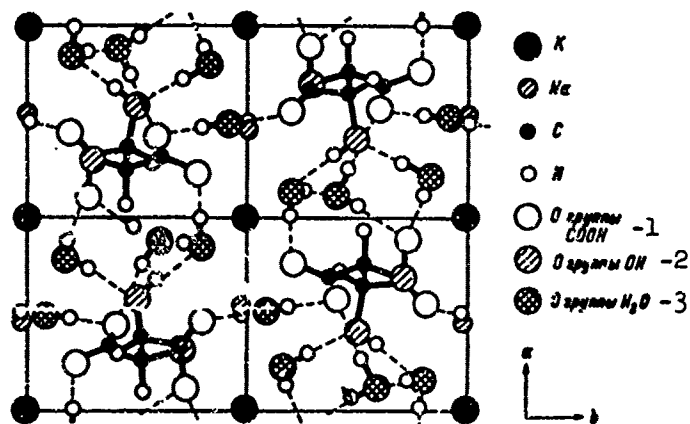


Figure 2.7. System of hydrogen bonds in Seignette's salt (broken lines) in projection onto the plane (001). (After Frazer et al. [11]).

Key: 1 -- O of the COOH group; 2 -- O of the OH group; 3 -- O of the H<sub>2</sub>O group.

In Figure 2.7 is shown a system of hydrogen bonds according to the data in [11]. This system agrees well with the conclusions drawn from a study of Raman-effect spectra. It should be noted that although crystallographic class of rhombic modification of Seignette's salt allows the existence of two enantiomorphous modifications the Seignette's-salt crystals usually belong to the right-handed form [3]. The most developed and typical forms are the c-faces {001} and prismatic m-faces {110}; the n-faces {120}, l-faces {210} and b-faces {010} whereas a-faces {100} are very small in most cases or are absent altogether.

### Par. 3. Potassium Dihydrophosphate

At room temperature, potassium dihydrophosphate ( $\text{KH}_2\text{PO}_4$ ) has a tetragonal lattice with the parameters  $a=7.453 \text{ \AA}$  and  $c=6.959 \text{ \AA}$ , belonging to the noncentrosymmetrical group  $D_{2d}^{12} \rightarrow \overline{14}2d$  [9]. Crystals described by this space group are piezoelectric. This unit cell contains 4 formulaic units. The crystal lattice

Table 2

The Lengths of Bonds in  $\text{KH}_2\text{PO}_4$  According to the Data in [13], Expressed in Å (OH is Oxygen With Neighboring Hydrogen)

Bond	Room Temperature	12° K	7° K
P-O <sub>H</sub>	} 1.541 ± 0.05	} 1.541 ± 0.004	1.586 ± 0.02
P-O			1.511 ± 0.02
O <sub>H</sub> -O <sub>H</sub>	} 2.533 ± 0.007	} 2.533 ± 0.005	2.578 ± 0.006
O-O			2.554 ± 0.008
O-O <sub>H</sub>	} 2.508 ± 0.003	} 2.508 ± 0.005	2.524 ± 0.02
O <sub>H</sub> -O			2.517 ± 0.02
O-H-O	2.422 ± 0.005	2.430 ± 0.004	2.491 ± 0.004
O <sub>H</sub> -H	1.07 ± 0.01	1.07 ± 0.01	1.05 ± 0.014
O-H	1.42 ± 0.01	1.41 ± 0.01	1.43 ± 0.014
K-O <sub>H</sub>	} 2.894 ± 0.008	} 2.876 ± 0.003	2.902 ± 0.03
K-O			2.839 ± 0.03
K-O <sub>H</sub>	} 2.825 ± 0.004	} 2.808 ± 0.005	2.818 ± 0.01
K-O			2.783 ± 0.01

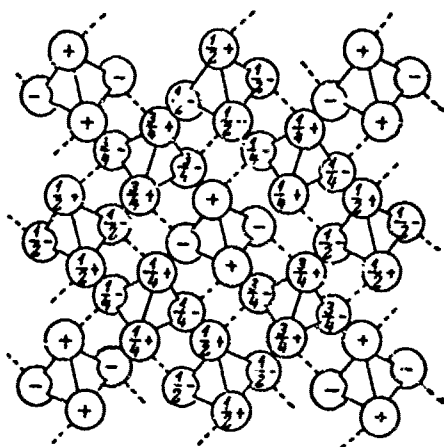


Figure 2.9. System of Hydrogen Bonds in  $\text{KH}_2\text{PO}_4$  (broken lines) in Projection onto the Plane (001). (After Frazer and Pepinsky [14]).

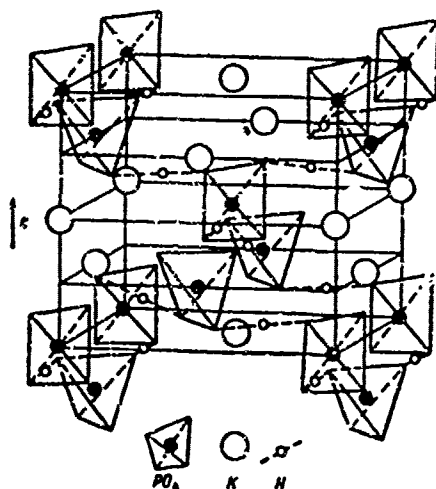


Figure 2.8. Unit cell of  $\text{KH}_2\text{PO}_4$  corresponding to the space group  $I\bar{4}2D$ . (After West [12]).

of  $\text{KH}_2\text{PO}_4$  may be described by using another tetragonal unit cell in which the edges forming the square base are diagonals of the square face of the cell mentioned above and accordingly are  $\sqrt{2}$  times larger (that is  $a=10.534 \text{ \AA}$  and  $c=6.959 \text{ \AA}$ ). However, in this case the space group will be  $D_2^{12} - F\bar{4}d2$ .

The arrangement of atoms in a tetragonal unit cell with  $a=7.453 \text{ \AA}$  is given in Figure 2.8. The lattice consists of  $\text{PO}_4$  tetrahedrons of nearly regular form. Potassium ions are located in the spaces between tetrahedrons. Each one of these ions is surrounded by eight oxygen atoms belonging to  $\text{PO}_4$  tetrahedrons with four of them lying somewhat closer to the potassium atom than the remaining four [13]. In Table 2 are given the interatomic distances in  $\text{KH}_2\text{PO}_4$ . Each  $\text{PO}_4$  group is linked with four neighboring  $\text{PO}_4$  groups by hydrogen bonds of about  $2.4 \text{ \AA}$  in length. As may be seen from Figure 2.8, hydrogen bonds are perpendicular to the  $c$ -axis and link the "lower" oxygen atoms in one tetrahedron of  $\text{PO}_4$  with the "upper" oxygen atoms in another tetrahedron. The system of hydrogen bonds in  $\text{KH}_2\text{PO}_4$  may

be seen from Figure 2.9 where a projection of the lattice onto the plane (001) is given. According to [13] the oscillations of hydrogen atoms have a high anisotropy with the amplitude of the oscillations being maximal along the direction of the bond. Hydrogen atoms in paraelectric phase of  $\text{KH}_2\text{PO}_4$  are statistically distributed in two positions lying on a straight line connecting the nearest oxygen atoms. The distance between these two positions amounts approximately to 0.35 Å (difference between the distances  $\text{O}_1\text{---H}$  and  $\text{O}_2\text{---H}$  in Table 2). Statistical distribution of hydrogen atoms in these two positions accounts for the absence of spontaneous electric moment in the substance.

Ferroelectric phase transition takes place in  $\text{KH}_2\text{PO}_4$  at  $-150^\circ\text{C}$  ( $123^\circ\text{K}$ ). In doing so, the lattice becomes rhombic and belongs to the space group  $\text{C}_{2v}^{19}\text{---Fdd}$ . An elongation of the unit cell with the space group  $\text{I}\bar{4}2d$  takes place along one of the diagonals of the square base and a contraction -- along the other diagonal so that a rhombic unit cell with  $a=10.44$ ,  $b=10.53$  and  $c=6.90$  Å at  $116^\circ\text{K}$  results upon transition to the other axes [3]. Distortion of the unit cell with the space group  $\text{F}\bar{4}d2$  consists in the elongation of the edges parallel to the b-axis and in shortening of the edges parallel to the a-axis. The polar axis is oriented along the tetragonal c-axis. The change in interatomic distances during the phase transition may be seen from Table 2.

The length of the hydrogen bond changes little during the phase transition but hydrogen atoms become ordered in such a manner that in a single-domain crystal all hydrogens are near the "upper" or "lower" oxygens according to the polarity of the crystal [3]. The change in the polarity of the crystal is connected with the displacement of hydrogen atoms along the directions of hydrogen bond from the "upper" oxygen atoms to the "lower" and from the "lower" to the "upper". The ordering of hydrogen atoms is accompanied by the displacements of the other atoms. Displacements of oxygen are very small. Potassium and phosphorus atoms are displaced along the c-axis in opposite directions relative to oxygen framework withdrawing from those oxygen atoms which the hydrogen atoms approach, i.e. the positive charge of proton approaching the oxygen atoms repulses the positive potassium and phosphorus ions adjacent to oxygen atoms. The magnitudes of the displacements of potassium atoms are evaluated at 0.04-0.05 Å and those of phosphorus [sic] atoms -- at 0.03-0.08 Å [13, 14].

Inasmuch as spontaneous polarization is oriented along the c-axis and hydrogen bonds are practically perpendicular to

the c-axis it is clear that appearance of spontaneous polarization can be explained only by displacements of heavy ions along the c-axis. Calculation of spontaneous polarization by the displacements of ions (ionic component) [13] on the assumption that phosphorus, potassium and oxygen ions have a charge of +5, +1 and -2 respectively gives a good agreement with the experimental value of spontaneous polarization. A good agreement, although with opposite sign of spontaneous polarization, also results with the assumption that phosphorus charge is equal to +3. Results of the study of  $\text{KH}_2\text{PO}_4$  using the method of anomalous scattering of x-rays agree with the assumption that phosphorus charge is equal to +5 [3].

In accordance with the results of structural investigations, the data of the study of infrared spectra and Raman-effect spectra indicate an absence of changes in the lengths of O--H bonds in the case of a phase transition [3]. This confirms the mechanism of transition, which consists in ordering of hydrogen atoms in two positions lying along the hydrogen bond and which follows from structural studies.

#### Par. 4. Triglycine Sulfate

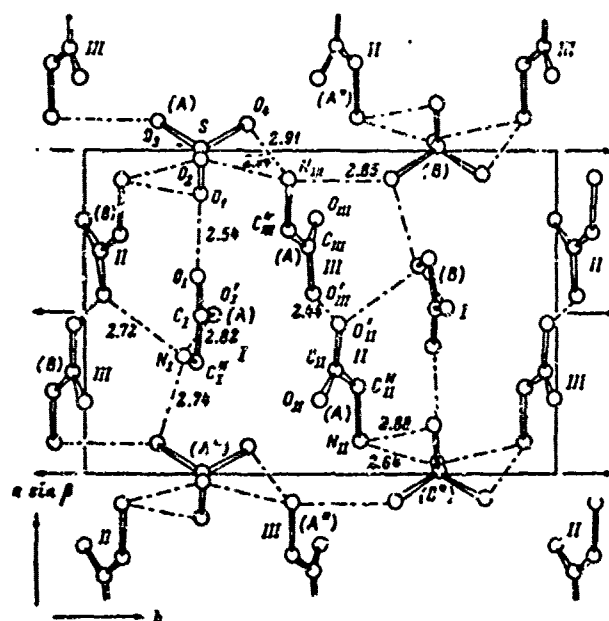


Figure 2.10. Projection of the structure of triglycine sulfate along c-axis. (After Hoshino et al. [16]).

Table 3

## Coordinates of Atoms in Triglycine Sulfate

Atoms	x	y	z
Sulfate ion Ион сульфата			
S	0.8295	0.2500	0.2250
O <sub>1</sub>	0.8583	0.2447	0.6051
O <sub>2</sub>	0.8699	0.2457	0.4572
O <sub>3</sub>	1.0820	0.1585	0.2234
O <sub>4</sub>	1.0769	0.3469	0.1941
Glycine Глицин I			
C	0.6064	0.2393	1.0746
C	0.4825	0.2715	0.6668
N	0.4905	0.2472	0.8727
O	0.3348	0.2361	0.9049
O	0.3585	0.2110	1.1639
Glycine Глицин II			
O	0.2218	0.4975	0.7646
O	0.4596	0.5397	0.7988
C	0.3153	0.5331	0.8787
N	0.2675	0.5734	0.4070
O	0.0939	0.5600	0.3063
Glycine Глицин III			
O	0.7824	0.4931	0.2229
O	0.5454	0.4825	0.2317
C	0.6937	0.4749	0.3281
N	0.7440	0.4320	0.5906
N	0.9068	0.4331	0.7059

Triglycine sulfate  $(\text{NH}_2\text{CH}_2\text{COOH})_3 \cdot \text{H}_2\text{SO}_4$  is a ferroelectric with a Curie temperature of  $49^\circ\text{C}$ . Above Curie point, triglycine sulfate has a monoclinic lattice belonging to the space group  $C_{2h}^2-P2_1/m$ . A unit cell of triglycine sulfate may be selected by two methods. The  $b$  and  $c$  parameters are the same for both unit cells but the angles  $\beta$  and parameters "a" differ. In both cases the unit cell contains two formulaic units. At room temperature, the lattice parameters in one selection are equal to:  $a=9.15$ ,  $b=12.69$ ,  $c=5.73 \pm 0.03 \text{ \AA}$ ,  $\beta = 105^\circ 40' \pm 20'$  according to the data in [15], and in the other selection  $a=9.42$ ,  $b=12.64$ ,  $c=5.73 \text{ \AA}$ ,  $\beta = 110^\circ 23'$  according to the data in [16].

Coordinates of atoms in triglycine sulfate at  $20^\circ\text{C}$  according to the data in [16] are given in Table 3 in fractions of the edge of the cell.

In the triglycine sulfate lattice, phosphorus atom is

in a distorted oxygen tetrahedron. The S--O distances lie in a range from 1.477 to 1.48<sub>1</sub> Å and are considerably shorter than in inorganic sulfates such as KH<sub>2</sub>SO<sub>4</sub> and MgSO<sub>4</sub>. The O--S--O angles lie in a range of from 105 to 115°.

In Figure 2.10 is given a projection of the structure of triglycine sulfate along c-axis. For convenience in description different groups of atoms are indicated by the letters A, B, A\* and B\* placed in parentheses. The numerals I, II and III indicate three glycine groups which are a part of the composition of the substance.

Glycine group II is a so-called "zwitterion", i.e. a molecular group one side of which has a positive charge and the other -- a negative charge, so that molecular group has a dipole moment. Glycine groups I and III carry only one charge -- a positive charge and, therefore, may be regarded as complex positive ions which are called glyciniums. Hence a second possible name for triglycine sulfate -- glycinedi-glycinium sulfate -- and the feasibility of writing the chemical formula in the form (NH<sub>3</sub><sup>+</sup>CH<sub>2</sub>COO<sup>-</sup>) (NH<sub>3</sub><sup>+</sup>CH<sub>2</sub>COOH)<sub>2</sub>SO<sub>4</sub><sup>2-</sup>.

Table 4

Displacements of Atoms From the  
Planes of Glycine Groups (in Å)

Atoms	Glycine groups		
	I	II	III
N	0.00 <sub>6</sub>	-0.26 <sub>6</sub>	-0.00 <sub>6</sub>
C	0.00 <sub>6</sub>	0.00 <sub>6</sub>	-0.04 <sub>6</sub>
O	0.03 <sub>6</sub>	-0.00 <sub>6</sub>	0.00 <sub>6</sub>
O'	-0.01 <sub>6</sub>	0.00 <sub>6</sub>	0.04 <sub>6</sub>
	-0.01 <sub>6</sub>	0.00 <sub>6</sub>	-0.06 <sub>6</sub>

As may be seen from Table 4, carbon, nitrogen and oxygen atoms in glyciniums I and III lie practically in one plane. In zwitter-ion of glycine (II) carbon and oxygen atoms also lie practically in one plane but nitrogen atom is displaced from this plane by 0.27 Å.

In paraelectric state above Curie point the planes  $y=\frac{1}{4}$  and  $\frac{3}{4}$  are crystallographic mirror-image planes. The planes of glycinium ions form an angle of 12.5° with the planes  $y=\frac{1}{4}$  and  $\frac{3}{4}$ . A glycinium molecule may go out of the

plane  $y=\frac{1}{4}$  (or  $y=\frac{3}{4}$ ) both on one and the other side of this plane with the direction of the deviation from this plane being different for each glycinium molecule and being in a chaotic state. Thus, above Curie point the planes  $y=\frac{1}{4}$  and  $y=\frac{3}{4}$  are mirror planes only statistically. With an ordered deviation of glycinium molecules below Curie point these planes cease to be mirror planes even statistically.

Determination of the system of hydrogen bonds in triglycine sulfate is of great importance. A possible system of hydrogen bonds assumed in [16] is shown in Figure 2.10 by dot-and-dash lines connecting different atoms. Attention is drawn by the short hydrogen bond between the  $O'_{III}(A)$  and  $O'_{II}(A)$  oxygens of 2.44 Å in length. It is assumed in [16] that proton is located closer to the atom of  $O'_{III}(A)$  oxygen of the completely plane glycinium III ion. Owing to this, group III is considered to be glycinium ion and glycine group II is regarded as a zwitter-ion.

The possibility of the transition of hydrogen from group III into group II along the short  $O'_{III}(A)\text{---H---}O'_{II}(A)$  bond accounts for the possibility of repolarization of the crystal. In doing so, the groups change roles: group III becomes a zwitter-ion and group II -- a glycinium ion.  $N_{II}(A)$  atom returns into the plane of the remaining atoms and  $N_{III}(A)$  atom leaves the respective plane. This regrouping of atoms in these groups leads to a change in the position of glycinium group which, as a result, assumes a symmetrical position relative to the plane  $y=\frac{1}{4}$ . Thus, repolarization in triglycine sulfate is not a simple change in the direction of the moment of one of glycinium groups but is connected with the disappearance of the moment in one glycinium group and transformation of the zwitter-ion of glycine into a glycinium group with a dipole moment of opposite direction.

Further studies confirmed that ferroelectric transition in triglycine sulfate is a transition of the order--disorder type and is in the main of the same nature as the transition in potassium dihydrophosphate but differs from it by a tighter bond between the motion of protons and the motion of heavy groups [17].

With the phase transition into paraelectric state the lattice remains monoclinic. In doing so, along the ferroelectric b-axis the crystal contracts during the heating and approach to Curie point and begins to expand in paraelectric phase while, conversely, along the a- and c-axes it expands during the heating in ferroelectric phase and begins to contract in paraelectric phase [18].

Par. 5. Sodium Nitrite

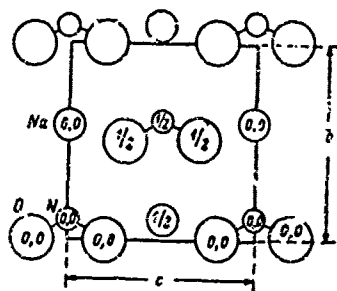


Figure 2.11. Projection of the structure of NaNO<sub>2</sub> onto the plane (100).

Small circles are nitrogen, medium-sized circles -- sodium, large circles -- oxygen (After Wyckoff [20]).

At room temperature sodium nitrite (NaNO<sub>2</sub>) has a rhombic structure belonging to space group  $C_{2v}^{20}--Im2M$  [19]. Unit cell has the parameters  $a=5.390$ ,  $b=5.578$  and  $c=5.70$  Å [20] and contains two formulaic units. The lattice of NaNO<sub>2</sub> may be represented as the lattice of NaCl in which chlorine ion is replaced with NO<sub>2</sub><sup>-</sup> ion with O--N--C angle equal to 115° whose bisector is oriented along b-axis of the NaNO<sub>2</sub> lattice and whose plane lies in the plane (101) of the cubic lattice of NaCl (Figure 2.11). Sodium atoms are surrounded respectively by six ions of NO<sub>2</sub><sup>-</sup> and the ions of NO<sub>2</sub><sup>-</sup> -- by six sodium atoms. The b-axis is the ferroelectric axis.

Approximately at 160°C the noncentrosymmetrical structure changes into a centrosymmetrical structure. Paraelectric phase is rhombic and belongs to space group  $D_{2h}^{22}--Immm$ . At 205°C, parameters of the unit cell are equal to:  $a=5.33$ ,  $b=5.68$  and  $c=3.69$  Å.

Above Curie point, oxygen atoms in NO<sub>2</sub> groups oscillate along the axis [010] near those positions which are defined by the centrosymmetrical space group.

With the assumption of a purely ionic structure the calculated value of spontaneous polarization proved to be equal to  $74 \cdot 10^{-6}$  coulombs/cm<sup>2</sup> [21]. This value exceeds by one order the experimental value of spontaneous polarization in NaNO<sub>2</sub>.

Agreement between the calculated and experimental values results if a charge equal to unity is assigned to a sodium ion, to nitrogen -- a charge equal to -0.36 and to oxygen -- a charge equal to -0.32 [21]. This indicates a strong covalence of bonds in NO<sub>2</sub> group.

#### BIBLIOGRAPHY

1. V. M. Goldschmidt. *Geochemische Verteilungsgesetze der Elemente*, VII. Oslo, 1926.
2. G. A. Smolenskiy, A. I. Agranovskaya, *ZhTF* [Journal of Technical Physics], Vol 28, p 1491 (1958).
3. F. Jona, D. Shirane. *Segnetoelektricheskiye Kristally* [Ferroelectric Crystals]. Mir Publishing House, Moscow, 1965.
4. H. T. Evans, *Acta Cryst.*, 14, 1019 (1961).
5. H. D. Megaw, *Acta Cryst.*, 15, 972 (1962).
6. G. Shirane, H. Danner, R. Pepinsky, *Phys. Rev.*, 105, 856 (1957).
7. H. F. Kay, P. Vousden, *Phil. Mag.*, 40, 1019 (1949).
8. C. A. Beevers, W. Hughes, *Proc. Roy. Soc.*, A177, 251 (1941).
9. V. Kentzig. *Segnetoelektriki i Antisegetoelektriki* [Ferroelectrics and Antiferroelectrics]. *IL* [Foreign Literature Press], Moscow, (1960).
10. F. Mazzi, F. Jona, R. Pepinsky, *Zs. f. Krist.*, 108, 359 (1957).
11. B. C. Frazer, M. McKeown, R. Pepinsky, *Phys. Rev.*, 94, 1435 (1954).
12. J. West, *Zs. f. Krist.*, 74, 306 (1930).
13. G. E. Bacon, R. S. Pease, *Proc. Roy.*, A220, 397 (1953); A230, 359 (1955).
14. B. C. Frazer, R. Pepinsky, *Acta Cryst.*, 6, 273 (1953).
15. E. A. Wood, A. N. Holden, *Acta Cryst.*, 10, 145 (1957).

16. S. Hoshino, Y. Okaya, R. Pepinsky, Phys. Rev., 124, 1036 (1961).
17. R. Blinc, S. Detoni, M. Pintar. Phys. Rev., 115, 323 (1959).
18. S. Ganesan, Acta Cryst., 15, 81 (1962).
19. F. Ormont. Struktury Neorganicheskikh Veshchestv. [Structures of Inorganic Substances]. GITTL [State Publishing House for Technical and Theoretical Literature], Moscow -- Leningrad. (1950).
20. R. W. Wyckoff. Crystal Structures, Vol 2, N. Y. (1951).
21. M. J. Kay, B. C. Frazer, Acta Cryst., 14, 56 (1961).

## CHAPTER 3. THERMODYNAMIC THEORY OF FERROELECTRICITY

Many physical properties of ferroelectrics are well described by thermodynamic theory (with the exception, perhaps, of their behavior in a narrow temperature range near transition point, and also with the exception of some nonlinear effects).

The principles of this theory were laid down by Ginzburg [1, 2] and Devonshire [3] who applied Landau [4] thermodynamic theory of phase transitions to ferroelectric crystals.

Thermodynamic theory makes it possible to describe phenomenologically thermal, mechanical and dielectric properties of ferroelectric crystals, predict possible changes in their symmetry in the case of transition of the second kind, to interconnect various physical quantities with anomalous temperature dependence, etc.

This chapter sets forth the principles and some results of thermodynamic theory, and also examines the question of the range of its applicability. Material presented in this chapter pertains only to single-domain crystals. The last circumstance is connected with the fact that thermodynamic theory of domain structure has been developed considerably less (a brief review of results of this theory may be found in chapter 7).

### Par. 1. Ferroelectric Phase Transition

The basis of Landau theory is representation of phase transition which takes place as a result of a change in symmetry and not in the state of aggregation of a body. From the standpoint of macroscopic theory the symmetry of a system is described by the so-called factor of order  $\eta(t, p)$  which is equal to zero in disordered phase and is nonzero in phases characterized by a lower symmetry. For ferroelectric transitions the order parameter may be provided by spontaneous polarization occurring as a result of displacement of atomic sublattices or ordering of atomic or molecular groups, which brings about the appearance of macroscopic dipole moment <sup>1)</sup>.

---

1) See footnote on next page.

If during the change in temperature the order factor of  $\eta$  changes suddenly, then a phase transition of the first kind exists, when the system permits in a certain region the existence of two phases within which thermodynamic functions are two-valued. Therefore, with the transition the state of the system changes suddenly, a temperature hysteresis is observed and, consequently, absorption or release of heat takes place.

In the case of a phase transition of the second kind  $\eta$ , as well as the thermodynamic functions, changes continuously, but a sudden change is experienced by their derivatives (thermal capacity, compressibility, specific inductive capacitance, etc.); however no release of latent heat takes place.

### 1. Phase Transition of the Second Kind

Suppose the state of a system is described by thermodynamic potential  $\Phi(p, T, \eta)$  <sup>2)</sup> which is postulated in the form of an expansion with respect to the powers of  $\eta$ , i.e.

$$\Phi(p, T, \eta) = \Phi_0(p, T) + a\eta + A\eta^2 + B\eta^3 + C\eta^4 + D\eta^5 + \dots \quad (3.1)$$

where coefficients  $a, A, B$ , etc. are functions of the temperature  $T$  and of the pressure  $p$ .

Inasmuch as the states with an  $\eta=0$  and  $\eta \neq 0$  are characterized by their symmetry and since at any point with an  $\eta \neq 0$  near the transition  $\Phi$  must be minimal, an  $a \equiv 0$  should be assumed in the entire range of temperature variation. It is also obvious that in symmetrical phase

$A > 0$  in accordance with the condition that  $\left(\frac{\partial^2 \Phi}{\partial \eta^2}\right) > 0$ . Conversely, with

an  $\eta \neq 0$ ,  $A < 0$  corresponds to the condition of minimum  $\Phi$  and  $C > 0$ . Consequently, at the transition point itself  $A_0 = 0$ . In addition to this, on the basis of these considerations  $B_0 = 0$ . Attention has to be paid here to one important circumstance: if in a certain region  $B(p, T)$  vanishes iden-

1) In the general case, lattice symmetry is symmetry of the density function  $\rho(x, y, z)$  [4] which defines the probability of different positions of particles, including electrons. The last is of basic significance inasmuch as a ferroelectric transition does not necessarily have to be imagined as a result of displacement of ions. As Jaynes and others [5, 6] have shown, in principle, transition may also take place as a result of a change in the symmetry of the function describing the state of lattice electrons.

2) It is assumed here that in the case of equilibrium  $\Phi(p, T, \eta)$  has a minimum in relation to the variable  $\eta$ .  $\Phi(p, T, \eta)$  is selected in such a manner that entropy  $S$  is connected with it by the relationship  $S = -\left(\frac{\partial \Phi}{\partial T}\right)_p$ . See Par. 3, subparagraph 2 concerning thermodynamic functions as applied to different external conditions.

tically because of the properties of symmetry, then only the condition  $A_0(p, T) = 0$  remains in this case, and a line of phase transitions exists in the  $p, T$  plane. If however,  $B(p, T)$  does not vanish identically, then only isolated points of the phase transitions exist in the  $p, T$  plane with these points being determined from the condition  $A_0(p, T) = 0$  and  $B_0(p, T) = 0$ . We will assume that the conditions  $B(p, T) = 0$  and  $D(p, T) = 0$  are satisfied.

Thus, on the basis of the above considerations the expression for thermodynamic potential has a form of expansion with respect to the even powers of  $\eta$

$$\Phi(p, T, \eta) = \Phi_0(p, T) + A\eta^2 + C\eta^4 + E\eta^6 + \dots \quad (3.2)$$

In addition to this, on the basis of the condition of minimum (i.e.  $A_T < \theta < 0$ ;  $A_T = \theta = 0$  and  $A_T > \theta > 0$ )  $A(T)$  may be written in the form of a linear temperature function:

$$A(T) = \left(\frac{\partial A}{\partial T}\right)_\theta (T - \theta) \quad (3.3)$$

( $\theta$  is Curie point).

Next, from the condition of the minimum  $\frac{\partial \Phi}{\partial \eta} = 0$  we will find

$$\eta^2 = -\frac{A}{2C} = -\frac{1}{2C} \left(\frac{\partial A}{\partial T}\right)_\theta (T - \theta) \quad (3.4)$$

after which the change in the entropy  $\Delta S$  and a sudden change in thermal capacity  $\Delta c_p$  with transition are determined as follows

$$\Delta S = S - S_0 \approx -\left(\frac{\partial A}{\partial T}\right)_\theta \eta^2 \quad (3.5)$$

$$\Delta c_p = c_p - c_{p0} \approx \left(\frac{\partial A}{\partial T}\right)_\theta^2 \frac{\partial}{\partial T} \quad (3.6)$$

where  $S_0$  and  $c_{p0}$  are respectively entropy and thermal capacity in disordered phase.

Representations set forth above and formulas (3.2)-(3.6) obtained on the basis of them are made use of in Ginzburg [2] thermodynamic theory of ferroelectricity. Inasmuch as spontaneous polarization  $P_s$  has properties which are characteristic of the order factor  $\eta$  ( $P_s = 0$  in disordered phase and  $P_s \neq 0$  in ordered phase), the expansion of  $\Phi(P_s)$  in the absence of external field  $E$  has a form similar to  $\Phi(\eta)$  (formula 3.2) <sup>1)</sup>. If the field  $E$  is nonzero, then total polarization  $P = P_s + P_i$  ( $P_i$  is polarization induced by the field) is present in the expression for  $\Phi$ .

1) Later, expansion of  $\Phi$  with respect to induction components  $D$  was made use of in [7]. With  $E = 0$ ,  $D_s = 4\pi P_s$ , i.e. expansions of  $\Phi(P_s)$  and  $\Phi(D_s)$  are equivalent. However, when  $E \neq 0$ , expansion of  $\Phi(D)$  is more correct. It can be shown that the total differential of polarization work function of a dielectric is  $(\frac{1}{2}\pi) E dD$ , and not  $E dP$ . The relative error when using  $\Phi(P)$  is of the order of  $E/P$  or  $\partial E/\partial P$  and is substantial only when sufficiently far from  $\theta(T > \theta)$  or is in the saturation region  $P(E)$ .

On the basis of this, we have:

$$\Phi = \Phi_0 + \alpha P^2 + \frac{\beta}{2} P^4 + \dots \quad (3.7)$$

whence the characteristics of ferroelectric with which we are concerned are determined. From the condition  $\frac{\partial \Phi}{\partial P} = 0$  and  $\frac{\partial^2 \Phi}{\partial P^2} > 0$  we have:

$$2\alpha P + 2\beta P^3 = E, \quad (3.6a)$$

$$2\alpha + 6\beta P^2 > 0. \quad (3.8b)$$

In the absence of field the equation (3.8a) gives:

$$P_1^2 = -\frac{\alpha}{\beta} = \frac{\theta}{\beta} (T - \theta); \quad T < \theta, \quad (3.9a)$$

$$P_1^2 = 0; \quad T > \theta. \quad (3.9b)$$

Next, making use of formula (3.5) and (3.6) we will obtain the following expression for the sudden change in thermal capacity:

$$\Delta c_p = (\alpha_1)^2 \frac{\theta}{\beta}. \quad (3.10)$$

Dielectric constant will be found after substituting the definition of  $P_s = \frac{\epsilon - 1}{4\pi} E$  in (3.8a) with account taken of (3.9):

$$\epsilon = 1 + \frac{2\kappa}{\alpha_1 (T - \theta)}; \quad T > \theta, \quad (3.11a)$$

$$\epsilon = 1 + \frac{\kappa}{\alpha_1 (\theta - T)}; \quad T < \theta. \quad (3.11b)$$

By analogy with the well known law for permeability  $\mu(T)$  the dependences  $\epsilon(T)$  have the name Curie-Weiss law and the quantity  $C = \frac{2\kappa}{\alpha_1 \theta}$  is called Curie constant.

It follows from the formulas (3.11a and b) that the slope of the straight line  $\frac{1}{\epsilon}(T)$  when  $T > \theta$  is smaller by one half than when  $T < \theta$ . This effect ("the law of dyad") is well confirmed by experiments. It should be underscored that formulas (3.11a and b) are valid if terms of the order of  $P_1^2$  and higher, i.e. when  $P_1 \ll P_s$  may be neglected in (3.9).  $P_1 \ll P_s$  occurs only in weak fields and at temperatures that are not very close to  $\theta$ . Nonlinear effects cannot be neglected in direct proximity to  $\theta$  even when  $E$  are very small.

## 2. Phase Transitions of the First Kind

The relationships  $P_s(T)$ ,  $\epsilon(T)$  and  $c_p(T)$  obtained on the basis of (3.8) are valid in the case of phase transitions of the second kind. However, in many cases experimental relationships contain explicit indications of transition of the first kind. The character of phase transitions may vary according to the values and signs of the coefficients of expansion of  $\Phi$ , forming a "continuous gamut" of transitions of the second and first kind. Indeed, in accordance with theory of phase transitions of the second kind, in the expression for  $\Phi$  (3.7) the coefficient  $\beta > 0$ . If  $\beta < 0$ , then we can no longer limit ourselves to the fourth-order terms (the condition of minimum  $\Phi$  is not satisfied) and, consequently, it is necessary to take the terms  $\sim P^6$  into account:

$$\Phi = \Phi_0 + \beta P^2 + \frac{\beta}{2} P^4 + \frac{\beta}{3} P^6. \quad (3.12)$$

Repeating the same considerations as before, we will find:

$$P_s^2 = \frac{-\beta}{2\beta} \left( 1 + \sqrt{1 - \frac{4\beta T}{\beta^2}} \right). \quad (3.13)$$

With a decrease of  $\beta$  the character of the transition starts to change and in the extreme case of  $\beta = 0$  we have the so-called critical Curie point below which:

$$P_s^2 = \sqrt{\frac{2\beta}{\beta}} (T - T_c) \quad (3.14)$$

$$c_p = c_{p0} + \frac{\beta c_{p0}}{2\beta^{3/2} \sqrt{T_c - T}}. \quad (3.15)$$

and, consequently, at the critical Curie point thermal capacity becomes infinite. Such a phase transition is also called  $\lambda$ -point.

The law of variation of dielectric constant when  $T > \Theta$  coincides with (3.11a). However, below Curie point

$$\epsilon \sim \frac{\epsilon}{2\beta(T_c - T)}, \quad \text{for } T < \Theta. \quad (3.16)$$

In the case under consideration  $\beta$  is identically equal to zero in a certain region adjacent to Curie point. However, crystals are also possible in which  $\beta$  vanishes at the Curie point itself or in its neighborhoods, i.e.  $\beta = \beta_0 (T - \Theta_c)$ . In doing so, the character of the relationships differs little from the case with a constant coefficient  $\beta = 0$  that has been examined. 1)

We will now examine a case of phase transition of the first kind ( $\beta < 0$ ).

1) In principle a case is possible when  $\beta(T) \rightarrow 0$  and changes sign when far from  $\Theta$ , i.e. in the case of finite values of  $\alpha(T)$ . Apparently this case is realized in ferroelectric-semiconductor SbSI near  $T = 230^\circ\text{K}$  (Curie point in SbSI corresponds to a temperature  $\Theta = 290^\circ\text{K}$ ).

Both phases (ordered and disordered) are in equilibrium and, consequently,  $\Phi_{P_S \neq 0} = \Phi_{P_S = 0}$  at the transition point (more exactly, in the transition region since temperature hysteresis is possible) and  $P_S$  changes suddenly. On the basis of equality of thermodynamic potentials and condition  $\frac{\partial \Phi}{\partial P_S} = 0$  we will find that at the transition point itself  $P_{S0}^2 = -\frac{3\beta}{4\gamma}$ .

With  $T = \theta_1$ ,  $\alpha$  does not vanish here. Unlike the phase transition of the second kind, in this case transition occurs as a result of the circumstance that one of the states  $\Phi_{P_S \neq 0}$  or  $\Phi_{P_S = 0}$  becomes metastable. Therefore, it is convenient to represent the quantity  $\alpha$  in transition region in the following form

$$\alpha = \alpha_0 + \alpha_1 (T - \theta_1). \quad (3.17)$$

Making use of (3.17), we will determine  $\varepsilon(T)$ :

$$\varepsilon = \frac{2\pi}{\alpha_0 + \alpha_1 (T - \theta_1)}, \quad T > \theta_1, \quad (3.18a)$$

$$\varepsilon = \frac{\pi}{2\alpha_0}, \quad T < \theta_1. \quad (3.18b)$$

Thus, the jump at the transition point  $\Delta \varepsilon = \frac{3\pi}{2\alpha_0 \theta_1}$ . Latent heat of the transition is determined in terms of entropy jump:

$$Q = \theta_1 \Delta S = \theta_1 \alpha_1 \rho_0^2 \chi_0. \quad (3.19)$$

In most of ferroelectrics known at the present time the phase transition is transition of the first kind approaching critical Curie point. In particular, temperature dependences of  $\alpha$ ,  $\beta$  and  $\gamma$  (Figure 3.1) calculated in [8] from empirical data of Meherhofer [9] indicate that precisely such a transition occurs near  $\theta = 120^\circ\text{C}$  in  $\text{BaTiO}_3$  single crystals.

Strictly speaking, the case examined here corresponds to phase transition of the first kind approaching critical Curie point, i.e.  $\alpha$  and  $\beta$  near  $T = \theta_1$  are very small. If this condition is not satisfied, i.e.  $\beta < 0$  and is large in absolute value, then we have a case of sharply marked phase transition of the first kind. With  $\beta < 0$ , very large  $|\beta|$  correspond to a typical pyroelectric differing from a ferroelectric (undergoing transition both of the first and second kind) in that all temperature, pressure and electric-field dependences are marked extremely slightly. The reason for this "hardness" can be easily understood if qualitative curves  $\Phi(E, P)$  shown in Figure 3.2 are compared.

It is obvious that with the transition from the case "a" to the case "b" the effect of external factors (field, pressure and temperature) will decrease owing to the build-up of the "activation barrier". At the limit, transition is not realized at all in the case "b" and, consequently, the temperature and nonlinear effects characteristic of ferroelectrics are absent.

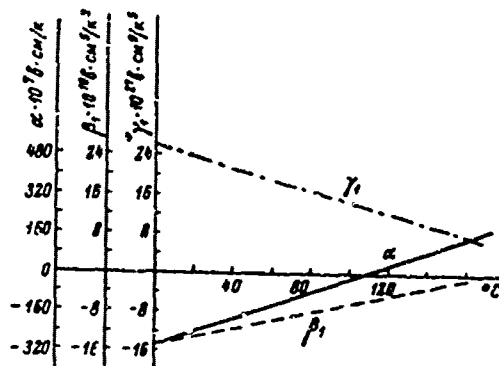


Figure 3.1. Temperature dependence of  $\alpha$ ,  $\beta$  and  $\gamma$  for  $\text{BaTiO}_3$ .

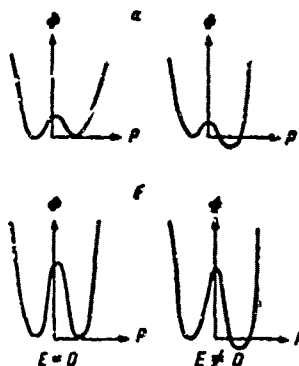


Figure 3.2. The function  $\Phi(P)$  for a ferroelectric (a) and for a pyroelectric (b).

The character of a phase transition depends on many factors: symmetry, interaction of atoms making up the crystal lattice, internal stresses, etc. Some of them are objects of microscopic theory; others, for example, symmetry and elastic effects (see Par. 2 and 3) may be examined within the framework of phenomenological theory.

### 3. Range of Applicability of Thermodynamic Theory and Effect of Fluctuations

Fluctuations of parameters characterizing the equilibrium of a thermodynamic system, in particular fluctuations of the order factor  $\eta$ , may materially increase near the phase transition points, i.e. during the rearrangement of crystal lattice. Therefore, description of a tran-

sition on the basis of representations concerning equilibrium thermodynamic functions cannot be justified, at least in the region directly adjacent to Curie point. Assumption of the fluctuations of order factor requires abandonment of examination of the spatially uniform case, and taking spatial distribution  $\eta(r)$  into account in the expression for  $\Phi$ , i.e.

$$\Phi = \Phi_0 + A\eta^2 + C\eta^4 + P\eta^6 + \delta_1(\text{grad } \eta)^2 + \dots \quad (3.20)$$

The term  $\delta_1(\text{grad } \eta)^2$  is called correlation energy in Ginzburg's works [10, 11]. This term is essential not only in the descriptions of fluctuations but also in all of those cases when regions of appreciable change of  $\eta(r)$  exist.

The range of applicability of thermodynamic theory on the basis of the expansion (3.20) was examined for the first time by Ginzburg [10]. His approach was developed to a certain extent by Kadonoff, et al. [12]. The theory in [12] as applied to ferroelectrics is also set forth in the lectures by Blinc [13].

Substituting  $\eta$  by  $P_S$  we will rewrite the expansion (3.20) for ferroelectrics limiting ourselves as before to a unidimensional case:

$$\Phi(p, T, P) = \Phi_0(p, T) + a(T)P^2 + \frac{b(T)}{2}P^4 + \delta_1(T)(\text{grad } P)^2. \quad (3.21)$$

Here  $\Phi$  is thermodynamic potential per unit of volume <sup>1)</sup>. Thermodynamic potential  $\Phi_V$  of the entire body is equal to

$$\Phi_V = \int \Phi(r) dv.$$

In equilibrium the quantity  $\Phi_V + \int E dv \sum P$  must remain invariable relative to infinitely small changes

$$P(r) \rightarrow P(r) + \delta P(r).$$

In other words it is necessary that

$$\delta \Phi = \int \delta P (2aP + 2bP^3 - 2\delta_1 \text{grad}^2 P - E) dv = 0.$$

From this we find:

$$2aP + 2bP^3 - 2\delta_1 \text{grad}^2 P = E. \quad (3.22)$$

With  $\delta_1=0$  the equation (3.22) changes into the equation (3.8a) and the results set forth above follow from it.

1) In the examination given below we neglect the change in volume. In this case it is of no difference whether free energy or thermodynamic potential is discussed.

We will expand the fluctuation of the quantity P

$$\Delta P(r) = P(r) - \bar{P}$$

into Fourier series

$$\Delta P(r) = \sum_q P_q e^{iqr}; \quad P_q = P_{-q}^*$$

Here the the probability of the fluctuation  $\Delta P(r)$  is proportional to:

$$w \sim e^{-\frac{\Delta \Phi_v}{kT}} \quad (3.23)$$

where  $\Delta \Phi_v$  is the change in thermodynamic potential owing to the fluctuation  $\Delta P(r)$ .

Taking into account that  $\Phi(\bar{P} + \Delta P) - \Phi(\bar{P}) = \Phi'_{P=\bar{P}} \frac{\Delta P^2}{2} + \delta_1 \text{grad}^2 \Delta P$  we will find

$$\Delta \Phi_v = \int [\Phi(P + \Delta P(r)) - \Phi(P)] \rho v = \nu \sum_q [2\alpha(T) + b_1 q^2] |P_q|^2 \quad (3.24)$$

In the expression (3.24) we limited ourselves to terms quadratic with respect to  $q$  and, consequently, it is valid when  $q$  are not too large. Substituting (3.24) into (3.23), we find:

$$|P_q|^2 = c \int_{-\infty}^{+\infty} |P_q|^2 e^{-\nu(|P_q|^2 [2\alpha(T) + 2b_1 q^2])} d|P_q| \quad (3.25)$$

Since in phase transition of the second kind  $\alpha \rightarrow 0$ , then for long-wave fluctuations  $P_q \rightarrow \infty$ , and consequently neglecting of fluctuations is impermissible. In phase transition of the first kind approaching critical point the value of  $\alpha(T_C) \neq 0$  but is small and accordingly the long-wave fluctuations sharply increase. Thus, Landau theory is inapplicable in direct proximity to the transition point.

Specifically, it becomes inapplicable in the temperature region in which the inequality

$$\overline{|P(r) - \bar{P}| |P(r') - \bar{P}|} \ll (\bar{P})^2 \quad (3.26)$$

is not satisfied. This inequality requires that fluctuations of the order parameter at distances of the order of coherent length  $\xi$  be much smaller than the parameter itself. Therefore, to evaluate the range of applicability of thermodynamic theory it is necessary to examine the correlation of fluctuations.

We will introduce the correlation function:

$$f(r, r') = \overline{|P(r) - \bar{P}| |P(r') - \bar{P}|}$$

The function  $f(r, r')$  can be calculated by following the theorem of classical statistical mechanics (see in greater detail in [12]) from which it follows that a small variation of the field  $S(r)$  brings about changes in polarization  $P(r)$ :

$$\delta P(r) = \frac{1}{kT} \int (r') \delta S(r') E(r) dr' \quad (3.27)$$

On the other hand, it follows from Landau theory (see 3.22) that

$$2\alpha \overline{P}(r) + \delta P^2(r) + 2\beta_1 \text{grad}^2 P(r) - 2\beta_1 \text{grad}^2 \delta P(r) = \delta E(r) \quad (3.28)$$

Substituting the expression (3.27) into (3.28), we find:

$$\int \{ (2\alpha + \delta P^2(r) - 2\beta_1 \text{grad}^2) f(r') - kT\delta(r-r') \} P(r') dr' = 0 \quad (3.29)$$

Since  $\delta P$  is arbitrary, the following is necessary to satisfy the equality (3.29):

$$\{ 2\alpha + \delta P^2(r) - 2\beta_1 \text{grad}^2 \} f(r') = kT\delta(r-r')$$

where  $\delta(r-r')$  is Dirac delta function.

With  $T > \theta$  and  $E=C$ ,  $\overline{P}=0$  and, consequently:

$$\{ 2\alpha(T-\theta) - 2\beta_1 \text{grad}^2 \} f(r') = kT\delta(r-r')$$

With  $T < \theta$  and  $E=0$ ,  $P^2 = -\frac{C}{\beta}$  (see 3.10)

$$\{ 4\alpha(T-\theta) - 2\beta_1 \text{grad}^2 \} f(r') = kT\delta(r-r')$$

Solution of these differential equations has the following form:

$$f(r') = \frac{e^{-\frac{r-r'}{\xi}}}{|r-r'|} \frac{kT}{8\alpha\beta_1} \quad (3.30)$$

where

$$\xi = \begin{cases} \left(\frac{\beta_1}{2\alpha}\right)^{1/2} (T-\theta)^{-1/2} & T > \theta \\ \left(\frac{\beta_1}{2\alpha}\right)^{1/2} (\theta-T)^{-1/2} & T < \theta \end{cases} \quad (3.31)$$

It is assumed here that  $r-r'$  is much larger than lattice constant.

It may be seen from (3.31) that coherent length  $\xi$  increases as  $(T-\theta)^{-1/2}$  when  $T \rightarrow \theta$  where, according to Landau theory,  $\nu = \frac{1}{2}$ . When  $T = \theta$ ,  $\xi$  becomes infinite and correlation between fluctuations decreases as  $1/r$  (see (3.30)).

It is of interest to note the correspondence between the divergence of the quantity  $\xi$  and Curie-Weiss Law. Indeed,

$$\epsilon = 1 + 4\pi \left( \frac{\partial P}{\partial E} \right)_{T=0} = 1 + \frac{4\pi}{kT} \int f(r, r') d\nu = 1 + \frac{2\pi}{\lambda^3} \xi. \quad (3.32)$$

Taking (3.31) into account we will obtain equalities coinciding with (3.11):

$$\epsilon = 1 + \frac{2\pi}{\alpha_0^2 (T - \theta)} \quad T > \theta,$$

$$\epsilon = 1 + \frac{\pi}{\alpha_0^2 (\theta - T)} \quad T < \theta.$$

This result indicates how divergence in coherent length brings about divergence in thermodynamic derivatives.

We will introduce the following parameter:

$$\tau = \frac{\Delta T}{\theta} = \frac{T - \theta}{\theta}.$$

Then, with account taken of (3.30), (3.31) and (3.10) the condition (3.26) gives:

$$\frac{k\theta}{8\pi\alpha_0^2 \xi(r)} \ll -\frac{\alpha}{\beta}.$$

From this we find the following for critical value of  $\tau$  limiting the range of applicability of thermodynamic theory:

$$\tau_c = \frac{k^2 \theta^2}{32\pi^2 \alpha_0^2 \alpha_0^2}. \quad (3.33)$$

Taking (3.6) into account, (3.33) may be written in the following form:

$$\tau_c = \left( \frac{2}{16\pi\epsilon^2} \cdot \frac{k}{\Delta c \lambda^3} \right)^2; \quad (3.34)$$

where  $\lambda = \left( \frac{\delta_1}{2\alpha_0 \theta} \right)^{\frac{1}{2}}$  is coherent length extrapolated to  $T=0$  and  $\Delta c$  is specific-heat jump.

According to Ginzburg's evaluations [10]  $\tau \sim 10^{-4}$  for  $\text{BaTiO}_3$ . In this work the value of  $\delta_1$  (the evaluation of which naturally goes beyond the framework of thermodynamic theory) is determined for the aggregate of dipoles whose moments change in accordance with the following formula:

$$p = p_0 e^{iqd}.$$

With  $qd \ll 1$  ( $d$  is the lattice constant) the energy of such a system

$$W_p = -\frac{2\pi}{3} p_0^2 \left\{ 1 - \frac{(qd)^2}{10} \right\}. \quad (3.35)$$

The first term in (3.35) is volume energy and the second -- correlation energy. It follows from (3.35) that  $\delta_1 \sim \frac{\pi}{15} d^3$ .

Experimental verification of Landau theory was carried out by means of checking Curie-Weiss law. It was found [14] that it is observed for triglycine sulfate,  $\text{KH}_2\text{PO}_4$  and upper Curie point of Salignette's salt up to  $\tau_c$  equal respectively to  $2 \cdot 10^{-4}$ ,  $3 \cdot 10^{-4}$  and  $4 \cdot 10^{-4}$ . It was found that near Curie point

$$\tau \sim (\tau - \tau_c)^{-\gamma} \quad (3.36)$$

with  $\gamma = 1 \pm 0.02$ .

The reasons that  $\tau$  is so small for ferroelectrics in comparison with the other transitions (for ferromagnetics  $\tau \sim 10^{-2}$ ) consist apparently in that spontaneous polarization is low in comparison with the maximum possible polarization, when ion sublattices are displaced by the lattice constant.

It should also be noted that evaluations for  $\delta_1$  and  $(\Delta P^2)_0$  obtained in [10, 11] coincide in regard to the order of value with the corresponding values determined with the aid of model theories [15, 16] based on representation of a self-consistent effective field (see chapter 4, Par. 1). In doing so, it proves to be that in general the condition for transition may be stated as a certain relationship between the energy of fluctuations in the displacements of ions and electrostatic energy of fluctuations of "hard" (i.e.  $\mu \neq 0$ ) sublattices.

The fact that undoubtedly there must be a connection between fluctuations and condition determining the transition of a crystal into a new phase is obvious enough since  $P_s$  fluctuates relative to its equilibrium value owing to the existence of thermal agitation of atoms which leads to a "disordering" of the system. With  $T > \theta$  the existence of fluctuations of  $P_s$  means that regions with a  $P_s \neq 0$  appear and disappear in nonferroelectric phase, i.e. nuclei of a phase with a lower symmetry appear. Conversely, with  $T < \theta$  regions with nonequilibrium values of  $P_s$  appear and disappear. At the phase transition point these fluctuations are restricted precisely by the interaction of atoms, i.e. by the presence of correlation energy.

Indeed, if the term  $\delta_1 (\text{grad } P)^2 = 0$ , then after the integration of (3.25) we will find for fluctuations a quantity  $\overline{\Delta P^2} = \frac{kT}{2\alpha |v|}$  which becomes infinite when  $\alpha \rightarrow 0$ .

As we see, taking nonuniformity into account leads to the result that  $\overline{\Delta P^2}$  remains a finite quantity also when  $T \rightarrow \theta$  with  $\overline{\Delta P^2}$  near the transition point being the smaller the higher the quantity  $\delta_1 \approx \alpha' \theta d^2$ , i.e. the larger the radius of intermolecular interaction  $d \sim (10^{-8} \text{ to } 10^{-7})$  cm.

Fluctuation corrections into expressions for  $\xi(T)$ ,  $c_p(T)$  and compressibility  $k(T)$  were determined in [17].

#### 4. Critical Indices in Thermodynamic Theory

Thermodynamic theory as well as model calculations, for example Ising model, etc., predicts that the basic physical quantities characterizing a phase transition are proportional to the quantity  $(T - T_c)^{\pm \gamma_i}$  when  $T \rightarrow T_c$ . The numbers  $\gamma_i$  are called critical indices. These indices predicted by thermodynamic theory for different physical quantities are given in Table 5.

Table 5  
Values of Critical Indices Predicted by Landau  
Thermodynamic Theory of Phase Transitions of the  
Second Kind

(1) Физическая величина	$\tau = \frac{T - T_c}{T_c}$	(3) Диаметр когерентного поля	(4) Поведение величины	(5) Значение критического индекса
P	$> 0$	0	0	—
	$< 0$	0	$\sim  \tau_T ^\beta$	$\beta = 1/2$
$\chi = \left(\frac{\partial P}{\partial E}\right)$	$> 0$	$\neq 0$	$\pm E^{1/\delta}$	$\delta = 3$
	$< 0$	0	$\sim  \tau_T ^{-\gamma}$	$\gamma = 1$
f( $\tau'$ ) и $\xi$ — когерентная длина (2)	$> 0$	0	$\sim  \tau_T ^{-\gamma'}$	$\gamma' = 1$
	$< 0$	0	$\sim  \tau_T ^{-\gamma'}$	$\gamma' = 1$
$c_p$	$> 0$	0	$\sim  \tau_T ^{-\nu}$	$\nu = 1/2$
	$< 0$	0	$\sim  \tau_T ^{-\nu'}$	$\nu' = 1/2$
$\alpha$	$> 0$	0	$\sim A_1 \tau_T^\alpha + B_1$	$\alpha = 0$
	$< 0$	0	$\sim A_2 \tau_T^{\alpha'} + B_2$	$\alpha' = 0$

Key: (1) Physical quantity (4) Behavior of the quantity  
(2) Coherent length (5) Value of critical index  
(3) Electric field

Except thermodynamic theory and two-dimensional Ising model (see chapter 5, par. 3) none of the theories could formerly predict the exact values of critical parameters  $\alpha$ ,  $\alpha'$ ,  $\beta$ ,  $\gamma$ ,  $\gamma'$ ,  $\delta$ ,  $\nu$ ,  $\nu'$  and  $\eta$  (critical indices are not to be confused with physical quantities which are indicated by the same letters).

A supposition (substantiated by model considerations) was expressed in a series of works [18-23] and in some of the others that the following relationships exist between critical indices:

$$\eta - \alpha = \nu - \alpha' = d\nu - d\nu' = \gamma + 2\beta = \gamma' + 2\beta' = \frac{\gamma d}{2 - \gamma} = \beta(b + 1) \quad (3.37)$$

and, thus, nine critical indices are expressed in terms of two fundamental quantities characterizing a transition (for example,  $\nu$  and  $\eta$ ). Here  $d$  is dimensionality of space for the model selected.

The relationships (3.37) are called similarity relationships.

It may be seen from Table 5 that the relationships (3.37) are satisfied for thermodynamic theory. Speaking in advance, we will note that they are also rigorously satisfied for the two-dimensional and approximately satisfied for the three-dimensional Ising model (see chapter 4, par. 3).

Similarity relationships are of great importance since it turns out [12] that they can provide certain information concerning the behavior of a system in "critical region", i.e. in the region of wavelengths of Fourier fluctuation components smaller than coherent length, i.e.  $\lambda \gg l$ . It should be noted that since  $\xi \rightarrow \infty$  when  $T \rightarrow \theta$ , this critical region extends up to the longest waves, i.e. up to  $q \rightarrow 0$ .

It is, therefore, understandable that experimental verification of the relationships is of a special interest. However, up to the present time, only the index  $\nu$ , i.e. Curie-Weiss law (see subparagraph 3 of this paragraph) has been measured with sufficient accuracy. For the remaining physical quantities characterizing ferroelectrics there has not as yet been made a study of their temperature behavior with sufficient accuracy near the transition point and, therefore, such a study remains to be one of important tasks for the future.

One of the latest achievements in the field of theoretical substantiation of similarity relationships is a work by Migdal [24]. The results he obtained will apparently make it possible to calculate in the future the critical indices for some of the microscopic models.

## Par. 2. Ferroelectric Transition and Symmetry of Crystals

Preceding paragraph investigated a unidimensional ferroelectric, i.e. it was assumed that spontaneous polarization is characterized by one component  $P_s$  and, accordingly, the crystal has only one ferroelectric axis.

Inasmuch as the basis of Landau theory is representation of phase transition connected with a change in the symmetry of the crystal for a three-dimensional case, it is necessary to find such a general form of notation for the thermodynamic potential  $\Phi$  which by itself would contain the possibility of different changes in the symmetry of a crystal in phase transitions. It is obvious that as before, a measure of this change must be the order factor  $\eta$  and both phases (more or less symmetrical) must satisfy the condition of minimum  $\Phi$ .

The approach to the description of phase transition from the positions of symmetry theory consists in that the thermodynamic potential of

of each phase must be invariant in relation to those symmetry operations the aggregate of which forms a symmetry group of this phase. In doing so, transition into a less symmetrical phase is connected with a disappearance of one or several symmetry elements, i.e. with a transition of the group into its subgroup. Therefore, order factor must be connected with symmetry operations in such a manner that its changes would lead to corresponding changes in the number of symmetry elements in the group. This method of describing the phase transitions was developed by Landau and Lifshits for phase transitions of the second kind [25, 26] and was used later by Indenbom [27, 28] for the analysis of possible realizations of ferroelectric phase transitions in crystals belonging to different classes of symmetry. In addition to this, it is possible to determine different changes in the symmetry of a crystal in the case of a ferroelectric transition on the basis of Curie principle which connects a change in the symmetry of a system during an external action upon it with the symmetry of this action.

Both of these approaches are based on group theory the basic principles of which are given in chapter 6. A bibliographic reference on literature devoted to the application of group theory in physics is also given there.

#### 1. Change in the Symmetry of Crystals in Phase Transitions of the Second Kind

In a phase transition of the second kind the order factor (for example, spontaneous polarization) continuously tends to zero during the approach to Curie point and vanishes at the transition point. However, the symmetry of a crystal changes at the transition point discontinuously since it is possible to show at every moment to which one of the two phases the body is related. At the transition point the states of both phases coincide and, therefore, symmetry must contain symmetry elements of both phases.

In the case of phase transitions of the first kind the order parameter changes discontinuously. Two different phases are in a state of equilibrium at the transition point. Therefore, on the basis of considerations similar to those set forth above no restrictions can be imposed on the change in symmetry in the case of a phase transition of the first kind. Of course, it is possible to attempt to extend such an examination to the phase transitions of the first kind that are close to the critical point but it should be remembered that such attempts have no rigorous substantiation.

A method, less general but one quickly leading to the accomplishment of the aim, is usually employed in the examination of phase transitions of the first kind. This method consists in that in the expression for  $\Phi$  only those combinations of coefficients at  $\eta$  are kept which leave  $\Phi$  invariant in relation to the operations of pre-set symmetry of the respective phases. In practice this was precisely what was done by the authors of

most of the works devoted to thermodynamic theory, for example in the determination of  $\Phi$  for the cubic, tetragonal, orthorhombic and rhombohedral phases of BaTiO<sub>3</sub>. This method can be connected with Curie principle (see subparagraph 3).

Two important inferences may be drawn from the foregoing for phase transitions of the second kind, stating them for convenience in terms of group theory (these inferences will be laid down as a basis for the further exposition):

1) symmetry group G of one of the phases is a subgroup of symmetry group G<sub>0</sub> of the other phase;

2) changes in the symmetry of a crystal correspond to one of the irreducible representations of a highly symmetrical phase.

We will explain the sense of the proposition 2. Suppose  $\rho_0(x, y, z)$  is a density function defining the distribution of probabilities of different positions of atoms in a crystal. The symmetry of a crystal lattice is an assemblage (group) of transformations of coordinates in relation to which  $\rho_0(x, y, z)$  is invariant. If a phase transition of the second kind takes place and, consequently, the state of the crystal changes continuously, then function  $\rho(x, y, z)$  of the new phase may be represented in the following form:

$$\rho(x, y, z) = \rho_0(x, y, z) + \psi_0(x, y, z).$$

The function  $\delta\rho_0$  may be expanded with respect to the base functions of irreducible representations of the group G<sub>0</sub>:<sup>1)</sup>

$$\psi_0 = \sum_n \sum_i c_i^{(n)} \psi_i^{(n)}. \quad (3.38)$$

Here n indicates the number of irreducible representation and i -- the number of the line of the n-th irreducible representation.

The term connected with that base function which is invariant in relation to all transformations of the G<sub>0</sub> group and consequently realizes a unit irreducible representation, can be simply included in  $\rho_0$  by re-writing the expansion (3.38) in the following form:

$$\psi_0 = \sum_n' \sum_i c_i^{(n)} \psi_i^{(n)}. \quad (3.39)$$

The prime shows here that the term corresponding to the unit representation is omitted.

1) The proof that base functions of irreducible representations form a complete set of functions is contained in any one of the courses on group theory listed in chapter 6.

Proposition 2 means that two different and two independent phase transitions may correspond to two different irreducible representations.

In accordance with this, we will henceforth omit the index  $n$  bearing in mind that the irreducible representation which is connected with the phase transition under consideration was left in (3.39).

If a phase transition of the second kind is examined, then  $\delta p_0 \rightarrow 0$  when  $T \rightarrow \Theta$  and, consequently, all values of  $c_i$  must also tend to zero when  $T \rightarrow \Theta$ . Therefore, we can expand thermodynamic potential  $\Phi(p, T, c_i)$  with respect to the powers of  $c_i$  near Curie point.

We will introduce the following notation:

$$z_i = \gamma_i; \quad \sum \gamma_i = 1. \quad (3.40)$$

It follows from (3.40) that:

$$\sum c_i^2 = \gamma^2. \quad (3.41)$$

Taking (3.40) and (3.41) into account, we can write the expansion for thermodynamic potential in the following form:

$$\phi = \phi_0(p, T) + \gamma^2 A(p, T) + \gamma^3 B(p, T) f^{(3)}(\gamma_i) + \gamma^4 \sum C_\alpha(p, T) f^{(4)}(\gamma_i). \quad (3.42)$$

Here  $f_\alpha^{(k)}$  is an invariant of the  $k$ -th order made up of quantities  $(\gamma_i)$ . In the sum over  $\alpha$  there are as many terms as there are fourth-order invariants. In writing (3.42) it was taken into account that there exists only

one second-order invariant  $\left( \sum_i \gamma_i^2 \right)$  equal in accordance with (3.41) to

unity. Also taken into account was theorem proven in [29] according to which there cannot be more than one third-order invariant for irreducible representations of the space groups.

This proposition which was put forth earlier as a hypothesis in the monograph [4] is very essential for thermodynamic theory. Indeed if third-order terms are absent in the expansion (3.42), then condition for the transition has the form  $A(p, \Theta) = 0$  and a whole line of phase transitions exists in the  $pT$  plane. If a third-order term is present (see [4], p 526), conditions  $B_\alpha(p, \Theta) = 0$  are added and, consequently, if one third-order invariant exists, then there are isolated phase transition points in the  $pT$  plane, which have not been observed up to the present time. If more than one third-order invariant existed, then more than two equations would result for the determination of two quantities  $p$  and  $\Theta$ , which has no physical sense. Therefore, we will limit ourselves to the case when a line of phase transitions exists in the  $pT$  plane and third-order terms are

absent owing to symmetry. In this case the expansion (3.42) may be re-written in the following form:

$$\phi = \phi_0 + A(p, T)\eta^2 + \eta^4 \sum_i C_i(p, T) \gamma_i^4 \quad (3.43)$$

Inasmuch as the second-order term does not contain the quantities  $\gamma_i$ , these quantities are determined from the condition of minimalness of the fourth-order terms, i.e. of the coefficient with  $\eta^4$  in (3.43) <sup>1)</sup>. If the minimal value of this coefficient is indicated by  $c(p, T)$ , we will obtain the expansion (3.7). Then the parameter  $\eta$  can be determined from the condition of minimum  $\Phi$  (as in 3.8 and 3.9) and, consequently,

$$\eta = \eta \sum_i \gamma_i \quad (3.44)$$

The functions  $\gamma_i$  found in this manner will define the change in symmetry during a phase transition.

Up to the present time we limited ourselves to a case of a homogeneous crystal. In order to examine a heterogeneous, for example stratified crystal, it is necessary to taken into account that  $\Phi$  depends not only on  $c_i^{(n)}$  but also on their derivatives with respect to coordinates.

Therefore, near the transition point, it is necessary to take into account in the expansion of thermodynamic potential  $\Phi$  the units of volume not only of the power of  $c_i$  but also their derivatives with respect to  $x$ ,  $y$  and  $z$ . In order that  $\Phi$  be minimal without stratification into regions characterized by different values of  $\eta$  varying with the coordinate (as this occurs, for example, during fluctuations), it is necessary to require that terms containing space derivatives  $\frac{\partial c_i}{\partial x}$  or derivatives  $c_k \frac{\partial c_i}{\partial x}$  be identically equal to zero in  $\Phi$ . In doing so, the thermo-

dynamic potential of the entire crystal must be minimal, i.e.  $\Phi_v = \int_v \Phi dv$

(minimum  $\Phi$  related to a unit of volume is determined in the case of a homogeneous crystal). It is, therefore, clear that after integration the quantity  $\int_v c_i$ , i.e. total derivatives, leads to the appearance of a constant in the expression for  $\Phi$ , which is not essential in the determination of the minimum  $\Phi_v$ . The same also applies to symmetrical combinations

$$c_k \frac{\partial c_i}{\partial x} + c_i \frac{\partial c_k}{\partial x} = \frac{\partial}{\partial x} (c_i c_k) + \dots$$

and, consequently, the following antisymmetrical combinations are essen-

1) Of course, in practice it is not possible to determine the quantities  $\gamma_i$  from the condition of minimalness of the fourth-order term in (3.43) since knowledge of the coefficients  $C_i(p, T)$  for different irreducible representations is necessary for such a procedure.

tial

$$c_k \frac{\partial c_l}{\partial x} - c_l \frac{\partial c_k}{\partial x}.$$

Quantities proportional to  $\left(\frac{\partial c_j}{\partial x}\right)^2$ , i.e. those which lead to the appearance of correlation energy  $\delta_1(\text{grad } \eta)^2$ , must be essentially positive. However, this does not impose any limitations on  $c_1$  and, consequently on  $\gamma_1 \eta$ , since similar quadratic forms exist for  $c_1$ , which are transformed in accordance with any one of irreducible representations (see [4, 30]). Therefore, henceforth we will be concerned first of all with the presence in  $\Phi$  of invariants which contain the following antisymmetrical combinations of derivatives

$$c_k \frac{\partial c_l}{\partial x}.$$

Thus, if a case is examined when we have a homogeneous crystal it is necessary to require an absence of invariants corresponding to expressions of the following type

$$c_k \frac{\partial c_l}{\partial x} - c_l \frac{\partial c_k}{\partial x}. \quad (3.45)$$

It follows from the foregoing that the range of possible changes in symmetry in phase transitions of the second kind may be limited by two requirements, namely: irreducible representation with which a phase transition is connected: a) must not allow the existence of a third-order invariant, b) must not allow invariants made up of quantities of the form (3.45). Irreducible representations which satisfy the conditions a) and b) are called active representations.

It can be shown that out of an infinite number of irreducible representations of every space group only a few prove to be active, and that they can be found by making use of the conditions a) and b) [26, 30].

Investigations in this direction have been carried out for ferroelectrics in the works [27, 28, 31] and in other works.

It is of interest to note that in a number of cases a conclusion concerning the character of a phase transition can be drawn on the basis of theory set forth above. Indeed, if a phase transition is connected with an active irreducible representation, it can be both of the first and second kind but if a transition is connected with an "inactive" irreducible representation, it must be only a transition of the first kind.

Making use of the condition a) and b) Landau [4] proved a theorem according to which phase transition of the second kind can exist for every change in the structure connected with a decrease in the number of symmetry elements by one half, and expressed a supposition (as yet unproven) according to which phase transitions of the second kind cannot

exist for changes in the structure, connected with a decrease in the number of symmetry transformations by 3 times.

An example of phase transitions with which the number of symmetry elements changes by half may be provided by  $\text{KH}_2\text{PO}_4$ , triglycine sulfate, Seignette's salt, etc.

But in a ferroelectric  $(\text{NH}_3\text{CH}_3)\text{Al}(\text{SO}_4)$ , for example, the number of symmetry elements in a space group of low-symmetrical phase is not equal to one half of the elements in a space group of paraelectric (highly symmetrical) phase (a group of paraelectric phase  $T^4$  (p23) of ferroelectric phase  $C_2^2$  (p2)). Transition is connected with a three-dimensional irreducible representation of F. It can be shown that one third-order invariant exists for this irreducible representation and, consequently, ferroelectric transition in this crystal is unquestionably of the first kind.

## 2. Ferroelectric Transitions in Crystals of Different Symmetry

Concrete expressions for  $\Phi(P)$  as applied to crystals belonging to different symmetry classes can be examined with the aid of formula (3.42). As before, we will assume an  $\eta = |P_s|$ . Now  $|P_s|$  is absolute value of the three-dimensional vector  $P_s$ . Unlike this equality, a dimensionless normalized quantity  $\eta$  is in (3.42). However, this should not cause difficulties since the normalizing factor  $\left(\frac{1}{|P_s|_{\max}}\right)^n$  can be intro-

duced into (3.42), i.e. into the respective coefficients A, B and C, ( $|P_s|_{\max}$  is maximum value of polarization in the least symmetrical phase and n is exponent of the corresponding term in  $\Phi$ ). On the basis of the foregoing we will rewrite (3.42) in the following form:

$$\Phi(T, P_{ij}, P_{ijk}) = \Phi_0(T) + \alpha_{ij} P_{ij} P_{ij} + \alpha_{ijkl} P_{ij} P_{ij} P_{kl} + \gamma_{ijklm} P_{ij} P_{ij} P_{kl} P_{lm} + \gamma_{ijklmn} P_{ij} P_{ij} P_{kl} P_{lm} P_{mn} \quad (3.46)$$

Summing is done over twice-repeating indices. In this expression the quantities  $P_{ij}$  are transformed in accordance with irreducible representations of the point group during the action of symmetry operations of the crystal class in question.

Thus, for cubic crystals (class T and O)  $P_{sx}$ ,  $P_{sy}$  and  $P_{sz}$  are transformed in accordance with a three-dimensional irreducible representation, and in the case of the so-called uniaxial crystals, for example for the class  $C_{4h}$ ,  $P_{sx}$  and  $P_{sy}$  they lie in the symmetry plane and are transformed in accordance with two-dimensional representation. Only one component of spontaneous polarization exists in biaxial crystals (for example, Seignette's salt, class  $D_2$ ). In transitions of the second kind the fifth- and sixth-order terms do not have to be taken into account in (3.46). In addition to this, it is necessary to require absence of third-order invariants since otherwise  $\Phi$  has no minimum when  $T = \Theta$  (isolated transition

points are not examined). Next, inasmuch as a homogeneous single-domain crystal without stratification is examined an absence of terms of the type  $P_{sj} \frac{\partial P_{si}}{\partial x_k} - P_{sj} \frac{\partial P_{si}}{\partial x_k}$  should be assumed regardless of the character of the transition.

The possibility of existence in the expansion of  $\Phi(P_s)$  of third-order invariants and of invariants which contain derivatives with respect to coordinates was determined for crystals of different symmetry classes in [27, 28]. It was found that in principle the classes  $D_2(222)$ ,  $D_{2d}$ ,  $S_4(4)$  and  $T(23)$  allow the invariant  $P_{sx}P_{sy}P_{sz}$ . In the class  $D_2$  (a biaxial crystal) the third-order term is not forbidden in  $\Phi$  by symmetry; however, it does not play any role anyway since the transition is determined by only one component of the vector  $P_s$  (for example, the transition  $D_{2h} \xrightarrow{C_{2v}}$  in  $SbSI$  and  $D_{2d} \xrightarrow{C_{2v}}$  in  $KH_2PO_4$ ).

In the class- $D_{2d}$  crystals, upon the appearance of polarization in the base plane, crystal symmetry also requires the appearance of secondary polarization along the second-order principal axis. Similar effects should be observed in the class- $S_4$  crystals (i.e. those having an axis of rotary reflection of the fourth order) in which invariants of the type  $P_{sx}P_{sy}P_{sz}$  and  $P_{sz}(P_{sx}^2 - P_{sy}^2)$  are allowed in principle.

Invariant  $P_{sx}P_{sy}P_{sz}$  is possible in the classes  $T$  and  $T_d$  (cubic crystals having no center of symmetry), and therefore phase transitions of the first kind may take place in these crystals. In principle, crystals of the class  $D_3$ ,  $D_{3h}$  and  $C_{3h}$  allow third-order invariants of the type  $P_{sx}(3P_{sy}^2 - P_{sx}^2)$  or  $P_{sy}(3P_{sx}^2 - P_{sy}^2)$ . Therefore, if ferroelectrics of this type exist, a phase transition of the second kind is possible in them only if spontaneous polarization appears along the third-order principal axis, i.e. when  $P_{sx}=P_{sy}=0$ .

Invariants requiring a stratification of the crystal may have the following form: a)  $P_{sx} \frac{\partial P_{sy}}{\partial z} - P_{sy} \frac{\partial P_{sx}}{\partial z}$  and b)  $P_s \text{ rot } P_s$  (a more general case). In principle the invariant  $P_{sx} \frac{\partial P_{xy}}{\partial z} - P_{sy} \frac{\partial P_{sx}}{\partial z}$  is allowed by the classes  $D_3$ ,  $D_4$  and  $D_6$  and, therefore, phase transitions of the second kind are possible in them only when  $P_{sx}=P_{sy}=0$ ;  $P_{sz} \neq 0$ , i.e. in the case of polarization oriented along the principal axis. The invariant  $P_s \text{ rot } P_s$  is allowed by the classes  $T$  and  $O$  (noncentrosymmetrical cubic crystals) and, therefore, ferroelectric transitions of the second kind are forbidden in these crystals. Thus, all crystals having a horizontal symmetry plane, i.e. crystals of the class  $C_{4h}$ ,  $D_{4h}$ ,  $D_{3h}$ ,  $C_{3h}$ ,  $D_{6h}$ ,  $T_6$  and  $O_h$  do not con-

tain in  $\Phi(P)$  odd-order invariants and invariants with antisymmetrical combinations  $\frac{\partial P_{si}}{\partial x_k}$ . In all of the remaining cases, phase transitions of the first kind having a number of special characteristics owing to the presence of odd-order invariants may be observed in uniaxial and cubic crystals.

On the basis of knowledge of crystal symmetry in the region  $P_s=0$ , the results obtained make it possible to "design" thermodynamic potential  $\Phi(P)$  for different ferroelectrics. In doing so, it should be born in mind that the expression  $\Phi(P)$  in ferroelectric phases, which results on the basis of expansion of  $\Phi(P)$  of the crystal in the initial paraelectric phase is sufficiently correct on the condition that electrostrictive distortions of the lattice, i.e. spontaneous deformations when  $P_s \neq 0$  are small. Strictly speaking this approximation is not always valid and, therefore, in a number of cases (for example, in the region of low-temperature transitions in BaTiO<sub>3</sub>) it rather bears the character of an illustration since the form of phase transition and even the very condition for its realization may considerably depend on that portion of  $\Phi$  which is brought about by electroelastic effects. (Effect of deformations, mechanical stresses and electrostriction is examined in paragraph 3 of this chapter). Analysis of expressions for  $\Phi$  without taking electromechanical properties of ferroelectrics into account is, nevertheless, not only a necessary stage in the "movement" toward a more complete and exact thermodynamical description of a ferroelectric transition but it also makes it possible to obtain formulas for a direct comparison of results of different microscopic theories of ferroelectrics, in which electromechanical effects are not, as a rule, taken into consideration.

We will examine the expansion of  $\Phi(P)$  for some of the crystals.

#### Seignette's Salt

The region of existence of spontaneous polarization is bounded by two Curie points: -18 and +24°C. Within this region the crystal belongs to the monoclinic symmetry class  $C_2$ . In nonferroelectric region the crystal belongs to the rhombic class  $D_2$  and is a piezoelectric (the center of symmetry is absent). In accordance with the foregoing the thermodynamic potential has the following form:

$$\Phi(T, P_s) = \Phi_0(T) + \alpha P_{1s} + \frac{\beta}{2} P_{1s}^2 + \frac{\gamma}{3} P_{1s}^3. \quad (3.47)$$

Apparently Seignette's salt undergoes phase transition of the second kind at both Curie points [32]. It does not appear possible to explain within the framework of the expression (3.31) the existence of a second, i.e. low-temperature Curie point, in other words a twofold transition through zero. According to representations of a number of authors the second Curie point is brought about by strong piezoeffect and electrostriction [33, 34] which are not taken into account in (3.47). Another explanation of anomalous behavior of  $P_s$  is based on microscopic representations concerning the nature of spontaneous polarization in Seignette's salt (see [5, 33-35] and par. 3, chapter 4).

#### Triglycine Sulfate (TGS)

In nonferroelectric region TGS belongs to centrosymmetrical class  $C_{2h}$  (symmetry elements -- second-order rotary axis  $C_2$  and horizontal sym-

metry plane  $C_h$ ). Below Curie point (40°C) the crystal has a lower symmetry group  $C_2$ . Second-order monoclinic axis is the ferroelectric axis. Consequently, third-order invariants and terms of the type  $\frac{\partial^3 \Phi}{\partial x_k^3}$  must be absent in the expansion. Thus, phase transition in triglycine sulfate, as well as in ferroelectrics isomorphous to it -- triglycine selenate and triglycine fluoroborate -- is described by thermodynamic potential of the type (3.47) which does not forbid phase transition of the second kind. According to experimental data [36, 37], all of these crystal modifications indeed undergo phase transition of the second kind.

#### Potassium Dihydrogen Phosphate $KH_2PO_4$

$KH_2PO_4$  and compounds isomorphous to it, for example  $KD_2PO_4$  and  $KH_2AsO_4$ , belong in nonferroelectric phase to the point group  $D_2$ . After the transition of the second kind approaching critical point ( $\theta = 123^\circ K$ )  $KH_2PO_4$  has symmetry  $C_{2v}$ . Inasmuch as polarization appears along the principal axis  $C_2$ , the expansion of  $\Phi$  is described by a formula analogous to (3.47) (notation of spontaneous polarization changes to  $P_{sz}$ ).

Alum (a family of double salts with a general formula  $M^{1+}M^{3+}(RO_4) \cdot 12 H_2O$  where  $M^{1+}$  is a monovalent metal,  $M^{3+}$  -- a trivalent metal R = S,

Se or Te)

Some of the alums, in particular ammonium or methyl ammonium alum, belong in nonferroelectric phase to the point group  $T(23)$ . According to other data they belong to nonpolar phase  $C_{3v}$  [37]. If cubic symmetry  $T$  exists, then, as noted earlier, existence of the third- and, consequently, fifth-order invariants is possible in the expansion of  $\Phi$ , with the phase transitions of the second kind being excluded:

$$\begin{aligned} \Phi(T, P_i) = & \Phi_0(T) + \alpha(P_{xx}^2 + P_{yy}^2 + P_{zz}^2) + \beta P_{xx}P_{yy}P_{zz} + \\ & + \frac{1}{2}\gamma_1(P_{xx}^4 + P_{yy}^4 + P_{zz}^4) + \gamma_2(P_{xx}^2P_{yy}^2 + P_{xx}^2P_{zz}^2 + P_{yy}^2P_{zz}^2) + \\ & + \gamma_3(P_{xx}^2P_{yy}P_{zz} + P_{yy}^2P_{xx}P_{zz} + P_{zz}^2P_{xx}P_{yy}) + \frac{1}{3}\gamma_4(P_{xx}^3 + P_{yy}^3 + P_{zz}^3) + \gamma_5(P_{xx}^2P_{yy}^2 + \\ & + P_{xx}^2P_{zz}^2 + P_{yy}^2P_{zz}^2) + \gamma_6(P_{xx}^2P_{yy}^2 + P_{xx}^2P_{zz}^2 + P_{yy}^2P_{zz}^2) + \gamma_7(P_{xx}^2 \cdot P_{yy}^2 - P_{zz}^2) \end{aligned}$$

(3.48)

According to the experiment, spontaneous polarization of aluminum methyl ammonium alum in the phase transition region ( $\theta_1 \approx 177^\circ K$ ) changes discontinuously clearly exhibiting the characteristics of phase transition of the first kind. If however, a less symmetrical configuration  $C_{3v}$  is realized above the transition point, then an expansion with respect to even powers, that is of the type (3.47), takes place. As it has already been found, with a certain relationship between the coefficients

( $\beta < 0$ ) this configuration also leads to a phase transition of the first kind.

### Barium Titanate

At a Curie temperature of 120°C above the transition point the crystals of BaTiO<sub>3</sub> and in general the entire group of perovskites, belong to the cubic centrosymmetrical class O<sub>h</sub>. Below  $\theta \sim 120^\circ\text{C}$ , the crystal of BaTiO<sub>3</sub> loses the horizontal plane and the center of symmetry as a result of phase transition of the first kind and changes to polar phase which has tetragonal symmetry C<sub>4v</sub>. At  $T < 5^\circ\text{C}$  the crystal has orthorhombic symmetry C<sub>2v</sub> and at  $T < -90^\circ\text{C}$  -- rhombohedral symmetry C<sub>3v</sub>.

Thus, taking the conclusions of the preceding section into account, we have an expansion in which odd-order invariants and the term  $P_x$  and  $P_y$  are absent:

$$\begin{aligned} \Phi(T, P_i) = & \Phi_0(T) + a(P_{xx}^2 + P_{yy}^2 + P_{zz}^2) + \frac{1}{2} \beta_1 (P_{xx}^4 + P_{yy}^4 + P_{zz}^4) + \\ & + \beta_2 (P_{xx}^2 P_{yy}^2 + P_{yy}^2 P_{zz}^2 + P_{xx}^2 P_{zz}^2) + \frac{1}{3} \gamma_1 (P_{xx}^3 + P_{yy}^3 + P_{zz}^3) + \\ & + \gamma_2 (P_{xx}^2 P_{yy} + P_{yy}^2 P_{xx} + P_{xx}^2 P_{zz}^2) + \beta_3^2 P_{xx}^2 P_{yy}^2 P_{zz}^2. \end{aligned} \quad (3.49)$$

Conditions of the minimum thermodynamic potential  $\frac{\partial \Phi}{\partial P_{sx}} = 0$ ,  $\frac{\partial \Phi}{\partial P_{sy}} = 0$  and  $\frac{\partial \Phi}{\partial P_{sz}} = 0$  give the following solutions for all four phases.

1. Cubic phase O<sub>h</sub>  $P_{sx} = P_{sy} = P_{sz} = 0$ ;
2. Tetragonal phase C<sub>4v</sub>  $P_{sx} = P_{sy} = 0$   $P_{sz} \neq 0$ ;
3. Orthorhombic phase C<sub>2v</sub>  $P_{sx} = 0$   $P_{sy} = P_{sz} \neq 0$ ;
4. Rhombohedral phase C<sub>3v</sub>  $P_{sx} = P_{sy} = P_{sz} \neq 0$ .

Stability conditions for each phase will be found as a result of satisfying the requirements in regard to the determinants made up of the second derivatives of  $\Phi$  (see [38, 39]), i.e.

$$\frac{\partial^2 \Phi}{\partial P_{sx}^2} > 0; \quad \begin{vmatrix} \frac{\partial^2 \Phi}{\partial P_{sx}^2} & \frac{\partial^2 \Phi}{\partial P_{sx} \partial P_{sy}} \\ \frac{\partial^2 \Phi}{\partial P_{sy} \partial P_{sx}} & \frac{\partial^2 \Phi}{\partial P_{sy}^2} \end{vmatrix} > 0; \quad \begin{vmatrix} \frac{\partial^2 \Phi}{\partial P_{sx}^2} & \frac{\partial^2 \Phi}{\partial P_{sx} \partial P_{sy}} & \frac{\partial^2 \Phi}{\partial P_{sx} \partial P_{sz}} \\ \frac{\partial^2 \Phi}{\partial P_{sy} \partial P_{sx}} & \frac{\partial^2 \Phi}{\partial P_{sy}^2} & \frac{\partial^2 \Phi}{\partial P_{sy} \partial P_{sz}} \\ \frac{\partial^2 \Phi}{\partial P_{sz} \partial P_{sx}} & \frac{\partial^2 \Phi}{\partial P_{sz} \partial P_{sy}} & \frac{\partial^2 \Phi}{\partial P_{sz}^2} \end{vmatrix} > 0 \quad (3.50)$$

If these inequalities are analyzed with account taken of the values of  $\Phi$  in the respective phases, then relationships can be obtained which

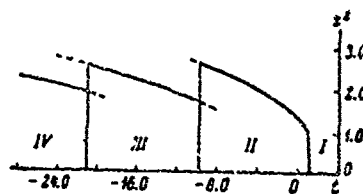


Figure 3.3. Relationship of  $P_{s1}^2$  to T  
(in relative units).

$$z = \frac{P_{s1}^2}{P_1^2}; P_1 \approx 10 \text{ microcoulombs/cm}^2;$$

$$t = \frac{T}{\theta_1 - \theta}; \theta = 118^\circ\text{C}; \theta_1 = 128^\circ\text{C}.$$

make it possible to determine which one of the phases is advantageous from the standpoint of energy in different temperature ranges. The relationship  $P^2(T)$  expressed in relative units and calculated by Devonshire [3] is shown in Figure 3.3. In particular, it follows from this figure that in the transition from phase  $C_{4v}$  to  $C_{2v}$  the value of  $P_{s2}$  decreases approximately as  $\frac{1}{\sqrt{2}}$  and in the transition from phase  $C_{2v}$  to  $C_{3v}$  -- as  $\frac{1}{\sqrt{3}}$ , i.e. turns, as it were, of the vector  $P_s(P_s(100) \rightarrow P_s(110) \rightarrow P_s(111))$  take place.

All transitions in  $\text{BaTiO}_3$  are transitions of the first kind. However, a big difference exists between the character of the transitions  $O_h \rightarrow C_{4v}$  on one hand, and transitions  $C_{4v} \rightarrow C_{2v}$  and  $C_{2v} \rightarrow C_{3v}$  -- on the other. In the former case, symmetry space group  $O_h$  passes into its subgroup in the transition region as a result of disappearance of the center of symmetry and horizontal reflection plane. As is known, in doing so, a phase transition approaching the critical point takes place and, consequently, even if the coefficients  $c_i^{(n)}$  in the expansion (3.39) do not vanish near the transition, they may be very small. In the case of low-temperature phase transitions none of the less symmetrical point groups  $C_{3v}$ ,  $C_{2v}$  and  $C_{4v}$  of the two neighboring phases is a subgroup of a more symmetrical phase although each one of them is a subgroup of the highly symmetrical point group  $O_h$ . In this case, phase transitions of the first kind take place and the coefficients  $c_i^{(n)}$  may be comparatively large.

### 3. Curie Principle and Tables of Possible Ferroelectric Transitions

As already noted above, theory of phase transitions of the second

kind imposes only certain restrictions on the class of possible changes in symmetry without predicting exactly precisely what change in symmetry from this class will take place with a phase transition. But strictly speaking, thermodynamic theory does not impose in general any restrictions on changes in symmetry in the case of phase transitions of the first kind.

However, possible changes in symmetry can be predicted for ferroelectrics in a large number of cases important from practical standpoint when transition parameter is spontaneous polarization [40, 41] regardless of the type of transition. 1) Curie principle is made use of for this purpose. According to this principle it is stated that if a crystal undergoes an external action, then it retains only symmetry elements that are common with the symmetry of the action.

The following rule for the determination of possible ferroelectric transitions follows from Curie principle: symmetry group of a ferroelectric phase must contain all symmetry elements common for the symmetry group of polarization vector (or, which is the same, of any other vector). An additional restriction is imposed on this rule: it is considered that in the case of successive ferroelectric phase transitions in a crystal the symmetry of each ferroelectric phase is connected not with the symmetry of the neighboring phase but with the symmetry of paraelectric phase [42, 43]. In other words, it is assumed that the structures of all ferroelectric phases represent a distorted structure of the initial paraelectric phase and that a change in the symmetry for each one of them takes place independently of the other. In addition to possible symmetry of ferroelectric structures such an approach makes it possible to also show the number of equivalent directions of spontaneous polarization  $N$ :

$$N = \frac{N_p}{N_f}, \quad (3.51)$$

where  $N_p$  and  $N_f$  are the orders of the groups of paraelectric and ferroelectric phases respectively.

The numbers and possible changes in equivalent directions of  $P$  in ferroelectric transitions obtained with the aid of Curie principle are given in Table 6.

We will examine some of the concrete examples.

For  $\text{BaTiO}_3$  the point group of paraelectric phase is  $O_h$  ( $m\bar{3}m$ ), the point group of tetragonal phase --  $C_{4v}$  ( $4mm$ ), the point group of rhombic phase --  $C_{2v}$  ( $mm2$ ), the point group of triclinic (rhombohedral) phase --  $C_{3v}$  ( $3m$ ). The numbers  $N$  of the equivalent possible directions of polarization are equal to 6, 8 and 12 respectively. For  $\text{KH}_2\text{PO}_4$  the point group of paraelectric phase is  $D_{2d}$  ( $\bar{4}2m$ ) and of the ferroelectric phase --  $C_{2h}$  ( $cm2$ ). The number  $N=2$ . For triglycine sulfate the group of paraelectric phase is  $C_{2v}$  ( $2/m$ ) and of the ferroelectric phase --  $C_2$  ( $2$ ).  $N=2$ .

1) Spontaneous polarization is not the only transition parameter, for example in boracite [42], and in general is not a transition parameter in the formation of superstructure. However, in the former case the method set forth below may be used after also taking the other transition parameters into account (see [17] for more details).

Table 6

Possible Changes in Symmetry in Ferroelectric Transitions

(1) Наименьшее число направлений для P	(2) Симметрия параллельной фазы				
	mm2 (O <sub>h</sub> )	432 (O <sub>h</sub> )	3m (Td)	m3 (Td)	23 (T)
	(3) точечная группа оптовольтных и числа эквивалентных направлений P				

(4) а) классом кубической сингонии

<100>	4mm2 (C <sub>4v</sub> ) N = 8	4 (C <sub>4</sub> ) N = 8	mm2 (C <sub>2v</sub> ) N = 8	mm2 (C <sub>2v</sub> ) N = 8	2 (C <sub>2</sub> ) N = 8
<111>	3m (C <sub>3v</sub> ) N = 6	3 (C <sub>2</sub> ) N = 6	3m (C <sub>2v</sub> ) N = 4	3 (C <sub>2</sub> ) N = 6	3 (C <sub>2</sub> ) N = 6
<110>	2 (C <sub>2v</sub> ) N = 12	2 (C <sub>2</sub> ) N = 12	m (C <sub>2</sub> ) N = 12	m (C <sub>2</sub> ) N = 12	1 (E) N = 13
<100>	m (C <sub>2</sub> ) N = 24	1 (E) N = 24	1 (E) N = 24	m (C <sub>2</sub> ) N = 12	1 (E) N = 12
<111>	3 (C <sub>2</sub> ) N = 24	1 (E) N = 24	m (C <sub>2</sub> ) N = 12	1 (E) N = 24	1 (E) N = 12
<110>	2 (C <sub>2</sub> ) N = 24	1 (E) N = 24	m (C <sub>2</sub> ) N = 12	1 (E) N = 24	1 (E) N = 12
<111>	1 (E) N = 48	1 (E) N = 24	1 (E) N = 24	1 (E) N = 24	1 (E) N = 12

(1) Наименьшее число направлений для P	(2) Симметрия параллельной фазы						
	6mm2 D <sub>3h</sub>	3m C <sub>3v</sub>	3m C <sub>2v</sub>	32 D <sub>3</sub>	3 C <sub>3</sub>	3m2 D <sub>3d</sub>	3 C <sub>3</sub>
	(3) точечная группа оптовольтных и числа эквивалентных направлений P						

<0001>	6mm2 (C <sub>3v</sub> ) N = 2	3m (C <sub>3v</sub> ) N = 1	6 (C <sub>2</sub> ) N = 2	6 (C <sub>2</sub> ) N = 2	3 (C <sub>2</sub> ) N = 1	3m (C <sub>3v</sub> ) N = 2	3 (C <sub>2</sub> ) N = 7
<1120>	3m2 (C <sub>2v</sub> ) N = 6	m (C <sub>2</sub> ) N = 6	m (C <sub>2</sub> ) N = 6	2 (C <sub>2</sub> ) N = 6	1 (E) N = 6	3m2 (C <sub>2v</sub> ) N = 3	3 (C <sub>2</sub> ) N = 3
<1010>	3m2 (C <sub>2v</sub> ) N = 6	m (C <sub>2</sub> ) N = 6	m (C <sub>2</sub> ) N = 6	2 (C <sub>2</sub> ) N = 6	1 (E) N = 6	m (C <sub>2</sub> ) N = 6	m (C <sub>2</sub> ) N = 3
<1110>	m (C <sub>2</sub> ) N = 12	1 (E) N = 12	1 (E) N = 12	1 (E) N = 12	1 (E) N = 6	m (C <sub>2</sub> ) N = 6	3 (C <sub>2</sub> ) N = 3
<11210>	m (C <sub>2</sub> ) N = 12	m (C <sub>2</sub> ) N = 3	1 (E) N = 12	1 (E) N = 12	1 (E) N = 6	m (C <sub>2</sub> ) N = 6	1 (E) N = 6
<11110>	m (C <sub>2</sub> ) N = 12	m (C <sub>2</sub> ) N = 6	1 (E) N = 12	1 (E) N = 12	1 (E) N = 6	3 (E) N = 12	1 (E) N = 6
<111110>	1 (E) N = 24	1 (E) N = 12	1 (E) N = 12	1 (E) N = 12	1 (E) N = 6	1 (E) N = 12	1 (E) N = 3

Table 6 (continued)

(1) Наименование группы для направ- ления P	(2) Симметрия параллельной фазы				
	$3m (C_{3v})$	$3 (C_3)$	$3m (C_{3h})$	$3 (D_3)$	$3 (C_2)$
	(3) Уточняем группы симметрии и числа эквивалентных направлений P				

b) б) классы тригональной симметрии

$\langle 0001 \rangle$	$3m (C_{3v})$ $N=2$	$6 (C_6)$ $N=2$	$3m (C_{3h})$ $N=1$	$2 (C_2)$ $N=2$	$3 (C_2)$ $N=3$
$\langle 1120 \rangle$	$2 (C_2)$ $N=6$	$1 (E)$ $N=6$	$1 (E)$ $N=6$	$2 (C_2)$ $N=3$	$1 (E)$ $N=3$
$\langle 10\bar{1}0 \rangle$	$2 (C_2)$ $N=6$	$1 (E)$ $N=6$	$m (C_2)$ $N=3$	$1 (E)$ $N=6$	$1 (E)$ $N=3$
$\langle hkl \rangle$	$1 (E)$ $N=12$	$1 (E)$ $N=6$	$1 (E)$ $N=6$	$1 (E)$ $N=6$	$1 (E)$ $N=3$
$\langle h_1h_2h_3 \rangle$	$1 (E)$ $N=12$	$1 (E)$ $N=6$	$1 (E)$ $N=6$	$1 (E)$ $N=6$	$1 (E)$ $N=3$
$\langle h_1h_1l \rangle$	$m (C_2)$ $N=6$	$1 (E)$ $N=6$	$m (C_2)$ $N=3$	$1 (E)$ $N=6$	$1 (E)$ $N=3$
$\langle h_1hl \rangle$	$1 (E)$ $N=12$	$1 (E)$ $N=6$	$1 (E)$ $N=6$	$1 (E)$ $N=6$	$1 (E)$ $N=3$

(1) Наименование группы для направ- ления P	(2) Симметрия параллельной фазы						
	$4/m (D_2d)$	$4/m (C_{4h})$	$4/m (C_{4v})$	$422 (D_4)$	$4 (C_4)$	$2/m (D_{2d})$	$1 (E)$
	(3) Уточняем группы симметрии и числа эквивалентных направлений P						

c) в) классы тетрагональной симметрии

$\langle 001 \rangle$	$4/m (C_{4h})$ $N=2$	$4/m (C_{2v})$ $N=1$	$4 (C_4)$ $N=2$	$4 (C_4)$ $N=2$	$4 (C_2)$ $N=1$	$2/m (C_{2v})$ $N=2$	$2 (C_2)$ $N=2$
$\langle 100 \rangle$	$2/m (C_{2v})$ $N=4$	$m (C_2)$ $N=4$	$m (C_2)$ $N=4$	$2 (C_2)$ $N=4$	$1 (E)$ $N=4$	$2 (C_2)$ $N=4$	$1 (E)$ $N=4$
$\langle 110 \rangle$	$2/m (C_{2v})$ $N=4$	$m (C_2)$ $N=4$	$m (C_2)$ $N=4$	$1 (E)$ $N=8$	$1 (E)$ $N=4$	$2 (C_2)$ $N=4$	$1 (E)$ $N=4$
$\langle h_1k_0 \rangle$	$m (C_2)$ $N=8$	$1 (E)$ $N=8$	$m (C_2)$ $N=4$	$1 (E)$ $N=8$	$1 (E)$ $N=4$	$1 (E)$ $N=8$	$1 (E)$ $N=4$
$\langle h_0l \rangle$	$m (C_2)$ $N=8$	$m (C_2)$ $N=4$	$1 (E)$ $N=8$	$1 (E)$ $N=8$	$1 (E)$ $N=4$	$1 (E)$ $N=8$	$1 (E)$ $N=4$
$\langle h_1hl \rangle$	$m (C_2)$ $N=8$	$m (C_2)$ $N=4$	$1 (E)$ $N=8$	$1 (E)$ $N=8$	$1 (E)$ $N=4$	$m (C_2)$ $N=4$	$1 (E)$ $N=4$
$\langle h_1kl \rangle$	$1 (E)$ $N=16$	$1 (E)$ $N=8$	$1 (E)$ $N=8$	$1 (E)$ $N=8$	$1 (E)$ $N=4$	$1 (E)$ $N=8$	$1 (E)$ $N=4$

Table 6 (continued)

(1) Надпись миллера для на- правления P	(2) Симметрия параэлектрической фазы						
	ччч (D <sub>3d</sub> )	чч1 (C <sub>3v</sub> )	22 (D <sub>2d</sub> )	2/m (C <sub>2h</sub> )	m (C <sub>2v</sub> )	1 C <sub>s</sub>	1
	(3) точечная группа ферроэлектриков и числа возможных направлений P						
	(7) d) r) классы ромбической, моноклинической и триклинической сингонии						
$\langle 111 \rangle$	ччч2 (C <sub>3v</sub> ) N=2	ччч2 (C <sub>3v</sub> ) N=1	2 (C <sub>2</sub> ) N=2	2 (C <sub>2</sub> ) N=2	m (C <sub>2v</sub> ) N=1	2 (C <sub>2</sub> ) N=1	1 (E) N=2
$\langle 110 \rangle$	ччч2 (C <sub>2v</sub> ) N=2	m (C <sub>s</sub> ) N=2	2 (C <sub>2</sub> ) N=2	m (C <sub>s</sub> ) N=2	1 (E) N=2	1 (E) N=2	1 (E) N=2
$\langle 100 \rangle$	ччч2 (C <sub>2v</sub> ) N=2	m (C <sub>s</sub> ) N=2	2 (C <sub>2</sub> ) N=2	m (C <sub>s</sub> ) N=2	m (C <sub>2v</sub> ) N=1	1 (E) N=2	1 (E) N=2
$\langle 100 \rangle$	m (C <sub>s</sub> ) N=4	1 (E) N=4	1 (E) N=4	1 (E) N=4	1 (E) N=2	1 (E) N=2	1 (E) N=2
$\langle 101 \rangle$	m (C <sub>s</sub> ) N=4	m (C <sub>s</sub> ) N=2	1 (E) N=4	m (C <sub>s</sub> ) N=2	m (C <sub>2v</sub> ) N=1	1 (E) N=2	1 (E) N=2
$\langle 011 \rangle$	m (C <sub>s</sub> ) N=4	m (C <sub>s</sub> ) N=2	1 (E) N=4	1 (E) N=4	1 (E) N=2	1 (E) N=2	1 (E) N=2
$\langle 111 \rangle$	1 (E) N=2	1 (E) N=4	1 (E) N=4	1 (E) N=4	1 (E) N=2	1 (E) N=2	1 (E) N=2

- Key: (1) Miller indices of the direction of P (4) Classes of cubic syngony  
 (2) Symmetry of paraelectric phase (5) Classes of trigonal syngony  
 (3) Point groups of ferroelectrics and the numbers of possible directions of P (6) Classes of tetragonal syngony  
 (7) Classes of rhombic, monoclinic and triclinic syngony

It is easy to see that these ferroelectric transitions (as well as an overwhelming majority of other transitions) are indeed predicted in Table 6.

All possibilities following from Curie principle are examined in this table but nothing is said as to precisely what transitions will be actually realized. Nevertheless, the results given there may prove to be useful, for example, in searching for new ferroelectrics. A major success of this "symmetry" method is, in particular, the prediction of ferroelectric properties in the crystals of NaNO<sub>2</sub> [44].

### Par. 3. Electroelastic Effects in Ferroelectrics

Rearrangement of crystal lattice taking place in the region of a ferroelectric transition leads to a substantial increase of the sensitivity of a crystal to a change in external conditions, in particular to the

application of external electric fields and mechanical stresses. The "pliantness" of a ferroelectric in regard to the action of an electric field is described by the relationship  $E_i = \epsilon E_i$  which was examined in paragraph 2. However, this examination bore a one-sided character.

It may be expected that "pliantness" in regard to mechanical actions, i.e. to the relationship  $\sigma_k = c_{kl} u_l$  (where  $\sigma_k$  is mechanical stress and  $u_l$  is deformation) and also the "cross" effects, for example, the relationships  $P_i = d_{ik} \sigma_k$  will also exhibit marked anomalies in the transition region. This will be reflected in appropriate manner on the behavior of elastic constant  $c_{kl}(T)$  and the piezomodulus  $d_{ik}(T)$ . At the same time, it is clear that electrical and mechanical properties of a ferroelectric must be interconnected.

Thus, it is necessary to examine ferroelectric transition with the electromechanical properties of the crystals taken in account. It is expedient to divide this examination into two parts:

1) examination of electroelastic effects appearing near the phase transition points in a free ferroelectric in the absence of external fields and mechanical forces, in other words, determination of the properties of a ferroelectric with spontaneous deformation taken into account;

2) investigation of electromechanical properties of a ferroelectric in the presence of various electrical and mechanical external actions.

### 1. Spontaneous Deformation

In the preceding paragraphs it was assumed that the state of a ferroelectric is determined by temperature, pressure and behavior of the order factor  $\eta$  appearing in a less symmetrical phase. The quantity  $\eta$  is directly connected with the components of spontaneous-polarization vector ( $P_{si} \sim \eta c_i$ ) the aggregate of which forms the basis of irreducible representation of the crystal's symmetry group in nonferroelectric phase. However, the state of the system may be determined not only by the aggregate of the variables  $\eta c_i$  but also by the set of other variables ( $u_{sk} \sim \xi \tau_k$ ) with the quantity  $\xi$  appearing like  $\eta$  in a less symmetrical phase. Such a situation occurs in a free (nonfixed) ferroelectric crystal in which, in addition to spontaneous polarization  $P_{si}$ , spontaneous deformation  $u_{sk}$  also appears in ordered state. Strictly speaking, now it is necessary to define anew the thermodynamic functions which describe transition when there are two parameters appearing in nonsymmetrical phase. It is also obvious that the complexity of this definition in the presence of even two parameters greatly increases, especially if  $\xi \tau_k$  is a tensor. Indeed, if  $\Phi$  is represented in the form of a series for the entire aggregate of the parameters  $\eta c_i$  and  $\xi \tau_k$ , then it is necessary to take into account not only terms of the type  $(\eta c_i)^n$  and  $(\xi \tau_k)^m$  but also the cross terms  $(\eta c_i)^n (\xi \tau_k)^m$  (n and m are integers). If these new terms are sufficiently large with respect to the order of magnitude, then conclusions drawn earlier concerning the structure of  $\Phi$  (for example, concerning the effect of odd-power invariants on the character of the transition) should be substantiated anew.

In the examination of a "unidimensional" approximation of phase transitions in the presence of several quantities appearing in ordered phase it was assumed in the work [17] that their role is dissimilar, namely, some are transition parameters while the others are of a secondary significance. For example, in a ferroelectric transition the quantity  $\eta \sim P_s$  is a transition parameter since it is the cause of it whereas the quantity  $\xi \sim u_k$  cannot be a transition parameter inasmuch as it is a result of the existence of  $\eta \neq 0$ . Another case is also possible when  $\eta \sim P_s$  is no longer a transition parameter, for example, if transition is connected with a change in the number of atoms in a unit cell, i.e. upon the appearance of a superstructure. An example of such a crystal is ammonium fluoroberyllate [37, 45] in which parameters of the cell are equal to  $a_T < \theta \approx 2a$ ;  $b_T < \theta = b$  and  $c_T < \theta = c$ . The appearance of this superstructure is accompanied by the appearance of spontaneous polarization. Another example is  $\alpha \rightarrow \beta$  transition in quartz. Here  $\eta$  characterizes the magnitude of displacement of several sublattices relative to each other without the appearance of spontaneous polarization.

According to [17], in ferroelectrics the parameter, i.e. the cause of transition, is spontaneous polarization  $P_s \sim \eta$  whereas spontaneous deformation merely accompanies polarization. The authors substantiate this statement by the following considerations: if a cubic crystal, for example  $\text{BaTiO}_3$ , is polarized, then under certain conditions a displacement deformation may be obtained whereas the displacement deformation itself is unable to lead in any manner to the appearance of polarization in a cubic crystal. The proof shown can hardly be considered exhaustive and, in our opinion, the question of whether spontaneous deformation may be a second transition parameter remains open. Indeed, interconnection between displacement deformation and polarization in phase transition in  $\text{BaTiO}_3$  may be regarded as applied to the phases corresponding to the symmetry  $C_{4v} \rightarrow C_{2v}$  and  $C_{2v} \rightarrow C_{3v}$ . In this case, displacement in the respective planes leads to the appearance of new polarization components. As regards the symmetry region  $O_h \rightarrow C_{4v}$ , not too far from the transition point the respective elongation and compression deformations (see subparagraph 3) displace the transition into the region of higher temperatures and, consequently, the state with  $P_s = 0$  becomes unstable.

Division of parameters characterizing the internal steady state of the system into cause and effect is apparently conditional. When discussion concerns the action on the system from without this division is quite obvious: application of external field and external forces is undoubtedly the cause of the appearance of induced polarization and deformation. However, relationships between different internal parameters, for example spontaneous polarization and spontaneous deformation, are not so clear. It may be considered that the aggregate of the variables  $P_{si} \sim \eta c_i$  and  $u_{sk} \sim \xi \tau_k$  forms a multidimensional space the points of which determine the thermodynamic state of the system. In this case, phase transition of the second kind will appear if the coordinates pass through zero at some of the quadratic terms of the expansion of  $\Phi$ . However, if the multidimensionality of the parameters  $P_s$  and  $u_{sk}$  is taken into account, transitions of this type have a complex character and have not as yet been investigated in detail. Therefore, henceforth it is postulated but not stated that  $P_s$  is the only transition parameter and spontaneous deformation appears as a result of polarization of the crystal.

Inasmuch as the system must now be minimal in regard to  $P_{si}$  and  $u_{sk}$ , the conclusions drawn in the preceding paragraph regarding the structure of thermodynamic functions describing a transition may be retained only on the condition that electromechanical effects produce little change in the symmetry of the crystal.

We will define now the expression for thermodynamic potential with spontaneous deformation taken into account. Suppose transition parameter is a three-dimensional spontaneous-polarization vector  $P_{si} \sim \eta c_i$  ( $i=1, 2, 3$ ). Spontaneous deformation whose components are represented by a row matrix  $u_{sk} \sim \xi \tau_k$  ( $k=1, 2, \dots, 6$ ) appears in the ordered phase. In addition to invariants containing different powers of  $(\eta c_i)$ , powers of  $(\xi \tau_k)$ , and cross terms of the type  $\eta \xi (c_i \tau_k)$ ;  $\eta^2 \xi (c_i c_j \tau_k)$ ;  $\eta \xi^2 (c_i \tau_k \tau_l)$ ;  $\eta^2 \xi^2 (c_i c_j \tau_k \tau_l)$ , etc. appear now in the expansion of thermodynamic potential.

We will dwell on these terms in a greater detail. The quantities  $\sim \eta \xi$  and  $\eta \xi^2$  are allowed if the substance in disordered phase has no center of symmetry and, consequently, has piezoelectric properties (for example, Seignette's salt). Invariants  $\sim \eta \xi^2$  exist for any crystal symmetry with the parameter  $\tau_k$  being transformed as  $c_i c_j$  if it is a second-rank tensor. It follows from this that invariants  $\sim \eta \xi^3$  are transformed as a third-rank tensor and invariants  $\sim \eta \xi^4$  -- as a fourth-rank tensor. We will note that the terms  $\eta \xi^2$  and  $\eta^2 \xi^2$  have a higher order than the remaining quantities and taking them into account is necessary only when determining non-linear dependence of deformation on the field (see par. 3, subparagraph 4).

Taking the foregoing into account and passing on from the variables  $c_i \tau_i$  and  $\tau_{ik}$  to  $P_{si}$  and  $u_{sk}$  we will find the following expression for free energy  $A_p$ :

$$\begin{aligned}
 A_p(T, P_{si}, u_{sk}) = & A_p^0(T) + \alpha_{ij} P_{si} P_{sj} + \omega_{ijl} P_{si} P_{sj} P_{sl} + \beta_{ijkl} P_{si} P_{sj} P_{sl} P_{lm} + \\
 & + \gamma_{ijklm} P_{si} P_{sj} P_{sl} P_{lm} P_{mn} + \zeta_{ijklmnp} P_{si} P_{sj} P_{sl} P_{lm} P_{np} P_{pq} + c_{2k} u_{sk} u_{kr} + \\
 & + b_{ik} P_{si} u_{sk} + g_{ijk} P_{si} P_{sj} u_{sk} + \dots
 \end{aligned} \tag{3.52}$$

where  $i, j, l, m, n, p=1, 2, 3$ ;  $k, r=1, 2, \dots, 6$ .

As usually, summation is carried out over twice-repeated indices. Determination of the structure of coefficients of the expansion (3.52) as applied to the symmetry of a ferroelectric in disordered phase is based on the following considerations. It is assumed that spontaneous deformation  $u_{sk}$  brings about a slight distortion of the crystal structure at transition into ferroelectric phase and may be regarded as a small disturbance  $\Delta p(P_s)$ . Properly speaking, this assumption is already contained in (3.52) inasmuch as in writing it, terms of higher order than  $u_{sk}^2$  and  $u_{sk} P_{si}^2$  were neglected. If this assumption is sufficiently correct (in the end its validity can be verified experimentally), then the rules for the selection of coefficients examined in paragraph 2, subparagraph 2 may be retained for  $\Delta p_1(P_s) = \alpha_{ij} P_{si} P_{sj} + \omega_{ijl} P_{si} P_{sj} P_{sl} + \dots$ , and consequently it

remains to determine the structure of

$$A_{P_i}(P_s, u_{sk}) = c_{kr} u_{sk} + h_{ik} P_{si} u_{sk} + q_{ijk} P_{si} P_{sj} u_{sk}$$

Coefficients  $c_{kr}$  have dimensionality and physical sense of elastic constants of the crystal and their aggregate is represented by a matrix whose structure is determined by crystal symmetry in nonferroelectric phase. The quantities  $h_{ik}$  have the sense of piezoelectric constants, and  $q_{ijk}$  -- the sense of coefficients of electrostriction. The aggregates of these constants are also defined by the respective matrices [46, 47] for a highly symmetrical phase.

We will examine expressions for  $A_{P_i}(P_s, u_{sk})$  as applied to barium titanate and Seignette's salt.

### Barium Titanate

The matrix of elastic constants for a cubic crystal  $O_h$  ( $m3m$ ) has the following form [46]:

$$\epsilon = \begin{pmatrix} c_{11} & c_{12} & c_{12} & 0 & 0 & 0 \\ c_{12} & c_{11} & c_{12} & 0 & 0 & 0 \\ c_{12} & c_{12} & c_{11} & 0 & 0 & 0 \\ 0 & 0 & 0 & c_{44} & 0 & 0 \\ 0 & 0 & 0 & 0 & c_{44} & 0 \\ 0 & 0 & 0 & 0 & 0 & c_{44} \end{pmatrix}$$

In this phase the crystal has no piezoeffect and, consequently,  $h_{ik}=0$ . The matrix of coefficients of electrostriction for crystals of the class  $O_h$  is analogous to  $\epsilon$ :

$$q = \begin{pmatrix} q_{11} & q_{12} & q_{12} & 0 & 0 & 0 \\ q_{12} & q_{11} & q_{12} & 0 & 0 & 0 \\ q_{12} & q_{12} & q_{11} & 0 & 0 & 0 \\ 0 & 0 & 0 & q_{14} & 0 & 0 \\ 0 & 0 & 0 & 0 & q_{14} & 0 \\ 0 & 0 & 0 & 0 & 0 & q_{14} \end{pmatrix}$$

and, consequently the expression for  $A_{P_i}(P_s, u_{sk})$  will be written in the following manner (for graphicalness the indices  $i=1, 2, 3$  are replaced by  $x, y, z$  and the indices  $k=1, 2, 3, 4, 5, 6$  by  $xx, yy, zz, yz, xz, xy$ ):

$$\begin{aligned} A_{P_i}(T, P_s, u_{sk}) = & A_0(T) + s(P_x^2 + P_y^2 + P_z^2) + \frac{\beta_1}{2}(P_{xx}^2 + P_{yy}^2 + P_{zz}^2) + \\ & + \beta_2(P_{xx}^2 P_{yy}^2 + P_{xx}^2 P_{zz}^2 + P_{yy}^2 P_{zz}^2) + \frac{\gamma_1}{3}(P_x^4 + P_y^4 + P_z^4) + \gamma_2(P_x^2(P_{yy}^2 + P_{zz}^2) + \\ & + P_y^2(P_{xx}^2 + P_{zz}^2) + P_z^2(P_{xx}^2 + P_{yy}^2)) + \gamma_3 P_x^2 P_y^2 P_z^2 + \frac{1}{2} c_{11}(u_{xx}^2 + u_{yy}^2 + u_{zz}^2) + \\ & + c_{12}(u_{xx} u_{yy} + u_{xx} u_{zz} + u_{yy} u_{zz}) + \frac{1}{2} c_{44}(u_{yz}^2 + u_{xz}^2 + u_{xy}^2) + \\ & + c_{11}(u_{xx} P_x^2 + u_{yy} P_y^2 + u_{zz} P_z^2) + c_{12}(u_{xx}(P_y^2 + P_z^2) + u_{yy}(P_x^2 + P_z^2) + \\ & + u_{zz}(P_x^2 + P_y^2)) + c_{14}(u_{xy} P_{xz} + u_{yz} P_{xx} + u_{zx} P_{yy}) + u_{xy} P_{xy} P_{zz} \end{aligned} \quad (3.53)$$

The quantities  $P_{Si}$  and  $u_{Sk}$  are determined as a result of solving a system of equations resulting from the equilibrium condition of the crystal:

$$\left. \begin{aligned} \frac{\partial A_p}{\partial P_{Si}} &= 0, \\ \frac{\partial A_j}{\partial u_{Sk}} &= 0. \end{aligned} \right\} \quad (3.54)$$

Solutions of these equations obtained for the first time for all ferroelectric phases of BaTiO<sub>3</sub> by Devonshire [3] are reduced to the following form:

1. Cubic phase

$$\begin{aligned} P_{xx} = P_{yy} = P_{zz} &= 0, \\ u_{xxx} = u_{yyy} = u_{zzz} &= 0, \\ u_{xyx} = u_{xzy} = u_{yzz} &= 0; \end{aligned}$$

2. Tetragonal phase

$$\begin{aligned} P_{xx} = P_{yy} &= 0, \quad P_{zz} \neq 0, \\ u_{xxx} &= \frac{2q_{11}c_{12} - q_{11}(c_{11} + c_{12})}{(c_{11} - c_{12})(c_{11} + 2c_{12})} (P_{zz}^2)_{11} = \theta_{22} (P_{zz}^2)_{11}, \\ u_{xzz} = u_{yzz} &= \frac{q_{11}c_{12} - q_{11}c_{11}}{(c_{11} - c_{12})(c_{11} + 2c_{12})} (P_{zz}^2)_{11} = \theta_{31} (P_{zz}^2)_{11}, \\ u_{xyx} = u_{xzy} = u_{yzz} &= 0; \end{aligned}$$

3. Orthorhombic phase

$$\begin{aligned} P_{xx} = P_{zz} &\neq 0, \quad P_{yy} = 0, \\ u_{xxx} = u_{yyy} &= \frac{-q_{11}c_{11} - q_{12}(c_{11} - 2c_{12})}{(c_{11} - c_{12})(c_{11} + 2c_{12})} (P_{zz}^2)_{11}, \\ u_{xzz} &= \frac{-2(q_{11}c_{12} - q_{12}c_{11})}{(c_{11} - c_{12})(c_{11} + 2c_{12})} (P_{zz}^2)_{11}, \\ u_{xyx} = u_{xzy} &= 0; \quad u_{yzz} = -\frac{q_{41}}{c_{44}} (P_{zz}^2)_{11}; \end{aligned} \quad (3.55)$$

4. Rhombic phase

$$\begin{aligned} P_{xx} = P_{yy} = P_{zz} &\neq 0, \\ u_{xxx} = u_{yyy} = u_{zzz} &= \frac{-(q_{11} - 2q_{41})}{c_{11} + 2c_{12}} (P_{zz}^2)_{11}, \\ u_{xyx} = u_{xzy} = u_{yzz} &= -\frac{q_{41}}{c_{44}} (P_{zz}^2)_{11}. \end{aligned}$$

It follows from (3.55) that temperature dependence of spontaneous deformation or, as it is also called, spontaneous electrostriction is determined in the main by the behavior of  $P_{Si}^2(T)$ . Theoretical relationships  $P_{Sj}^2(T)$  calculated in [3] for the phases 2, 3 and 4 and defining  $u_{Sik}(T)$  are shown in Figure 3.3.

It should be noted that spontaneous electrostriction "displaces"

the character of transition in the direction of phase transitions of the first kind. In particular, for perovskites (if transition of the second kind takes place) in tetragonal phase the expression (3.9a) is replaced by [48, 49]:

$$P_{22}^2 = \frac{q_1^2(\theta - 1)}{p_1 - \theta}, \quad (3.56)$$

where  $\theta = - (q_{11}^2 \vartheta_{33} + 2q_{12}^2 \vartheta_{31}) = \frac{q_{11}^2(c_{11} + c_{12}) + 2q_{12}^2 c_{11} - 4q_{11} q_{12} c_{11}}{(c_{11} - c_{12})(c_{11} + 2c_{12})} > 0$   
 since volume electrostriction  $u_{szz} + 2u_{sxx} > 0$ .

This inference is also confirmed by the increase of the jump of the thermal capacity  $\Delta c_p$  determined with the effect of spontaneous deformation of the crystal taken into account [49].

### Seignette's Salt

For ferroelectric phase [rhombohedral symmetry  $D_2 (222)$ ] we have the following matrices defining the structure of  $A_p(P_{si} u_{sk})$ .

Matrix of elastic constants:

$$c_{mn} = \begin{pmatrix} c_{11} & c_{12} & c_{13} & 0 & 0 & 0 \\ c_{12} & c_{22} & c_{23} & 0 & 0 & 0 \\ c_{13} & c_{23} & c_{33} & 0 & 0 & 0 \\ 0 & 0 & 0 & c_{44} & 0 & 0 \\ 0 & 0 & 0 & 0 & c_{55} & 0 \\ 0 & 0 & 0 & 0 & 0 & c_{66} \end{pmatrix}$$

Matrix of piezoelectric constants:

$$h_{mn} = \begin{pmatrix} 0 & 0 & 0 & h_{14} & 0 & 0 \\ 0 & 0 & 0 & 0 & h_{25} & 0 \\ 0 & 0 & 0 & 0 & 0 & h_{36} \end{pmatrix}$$

Matrix of electrostriction coefficients:

$$q_{mn} = \begin{pmatrix} q_{11} & q_{12} & q_{13} & 0 & 0 & 0 \\ q_{12} & q_{22} & q_{23} & 0 & 0 & q \\ q_{13} & q_{23} & q_{33} & 0 & 0 & 0 \\ 0 & 0 & 0 & q_{44} & 0 & 0 \\ 0 & 0 & 0 & 0 & q_{55} & 0 \\ 0 & 0 & 0 & 0 & 0 & q_{66} \end{pmatrix}$$

In view of the relatively low symmetry of Seignette's salt the expression for  $A_p$  is considerably more complex than in the case of  $BaTiO_3$ . However, a number of simplifications are possible. Inasmuch as it is as-

sumed that phase transition of the second kind takes place in Seignette's salt we may limit ourselves only to the terms  $P_S^4$ . And next, since a free crystal is examined (external mechanical stresses and electric field are absent), we may limit ourselves to taking into account only one component  $P_{SX}$ , precisely the one which appears in a less symmetrical phase:

$$\begin{aligned}
 A_F(T, P, u_{sz}) = & A_{F0}(T) + \alpha P_{SX}^2 + \frac{\beta}{2} P_{SX}^4 + \frac{1}{2} (c_{11}u_{sz}^2 + c_{22}u_{yy}^2 + c_{33}u_{zz}^2) + \\
 & + c_{12}u_{sz}u_{yy} + c_{13}u_{sz}u_{zz} + c_{23}u_{yy}u_{zz} + \frac{1}{2} c_{44}u_{yy}^2 + \frac{1}{2} c_{55}u_{zz}^2 + c_{66}u_{xy}^2 + \\
 & + h_{11}P_{SX}u_{yy} + q_1P_{SX}u_{sz} + q_{12}P_{SX}u_{yy} + q_{13}P_{SX}u_{zz} + q_{14}P_{SX}u_{xy}. \quad (3.57)
 \end{aligned}$$

Further simplifications are possible if we limit ourselves to the examination of the displacement deformation  $u_{sz}$  which has an anomalously large magnitude

$$\left. \begin{aligned}
 u_{yy} = & - \left( \frac{h_{11}}{c_{44}} P_{SX} + \frac{q_{11}}{c_{44}} P_{SX}^2 \right), \\
 P_{SX} = & \frac{3}{8} \frac{h_{11}q_{11}/c_{44}}{\beta - q_{11}^2/c_{44}} - \sqrt{\frac{9}{16} \frac{(h_{11}q_{11}/c_{44})^2}{(\beta - q_{11}^2/c_{44})^2} - \frac{2\alpha - h_{11}/c_{44}}{2(\beta - q_{11}^2/c_{44})}}. \quad (3.58)
 \end{aligned} \right\}$$

The expression (3.58) considerably differs from a similar relationship for BaTiO<sub>3</sub> owing to the influence of linear piezoeffect. We will also note that the condition  $P_{SX}=0$  is satisfied when  $2\alpha - \frac{h_{11}}{c_{44}} = 0$  and in addition to this,  $P_{SX}$  becomes complex when

$$\frac{9}{8} \frac{(h_{11}q_{11}/c_{44})^2}{\beta - q_{11}^2/c_{44}} < \left( 2\alpha - \frac{h_{11}}{c_{44}} \right).$$

This creates a formal possibility of explaining the existence of a second Curie point owing to the influence of strong piezoeffect and electrostriction.

## 2. Thermodynamic Potentials and Elastic Electric Constants in Ferroelectrics

In the examination of the properties of a ferroelectric crystal, in particular in the determination of behavior of such of its internal parameters as  $P_{Si}(T)$  and  $u_{Sk}(T)$ , the differences between a thermodynamic potential and free energy were not determined. These differences become all the more important when describing the behavior of a crystal which is under the effect of external forces and electric fields. Thus, a question arises concerning the selection of a thermodynamic function (i.e. a thermodynamic potential in the broad sense of this word) for describing the processes taking place in a ferroelectric upon a change in temperature and during the action of external electric and mechanical fields.

According to the definition (see, for example, [4, 7]), free energy

(it is also called Helmholtz free energy) is equal to

$$A = U - TS, \quad (3.59)$$

where  $U$  is the energy of the system. Passing on to differential relationships we have

$$dA = dU - TdS - SdT, \quad (3.60)$$

$$dU = TdS - pdv \quad (3.61)$$

and consequently

$$dA = -SdT - pdv, \quad (3.62)$$

i.e. the change in free energy is equal to work done on the system in the case of a reversible isothermal process, or to the change in the amount of heat with a constant volume. When other parameters  $\lambda_i$  and  $\Lambda_i$  defining the state of the system (for example, components of electric polarization  $P_i$  and external electric fields  $E_i$ ) are present, elementary work  $\sum_i \Lambda_i d\lambda_i$

defining the corresponding change in the system's energy must be added in (3.60). Here  $\Lambda_i d\lambda_i$  has the dimensionality of energy or, if  $A$  is related to a unit of volume -- the dimensionality of energy density:

$$dA = -SdT - pdv + \sum_i \Lambda_i d\lambda_i. \quad (3.63)$$

From this we have the following relationships:

$$\left(\frac{\partial A}{\partial \lambda_i}\right)_T = \Lambda_i; \quad \left(\frac{\partial A}{\partial T}\right)_{v, \lambda} = -S; \quad \left(\frac{\partial A}{\partial v}\right)_{T, \lambda} = -p \quad (3.64)$$

(indices indicate which quantities are considered constant in differentiation).

If all  $\Lambda_i = 0$ , then (3.64) is equilibrium condition of the system with constant volume and temperature.

We will note that determination of the relationship  $P_{iS}(T)$  and  $\xi(T)$  was based on the condition  $\left(\frac{\partial A}{\partial P_i}\right) = E_i$ .

If independent variables in the initial function are  $T$  and  $p$ , then the thermodynamic function resulting in this case is called thermodynamic potential  $\Phi$  (in the narrow sense of this word). It is also called free energy or Gibbs function (for gas and liquids).

Connection between  $\Phi$  and  $A$  follows from the definition

$$\Phi = U - TS + pv = A + pv. \quad (3.65)$$

The total differential of  $\Phi$  is equal to:

$$d\Phi = dA + d(pv) = -SdT + vdp. \quad (3.66)$$

Consequently, the increment of  $\Phi$  is numerically equal to work done by the system at a constant temperature, or to the change in the amount of heat at a constant pressure.

If in addition to the variables  $S$ ,  $T$ ,  $p$  and  $v$  the state of the system is also defined by a set of other variables  $\Lambda_i$  and  $\lambda_i$ , then inasmuch as the differential transformation of  $dA$  to  $d\Phi$  does not affect the variables  $\lambda_i$  and  $\Lambda_i$

$$d\Phi = dA + d(pv) = -SdT + vdp + \sum_i \Lambda_i d\lambda_i, \quad (3.67)$$

and consequently

$$\left(\frac{\partial \Phi}{\partial T}\right)_{p, \lambda_i} = -S; \quad \left(\frac{\partial \Phi}{\partial p}\right)_{T, \lambda_i} = v; \quad \left(\frac{\partial \Phi}{\partial \lambda_i}\right)_{T, p} = \Lambda_i. \quad (3.68)$$

As long as a change in the volume (i.e. dimensions of the system) and pressure plays no role, the differences between  $\Phi$  and  $A$  are unessential. Therefore, in setting up the equations defining the state of a ferroelectric the question of precisely which thermodynamic function is involved arose for the first time in taking spontaneous deformation into account. With the action of external forces it is necessary to strictly differentiate precisely which function is meant and, consequently, pressure or volume should be considered constant in defining the equilibrium condition of the system.

Unlike a gas or liquid for which formulas (3.59)-(3.68) are valid, a complex state of stress described by tensors of mechanical stresses  $\sigma_k$  and deformation  $u_k$  appears in the crystal during the action of external forces. Therefore, the quantity  $p$  in the expression for  $\Phi$  must be substituted by a sum of the type  $\sum_k \sigma_k u_k$  (work done during the deformation of the crystal). Differential relationships must be changed in accordance with this, i.e.

$$\Phi_p(T, P_i, u_k) = U - TS - \sum_k u_k \sigma_k, \quad (3.69)$$

$$d\Phi_p = -SdT - \sum_k u_k d\sigma_k + \sum_i E_i dP_i. \quad (3.70)$$

The function defined by formulas (3.69) and (3.70) is called elastic thermodynamic potential or elastic Gibbs function (for crystals).

Upon passing to the new variables  $U_k$ ,  $T$  and  $P_i$ , free energy is expressed as

$$A_p(T, P_i, u_k) = U - TS, \quad (3.71)$$

$$dA_p = -SdT + \sum_k u_k d\sigma_k + \sum_i E_i dP_i. \quad (3.72)$$

We find the following important relationships from (3.70) and (3.72):

$$\left(\frac{\partial \Phi_P}{\partial P_i}\right)_{T, \sigma_k} = \varepsilon_{ii}; \quad \left(\frac{\partial \Phi_P}{\partial \sigma_k}\right)_{T, P} = -u_k; \quad (3.73)$$

$$\left(\frac{\partial A_P}{\partial P_i}\right)_{T, \sigma_k} = \varepsilon_{ii}; \quad \left(\frac{\partial A_P}{\partial \sigma_k}\right)_{T, P} = -u_k; \quad (3.74)$$

$$A_P = (\Phi_P)_{T, \sigma_k}; \quad \left(\frac{\partial A_P}{\partial P_i}\right)_{T, \sigma_k} = \left(\frac{\partial \Phi_P}{\partial P_i}\right)_{T, \sigma_k}. \quad (3.75)$$

If it is assumed that connection between  $\varepsilon_{ik}$  and  $u_k$  is linear, i.e.  $u_k = \sum_l s_{kl} \sigma_l$ , then we have the following for  $\Phi_P$ :

$$\Phi_P(T, P_i, \sigma_k) = U - TS - \frac{1}{2} \sum_k \sum_l s_{kl}^P \sigma_k \sigma_l, \quad (3.76)$$

where  $s_{kl}^P = \left(\frac{\partial^2 \Phi}{\partial \sigma_k \partial \sigma_l}\right)_{P, T}$  is matrix of moduli of elasticity at a constant polarization (induction).

In a similar manner a group of terms represented by the sum  $\sum_k \sum_l c_{kl}^P u_k u_l$  can be singled out in the expression  $A_P$ . In this sum

$$c_{ik}^P = \left(\frac{\partial^2 A_P}{\partial u_k \partial u_i}\right)_{T, P} \quad (3.77)$$

are components of the matrix of elastic constants of the crystal, measured at constant polarization and with  $c_{ik}^P = (s_{ik}^P)^{-1}$ .

Forming second derivatives of thermodynamic functions with respect to polarization we will find:

$$\left(\frac{\partial^2 A_P}{\partial P_i \partial P_k}\right)_{T, \sigma_k} = \chi_{ik}^u; \quad \left(\frac{\partial^2 \Phi_P}{\partial P_i \partial P_k}\right)_{T, \sigma_k} = \chi_{ik}^{\sigma}, \quad (3.78)$$

where  $\chi_{ik}^u$  and  $\chi_{ik}^{\sigma}$  are tensors of inverse dielectric susceptibility, determined respectively with a constant deformation or a constant mechanical stress. We will note that dielectric-susceptibility tensor is equal to  $\chi_{ik}^{\sigma} = (\chi_{ik}^u)^{-1}$  and, consequently, components of dielectric-susceptibility tensor, determined from (3.78) will be written as

$$\chi_{ik}^{\sigma} = 1 + 4\pi \chi_{ik}^u; \quad \chi_{ik}^u = 1 + 4\pi \chi_{ik}^{\sigma}. \quad (3.79)$$

If  $T$ ,  $\sigma$  and  $E$  are selected as independent variables, then we will obtain a function which is called thermodynamic potential or Gibbs function (for crystals):

$$\Phi_{12}(T, \sigma_i, \sigma_k) = \Phi_P - PE = U - TS - \sum_k u_k \sigma_k - PE; \quad (3.80)$$

$$d\Phi_{12} = d\Phi_P - d(PE) = - \sum_k u_k d\sigma_k - SdT - \sum_i P_i dE_i. \quad (3.81)$$

If independent variables are T, E and  $u_k$ , then we have electric thermodynamic potential (electric Gibbs function):

$$\Phi_{2E}(T, E, u_k) = A_p - P_i E_i = U - TS - \sum_i P_i E_i, \quad (3.82)$$

$$d\Phi_{2E} = dA_p - d(P_i E_i) = -SdT - \sum_i P_i dE_i + \sum_i u_i du_i. \quad (3.83)$$

After differentiating  $\Phi_{1E}$  and  $\Phi_{2E}$  with respect to  $\epsilon_k$  and  $u_k$  we will find:

$$d_{ik}^E = \left( \frac{\partial^2 \Phi_{1E}}{\partial \epsilon_i \partial \epsilon_j} \right)_{E, T} = c_{ki}^E = \left( \frac{\partial^2 \Phi_{2E}}{\partial u_k \partial u_l} \right)_{E, T}. \quad (3.84)$$

To obtain fundamental equations describing the state of a piezoelectric crystal, use should be made of the fact that expressions for total differentials of the respective thermodynamic potentials are given in (3.72), (3.81) and (3.83).

Making use of thermodynamic potentials  $A_p$ ,  $\Phi_p$ ,  $\Phi_{1E}$  and  $\Phi_{2E}$  represented in the form of polynomials with addends of the order of  $P_i P_j$ ;  $E_i E_j$ ;  $\epsilon_k \epsilon_l$ ;  $u_k u_l$ ;  $\epsilon_k P_i P_j$ ;  $u_k E_i E_j$ , etc. we will obtain canonical equations (written in matrix form) defining elastic electric effects in a crystal:

$$\begin{aligned} a) \begin{cases} \epsilon_i = -\epsilon^E u + h \beta \\ E = -h u + \epsilon^E \beta \end{cases} & \begin{cases} \epsilon = -\epsilon^E u + \epsilon^E E \\ \beta = \epsilon u + \epsilon^E E \end{cases} \\ b) \begin{cases} u = -\epsilon^E \epsilon + \epsilon \beta \\ E = \epsilon u - \epsilon^E \beta \end{cases} & \begin{cases} \epsilon = -\epsilon^E \epsilon + \epsilon E \\ \beta = -\epsilon u + \epsilon^E E \end{cases} \end{aligned} \quad (3.85)$$

Equations (3.85) define physical sense of piezoelectric constants  $h_{ik}$ ,  $g_{ik}$ ,  $\epsilon_{ik}^E$  and  $d_{ik}$  (the constants  $d_{ik}$  are usually called piezomoduli). The following relationships exist between these constants:

$$\begin{aligned} h = \epsilon^E \epsilon = \epsilon \beta; \quad \epsilon = \epsilon^E h = \epsilon \beta; \\ \epsilon = \epsilon^E d = h \beta; \quad d = \epsilon^E \epsilon = \epsilon \beta \end{aligned}$$

Making use of these relationships and the equations (3.85) it is possible to find connection between elastic constants determined for a crystal with short-circuited and open electrodes ( $s_{ik}^E$ ,  $c_{ik}^E$  and  $s_{ik}^P$ ,  $c_{ik}^P$ ), for example:

$$s_{ik}^E = s_{ik}^P + \sum_l \epsilon_{il} \epsilon_{lk}^E.$$

For components of the tensor of inverse dielectric susceptibility of a "clamped" ( $\epsilon_{ik}^E$ ) and "free" ( $\epsilon_{ik}^P$ ) crystal we have:

$$\epsilon_{ik}^E = \epsilon_{ik}^P + \sum_l h_{il} d_{lk}^E.$$

A special characteristic of a ferroelectric is that the free energy  $A_p$ , which is a component of thermodynamic potentials  $\Phi_p$ ,  $\Phi_{1E}$  and  $\Phi_{2E}$  represents an expansion containing terms of a higher order than  $P_i P_j$ ;  $E_i E_j$ ;  $\epsilon_k \epsilon_l$ ;  $\epsilon_k P_i P_j$ , etc. with some of the coefficients of the expansion being highly dependent on temperature. Therefore, some of the elastic

and elastic-electric constants must undergo appreciable temperature anomalies in the phase transition region.

Relationships being sought may be found on the basis of Ehrenfest equations connecting the discontinuities of various physical quantities in a phase transition (see [4]). However, Ehrenfest equations are inapplicable in the case of phase transitions approaching critical point when the quantities mentioned tend to infinity.

To establish connection between these quantities for ferroelectric transitions, Janovec [50] recently made use of Pippard's [51] and Gurland's [52] generalized equations and procedure used for a thermodynamic description of transition in liquid helium by Buckingham and Fairbank [53]. We will cite the basic results obtained in the work [50]:

$$\left. \begin{aligned} \alpha_k^0 &= \gamma_k^0 \frac{c^0}{T} + \alpha_k^0 \\ s_{ii}^0 &= \gamma_i^0 \alpha_i^0 + s_{ii}^0 \\ d_{ii} &= \gamma_i^0 p_i^0 + d_{ii}^0 \\ s_{ii}^0 &= \gamma_i^0 \frac{c^0}{T} + s_{ii}^0 + \alpha_i^0 \gamma_i^0 \end{aligned} \right\} (3.86)$$

Here  $c^0, E$  is specific heat,  $\alpha_k^0, E$  are the coefficients of thermal expansion,  $s_{kl}^0, E$  are moduli of elasticity,  $(p_i)_E = \left(\frac{\partial S}{\partial E}\right)_E$  are pyroelectric coefficients, and  $d_{ik}$  are piezoelectric moduli.

Quantities with the index "0" have a "normal", i.e. weak temperature dependence; the quantity  $\gamma_k^0 = -\left(\frac{\partial \theta}{\partial \sigma_k}\right)_R$  is weakly dependent on temperature according to the definition. As an example, the relationships (3.86) were used to describe a ferroelectric transition in triglycine sulfate [50]. In doing so, it was found that experimental data for TGS agree well with the equalities (3.86). Thus, these relationships represent a convenient method of checking the consistency of experimental data describing a ferroelectric transition of A-type.

Coming back to the question of selection of this or other thermodynamic potential when describing the properties of a ferroelectric, we will note the following. In the absence of electric field ( $E_i=0$ ), we have:

$$A_p = \Phi_p - \Phi_{iE} + PE = \Phi_{iE} + PE.$$

for a free crystal ( $\sigma_k=0$ ) if spontaneous deformations ( $u_{sk}=0$ )  $A_p = \Phi_p = \Phi_{1E} = \Phi_{2E}$  are neglected, and for a free crystal located in an external field when electrostriction and piezoeffect are neglected.

The variables  $T$ ,  $u_{sk}$  and  $P_i$  were made use of in paragraph 3, subparagraph 3 in the examination of special features appearing when taking account of spontaneous deformations in a free ferroelectric and, consequently, the expression (3.52) is free energy  $A_p(T, P_i, u_{sk})$ . The

same results could have been obtained by using elastic Gibbs function  $\Phi_p(T, P_i, \sigma_k)$  if a representation for spontaneous mechanical stresses leading to the formation of spontaneous deformations, i.e.  $u_{sk} = \sum_l^p s_{kl}^p \sigma_{sl}$  were introduced.

In describing the properties of a fixed ferroelectric it is preferable to "work" with the variables  $P_s, u_s$ , i.e. to make use of the free energy  $A_p(T, P_i, u_k)$ . Conversely, in the examination of behavior of a free crystal and of a crystal to which external forces are applied it is more convenient to use elastic thermodynamic potential  $\Phi_p(P, \sigma)$  since the equations resulting with its differentiation are simpler and accomplish the aim faster. It should be noted that both approaches have been used sufficiently often in the studies of ferroelectrics. For example, elastic thermodynamic potential  $\Phi_p(T, P_i, \sigma_k)$  was used in the works [2, 38, 39] in the determination of effect of mechanical stresses on the properties, and free energy  $A_p(T, P_i, u_k)$  was used in (3.49) with the results of these studies agreeing with each other.

### 3. Ferroelectrics in the Case of Weak External Influences

According to Curie principle, during the action of external forces crystal symmetry contains only elements common with the symmetry group of the external influence. Therefore, in satisfying the equilibrium condition the expression for thermodynamic potential of the crystal (most often  $A_p(T, u_k, P_i)$  or  $\Phi_p(T, \sigma, P_i)$ ) must contain only the invariants determined by this symmetry. Finding of the values of variables with which equilibrium is provided is reduced to finding the minimum of  $\Phi_p$  with the specified external forces, i.e. to the solution of a set of equations of the following type 1)

$$\left. \begin{aligned} \frac{\partial \Phi_p}{\partial P_i} &= E_i \quad i=1, 2, 3; \\ \frac{\partial \Phi_p}{\partial \sigma_k} &= -u_k \quad k=1, \dots, 6. \end{aligned} \right\} \quad (3.87)$$

In order that the solutions of (3.87) indeed correspond to the minimum of  $\Phi_p$  in accordance with the rules for finding the minimum of a function of many variables, it is necessary to require the satisfaction of stability conditions, i.e. of a series of inequalities for determinants made up of the second derivatives of  $\Phi_p$  with respect to independent variables [see, for example, (3.50)].

In those cases when a phase transition of the first kind takes place and two different phases coexist at a specified temperature and stresses, the absolute values of  $\Phi_p$  of each phase are compared and in this manner it is determined which one of them is metastable.

When solving the equations (3.87) simultaneously with stability conditions (3.50) Curie principle is satisfied automatically and, conse-

1) For the other thermodynamic potentials  $A_p, \Phi_{1E}$  and  $\Phi_{2E}$  equilibrium conditions are written in a similar manner; physical sense of independent variables changes.

quently, when constructing the function  $\Phi_p$  there is no need to be concerned with its resultant symmetry. In other words, the expression for  $\Phi_p$  may contain all invariants of the highly symmetrical phase similarly to the way this was done in the determination of the components  $P_{Si}$  and  $u_{Sk}$  (3.53), (3.57). Another approach is permitted, which in a number of cases substantially simplifies the investigations, when terms the existence of which in a set of final solutions clearly contradicts the properties of symmetry of the external forces are excluded from  $\Phi_p$  in advance (for example, in the  $\Phi_p$  of a cubic crystal there is no need to take into account the displacement components during the action of mechanical forces and fields along the major symmetry axes).

We will note that equations for piezoeffect (3.85), which are nothing else but a generalized matrix form of writing the solution of linearized equations (3.87), also satisfy the requirements of Curie principle if matrices whose structures satisfy the requirements of symmetry of the phase with which we are concerned in a ferroelectric appear in them. However, the equations (3.84) do not contain by themselves the information on temperature dependences of parameters of a ferroelectric and on stability of its phases under different conditions inasmuch as they have no specific features characterizing the crystal near a phase transition.

In the case of weak external influences when the effects brought about by them are sufficiently small in comparison with some of the parameters characteristic of a system (for example, when polarization  $P_{Ui}$  and deformation  $u_{Uk}$  induced by the field and mechanical stresses are small in comparison with  $P_{Sk}$  and  $u_{Sk}$ ) the system (3.87) may be reduced to equations linear with respect to  $P_{Ui}$  and  $u_{Uk}$ . Of course, in direct proximity to the transition point the assumption concerning the relative smallness of  $P_{Ui}$  and  $u_{Ui}$  is conditional.

We will examine solution of the equations (3.87) as applied to ferroelectrics having symmetry  $O_h$  above Curie point and to ferroelectrics which exhibit piezoelectric properties in the highly symmetrical phase.

#### Barium Titanate Group

Thermodynamic theory of electromechanical properties of barium titanate was developed in the works of V. L. Ginzburg [1, 2], Devonshire [3], L. P. Kholodovko [38, 39, 54, 55] and other authors [48, 49]. In the works [1, 2, 38, 39] the authors examine conditions for the minimum of elastic thermodynamic potential  $\Phi_p(T, P_i, \sigma_k)$ , and the minimum of free energy  $A_p(T, P_i, u_k)$  is determined in [3, 48, 49]. As already pointed out, this difference does not lead to contradictions. However, in the determination of electrostriction corrections to the coefficients of the expansion it is preferable to use the second method. This was done in subparagraph 1 of this paragraph. When mechanical stresses brought about by external forces are present in the crystal the first method proves to be more effective.

The expression for  $\Phi_P(T, P_i, \epsilon_k)$  will now be written in the following form: 1)

$$\begin{aligned}
 \Phi_P(T, P_i, \epsilon_k) = & \Phi_0(T) + a(P_x^2 + P_y^2 + P_z^2) + \frac{3}{2}(P_x^4 + P_y^4 + P_z^4) + \\
 & + \beta_2(P_x^2 P_y^2 + P_x^2 P_z^2 + P_y^2 P_z^2) + \frac{1}{3} \gamma_1 (P_x^4 + P_y^4 + P_z^4) + \gamma_2 P_x^2 (P_x^2 + P_y^2) + \\
 & + P_y^2 (P_x^2 + P_y^2) + P_z^2 (P_x^2 + P_y^2) + \gamma_3 (P_x^2 P_y^2 P_z^2) - \epsilon_{11} (\epsilon_{xx} P_x^2 + \epsilon_{yy} P_y^2 + \epsilon_{zz} P_z^2) - \\
 & - \epsilon_{12} (\epsilon_{xx} P_x^2 + P_y^2) + \epsilon_{yy} (P_x^2 + P_y^2) + \epsilon_{zz} (P_x^2 + P_y^2) - 2\epsilon_{13} (\epsilon_{xy} P_x P_y + \\
 & + \epsilon_{yz} P_y P_z + \epsilon_{zx} P_z P_x) - \frac{1}{2} \epsilon_{14} (\epsilon_{xx}^2 + \epsilon_{yy}^2 + \epsilon_{zz}^2) - \epsilon_{15} (\epsilon_{xx} \epsilon_{yy} + \epsilon_{xx} \epsilon_{zz} + \epsilon_{yy} \epsilon_{zz}) - \\
 & - \frac{1}{2} \epsilon_{16} (\epsilon_{xy}^2 + \epsilon_{yz}^2 + \epsilon_{zx}^2). \tag{3.88}
 \end{aligned}$$

Comparing this expression with formula (3.53) we see that their structure completely coincides [if, of course, in (3.53)  $P_{Si}$  is substituted by  $P_i$  and  $u_{Sik}$  by  $u_k$ ]. The difference in signs before the mechanical and mixed terms is explained by that a system of signs different from [3, 48, 49] is used in [38, 39] and, consequently, in (3.88). Namely, it is assumed in [38, 39] that elongation deformations and stresses are positive whereas in the works [3, 48, 49] and other works elongation deformations and compression stress are positive. In the examination of spontaneous deformation this was of no significance. However, henceforth, when comparing the results we will use the more natural system of signs used in the works [38, 39], i.e.  $u_{elong} > 0$ ,  $\epsilon_{elong} > 0$ .

In addition to this, in  $\Phi_P(T, P, u_k)$  the coefficients  $a$ ,  $\beta_1$ ,  $\beta_2$ , etc. should be provided with the symbol "u" in conformity with the fact that they are taken with a constant deformation whereas in  $\Phi_P(T, P_i, \epsilon_k)$  these coefficients are taken with a constant mechanical stress in the crystal.

It can be shown that, for example,  $\beta_1^e = \beta_1^u - \mathcal{D}$ . It is also obvious that elastic constants  $c_{ik}^P$  enter (3.53). The matrix of electrostriction constants  $\alpha_{ik}$  has the same form as  $q_{ik}$  in (3.53)

1) Notation of  $\Phi_P(T_i, P_i, \epsilon_k)$  from [38, 39] differs from (3.88) in that terms of the form  $\beta_1^4 P_s^4$  and  $\gamma_1^6 P_s^6$  instead of  $\beta_1^4 (P_{sx}^4 + P_{sy}^4 + P_{sz}^4)$  and  $\gamma_1^6 (P_{sx}^6 + P_{sy}^6 + P_{sz}^6)$  appear in [38, 39]. Both notations and all results are identical if coefficients of the expansion  $\beta_2^e$ ,  $\gamma_2^e$  and  $\gamma_3^e$  are substituted respectively by  $\beta_2^u - \beta_1^u$ ,  $\gamma_2^u - \gamma_1^u$  and  $\gamma_3^u - 2\gamma_1^u$  from (3.88). The advantages of formula (3.88) consist in that it does not contain superfluous invariants of the type  $P_x^2 P_y^2$  and  $P_j^4 P_i^2$ . In addition to this, comparison with the results of the other works, for example [3, 48, 49], and of the preceding sections of this chapter [compare with formulas (3.46), (3.48), (3.49), (3.52), (3.53)] is made easier.

The main results of solution of the set of equations (3.87) according to [38] and [39] are given below.

1) Spontaneous Polarization. Solutions of the equations  $\left(\frac{\partial \Phi}{\partial P_i}\right)_{\sigma_k=0} = 0$  with the additional conditions (3.50) are sought.

Solutions have the following form (see also 3.49).

1. Cubic phase

$$P_i^2 = 0;$$

2. Tetragonal phase

$$P_{1z}^2 = \frac{1}{2\gamma_1} (-\beta_1 - \sqrt{\beta_1^2 - 4\alpha\gamma_1});$$

$$P_{1y} = P_{1x} = 0;$$

3. Orthorhombic phase

$$P_{1z}^2 = P_{1y}^2 = \frac{1}{2(\gamma_1 + 3\gamma_2)} [-(\beta_1 + \beta_2) + \sqrt{(\beta_1 + \beta_2)^2 - 4\alpha(\gamma_1 + 3\gamma_2)}];$$

$$P_{1x} = 0;$$

4. Rhombohedral phase

$$P_{1z}^2 = P_{1y}^2 = P_{1x}^2 = \frac{1}{2(\gamma_1 + 6\gamma_2 + \gamma_3)} [-(\beta_1 + \beta_2) + \sqrt{(\beta_1 + \beta_2)^2 - 4\alpha(\gamma_1 + 6\gamma_2 + \gamma_3)}].$$

(3.89)

Stability conditions (3.50) give the following inequalities for all of the four phases: <sup>1)</sup>

$$\left. \begin{array}{l} I) \alpha > 0; \\ II) 1) \beta_1 + 2\gamma_1 P_{1z}^2 > 0; 2) \beta_2 - \beta_1 + 2(\gamma_2 - \gamma_1) P_{1z}^2 > 0; \\ III) 1) \beta_2 - \beta_1 - (\gamma_2 - 3\gamma_1 - \gamma_3) P_{1z}^2 > 0; 2) \beta_2 - \beta_1 + 2(\gamma_2 - \gamma_1) P_{1z}^2 < 0; \\ 3) \beta_1 + \beta_2 - 2(\gamma_1 + 5\gamma_2) P_{1z}^2 > 0; \\ IV) 1) \beta_1 + (\gamma_1 + 2\gamma_2) P_{1z}^2 > 0; 2) \beta_2 - \beta_1 + (\gamma_2 - 2\gamma_1) P_{1z}^2 < 0; \\ 3) (\beta_1 - \beta_2) + 2(\gamma_1 + 6\gamma_2 + \gamma_3) P_{1z}^2 > 0. \end{array} \right\} (3.90)$$

A very interesting conclusion follows from (3.90): when  $\gamma_1 = \gamma_2 = \gamma_3 = 0$ , phase 3 is unstable since the first two conditions in (3.90) for 3 are inconsistent. In other words, the terms  $\sim P_{si}^6$  have to be taken into account to explain the low-temperature transitions.

2. Spontaneous Deformation. Components of spontaneous-deformation tensor were defined in subparagraph 1, paragraph 3 (see (3.55) on the basis of conditions of minimum for the free energy  $A_p(T, P_{is}, u_s)$ .

For  $\Phi_p(T, P_i, \sigma_k)$ , expressions for  $u_{sk}$  will be found from the equations  $\left(\frac{\partial \Phi_p}{\partial \sigma_k}\right)_{\sigma_k=0} = -u_{sk}$  upon substituting in them the solutions (3.89). For

1) The relationship  $P_{si}^2(T)$  calculated by Devonshire [3] is shown in Figure 3.3.

example, for phase 2 we have:

$$\left. \begin{aligned} u_{xx} &= x_{11} P_{21}^2; u_{yy} = u_{zz} = x_{12} P_{21}^2; \\ u_{xy} &= u_{yz} = u_{zx} = 0. \end{aligned} \right\} \quad (3.91)$$

Comparing these equalities with the formulas from (3.55), the electrostrictive constant  $\chi_{ik}$  may be expressed in terms of coefficients of electrostriction  $q_{ik}$  and elastic constants  $c_{ik}^P$  ( $\chi_{33} = q_{33}$ ,  $\chi_{31} = q_{31}$  from (3.55))

3) Dielectric-Constant Tensor. To find the component  $\epsilon_{ik}$  of the dielectric-constant tensor in the absence of mechanical stresses the following set of equations is solved

$$\left( \frac{\partial \phi}{\partial P_i} \right)_{P_j=0} = E_i.$$

The condition of smallness of the quantity  $E$  makes it possible to linearize these equations. For this purpose, polarization is represented in the following form:

$$[P_{ni} = P_{ii}] \quad P_i = P_{ii} + P_{ni}(E), \quad (3.92)$$

where  $P_{ii}$  is a small quantity. Making use of (3.92) and neglecting terms containing the quantities  $\sim P_{ii}^2$  and higher, we will obtain a set of equations linear with respect to  $P_{ii}^2$ . Next, making use of the definition of

$$P_{ii} = \frac{\epsilon_{ik}^e - 1}{4\pi} E_k$$

we will obtain the following:

Phase 1.

$$\epsilon^e = \begin{pmatrix} \epsilon_{xx}^e & 0 & 0 \\ 0 & \epsilon_{yy}^e & 0 \\ 0 & 0 & \epsilon_{zz}^e \end{pmatrix}; \quad \epsilon_{xx}^e = \epsilon_{yy}^e = \epsilon_{zz}^e = \frac{2\pi}{\tau}.$$

Phase 2.

$$\epsilon^e = \begin{pmatrix} \epsilon_{xx}^e & 0 & 0 \\ 0 & \epsilon_{yy}^e & 0 \\ 0 & 0 & \epsilon_{zz}^e \end{pmatrix};$$

$$\epsilon_{xx}^e = \frac{2\pi}{\tau};$$

$$\epsilon_{zz}^e = \frac{2\pi}{\tau} \frac{1}{1 - \tau_1 + (\tau_2 - \tau_1) P_{21}^2 P_{21}^2}.$$

Phase 3. Expressions for  $\epsilon_{ik}$  are very cumbersome and are transverse components of the type  $\epsilon_{xy}$ . However, after reduction to the major symmetry axes they acquire a sufficiently compact form:

$$\begin{aligned} (\epsilon_{xx}') &= \frac{2\pi}{[\beta_2 - \beta_1 + (\gamma_2 - \gamma_1 - \gamma_2) P_{22}^1 P_{22}^1]}; \\ (\epsilon_{yy}') &= -\frac{\pi}{[\beta_2 - \beta_1 + 2(\gamma_1 - \gamma_2) P_{22}^1 P_{22}^1]}; \quad (\epsilon_{zz}') = -\frac{\pi}{2\alpha + (\beta_2 + \beta_2) P_{22}^1}. \end{aligned}$$

Phase 4. After reduction to the major axes:

$$\left. \begin{aligned} (\epsilon_{xx}') &= (\epsilon_{yy}') = -\frac{\pi}{[\beta_2 - \beta_1 + (\gamma_2 - 2\gamma_1) P_{22}^1 P_{22}^1]}; \\ (\epsilon_{zz}') &= -\frac{\pi}{2\alpha + (\beta_1 + 2\beta_2) P_{22}^1}. \end{aligned} \right\} \quad (3.93)$$

In Figure 3.4 are shown temperature dependences of the values of  $\epsilon'_{ik}$  calculated for BaTiO<sub>3</sub> in [3] and reduced to major axes.

Temperature dependences of dielectric constants of a "clamped" crystal are considerably less marked [3, 37, 42].

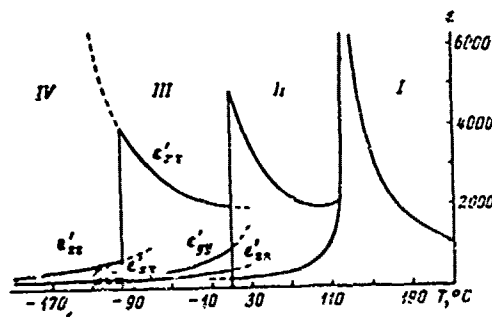


Figure 3.4. Temperature dependence of components of dielectric-constant tensor for BaTiO<sub>3</sub> [3].

I -- cubic phase; II -- tetragonal phase;  
III -- orthogonal phase; IV -- rhombic phase.

4) Piezomoduli Tensor. To determine piezoelectric properties it is necessary to solve simultaneously the following set of equations:

$$\frac{\partial \phi_P}{\partial P_i} = 0; \quad -\frac{\partial \phi_P}{\partial x_k} = u_k \quad (3.94)$$

(direct piezoelectric effect  $E_i=0$ ;  $\epsilon_k \neq 0$ ) or

$$\frac{\partial \phi_P}{\partial P_i} = E_i; \quad -\frac{\partial \phi_P}{\partial x_k} = 0 \quad (3.95)$$

( $E_i \neq 0$ ;  $\epsilon_k = 0$ ; inverse piezoelectric effect). When using formulas (3.95) for region II the inverse piezoelectric effect is expressed as:

$$u_{ik} = u_{ik}^{(0)} + u_{ik} (P_{22}^1 + 2P_{22}^1 P_{22}^1) = u_{ik} + \frac{u_{ik} P_{22}^1}{2\pi} E_i. \quad (3.96)$$

In other words, inverse piezoelectric effect in BaTiO<sub>3</sub> and in ferroelectrics isophormous to it is in essence linearized electrostriction. It is obvious that the results of both methods of determining the d<sub>ik</sub> must coincide.

Calculated components of piezomoduli are given below (for phases 3 and 4 the values of d<sub>ik</sub> are reduced to major axes).

Phase 2.

$$d = \begin{pmatrix} 0 & 0 & 0 & 0 & d_{15} & 0 \\ 0 & 0 & 0 & d_{15} & 0 & 0 \\ d_{31} & d_{31} & d_{33} & 0 & 0 & 0 \end{pmatrix};$$

$$d_{33} = -\frac{x_{11} P_{ee}}{2(\beta_2 + \beta_1 P_{ee}^2)} = \frac{x_{11} P_{ee}}{2\pi};$$

$$d_{31} = d_{32} = \frac{x_{12} P_{ee}}{2(\beta_2 + \beta_1 P_{ee}^2)} = \frac{x_{12} P_{ee}}{2\pi};$$

$$d_{15} = d_{16} = \frac{x_{14}}{[(\gamma_2 - \gamma_1) + (\gamma_2 - \gamma_1) P_{ee}^2] P_{ee}} = \frac{x_{14} P_{ee}}{2\pi}.$$

Phase 3.

$$d'_{33} = -\frac{(x_{11} + x_{12} + 2x_{44}) P_{ee}}{2\sqrt{2} [2\alpha + (\beta_1 + \beta_2) P_{ee}^2]}; \quad d'_{31} = -\frac{x_{12} P_{ee}}{2\sqrt{2} [2\alpha + (\beta_1 + \beta_2) P_{ee}^2]};$$

$$d'_{32} = -\frac{(x_{12} + x_{11} - 2x_{44}) P_{ee}}{2\sqrt{2} [2\alpha + (\beta_1 + \beta_2) P_{ee}^2]}; \quad d'_{15} = \frac{x_{12} - x_{11}}{2\sqrt{2} [\beta_2 - \beta_1 + 2(\gamma_2 - \gamma_1) P_{ee}^2]};$$

$$d'_{16} = \frac{\sqrt{2} x_{14}}{\beta_2 - \beta_1 + (\gamma_2 - \gamma_1) P_{ee}^2}.$$

Phase 4.

$$d'_{33} = -\frac{(x_{11} + 2x_{12} + 2x_{44}) P_{ee}}{2\sqrt{3} [2\alpha + (\beta_1 + 2\beta_2) P_{ee}^2]};$$

$$d'_{31} = d'_{32} = -\frac{(x_{11} + 2x_{12} - x_{44}) P_{ee}}{2\sqrt{3} [2\alpha + (\beta_1 + 2\beta_2) P_{ee}^2]};$$

$$d'_{15} = -d'_{16} = -\frac{1}{2} d'_{16} = -\frac{x_{12} - x_{11} + x_{44}}{2\sqrt{6} [\beta_2 - \beta_1 + (\gamma_2 - 2\gamma_1) P_{ee}^2]};$$

$$d'_{17} = d'_{18} = -\frac{2x_{11} - 3x_{12} + x_{44}}{2\sqrt{3} [\beta_2 - \beta_1 + (\gamma_2 - 2\gamma_1) P_{ee}^2] P_{ee}}.$$

Relationships of piezomoduli to T (not in the major axes) calculated in [3] are shown in Figure 3.5.

It can be shown [3] that components of piezomoduli and dielectric constant are connected by the general relationships:

$$\frac{c_{12}}{d'_{12}} = -4\pi \left( \frac{\partial^2 \Phi_p}{\partial P_{ee}^2} \right)_0. \quad (3.97)$$

where all quantities are taken relative to the major axes. The relationship (3.97) follows from the obvious fact that upon the application of the field both P<sub>ik</sub> and u<sub>ik</sub> are brought about by the displacement of the charge.

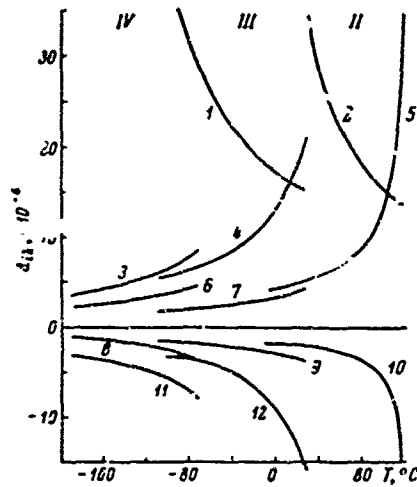


Figure 3.5. Temperature dependence of the components of piezomoduli for BaTiO<sub>3</sub> [3].

II -- tetragonal phase; III -- orthorhombic phase; IV -- rhombohedral phase. 1 --  $d_{15} = d_{16}$ ; 2 --  $d_{15} = d_{24}$ ; 3 --  $d_{11} = d_{12} = d_{33}$ ; 4 --  $d_{22} = d_{33}$ ; 5 --  $d_{33}$ ; 6 --  $d_{15} = d_{16} = d_{24} = d_{26} = d_{34} = d_{35}$ ; 7 --  $d_{24} = d_{34}$ ; 8 --  $d_{14} = d_{25} = d_{36}$ ; 9 --  $d_{21} = d_{31}$ ; 10 --  $d_{31} = d_{32}$ ; 11 --  $d_{13} = d_{21} = d_{23} = d_{32}$ ; 12 --  $d_{23} = d_{32}$ .

5) Moduli of Elasticity  $s_{ik}^{(P)}$  and  $s_{ik}^{(E)}$ . Analysis of the equations (3.85) simultaneously with (3.86) shows that behavior of the constants  $c_{ik}^P$  and  $s_{ik}^P$  and of the constants  $c_{ik}^{(E)}$  and  $s_{ik}^{(E)}$  which appear in thermodynamic potentials  $\Phi_{iE}$  and  $\Phi_{2E}$  is very dissimilar.

Whereas the former are continuous and relatively weak temperature functions, the latter, i.e. the quantities  $c_{ik}^{(E)}$  and  $s_{ik}^{(E)}$ , either undergo a discontinuity or experience a sharp change in the phase transition region (Figure 3.6).

6) Displacement of Curie Point. It follows from (3.88) that in the presence of mechanical stresses the term  $\sim \alpha P^2$  may be combined with invariants of the type  $\alpha_{in} P_{ik}^2$  and, consequently,  $\alpha_i = \alpha - \alpha_{in} P_{ik}^2$ . The condition for phase transition changes in accordance with this. For example, in the region of tetragonal symmetry the condition  $\alpha_{in} = 0$  leads to the following formulas [39]:

$$s_{1,22} = 0 + \frac{2\alpha}{\epsilon_0^2} s_{22}; \quad s_{1,33} = 0 + \frac{2\alpha}{\epsilon_0^2} s_{33}.$$

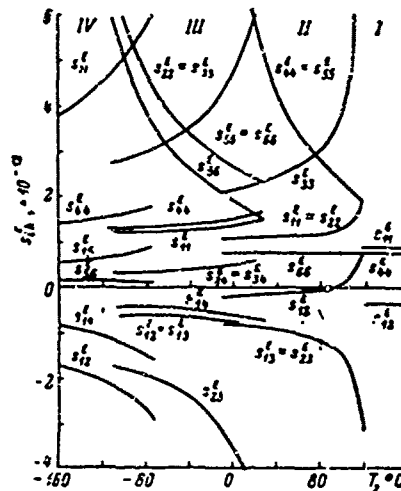


Figure 3.6. Moduli of elasticity with a permanent field for BaTiO<sub>3</sub> in relation to temperature [3].

I -- cubic phase; II -- tetragonal phase;  
 III -- orthorhombic phase; IV -- rhomboidal phase.

On the basis of these relationships the appearance of additional polarization may be represented as a change in spontaneous polarization  $P_{sz}$ , brought about by a "displacement" of the entire curve  $P_{sz}(T)$  to the right or to the left of some point  $T$ . From this, a conclusion may be drawn that appearance of piezopolarization and displacement of the transition point  $\theta$  are essentially equivalent effects brought about by a change [49] of the state of the ferroelectric as a result of application of external forces.

#### Seignette's Salt

Elastic thermodynamic potential for Seignette's salt may be easily obtained from (3.57) after appropriate substitution of variables and coefficients of expansion, i.e.  $c_{ik}^p \rightarrow s_{ik}^p$ ,  $u_{sk} \rightarrow \epsilon_{sk}$ ;  $q_{ik} \rightarrow x_{ik}$ ;  $h_{ik} \rightarrow g_{ik}$ ;  $\alpha \rightarrow \alpha^e$ ;  $\beta \rightarrow \beta^e$ . Owing to the presence of a linear piezoelectric term in  $\Phi$ , solutions of the equations (3.87) are expressed by very cumbersome formulas that lend themselves with difficulty to analysis. If we limit ourselves to a unidimensional approximation [1, 2], i.e. if  $\Phi_p$  is rep-

resented in the following form

$$\Phi_p(T, P_i, \sigma_k) = \Phi_c(T) + \epsilon P_i^2 + \frac{\beta}{2} P_i^4 - \frac{1}{2} \epsilon_{ij}^p \sigma_j \sigma_i - \epsilon_{11}^p \sigma_x^2 - \epsilon_{22}^p \sigma_y^2, \quad (3.98)$$

then a connection may be established between certain parameters in (3.98) and (3.57), in particular

$$\epsilon_{11} = -\frac{h_{11}}{c_{44}}; \quad \epsilon_{22} = -\frac{h_{22}}{c_{44}}.$$

Above Curie point, when the terms  $P_x^4$ ,  $\alpha^6 \approx \alpha - \frac{h_{14}^2}{c_{44}}$  and consequently,

$$\epsilon_{xx}^* = 1 + \frac{4\pi}{2\epsilon - \frac{h_{14}^2}{c_{44}}}; \quad d_{11} = \frac{1}{\frac{2\pi c_{44}^p}{h_{11}} - h_{11}}; \quad \epsilon_{11}^* = \frac{1}{c_{44}^p - \frac{h_{14}^2}{2\epsilon}}.$$

#### 4. Some Comments on Thermodynamic Description of Nonlinear Properties in Ferroelectrics

At the first glance the attempt at a theoretical description of nonlinear effects on the basis of thermodynamic theory of phase transitions appears very natural and substantiated by its extrapolation. It may be assumed that the problem is reduced merely to the calculation of high powers of the field and mechanical stresses in the equations of state

$$\frac{\delta \Phi_p}{\delta P_i} = E_i; \quad - \frac{\delta \Phi_p}{\delta \sigma_k} = u_k.$$

It would seem that solution of these equations in the following form

$$P_i(T, E_i, \sigma_k) \quad \text{and} \quad u_k(T, E, \sigma_k)$$

would make it possible to calculate the relationships of dielectric and piezoelectric constants to the field and mechanical stresses. Actually, physical statement of the problem must be considerably more complex.

The fact is that in the case of intense external influences nonlinear change in polarization (the main physical substance of nonlinear effects in ferroelectrics amounts precisely to this change) is accompanied by an extensive transformation of mechanical and electric energy into heat. In other words, the process becomes irreversible and must be examined using the methods of irreversible thermodynamics. There is no doubt that energy dissipation takes place in the case of weak excitations also, i.e. in the region of linear dependence  $P(T, E_i, \sigma_k)$ . However, here, owing precisely to nonlinearity the reversible and irreversible components of the process can be separated and examined. For example, the relationship  $E(T)$  can be examined within the framework of reversible thermodynamics,

and  $\text{tg } \delta(T)$  -- by means of solving differential equations describing the stabilization of the process in time. In the case of large exciting fields, such a separation proves to be impossible owing to nonlinearities -- hysteresis loop is brought about both by the reversible change in polarization during the cycle of the change in the field and by irreversible transformation of electric energy into heat.

A rigorous application of irreversible thermodynamics for describing these processes encounters great difficulties inasmuch as irreversible thermodynamics of electromagnetic process is applicable only to linear systems [56, 57]. Some of the basic theorems underlying irreversible thermodynamics, the so-called Onsager reciprocity relationships which establish the connection between thermodynamic forces and flows in cross events, are valid only in the case when these flows (for example, currents and deformations) are linear functions of thermodynamic forces (the field, mechanical stresses, etc.). However, precisely these connections, both the direct and cross connections, are assumed to be nonlinear. Thus, in the attempt to create a rigorous thermodynamic theory of hysteresis loop with energy dissipation taken into account, we encounter a series of basic difficulties which increase still more for polydomain structures inasmuch as a sufficiently correct theory, even within the framework of reversible thermodynamics, has not been created for their description. It should also be noted that according to experimental observation of behavior of a single-domain crystal in a strong field, repolarization always occurs by means of appearance and growth of the nuclei of polarization  $-P$ , inverse in relation to  $P_s$ , and not as a result of a simultaneous repolarization of the entire crystal. The growth of these nuclei is a complex statistical process in which, in addition, the effect of their interaction also plays a role (see chapter 7).

In considering all of the foregoing, no surprise should be caused by the fact that coercive field calculated on the basis of representations concerning reversible thermodynamic process in single-domain ferroelectrics exceeds approximately by 20 times the value of  $E_g$  observed experimentally.

At the same time, the application of "conventional" thermodynamic representations by no means proves to be in vain if attention is focused on the explanation of qualitative characteristics of ferroelectrics.

For a number of cases this approximation amounts to the following: a comparison is made of the theoretical (obtained using the methods of reversible thermodynamics) and experimental cyclic relationships  $P_i(E_i, \sigma_k, T)$ , i.e. hysteresis loops, plotted in a quasi-static state. Next, theoretical loop is recorded in dimensionless coordinates and identified with the experimental loop. After this, all relationships of the parameters can be determined on the basis of reversible theory in terms of the parameters of the theoretical loop recorded in the scale of experimental hysteresis loop. This method used in [9, 58-60] cannot be used for a quantitative description of parameters which characterize energy dissipation. Effects observed in "aging the test samples in a strong field" and the so-called aging effect also drop out from the consideration. However, this method gives

quite satisfactory results in the explanation and even quantitative evaluation of nonlinear dependences of dielectric and piezoelectric constants determined after the completion of these transient processes.

We will illustrate the foregoing by examining the behavior of dielectric constant  $\epsilon$  and piezomoduli  $d_{33}$  and  $d_{31}$  for tetragonal phase of  $\text{BaTiO}_3$ . We have:

$$\Phi_p(T, P_s, \sigma_k) = \Phi_0(T) + \alpha P_s^2 + \frac{1}{2} \beta_1 P_s^4 + \frac{1}{3} \gamma P_s^6 - (\beta_{33} \sigma_{zz} + 2\beta_{31} \sigma_{xx}) P_s^2 - \frac{1}{2} \epsilon_{11}' (\sigma_{zz}^2 + 2\sigma_{xx}^2) - \epsilon_{12}' (\sigma_{zz}^2 + 2\sigma_{xx} \sigma_{zz}).$$

Here  $\epsilon_{xx} = \epsilon_{yy}$ ;  $\gamma_{11} = \beta_{33} \approx 2.7 \cdot 10^{-12} \text{ bar}^{-1}$ ;  $\alpha_{12} = \beta_{31} = -1.2 \cdot 10^{-12} \text{ bar}^{-1}$ . The circumstance that in the expression for  $\Phi_p$  we limited ourselves only to the terms  $\sim \sigma_k^2$  is connected with the fact that according to measurements moduli of elasticity are practically constant in a wide range of values of  $\sigma_k$ . As regards electromechanical "cross" terms of the type  $\sigma_k P_i^4$  and  $\sigma_k^2 P_i^2$ , neglecting of higher powers when excitations are sufficiently intense indeed does not always prove to be correct.

Next, as usually, we write the equations of state ( $\sigma_k = 0$ ) with an additional condition  $\frac{\partial^2 \Phi_p}{\partial P_s^2} > 0$ , i.e.

$$2P_s (\alpha + \beta P_s^2 + \gamma P_s^4) = E_s, \quad (3.99a)$$

$$\beta_{33} P_s^2 = u_{zz}, \quad (3.99b)$$

$$\beta_{31} P_s^2 = u_{xx}, \quad (3.99c)$$

$$\alpha + 3\beta P_s^2 + 5\gamma P_s^4 > 0. \quad (3.100)$$

Inasmuch as the region of tetragonal symmetry is being examined, the subscript  $z$  will henceforth be omitted for the sake of brevity.

The equation (3.99a) and inequality (3.100) were investigated by L. P. Kholodenko [58, 60] who found the relationship  $P(E)$  and the magnitude of coercive force  $E_c$ , i.e. those values of the field for which (3.99a) and (3.100) are incompatible and the system is unstable. The expressions (3.99a) and (3.100) prove to be compatible upon changing the sign in front of  $P$  to the opposite sign, i.e. upon turning the polarization vector by  $180^\circ$ . The relationship  $P(E)$  obtained in this manner proves to be ambiguous and has a characteristic shape of a hysteresis loop (Figure 3.7). However, the value of  $E_c$  found from (3.99a) and (3.100) proves to be considerably higher than the measured values. As already mentioned above, it is possible to surmount this difficulty to a certain extent since the relationships  $\epsilon(E)$  and  $d_{jk}(E)$  with which we are concerned are determined in the final analysis by the relationship

where  $P_M$  is induced polarization. Consequently, if  $E$ 's measured in the values of  $E_c$ , and  $P$  -- in the values of  $P_s$ , then the shape of the

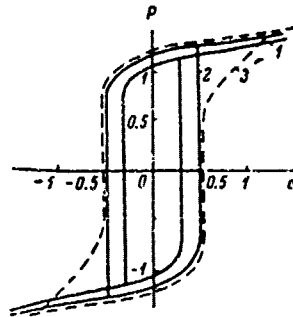


Figure 3.7. Theoretical [60] and experimental [61] hysteresis loops for BaTiO<sub>3</sub> (in relative units).

1 -- theoretical curve for T=80°C; 2 -- theoretical curve for T=20°C; 3 -- experimental curve for T=20°C.

loop, and not the absolute value, becomes the determinant as a result of such an identification of the scale. If in doing so, a satisfactory coincidence of the shapes of the experimental and theoretical hysteresis loop takes place, then an agreement between the calculated and measured relationships  $\mathcal{E}\left(\frac{E}{E_C}\right)$  and  $d_{ik}\left(\frac{E}{E_C}\right)$  may be expected. With this aim, the following dimensionless quantities are introduced into (3.99) and (3.100):

$$p = p_0 + p_1 = \frac{P_0 + P_1}{\sqrt{-\frac{p}{T}}}, \quad (3.101)$$

$$e = -\frac{E}{2\sqrt{-\frac{p}{T}}} \quad \text{and} \quad \alpha = -\frac{a^3}{T}. \quad (3.102)$$

After this, (3.99) and (3.100) are solved graphically in these relative units (Figure 3.7).

We will now investigate  $P_M(e)$  in the range of values  $|e| < 0.5$ , i.e. with fields whose amplitudes do not exceed the magnitude of coercive field.  $P_M(e)$  is sought in the form of an expansion with respect to the powers of  $e$  up to the terms  $e^5$ :

$$P_M = \sum_{n=1}^5 c_n(T) e^n. \quad (3.103)$$

After the substitution of (3.103) into (3.99) and equating the coefficients placed at the same powers of  $e$  on the right and on the left, we obtain a set of equations by solving which we define  $c_n$  as a function of

$P_S$  and  $\xi$ , i.e. in the final analysis, as a function of temperature.

Suppose  $e=e_0 \sin \omega t$  <sup>1)</sup>. Then, after a series of transformations [9] we will obtain  $P_M(e)$  in the form of an expansion with respect to harmonics:

$$P_M(e, T) = \sum_{n=0}^k P_M^{(n)}(a_n, e_0) \sin(n\omega t - \varphi_n), \quad (3.104)$$

where the amplitudes of  $P_M$  are the known field-amplitude functions  $e_0$  and  $a_n(T)$ .

The expression (3.104) makes it possible to calculate both the total dielectric constant and that portion of it  $\epsilon^{(n)}$  which is determined as a result of measuring a certain harmonic of the displacement current  $P_M^{(n)}$  flowing through a nonlinear capacitor:

$$\left. \begin{aligned} \epsilon &= 4\pi \frac{P_M(E)}{E} = A \cdot 4\pi \frac{P_M(e)}{e_0}, \\ \epsilon^{(n)} &= 4\pi \frac{P_M^{(n)}(E)}{E} = A \cdot 4\pi \frac{P_M^{(n)}(e_0)}{e_0}, \\ A &= \frac{2\epsilon}{\beta T}. \end{aligned} \right\} \quad (3.105)$$

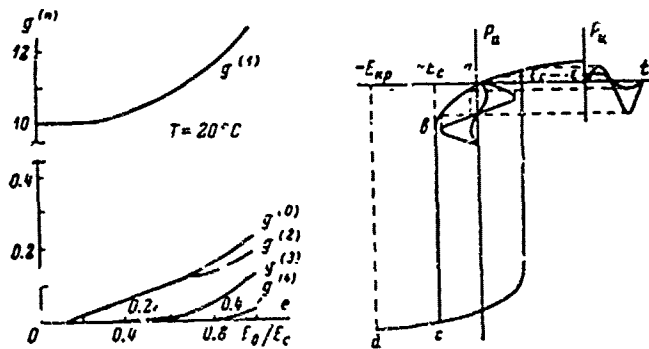


Figure 3.8. Relationship of  $g^{(n)}$  to field amplitude.

Figure 3.9. For the explanation of the relationship  $g^{(1)} = \frac{\epsilon^{(1)}}{\epsilon_0}(e)$ .

Next we will introduce the quantity  $g^{(n)}(e_0) = \frac{\epsilon^{(n)}(e_0)}{\epsilon_0}$  where

$$g^{(n)}(e_0) = \frac{4\pi P_M^{(n)}(E_0)}{E_0}.$$

Thus,  $g^{(n)}(e_0)$  defines the weight of the respective "harmonic"  $e^{(n)}$ , i.e. its value in relation to the normal value of  $\epsilon_0$  measured in small fields in the case of which nonlinear effects may be neglected. The amplitudes of  $g^{(n)}(e_0)$  calculated for  $T=20^\circ\text{C}$  are shown in Figure 3.8 the X-axis of which has a second scale expressed in units of  $\frac{E_0}{E_c}$ . This makes it possible to connect  $g^{(n)}$  with the concrete values of the fields

1) Of course, the question concerns very low frequencies, i.e.  $\omega \ll \omega_0$  where  $\omega_0$  is resonance frequency of the crystal sample.

and apply the curves shown in Figure 3.8 to ferroelectrics having different  $E_c$ . As may be seen from Figure 3.8, the amplitudes of all harmonics grow, with the rate of their growth appreciably increasing as the field amplitude approaches  $E_c$ .

Nonlinear growth of the first harmonic which is of the greatest interest inasmuch as this is the harmonic that is usually determined in measurements, and the growth of high harmonics and direct component of the current may be explained physically on the basis of the following (Figure 3.9). During the action of a variable field  $E < E_c$  on a ferroelectric the induced polarization  $P_M$  (and, consequently, the current also) will vary as shown in Figure 3.9, i.e. it will be assuming values defined by the upper branch of the loop (the section ab of the loop), with a positive half-wave of the field  $P$  increasing gradually and with a negative half-wave -- more sharply. It is easy to see that such a relationship of  $P_M(t)$  leads to a nonlinear growth of the first harmonic and to the appearance of higher harmonics and a negative (in relation to  $P_S$ ) direct component of the current. This direct component of the current is equivalent to a certain negative increment  $\Delta P_S$  of residual polarization:

$$\Delta P_S = P_S^{(0)} = -\frac{\epsilon_0 E_c}{4\pi} g^{(1)}(\omega). \quad (3.106)$$

Actually  $P_M^{(0)}$  does not change the relationships  $\epsilon(E)$ . However, as we shall see, it appreciably affects the shape of the curve  $d_{ik}(E)$ . With the fields  $E_0 \gg E_c$  ( $\epsilon_0 \gg 0.5$ ), expressions for  $g^{(n)}$  become invalid in view of incompatibility of (3.99a) and (3.100).

Thus, we have arrived at a rather obvious conclusion which apparently may be taken into account in explaining a considerable portion of nonlinear effects observed in ferroelectrics.

The relationship  $\epsilon(E)$ , i.e. in the final analysis  $P_M(E)$ , is marked the more strictly the sharper the slope of the ascending branch of the hysteresis loop changes, the smaller the coercive field  $E_c$  and the closer the "quiescent point" relative to which the field changes the state of the ferroelectric, adjoins the region of the maximum change in the slope of the loop.

We will now determine the relationship of the piezomoduli  $d_{33}$  and  $d_{31}$  to the amplitude of electric field. Substituting polarization  $P = P_S + P_M$  and separating that portion of the deformation which is brought about by the electric field applied, we will obtain

$$u_{33} = d_{33} [2P_S P_M(E) + P_M^2(E)]. \quad (3.107)$$

Simultaneous examination of this relationship expressed in terms of dimensionless quantities  $P_S$ ,  $P_M$  and  $\epsilon$  and hysteresis loop leads to the well known relationship  $u_{33}(E)$  of the "butterfly" type (see [62]).

Substituting then the  $P_M(e)$  from (3.104) into the relationships obtained, we have

$$u_{ik} = \epsilon_{ijk} \sum_{n=1}^{\infty} d_{ik}^{(n)}(T) e^{in\omega t} \quad (3.108)$$

and introducing then  $e = \epsilon_0 \sin \omega t$ , we will obtain (3.108) in the form of an expansion with respect to harmonics.

We will examine behavior of the first harmonic of the deformation  $u_{ik}$  and will introduce the value of piezomodulus  $d_{ik}^{(1)} = \frac{u_{ik}}{E_0}$ .

In general the matrix  $\hat{d}$  "splits" into the harmonics

$$d_{ik}^{(n)} = \frac{u_{ik}^{(n)}}{E_0} \quad (3.109)$$

If we limit ourselves to such fields (actually not very small in comparison with  $E_c$ ) with which, according to Figure 3.9,  $P_{11}$  is small in comparison with  $P_S$ , then the second terms in formula (3.107) could be neglected and in that case  $u_{ik} = 2 \epsilon_{ijk} P_S P_M(E)$ .

Taking into account that  $\epsilon^{(n)} = \frac{4\pi P_M^{(n)}}{E_0}$ , we have

$$d_{ik}^{(n)} = \frac{\epsilon_{ijk} P_S}{2\pi} \epsilon^{(n)}(E) \quad (3.110)$$

and, consequently,

$$\frac{\epsilon^{(n)}}{\epsilon_0} = \frac{d_{ik}^{(n)}(E)}{d_{0ik}} = d^{(n)}(\epsilon_0); \quad d_{0ik} = \lim_{E \rightarrow 0} d_{ik}$$

If  $|E| > |E_c|$ , then the relationships obtained are invalid.

It is easy to perceive that with an increase in temperature the relationship  $\frac{d_{ik}^{(1)}(E)}{d_{0ik}}$ , like the relationship  $\frac{\epsilon^{(1)}(E)}{\epsilon_0}$ , becomes more marked.

Relationships obtained above in general make it possible to determine the trend of the change in  $d_{ik0}(E)$ . However, a direct comparison of  $d_{in}^{(1)}(E)$  and  $\frac{\epsilon^{(1)}(E)}{\epsilon_0}$  indicates a slight quantitative lack of coincidence of these relationships, which is explained by the fact that in formula (3.108) the direct component does not appear in explicit form and the terms  $\sim (P_0 + P_M)^6$  also do not appear. This was already discussed earlier.

The effect of permanent electric field  $E_{\perp}$  may be analyzed using similar methods.

The relationship  $\epsilon(T, E_{\perp})$  was determined in a number of works [36,

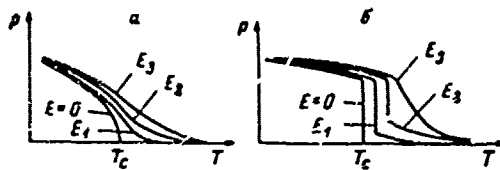


Figure 3.10. Temperature dependence of polarization in the presence and in the absence of displacing field  $E$  [63].

a -- phase transition of the second kind;  
b -- phase transition of the first kind.

39, 63] and it was found that near the phase transition of the first kind

$$\frac{4\pi P_s}{E} = \epsilon_{11}(T, E_{\perp}) = \frac{\pi}{2a} - \frac{4\pi}{10P_s} E_{\perp}$$

In the case of phase transition of the second kind the relationship is more complex:

$$\frac{4\pi P_s}{E} = \epsilon_{11} = \frac{1}{b} \sqrt{\frac{4}{\beta_1 E_{\perp}^2} \left( \frac{z^2}{q^2} + q^2 \right)^{-1}}$$

where

$$z = \frac{2a}{E_{\perp}} P_s; \quad q = \frac{4\pi^2}{\beta_1 E_{\perp}^2}$$

The curve of total polarization, i.e.  $P_s + P_M(E_{\perp})$  shown in Figure 3.10 indicates that with the growth of  $E_{\perp}$  the phase transition becomes "blurred".

Attempt to explain the observed relationships  $\epsilon_{ij}(\sigma_k)$  and  $d_{ijk}(\sigma_k)$  in an analogous manner encounters great difficulties. As an illustration we will examine changes taking place in tetragonal  $\text{BaTiO}_3$  during the action of mechanical stresses applied along and perpendicularly to  $P_s$ .

Expanding  $P_{s,ij}$  from (3.99) ( $\sigma_k \neq 0$ ) into a series and substituting into the expression for  $\epsilon_{S2}$  and  $d_{ijk}$ , we will obtain:

$$P_{s,ij}(\sigma_{22}) = P_{0ij} + d_{333}^i \sigma_{22}; \quad P_{s,ij}(\sigma_{33}) = P_{0ij} + d_{331}^i \sigma_{33};$$

$$\epsilon_{11}(\sigma_{22}) \approx \epsilon_{011} \left[ 1 + \frac{2}{\pi} (\beta_{22}^i \sigma_{22} - \beta_1 d_{333} P_{011}) \sigma_{22} \right];$$

$$\epsilon_{11}(\sigma_{33}) \approx \epsilon_{011} \left[ 1 + \frac{2}{\pi} (\beta_{31}^i \sigma_{33} - \beta_1 d_{331} P_{011}) \sigma_{33} \right];$$

$$d_{33}(\sigma_{22}) = d_{330} (1 + d_{33}^i \sigma_{22} / P_{011}) \left[ 1 + \frac{2}{\pi} (\beta_{22}^i \sigma_{22} - 2\beta_1 d_{333} P_{011}) \sigma_{22} \right];$$

$$d_{33}(\sigma_{33}) = d_{330} (1 + d_{33}^i \sigma_{33} / P_{011}) \left[ 1 + \frac{2}{\pi} (\beta_{31}^i \sigma_{33} - 2\beta_1 d_{331} P_{011}) \sigma_{33} \right].$$

In these formulas, quantities having the subscript "0" were taken with a  $\sigma_k = 0$ . These expressions accurately convey the main trends (decrease, increase) of the relationships  $P_{sz}(\sigma_k)$ ,  $\epsilon_i(\sigma_k)$  and  $d_{ik}(\sigma_k)$  observed in single crystals and even in piezoceramics.

However, quantitative evaluations lead to considerable divergences even with small stresses ( $\sigma_{zz} \sim 50-100$  kilograms/cm<sup>2</sup>). Taking into account of the terms containing higher powers of  $\sigma_k$  in (3.88) and in above formulas does not change the situation. The essence of the matter consists in that solution of (3.88), i.e.  $P_{sz}(\sigma_k)$  has to be examined together with the stability conditions (3.80) which change substantially even when  $\sigma_k$  are small. As it was shown in [39], for a single crystal of BaTiO<sub>3</sub>, with a  $\sigma_k \neq 0$  the most advantageous of the solutions will be that with which  $P_s$  will be oriented along the highest of the elongating stresses or along the smallest of the compressing stresses. For example, compression stress  $\sigma_{zz}$  leads not only to the appearance of piezopolarization inverse to  $P_s$  but also to its turning by 90°. In accordance with this,  $\epsilon_i(\sigma_k)$  and  $d_{ik}(\sigma_k)$  change more than this follows from the formulas cited above. A certain set of minimal stresses which can change the direction of  $P_s$  of the separate domains must exist in an actual crystal. In other words, a quantitative description of the relationships  $\epsilon_i(\sigma)$  and  $d_{ik}(\sigma_k)$  is possible only as a result of examination of "mechanical hysteresis" with the behavior characteristics of the domains taken into account.

#### Par. 4. Thermodynamic Theory of Antiferroelectricity

Some crystals (often isomorphous or close in structure to ferroelectric crystals) undergo with a change in temperature a phase transition into a state with a lower symmetry. As a rule, twinning (analogue of the domain structure of ferroelectrics) takes place in this process but unlike the ferroelectric transitions no resultant dipole moment appears. If the structure of the low-symmetry phase is broken up into two sublattices having an equal but opposite dipole moment, then the crystal undergoing such a phase transition is called antiferroelectric. The principles of thermodynamic theory of antiferroelectrics were laid down by Kittel [64].

Following Kittel, we will examine a crystal lattice consisting of two identical interpenetrating sublattices with the polarization  $P_a$  and  $P_b$  corresponding to these sublattices. In the case of a phase transition, expansion of free energy  $A_p$  with respect to the powers of  $P_a$  and  $P_b$  may be written in the following form (compare with 3.7):

$$A_p(P_a, P_b, T) = A_0 + f(P_a^2 + P_b^2) + gP_aP_b + h(P_a^4 + P_b^4). \quad (3.111)$$

The coefficients  $f$ ,  $g$  and  $h$  in (3.111) are functions of temperature. From (3.111) we find:

$$E = \frac{\partial A_p}{\partial P_a} = 2fP_a + gP_b + 4hP_a^3. \quad (3.112)$$

And thus, spontaneous polarization of one sublattice  $P_{sa} = -P_{sb}$  is equal to:

$$P_{sa}^2 = \frac{f-2f}{4h}. \quad (3.113)$$

Polarization  $\Delta P = P_a + P_b \ll P_a$  in a weak electric field  $\Delta E$  may also be determined from (3.112):

$$2\Delta E = 2f\Delta P + g\Delta P + 12\lambda P_{sa}^2 \Delta P. \quad (3.114)$$

Hence we find dielectric susceptibility:

$$\chi = \frac{\Delta P}{\Delta E} = \frac{1}{2(g-f)}. \quad (3.115)$$

At Curie point  $P_{sa}^2 = 0$  and, consequently (see 3.113),  $f=2g$ . Therefore we find the following from (3.115):

$$\epsilon = 1 + 4\pi\chi_{T=\theta} = 1 + \frac{4\pi}{g} \quad (3.116)$$

in approaching Curie point from antiferroelectric modification. In unpolarized state, fourth-order terms in (3.114) should be neglected. After this, we will find:

$$\epsilon = 1 + 4\pi\chi = 1 + \frac{8\pi}{2f+g}. \quad (3.117)$$

When  $T=\theta$ , (3.117) is reduced to the equality (3.116). Thus, dielectric constant is continuous at the transition point. In doing so, it does not necessarily reach large values. If it is assumed that the value of  $f$  near  $\theta$  changes in accordance with the formula (compare with 3.3)

$$f = \frac{1}{2}g + \lambda(T-\theta), \quad (3.118)$$

we will obtain the following from formulas cited above (when  $\lambda > 0$ ):

$$P_{sa}^2 = P_{sb}^2 = \frac{\lambda(T-\theta)}{2\lambda}. \quad (3.119)$$

$$\epsilon = 1 + 4\pi\chi = 1 + \frac{4\pi}{g + 2\lambda(T-\theta)}. \quad (3.120)$$

$$\epsilon = 1 + 4\pi\chi = 1 + \frac{4\pi}{g + \lambda(T-\theta)}. \quad (3.121)$$

With  $\lambda > 0$  the low-temperature phase will be antiferroelectric and dielectric constant has a maximum at  $T=\theta$ . With  $\lambda < 0$  the high-temperature modification will be antiferroelectric and dielectric constant has a minimum at the transition point.

If it is assumed that the coefficients  $g$  and  $h$  weakly depend on temperature, then the jump in entropy  $\Delta S$  and thermal capacity at a constant pressure  $\Delta c_p$  may be found from (3.111) in the case of antiferroelectric transition:

$$\Delta S = -(f_{1a} + P_{1a}^2) \left( \frac{\partial f}{\partial T} \right)_{P_a} \quad (3.122)$$

$$\Delta C_p = \theta \left( \frac{\partial^2 f}{\partial T^2} \right)_{P_a} = \frac{\theta}{k} \left( \frac{\partial f}{\partial T} \right)_{P_a} \left( \frac{\partial^2 f}{\partial P_a^2} \right)_{P_a} \quad (3.123)$$

We will examine now phase transitions of the first kind. For this purpose, as well as also for the case of ferroelectrics, it is necessary to take into account the sixth-order terms in the expansion of free energy with respect to the powers of polarization:

$$A_p = A_0 + f(P_a^2 + P_b^2) + gP_aP_b + h(P_a^4 + P_b^4) + j(P_a^6 + P_b^6) \quad (3.124)$$

We find the following from (3.124):

$$E = \frac{\partial A_p}{\partial P_a} = 2fP_a + gP_b + 4hP_a^3 + 6jP_a^5 \quad (3.125)$$

Thus, spontaneous polarization of one sublattice in antiferroelectric phase ( $P_{1a} = -P_{1b}$ ) will be defined by the equation:

$$6jP_{1a}^5 + 4hP_{1a}^3 + (2f - g) = 0 \quad (3.125a)$$

At Curie point the thermodynamic potential with  $P_{1a} = -P_{1b} \neq 0$  and  $P_{1a} = P_{1b} = 0$  must have one and the same value.

Taking (3.124) into account, we find the following from that condition:

$$(2f - g) + 2hP_{1a}^2 + 2jP_{1a}^4 = 0 \quad (3.126)$$

Solution of the equations (3.125) and (3.126) gives:

$$\left. \begin{aligned} P_{1a}^2 &= \frac{g - 2f}{h} \\ P_{1a}^4 &= \frac{2f - g}{2j} \end{aligned} \right\} T = \theta \quad (3.127)$$

From (3.127), we find:

$$2f(2f - g) = h^2; \quad T = \theta \quad (3.128)$$

The relationship (3.128) is a condition defining the transition point and, therefore, it is natural to assume the temperature dependence of the quantity  $f$  near  $\theta$  to be in the following form:

$$f = \frac{g}{2} + \frac{h^2}{4j} + \lambda(T - \theta)$$

In the approach from the antiferroelectric and unpolarized phases the dielectric constants  $\epsilon^-$  and  $\epsilon^+$  at the transition point prove to be equal respectively to:

$$\left. \begin{aligned} \epsilon^- &= 1 + 4\pi\chi^- = 1 + \frac{4\pi}{4f - g} \\ \epsilon^+ &= 1 + 4\pi\chi^+ = 1 + \frac{8\pi}{2f + g} \end{aligned} \right\} \quad (3.129)$$

And thus, in the phase transition of the first kind the dielectric constant experiences a jump at  $T = \theta$ .

It should be noted that the character of a transition is determined by the sign of the coefficient  $h$ . An investigation similar to that carried out in subparagraph 2, paragraph 1 of this chapter for ferroelectrics indicates that transition of the first kind occurs when  $h < 0$ .

Kittel theory set forth above was later supplemented by Tessmann [65] who examined the behavior of an antiferroelectric in an external electric field, and by Mason [66] who took electromechanical effects into account using antiferroelectrics of the type  $\text{NH}_4\text{H}_2\text{PO}_4$  as an example.

In the work [67] in which Kittel theory was generalized for a three-dimensional case, a study was made not only of the transition from antiferroelectric state into a paraelectric state, but also a study of phase transition from antiferroelectric state into ferroelectric state. In doing so, transition of the first kind was examined with anisotropy and deformations taken into account. Behavior of an antiferroelectric in an external electric field was also examined in the work [67].

In the investigation of phase transition from antiferroelectric state into paraelectric state the free energy  $A_p$  was written in the form of a series with respect to the powers of components of polarization of sublattices  $P_a$  and  $P_b$  and of the deformation tensor with accuracy to the fourth-order terms. After this, solutions were found from the following set of equations:

$$\left. \begin{aligned} \frac{\partial A_p}{\partial P_{ei}} &= E_i, \\ \frac{\partial A_p}{\partial P_{bi}} &= E_i, \\ \frac{\partial A_p}{\partial u_k} &= -\sigma_k. \end{aligned} \right\} \quad (3.130)$$

where  $\sigma_k$  are components of elastic-stress tensor. A study of the set of equations (3.130) leads to the following results (which coincide with the results of the work [64]).

Piezoelectric effect must be absent in an antiferroelectric; lattice symmetry decreases during the transition owing to the presence of spontaneous deformations. In the approximation used, Curie point of an antiferroelectric does not depend on pressure. In addition to this, spontaneous polarizations  $P_{as}$  ( $P_{bs}$ ), thermal-capacity jump and dielectric constant near Curie point were determined in the work [67] more rigorously than in [64].

More complex cases are examined in [67] only for unidimensional model. Analysis of phase transitions of the first kind differs from that carried out in the work [64] by taking into account all possible invariants (for example, invariants of the type  $P_a^2 P_b^3$  omitted in writing the (3.124)). In doing so, the qualitative conclusions remain the same.

To investigate transitions in crystals in which antiferroelectric,

ferroelectric and paraelectric states are possible in the absence of an external field,  $A_p$  is written in the form of (3.111). The values of  $P_{as}$  and  $P_{bs}$  are found from the following equations:

$$\frac{\partial A_p}{\partial P_{as}} = 0; \quad \frac{\partial A_p}{\partial P_{bs}} = 0. \quad (3.131)$$

Stability conditions (i.e. conditions for the minimum of thermodynamic potential (3.111)) have the following form:

$$\frac{\partial^2 A_p}{\partial P_{as}^2} > 0; \quad \frac{\partial^2 A_p}{\partial P_{bs}^2} > 0; \quad (3.132)$$

$$\begin{vmatrix} \frac{\partial^2 A_p}{\partial P_{as}^2} & \frac{\partial^2 A_p}{\partial P_{as} \partial P_{bs}} \\ \frac{\partial^2 A_p}{\partial P_{as} \partial P_{bs}} & \frac{\partial^2 A_p}{\partial P_{bs}^2} \end{vmatrix} > 0. \quad (3.133)$$

We find the following from (3.131), (3.132) and (3.133).

1. Paraelectric state ( $P_{as}=P_{bs}=0$ ) is achieved if  $f > 0$ ,  $-f < g/2 < f$ .
2. Ferroelectric state ( $P_{as}=P_{bs}$ ) is achieved if  $f+g/2 < 0$ ,  $f+g < 0$ .

In this case

$$P_{as}^2 = -\frac{g + 2f}{4h}.$$

3. Antiferroelectric state is achieved when

$$\frac{g}{2} - f > 0; \quad g - f > 0.$$

$$P_{as}^2 = \frac{g - 2f}{4h}.$$

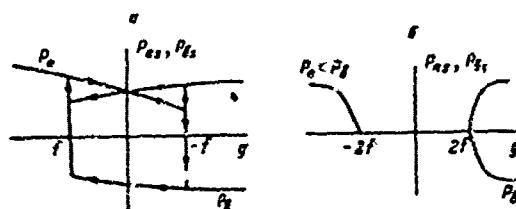


Figure 3.11. Relationship of  $P_{as}$  and  $P_{sb}$  to  $g$ .

a --  $f < 0$ ; b --  $f > 0$ .

With a change of temperature, relationships between the coefficients  $f$  and  $g$  may change and accordingly phase transitions will take place. Relation of spontaneous polarization of sublattices  $P_{as}$ ,  $P_{bs}$  to the parameter  $g$  with different signs of the parameter for the case of phase transition of the second kind (i.e.  $h > 0$ ) is shown in Figure 3.11.

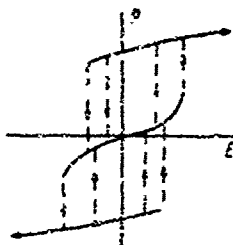


Figure 3.12. Hysteresis loop for an antiferroelectric.

Results of investigation carried out in [67] on the behavior of an antiferroelectric in an external electric field are reduced in the main to the following: at transition from ferroelectric into antiferroelectric state (in the case of a phase transition of the second kind), dielectric constant decreases by four times. In a reverse transition it also undergoes discontinuity but becomes infinite at the transition point. In strong electric fields the crystal changes from antiferroelectric into ferroelectric state with an unusual hysteresis loop forming in this process (Figure 3.12). Critical field strength  $E_{CR}$  corresponding to transition into ferroelectric state was calculated in [67]:

$$E_{CR} = \frac{4}{3} \sqrt{3k} (g-1)^{3/4}. \quad (3.134)$$

A later attempt to generalize thermodynamic theory of antiferroelectrics for a three-dimensional case was undertaken by Cross [68]. Cross examined a pseudocubic crystal consisting of two interpenetrating sublattices with the polarization  $P_1$  and  $P_2$ . Cross represents free energy in the form of a series according to the even powers of the quantities:

$$\begin{aligned} P_x &= P_{1x} + P_{2x}; & P_y &= P_{1y} - P_{2y}; \\ P_y &= P_{1y} + P_{2y}; & P_x &= P_{1x} - P_{2x}; \\ P_z &= P_{1z}; & P_z &= P_{1z} - P_{2z}. \end{aligned}$$

writing it in a form analogous to Devonshire's expression (3.69). Making use of such a free-energy function it is possible to describe dielectric properties of  $\text{NaNbO}_3$  in all phases.

It should be noted that as in the case of ferroelectric transition, to construct a consistent thermodynamic theory of antiferroelectricity it is necessary to determine the transformation properties of parameter which characterizes antiferroelectric transition [69]. This question is examined in detail in the work [69] using antiferroelectric transition in  $(\text{NH}_4)_2\text{PO}_4$  as an example and employing the general group method.

## BIBLIOGRAPHY

1. V. L. Ginzburg, ZhETF [Journal of Experimental and Theoretical Physics], Vol 19, p 36 (1949).
2. V. L. Ginzburg, UFN [Achievements of Physical Sciences], Vol 38, p 430 (1949).
3. A. F. Devonshire, Phil. Mag., Vol 40, p 1040 (1949); Vol 42, p 1065 (1951).
4. L. D. Landau and Ye. M. Lifshits. Statisticheskaya Fizika [Statistical Physics]. Nauka Publishing House, Moscow, (1964).
5. E. Jaynes, Ferroelectricity. Princeton Univ. Press (1953).
6. V. A. Popov, Izv. AN SSR, ser. fiz. [Bulletin of USSR Academy of Sciences, Physics Series], Vol 31, p 1038 (1967).
7. L. D. Landau and Ye. M. Lifshits. Elektrodinamika Sploshnykh Sred [Electrodynamics of Solid Media]. GITTL [State Publishing House for Technical and Theoretical Literature], Moscow, (1957).
8. D. Meherhoter, Phys. Rev., Vol 112, p 413 (1958).
9. R. Ye. Pasyukov, FTT, Vol 3, p 1587 (1961).
10. V. L. Ginzburg, FTT, Vol 2, p 2061 (1960).
11. V. L. Ginzburg, A. P. Levanyuk, in the book: Sbornik pamyati G. S. Landsberg [Collection in Memory of G. S. Landsberg]. USSR Academy of Sciences Press, Moscow, p 104 (1959).
12. L. P. Kadonoff, et al., Rev. Mod. Phys., Vol 39, p 395 (1967).
13. R. Blinc. Ferroelectricity (in lectures on condensed matter, Trieste) (1968).
14. P. P. Craig, Phys. Letters, Vol 20, p 140 (1966).
15. R. Ye. Pasyukov, Izv. AN SSSR, ser. fiz., Vol 21, p 340 (1957).
16. G. A. Smolenskiy, R. Ye. Pasyukov, ZhETF, Vol 25, p 57 (1952).
17. A. P. Levanyuk, D. G. Sannikov, ZhETF, Vol 55, p 256 (1968).
18. L. P. Kadonoff, Physics, Vol 2, p 263 (1966).
19. C. Domb, Ann. Acad. Sci. Fennicae, ser. A. VI, Physica, 210, Helsinki (1966).

20. M. E. Fisher, J. Appl. Phys., Vol 38, p 1981 (1967).
21. B. Sidom, J. Chem. Phys., Vol 38, p 981 (1967).
22. A. Patashinskiy, V. L. Pokrovskiy, ZhETF, Vol 50, p 439 (1966).
23. V. L. Pokrovskiy, UFN, Vol 94, p 128 (1968).
24. A. Migdal, ZhETF, Vol 55, p 1964 (1963).
25. L. D. Landau, Sov. Phys., Vol 11, pp 255, 269 (1941).
26. Ye. M. Lifshits, ZhETF, Vol 11, pp 255, 259 (1941).
27. V. L. Indenbom, Izv. AN SSSR, ser. fiz., p 1180 (1960).
28. V. L. Indenbom, Kristallografiya [Crystallography], Vol 5, p 115 (1960).
29. M. S. Shur, ZhETF, Vol 51, p 1260 (1966).
30. G. Ye. L. Ye. Lyubarskiy. Teoriya Grupp i yeyo Primeneniye v Fizike [Theory of Groups and Its Application in Physics]. GIFML [State Publishing House for Physical and Mathematical Literature], Moscow, (1958).
31. K. Aizu, Phys. Rev., Vol 136, A. p 753 (1964).
32. I. Halblützel, Heiv. Phys. Acta, Vol 12, p 489 (1939).
33. A. Devonshire, Phil. Mag. Suppl., Vol 3, p 85 (1954).
34. W. P. Mason, Bell Syst. Techn. Journ., Vol 26, p 80 (1947).
35. V. G. Vaks, P. I. Larkin, Yu. N. Ovchinnikov, ZhETF, Vol 49, p 1180 (1965).
36. T. Mitsui, Phys. Rev., Vol 111, p 1259 (1958).
37. F. Jona, D. Shirane. Segnetoelektricheskiye Kristaly [Ferroelectric Crystals]. Mir Publishing House, Moscow (1965).
38. L. P. Kholodenko and M. Ye. Shirobokov, ZhETF, Vol 21, p 1250 (1951).
39. M. Ye. Shirobokov and L. P. Kholodenko, ZhETF, Vol 21, p 1239 (1951).
40. I. S. Zheludev, L. A. Shuvalov, Kristallografiya, Vol 1, p 681 (1956).
41. I. S. Zheludev, L. A. Shuvalov, Izv. AN SSSR, ser. fiz., Vol 21m p 264 (1957).

42. L. A. Shuvalov. Printsipy Simmetrii i Mikroskopicheskiye Svoystva Kristalov [Principles of Symmetry and Microscopic Properties of Crystals]. Prague, (1967).
43. I. S. Zheludev. Fizika Kristallicheskikh Dielektrikov [Physics of Crystalline Dielectrics]. Nauka Publishing House, Moscow (1968).
44. A. S. Sonin, I. S. Zheludev, G. F. Dobrzhanskiy, Izv. AN SSSR, ser. fiz., Vol 24, p 1209 (1960).
45. B. A. Strukov, N. D. Gavrilova, V. A. Kopshchik, Kristallografiya, Vol 6, p 780 (1961).
46. W. Gady. P'yezoelektrichestvo i Yego Prakticheskiye Primeneniya [Piezoelectricity and Its Practical Applications]. IL [Foreign Literature Press], Moscow (1952).
47. W. Mason. P'yezoelektricheskiye Kristally i ikh Primeneniye v Ul'traakustike [Piezoelectric Crystals and Their Application in Ultrasonics]. IL, Moscow (1952).
48. G. A. Smolenskiy, R. Ye. Pasynkov, DAN SSSR [Proceedings of USSR Academy of Sciences], Vol 79, p 431 (1951).
49. G. A. Smolenskiy, R. Ye. Pasynkov, ZhETF, Vol 24, p 69 (1953).
50. V. Janovec, J. Chem. Phys., Vol 45, p 1874 (1966).
51. E. B. Pippard. Classical Thermodynamics. Cambridge Univ. Press (1960).
52. C. W. Garland, J. Chem. Phys., Vol 41, p 1005 (1964).
53. M. J. Buckingham, W. M. Fairbank. Progress in Low-Temperature Physics, Vol 3, Amsterdam (1961).
54. L. P. Kholodenko, ZhETF, Vol 31, p 244 (1956).
55. L. P. Kholodenko, FIT, Vol 5, p 897 (1963).
56. S. Groot. Termodinamika Neobratimyykh Protssessov [Thermodynamics of Irreversible Processes]. GITTL, Moscow, (1956).
57. Z. Onsager, Phys. Rev., 3, 7, 405 (1931).
58. L. P. Kholodenko, Izv. AN SSSR, ser. fiz., Vol 21, p 369, (1957).
59. V. N. Zaytseva, R. Ye. Pasynkov, V. I. Pozern and A. M. El'gard, Izv. AN SSSR, ser. fiz., Vol 11, p 1357 (1960).
60. L. P. Kholodenko, Kristallografiya, Vol 1, No 4, p 393 (1956).

61. G. A. Velyukhanova, R. Ye. Pasyukov, V. I. Pozern and A. M. El'gard, Izv. AN SSSR, ser. fiz., Vol 11, p 1362 (1960).
62. H. L. Allsopp, D. F. Gibbs, Phil. Mag., Vol 4, p 359 (1959).
63. A. Devonshire, Phil. Mag. Suppl., Vol 3, p 85 (1954).
64. C. Kittel, Phys. Rev., Vol 8, pp 2, 729 (1951).
65. J. R. Tessmann, Phys. Rev., Vol 91, p 447 (1953).
66. W. P. Mason, Phys. Rev., Vol 88, p 480 (1952) (see translation in the collection Problemy Sovremennoy Fiziki [Problems of Modern Physics, No 6, IL, Moscow (1953)]).
67. G. A. Smolenskiy, V. Kh. Kozlovskiy, ZhETF, Vol 26, p 684 (1954).
68. L. E. Cross, Phil. Mag., (8), pp 1, 76 (1956).
69. Yu. Sirotin and L. M. Mikhel'son, FIT, Vol 10, p 1843 (1968).

#### CHAPTER 4. MICROSCOPIC (MODEL) THEORY OF FERROELECTRICITY

The first attempts to explain the appearance of spontaneous polarization by means of some atomic mechanism date back to the time when the only known ferroelectric was Seignette's salt.

According to hypothesis stated by I. V. Kurchatov and P. P. Kobeko the reason for the anomaly of the properties of Seignette's salt is the appearance within a certain temperature range of preferred orientation of rotating dipole groups, which disappears at a certain temperature similarly to the way this takes place in Langevin theory. The interest in microscopic theory of spontaneous polarization considerably increased immediately after the discovery of ferroelectric properties of  $\text{BaTiO}_3$ .

Most of theoretical investigations were based on the assumption that spontaneous polarization is a result of displacement of these or other ions ( $\text{T}'$  or  $\text{O}$  ions in  $\text{BaTiO}_3$ , protons in Seignette's salt or  $\text{KH}_2$ ). This state is maintained by a self-consistent field (i.e. by the field defined by the displacements of these ions). Phase transition, i.e. the disappearance of  $P_S$ , is brought about by the preponderance of disordering action of thermal movements of ions over the action of effective field which holds the ions in displaced positions or provides a certain preferred direction of statistical distribution of elementary dipole moments.

Two types of models have appeared in the process of forming these representations which are considered valid even at the present time in spite of these or other refinements.

1) Model of order-disorder type in which it is assumed that "active" ions may be in one of the minima (displaced relative to the center of the cell) of potential function describing its state (Figure 4.1a). In this case, spontaneous polarization is a result of preponderance of the number of ions located, for example, in the potential well 1. This model was used to explain the nature of ferroelectricity in  $\text{BaTiO}_3$  [1], Seignette's salt [2],  $\text{KH}_2\text{PO}_4$  [3], etc., and is also known under the name of "model of local minima."

2) Model of "displacement" type. Above Curie point, active ions are on the average in the center of potential well which as a result of the action of self-consistent field becomes asymmetrical when  $T < \theta$ , i.e.

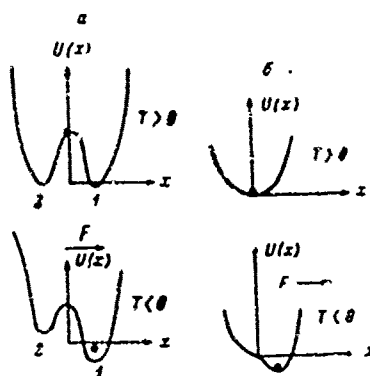


Figure 4.1. Potential function with two minima (a) and with one minimum (b).

its minimum is displaced along one of the directions allowed by the lattice symmetry (Figure 4.1b). Thus, the average position of an ion proves to be displaced and this leads to the appearance of  $P_S$ . This model which is also called a model of anharmonic oscillators, was successfully used in a whole series of works devoted to theory of  $\text{BaTiO}_3$  [4, 3] and other ferroelectrics.

Phase transitions of the "order-disorder" type and transitions of the "displacement" type are differentiated in accordance with these two models. Of course, in actual cases these models do not "countervail" each other and transitions of mixed type, for example in  $\text{KH}_2\text{PO}_4$ , apparently exist (see also chapter 5, paragraph 4, subparagraph 3).

It should be noted that the entire process of formation of microscopic theory of ferroelectricity may be characterized by two main directions of their development, which by no means exclude each other.

1) Model theories of the above-mentioned type, constructed on the basis of these or other assumptions concerning the form of potential relief along which active ions are displaced. The movement of these ions takes place in a time-averaged self-consistent field. The question of the region of existence of  $P_S \neq 0$  is reduced to a determination of conditions under which nonzero displacements of ions averaged over the ensemble (or time) are allowed.

2). Dynamic theories, developed somewhat later, in which the field is considered to be dependent on instantaneous positions of all ions which perform related vibrations relative to the equilibrium positions in the lattice. Phase transition points are defined as points of a loss of dynamic stability of the lattice relative to one of its normal vibrations. An advantage of this approach is that it makes it possible to connect the characteristics of the vibration spectrum of the lattice with anomalies in the transition region.

Dynamic theory to which chapter 5 is devoted, has very many common points of contact with model theories examined in the present chapter.

Jaynes and Wigner [6] theory in which spontaneous polarization is viewed as a result of spontaneous change in the symmetry of functions defining the state of lattice electrons appeared in the beginning of the 1950s. These representations give rise to certain objections on points of principle. However, at the present time, marked trends toward the further development and refinement of the so-called electron theory of ferroelectricity exist.

It should be noted that perfection of theories based on representations concerning displacements of ions is possible not only by means of using the apparatus of dynamics of crystal lattices. Considerable refinements can also be achieved within the framework of statistical methods if rough model representations are abandoned and if the short range of ions is taken into account on the basis of more accurate representations, in particular those involving the use of Bogolyubov method, as this was done in the works [7, 8].

Interest in the models of local minima has also resumed at the present time. Examination of phase transitions of the order-disorder type in terms of Ising model with lattice vibrations and quantum effects taken into account [9] opens new possibilities of explaining and classifying the characteristics of ferroelectric transitions in different crystals.

Big progress has been recently achieved in theory of phase transitions in hydrogen-containing ferroelectrics. The latest works by Blinc, et al. [10, 11] and a number of works [12-16] on two-dimensional models of such crystals qualitatively explain many important features of phenomena taking place in them.

#### Par. 1. Free Energy in Self-Consistent-Field Method

General relationships which are used in various model theories based on representations on the displacements of ions are derived in this paragraph. Expressions obtained on the basis of self-consistent-field method are not connected with any concrete form of potential relief and can be made use of in the analysis of models of local minima and anharmonic oscillators.

##### 1. Free Energy

Displacements of ions bring about the appearance of strong effective fields whose action is conducive to fixing the ions in their displaced positions. Spontaneous polarization developing in this process is also accounted for by electric dipole moments the appearance of which is connected with the action of effective fields on the electron shells of ions. Interaction of ions is taken into account in two ways: interaction of the nearest neighbors is defined by a certain function of coordinates  $U_k(x,$

y, z) which reproduces the energy relief along which ions belonging to the k-th sublattice "move"; interaction forces, i.e. electrostatic forces, are introduced by an addition to  $U_k(x, y, z)$  of the term  $z'_k (F_k r_k)$  which is equal to potential energy of the ion with a charge  $z'_k$ , displaced in the effective field  $F_k$  by the quantity  $r_k$ . Effective field depends not on the instantaneous but on the average coordinates of all of the remaining ions, and consequently, on statistical properties of the entire crystal lattice as a whole.

In accordance with these representations the investigation is reduced to the solution of two problems, independent in a certain sense:

1) calculation of effective fields acting on different ions, and also calculation of total polarization as functions of applied field and average displacements of ions;

2) writing and solving equations defining the electric and thermal state of the crystal under the conditions of thermodynamic equilibrium; these equations make it possible to determine the phase transition points, temperature dependence of spontaneous polarization and dielectric constant, entropy jump, etc.

Lorenz method or Ewald method (see par. 2) is used in the calculation of effective fields acting on different lattice ions. The calculation in the process of which the crystal lattice is divided into  $m$  simple monatomic cubic sublattices (for  $\text{BaTiO}_3$   $m=5$ ), leads to the following formulas for cubic and tetragonal crystals [3, 17]:

$$F_{kx} = \gamma_k E_x + \sum_{k=1}^m \beta_{kk} P_{kx} \quad (4.1)$$

$$P_x = \gamma_p E_x + \sum_{k=1}^m \rho_k P_{kx} \quad (4.2)$$

$P_x$  is here component of total polarization of the crystal,  $P_{gk'x}$  is electric moment of a unit of volume, forming as a result of displacement of ions of the k-th sublattice from the symmetric position ( $P_{gk'x} = Nz'_k s_k$ , where  $N$  is the number of cells in a unit of volume and  $s_k$  -- components of the average ion displacement),  $E$  is component of the applied field,  $\gamma_k$ ,  $\gamma_p$ ,  $\beta_{kk}$ , and  $\rho_k$  are coefficients dependent on the polarizabilities and charges of ions and on the lattice structure.

It is essential to underscore that all of these coefficients were calculated on the assumption that the ions are point ions. Therefore, an exact coincidence of theory and experiment can hardly be expected, and it is expedient to focus attention on obtaining the most important qualitative characteristics of ferroelectrics. It should also be remembered that (4.1) is a linear approximation of the relationship  $F_{kx}(E_i, P_i)$ .

If it is assumed that appearance of spontaneous polarization is

brought about by ions belonging to one sublattice (for example, titanium ions), then the sums in (4.1) and (4.2) will contain only one term:

$$F_{2s} = \gamma_s E_s + \beta_s P_{2s}, \quad (4.3)$$

$$P_{2s} = \gamma_s' E_s + \beta_s' P_{2s}. \quad (4.4)$$

Equation of state for a crystal lattice are determined by means of free energy of the following system:

$$A = -Nk \ln Z, \quad (4.5)$$

where  $Z$  is a statistical integral.

In most cases the calculation of  $Z$  is carried out without taking the quantum-mechanical effects into account and is based on the following assumptions:

1) potential energy of the ion is defined by the function  $U_k(x, y, z) = z_k(F_k r_k)$ , and integrals describing the state of the separate ions are multiplicative, which is equivalent to neglecting the correlations between instantaneous positions of these ions;

2) appearance of spontaneous polarization is brought about by ions called henceforth ferroactive, which belong to one sublattice (for example,  $Ti^{+4}$  ions in  $BaTiO_3$ ). Because of this, statistical distribution of these ions alone is taken into account and temperature effects connected with the vibrations of the structural elements of a crystal lattice are ignored.

In accordance with these representations, statistical integral  $Z$  is written in the following form:

$$Z = \frac{1}{N} \left\{ \frac{(2\pi kT m_k)^{3/2}}{h^3} \int_{v_k} \exp \left\{ - \left[ \frac{(x, y, z) - z_k(F_k r_k)}{kT} \right] \right\} dv_k \right\}^N, \quad (4.6)$$

where  $m_k$  is ion mass and  $h$  -- Planck constant.

Substituting (4.6) into (4.5) and differentiating with respect to  $F_{kx}$ , we will find the following relation:

$$P_{2s} = \frac{\partial A}{\partial F_{2s}}. \quad (4.7)$$

Expressing the  $F_{kx}$  in this formula according to (4.1) and (4.2) in terms of  $P_{gkx}$  and  $E$ , we will obtain an equation the solution of which gives temperature dependence of spontaneous polarization (with  $E_x=0$ ) and dielectric constant.

Such is the scheme and basic approximations of theories of ionic displacements developed at the present time. They differ from each other by the form and methods of defining the function  $U_k(x, y, z)$ . Thus, in Mason and Mattias [1] theory,  $U_k(x, y, z)$  for  $BaTiO_3$  is given in the form of six local minima displaced relative to the center of the cell. Devon-

shire [4] and Slater [5] write  $U_k(x, y, z)$  in a form characteristic of an anharmonic oscillator.

We will examine a more general case based on the assumption [17] that oscillations of all ions of a crystal lattice take place. In doing so, we keep the assumptions made earlier as being valid.

In accordance with the foregoing, we will now write the statistical integral in the following manner:

$$Z = \frac{1}{N!} \prod_{k=1}^m \left[ \left( \frac{(2\pi k T m_k)^{3/2}}{h^3} \right)^{v_k} \int \exp \left[ - \left( \frac{U_k(x, y, z) - s_k^i (F_k r_k)}{kT} \right) dv_k \right] \right]^{v_k} \quad (4.8)$$

where  $m$  is the number of sublattices.

In a particular case (for example, the model of local minima in Mason's and Mattis' interpretation), when  $U_k(x, y, z)$  can assume only discrete values, the integral in (4.8) should be written in the form of the following sum:

$$\sum_{j=1}^n \exp \left[ - \frac{U_{jk} - s_k^i (F_k r_k)}{kT} \right] v_j \quad (4.9)$$

where  $n$  is the number of discrete states with energy  $U_{jk}$ ,  $v_j$  is volume determined by statistical weight of the state  $U_{jk}$ , in the case in question  $r_k$  is the average coordinate of an ion which is in this state.

We will limit ourselves to the assumption that  $U_k$  has reflection symmetry and that the integrand decreases so rapidly with the increase of  $r_k$  that without impairing accuracy, integration with respect to the volume of unit cell may be replaced by integration with infinite limits.

For this case, free energy is equal to:

$$A = -NkT \left\{ \ln \frac{1}{N} \prod_{k=1}^m \left( \frac{(2\pi k T m_k)^{3/2}}{h^3} \right)^{v_k} - \sum_{k=1}^m \ln \left[ \int \exp \left( - \frac{U_k - s_k^i (F_k r_k)}{kT} \right) dv_k \right] \right\} \quad (4.10)$$

Next, we have:

$$P_{k\alpha} = N s_k^i s_{k\alpha} = \frac{N s_k^i \int s_{k\alpha} \exp \left[ - \frac{U_k - s_k^i (F_k r_k)}{kT} \right] dv_k}{\int \exp \left[ - \frac{U_k - s_k^i (F_k r_k)}{kT} \right] dv_k} = \frac{\partial A}{\partial F_{k\alpha}} \quad (4.11)$$

Differentiating (4.10) with respect to all  $F_{k\alpha}$ , we will obtain a system of  $3m$  equations of the following form:

$$P_{k\alpha} - \varphi_{k\alpha}(T, E_1, E_2, E_3; P_{11}, \dots, P_{13}, \dots, P_{m1}, \dots, P_{m3}) = 0 \quad (4.12)$$

where

$$\varphi_{k\alpha}(T, E_1, \dots; P_{\alpha\alpha}) = \left( \frac{\partial A}{\partial F_{k\alpha}} \right)_{F_{k\alpha} = (E, P_{\alpha})}$$

Assuming all  $E_i=0$ , we will obtain an equation of state for a ferroelectric, which defines the temperature dependence of spontaneous polarization:

$$P_{gkx} - \tau A_k(T; P_{g1x}, \dots, P_{gkx}, \dots, P_{gmx}) = 0. \quad (4.13)$$

We will examine first a particular case important for the further examination. We will assume that all ions make purely harmonic oscillations, i.e. all

$$U_k(x, y, z) = a_k(x^2 + y^2 + z^2).$$

In this case, integration of (4.6) can be easily carried out and, therefore, (4.12) will be written in the following form:

$$P_{gkx} - \alpha_k^i F_{kx} = 0. \quad (4.14)$$

where  $\alpha_k^i = \frac{Na_k}{2}$  is polarizability of ionic displacements.

Substituting (4.14) into the preceding expression (4.13), we will obtain a system of linear equations of the following form:

$$\sum_{k'=1}^n (\alpha_k^i \beta_{kk'} + \delta_{kk'}) P_{gk'x} = 0,$$

where

$$\delta_{kk'} = \begin{cases} 1 & \text{when } k'=k \\ 0 & \text{when } k' \neq k. \end{cases}$$

Generally speaking such a system has only zero solutions, i.e. the crystal is paraelectric. However, in a particular case when the determinant of the system with the elements  $\alpha_k^i \beta_{kk'} + \delta_{kk'}$  vanishes, nonzero solutions of the following form are possible

$$P_{gkx}^s = \tau A_k$$

where  $A_k$  is an algebraic complement of the  $k$ -th line and  $\tau$  is some arbitrary constant. However, these solutions are unstable. This can be easily shown if we calculated directly the free energy which in this case is a function of the squares of  $P_{gkx}^s$  which is infinitely decreasing with the increase of  $P_{gkx}^s$ .

A stable ferroelectric configuration can exist only when the expression for free energy of the crystal contains terms that are proportional at least to  $(P_{gkx}^s)^2$  and the aggregate of which forms a quantity smaller than zero, and the higher powers of  $P_{gkx}^s$  making up together a positive quantity.

Terms containing high powers of  $P_{gkx}^S$  provide the saturation effect of spontaneous polarization and may appear in the expression for free energy if the ions of at least one sublattice move under the conditions when nonlinear forces are in operation; in other words, if at least one of the functions  $U_k(x, y, z)$  contains terms of higher powers than  $x^2, y^2, z^2$ . It is precisely these terms that account for the temperature and nonlinear effects characteristic of ferroelectrics.

As regards the first condition -- the requirement that terms proportional to  $(P_{gkx}^S)^2$  make up a negative quantity, it is necessary in order that the free energy  $A(P_S)$  have a minimum when  $x_k \sim P_S \neq 0$ . This condition is realized owing to a strong long-range action -- effective field  $F_k(P_S)$  which "breaks" the symmetry of the function  $U_k(xyz)$ .

Ions performing harmonic oscillations indirectly affect the temperature characteristics of a ferroelectric; taking them into account when calculating the effective fields and polarization will introduce corrections into the expressions for the coefficients in (4.3) and (4.4).

## 2. Conditions for a Ferroelectric Transition

According to the theorem on implicit functions [18] the existence of a unique and finite nontrivial system of solutions of equations of the type (4.12) is possible with those values of  $P_{gks}^S$  with which the functional determinant

$$\begin{pmatrix} 1 - \frac{\partial^2 \varphi_{1x}}{\partial P_{1x}^2} & \dots & - \frac{\partial^2 \varphi_{1x}}{\partial P_{1y}^2} \\ \dots & \dots & \dots \\ - \frac{\partial^2 \varphi_{1y}}{\partial P_{1x}^2} & \dots & 1 - \frac{\partial^2 \varphi_{1y}}{\partial P_{1y}^2} \end{pmatrix} \quad (4.15)$$

is not equal to zero.

The equality of the determinant to zero indicates a loss of "stability" by the system (4.12). It is obvious that the temperature of transition into paraelectric state will be found by substituting into (4.15) the trivial solutions of the system (4.12):

$$P_{g1x}^S \dots P_{g1y}^S \dots P_{gmx}^S \dots P_{gmy}^S = 0.$$

A study of the condition of equality of the determinant (4.15) to zero together with the equations (4.12) makes it possible to draw a number of conclusions concerning permissible types of solutions of these equations.

1) With a phase transition of the first kind (4.15) may vanish or become a complex quantity when  $P_{gij}^S \neq 0$ .

1) The system (4.12) is satisfied with the solutions of the following form:

$$P_{12} \equiv 0, \text{ or } P_{g12}^0 = P_{g12}^1 = \dots = P_{gmn}^0 \equiv 0; P_{12} \neq 0; P_{mn} \neq 0. \quad (4.16)$$

In other words, low-temperature transitions similar to those which take place in BaTiO<sub>3</sub> are allowed in principle when several active lattices are present.

2) Solutions of the following form

$$P_{12} \neq 0, \text{ or } P_{g12}^0 \equiv 0 \text{ or } P_{g12}^1, \dots, P_{gmn}^0 \neq 0$$

are not allowed, i.e. for each specified component  $P_{g1}$ , one and only one transition is possible with which all spontaneous displacements of several active sublattices disappear at once.

3) Solutions of the following form

$$P_{12} \equiv 0; P_{g12}^1, \dots, P_{g12}^n, \dots, P_{gmn}^0 \neq 0$$

do not satisfy the system (4.12). In other words, antiferroelectric configuration can appear only as a result of "opposing" displacements of ions belonging to one and the same sublattice. From the standpoint of microscopic theories examined here this assumption is reduced to a formal division of statistical integral pertaining to a given sublattice, into two multiplicative groups

$$Z_k = (Z_k^+)^{1/2} (Z_k^-)^{1/2}$$

and to a doubling of the number of equations of state. However, with such an approach the question of the causes of appearance of antiferroelectricity does not gain a more thorough (atomistic) interpretation in comparison with the application of Kittel thermodynamic theory (see paragraph 4 in chapter 3).

We will return to the equations (4.12). It does not appear possible to find a solution of these systems of equations in a general form with arbitrary  $U_k(x, y, z)$ . It is, therefore, expedient to search for approximate methods of solving these equations for each concrete form of  $U_k(x, y, z)$ , i.e. separately for each model theory proposed.

For all methods of defining  $U_k(x, y, z)$ , when determining Curie point it is necessary to use the condition of the functional determinant becoming zero or appearance of complex solutions.

As an illustration we will examine this rule as applied to the existing model theories in which the presence of one ferroactive lattice is assumed. Equations of state are written in the following form:

$$\frac{P_{sx}}{\beta} - \varphi_x^0(T, P_{sx}, P_{sy}, P_{sz}) = 0,$$

$$\frac{P_{sy}}{\beta} - \varphi_y^0(T, P_{sx}, P_{sy}, P_{sz}) = 0,$$

$$\frac{P_{sz}}{\beta} - \varphi_z^0(T, P_{sx}, P_{sy}, P_{sz}) = 0.$$

Inasmuch as  $F_{sx} = \beta P_{sx}$  and  $\epsilon_{sx} = \rho P_{sx}$  it becomes easy to express here the equations in terms of the components of total spontaneous polarization. These equations must coincide with respect to the sense with the equations of state obtained as a result of differentiation of free energy  $A(T, P_{sx}, P_{sy}, P_{sz})$  formed according to thermodynamic theory of ferroelectricity [19]. Therefore, the following may be written:

$$\tau \left[ \frac{P_{sx}}{\beta} - \varphi_x^0(T, P_{sx}, P_{sy}, P_{sz}) \right] = \frac{\partial A(T, P_{sx}, P_{sy}, P_{sz})}{\partial P_{sx}},$$

where  $\tau$  is a dimensionless multiplier.

Next, we have the following for the determinants:

$$\tau \left| \delta_{ij} \frac{1}{\beta} - \frac{\partial \varphi_i^0}{\partial P_{sj}} \right| = \left| \frac{\partial^2 A}{\partial P_{si} \partial P_{sj}} \right|. \quad (4.17)$$

It follows from this that in transitions of the second kind the vanishing of the functional determinant takes place when the right member of (4.17) is equal to zero. According to thermodynamic theory of ferroelectricity this indicates a loss of stability, i.e. an absence of the minimum of free energy. In the case of transitions of the first kind it may be expected that (4.17) will vanish when  $T \rightarrow \Theta$  ( $T > \Theta$ ).

In the region of tetragonal symmetry and above Curie point the determinant has only diagonal terms:

$$\begin{vmatrix} \frac{1}{\beta} - \frac{\partial \varphi_x^0}{\partial P_{sx}} & 0 & 0 \\ 0 & \frac{1}{\beta} - \frac{\partial \varphi_y^0}{\partial P_{sy}} & 0 \\ 0 & 0 & \frac{1}{\beta} - \frac{\partial \varphi_z^0}{\partial P_{sz}} \end{vmatrix}$$

Therefore, one of the conditions for the determinant becoming zero will be:

$$\frac{1}{\beta} - \frac{\partial \varphi_x^0}{\partial P_{sx}} = 0.$$

Making use of (4.12) and (4.10) we will find:

$$k\theta = 6N\alpha^2(x-x)^2 \quad (4.18)$$

or if  $x=0$  at Curie point, then

$$k\theta = 6N\alpha^2 T_c^2. \quad (4.19)$$

Inasmuch as  $\beta Nz'x$  is effective field upon displacement of all ions by a quantity  $x$ , the relationship obtained defines the magnitude of its average potential energy as of the entire field upon the displacement of the sublattice. This corresponds to the case of the so-called maximum oscillations ( $q=0$ ) which play the main role in dynamic theory of ferroelectricity (see chapter 5).

Formulas (4.18) and (4.19) are also a condition for phase transition, expressed in the language of fluctuations in the displacements of active ions. In the case of a phase transition of the second kind, when  $T = \theta$ ,  $x=0$ ,  $\Delta x^2 = x^2$  and the condition (4.18) exists. In the case of a phase transition of the first kind, at the transition point  $x \neq 0$  the nuclei of the new phase appear in the form of fluctuations even before the disappearance of spontaneous polarization and, consequently, the condition must be more complex. We will note that fluctuations in transition region are finite owing to the "self-consistency" of the field  $F$ , which does not allow the appearance of large values of  $P_i$  in (4.11).

Formula (4.18) makes it possible to determine the order of fluctuations of polarization:

$$\Delta P_i^2 \approx N^2(x')^2 \overline{\Delta x^2} = \frac{k\theta N}{3} \approx 10^7 \text{ ex. C/CE,}$$

which agrees well with the results of thermodynamic theory (see chapter 3, paragraph 1, subparagraph 3).

#### Par. Calculation of Internal Electric Fields

##### 1. Determination of Internal (Effective) Field

Internal field  $F$  acting on an atom in a crystal lattice may be represented in the following form:

$$F = E_0 + E_1 \quad (4.20)$$

Here  $E_0$  is an external electric field and  $E_1$  is a field acting on the atom in question from the side of the other atoms of a unit cell. The field  $E_1$  is defined as follows:

$$E_1 = \sum_i \frac{3(p_i r_i - r_i^2 p_i)}{r_i^5} \quad (4.21)$$

where  $p_i$  is dipole moment and  $r_i$  -- the radius of the vector of the  $i$ -th atom of the lattice.

We will examine first the simplest case of a diatomic cubic crystal (for example, of NaCl type). In this case, to calculate the field  $E_1$  it is convenient to separate mentally from the entire volume of the crystal a sphere surrounding the atom in question and having a radius of several

lattice constant. (the so-called Lorentz sphere). Taking of the microscopic structure of the crystal into account, i.e. making use of the expression (4.21) for the calculation of internal field, and the calculation of the lattice sums are necessary only inside the Lorentz sphere. However, for diatomic cubic crystals the corresponding contribution of  $E_1^i$  into the field  $E_1$  is identically equal to zero. This follows from the considerations of symmetry. Outside the Lorentz sphere one may examine the crystal approximately as a homogeneous continuous medium with polarization  $P$  on the surface of the specimen. Calculation of the field  $E_1^d$  in the center of spherical plane in such a medium is a classical problem in electrostatics. The result of the solution of this problem has the following form:

$$E_1^d = \frac{4\pi}{3} P. \quad (4.22)$$

Finally, charges which had appeared owing to polarization on the surface of the specimen (depolarizing field  $E_1^d$ ) will make a contribution to the field  $E_1$ . In the simplest case when the crystal is an ellipsoid (or a shape which is an extreme case of an ellipsoid) and the external field  $E_0$  is oriented along one of its principal axes, the depolarizing field is connected with the polarization of the specimen by the simple relationship:

$$E_1^d = -MP. \quad (4.23)$$

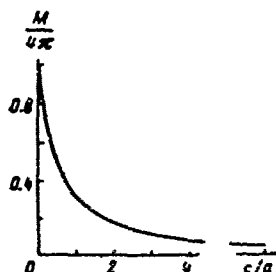


Figure 4.2. Relation of depolarizing factor  $M$  to the  $c/a$  ratio of the principal axes of ellipsoid.

The quantity  $M$  is called depolarizing factor. Its values for different shapes of the specimens have been calculated in the works [20, 21] (see also approximate calculations for the other shapes of the crystal [22, 23]). In Figure 4.2 is shown the relation of  $M$  to the ratio of the axes of ellipsoids of revolution [24]. We will also note an important property of depolarizing factors:  $M_a + M_b + M_c = 4\pi$  where  $M_a$ ,  $M_b$  and  $M_c$  are depolarizing factors in the direction of three principal axes of the ellipsoid.

We will now examine an internal field acting on an atom in a cubic crystal placed between capacitor plates:

$$F = E_0 + 4\pi P - 4\pi P + \frac{4\pi}{3} P. \quad (4.24)$$

Here  $E_0$  is the field between capacitor plates in the absence of a dielectric. Upon insertion of a dielectric the field in the gap between the surface of the dielectric and capacitor plate becomes equal to  $E_0 + 4\pi P$ , the third addend in (4.24) corresponds to a depolarizing field, the fourth -- to the field of Lorentz cavity. In a noncubic crystal, one more addend corresponding to the field created by atoms inside Lorentz sphere would appear in (4.24). We have the following from (4.24):

$$F = E_0 + \frac{4\pi}{3} P. \quad (4.25)$$

It may be seen from (4.25) that macroscopic (i.e. averaged over a volume which is large in comparison with the unit cell) field in the crystal in the case under consideration is simply equal to the field  $E_0$ .

Considerations given above bear first of all an illustrative character. Ewald transform [25, 26] which gives a systematic basis for the examination of the internal and macroscopic field in an arbitrary dipole lattice should be made use of in more complex cases.

## 2. Macroscopic Field in Dipole Lattice and Ewald Method

We will examine the dipoles

$$p(h) = p_0 e^{iQ(h)}, \quad (4.26)$$

located at the points of Bravais lattice ( $x(h) = h_1 a_1 + h_2 a_2 + h_3 a_3$  where  $a_1, a_2$  and  $a_3$  are base vectors). If  $qa \ll 1$ , where "a" is lattice constant, then such a Bravais lattice may be approximately examined as a continuous polarized medium with macroscopic polarization:

$$p(x) = \frac{p}{v} e^{iQx}. \quad (4.27a)$$

(Here  $v$  is the volume of unit cell). Correspondingly, it is possible to determine the macroscopic (i.e. changing little at distances comparable with "a") electric field  $E$  with the aid of electrostatics equation:

$$\text{div} \{E(x) + 4\pi P(x)\} = 0. \quad (4.27b)$$

Only the irrotational component  $P(x)$  makes a contribution in (4.27a). It is easy to ascertain that this component is parallel to  $q$ . Therefore, on the basis of (4.27b) we have:

$$E(x) = -4\pi P(x). \quad (4.28)$$

Taking (4.26) into account we find from (4.28):

$$E(x) = -\frac{4\pi}{v} \left(\frac{q}{q}\right) \cdot \frac{qp}{q} \quad (4.29)$$

The relationship of macroscopic electric field to the direction  $q \rightarrow 0$  has the same physical sense as the depolarizing factor  $M$  in the calculation of internal field by Lorentz method: it takes account of the dependence of depolarizing field on the shape of the specimen.

Effective field  $F$  naturally differs from the macroscopic field  $E$ . An exact expression for the field  $F(x)$  has the form:

$$F_2(x) = \sum_i p_i \frac{\partial^2}{\partial x_i \partial x_k} \sum_n \frac{e^{iqz(h)}}{|x'(h) - x|} \quad (4.30)$$

Using Ewald transform it is possible to reduce the expression for  $F(x)$  to the sum  $\Sigma_k(x)$  and to the rapidly converging series not dependent on the direction  $q \rightarrow 0$ , i.e. Ewald method makes it possible to separate a macroscopic field from a Coulomb field and ensures rapid convergence of lattice sums.

Following Ewald, we will make use of the integral relationships:

$$\frac{2}{\sqrt{\pi}} \int_0^{\infty} e^{-|x(h)-x|p} dp = \frac{1}{x(h)-x} \quad (4.31)$$

Making use of (4.31), (4.30) may be written in the following form:

$$\sum_i p_i \frac{\partial^2}{\partial x_i \partial x_k} \int_0^{\infty} \left\{ \frac{2}{\pi} \sum_n \exp(-|x(h)-x|p^2 + iq|x(h)-x|) \right\} e^{iqz} dp \quad (4.32)$$

It is easy to verify that the expression in braces is a function  $x$  with the periodicity of the lattice. Consequently, it may be represented in the form of an expansion into Fourier series whose coefficients will be equal to [27]:

$$\left[ \begin{array}{l} \text{по ячейке} = \\ \text{with respect} \\ \text{to the cell} \end{array} \right] \quad g(l_1, l_2, l_3) = \frac{1}{v} \sum_n \int_{-h}^h \left\{ \frac{2}{\sqrt{\pi}} e^{-|x'(h)-x|p^2 - i(qz)q|h|} \right\} dx' \quad (4.33)$$

[The summing in (4.33) is done over all vectors of reciprocal lattice].

The sum in (4.33) is equivalent to integration by space with the computation of the integral giving

$$g(l_1, l_2, l_3) = \frac{2\pi}{v} \frac{1}{p^2} \exp\left\{-\frac{|g(l) + q|^2}{4p^2}\right\} \quad (4.34)$$

Thus, the sum within the braces of the expression (4.32) may be written in the following form:

$$\frac{2}{\sqrt{\pi}} \sum_n \exp(-|x(h)-x|p^2 + iq|x(h)-x|) = \sum_l g(l) e^{iq(l)x} = -\frac{2\pi}{v} \sum_l \frac{1}{p^2} e^{-\frac{|g(l)+q|^2}{4p^2} + iq(l)x} \quad (4.35)$$

The equality (4.35) is called theta-function transform. The series in both members of (4.35) converge with large and small values of  $\rho$  respectively. If the integral in (4.35) is divided into two parts and both expressions are made use of, then by a successful selection of the partition parameter it is possible to achieve a rapid convergence of the series. With  $q \rightarrow 0$ , effective field (the calculation of which is especially imperative for ferroelectrics) calculated with the aid of Ewald method has the following form:

$$F_i = - \sum_k \lim_{q \rightarrow 0} \frac{4\pi}{v} \cdot \frac{q N_k}{|q|^2} \cdot p_k + \frac{1}{v} \sum_k \beta_{ik} p_k. \quad (4.36)$$

This result is easily generalized for the case of a complex lattice. We will number different atoms of the base with the symbols  $\mu, \nu$ . Then we have:

$$F_i = - \frac{4\pi}{v} \sum_k \frac{q N_k}{|q|^2} \sum_\mu p_k^\mu + \frac{1}{v} \sum_{\mu, \nu} \beta_{ik}^{\mu\nu} p_k^\nu. \quad (4.37)$$

Here  $\beta_{ik}^{\mu\nu}$  and  $\beta_{ik}^{\nu\mu}$  are structural coefficients of internal Lorentz field, calculated in Ewald method by the following formula:

$$\begin{aligned} \beta_{ik}^{\mu\nu} = R^{2\nu} \sum_h H_{ik}(R x_{\mu\nu}^h) - \\ - \frac{\pi}{R^{2\nu}} \sum_h q_\nu(h) q_\mu(h) G\left(\frac{|q(h)|^2}{4R^2}\right) \exp(iq(h)(x^\mu - x^\nu). \end{aligned} \quad (4.38)$$

Here  $x^\mu$  and  $x^\nu$  are vectors connecting the origin of coordinates with the atoms  $\mu$  and  $\nu$  of the zero unit cell,  $x_{\mu\nu}^h$  is a vector drawn from the point corresponding to atom  $\mu$  of the zero unit cell to the point corresponding to atom  $\nu$  of the cell with the number  $h$ , and  $R$  is partition parameter of the series.

In addition to this, the following notations have been introduced:

$$H_{ik} = \frac{\partial^2}{\partial x_i \partial x_k} H(|z|),$$

where

$$H(|z|) = \frac{2}{\sqrt{\pi}} \int_0^\infty e^{-z^2 s} ds,$$

$$G(s) = \frac{e^{-s}}{s}.$$

A program for the calculation of Lorentz coefficients [28] on the electronic computer BESM-2 using formula (4.38) has been drawn up at the FTI [Physical Engineering Institute] imeni A. F. Ioffe. The program provides a quick and accurate (with accuracy to the sixth decimal point) calculation of the coefficients  $\beta_{ik}^{\mu\nu}$  for crystals of any structure.

In numerical calculations by Ewald method without the employment of electronic computers it is convenient to use tables of special functions given in the work [29]. These tables, used in the calculations of Lorentz coefficients for the ferroelectrics  $\text{KH}_2\text{PO}_4$  [30, 31] and  $\text{NaNO}_2$  [32, 33] considerably reduce the labor consumption of numerical calculations.

### 3. Effective Fields in Complex Dipole Structures

In the preceding subparagraph we examined an internal field acting in a dipole lattice and considered in doing so that the distribution of dipoles on the crystal lattice was known to us. However, in the examination of internal fields in ferroelectrics the electron polarizability and effective charges of ions are usually considered known. But the dipole moments are determined by calculation. With such a method (see, for example, [34] and the bibliography given in this work) the calculation of internal fields is carried out in the following manner.

The internal field  $F$  is written in the following form:

$$F = F_3 + F_g \quad (4.39)$$

where  $F_3$  is an internal field created by the point charges of ions, and  $F_g$  is an internal field created by point dipoles. In accordance with the foregoing, the internal field  $F_g^\mu$  acting on the atom  $\mu$  is equal to:

$$F_g^\mu = \frac{1}{v} \sum_{\nu} \beta_{ik}^{i\nu} p_i \quad (4.40)$$

The field  $F_3^\mu$  may also be represented in the following form:

$$F_3^\mu = \frac{1}{v^{\mu\nu}} \sum_{\nu} f_1^{i\nu} z_\nu \quad (4.41)$$

Here  $\beta_{ik}^{i\nu}$  are structural coefficients of the internal field,  $f_1^{i\nu}$  are structural sums for a lattice of point charges which can also be calculated with the aid of Ewald method [34], and  $z_\nu$  is effective charge of the atom  $\nu$ . The depolarizing field was omitted in (4.40). As may be seen from the subparagraph 1 of the preceding paragraph, this imposes certain restrictions on the shape of the crystal or its external conditions. If there are  $s$  atoms in a unit cell, then defining the polarizability of the atom  $\mu$  as [34]

$$\alpha_\mu = \frac{p_\mu}{E_\mu} \quad (4.42)$$

we will obtain a system of  $3s$  equations for the calculation of  $3s$  values of  $F_i^\mu$ :

$$\frac{1}{v^{\mu\nu}} \sum_{\nu} (\delta_{ik} z_\nu - f_{ik}^{\nu\mu}) p_i = \sum_{\nu} \alpha_\nu F_i^\nu \quad (4.43)$$

Here  $\delta_{ik}$  and  $\delta_{\mu\nu}$  are Kronecker symbols.

We will note that in writing (4.43) it was assumed for simplicity that the polarizability  $\alpha_\mu$  is a scalar quantity, but it is not difficult

to generalize (4.43) for a more complex case also. With a sufficiently large number  $s$ , solution of the system (4.43) may prove to be a complex problem. However, as shown in [34], in a number of cases this problem can be simplified if the symmetry of the structure is taken into account.

In conclusion we will list some of the works devoted to calculations of internal fields in ferroelectrics. Effective fields in crystals of perovskite structure are calculated in the works [35, 36]. The work [37] is devoted to the calculation of internal fields in  $\text{PbTiO}_3$ . Internal fields acting in ferroelectric and antiferroelectric crystals of perovskite type are compared in the works [38, 39]. The work [40] gives a comparison of theory of polarization of ionic crystals based on a representation of internal field, with the respective theories based on dynamic models. A more detailed bibliography and references to previous investigations in this direction may be found in the works listed above.

#### Par. Model Theories for Transitions of Order-Disorder Type

Representations and methods set forth in paragraphs 1 and 2 in these or other modifications were used to explain atomic nature of phase transitions observed in some crystals of the perovskite group and other crystals, in particular in hydrogen-containing ferroelectrics. In the last case the complexity of crystal structure and interaction forces led to the necessity of a number of refinements of the initial model, for example, taking into account the piezoelectric effect in Seignette's salt and tunneling of active ions in  $\text{KH}_2\text{PO}_4$ .

A model of local minima, i.e. representation of potential relief, along which an ion moves, in the form of deep "rectangular" wells was proposed at the earliest stage of development of microscopic theory of ferroelectricity.

In spite of the fact that after a sufficiently long discussion a quite definite opinion formed concerning its inapplicability to barium titanate, this model has a wide field of application for explaining transitions of the order-disorder type and, possibly, some of the cases of phase transitions of the first kind in ferroelectrics with a structure of perovskite type.

##### 1. Model of Local Minima

Suppose potential energy  $U$  from (4.8) has  $n$  deep minima removed to a distance of  $2s$  from each other. We will limit ourselves to an examination of those crystals where these minima are located in pairs on these or other symmetry axes. The position of a minimum is characterized by the subscripts  $j$  and  $k$  where  $j$  is the number of displacement axis and  $k$  -- the number of minimum on this axis ( $j=1, \dots, n/2$ , and  $k=1, 2$ ). In the absence of an external field and with a uniform statistical distribution of active ions in a cell  $U_{jk} = U_{j'k'}$ , and, consequently, the numbers of ions  $N_{jk} = N_{j'k'}$ , with any values of the subscripts. For convenience we will

use a  $U_{jk} = U_{j'k'} = 0$ . Assuming that only ions of one kind can be displaced and making use of (4.9) and (4.10) we will obtain the following expression for free energy:

$$A = A_0(T) - NkT \ln \left\{ \sum_{\alpha} \exp \left\{ \frac{z'F_j \rho}{kT} \right\} + \exp \left\{ \frac{-z'F_j \rho}{kT} \right\} \right\}. \quad (4.43a)$$

If all axes  $j$  are orthogonal (the case of nonorthogonal axes was examined in [41]), then after the differentiation of  $\frac{\partial A}{\partial F_j}$  the equation of state (4.12) will be written in the following form:

$$P_{jj} - N_{\text{res}} \frac{\text{sh} \frac{z'F_j \rho}{kT}}{\sum_j \text{ch} \frac{z'F_j \rho}{kT}} = 0. \quad (4.44)$$

In the absence of an external field it is convenient to write the equation of state (4.44) in the following form:

$$\eta_j = \frac{\text{sh} a_j \eta_j}{\sum_j \text{ch} a_j \eta_j} = 0. \quad (4.45)$$

where  $\eta_j = \left( \frac{N_{j1} - N_{j2}}{N} \right)_{E=0}$  and for the case when there is only one axis  $j$ , has the sense of the order factor  $\eta$

$$a_j = \frac{\beta_j N (z_s)^2}{kT}$$

where  $\beta_j$  is the coefficient of internal field from (4.3). The equation (4.45) corresponds to the equation (4.12) normalized for the maximum dipole polarization  $(P_{\text{sg}})_{\text{max}} = Nsz'$ . Formulas from the theory suggested by Mason and Mattis for  $\text{BaTiO}_3$  are also reduced to this equation if certain inaccuracies permitted in [1] are eliminated. It is assumed in [1] that minima are situated on the principal axes of cubic cell between the  $\text{Ti}^{4+}$  and  $\text{O}^{2-}$  ions ( $j=1, 2, 3$ ) and that owing to a small radius and large space inside the oxygen octahedron the Ti ions can be displaced (Figure 4.3).

With account taken of stability conditions (4.15), for the case shown in Figure 4.3 the system of equations (4.45) has nonzero solutions when  $a_j \gg 3$ , i.e.  $\theta = \frac{\beta_j N (z_s)^2}{3k}$ .

We will compare the results following from the application of the model of local minima to  $\text{BaTiO}_3$ , with the main experimental data.

We will examine different possible solutions of the system (4.45).

I. The region of cubic symmetry:

$$\eta_1 = \eta_2 = \eta_3 = 0. \quad (4.46)$$

II. The region of tetragonal symmetry:

$$\left. \begin{array}{l} \eta_1 \neq 0; \eta_2 = \eta_3 = 0; \\ \eta_1 - \frac{\operatorname{sh} a \eta_1}{2 + \operatorname{ch} A \eta_1} = 0. \end{array} \right\} \quad (4.47)$$

III. The region of orthorhombic symmetry:

$$\left. \begin{array}{l} \eta_1 = \eta_2 \neq 0; \eta_3 = 0; \\ \eta_1 - \frac{\operatorname{sh} a \eta_1}{1 + 2 \operatorname{ch} a \eta_1} = 0. \end{array} \right\} \quad (4.48)$$

IV. The region of rhombohedral symmetry:

$$\left. \begin{array}{l} \eta_1 = \eta_2 = \eta_3 \neq 0; \\ \eta_1 - \frac{1}{3} \operatorname{tg} a \eta_1 = 0. \end{array} \right\} \quad (4.49)$$

On the basis of (4.46)-(4.49) and (4.15) it may be stated that tetragonal phase proves to be stable in a temperature range of from  $0^\circ$  to  $\Theta$ . The orthorhombic and rhombohedral phases prove to be unstable in the temperature range with which we are concerned from the standpoint of the experiment. In addition to this, the following has to be noted. If the regions of fulfillment of conditions for the stability of solutions for the orthorhombic and rhombohedral phases would correspond to experimental data, there would nevertheless exist a considerable contradiction between the theory under consideration and the experiment.

According to calculations, below transition point and in direct proximity to it  $\eta^{\text{III}} \sim \text{const} = \frac{1}{2}$  and  $\eta^{\text{IV}} = \text{const} = \frac{1}{3}$ . However, measurements show that spontaneous polarization along the axis decreases by  $\sqrt{2}$  times after the emergence from the tetragonal into orthorhombic phase [42]. This experimental fact indicates that a turning of ionic displacement axis by  $45^\circ$  takes place with the average magnitude of the displacement of ions remaining constant, and not a redistribution of ions in potential wells in two mutually perpendicular directions the way this follows from the examination of the model theory in question. In precisely the same way the experimental value of  $\eta^{\text{IV}} \sim \frac{1}{3}$  indicates a turning of ionic displacement axis along the volume diagonal of the cube without a change in the magnitude of displacement, and not a redistribution of the displacements of ions in three mutually perpendicular directions.

Thus, as a result of examination of low-temperature phase transitions a conclusion has to be drawn concerning the inconsistency of the application of a model of local minima in the entire temperature range to explain the properties of barium titanate.

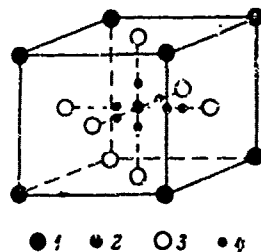


Figure 4.3. Unit cell of BaTiO<sub>3</sub>.  
1 -- Ba; 2 -- Ti; 3 -- O; 4 --  
local minima

We will determine now with the aid of (4.4, 4.43, 4.45) an expression for free energy  $A(T)$  for a tetragonal region in the form of an expansion with respect to  $P_3$ :

$$A(P, T) = A_0(T) + \frac{T-\theta}{6} P_3^2 + \frac{\beta_2^2 N_s^2 \epsilon^2}{3\beta_2^2 \cdot 10^3 (kT)^2} P_3^4 + \dots \quad (4.50)$$

Comparing with (3.12), we see that

$$a = \frac{T-\theta}{6}; \quad \beta \equiv 0; \quad \gamma = \frac{\beta_2^2 N_s^2 \epsilon^2}{3\beta_2^2 \cdot 10^3 (kT)^2}$$

and, consequently, a model with local minima situated in pairs on three mutually perpendicular axes leads to a phase transition of  $\lambda$ -type (critical Curie point).

Making use of (4.50), we will obtain the following relationships characteristic of critical Curie point:

$$P_3^2 = \sqrt{\frac{a}{\gamma}} (\theta - T)^{1/2} = \left( \frac{10^3 \beta_2^2 (kT)^2}{20 \beta_2^2 N_s^2 \epsilon^2} \right)^{1/2} (\theta - T)^{1/2}, \quad (4.51)$$

$$c_p - (c_p)_0 = \frac{2a^2 \theta}{27 \gamma^2} (\theta - T)^{-1/2} = \left( \frac{10^6 \beta_2^4 (kT)^4}{81 \beta_2^4 N_s^4 \epsilon^4} \right)^{1/2} (\theta - T)^{-1/2}, \quad (4.52)$$

$$c_{T>\theta} = \frac{2\pi}{a} = \frac{2\pi}{T-\theta}. \quad (4.53)$$

Upon a substitution of numerical values, Curie constant in (4.53) proves to be lower than the experimental value by more than one order. It is necessary to underscore that attempts at this or other improvement of agreement of theoretical results with experimental results encounter the following difficulty in the case of the model of local minima.

According to the definition the magnitude of entropy jump in a

transition will amount to:

$$\Delta S \approx Nk (\ln W_{T>T_0} - \ln W_{T<T_0}), \quad (4.54)$$

where  $W$  is thermodynamic probability

$$\Delta S = Nk (\ln 6 - \ln 1) \approx 1.79 kN,$$

whereas the experimental value of  $\Delta S \approx (0.02 \text{ to } 0.1) kN$  (see chapter 12, paragraph 1). Such a wide divergence makes the attempts at "adjusting" the model of local minima for describing  $\text{BaTiO}_3$  by means of correction and refinement of its separate components impractical.

We will note one important feature of this model. If it is assumed that there is only one axis  $j$ , i.e. active ions may be only in two wells, then the self-adjoint equation (4.45) has the following form:

$$\eta - \text{th } a_1 \eta = 0, \quad (4.55)$$

whence  $\eta \neq 0$  when  $a_1 > 1$  and, consequently, free energy will be expressed in terms of  $P_S^2$  as

$$A(P_S, T) = A_0(T) + \frac{T-0}{2\theta} P_S^2 + \frac{P_S^3 N (x_1 x_2)^4}{\theta^2 (kT)^2} P_S^4 + \dots$$

i.e.

$$a = \frac{T-0}{2\theta}; \quad \beta = \frac{P_S^3 N (x_1 x_2)^4}{\theta^2 (kT)^2} \quad (\text{см. 3.12}).$$

In other words, in this case the order-disorder transition contains characteristic signs of a phase transition of the second kind. However, the change in entropy is also big in this case:

$$\Delta S = Nk \ln 2 = +0.69 Nk.$$

The large value of  $\Delta S$  is accounted for by the fact that coordinate space of active ions has a discrete character determined by the model selected. If it is assumed that active ions occupy both above and considerably below the transition point a large portion of the "phaseal space" of the cell, i.e. the potential relief is less sharp, then the change in entropy should materially decrease.

The fact that the depth of the minima cannot be too great is indicated by the contradiction which arises upon a comparison of Curie constants and of the quantity characterizing the change in spontaneous polarization at low temperatures in the case of applying theory to  $\text{BaTiO}_3$ . It is natural that assumption concerning sloping wells requires a passing-on from (4.9) to continuous integration when calculating free energy, i.e. to formula (4.10).

## 2. Potential Relief for Ions in BaTiO<sub>3</sub> Crystals

Selection of the shape of potential relief for Ti ions in [1] was based to a considerable degree on the assumption that the bonds between BaTiO<sub>3</sub> ions have to a high degree a covalent character. In addition to this, naturally, the overlapping of electron shells must not be too big so that ion charges would not be very small since otherwise it does not appear possible to explain the large value of spontaneous polarization in BaTiO<sub>3</sub>. Therefore, it is obvious that the bonds in this crystal must have nevertheless a sufficiently well marked ionic character.

Because of the foregoing, a question arises: what may the shape of potential relief be like for different ions and, in particular, is the assumption concerning covalent character of the bonds absolutely necessary for using local minima in the model?

Works by Hagedorn [43], Devonshire [4], Syrkin [44] and by other authors were devoted to the calculation of potential energy of ions of a unit cell. In carrying out the calculations the authors of [4, 44] proceeded from Born treatment of the forces acting between ions in the crystals, i.e. they wrote the expression for potential energy of the ions in the following form:

$$U(x, y, z) = \sum_{ik} U_{ik}(x, y, z) = \sum_{ik} \frac{q_i q_k}{r_{ik}} + \lambda_k (r_{ik})^{-9} - \mu_k (r_{ik})^{-6}. \quad (4.56)$$

All ions in this formula are assumed to be unpolarizable and the subscripts *i* and *k* indicate respectively the number of the ion in the sublattice and the number of the sublattice. According to [44], in taking polarizability into account, additional energy  $U_p$  of an ion having the polarizability  $\alpha_i$  with a small displacement is introduced into the formula (4.56), i.e.  $U_p = -\frac{1}{2} \alpha_i E_0^2(x, y, z)$  where  $E_0(x, y, z)$  is the field acting on the displaced ion.

In [4] it is assumed that the ion is in a spherically symmetric field. In [44] the formulas are determined more precisely with anisotropy taken into account.

As a result of calculations it was found that the only stable position for Ba<sup>2+</sup> and Ti<sup>4+</sup> ions (in the absence of effective field brought about by spontaneous polarization) is the center of a cubic cell. In other words, for the Ti<sup>4+</sup> and Ba<sup>2+</sup> ions there are no potential minima displaced relative to the center of the cell. In doing so, anharmonicalness for the Ba<sup>2+</sup> ions is less marked than for the Ti<sup>4+</sup> ions, i.e. the position of the Ba<sup>2+</sup> ions is the most stable. It was also found that the deviation of the field acting on the O<sup>2-</sup> ions being displaced, from the spherical symmetry is marked considerably more strongly. The

potential energy of  $O^{2-}$  has two minima of  $U_0 \sim 0.5$  electron-volts situated on a line connecting it with two  $Ti^{4+}$  ions at a distance of  $0.33 \text{ \AA}$  from the normal undisplaced position of the  $O^{2-}$  ion. We will note that according to experimental data the displacement of ions amounts to  $\delta_{Ti^{4+}} \sim 0.06 \text{ \AA}$ ;  $\delta_{O^{2-}} \sim 0.12 \text{ \AA}$ ;  $\delta_{Ba^{2+}} \sim 0.00 \text{ \AA}$ .

The results obtained in [44] indicate that the minima of  $U_k(x, y, z)$  displaced from the center of the cell may appear also in purely ionic crystals. Of course, it should be remembered that taking the short-range covalent forces into account may materially affect the results of these calculations and, in particular, it may be found that the potential energy of  $Ti^{4+}$  ions also has minima. It should be noted that Hagedorn's calculations carried out on the basis of using Madelung method lead to similar conclusions regarding the potential energy of  $O^{2-}$ . However, the use of results contained in [43] leads to a big divergence of the magnitudes of the calculated and experimental polarizations at low temperatures. The author of [43] attempts to decrease the value of theoretical polarization by introducing decreased effective charges and polarizability into calculations. In other words, it is assumed that the crystal is not a purely ionic crystal. In this case it is possible to achieve agreement with experimental data. However, in doing so, the values of the charges prove to be very small and the contribution made by the displacement of ions into total polarization amounts to about 6 percent.

Abandonment of a static model and taking the oscillations of ions into account would have made it possible to introduce more accuracy into the calculations of potential energy.

Coming back to the question of applicability of the model of local minima to barium titanate we will note that although the use of active  $O^{2-}$  ions within the framework of the Mason and Mattis theory would have led to a certain improvement of it, it would leave valid a large portion of divergences between the results of theory and experiment. A model of anharmonic oscillators leading to transitions of displacement type (see paragraph 4) proves to be more proper for  $BaTiO_3$ . However, the use of a model of intermediate type with oxygens as the active ions moving between two sloping and shallow potential wells is not precluded for the other ferroelectrics having a structure of perovskite type.

A model in which active ions have two stable equilibrium positions along some of selective directions of displacement is used to explain the properties of some hydrogen-containing ferroelectrics (see below). However, in this case also physical representations and methods of theoretical investigation greatly differ from [1]. We mean, in particular, taking account of correlation, taking account of tunneling through the potential barrier between the minima, failure to use a self-consistent field, etc.

### 3. Phase Transitions of Order-Disorder Type in Hydrogen-Containing Ferroelectrics

In a whole series of hydrogen-containing ferroelectrics a typical example of which may be provided by  $\text{KH}_2\text{PO}_4$ , ferroelectric transition is connected with the ordering of protons. In this case, proton has two possible equilibrium positions on the hydrogen bond with its presence in each one of these equilibrium positions bringing about the appearance of dipole moment. If the protons are ordered, then the dipole moments corresponding to them are combined and the crystals have spontaneous polarization. Upon a change in temperature, protons on the bonds become disordered and spontaneous polarization disappears.

The circumstance that a ferroelectric transition in  $\text{KH}_2\text{PO}_4$  is accompanied by a disordering of protons with a rise of temperature is confirmed by neutron-diffraction [45] and x-ray data [46], by a high isotopic effect for Curie temperature upon replacement of hydrogen with deuterium, and by the measurements of relaxation time of deuterons [47].

Theory of phase transition in  $\text{KH}_2\text{PO}_4$  is illuminated in two detailed surveys [11, 47]. Therefore, we will dwell here only on the basic premises and results of the theory.

The first theory which described comparatively successfully the phase transition in  $\text{KH}_2\text{PO}_4$  was Slater theory [3]. Slater assumed that each proton has two symmetrical positions on the hydrogen bond and that there is only one proton for each hydrogen bond, and that only two hydrogen atoms may be near each  $\text{PO}_4$  group. Only the short-range interactions between protons were taken into account in Slater's calculations which were later improved by Takagi [49]. Slater theory predicts phase transition at a temperature

$$T = \frac{I}{k \ln 2} \quad (4.57)$$

where  $I$  is the difference of dipole energies oriented along and perpendicular to the tetragonal axis. Modified by Yomosa and Nagamida [50] Slater theory, which takes piezoelectric effect into account, predicts anomaly of elastic properties agreeing qualitatively with the experiment, and the magnitude of spontaneous deformation of the crystal which coincides exactly with the experiment. However, Slater theory cannot explain a high isotopic effect -- a nearly twofold rise of Curie temperature upon replacement of hydrogen with deuterium. An attempt to examine long-range forces in Slater's model was made in the work [51]. Theory in [51] satisfactorily describes most of the experimental data with two exceptions: it also predicts too large an entropy of transition (see subparagraph 1 of this paragraph) and does not give a clear explanation of isotopic effect.

The last circumstance is explained by the fact that it does not take account of quantum phenomena (the tunneling of protons) the impor-

tance of which was pointed out by Blinc [52] and which may satisfactorily explain the isotopic effect. Blinc and Svetina [10] suggested a new version of the theory based on the method of group decompositions. Both the short-range and long-range forces, and quantum effects are taken into account in their calculations. Blinc and Svetina theory explains the isotopic effect and predicts correct value of entropy of transition. In the classical extreme it is reduced to the work model [51].

In 1963, de Gennes [53] introduced for the description of transition in  $\text{KH}_2\text{PO}_4$  the so-called isospin method which was used in the works [54, 55, 56] for the study of collective excitations of protons (see in [11] a detailed review of results obtained in [54-55]).

In the investigation of elementary excitations the Hamiltonian of the system is written in the following form:

$$H = H_p + H_L + H_{pL}. \quad (4.58)$$

Here  $H_p$  is the Hamiltonian of proton subsystem in the lattice whose motion is fixed,  $H_L$  is the Hamiltonian of lattice vibrations with the protons at rest, the term  $H_{pL}$  describes the interaction of the proton and lattice subsystems.

Following de Gennes [53], introduction of "isospin" is usually made use of in writing the  $H_p$ . In doing so, each proton is assigned a fictitious spin equal to  $(\frac{1}{2})$  if the proton is in one of the two equilibrium positions, and to  $(-\frac{1}{2})$  if it is in the other equilibrium position. In this case the Hamiltonian  $H_p$  (see [11]) has the following form:

$$-H_p = -2\Gamma \sum_{f=1}^N \sum_{g=1}^N S_{fg}^x + \sum_{f,g=1}^N \sum_{\alpha,\beta} (J_{fg}^{\alpha\beta} S_{f,\alpha}^z S_{g,\beta}^z + J_{fg}^{\beta\alpha} S_{f,\beta}^z S_{g,\alpha}^z) + U_3(S^z) + U_4(S^z). \quad (4.59)$$

Here  $\Gamma$  is proton tunneling frequency [11], the second term describes the tunneling of one proton at the tunneling frequency of the other, the following terms describe respectively the two-, three- and four-part interactions, the subscripts  $f$  and  $g$  number the lattice points, the subscripts  $\alpha$  and  $\beta$  number the protons at the point, the operators  $S_{f,\alpha}^x$  and  $S_{f,\alpha}^z$  are described by Pauli matrices:

$$S^x = \begin{pmatrix} 0 & \frac{1}{2} \\ \frac{1}{2} & 0 \end{pmatrix}; \quad S^z = \begin{pmatrix} \frac{1}{2} & 0 \\ 0 & -\frac{1}{2} \end{pmatrix} \quad (4.60)$$

and act on the eigenfunctions:

$$|\Phi_1\rangle = \begin{pmatrix} 1 \\ 0 \end{pmatrix}; \quad |\Phi_2\rangle = \begin{pmatrix} 0 \\ 1 \end{pmatrix}.$$

If the interaction of protons with the lattice, and the terms of the third ( $U_3$ ) and of the fourth ( $U_4$ ) order in (4.59) are neglected, then the Hamiltonian  $H_p$  will acquire a comparatively simple form:

$$-H_p = 2T \sum_{j=1}^N \sum_{\alpha=1}^2 S_{j\alpha}^2 + \sum_{j, j'} \sum_{\alpha, \beta} (B_{jj'}^{\alpha\beta} S_{j\alpha}^2 S_{j'\beta}^2 + I_{jj'}^{\alpha\beta} S_{j\alpha}^2 S_{j'\beta}^2). \quad (4.61)$$

In the approximation of molecular field (4.61) may be rewritten in the following form:

$$-H_p = H_a \sum_j \sum_{\alpha} S_{j\alpha}^2 + H_b \sum_j \sum_{\alpha} S_{j\alpha}^2. \quad (4.62)$$

where

$$\begin{aligned} H_a &= 2T + 2D \langle S_{j\alpha}^2 \rangle; \\ H_b &= 2I \langle S_{j\alpha}^2 \rangle; \\ D &= \sum_{j, j'} B_{jj'}^{\alpha\beta}; \quad I = \sum_{j, j'} I_{jj'}^{\alpha\beta}; \end{aligned}$$

$\langle S^2 \rangle$  indicates thermal average  $S^2$ .

An examination of the Hamiltonian (4.62) makes it possible to find the frequencies of quantitative "quasi-spin" proton modes and determine (in the approximation of chaotic phases) their temperature dependence. The main result of such an examination amounts to that one of the frequencies of proton modes in  $\text{KH}_2\text{PO}_4$  near Curie point changes with temperature in accordance with the following law:

$$\omega_1^2(q) = \eta(T - \theta) + \epsilon q^2. \quad (4.63)$$

i.e. with  $T \rightarrow \theta$   $\omega_1 \rightarrow 0$  when  $q \rightarrow 0$ . Thus, the behavior of this quasi-spin mode is similar to the behavior near Curie point of ferroelectric lattice vibration (soft mode) in ferroelectrics of displacement type.

Taking into account the interaction of proton subsystem with lattice vibrations, the importance of which was first pointed out by Blinc [57], changes the results set forth above in the following manner [58]. One of proton modes is highly "interlaced" with the frequency of optical lattice vibrations, and the frequency of one of the two bound proton-lattice modes vanishes at the transition point (see in more detail in subparagraph 3, paragraph 4, chapter 5).

Another new interesting result in theory of phase transition in  $\text{KH}_2\text{PO}_4$  is an exact solution recently found by a group of authors [12-16] for a two-dimensional Slater model. In this case, phase transition proves to be of the first kind with a release of latent heat. As in Slater theory,

Curie temperature is equal to

$$\theta = \frac{I}{k \ln 2}.$$

Thermal capacity proves to be above and near  $\theta$   $c_p \sim (T - \theta)^{\frac{1}{2}}$  unlike Slater model in which thermal capacity at  $T = \theta$  remains finite. Dielectric constant is governed by Curie-Weiss law.

#### 4. Ising Model

Different model theories connected with the use of a self-consistent field, as well as Landau phenomenological theory of phase transitions, are applicable only in the case if fluctuations do not play a determinant role, i.e. if the radius of their correlation is small in comparison with the radius of interaction characteristic of the system in which phase transition takes place.

As shown in subparagraph 3, paragraph 1, chapter 3, this region is small for ferroelectric transitions (it amounts to fractions of a degree). However, the behavior of physical quantities in direct proximity to Curie point is of a special interest.

In the region where fluctuations are substantial it was possible to create microscopic theory of phase transitions only for a two-dimensional Ising model. By Ising model is meant a lattice of dipoles each one of which occupies only two positions and interacts only with the nearest neighbors. In a two-dimensional lattice each dipole interacts with four neighbors so that the energies of the parallel and antiparallel dipoles are dissimilar (we will indicate their difference by  $I$ ). Statistical sum for such a lattice can be calculated exactly (see [56]), and free energy related to one dipole proves to be equal to:

$$A(T) = -kT \left\{ \frac{1}{2} \ln 2 + \frac{1}{2\pi} \int_0^\pi \int_0^\pi \ln \left[ \text{ch}^2 \frac{I}{kT} - \text{sh} \frac{I}{kT} (\cos \omega + \cos \omega') \right] \cdot d\omega \cdot d\omega' \right\}. \quad (4.64)$$

The function  $A(T)$  has a singularity at a temperature  $\theta$ , determined from the following condition:

$$\text{sh}^2 \frac{I}{kT} = 1. \quad (4.65)$$

With  $T < \theta$  the lattice is in an ordered state, with  $T > \theta$  it is in a disordered state, and with  $T = \theta$  a phase transition of the second kind takes place. Free energy near the transition point has the following form:

$$A(T) = a - \frac{1}{2} b (T - \theta)^2 \ln |T - \theta|, \quad (4.66)$$

where  $a$  and  $b$  are constants (with  $b > 0$ ) and thus, thermal capacity at the transition point becomes infinite in accordance with the following law:

$$C \sim -\ln|T-\theta|. \quad (4.67)$$

If a phase transition in Ising model is approached from the standpoint of Landau theory, the role of order parameter will be played by the average dipole moment at the point P ("spontaneous polarization" of the lattice). With the approach to the transition point P vanishes as

$$P \sim (T-\theta)^{1/2}. \quad (4.68)$$

Finally, the correlation function  $f(r_{i,k}; r_{i',k'})$  of dipole moments at the lattice points with the coordinates  $r_{i,k}$  and  $r_{i',k'}$  has a singularity at a  $T=\theta$ . For  $T \neq \theta$  the correlation function decreases exponentially from  $r_{i,k} - r_{i',k'}$ . With a  $T=\theta$  the correlation proves to be very strong and  $f$  decreases slowly:

$$f \sim |r_{i,k} - r_{i',k'}|^{-1/2}$$

[compare with formula (3.30)].

Table 7

Behavior of Physical Quantities Describing Phase Transition With  $T \rightarrow \theta$  for a Two-Dimensional Ising Model [60]

Физическая величина	$\nu, \frac{T-\theta}{\theta}$	Электрическое поле E	Поведение величин	Значение критических индексов
2- Спонтанная поляризация $\bar{P}_s$	$\begin{cases} > 0 \\ < 0 \\ 0 \end{cases}$	$\begin{cases} 0 \\ \neq 0 \end{cases}$	$\begin{cases} P_s = 0 \\ P_s \approx \pm  T-\theta ^\beta \\ \pm E^{1/\delta} \end{cases}$	$\begin{cases} - \\ \beta = 1/2 \\ \delta = 15 \end{cases}$
3- Диэлектрическая проницаемость $\epsilon = 4\pi \left(\frac{\partial P}{\partial E}\right)$	$\begin{cases} > 0 \\ < 0 \end{cases}$	$\begin{cases} 0 \\ 0 \end{cases}$	$\begin{cases} \sim T^{-1} \\ \sim  T-\theta ^{-\gamma} \end{cases}$	$\begin{cases} \gamma = 7/4 \\ \gamma' = 7/4 \end{cases}$
4- Корреляционная функция $f(r, r')$ или $\langle P_s(r) P_s(r') - P_s^2 \rangle$	$\begin{cases} > 0 \\ < 0 \end{cases}$	$\begin{cases} 0 \\ 0 \end{cases}$	$\begin{cases}  r-r' ^{-1/2-\nu} \\ \sim T^{-\nu} \\ \sim T^{-\nu'} \end{cases}$	$\begin{cases} \nu = 1/4 \\ \nu = 1 \\ \nu' = 1 \end{cases}$
5- Коherentный длины $\xi$	$\begin{cases} > 0 \\ < 0 \end{cases}$	$\begin{cases} 0 \\ 0 \end{cases}$	$\begin{cases} \sim T^{-\nu} \\ \sim T^{-\nu'} \end{cases}$	$\begin{cases} \nu = 1 \\ \nu' = 1 \end{cases}$

Key: (1) Physical Quantity (5) Coherent length  
 (2) Spontaneous polarization  $\bar{P}_s$  (6) Electric field E  
 (3) Dielectric constant (7) Behavior of the quantity  
 (4) Correlation function (8) Value of critical indices

Physical quantities describing phase transitions in Ising model are systematized in Table 7 where all "critical" indices (see paragraph 1, chapter 3) describing their behavior when  $T \rightarrow \theta$  are given. With the aid of Table 7 it is possible to verify that (as already noted in subparagraph 3, paragraph 1, chapter 3) similarity relationships making it possible

to express critical indices in terms of two fundamental quantities are satisfied for a two-dimensional Ising model.

It is of interest to compare Table 7 with Table 6 (see chapter 3) in which similar results obtained with the aid of Landau theory are given. This comparison indicates the considerable difference in the results obtained on the basis of Ising model and phenomenological theory, and thus underscores the advantage of investigating the microscopic models.

Unfortunately, an analytical solution has not as yet been found for a three-dimensional Ising model. However, there are numerical computerized calculations [61] the main results of which are reduced to the following. With the approach to the transition point from the side of high temperatures, thermal capacity diverges as  $a_1(1 - \Theta)^{0.2}$ , and with the approach from the side of low temperatures it diverges logarithmically as  $a_2 \ln(\Theta - T)$ . In this process, spontaneous polarization  $P_s \sim (\Theta - T)^{5/16}$  and dielectric constant behaves as  $(T)^{-5/4}$ .

Results of numerical calculations for a three-dimensional model are of interest in connection with the results in the work [62] in which it is shown that with a certain relationship of lattice constants the characteristics of thermodynamic quantities in phase transitions of the second kind in crystals must have the same form with a change in symmetry as in a three-dimensional Ising model. The available experimental data for ferroelectrics qualitatively agree with this conclusion (see chapters 8 and 12) in the sense that when thermal capacity exhibits a  $\lambda$ -peak, the shape of the curve on the side of ferroelectric phase is steeper. A more detailed comparison with the experiment has not as yet been made. The work [62] also examines the effect of the oscillations of atoms and quantum effects and it has been found that taking the oscillations of the atoms into account leads to a necessity of adding terms describing the interaction between non-nearest neighbors and also the multi-part interactions, and quantum effects lead to the appearance of a transverse field.

It is shown in [62] that this field may be responsible for the isotopic displacement of transition point, which occurs, for example, in the ferroelectrics  $\text{KH}_2\text{PO}_4$  and  $\text{KD}_2\text{PO}_4$ . (A similar result was also obtained in the works [10, 63]). Apparently these effects do not change the character of characteristics near the transition point.

A qualitative argument in favor of the last statement are the results of an investigation of a two-dimensional Ising model with the interaction of non-nearest neighbors taken into account. Such an investigation carried out in the work [64] in which interaction with dipoles following after the nearest neighbors was taken into account, showed that the shape of the characteristic and the asymptote of the correlation function remain the same as for the usual two-dimensional Ising lattice.

An important distinction in such a case is only that with a certain relationship between the constants the system undergoes three successive

1) Numerical calculations were carried out for a face-centered cubic lattice.

phase transitions with a drop of temperature: first from paraelectric state to ferroelectric state, then from ferroelectric state again to paraelectric state and, finally, to antiferroelectric state.

A situation when transition to ferroelectric state takes place with a rise, and not a drop of temperature, occurs, for example, in Seignette's salt. In the interaction with non-nearest neighbors, Ising model permits such transitions only in a very narrow range of numerical values of the interaction constants. This may correspond to the observed rarity of such transitions.

In the light of the foregoing the importance of experimental investigations of characteristics of physical quantities in transition region should be pointed out once more in order to attempt to understand whether these characteristics correspond to results obtained for a three-dimensional Ising model both in the qualitative and quantitative respect.

#### Par. 4. Model Theories for Displacement-Type Transitions

##### 1. Model of Anharmonic Oscillators

An attempt to utilize representations for nonlinear oscillations of titanium ions to explain the nature of ferroelectricity in BaTiO<sub>3</sub> was made for the first time in a work by Ginzburg [19]. Later these representations were analyzed in detail and developed by Devonshire [4] and Slater [5]. Some problems pertaining to the model of anharmonic oscillators were also examined in [41, 65-67] and in other works.

The main distinction of this model from the model of local minima is assumption of a smooth change of the relationship  $U_k(x, y, z)$  and abandonment of assumption concerning the existence of potential minima "prepared in advance." Owing to the appearance of a self-consistent field when  $T < \theta$  the function  $U_k(xyz)$ , symmetrical for cubic crystals, loses the center of symmetry and a nonzero average displacement of ions takes place. This situation can occur only in the case (see subparagraph 1, paragraph 1) if the oscillations of active ions have a marked anharmonic character, i.e.

$$U_k = a_k(x^2 + y^2 + z^2) + b_{1k}(x^4 + y^4 + z^4) + 2b_{2k}(x^2y^2 + x^2z^2 + y^2z^2). \quad (4.69)$$

Instantaneous positions of the point dipoles appearing upon the displacement of an active ion relative to the center of the cell are considered to be independent of each other. The interaction of the dipoles is taken into account by the introduction of an averaged field determined by the action of all of the remaining dipoles. For this purpose, a term  $z'F$  is introduced into (4.69). In this term  $z'$  is effective charge of the central ion,  $F$  is effective field acting on the ion, and  $r$  is a radius vector connecting the center of symmetry of the cell with the ion. Thus, we have here anharmonic oscillations relative to the center the position of which depends on the magnitude of effective field.

In the integration of (4.8) the anharmonic portion (4.69) is considered to be a small quantity. This makes it possible to expand the exponent under the integral sign into a series with respect to the anharmonic portion. In that case we have:

$$\begin{aligned}
 A = & -NkT \ln \left[ \frac{e}{NkT} (\pi kT)^3 \left( \frac{2\pi}{a} \right)^{3/2} \right] - \frac{Nz^2 F^2}{4\epsilon} + \frac{5N(kT)^2}{4\pi^2} (3b_1 + 2b_2) + \\
 & + NkT (3b_1 + 3b_2) \cdot \frac{z^2 F^2}{4a^3} + \frac{Nz^4}{16a^3} [b_1 (F_x^4 + F_y^4 + F_z^4) + \\
 & + 2b_2 (F_x^2 F_y^2 + F_x^2 F_z^2 + F_y^2 F_z^2)].
 \end{aligned}
 \tag{4.70}$$

Differentiating A with respect to the field F we will obtain a system of equations (4.12). However, inasmuch as free energy is expressed here not in terms of exponents but in the form of a power series it is more convenient, by using (4.12), to represent it as a function of total polarization. This makes it possible to make an immediate comparison with thermodynamic theory, i.e.

$$\begin{aligned}
 A_P(P) = & -NkT \ln \left[ \frac{e}{NkT} (\pi kT)^3 \left( \frac{2\pi}{a} \right)^{3/2} \right] + \frac{N(kT)^2}{a^3} \cdot \frac{3}{2} (3b_1 + 2b_2) + \\
 & + \beta^2 \left( \frac{Nz^2}{4a^3} \right) (2b_1 + 2b_2) \cdot (T - \theta) (P_x^2 + P_y^2 + P_z^2) + \beta^4 \left( \frac{Nz^4}{16a^3} \right) b_1 (P_x^4 + P_y^4 + P_z^4) + \\
 & + 2b_2 (P_x^2 P_y^2 + P_x^2 P_z^2 + P_y^2 P_z^2) + \dots
 \end{aligned}
 \tag{4.71}$$

where  $\theta$  is determined from the condition of the coefficient at  $P^2$  becoming zero, i.e.

$$\theta = \left( \beta^2 \frac{Nz^2}{2} - a \right) \frac{a}{k(3b_1 + 2b_2)}.
 \tag{4.72}$$

According to the calculations in [5]

$$\beta \approx 5.09 \frac{4\pi}{3}; \quad \beta_1 \approx 16.4 \cdot \frac{4\pi}{3}.$$

Formula (4.72) has a sufficiently definite physical sense: namely, a ferroelectric transition ( $\theta > 0$ ) takes place if the constant  $\frac{2Nz^2}{2}$  which characterizes Coulomb forces tending to displace the ion, is larger than the constant which characterizes elastic force tending to return the ion into initial position. In dynamic theory (see chapter 5, paragraph 4) this qualitative definition of condition for existence of phase transition acquires an additional sense in terms of stability of lattice vibrations. The role of anharmonic terms in a phase transition may be explained in the following manner: initial equation defining the relationship P(F) is easily transformed to the form:

$$P_x = \frac{Nz^2 F_x}{2a} - \frac{4z^2 F_x}{2a} \left[ \frac{(3b_1 + 2b_2) kT}{a^2} + \frac{z^2 F_x^2 b_1}{2a^3} \right],
 \tag{4.73}$$

whence it may be seen that taking anharmonic terms into account leads to the appearance in the expression for  $P$  of a term dependent on  $T$ , and accordingly to a weak temperature dependence of atomic polarizability. However, precisely this temperature dependence of the constant leads to a "ferroelectric catastrophe."

It is easy to perceive from (4.71) that the model of anharmonic oscillators makes it possible to "design" phase transitions of different types without coming into contradiction with the experiment, as this takes place in the case of the model of local minima. It may also be seen that the model of anharmonic oscillators describes a very "smooth" phase transition of the second kind with a small change in entropy.

In general, in this model the difficulty is of an opposite character in comparison with the case of Mason model. According to Jaynes' [6] comment, in this case the ferroelectric transition is brought about too "easily." In other words, owing to the presence of electron polarizability in all ions, the effect resulting with a displacement of Ti ions proves to be very strong and it becomes necessary to assume very small values of polarizabilities in order to explain why Curie point is at relatively low temperatures. In accordance with this, the " $4/3$   $\mathcal{N}$ -catastrophe" takes place here in a very mild form. In the case of displacement-type transition in question the entropy jump is relatively small. Physically this is clear from the simple fact that unlike the model of local minima, phase spaces differ little from each other before and after a transition (see Figure 4.1).

It should be noted that for the model of anharmonic oscillators there are many ways for matching with the experiment, in particular, introduction of reasonable values of effective charges and polarizabilities makes it possible to reduce the effect from displacement of active ions: when electrostrictive terms are taken into account the character of a phase transition shifts in the direction of phase transitions of the first kind, etc. In our opinion, a substantial improvement in the accuracy of the model of displacement-type transitions would be that at least two sublattices perform anharmonic oscillations. Indeed, assumption of the existence of only one active sublattice in the presence of an elastic bond [17] with all of the remaining ions appears to be of small probability. Undoubtedly, the case examined in paragraph 1 when all ions perform oscillations that are anharmonic to one or another degree is more practicable.

## 2. Anharmonicity and Fluctuations of Displacements of Active Ions

The method of mathematical treatment of the model of anharmonic oscillators is nothing else but application of thermodynamic perturbation theory to the calculation of free energy of anharmonically oscillating

ions [41]. The energy of an anharmonically oscillating oscillator with its kinetic energy  $p^2/2m$  taken into account has the following form:

$$E = \frac{p^2}{2m} + a(x^2 + y^2 + z^2) + b_1(x^4 + y^4 + z^4) + 2b_2(x^2y^2 + x^2z^2 + y^2z^2) - s'Fx, \quad (4.74)$$

where  $p$  is a pulse. In this case the role of the minor term  $V$  is played by the "anharmonic" portion of potential energy:

$$V = b_1(x^4 + y^4 + z^4) + 2b_2(x^2y^2 + x^2z^2 + y^2z^2).$$

According to thermodynamic perturbation theory [59], free energy may be represented in the following manner:

$$A = A_1 + NV - \frac{N}{2kT} \overline{(V - \bar{V})^2}. \quad (4.75)$$

Here

$$A_1 = -kT \ln \frac{1}{N!} \left[ \int \int \exp\left(-\frac{E_0}{kT}\right) dx \dots dp_s \right]^N, \quad (4.76)$$

$$\bar{V} = \frac{\int \int \exp\left(-\frac{E_0}{kT}\right) V dx \dots dp_s}{\int \int \exp\left(-\frac{E_0}{kT}\right) dx \dots dp_s}, \quad (4.77)$$

$$\overline{V^2} = \frac{\int \int \exp\left(-\frac{E_0}{kT}\right) V^2 dx \dots dp_s}{\int \int \exp\left(-\frac{E_0}{kT}\right) dx \dots dp_s}, \quad (4.78)$$

$$E_0 = \frac{p^2}{2m} + a(x^2 + y^2 + z^2) - s'Fx. \quad (4.79)$$

In (4.75),  $A_1$  indicates "unperturbed" free energy calculated with  $V=0$ ;  $\bar{V}$  is the average value of the perturbing energy, in this case the average value of anharmonic portion of ion energy;  $\overline{V^2} = \overline{(V - \bar{V})^2}$  is the average quadratic fluctuation of the quantity  $V$ .

In the determination of free energy in [5], only the first approximation was obtained which is given by thermodynamic perturbation theory. The average quadratic fluctuation of anharmonic portion of potential energy of the ion, having terms with  $b_1^2$  and  $b_2^2$  is not contained in the expression for free energy (4.71) obtained in these works. The situation is different in regard to polarization. As will be shown below, in this case fluctuations already appear in the first approximation.

Taking (4.71) into account, we find in the first approximation the component of polarization vector along the axis:

$$P_s = \frac{\partial A}{\partial F_s} = -\frac{\partial A_1}{\partial F_s} - N \frac{\partial V}{\partial F_s}. \quad (4.80)$$

We will note that

$$\int_{(p_s y_p z_s)} \int_{(x y z)} f(p_s y_p z_s) f_1(x y z) dx \dots dp_s = \int_{(p_s y_p z_s)} f(p_s y_p z_s) dp_s \dots dp_s \int_{(x y z)} f_1(x y z) dx \dots dx$$

and, therefore, when using the expressions (4.77) and (4.78) the kinetic portion of the energy  $E_0$  does not have to be taken into account at all. Henceforth we will mean by  $E_0$  only the potential energy of an ion performing harmonic oscillations.

Substituting (4.76) and (4.77) into (4.80) we obtain the following after simple transformations (see [41])

$$P_z = Ns'z - \frac{Ns'}{kT} (\bar{zV} - zV), \quad (4.81)$$

where

$$z = \int_{-\infty}^{+\infty} z \exp\left(-\frac{ax^2 - z'F_z x}{kT}\right) dx \int_{-\infty}^{+\infty} \exp\left(-\frac{ax^2 - z'F_z x}{kT}\right) dx, \quad (4.82)$$

$$\bar{zV} = \int_{-\infty}^{+\infty} zV \exp\left(-\frac{ax^2 - z'F_z x}{kT}\right) dx \int_{-\infty}^{+\infty} \exp\left(-\frac{ax^2 - z'F_z x}{kT}\right) dx. \quad (4.83)$$

It should be born in mind that in (4.81) the averaging is done in relation to a harmonically oscillating ion. The first term of this expression represents the average electric moment of a unit of volume brought about by a displacement of the center of oscillations of the oscillators. The second term is explained by the perturbing action of anharmonic oscillations. We will show that it represents a disordering effect of the fluctuation of ion displacements:

$$\bar{zV} - zV = b_1(z^2 - x^4) + 4b_2y^2(z^2 - x^2z).$$

Statistical independence of the coordinates  $xyz$  and the fact that  $\bar{y}_b^2 = \bar{z}^2$  if  $F_x \neq 0$  and  $F_y = F_z = 0$  were taken into account in the calculation.

It easy to see that  $\overline{x^3} = \overline{x^2} \cdot \overline{x} = 2\overline{x}(\overline{\Delta x})^2$  and  $\overline{x^5} = \overline{x^4} \cdot \overline{x} = 4\overline{x}(\overline{\Delta x})^4 + 4\overline{x^3}(\overline{\Delta x^2})$  since  $(\overline{\Delta x^{2n+1}})$ .

In addition to this,  $\overline{y^2} = (\overline{\Delta x})^2$  and  $\overline{(\Delta x)^4} = 3[\overline{(\Delta x)^2}]^2$ . Finally,

$$P_z = Ns'z - \frac{4Ns'z}{kT} \left\{ (3b_1 + 2b_2) [\overline{(\Delta x)^2}]^2 + b_1 \overline{x^2} (\overline{\Delta x})^2 \right\}. \quad (4.84)$$

We find from (4.82) that

$$\left. \begin{aligned} z &= z'F_z/2a, \\ \overline{(\Delta x)^2} &= \frac{\int_{-\infty}^{+\infty} (x-z)^2 \exp\left(-\frac{ax^2 - z'F_z x}{kT}\right) dx}{\int_{-\infty}^{+\infty} \exp\left(-\frac{ax^2 - z'F_z x}{kT}\right) dx} = \frac{kT}{2a}. \end{aligned} \right\} \quad (4.85)$$

Substituting the values of  $x$  and  $\overline{(\Delta x)^2}$  from (4.85) into (4.84), we find (4.73).

The difference between  $\overline{\Delta x^2}$  from (4.18) and (4.85) is explained by the fact that in the former case the averaging was done relative to the total and in the latter -- relative to the unperturbed energy of the oscillator. The absence of singularity in the relationship  $\overline{\Delta x^2}(T) \rightarrow \Theta$  apparently indicates the "hardness" of the oscillator system in a uniform self-consistent field.

Thus, dependence of polarization from (4.73) and dielectric constant on temperature and field strength, characteristic of ferroelectrics, is connected with the fluctuations of ion displacements. With a  $P \rightarrow \Theta$  these fluctuations act as a disordering factor, i.e. they decrease polarization.

Thermodynamic perturbation theory is also applied in the determination of average values of displacements in dynamic theory but with the use of a Hamiltonian expressed in terms of normal mode of the acoustic and optical branches (see subparagraph 2, paragraph 3, chapter 5).

### 3. Statistical Theory of Ferro- and Antiferroelectric transitions

In essence, theories for displacement-type transitions examined above have a semiphenomenological character. Assumption concerning a self-consistent field in (4.8) which "breaks" the lattice symmetry predetermines in advance the possibility, in principle, of the existence of nonzero average ion displacements. In particular, this explains the inability of this theory to explain antiferroelectric transitions from the standpoint of microscopic representations on interaction forces. Naturally, a desire arises to obtain conditions for the existence of  $P_g$  on the basis of internal dynamic and statistical characteristics of a system without resorting to an a priori introduction of the self-consistent field  $F$ .

In other words, the question concerns the construction of a displacement-type model with the correlation of the states taken into account similarly to the way this was done in Ising model. An attempt to construct such a theory was made by V. I. Klyachkin [7, 8, 68]. The distribution of ion displacements in a crystal is examined in the works mentioned from the standpoint of Bogolyubov statistical method [69]. Transition to an ordered state is equivalent to the appearance of a nonzero projection of electric moment  $P_g = z \langle s \rangle$  where  $\langle s \rangle$  is the average displacement of an ion. Next, a sequence of distribution functions  $F_1(s)$ ,  $F_2(s_1 s_2) \dots \dots F_k(s_1 \dots s_k)$  is set up in the configuration space of  $P_g$ . These functions define the probability of the fact that the ions 1, 2, 3... will be displaced from their equilibrium positions by the vectors  $s_1, s_2 \dots, s_k$ . To determine  $s_i$  in accordance with general procedure, systems of integro-differential equations are constructed, which connect a sequence of distribution function:

$$DF_k = LF_{k+1}, \quad (4.86)$$

where  $D$  and  $L$  are differential and integral operators.

In the examination of odd-order statistical moments as the functions of components of ionic displacements it was found that they vanish only in the case if potential energy of a displaced ion, determined from Bogolyubov equations becomes an even function relative to the corresponding space coordinate.

In other words, the appearance of nonzero odd moments, including those of the first order, i.e. of the components of average displacements, is connected with the disappearance of reflection symmetry of potential energy of an ion relative to the respective plane. Thus, a phase transition in a ferroelectric crystal is a transition from a state with a smaller number of the planes of reflection symmetry of potential energy of an ion to a state with a larger number of these planes. Ways for finding the phase transition points appear in accordance with the foregoing.

Setting up a system of nonlinear integro-differential equations for the antisymmetric -- with respect to the respective coordinate -- portion of potential energy of the ion and application of an approximation of the form (4.86) makes it possible to reduce the problem of determination of the phase transition points to a determination of the branching points of nonlinear integral equations with these points corresponding to those temperatures below which a state with a zero antisymmetric portion of potential energy of a displaced ion becomes unstable.

The respective criteria have the following form:

for a ferroelectric

$$[\beta_{\alpha l} - \beta_{\alpha} \langle x^2 \rangle_{\alpha} \beta_{\alpha \alpha}^{kl}] = 0; \quad \alpha = 1, 2, 3;$$

for an antiferroelectric

$$[\beta_{\alpha l} - \beta_{\alpha} \langle x^2 \rangle_{\alpha} \beta_{\alpha \alpha}^{kl}] = 0; \quad l, k = 1, \dots, n.$$

In these formulas  $\beta_{\alpha \alpha}^{kl}$  and  $\beta_{\alpha \alpha}^{kl}$  are elastic moduli of respective states, defined as structural sums of the second derivatives of effective potential energy for the respective coordinate. In doing so, it was taken into account that in the ferroelectric case spontaneous displacements of the separate superstructural sublattices are on the average equal and parallel, and in an antiferroelectric they are equal and antiparallel. It is important that  $\langle x^2 \rangle_{\alpha}$  relates to a state lying above the temperature of transition with the direction  $x_{\alpha}$  being the direction in which the symmetry of potential energy changes during the transition. These same conditions may also be obtained as a result of requirements of thermodynamic stability of the system for the free-energy functional [compare formulas (3.50) and (4.15)].

The simplest case of one lattice undergoing a displacement was examined in [68]. It was found that by expanding the energy of pair interaction with respect to the powers of relative ion displacements up to the fourth-order terms and applying thermodynamic perturbation theory relative to the anharmonic portion of energy it is possible to obtain an expression for  $\langle x_{\alpha}^2 \rangle_k$  and the temperature of transition to tetragonal phase (for perovskite structures). In doing so

$$\left. \begin{matrix} x_{\alpha}^k \\ x_{\beta}^k \end{matrix} \right\} = \xi^k \left[ \sum_{\alpha\beta} (2 + \epsilon_{\alpha\beta}) \frac{\xi_{\alpha\beta}^k}{\xi_{\alpha\beta}^k} \right]^{-1} \begin{pmatrix} 1 - \frac{\xi_{\alpha\alpha}^k}{\xi_{\alpha\alpha}^k} \\ 1 - \frac{\xi_{\beta\beta}^k}{\xi_{\beta\beta}^k} \end{pmatrix}. \quad (4.87)$$

Here  $\xi_{\alpha}^k$  and  $\xi_{\alpha\beta}^k$  are structural sums of the second and fourth derivatives of effective potential energy;  $\xi_{\alpha s}^{kk}$  and  $\xi_{\alpha a}^{kk}$  are the respective sums extended only over a lattice undergoing displacement in a ferro- and antiferroelectric case.

Dynamic criteria of the appearance of ordered structures have the following form:

$$\xi_{\alpha}^k > \xi_{\beta}^k; \quad \xi_{\alpha}^k > \xi_{\beta}^k; \quad \xi_{\alpha}^k > 0.$$

These inequalities are possible with the condition of strong compensation of the positive and negative contributions in the quantity  $\xi_{\alpha}^k$ . Calculation of the average spontaneous displacements indicates that a phase transition of the second kind [ $\langle x_{\alpha} \rangle_k^2 \sim \theta - T$ ] takes place in this case.

Similarly, the values of dielectric susceptibility of each configuration determined in the usual way prove to be exactly coinciding with Ginzburg's [19] and Kittel's [70] thermodynamic expressions:

$$\chi_{\alpha}^k = \frac{C_k}{T - \theta_k}; \quad T > \theta_k; \quad \chi_{\alpha}^k = \frac{1}{2} \frac{C_k}{\theta_k - T}; \quad T < \theta_k,$$

for a ferroelectric, and

$$\chi_{\alpha}^k = |s_k + a_k (T - \theta_k)|^{-1}; \quad T > \theta_k, \\ \chi_{\alpha}^k = |s_k + 2b_k (\theta_k - T)|^{-1}; \quad T < \theta_k,$$

for an antiferroelectric.

A study of thermal capacity jump indicates that the following equality is satisfied in the approximation used:

$$\Delta c_s = \Delta c_a,$$

i.e. it is impossible to identify the ferroelectric or antiferroelectric configurations on the basis of purely calorimetric measurements.

The question of relative stability of the states was also investi-

gated by means of comparing thermodynamic potentials of the ferroelectrics and antiferroelectrics. In doing so, it was found that

$$\Phi_s > \Phi_a \quad \text{when } \theta_a > \theta_s$$

$$\Phi_s < \Phi_a \quad \text{when } \theta_s > \theta_a$$

( $\Phi$  is thermodynamic potential), i.e. a state having a higher Curie temperature is more advantageous.

A necessary condition for setting up appropriate structures is considerable mutual compensation in the coefficient of elasticity of potential energy of the displaced ion by energy brought about by the attractive and repulsive forces in an ionic crystal. This compensation must be considerable to such an extent that elastic coefficient of only one sublattice undergoing a displacement would turn out to be larger than the total elastic coefficient linked with all sublattices of the crystal (compare with subparagraph 1, paragraph 3, chapter 4 and paragraph 4, chapter 5).

The inference mentioned relates to the case of one ferroactive sublattice and is similarly valid both for ferroelectric and antiferroelectric crystals.

In principle, ferroelectric configurations prove to be possible even in the absence of strong Coulomb long-range forces. A necessary condition in this case is the existence of strong exchange interaction which must make negative contributions to the coefficient of elasticity of a displaced ion.

A numerical investigation of the force factors of energy of a pair interaction of ions carried out for perovskite structure indicates that conditions for the appearance of ferroactive state cannot be realized for a B-type lattice in the  $ABO_3$  compound owing to a high symmetry of potential energy of the B ion. Conversely, for an O ion conditions of this kind can be satisfied with reasonable values of polarizabilities, effective charge and of the constants of non-electrostatic interactions (compare with [44] and paragraph 3, subparagraph 2).

In the approximation of one lattice undergoing displacement it turns out that an increase in polarizability of a central B ion leads to difficult conditions for the appearance of ferroactive structures. It turns out that in this same approximation the polarizability of an A ion has very little effect on the appearance of ferroelectricity.

Like the model theories of Devonshire and Slater, statistical theory of phase transition of the second kind based on the representation of one sublattice undergoing a displacement leads to an insufficiently rapid fall-off of spontaneous polarization near Curie point and, as a result of this, to an understated value of the thermal capacity jump. In this connection it may be believed that taking account of ion displacements, which becomes necessary in the investigation of several sub-

lattices undergoing a displacement, will lead to an increase of the rate of growth of spontaneous polarization near the transition point, i.e. it will shift transition of the second kind in the direction of critical Curie point.

### Par. 5. Electron Theory

#### .. Jaynes-Wigner Theory

Microscopic theories examined in the preceding paragraphs are based on the assumption that spontaneous polarization is a result of displacements of ions in a certain internal field determined by these same displacements. In doing so, electron polarization plays an auxiliary part (in spite of the fact that its magnitude may even be larger than ion polarization): electron component of the effective field  $F_e$  grows in proportion to the displacement of ions and thereby increases the forces that are conducive to the formation of spontaneous polarization until the disordering thermal factors and a sharper growth of the restoring forces stops this process. In the case of transitions of the order-disorder type, electron member in the effective field increases the preponderance of ions concentrated in one of discrete states.

From the formal point of view this mechanism is described by the equations of a self-consistent field, which are given here in a maximally simplified form: ( $E=0$ )

$$\left. \begin{aligned} \text{a) } F_{e1} &= \beta_e (P_{e1} + P_{i1}), \\ \text{b) } P_{e1} &= \gamma_e P_{i1}, \\ \text{c) } F_{i1} &= \frac{\beta_i P_{i1}}{1 + \beta_i \gamma_e}, \end{aligned} \right\} \quad (4.88)$$

whence, taking (4.12) into account, we have:

$$\text{r) } P_{i1} - \gamma_e \left( \gamma_e \frac{\beta_e P_{i1}}{1 + \beta_e \gamma_e} \right) = 0,$$

where  $\varphi_e$  is a nonlinear function. In principle we may imagine a reverse case, i.e. transpose the cause and effect:

$$\left. \begin{aligned} \text{a) } F_{i1} &= \beta_i (P_{i1} + F_{e1}), \\ \text{b) } P_{i1} &= \gamma_i F_{e1}, \\ \text{c) } F_{e1} &= \frac{\beta_e P_{i1}}{1 + \beta_e \gamma_i}, \\ \text{r) } P_{e1} - \gamma_e \left( \gamma_e \frac{\beta_e P_{i1}}{1 + \beta_e \gamma_e} \right) &= 0. \end{aligned} \right\} \quad (4.89)$$

The equation (4.89) leads to a phase transition if there is a certain electron statistical mechanism responsible for the nonlinearity of  $\varphi_e(T, P_{se})$ . We will note that this situation does not contradict in principle the thermodynamic theory inasmuch as the order factor  $\eta$  may be expressed in terms of probability of different states of the particles, including electrons (see footnote to chapter 3, paragraph 1, subparagraph 1).

This electron mechanism was suggested for the first time by Wigner and Jaynes [6]. Its essence consists (as applied to BaTiO<sub>3</sub>) in the following.

Barium titanate is not a purely ionic compound and the electron structure is such that the octahedron should be regarded as something whole, and not as a system consisting of independent parts. At the same time, inasmuch as the octahedron consists of closely packed highly polarizable ions, a good shielding of internal Ti ions from external actions exists so that in the first approximation each octahedron may be assigned its own internal electron state not dependent on the state of the neighboring unit cells. Owing to the presence of central symmetry of the cell in the absence of electric field each state must have a definite parity, and in this case the dipole moment does not appear.

However, if two states of opposite parity have close energies, then the interaction between octahedrons will lead to the result that the crystal as a whole will have a minimum of energy and the internal state of each octahedron will be represented in the form of a linear combination of symmetric states. This linear combination of states will have a non-vanishing dipole moment, i.e. spontaneous polarization and an internal field appear.

Thus, the oxygen octahedron is polarized under the effect of the internal field with the magnitude of polarization brought about by the "mixing" of electron states being equal to  $P_e(F_e, T)$ .

Total macroscopic polarization  $P$  consists of the sum of  $P_e + P_i$  and the term  $P_i$ , which represent polarization of ionic residues (including the polarizability of Ba ions and, possibly, of the Ti and O ions). Next, an assumption is made concerning statistical independence of the neighboring cells. The average dipole moment is one and the same in all cells and this average polarization is used for the calculation of local field acting on the cells. Actually the state of a given cell is affected by the neighboring cells more strongly than this is believed and a considerably stronger correlation between the dipole moments of the cells should be expected. This correlation may be taken into account by using the method employed in Ising model for transitions (order-disorder). However, the method of self-consistent field is applied in the work [6].

In the absence of internal field  $F_{se} = \frac{P_e P_{se}}{1 + \beta_e \gamma_i}$ , the electron state of

the octahedron is invariant relative to the symmetry group  $O_h$ . The polarization of the octahedron is brought about by the existence of excited states connected with the fundamental state through the interactions determined with the change of the dipole moment. In the work [6] it is assumed that the electronic excited state of the octahedron has the symmetry  $F_{1u}$  (see chapter 6), i.e. it is thrice degenerated; it was verified that the matrix element of the dipole moment between the fundamental and excited state in this case is not identically equal to zero because of considerations of symmetry. Then, indicating the difference between the energies of the fundamental state and excited states with  $2\epsilon$  and se-

lecting the energy zero in the middle between them, we will obtain the following for an unperturbed Hamiltonian:

$$H_0 = \begin{pmatrix} -\epsilon & 0 & 0 & 0 \\ 0 & \epsilon & 0 & 0 \\ 0 & 0 & \epsilon & 0 \\ 0 & 0 & 0 & \epsilon \end{pmatrix}$$

If the field  $F_{se}$  is applied in the direction of X-axis, the perturbed Hamiltonian is represented in the following form:

$$H = \begin{pmatrix} -\epsilon & v & 0 & 0 \\ v & \epsilon & 0 & 0 \\ 0 & 0 & \epsilon & 0 \\ 0 & 0 & 0 & \epsilon \end{pmatrix}$$

where  $v = -eF_{se} \int_V \psi_0 x \psi_1 dv = \mu F$ ;  $v$  is the volume of unit cell;  $\mu$  is a dipole moment appearing due to the overlapping ("mixing") of the fundamental and excited states. The Hamiltonian  $H$  is diagonalized by means of the transformation matrix

$$S = \begin{pmatrix} \cos \theta & -\sin \theta & 0 & 0 \\ \sin \theta & \cos \theta & 0 & 0 \\ 0 & 0 & 1 & 0 \\ 0 & 0 & 0 & 1 \end{pmatrix}$$

where

$$\tan \theta = \frac{\mu F}{\epsilon}$$

The transformation of  $H$  with the aid of the matrix  $S$  gives

$$SHS^{-1} = \begin{pmatrix} -b\epsilon & 0 & 0 & 0 \\ 0 & b\epsilon & 0 & 0 \\ 0 & 0 & \epsilon & 0 \\ 0 & 0 & 0 & \epsilon \end{pmatrix}$$

where

$$b = \sec 2\theta = \left(1 + \frac{\mu^2 F^2}{\epsilon^2}\right)^{1/2}$$

Therefore, the perturbed cell has the sum of the states:

$$Z = e^{-\frac{\mu\epsilon}{kT}} + e^{-\frac{\mu\epsilon}{kT}} + 2e^{-\frac{\epsilon}{kT}} = 2[e^{-\frac{\mu\epsilon}{kT}} + e^{-\frac{\epsilon}{kT}}]$$

where  $x = \frac{\epsilon}{kT}$  and, consequently, the free energy of the cell will as usually be:

$$A = -NkT \ln Z,$$

whence polarization

$$P_{se} = \frac{\mu}{v} \frac{\sqrt{h^2 - 1}}{b} \cdot \frac{\text{sh } bx}{\text{ch } bx + e^{-2}} \quad (4.90)$$

(4.90) is the unknown nonlinear self-consistent equation (4.89d) for  $P_{se}$ , which under certain conditions has nonzero solutions. Curie point is determined from the condition that  $b=1$ . The model examined makes possible a qualitative description of the basic relationships of ferroelectrics above (for example, Curie-Weiss law) and below (the growth of spontaneous polarization  $P_{se}$ ) Curie point. In spite of this, at the present time electron theory in this version can hardly be considered as something more than an interesting attempt to prove the possibility, in principle, of the existence of an electron mechanism of the appearance of spontaneous polarization. The necessity of using such a mechanism, at least for explaining the properties of  $\text{BaTiO}_3$ , encounters certain objections.

Originally, electron theory was based on a series of x-ray diffraction studies as a result of which no displacements of  $\text{BaTiO}_3$  ions were detected at all. At the present time, the existence of displacements of all  $\text{BaTiO}_3$  ions leaves no doubts. Jaynes considers that this fact in itself does not refute electron theory inasmuch as these displacements are from the standpoint of electron theory a result of the action of a field initially brought about by electronic processes.

However, while acknowledging the existence of ion displacements one must not fail to examine these ions in their statistical interaction. This should introduce substantial corrections into the conditions of the appearance of spontaneous polarization and into the temperatures characteristics obtained on the basis of electron theory. The question of which takes place first -- deformation of electron shells or displacement of ions belongs rather to the field of kinetics of appearance of spontaneous polarization.

According to [71] and [72], ferroelectricity appears in those crystals which contain positive ions with closed electron shells of noble-gas atoms, surrounded by oxygen octahedrons. Jaynes considers this as one of the proofs in favor of electron theory. However, this also indicates that possibly a formation of covalent bonds takes place, which is conducive to a mutual drawing together of positive ions and oxygen ions, forming an octahedron.

Jaynes points out the large value of refractive index in ferroelectrics indicating the large magnitude of electron polarizabilities, which is brought about by the exchange of electrons between oxygen and titanium ions. In addition to this, in his opinion the existence of a maximum in refractive index near Curie point also indicates a change in the electron structure of the crystal. However, these facts are not a proof of inconsistency of ionic theories. There is no doubt that a certain rearrangement of electron shells near Curie point (even from

the standpoint of ionic theories) must take place. However, it should be noted that the maximum of optical refractive index is very insignificant and amounts to  $\sim 3$  percent of its normal value. And the existence of a frequency relaxation effect with which  $\epsilon$  decreases approximately by hundreds of times, indicates by itself the enormous role which the displacements of ions play.

Finally, one of the main inferences in [6] -- prediction of absorption line in the region of 10 mc which corresponds to an initial energy level of  $\sim 4 k\theta$ , is not confirmed by the present-day data on infrared spectra of barium titanate (see chapter 15).

Modernized versions of electron theory of ferroelectricity are set forth in the works [73, 74].

With a combining of atoms into a crystal lattice, electron density considerably changes. A hybridization of atomic orbitals, for example, sp- or pd-hybridization may take place in this process. Hybridization of states with the quantum numbers of orbital moment differing by unity leads to the appearance of dipole moment of the atom. In the work [73] appearance of spontaneous polarization is linked with the hybridization of electron orbits. In doing so, a system of  $N$  identical atoms is examined in [73] with there being one valent electron for each atom. The Hamiltonian of the system is written in the same form as in the work [75] but terms describing the exchange interaction are omitted (these terms may prove to be essential in describing the ferronagnetics). Next, the dielectric constant is calculated using the procedure of double-time Green functions. The main results of the work [73] amount to an explanation of Curie-Weiss law and of the law of "dyad" for dielectric constant, and also to a prediction of existence of resonance absorption of electromagnetic field at the frequency of collective excitation of electron subsystem (Frenkel exciton)  $\Omega \sim 2\theta$ . At a  $\theta \sim 400^\circ K$ , an absorption of electromagnetic field with a wavelength  $\lambda \sim 3.5 \cdot 10^3$  cm should correspond to such a "ferroelectric exciton."

An attempt is made in the work [74] to take into account the correlation effects between electrons in the vacant sheaths of the A and B ions in ferroelectric crystals of  $ABO_3$  type.

An inference is drawn that, in principle, correlation effects may lead to the appearance of spontaneous polarization. Their role depends on the difference in the energies of the levels of electrons of A and B atoms and more considerably, for example, for  $BaTiO_3$  than for  $BaZrO_3$  or for  $CaTiO_3$ .

## 2. Pseudo-Yang-Teller Effect and Ferroelectric Transitions

Dynamic approach based on the conception of ferroelectric mode the frequency of which  $\omega_T$  becomes zero or reaches anomalously small values at the transition point (see paragraph 4, chapter 5), has become a standard approach to the description of ferroelectric transitions of displacement type.

In adiabatic approximation (see subparagraph 1, paragraph 1, chapter 5) underlies theory of crystal lattices. The sense of this approximation amounts to that the motion of electron and nuclear subsystems of the crystal is separated, with the electron term dependent on the coordinates of nuclei as on parameters being a potential function describing their oscillations. Therefore, an inference has to be drawn that when  $\omega_T \rightarrow 0$  substantial changes also take place in electron terms responsible for such anomalous behaviors of  $\omega_T$  (see also [81]).

An assumption, illustrated on models, that pseudo-Yang-Teller effect may be a cause of the appearance of spontaneous polarization for ferroelectrics of displacement type was expressed in a whole series of theoretical works [76-80].

We will recall at first the sense of Yang-Teller theorem [81]. In molecules or crystals with a sufficiently high symmetry the fundamental electron state could prove to be degenerate (degeneracy not connected with spin is meant). In order that the respective configuration of the system be stable, the energy of electron term as a function of distances between atoms must have a minimum. It follows from this that with small displacements of nuclei a change in the energy of the term must not contain terms linear with respect to displacements. Yang-Teller theorem states that such linear terms always exist for a degenerate fundamental state.

We will expand the Hamiltonian of the electron subsystem  $\mathcal{H}_e$  with respect to the powers of normal vibrations of the lattice:

$$\pi_e = \pi_0 + \sum_j \frac{\partial \pi}{\partial Q_j} Q_j + \frac{1}{2} \sum_{j,k} \frac{\partial^2 \pi}{\partial Q_j \partial Q_k} Q_j Q_k. \quad (4.91)$$

If the fundamental state is degenerate, then linear terms in (4.91) are not equal to zero and the splitting of the electron term may be found with the aid of theory of perturbations for degenerate levels. We will examine the simplest case of a twice degenerated level unstable relative to the normal vibration Y. We will denote the nondiagonal matrix element of the linear term in (4.91) with  $N^{-1/2} VY$  where N is the number of electrons, and the diagonal matrix element -- with  $E_0$ . Secular equation of perturbation theory will have the following form:

$$\begin{vmatrix} E_0 - E & N^{-1/2} VY \\ N^{-1/2} VY & E_0 - E \end{vmatrix} = 0. \quad (4.92)$$

The degenerate term will split in this manner into two levels with the magnitude of the split being equal to  $2N^{-1/2} VY$ , as may be seen from (4.92).

We will now pass on to a case of two nondegenerate but near levels. It turns out that in this case the linear terms in (4.91) are also nonzero until the distance between the levels is less than  $2N^{1/2} VY$  (notation for nondiagonal matrix element has been retained here).

The interaction of two near levels through lattice vibrations, connected with linear terms in (4.91) has the name of pseudo-Yang-Teller effect.

Following the work [79], we will show, using the simplest model as an example, how pseudo-Yang-Teller effect may lead to the appearance of spontaneous polarization. We will examine an ionic crystal with two near zones. In doing so, we will neglect their dispersion (the distance between the zones  $\Delta$ ). We will assume that these zones are of different parity. In this case, antisymmetric normal vibration  $Y_U$  is responsible for the pseudo-Yang-Teller effect. A macroscopic dipole moment appears when there are distortions connected with it. 1)

In the presence of two near levels, perturbation theory gives:

$$E_{1,2} = \frac{\Delta}{2} \pm \sqrt{\frac{\Delta^2}{4} + \frac{v^2 Y^2}{N}}. \quad (4.93)$$

With account taken of (4.93) we will obtain the following for the portion of crystal energy  $E$  dependent on the normal coordinate  $Y$ :

$$E(Y) = n_1 \left( \frac{\Delta}{2} - \sqrt{\frac{\Delta^2}{4} + \frac{v^2 Y^2}{N}} \right) + n_2 \left( \frac{\Delta}{2} + \sqrt{\frac{\Delta^2}{4} + \frac{v^2 Y^2}{N}} \right) + \frac{1}{2} M \omega^2 Y^2. \quad (4.94)$$

$M$  and  $\omega$  are here the reduced mass and the frequency of normal vibration.

$$n_1 = f_1 N = \frac{\lambda}{2 \pi \nu \tau}, \quad (4.95)$$

$$W = \frac{1}{2} \left( \Delta + \frac{V}{M \omega^2} + \frac{2 v^2 Y^2}{4 V^2} \right). \quad (4.96)$$

An analysis of these expressions shows that if

$$\frac{M \omega^2 \Delta}{2 V^2} < 1, \quad (4.97)$$

the equilibrium position of ions changes by the amount:

$$Y_0 = N^{1/2} \left\{ \frac{V - f_1 V^2}{2 V^2} - \frac{\Delta^2}{4 V^2} \right\}. \quad (4.98)$$

This means that two equivalent lower-symmetry configurations exist in each one of which the crystal has a permanent dipole moment. The value of  $Y$  and accordingly of spontaneous polarization is maximum when  $T=0$  and decreases with an increase of  $T$ .

At Curie temperature:

$$T_0 = V \left[ \frac{2 V^2 + M \omega^2 \Delta}{2 V^2 - M \omega^2 \Delta} \right]^{-1} \quad (4.99)$$

1) It was shown in the works [78, 82] that near zones of opposite parity must exist in  $\text{PbTiO}_3$ . If the zones had the same parity the distortions of the crystals would be connected with symmetric vibration and no macroscopic dipole moment would appear with them. If the zones are degenerate, the "active" normal vibration must also be degenerate and a whole series of low-symmetry configurations is possible.

the distortion of the lattice disappears and the crystal undergoes a phase transition of the second kind.

The effect under consideration leads to a high overnormalization of the frequency of the vibration  $\gamma$ , dependent on temperature. The frequencies of this vibration  $\omega_{c+}$  and  $\omega_{c-}$  prove to be respectively equal to the following with the approach to Curie point from the side of high and low temperatures:

$$\left. \begin{aligned} \left(\frac{\omega_{c+}}{\omega}\right)^2 &= \frac{2V^2}{M\omega^2\Delta} (j_+ - j_-) + 1, \\ \left(\frac{\omega_{c-}}{\omega}\right)^2 &= 1 - \left[ \frac{M\omega^2\Delta}{2V^2(j_+ - j_-)} \right]^2. \end{aligned} \right\} \quad (4.100)$$

With a  $T = \theta$   $\omega_{c+} = \omega_{c-} = 0$  (compare with paragraph 4, chapter 5).

The expansion (4.100) gives the following near  $\theta$  with accuracy to linear terms:

$$\left(\frac{\omega_{c+}}{\omega_{c-}}\right)^2 = 2. \quad (4.101)$$

i.e. the law of dyad well known from phenomenological theory (see paragraph 4, chapter 6).

It may already be seen from the foregoing that "interzone" theory of ferroelectricity is very promising. Very recently such an approach was used to describe spontaneous polarization [83] and successive phase transitions in  $\text{BaTiO}_3$  [84] and for the calculation of behavior of ferroelectric modes in an electric field [85].

Microscopic model theories examined in this chapter contributed to a considerable degree to the formation of representations concerning the nature of ferroelectric transitions. At the same time, there is no doubt that in their further development microscopic theories must be constructed on the basis of more improved physical approximations.

In the investigations of ferroelectrics within the framework of statistical method it is desirable to abandon the use of representations concerning self-consistent field, which convey to the theory a semi-macroscopic character. In other words, the question concerns the further development of an approach in which correlation between the states of active ions is taken into account. It is also obvious that it is necessary to abandon the separation of lattice elements into ferroactive and inactive elements, and examine the state of a crystal on the assumption that all of its elements perform anharmonic oscillations to one or another degree.

Development of Ising model and of interzone theory of spontaneous polarization also appears important.

The use of purely statistical methods precludes the possibility

of obtaining information on the special features of vibration spectrum of ferroelectrics. This gap is filled by dynamic theory which examines lattice vibrations. However, an explanation of temperature dependences of the parameters of the crystals and in general of the mechanism of ferroelectric transitions is possible at the present on the basis of representations concerning anharmonicity of oscillations and, consequently, with the condition of examination of interaction of different modes using the means of perturbation theory. This makes clear the reasons for the consolidation of dynamic and statistical methods of investigation, taking place at the present time.

#### BIBLIOGRAPHY

1. W. P. Mason, B. T. Matthias, Phys. Rev., Vol 74, p 1661 (1948).
2. W. Mason. P'yezoelektricheskiye Kristally i Ikh Primeneniye v Ul'traakustike [Piezoelectric Crystals and Their Application in Ultrasonics]. IL [Foreign Literature Press], Moscow. (1962).
3. I. C. Slater, J. Chem. Phys., Vol 9, p 16 (1941).
4. A. G. Devonshire, Phil. Mag., Vol 40, p 1040 (1949).
5. I. C. Slater, Phys. Rev., Vol 78, p 748 (1950).
6. E. Jaynes. Ferroelectricity. Princeton University Press (1953).
7. V. I. Klyachkin, FTT, Vol 2, p 5 (1960).
8. V. I. Klyachkin. In a book: Fizika Dielektrikov [Physics of Dielectrics], Works of the 2nd Conference on the Physics of Dielectrics, USSR Academy of Sciences Press, Moscow. p 297 (1960).
9. V. G. Vaks. Voprosy Teorii Fazovykh Prevrashcheniy i Spektrov Vozbuzhdeniy v Sistemakh Mnogikh Tel [Problems of Theory of Phase Transformations and Excitation Spectra in Multibody Systems]. Doctoral dissertation, IPAN SSSR [USSR Institute of Applied Atomic Science], Leningrad. (1967).
10. R. Blinc, S. Svetina, Phys. Rev., Vol 147, pp 423, 430 (1966).
11. R. Blinc. Ferroelectricity (in lectures on condensed matter). Trieste (1968).
12. F. I. Wu, Phys. Rev. Lett., Vol 18, p 605 (1967).
13. E. H. Lieb, Phys. Rev. Lett., Vol 19, p 198 (1967); Vol 18, p 1046 (1967).
14. B. Sutherland, Phys. Rev. Lett., Vol 19, p 103 (1967).

15. C. P. Yang, Phys. Rev. Lett., Vol 19, p 586 (1967).
16. B. Sutherland, C. N. Yang, C. P. Yang, Phys. Rev. Lett., Vol 19, p 588 (1967).
17. R. Ye. Pasyukov, Izv. AN SSSR, ser. fiz. [Bulletin of USSR Academy of Sciences, physical series], Vol 21, p 340 (1956).
18. V. I. Smirnov. Kurs Matematiki, [A Course in Mathematics], Vol 3. GITL [State Publishing House for Technical and Theoretical Literature], Moscow--Leningrad, pp 63-70 (1953).
19. V. L. Ginzburg, UFN [Achievements of Physical Sciences], Vol 38, p 430 (1949).
20. I. A. Osborn, Phys. Rev., Vol 67, p 351 (1945).
21. E. C. Stoner, Phil. Mag., Vol 36, p 803 (1945).
22. I. L. Snock, Physica, Vol 1, p 649 (1933).
23. R. M. Bozorth, D. M. Chapin, J. Appl. Phys., Vol 13, p 320, (1942).
24. Ch. Kittel. Vvedeniye v Fiziky Tverdogo Tela [Introduction to Solid State Physics]. GIFML [State Publishing House for Physics and Mathematics Literature], Moscow (1962).
25. P. P. Ewald, Ann. Phys., Vol 64, p 253 (1921).
26. H. Kornfeld, Z. Phys., Vol 22, p 27, (1924).
27. M. Born and K. Huang. Dinamicheskaya Teoriya [Dynamic Theory]. IL, Moscow (1958).
28. M. S. Shur, Yu. N. Tsarev, FTT, Vol 10, p 2899 (1968).
29. M. S. Shur, Primeneniye Teorii Grupp dlya Zanaliza i Rascheta Kolebatel'nykh Spektrov Kristalov [Application of Group Theory for Analysis and Calculation of Vibration Spectra in Crystals], FTI AN SSSR [Physical Engineering Institute, Academy of Sciences USSR], Ph.D. Candidate's dissertation. Leningrad (1967).
30. M. S. Shur, FTT, Vol 8, p 57 (1967).
31. M. S. Shur, FTT, Vol 8, p 1267 (1967).
32. E. V. Chisler, M. S. Shur, Phys. Stat. Sol., Vol 47, p 163, (1966).
33. E. V. Chisler, M. S. Shur, Izv. AN SSSR, ser. fiz., Vol 31, p 1098 (1967).

34. S. P. Solov'yov, Yu. N. Venevtsev, G. S. Zhdanov, Kristallografiya [Crystallography], Vol 5, p 718 (1960).
35. V. Kh. Kozlovskiy, ZhTF [Journal of Technical Physics], Vol 21, p 1388 (1951).
36. Yu. N. Venevtsev, S. P. Solov'yov, G. S. Zhdanov, Kristallografiya, Vol 4, p 576 (1959).
37. Yu. N. Venevtsev, G. S. Zhdanov, S. P. Solov'yov and V. V. Ivanova, Kristallografiya, Vol 4, p 255 (1959).
38. N. N. Kravnik, FTT [Solid State Physics], Vole 2, p 993 (1960).
39. N. N. Kraynik, Izv. AN SSSR, ser. fiz., Vol 24, p 1187 (1960).
40. S. N. Koykov, FTT, Vol 9, p 2915 (1967).
41. G. A. Smolenskiy and R. Ye. Pasyukov, ZhETF [Journal of Experimental and Theoretical Physics], Vol 25, p 57 (1953).
42. F. Jona, D. Shirane. Segnetoelektricheskiye Kristaly [Ferroelectric Crystals]. Mir Publishing House, Moscow (1965).
43. P. Hagedorn, Z. Phys., Vol 133, p 394 (1952).
44. L. N. Syrkin, Kristallografiya, Vol 1, p 274 (1956).
45. G. E. Bacon, R. S. Pease, Proc. Roy. Soc. London, Vol 230, p 359 (1955).
46. B. C. Frager, R. Pepinsky, Acta Cryst., Vol 6, p 273 (1953).
47. V. H. Schmidt, E. A. Vehling, Phys. Rev., Vol 126, p 477 (1962).
48. E. A. Vehling. Lectures on Theoretical Physics, Vol 5, N.Y. (1963).
49. Y. Takagi, J. Phys. Sci. Japan, Vol 3, p 271 (1948); Proc. Phys. Math. Soc. Japan, Vol 23, p 44 (1941).
50. S. Yomosa, T. Nagamiga, Progr. Theor. Phys., Vol 4, p 263 (1949).
51. H. B. Silsbec, E. A. Vehling, V. H. Schmidt, Phys. Rev., Vol 133, p A 165 (1964).
52. R. Blinc, J. Phys. Chem. Sol., Vol 13, p 204 (1960).
53. P. G. de Gennes, Solid State Comm., Vol 1, p 132 (1963).
54. M. Tokunada, T. Matsubara, Progr. Theor. Phys., Vol 35, p 581 (1966); ibid., Vol 36, p 857 (1966).

55. I. Villain, S. Stamenovic, *Phys. State Solid*, Vol 15, p 585 (1966)
56. R. Brout, K. A. Mueller, H. Thomas, *Solid State Comm.*, Vol 4, p 507 (1960).
57. R. Blinc, M. Ribaric, *Phys. Rev.*, Vol 130, p 1816 (1963).
58. K. Kobayashi, *J. Phys. Soc. Japan*, Vol 24, p 497 (1968).
59. L. D. Landau and Ye. M. Lifshits. Statisticheskaya Fizika [Statistical Physics]. Nauka Publishing House, Moscow (1964).
60. L. P. Kodanoff et al., *Rev. Mod. Phys.*, Vol 39, p 395 (1967)
61. C. DoMb, A. R. Miedema. *Progress in Low-Temperature Physics*, Vol 4, New York, p 296 (1964).
62. V. G. Baks, A. I. Larkin, ZhETF, Vol 49, p 975 (1965).
63. T. Matsubara, M. Takunaga, *Progr. Theor. Phys.*, Vol 35, p 581 (1966).
64. V. G. Vaks, A. I. Larkin, Yu. N. Ovchinnikov, ZhETF, Vol 49, p 1180 (1965).
65. V. Kh. Kozlovskiy, FTI, Vol 2, p 1733 (1960).
66. V. Kh. Kozlovskiy, Kristallografiya, Vol 8, p 819 (1963).
67. H. C. Schweinler, *Phys. Rev.*, Vol 87, p 5 (1952).
68. V. I. Klyachkin, FTI, Vol 1, p 1874 (1959).
69. N. N. Bogolyubov. Problemy Dinamicheskoy Teorii v Statisticheskoy Fizike [Problems of Dynamic Theory in Statistical Physics]. GITTL, Moscow--Leningrad (1966).
70. C. Kittel, *Phys. Rev.*, Vol 82, p 729 (1951).
71. B. T. Matthias, *Phys. Rev.*, Vol 35, p 1771 (1949).
72. G. A. Smolenskiy, I. V. Kozhevnikova, DAN SSSR [Proceedings of USSR Academy of Sciences], Vol 76, p 519 (1951).
73. V. A. Popov, Izv. AN SSSR, ser. fiz., Vol 31, p 1038 (1967).
74. V. T. Khozyainov, Izv. AN SSSR, Vol 28, p 620 (1964).
75. N. N. Bogolyubov, S. V. Tyablikov, ZhETF, Vol 19, p 251 (1949).
76. K. P. Sinha, A. P. Sinha, *Indian. J. Pure Appl. Phys.*, Vol 2, p 91 (1964).

77. R. Engeman. Microscopic Theory of Ionic Dielectrics. A.E.C., A19129, Rept 1, A 934 (1964).
78. Bersuker, Phys. Lett., Vol 20, p 589 (1966).
79. N. Kristoffel, P. Konsin, Physica Status Solidi, Vol 21, K39 (1967).
80. B. D. Silverman, Proc. Int. Meet. on Ferroelectricity, Vol 1, Prague (1966).
81. L. D. Landau and Ye. M. Lifshits. Kvantovaya Mekhanika [Quantum Mechanics]. GIFML, Moscow (1963).
82. W. Cochran, Phys. Rev. Lett., Vol 3, p 412 (1959).
83. I. B. Bersuker, B. G. Vekhter, FTT, Vol 9, p 2652 (1967).
84. I. B. Bersuke, B. G. Vekhter. Tez. dokl. 6-y Vsesoyuzn. konf. po Segnetoelektrichestvu [Thesees of Reports at the 6th All-Union Conference on Ferroelectricity], Riga, p 17 (1968).
85. N. N. Kristofel', P. I. Konsin. Tez. dokl. 6-y Vsesoyuzn. konf. po Segnetoelektrichestvu, Riga, p 17 (1968).

## CHAPTER 5. DYNAMIC THEORY OF FERROELECTRICITY

Owing to thermal agitation the atoms in a crystal perform small oscillations near equilibrium positions. The smallness of oscillatory displacements in comparison with lattice constants makes it possible to regard them (in the first approximation) as an aggregate of so-called normal oscillations, i.e. independent plane waves to each one of which corresponds its own frequency and wavelength.

Normal oscillations representing displacements of atomic sublattices of a crystal as a whole relative to each other are called limit oscillations. Some of the limit oscillations may be connected with a change of the macroscopic dipole moment of a crystal. Such oscillations are usually called dipole oscillations.

The equations of motion for a normal coordinate  $Q$  of a limit dipole oscillation in an electric field  $Ee^{i\omega t}$  may be written in the following form without taking damping into account:

$$\ddot{Q} + \omega_0^2 Q = \frac{z^*}{m} E e^{i\omega t}. \quad (5.1)$$

The equation (5.1) represents equation of motion of a harmonic oscillator. Here  $\omega_0$  is the frequency of normal oscillation,  $z^*$  -- effective dynamic charge of the mode in question (equal for the simplest model to ionic charge), and  $m$  -- reduced mass for a given normal oscillation.

Polarization  $P$  connected with the normal coordinate  $Q$  is equal to:

$$P = z^* N Q. \quad (5.2)$$

We will substitute (5.2) into (5.1) and will seek solution in the following form:

$$P = P_0 e^{i\omega t}. \quad (5.3)$$

Then we have:

$$-\omega^2 P_A + \omega_0^2 P_A = \frac{z^2 N}{m} E. \quad (5.4)$$

It follows from (5.4) that

$$\epsilon_g = 4\pi \frac{\partial P_A}{\partial E} = \frac{a}{\omega_0^2 - \omega^2}, \quad (5.5)$$

where  $\epsilon_g$  is contribution to the dielectric constant of the crystal  $\epsilon$  owing to the normal oscillation  $Q$ ,  $a = \frac{z^2 N}{m}$ .

If the crystal has several limit dipole oscillations, the expression for  $\epsilon$  acquires the following form:

$$\epsilon = \epsilon_\infty + \sum_k \frac{a_k}{\omega_k^2 - \omega^2}. \quad (5.6)$$

Here  $\epsilon_\infty$  is the high-frequency dielectric constant, i.e. at the frequencies  $\omega \gg \omega_k$ ,  $\omega_k$  indicates frequencies of the limit dipole oscillations, and  $a_k$  -- the forces of the oscillators.

In the expression (5.6) the damping of normal oscillations may be taken into account phenomenologically by assigning to each mode the damping constant  $\gamma_k$ :

$$\epsilon = \epsilon_\infty + \sum_k \frac{a_k}{\omega_k^2 - \omega^2 + 2i\omega_k \gamma_k}. \quad (5.7)$$

It may be seen from (5.7) that if in a certain temperature range the dielectric constant  $\epsilon$  (with  $\omega \ll \omega_k$ ) sharply increases and damping is small (i.e.  $\gamma_k \ll \omega_k$ ), then one of the frequencies  $\omega_k$  must sharply decrease at these temperatures. It follows from this that in a ferroelectric transition (in any case in a transition of displacement type) the frequency of one of the limit dipole oscillations of the lattice must sharply decrease with the approach to Curie point.

An oscillation whose frequency sharply decreases when  $T \rightarrow \Theta$  is usually called "ferroelectric oscillation" or "soft mode." The concept of "soft mode" was put forth by V. L. Ginzburg in 1949 for ferroelectric transitions.

Proceeding from phenomenological theory, Ginzburg showed [1-3] that in the case of a phase transition of the second kind (or of the first kind approaching critical point) the frequency of one of normal oscillations of the crystal lattice  $\omega_k$  must become zero, with the phase transition being ferroelectric if  $\omega_k$  is the frequency of the limit dipole oscillation.

Later, Anderson [4] obtained the same results on the basis of microscopic theory. This problem was investigated in a greater detail by Cochran [5-7] who examined it using a microscopic model of a diatomic ionic crystal as an example.

From the standpoint of Ginzburg--Anderson--Cochran theory, investigation of micromechanism of a ferroelectric transition of displacement type means, first of all, finding the mode of ferroelectric oscillation and following up the change in its frequency in phase transition. Therefore, the special interest shown of late in the dynamic theory and vibration spectra of ferroelectrics is understandable.

This chapter sets forth in brief form the fundamentals of dynamic theory, gives results of calculations of vibration spectra of ferroelectric crystals, which may prove to be helpful in the interpretation of respective experimental results, and makes an attempt to set forth the basic ideas of a theoretical approach to the problem of dynamics of crystal lattices.

### Par. 1. Elements of Dynamic Theory of Crystal Lattices

This paragraph sets forth basic information from dynamic theory of crystal lattices, necessary for the understanding of dynamic approach to the problem of ferroelectricity.

#### 1. Oscillations of a Linear Chain

Many characteristic properties of lattice vibrations show themselves in the simplest model of a linear chain of alternating atoms of two kinds (Figure 5.1a).

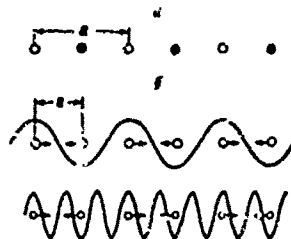


Figure 5.1. Oscillations of a linear chain.  
 a -- linear chain of alternating atoms of two kinds (black and white circles); b -- oscillations of a linear chain of the same items with wave vectors  $q = \frac{\pi}{a}$  and  $q = \frac{3\pi}{a}$ . Arrowheads indicate atomic displacements.

It is also convenient to trace on this model the basic approximations used in lattice vibration theory. One of them is the so-called adiabatic approximation. In this case, the wave function of a crystal, dependent on the coordinates of electrons and nuclei is reduced to a simple product of multiplication of the wave function of electronic subsystem with fixed positions of the nuclei by the wave function of nuclear subsystem, i.e. variables describing the motion of the electronic and nuclear subsystems are separated. The energy in electron term depends on the coordinates of nuclei as on parameters. The motion of nuclei is characterized by the potential energy  $U$  equal to the energy in electron term. Such a separation and introduction of potential function  $U$  for nuclei proves to be possible owing to the circumstance that kinetic energy of electrons is small in comparison with kinetic energy of nuclei, and the motion of electrons is much faster. Owing to this, during the oscillations of nuclei, electrons immediately (adiabatically) change their energy according to nuclear displacements.

We will use the following system of notations, which can be easily generalized later for a three-dimensional case: we will indicate by  $X_{\mu}^l$  displacements of an atom of the kind  $\mu$  ( $\mu=1, 2, \dots, s$ ) in the  $l$ -th unit cell ( $l=0; \pm 1; \pm 2; \pm 3; \dots$ ).

Making use of the smallness of the values of  $X_{\mu}^l$  in comparison with lattice constant, potential energy of the system  $U$  may be expanded into a series with respect to the powers of displacement: 1)

$$U = U_0 + \frac{1}{2} \left. \frac{\partial^2 U}{\partial X_{\mu}^l \partial X_{\nu}^{l'}} \right|_{\text{at } X_{\mu}^l = 0} X_{\mu}^l X_{\nu}^{l'} + \dots \quad (5.8)$$

The quantities

$$\Phi_{\mu\nu}^{ll'} = \left. \frac{\partial^2 U}{\partial X_{\mu}^l \partial X_{\nu}^{l'}} \right|_{\text{at } X_{\mu}^l = 0} \quad (5.9)$$

are called force constants.

It follows from translation symmetry that the values of  $\Phi_{\mu\nu}^{ll'}$  depend only on the difference  $l - l' = h$ . Therefore, later it will sometimes be more convenient to use for them the notation  $\Phi_{\mu\nu}^h$ .

The force constant  $\Phi_{\mu\nu}^{ll'}$  is numerically equal to the force acting on the  $\mu$ -th atom in the  $l$ -th unit from the side of atom  $\nu$  in the unit cell  $l'$  if the latter atom is displaced by one unit of length. The absence of first-order terms in (5.8) corresponds to equilibrium conditions of the chain. Neglecting of terms of higher than second order constitutes the basis of the so-called harmonic approximation.

---

1) Summing over repetitive indices is meant in (5.8).

The equations of motion for atoms have the form:

$$m_p \ddot{x}_p^i = - \sum_{q \neq p} \phi_{pq}^i x_q^i. \quad (5.10)$$

We will seek solutions in the following form:

$$x_p^i = a \sqrt{m_p} X_p^i e^{i(qa - \omega t)}. \quad (5.11)$$

i.e. in the form of plane waves propagating over the chain. Here "a" is lattice constant, q -- a wave vector, and  $\omega$  -- frequency of vibrations.

A substitution of (5.11) into (5.10) gives:

$$-\omega^2 X_p^i + \sum_{\mu \neq p} [\mu \nu] (q) X_p^i = 0, \quad (5.12)$$

where

$$[\mu \nu] (q) = \frac{1}{\sqrt{m_\mu m_\nu}} \sum_A \phi_{\mu\nu}^A e^{i(qaA)}. \quad (5.12a)$$

The following relationship exists between the quantities  $[\mu \nu] (q)$ :

$$\sum_\nu \sqrt{m_\mu m_\nu} [\mu \nu] (q) = 0, \quad (5.12b)$$

which follows from the requirement of an absence of appearance of internal forces acting on the atoms in a parallel translation of the crystal as a whole.

Thus, a set of an infinite number of equations for an infinite chain has been reduced to a set of systems of s order (s is the number of atoms in unit cell) for each value of q. The possible values of q may be determined from boundary conditions.

The so-called periodic boundary conditions are usually selected. In this case, an infinite crystal is divided into periodically arranged volumes and condition of a corresponding periodicity of displacements is imposed. Periodic boundary conditions are convenient in a mathematical scheme but, of course, they are artificial. However, rigorous proofs exist [8, 9] that the lattice vibration spectra calculated with the use of periodic and some other more realistic boundary conditions will hardly differ from each other when periodic volume is sufficiently large.

For a linear chain, periodic boundary conditions are equivalent to the relationships:

$$x_p^{i+N} = x_p^i \quad (5.13)$$

for all  $\mu$  and  $i$ , where N is the number of atoms on a periodic length.

In order that the expression (5.11) satisfy the requirement of

periodicity (5.13) it is necessary that:

$$q = \frac{2\pi}{Na} m, \quad m = 0; \pm 1; \pm 2, \dots, \pm \frac{N}{2} - 1; \frac{N}{2}. \quad (5.14)$$

In doing so,

$$-\frac{\pi}{a} < q < \frac{\pi}{a}, \quad (5.15)$$

since the number of  $N$ s solutions equal to the number of degrees of freedom of the "periodic length" of the chain is already contained in this range. 1)

The smallest range of the values of  $q$  corresponding to all possible physically unequivalent vibrations is called Brillouin zone. We will explain by using an example, the circumstance that the range (5.15) is a Brillouin zone for a linear chain. We will examine oscillations of a linear monatomic chain with a  $q = \frac{\pi}{a}$  and a  $q = \frac{3\pi}{a}$  respectively (Figure 5.1b).

It may be seen from the figure and the expression (5.11) that the same displacements of the atoms of the chain correspond to these two waves. These waves assume a different form only at the places where there are no atoms, i.e. where they have no physical sense.

Thus, the problem on the spectrum of a linear chain has been reduced to the solution of the sets of equations (5.12) of the  $s$  order for  $N$  values of the wave vector  $q$ .

We will examine the simplest model of a linear chain with atoms of two kinds (Figure 5.1) in which the nearest neighbors are coupled by springs having an elastic constant  $k$ . Then we have the following for the quantities  $[\mu\nu](q)$  ( $\mu, \nu = 1, 2$ )

$$\begin{aligned} [12](q) = [21](q) &= -\frac{k}{\sqrt{m_1 m_2}} (e^{iqa} + e^{-iqa}) = -\frac{2k}{\sqrt{m_1 m_2}} \cos qa, \\ [11](q) = [11](0) &= \frac{1}{m_1} \phi_{11}^0 = \frac{2k}{m_1}, \\ [22](q) = [22](0) &= \frac{1}{m_2} \phi_{22}^0 = \frac{2k}{m_2}. \end{aligned}$$

Here the quantities  $[11](0)$  and  $[22](0)$  were calculated with the aid of the relationship (5.12b).

Condition of solvability of the set (5.12) (dispersion equation defining the relationships  $\omega(q)$ ):

$$[\mu\nu](q) - \omega^2 \delta_{\mu\nu} = 0, \quad (5.16)$$

where  $\delta_{\mu\nu}$  is Kronecker symbol, acquires the following form:

1) For convenience in writing (5.14),  $N$  is assumed to be an even number.

$$\begin{vmatrix} \frac{2k}{m_1} - \omega^2 & -\frac{2k}{\sqrt{m_1 m_2}} \cos qa \\ -\frac{2k}{\sqrt{m_1 m_2}} \cos qa & \frac{2k}{m_2} - \omega^2 \end{vmatrix} = 0. \quad (5.17)$$

From (5.17) we find the dispersion curves:

$$\omega_{\pm}^2(q) = \frac{k}{m_1 m_2} (m_1 + m_2 \pm \sqrt{m_1^2 + m_2^2 + 2m_1 m_2 \cos 2qa}). \quad (5.18)$$

The ratios of the amplitudes of atomic displacements may be found from the equations of motion (5.11):

$$\frac{X_1}{X_2} = \frac{\frac{2k}{m_2} \cos qa}{\omega^2 - \frac{2k}{m_1}} = \frac{\omega^2 - \frac{2k}{m_2}}{\frac{2k}{m_2} \cos \frac{qa}{2}}. \quad (5.19)$$

In Figure 5.2 is shown the form of the spectrum  $\omega(q)$  and the density function of the states  $g(\omega)$  ( $g(\omega)d\omega$  is equal to the number of states in a range of from  $\omega$  to  $\omega + d\omega$ ) for a different mass ratio  $\frac{m_1}{m_2}$ . The two branches  $\omega_+$  and  $\omega_-$  corresponds to two roots of (5.18).

The vibrations  $\omega_-(q)$  for which  $\omega \rightarrow 0$  when  $q \rightarrow 0$ , are called acoustic vibrations. This name is connected with the fact that when  $q$  are small these vibrations correspond to sound: in this case the particles in one unit cell move practically as one whole and a discrete structure of the lattice is not very essential, i.e. it may be regarded simply as an elastic continuum. Conversely, for vibrations  $\omega_+(q)$  when  $q$  are small, two sublattices of the crystal as a whole vibrate in anti-phase with respect to each other. In ionic crystals, precisely such vibrations (with  $q \rightarrow 0$ ) may be coupled with a large dipole moment and strongly interact with electromagnetic field. Therefore, branches for which  $\omega(q) \neq 0$  when  $q \rightarrow 0$  are called optical vibrations. With a  $q = \frac{\pi}{a}$  only atoms of one kind vibrate (light atoms for optical branch and heavy for acoustical branch) and the atoms of the other kind are at rest. With any  $q$ , in acoustical branch the displacements of the nearest neighbors are of the same sign, and in the optical branch -- of the opposite sign.

It is of interest to follow up the change in vibration spectrum with a change in the ratio of atomic masses. With  $m_1 = m_2$  the linear chain actually has a lattice constant smaller by one half. The curve  $\omega(q)$  for a linear chain with the same atoms, with the same force constant and a lattice constant smaller by one half (Figure 5.1) is shown in Figure 5.2 with dashes. In this case the optical branch is absent. Solutions of  $\omega_{\pm}(q)$  have been obtained for a linear chain with formally distinctive atoms and with  $m_1 = m_2$  represent the same curve  $\omega(q)$  but reduced to a Brillouin zone which is smaller by one half. With  $\frac{m_1}{m_2} =$

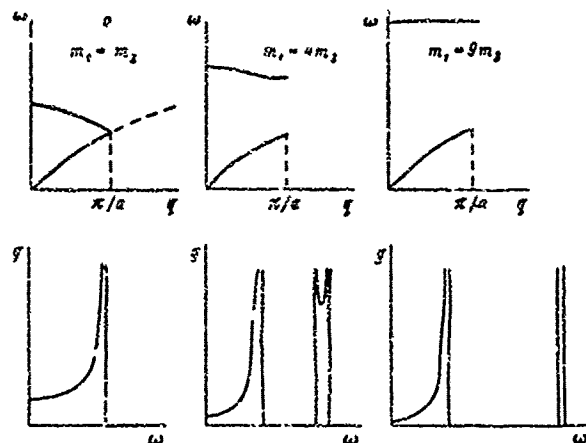


Figure 5.2. Dispersion curves  $\omega \pm(q)$  and density of states  $g(\omega)$  for a linear chain of atoms of two kinds with different ratios of atomic masses.

As the spectrum considerably changes. A slit appears in it. The dispersion of optical branch (i.e. dependence on  $q$ ) becomes weaker. Finally,

with  $\frac{m_1}{m_2} = 9$  the frequencies of the optical branch are confined in a very narrow range. These vibrations are reduced chiefly to the motion of light atoms whereas heavy particles remain practically motionless. Inasmuch as in the approximation of the nearest neighbors the particles affect each other only through the displacements of heavy particles, their vibrations

in the optical branch are to a large degree independent when  $\frac{m_1}{m_2} = 9$  and

vibration frequencies do not differ very perceptibly from the frequency of vibrations of the light particle between two fixed particles.

## 2. Generalization for a Three-Dimensional Case

This generalization is reduced in principle to the introduction of the subscripts  $i, k=1, 2, 3$  corresponding to Cartesian coordinates. The formulas (5/12) acquire the form:

$$-\Delta^2 X_i^q + \left[ \begin{matrix} i & i \\ & k \end{matrix} \right] (q) X_k^q = 0, \quad (5.20a)$$

$$\left[ \begin{matrix} i & i \\ & k \end{matrix} \right] (q) = \frac{1}{\sqrt{m_i m_k}} \sum_{\alpha} \Phi_{ik}^{\alpha} e^{iq \cdot \alpha}, \quad (5.20b)$$

where  $h_1=0; \pm 1; \pm 2; \pm 3; \dots$ ,

$$\phi_{1s}^{h=1-1'} = \frac{1 \partial^2 U}{\partial X_1^2 \partial X_2^2}$$

and  $\hat{A}$  is a matrix of the base vectors of translations (equal for example, for a simple cubic lattice to the unit three-dimensional matrix multiplied by lattice constant). In a three-dimensional case the components  $\begin{bmatrix} \mu & \nu \\ i & k \end{bmatrix} (q)$  are called components of frequency tensor.

Physical unequivalent values of the wave vector will now be determined from the condition:

$$q = \frac{2\pi}{N} B h \left( h_1 = 0, \pm 1; \pm 2; \dots; \pm \frac{iN}{2} - 1; \frac{iN}{2} \right), \quad (5.21)$$

where  $\hat{B}$  is a matrix of the base vectors of reciprocal lattice (see chapter 6).

For a three-dimensional case, Brillouin zone will represent a unit cell of reciprocal lattice.

With a specified value of the wave vector  $q$ , dispersion equation for the determination of the vibration frequencies of the crystal now has a 3s order:

$$\left| \begin{bmatrix} \mu & \nu \\ i & k \end{bmatrix} (q) - \lambda, \delta_{ik} \right| = 0. \quad (5.22)$$

Out of the 3s branches of the vibration spectrum three branches will be acoustical ( $\omega \rightarrow 0$  when  $q \rightarrow 0$ ) and 3s-3 will be optical branches. The vibrations will now also be differentiated by the direction of displacements with respect to the wave vector.

In some particular cases (for example, if  $q$  is oriented along the symmetry axis) atomic displacements will be purely longitudinal (i.e. oriented along the wave vector) for certain branches, and purely transverse (perpendicular to the wave vector) for the other branches.

### 3. Lattice Vibrations in Ionic Crystals

Ionic crystals should be specially examined for two reasons. Firstly, in the determination of vibrations it is necessary to take into account electric fields appearing on the surface of a crystal with the displacement of sublattices; secondly, for long-range Coulomb forces it is necessary to take into account the effects of delay, i.e. the circumstance that electromagnetic field does propagate instantaneously.

Both of these factors are important only in the case of long waves. Indeed, owing to the multiplier  $e^{iq \cdot h}$  the series of  $\begin{bmatrix} \mu & \nu \\ i & k \end{bmatrix} (q)$

(see 5.20b) converge. In addition to this, at distances of the order of vibration length  $\lambda_{lat} \approx 2\pi/q$  the constants should be taken into account. On the other hand, while the wavelength  $\lambda$  of light corresponding to the lattice vibration frequency  $\omega$  ( $\lambda = \frac{2\pi c}{\omega}$ ) is much larger than  $\lambda_{lat}$ , the effects of delay may be neglected. Since the frequencies of optical vibrations  $\omega \sim 10^{13} \text{ sec}^{-1}$ ,  $\lambda \sim 10^{-2} \text{ cm}$  ( $\lambda_{lat} \sim 10^{-8} \text{ cm}$ ), i.e. the effects of delay are considerable only in the portion amounting to  $10^{-6}$  of Brillouin zone.

Lattice vibrations with a  $q=0$  in which crystal sublattices are displaced as one whole are connected with the change in its macroscopic dipole moment and appear in infrared absorption and reflection spectra. Therefore, we should dwell in greater detail on these vibrations. It is convenient to do this with the aid of a simple phenomenological model for optical vibrations of diatomic ionic crystals.

We will first examine the problem without taking the effects of delay into account. The set of equations describing the limit optical ( $q \rightarrow 0$ ) vibrations of such crystals are written in the following form 1) [10, 11]:

$$\dot{W} = b_{11}W + b_{12}E, \quad (5.23a)$$

$$P = b_{21}W + b_{22}E. \quad (5.23b)$$

Here  $W = \sqrt{\mu}X$  where  $\mu = \frac{m_1 m_2}{m_1 + m_2}$  is reduced mass,  $X$  is the relative displacement of sublattices of the positive and negative ions,  $P$  is lattice polarization and  $E$  is electric field.

We seek a solution of the set (5.23) in the form:

$$\left. \begin{aligned} E &= E_0 \\ W &= W_0 \\ P &= P_0 \end{aligned} \right\} \times e^{i\omega t}.$$

Then we will obtain:

$$\left. \begin{aligned} -i\omega W_0 &= b_{11}W_0 + b_{12}E_0 \\ P_0 &= b_{21}W_0 + b_{22}E_0 \end{aligned} \right\} \quad (5.24)$$

Eliminating  $W_0$  from (5.24), we will obtain:

$$P_0 = \left( b_{22} + \frac{b_{12}b_{21}}{-b_{11} - i\omega} \right) E_0. \quad (5.25)$$

After comparing (5.25) with the definition:

$$E_0 + 4\pi P_0 = (-i) E_0. \quad (5.26)$$

we will find dispersion formula for dielectric constant:

---

1) It can be shown [10, 11] that it follows from the law of conservation of energy that  $b_{12} = b_{21}$ .

$$\epsilon(\omega) = 1 + 4\pi b_{22} + \frac{4\pi b_{12} b_{21}}{-b_{11} - \omega^2} \quad (5.27)$$

which it is convenient to write in the following form:

$$\epsilon(\omega) = \epsilon_\infty + \frac{\omega_0^2}{\omega_0^2 - \omega^2} \quad (5.28)$$

In formula (5.28),  $\omega_0 = \sqrt{-b_{11}}$  is infrared dispersion frequency, i.e. natural frequency of the lattice at which  $\epsilon(\omega) \rightarrow \infty$ ;  $\epsilon_0 = 1 + 4\pi b_{22} - \frac{4\pi b_{12} b_{21}}{b_{11}}$  is static (i.e. measured in a field with a frequency  $\omega \ll \omega_0$ ) dielectric constant;  $\epsilon_\infty = 1 + 4\pi b_{22}$  is optical (measured at  $\omega \gg \omega_0$ ) dielectric constant.

In order to examine the frequencies of limit optical vibrations the following equation of electrostatics should be added to the set (5.23):

$$\text{div}(\mathbf{E} + 4\pi\mathbf{P}) = 0. \quad (5.29)$$

Substituting  $\mathbf{P}$  from (5.23b), we will find:

$$\text{div} \mathbf{E} = -\frac{4\pi b_{11}}{1 + 4\pi b_{22}} \text{div} \mathbf{W} \quad (5.30)$$

We will separate the vector  $\mathbf{W}$  into its potential and solenoidal parts:

$$\mathbf{W} = \mathbf{W}_t + \mathbf{W}_s, \quad (5.31)$$

$$\text{div} \mathbf{W}_s = 0,$$

$$\text{rot} \mathbf{W}_t = 0. \quad (5.32)$$

$$(5.33)$$

Then, for  $\mathbf{W}_t$  we have:

$$\left. \begin{aligned} E_t &= 0, \\ \dot{W}_t &= b_{11} W_t = -\omega_0^2 W_t, \end{aligned} \right\} \quad (5.34)$$

whence it follows that:

$$W_t = W_t^0 e^{i\omega t} = W_t^0 e^{-\omega_0 t} \quad (5.35)$$

For  $\mathbf{W}_s$  we have:

$$\text{div} \mathbf{E} = -\frac{4\pi b_{21}}{1 + 4\pi b_{22}} \text{div} \mathbf{W}_s \quad (5.36)$$

and consequently:

$$\mathbf{E} = -\frac{4\pi b_{21}}{1 + 4\pi b_{22}} \mathbf{W}_s, \quad (5.37)$$

$$\dot{W}_s = \left( b_{11} - \frac{4\pi b_{12} b_{21}}{1 + 4\pi b_{22}} \right) W_s = -\frac{\omega_0^2}{\epsilon_\infty} W_s, \quad (5.38)$$

from which it follows that:

$$W_s = W_s^0 e^{i\omega t}, \quad (5.39)$$

with

$$\frac{\omega_l}{\omega_t} = \frac{\omega_l}{\omega_0} = \left(\frac{\epsilon_0}{\epsilon_\infty}\right)^{1/2}. \quad (5.40)$$

We will note that the transverse and longitudinal waves (when  $q \rightarrow 0$ ) are particular cases of solutions of  $W_l$  and  $W_t$ . Therefore,  $\omega_l$  and  $\omega_t$  are usually called the frequencies of longitudinal and transverse vibrations respectively. We will explain the physical sense of the results obtained by examining vibrations with a small but finite  $q$  ( $\lambda_{lat} = \frac{2\pi}{q} \ll L$  where  $L$  is the dimensions of the crystal). 1) For transverse waves, regions of a positive and negative charge alternating with a period  $\lambda_{lat}$  will appear on the surface of the crystal. In doing so, the aggregate field from these regions will be equal to zero in the center of the crystal. But in the case of longitudinal vibrations the following field appears:

$$(5.41)$$

which will be added to the restoring force. If it is taken into account that  $P = b_{21}W + b_{22}E$  (see 5.23a), then (5.37) is immediately obtained from (5.41).

In nonionic crystals  $b_{21} \rightarrow 0$  and the frequencies  $\omega_l$  and  $\omega_t$  coincide.

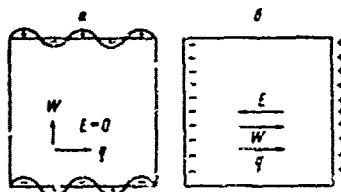


Figure 5.3. Charges appearing on the surface of a crystal with limit dipole vibrations of the lattice.

a -- transverse vibrations; b -- longitudinal vibrations.

It should be noted that the difference between  $\omega_l$  and  $\omega_t$  is of paramount significance upon the appearance of a situation conducive to a ferroelectric transition. From the microscopic point of view, for ionic crystals this difference is connected with the circumstance that components of effective field which coincide with the direction of propagation of vibrations and are perpendicular to it differ substantially from each other. This was already discussed above. This feature becomes even more

1) If this condition is not satisfied, the frequencies of limit vibrations will depend on the shape of the crystal (see below for more details).

obvious in the most interesting case of long waves for simple crystals having high symmetry. The field acting on an ion of a polarized crystal lattice is equal to the sum of the average macroscopic field  $E$  and the field  $E_1$  which takes account of the action of dipoles situated inside Larentz sphere (see paragraph 2, chapter 4):

$$F = E + E_1.$$

Leaving aside the question of the values of  $E_1$  (in the case of diatomic cubic crystals  $E_1 \neq 0$ ) we have, according to [11], when  $q \rightarrow 0$ :

$$E = -\lim_{q \rightarrow 0} 4\pi \cdot \frac{q}{|q|} \cdot \frac{pq}{v_s |q|},$$

where  $p$  is dipole moment of a unit cell. It follows from this that  $E \perp q = 0$  and  $E \parallel q = -4\pi P$ .

Thus, for longitudinal vibrations the crystal lattice is more rigid and the frequencies  $\omega_l$  are always higher than  $\omega_t$ .

Similar results may also be obtained for ionic crystals by using Ewald method [11, 12] (see also chapter 4, paragraph 2).

It can be shown that the components  $\begin{bmatrix} \mu & \nu \\ i & k \end{bmatrix}$  ( $q \rightarrow 0$ ) for a lattice of point ions will contain terms which depend on the direction of  $q \rightarrow 0$ :

$$\frac{4\pi}{v} \cdot \frac{q_i q_k}{q^2} \cdot \frac{z_\mu z_\nu}{v m_\mu m_\nu}. \quad (5.42)$$

Here  $z_\mu$  and  $z_\nu$  are ionic charges;  $\mu$ ,  $\nu$  and  $v$  are the volume of a unit cell. The expression (5.42) depends on the direction of  $q \rightarrow 0$  and, therefore, for different directions of  $q \rightarrow 0$ , different frequencies will be obtained from the equation (5.22). It can be shown that in the simplest case of diatomic optically isotropic cubic crystals everything will be reduced to the appearance of the frequencies  $\omega_l$  and  $\omega_t$  which do not depend on the direction of  $q \rightarrow 0$ . The ratio (5.40) is called Liddan-Saks-Teller ratio. On the basis of this ratio we may also point out the existence of a soft mode: it may be seen that if  $\epsilon_0$  sharply increases in some temperature range, the frequency of the transverse dipole vibration  $\omega_t$  should decrease in order that the relationship (5.40) be satisfied.

Cochran [6] generalized Liddan-Saks-Teller ratio for the case of cubic crystals with an arbitrary number of sublattices:

$$\frac{\epsilon_0}{\epsilon_\infty} = \prod_{j=1}^n \frac{(\omega_j)_l^2}{(\omega_j)_t^2}. \quad (5.43)$$

Here  $n$  is the number of dipole optical vibrations.

Thus, in this case, the frequency of each limit dipole vibration will be split into a longitudinal and transverse frequency.

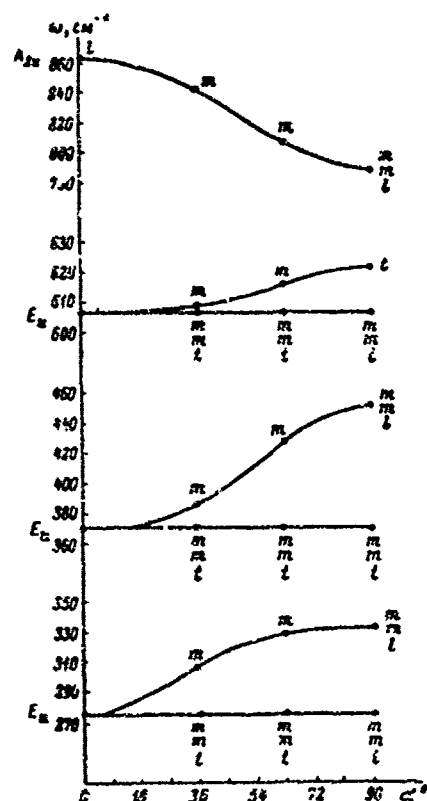


Figure 5.4. The curves  $\omega(q)$  with  $q \rightarrow 0$  for rutile.

$\alpha$  is the angle formed by direction with the tetragonal axis of the crystal. The letters m, l and t indicate the character of the respective vibration (m -- mixed, l -- longitudinal, t -- transverse). The upper letter pertains to a case when  $q$  lies in the plane (110), and the lower -- when  $q$  lies in the plane (100), the middle letter pertains to an intermediate case.

In noncubic crystals the dependence on the direction of  $q \rightarrow 0$  will bear a more complex character. With an arbitrary direction of  $q \rightarrow 0$  the limit dipole vibrations will not be purely longitudinal or transverse. In Figure 5.4 are shown the curves  $\omega(q \rightarrow 0)$  showing the dependence on the direction of  $q \rightarrow 0$  for rutile [13].<sup>1)</sup> The indices  $E_{2u}$  and  $A_{2u}$  in the

1) In the work [13], corresponding calculations were also carried out for the crystals of  $MgF_2$ ,  $ZnF_2$ ,  $FeF_2$  and  $MnF_2$ . As far as we know, no such calculations as yet exist for concrete noncubic crystals.

figure indicate irreducible representations of the point group of rutile  $D_{4h}$  ( $4/mmm$ ), to which the respective normal vibrations are related (see below for more details concerning this classification).

In addition to dipole limit vibrations, crystals of rutile structure have limit vibrations not connected with the change in dipole moment. The calculation naturally confirms the circumstance that their frequencies do not depend on the direction of  $q \rightarrow 0$ .

We will examine now the influence of the effects of delay. 1) For this purpose, one should examine the equation of lattice dynamics simultaneously with Maxwell equations. In Figure 5.5 are shown two sets of solutions characterizing a lattice in two extreme cases:

a) solution without taking delay into account (electrostatic approximation);

b) solutions corresponding to a lattice in which the motion of ions is fixed and which functions as a normal medium with a refraction index  $n = \sqrt{\epsilon_{\infty}}$ , and also exact solutions which (see in greater detail in [11], p 108) represent an interlacing of these two groups of approximate solutions.

Longitudinal vibrations are not affected by the effects of delay, but when  $q \rightarrow 0$  the transverse vibrations begin to bear not a purely mechanical but a mixed radiation-mechanical character with the percentage of energy of these excitations falling to the share of electromagnetic waves increasing with the approach of wave vector to zero (Figure 5.6).

As already mentioned above, electrostatic approximation is not suitable for transverse vibrations with phase velocities higher than  $c$  (with a wavelength  $\lambda \approx 10^{-2}$  cm). Of late, the term polaritons started to be used (see, for example, [14]) for excitations connected with the ascending section of the lower branch of the spectrum shown in Figure 5.5. Experiments in [15] for quartz confirmed the law of dispersion predicted theoretically for polaritons.

We will note that when  $\lambda_{\text{lat}} \approx L$ , where  $L$  is linear dimensions of the crystal, the spectrum of an ionic crystal begins to depend on its shape [16, 17] and results illustrated in Figure 5.5 become invalid. In connection with this, we will point out an important result (see [11], p 144) according to which the infrared dispersion frequency  $\omega_0$  (see the expression 5.28) is equal to the frequency  $\omega_t$  when the thickness of the film is small (in comparison with the wavelength  $\lambda = \frac{2\pi c}{\omega_0}$ ). This result makes it possible to investigate vibration frequencies of a crystal from the reflection spectra of thin films.

We will now discuss in the light of the results set forth above the physical sense of the crystal vibration frequencies calculated with  $q \rightarrow 0$  in electrostatic approximation, i.e. without taking the effects of delay into account. For the limit vibrations not connected with a change

1) The effect of delay on lattice vibrations was examined for the first time by K. B. Tolpygo.

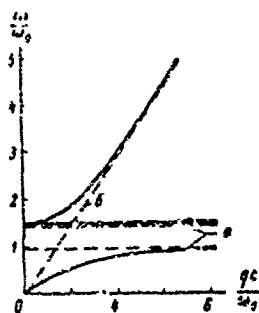


Figure 5.5. Effect of delay on lattice vibrations.  
(see explanation in the text)

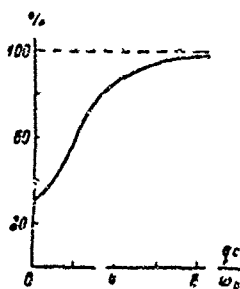


Figure 5.6. Proportion of mechanical energy in transverse lattice vibrations when  $q \rightarrow 0$ .

in dipole moment, and for longitudinal limit normal vibrations these results should be related to small but finite wave vectors  $q \left( \frac{2\pi}{q} \ll L \right)$  where  $L$  is the length of the crystal. For the transverse (and mixed) limit dipole vibrations these results are related to the wavelengths of lattice vibrations  $\lambda_{cr} \leq \frac{c}{\omega \sqrt{\epsilon_{\infty}}} \sim 10^{-2}$  cm. The corresponding values of wave vectors  $q$  are much smaller than the maximum value of the wave vector  $q_m \sim \frac{\pi}{a}$  where "a" is lattice constant.

Linear terms are absent in the expansion of the relationship  $\omega(q)$ , calculated in electrostatic limit, according to the powers of  $q$  with small  $q$  for a specified direction of  $q \rightarrow 0$  (see [18], p 225). Therefore, if calculations are carried out for  $q \rightarrow 0$  and for  $q \sim 10^2$  cm $^{-1}$ , the results will coincide with accuracy to  $\left( \frac{q}{q_m} \right)^2 \sim 10^{-9}$  percent. In all works on the "soft" ferroelectric mode, a  $\omega_t(q \rightarrow 0)$  is meant for  $q \sim 10^2$  cm $^{-1}$  and  $\omega_t(q \rightarrow 0)$  is calculated in electrostatic limit. However, it may be seen from Figure 5.5 that when  $\omega_t \rightarrow 0$ ,  $q_p$  also tends to zero. Nevertheless, it should be remembered that it is not worthwhile to examine the values of  $q_p < 1/L$  within the framework of the diagram shown in Figure 5.5.

When  $\omega_t \rightarrow 0$ , it is obvious that fundamental changes must also occur in the spectrum of polaritons. But this question has not as yet been investigated in detail.

#### 4. Models of "Hard" and Polarizable Ions

It follows from adiabatic approximation which underlies theory of dynamics of crystal lattices (see subparagraph 1 of this paragraph)

that to calculate the vibration spectrum of a crystal, the energy of the fundamental electronic state  $\mathcal{E}(R)$  should first be calculated for different positions of the nuclei  $R$  as the parameters, and then, regarding  $\mathcal{E}(R)$  as potential energy for the motion of nuclei the force constants and components of the frequency tensor should be calculated and the equation (5.22) solved for a set of values of  $q$  in Brillouin zone. However, at the present time it is difficult to carry out this program, especially for crystals of complex structure. Therefore, approximate models are usually employed for potential functions describing the motions of nuclei. In the simplest model, potential function is considered to be corresponding to a set of "springs" binding only the nearest atoms. Such a model was used, for example, in subpara. graph 1 of this paragraph to describe the vibration spectrum of a linear chain. For a rigorous description of the spectrum of actual crystals it often proves to be unsatisfactory and it is necessary to take into account the interaction with the following coordination spheres.

As already noted above, in ionic crystals electrostatic forces bear a long-range character. Therefore, Coulomb interaction forces have to be taken into account for all coordination spheres using special methods of summing the lattice sums, for example Ewald method (see paragraph 2, chapter 4). For an ionic crystal the simplest model of potential function requires an examination of Coulomb forces between the point ions. The repulsive forces are taken into account only between the nearest neighbors. A potential with a power or exponential dependence on the distance between atoms is usually selected for them:

$$U = \frac{\lambda_{\mu\nu}}{R_{\mu\nu}^n} \quad (5.44a)$$

or

$$U = B_{\mu\nu} e^{-\frac{r_{\mu\nu}}{r}} \quad (5.44b)$$

An exponent equal to 9 is usually selected. The subscripts  $\mu$  and  $\nu$  pertain to the kinds of atoms. The repulsion constant  $\lambda_{\mu\nu}$  may be evaluated in terms of ionic radii using Pauling empirical formula: <sup>1)</sup>

$$\lambda_{\mu\nu} = 0.02963e^2 (r_{\mu} + r_{\nu})^9 \quad (5.45)$$

Here  $e$  is electron charge and  $r_{\mu}$  and  $r_{\nu}$  are ionic radii of the ions  $\mu$  and  $\nu$  (see [11], p 45).

In the simplest case of a cubic diatomic crystal, lattice energy in the model under consideration has the following form without the vibrations taken into account:

$$U_0 = A \frac{\lambda_{\mu\nu}}{a^3} - e \frac{e^2}{a} \quad (5.46)$$

---

1) Physical cause of the appearance of repulsive forces is connected in essence with Pauli principle which forbids the existence at one point of two electrons with the same quantum numbers.

Here "a" is lattice constant,  $A_n$  and  $\alpha$  are dimensionless constants determined by geometry of the lattice, 1)  $e_{\text{eff}}$  is ionic charge. Lattice constant "a" may be determined from the condition of potential-energy minimum (Figure 5.7).

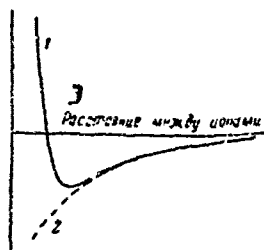


Figure 5.7. Curve of potential energy of the crystal of lattice constant.

1 -- potential energy; 2 -- Coulomb energy;  
3 -- distance between ions.

In the case of crystals having a high degree of ionicity of the bond (for example, alkaline-haloid crystals) the model of hard ions gives results which agree qualitatively with experimental data [19]. For some crystals with a partial fraction of covalent bond this model should be modified even for a qualitative comparison with the experiment, by taking into account (in the first approximation) the covalence of the bonds through the introduction of effective ionic charges which serve as the adjusting parameters [13, 20].

A modified version of the model of point ions may be used for complex structures consisting of ions of alkaline metals and closely packed atomic groups (for example, such as the ferroelectrics  $\text{KH}_2\text{PO}_4$ ,  $\text{NaNO}_2$ , etc.) [21-23]. In doing so, in calculating the long-range Coulomb forces a point negative charge equal to the charge of alkaline-haloid ion and situated in the center of the ion is assigned to the atomic groups constituting an anion, and the short-range repulsive forces are introduced with the atomic structure of the groups taken into account. In this case the internal (high-frequency) vibrations of the anion are omitted from the examination and only the relative vibrations of the sublattices of cations and anions as one whole, that are of the greatest interest for ferroelectrics are calculated.

For some of the alkaline-haloid crystals [24, 25] and  $\text{SrTiO}_3$  [26] the vibration spectra were calculated with the aid of the so-called model of deformed ions 2) examined for the first time by Tolpygo and Mashkevich and then by Dick and Overhauser [28].

1) The constant  $\alpha$  characterizing the contribution of Coulomb energy to lattice energy is called Madelung constant.

2) It is also called shell model.

According to this model a crystal is considered to be consisting of cores (nuclei+internal filled electron shells) located at the lattice points, and valence electrons, i.e. the outer shells. The cores and shells are considered to be independent sublattices bound with each other both by the short-range and long-range forces. In such a description of the properties of a crystal, account is taken of the interaction between different ions, ions and electrons in the outer shells and also interactions between outer electrons.

### 5. Shell Model and Dynamic Stability of the Lattice

We will write equations of motion for cores and shells.

In a shell model, potential energy depends not only on the displacements of ions  $X_{\mu}^I$  but also on the displacements of electrons in the outer shells  $S_i^I$ :

$$U = U_0 + \frac{1}{2} \left( \sum_{\mu, \nu} \Phi_{\mu\nu}^{II'} X_{\mu}^I X_{\nu}^I + \sum_{\mu} \alpha_{\mu}^{-1} \left( \sum_i P_i^{\mu} \right)^2 + \sum_i \left[ P_i^{\mu} + \sum_{\nu} X_{\nu}^I \right] E_i^{\mu} \right) + \dots \quad (5.47)$$

The following notations have been introduced in (5.47)  $z_{\mu}$  and  $Y_{\mu}$  are effective charges of ions and outer electrons respectively;  $\Phi_{\mu\nu}^{II'}$ ,  $\Phi_{Tik}^{II'}$  and  $\Phi_{Sik}^{II'}$  are force constants describing short-range forces between ions and between electrons respectively. The term  $\alpha_{\mu}^{-1} \left( \sum_i P_i^{\mu} \right)^2$  takes account of the interaction of electrons with their ions, and the last addend is the total Coulomb interaction of all electrons and ions of the crystal;  $\alpha_{\mu}$  is electron polarizability of the ion  $\mu$ ;  $P_i^{\mu} = Y_{\mu} S_i^{\mu}$  is dipole moment appearing with the displacement of electron relative to its core;  $E_i^{\mu}$  is a field acting on the  $\mu$ -th ion at the point I.

If electron mass is considered to be negligibly small in comparison with ion mass (this corresponds to the circumstance that at the frequencies under consideration, electron follows the field without lag), then the equations of motion for electrons and ions will acquire the following form:

$$\left. \begin{aligned} \ddot{X}_{\mu}^I &= - \frac{\partial U}{\partial X_{\mu}^I} \\ \ddot{S}_i^I &= - \frac{\partial U}{\partial S_i^I} \end{aligned} \right\} \quad (5.48)$$

Here  $m_\mu$  is the mass of the  $\mu$ -th ion.

We will seek solutions for the displacements of ions, electrons and other quantities connected with them, in the following form:

$$x^i = X^i \exp i(qX^i - \omega t), \quad (5.49)$$

where  $\omega$ ,  $q$  ( $q = \frac{2\pi}{\lambda}$ ) and  $\lambda$  are the frequency, wave vector and wavelength of the respective normal vibration.

After a substitution of (5.49) into (5.48) we will obtain the following set of equations:

$$\left. \begin{aligned} \omega^2 m_\mu X^i &= \left[ \sum_k R_{ik}^{\mu\nu} + i C_{ik}^{\mu\nu} \right] X_k^i + \left[ \sum_k T_{ik}^{\mu\nu} + i C_{ik}^{\mu\nu} Y_k \right] S_k^i \\ 0 &= \sum_k \left[ T_{ik}^{\mu\nu} + i C_{ik}^{\mu\nu} \right] X_k^i + \left[ \sum_k \phi_{ik}^{\mu\nu} + Y_k C_{ik}^{\mu\nu} Y_k \right] S_k^i \end{aligned} \right\} \quad (5.50)$$

Notations of the following type have been introduced in (5.50):

$$R_{ik}^{\mu\nu} = - \sum_h \phi_{hik}^{\mu\nu} \exp i(qAh + B^h - B^i).$$

The quantities  $C_{ik}^{\mu\nu}$  represent structural coefficients of internal field (see in more detail [11, 29] and paragraph 2, chapter 4).

It is convenient to rewrite the set of equations (5.50) in matrix form:

$$\left. \begin{aligned} \omega^2 m_\mu X &= (R + iC_2) X + (T + iCY) S \\ 0 &= (T + YC_2) X + (\phi + YCY) S \end{aligned} \right\} \quad (5.51)$$

Eliminating  $S$  from the equations (5.51), we will obtain equations for ionic displacements:

$$\omega^2 m_\mu X = \Phi X, \quad (5.52)$$

where  $\Phi$  is a matrix -- a component of "effective" frequency tensor -- having the following form:

$$\Phi = R + iC_2 - (T + iCY)(\phi + YCY)^{-1}(T + YC_2). \quad (5.53)$$

The set (5.52) has nonzero solutions when and only when

$$|\Phi_{ik}^{\mu\nu} - \omega^2 m_\mu \delta_{ik}| = 0 \quad (5.54)$$

The secular equation (5.54) is analogous to the equation (5.22) and, thus, shell model is reduced to Born-Karman theory. In doing so, it points out a physically clear method for the calculation of components of the frequency tensor with account taken of the long-range and short-range forces and polarizabilities of ions. However, in the calculations within the framework of this model (see below, paragraph 3 of this chap-

ter) it is necessary to use a large number of adjusting parameters. Therefore, at the first stage it is often expedient to make an attempt to interpret the vibration spectrum with the aid of simpler models, and then pass on to several shell models of increasing complexity, correcting the imperfections of preliminary calculations and achieving a more detailed agreement with the experiment, the way this was done, for example, in the work [26] for  $\text{SrTiO}_3$ .

One of important features of dispersion equations (5.54) is that when  $q \rightarrow 0$  the frequencies of acoustical branches tend to zero whereas the frequencies of optical branches remain, generally speaking, finite even in the case of infinitely long waves. The circumstance that when  $q=0$  one of the solutions of (5.54) is  $\omega^2=0$ , follows from the special characteristic of all square matrices,  $R$ ,  $T$  and, consequently, of the matrix  $\Phi$  with this characteristic consisting in a decrease of the rank of these matrices by three unities when  $q=0$ , i.e.  $|\Phi_{ik}^{(s)}|_{3s}=0$ .

In particular, this condition follows directly from an examination of equilibrium of the crystal upon its translation as one whole ( $q=0$ ). Another important feature of dispersion equation is the difference in the character of  $\omega(q)$  of the transverse and longitudinal vibrations, which is connected with the above-mentioned feature of the macroscopic field  $E$ , with this feature consisting in that the components of the field coinciding with the direction of the propagation of vibrations and perpendicular to it substantially differ from each other. This may be shown directly as a result of analyzing Coulomb terms contained in  $\Phi$ .

A necessary condition for stability of vibration process taking place in a crystal is the reality and difference from zero of all of its characteristic frequencies. This condition is defined by the secular equation (5.54). Naturally, this statement does not extend to the trivial solution, i.e. vanishing of the frequencies of the transverse and longitudinal vibrations of acoustical branch when  $q=0$ , which describes extreme case of vibrations, i.e. a uniform displacement of the crystal. Complexity or equality to zero of the frequencies of any one of the vibration modes indicates the presence of an aperiodic component in the time factor of the solutions (5.54). This is equivalent to a destruction of the lattices or to such a change in its structure with which the vibrations again become stable. In accordance with the well-known theorem in [30], condition for the existence of only positive solutions is satisfied if all principal minors of the determinant made up of the elements of the matrix  $\Phi$  are positive, i.e.

$$\text{Det}^{(s-1)}|\Phi| > 0, \quad (5.55)$$

and, consequently, vanishing of one of the principal minors of  $(\Phi)$  indicates instability of the crystal structure in question. 1)

1) It may be considered that a phase transition of the first kind takes place when the values of the principal minors of  $\Phi$  are positive or differ little from zero (compare with chapter 4, paragraph 1, subparagraph 2).

The condition (5.55) is a general expression defining the stability of a crystal and could be laid down as a basis of a general theory of phase transitions. In particular, the expression (5.55) was used by Thompson to determine the melting points in crystals [31]. It is obvious that in order to obtain temperature dependences of the quantities contained in  $\Phi$ , as a result of which the condition (5.55) will be disturbed at a certain temperature, we cannot limit ourselves to a purely harmonic approximation in the initial equations. It should be noted that introduction of anharmonicity into these equations even when it is regarded as a small perturbation, leads to a considerable complication of the entire problem (see, for example, [32]) inasmuch as the normalcy (i.e. independence) of vibration modes proves to be, strictly speaking, disturbed.

In Cochran theory [6, 7] this difficulty is circumvented by that the temperature dependences of the parameters of  $\Phi$  are either postulated or are introduced conditionally on the basis of a comparison with expressions which follow from phenomenological representations. Naturally, this reduces somewhat the "effectiveness" of stability condition and limits the possibilities of analysis of microscopic mechanism responsible for the appearance of phase transitions in terms of dynamic theory. At the same time, the application of the condition (5.55) is of value in itself even in a harmonic approximation inasmuch as it makes it possible, in principle, to connect the vibration spectrum of a crystal with the phase-transition points with these transitions having a diverse nature -- they include melting, transitions connected with polymorphism of the crystals and, finally, the ferro- and antiferroelectric transitions.

To determine phase-transition points connected with a change in the symmetry of a crystal it proves to be expedient to look for points of disturbance of the condition (5.55) in conformity with some definite modes of vibrations. In this case it is possible to simplify the structure and decrease the order of the minors (to break them up into units). For example, for crystals of cubic symmetry, if vibrations propagate along one of the principal axes of symmetry the sets of equations (5.52) are broken up into three independent subsets each one of which has an order  $s$  (two of them corresponding to two transverse waves prove to be alike), and accordingly, the order of the matrix appearing in each one of these equations is equal to  $s$ . As will be seen later, another advantage of examining the disturbance of stability of the crystals for one of the modes is the possibility of a more certain interpretation of the physical mechanism which is the cause of a transition. 1)

Vibrations corresponding to acoustical branch do not bring about an appearance of electric fields in a nonpiezoelectric crystal and, therefore, it is natural to connect the instability of electric state of a crystal (ferroelectric transition) with the instability of the system of electric oscillators, i.e. with a nonfulfillment of the condition (5.55)

1) See paragraph 2 of this chapter concerning the methods of decreasing the order of the determinant of a secular equation using the group-theory methods.

for frequencies of the dipole limit optical branch of the spectrum. Here the case of anomalously low frequencies of the optical branch is of the greatest interest. This statement playing the role of the basic thesis of dynamic theory of ferroelectricity is at the same time a "null approximation" and, as will be clear later, is valid only for crystals with weakly marked piezoelectric properties.

We will now examine dielectric properties of a crystal in an external field  $E = E_0 e^{i\omega t}$ . For this case the equation of shell model may be written in the following form:

$$\left. \begin{aligned} \omega^2 m_x X &= (R + zCs) X + (Y + zCY) S - \epsilon E_x z, \\ 0 &= (T - YCs) X + (\Phi + YCY) S - \epsilon E_x Y. \end{aligned} \right\} \quad (5.56)$$

From these expressions we can find the dielectric constant

$$\epsilon = 1 + 4\pi \frac{\partial P}{\partial E_x},$$

where

$$P = \frac{e}{v} (zX + YS).$$

A corresponding calculation carried out in the work [6] leads to the following expression for static ( $\omega = 0$ ) dielectric constant  $\epsilon_0$ :

$$\epsilon_0 = \epsilon_\infty + 4\pi \frac{e^2}{v} z' [\text{Det } \Phi(0)]^{-1} z''. \quad (5.57)$$

Here  $z'$  and  $z''$  are dynamic ionic charges with the numbers of the row and column of the matrix  $\Phi(0)$  which were crossed out in the calculation of the principal minor of  $\Phi$ . It is clear from (5.57) that when  $\text{Det } \Phi(0) \rightarrow 0$ ,  $\epsilon_0 \rightarrow \infty$ . Thus, an inference follows from the expression (5.57) that an attempt can be made to interpret the anomalous increase of  $\epsilon_0$ , i.e. the phase transition, as a loss of stability by the lattice with respect to one of the normal vibrations whose frequency becomes imaginary. Such an approach is equivalent to the concept of "soft mode" examined by Ginzburg. This concept was already discussed in the introduction to this chapter and will be examined in detail in paragraph 4 which will also examine the question of the role of anharmonicity of vibrations. This role is extremely important in describing a ferroelectric transition. Application of the expressions (5.52-5.54) is illustrated in paragraph 4 using simple examples.

#### 6. Application of Theory to Crystals With Piezoelectric Properties in Symmetrical Phase

An attempt was made in the work [7] to apply the representations of dynamic theory to ferroelectrics with a more complex symmetry than cubic crystals and having a strong piezoelectric effect in paraelectric region.

One of important features of this case is the necessity of examining vibrations with a wave vector  $q \neq 0$ . This is connected with the interaction, characteristic of piezoelectrics, of waves belonging to acoustical and optical branches of the spectrum. 1) Thus, the discussion concerns an attempt to examine dielectric, elastic and piezoelectric anomalies from a single point of view, i.e. in terms of stability of a crystal lattice.

Theory of electroelastic properties of crystals was developed by Born and Huang [11] on the basis of a model of hard ions. Later, their theory was refined by Cowley [33] who included in the examination effects connected with electron polarization. However, for the purposes of this examination it proves to be possible to limit ourselves to a model of hard ions. Neglecting of electron polarizability of ions is reflected chiefly on the results of quantitative evaluations. In doing so, quantitative characteristics of a crystal change immaterially. In this case, the equation  $\omega^2 m X = \Phi X - zE$  contains the matrix  $\Phi = R + zCz$  and  $E$  -- a columnar matrix the elements of which represent the amplitude of depolarizing macroscopic field equal for longitudinal waves propagating in a diatomic crystal to  $-4\pi P$ .

The matrix  $\Phi$  is expanded into a series with respect to  $q$ :

$$\Phi = \Phi^0 + \sum_{\nu=1}^{\infty} \Phi_{\nu}^{(1)} q_{\nu} + \frac{1}{2} \sum_{\nu=2}^{\infty} \Phi_{\nu}^{(2)} q_{\nu}^2. \quad (5.58)$$

$\Phi^0$  is a matrix having an order of  $3s \times 3s$  and a rank of  $(3n - 3)$  (i.e.  $q=0$ ).

Next, a matrix  $H_{ik}^{\mu\nu}$  is constructed. The elements of this matrix satisfy the conditions that  $H_{ik}^{\mu\nu}$  if  $\mu=1$  and  $\nu=1$ :

$$\sum_{\nu} H_{ik}^{\mu\nu} \Phi_{\nu}^{(1)} = \delta_{ik} \lambda_{\mu}, \quad \mu, \nu = 2, 3 \dots$$

The elements of the tensors of elastic constants  $c_{iklm}^E$ , of dielectric susceptibility  $\chi_{ik}$  and piezoelectric constants  $e_{ikl}$  are expressed in terms of the elements of the matrices  $\Phi$  and  $H$  in the following manner:

$$c_{(i, km)} = \frac{1}{2\nu} \sum_{\nu} \Phi_{\nu}^{(2)} c_{ikm}^{\nu}, \quad (5.59)$$

where

$$c_{(ik, jm)} = -\frac{1}{\nu} \sum_{\nu} (\Phi_{\nu}^{(1)} H_{\nu}^{\mu})_{ikj};$$

piezoelectric constant

$$e_{ikl} = -\frac{1}{\nu} \sum_{\nu} (\Phi_{\nu}^{(1)} H_{\nu}^{\mu})_{klt} \quad (5.60)$$

1) Examination of vibrations with  $q \neq 0$  is also necessary in describing an antiferroelectric transition.

and dielectric susceptibility

$$\chi_{ik} = \frac{1}{v} \sum_{\alpha} (\epsilon H^{\alpha})_{ik}. \quad (5.61)$$

Each one of the summations given here is done over all elements of the matrix with the other indices being constant, i.e.

$$\sum_{\alpha} A_{ik} = \sum_{\alpha} A_{ik}^{\alpha}.$$

The matrix  $H$  is connected with the frequencies and amplitudes of normal vibrations in the following manner:

$$\sum_{j=1}^{3q} (\omega_j)^{-2} X_i^j X_k^j = H_{ik}^{\alpha}. \quad (5.62)$$

Here the summation is done over all of the normal modes of vibrations ( $j=1, 2, 3$  for  $q=0$  are omitted inasmuch as they correspond to the three acoustic modes).

Formula (5.62) makes it possible to express the elements of the matrix  $H$  in terms of the frequency of normal vibrations. If it is assumed, as before, that owing to a weak temperature dependence (i.e. anharmonicity) instability occurs for any one of the modes  $j=f$  when  $q \rightarrow 0$ , then  $\omega_f^2 \sim (T - \theta)$  near the transition as in the case of nonpiezoelectric cubic crystals, while the elements of the matrix  $\Phi^0$  and the values of  $X_i^j$  remain approximately constant. Taking into account (5.62) and the circumstance that the element of the matrix  $\Phi^0$  dependent on  $(T - \theta)$  is contained in the expressions for  $c_{iklm}$  and  $e_{ikl}$ , an inference should be drawn that the separate elements of these tensors will follow Curie-Weiss law in the transition region.

For illustration, the properties of a diatomic cubic crystal of the zinc-blende (ZnS) type are examined in [7]. Crystals of this structure are characterized by three different elastic constants  $c_{11}$ ,  $c_{12}$  and  $c_{14}$ , by a dielectric constant  $\epsilon_0''$  of a fixed crystal and  $\epsilon_0'$  of a free crystal, and by one piezoelectric constant  $e_{14}$ . As in the case of nonpiezoelectric crystals, conditions with which a ferroelectric transition will be observed can be obtained by an appropriate selection of the constants characterizing the interaction of lattice elements and of the coefficients before anharmonic terms. A new circumstance in comparison with the results set forth above, is the necessity of taking here into account the piezoelectric effect in paraelectric phase, i.e. taking into account the interaction of optical and acoustic modes of vibrations. In this scheme an essential difference is the following. In the case under consideration the equation (5.40) is formulated as follows:

$$\left(\frac{\omega_l}{\omega_l^0}\right)^2 = \frac{1}{\epsilon_{\infty}}. \quad (5.63)$$

Dielectric constant of a fixed crystal consisting of hard ions is defined by the expression (see in greater detail in [7]):

$$\epsilon_0^D = \frac{1 + 8\pi(z_1)^2/3R_0\omega}{1 - 4\pi(z_1)^2/3R_0\omega}$$

with  $\epsilon_0^E = \epsilon_0^D c_{44}^D / c_{44}^E$ .

The quantities  $c_{44}^E$  and  $c_{44}^D$  and the piezoelectric constant  $e_{44}$  are defined by the relationships:

$$e_{44} = \frac{1}{\nu} \left[ \eta_0 (1 - \gamma)^2 + 2.96 \frac{z_1^2}{\nu} - 2\pi (\epsilon_0^D + 2) \left( 1.2 - \frac{1}{2} \gamma \right) \frac{z_1^2}{9\nu} \right], \quad (5.64)$$

$$\left. \begin{aligned} c_{44}^E &= \frac{1}{\nu} \left[ R_0 (1 - \gamma^2) / 8 - 1.57 \frac{z_1^2}{\nu} + 4\pi (\epsilon_0^D + 2) \left( 0.60 - \frac{1}{2} \gamma \right)^2 \left( \frac{z_1^2}{9\nu} \right) \right], \\ c_{44}^D &= \frac{z_1 z_2 (\epsilon_0^D + 2)}{3\nu} \left[ \frac{5.03 (z_1)^2}{\nu R_0} - \frac{1}{2} \gamma \right]. \end{aligned} \right\} \quad (5.65)$$

Here  $R_0$  is the constant of interaction between the ions of Zn (1) and of S (2) with  $q=0$ ;  $\gamma$  is defined as a ratio of the force constants

$$\Phi_{Rxy}^{12} / \Phi_{Rxy}^{12}$$

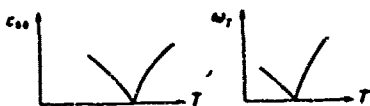


Figure 5.8. Qualitative temperature dependence of the quantities  $c_{44}^E$  and  $\nu_T$  for a model of a ferroelectric with piezoelectric properties.

If the force constants are such that  $\omega_t$  in the equation (5.63) differs little from zero and that owing to anharmonicity in transition region

$$\begin{aligned} 1 - 4\pi (\epsilon_0^D + 2) \frac{z_1^2}{3\nu R_0} &= \\ &= \pi \omega_t \frac{z_1^2}{R_0} = C_0 (T - \theta). \end{aligned}$$

then substituting this expression into (5.63) and then into (5.64) and (5.65) it can be shown that at a certain temperature the quantity  $c_{44}^E$  must vanish and, consequently, with a decrease of temperature the crystal becomes unstable with respect to the transverse acoustic mode before it becomes unstable with respect to the transverse optical mode (figure 5.8).

In principle, using an appropriate selection of the constants of a crystal it is possible to "design" a transition in which crystals, in particular those of ZnS, will exhibit antiferroelectric properties. For this purpose it is necessary to assume [7] that the instability of the

transverse optical mode takes place when  $q = \frac{\pi}{2a}$  (which corresponds to the motion of like ions toward each other over one lattice spacing). This type of transition may materialize if the temperature  $T_A$  at which it is to be observed proves to be considerably higher than  $\Theta$  (compare with chapter 4, paragraph 4, subparagraph 3). Such a situation apparently arises in  $\text{NH}_4\text{H}_2\text{PO}_4$ . According to the data of Nagamija [34] an antiferroelectric transition of this crystal may be defined from the standpoint of his examination as instability with respect to the mode of vibrations having a lower frequency than the ferroelectric mode.

Application of representations on the mechanism of a ferroelectric transition on the basis of displacement of ions in hydrogen-containing ferroelectrics (for example, Seignette's salt and  $\text{KH}_2\text{PO}_4$ ) leads to a number of difficulties. It might be assumed that the double transition in Seignette's salt is connected with the situation examined above when the crystal has two transition points one of which is brought about by a strong piezoelectric effect (see paragraph 3, chapter 3), i.e. by instability with respect to acoustic mode of vibrations. However, at the present time, physical mechanism of ferroelectric transition in these crystals is as yet insufficiently clear (see also paragraph 3 of this chapter).

## Par. 2. Group-Theory Analysis of Vibration Spectra in Crystals

Calculations of vibration spectra of actual crystals are connected with considerable difficulties. In addition to a large amount of calculations these difficulties are brought about by insufficient information on potential function of a crystal. The last is especially essential for ferroelectrics representing chiefly crystals with a complex structure and a large number of atoms in the unit cell.

The results of calculations of vibration spectra may greatly depend on the model used, with the simple models proving to be insufficiently effective in a number of cases; on the other hand, in complex models it is necessary to introduce a large number of adjusting parameters which impair the reliability of theory. Because of this, results which can be obtained on the basis of general principles without resorting to concrete models and to the approximation connected with them, acquire special significance.

Such results may be obtained first of all with a consistent taking into account of the crystal symmetry using group-theory methods. Group-theory approach affords the following possibilities.

a. It makes it possible to predict the number of bands in a vibration spectrum for a specified value of the wave vector  $q$ , the multiplicity of degeneration of the bands, the character of their polarization and the types of splittings in the case of minor changes in the wave vector.

b. Using the projection operators it is possible to find at the singular (symmetrical) points of Brillouin zone <sup>1)</sup> the symmetry coordinates the linear combinations of which are normal vibrations; in this manner the mode of normal vibrations is determined directly in a number of important particular cases (see paragraph 3 of this chapter).

c. The determinant of secular equation (5.22) at the symmetrical points of Brillouin zone can be reduced to a product of several determinants of lower order. This makes the calculations considerably easier making it possible in a number of cases to obtain results in analytical form even for complex crystals.

d. Group-theory analysis also makes it possible to follow up a change in vibration spectra (i.e. to predict a change in the number of lines and the splitting of the bands) in the case of phase transitions and external actions on a crystal.

e. For displacement-type transitions, in particular for ferroelectric transitions, using the concept of "soft mode" it is possible to limit the class of possible changes -- predicted by Landau theory -- in the symmetry of a crystal during a phase transition.

#### 1. Principles of Group-Theory Analysis of Vibration Spectra in Crystals

Group-theory analysis of vibration spectra is based on the circumstance that each normal vibration is transformed in accordance with an irreducible representation of a symmetry group, with the multiplicity of the degeneration of a vibration being equal to the dimensionality of the representation (see, for example, [35, 36]). Therefore, for a group-theory analysis it is necessary to find the characters of reducible representation according to which the entire assemblage of normal vibrations is transformed for a specified value of the wave vector  $q$  (such a reducible representation is called mechanical representation) and it is also necessary to expand the mechanical representation into irreducible representations of the wave-vector group.

The characters of a mechanical representation  $\chi_q$  may be found from simple geometrical considerations. With a turn by an angle  $\varphi$  about the z-axis the coordinates  $x$ ,  $y$  and  $z$  of Cartesian system are transformed in accordance with the following rule:

$$\left. \begin{aligned} x &= X \cos \varphi - Y \sin \varphi, \\ y &= X \sin \varphi + Y \cos \varphi, \\ z &= Z. \end{aligned} \right\} \quad (5.66)$$

<sup>1)</sup> Basic concepts connected with irreducible representations of space groups and projection operators are set forth in brief form in chapter 6 where references to respective literature are also given.

With a mirror turn by an angle  $\varphi$  we have:

$$\left. \begin{aligned} x &= X \cos \varphi - Y \sin \varphi, \\ y &= X \sin \varphi + Y \cos \varphi, \\ z &= Z. \end{aligned} \right\} \quad (5.67)$$

The traces of the matrices (5.66) and (5.67) are equal to  $1+2 \cos \varphi$  and  $-1+2 \cos \varphi$  respectively. Taking also into account that translations to the lattice vector  $\hat{A}h$  (here  $\hat{A}$  is a matrix of the base vectors of the lattice) in an irreducible representation of a space group (see chapter 6) corresponds to a multiplication by  $\exp - iq\hat{A}h$ , we obtain [36]:

$$\chi_q(g) = (\pm 1 + 2 \cos \varphi) \sum_n n_h e^{-iq\hat{A}h}. \quad (5.68)$$

Here the group element  $g = t_{\alpha} S$  where  $t_{\alpha}$  is a "nonelementary translation" (i.e. translation over a portion of the lattice spacing) and  $S$  is a turn or a mirror turn. The plus sign corresponds to a turn and the minus sign -- to a mirror turn;  $n_h$  indicates the numbers of atoms in a unit cell with number zero, which passed into the unit cell  $h$  under the action of the symmetry element  $g$  without changing their number.

After the characters of mechanical representation have been calculated the numbers  $m_{qp}$  of the normal vibrations transformed in accordance with irreducible representation of  $\tau_{qp}$  of the wave-vector group  $G_q$ , can be found using the following formula:

$$m_{qp} = \frac{1}{N_q} \sum_{g \in G_q} \chi_q(g) \chi_{qp}^*(g). \quad (5.69)$$

Here  $N_q$  is the order of the group  $G_q$ ,  $\chi_{qp}(g)$  is the character corresponding to the element  $g$  in the irreducible representation of  $\tau_{qp}$ :

$$\chi_{qp}(g) = \chi_{qp}(S) e^{-iq\hat{A}h}, \quad (5.70)$$

where  $\chi_{qp}$  is the corresponding character of a loaded irreducible representation. The characters of loaded representations for all irreducible representations of the space groups are given in the monograph [37].

Compatibility relationships (they are also sometimes called correlation relationships) are also found in group-theory analysis. These relationships show the change in irreducible representations in accordance with which normal vibrations are transformed with such a small change in the wave vector  $q$  that its group changes. Compatibility relationships define, in particular, the adhesion or splitting of the branches of vibration spectrum with a change in  $q$ .

In order to determine them it is necessary to calculate the numbers  $m_{qp}, q'p'$  which show how many times the irreducible representation is contained in the representation  $\tau_{qp}$ :

$$m_{q'p'} = \frac{1}{N} \sum_{S \in G_0} \chi_{q'p'}(S) \chi_{qp}^*(S) \quad (5.71)$$

Relationships similar to (5.71) also make it possible to follow a change in vibration spectrum in phase transitions in the case when a symmetry group of one of the phases is a subgroup of a symmetry group of another phase.

For example, for the limit normal vibrations such an investigation is reduced to a calculation of the numbers:

$$m_{jj'} = \frac{1}{N} \sum_{S \in G_0} \chi_j(S) \chi_{j'}^*(S) \quad (5.72)$$

Here  $N$  is the order of the point group of a low-symmetry phase, and  $j$  and  $j'$  are the numbers of irreducible representations of the symmetry groups  $G_n$  and  $G_c$  of the high-symmetry and low-symmetry phases respectively.

The problem of change in vibration spectrum in the case of an external action on the crystal is reduced in essence to the preceding problem if, in accordance with Curie principle, we mean by the symmetry group of a crystal in the presence of an external influence a group consisting of symmetry elements common for the crystal and external influence.

Examples of using the relationships (5.71) and (5.72) will be given in paragraph 3 of this chapter. Paragraph 3 is devoted to the analysis and calculation of vibration spectra of concrete ferroelectric crystals.

## 2. Symmetry Coordinates and Splitting of Secular Equation at the Symmetric Points of Brillouin Zone

Initial equations of Born-Karman theory (see 5.20)

$$m \ddot{x}_i^a = - \sum_j^N \chi_{ij}^a \quad (5.73)$$

are written in Cartesian coordinates of displacements of all atoms of a crystal. However, a substitution of the following form

$$x_i^a = \chi_i^a(\mathbf{q}) e^{i\mathbf{q} \cdot \mathbf{R}_i} \quad (5.74)$$

i.e. making use of translation symmetry of the lattice makes it possible

to reduce the initial system of equations of the order of  $3Ns$ , where  $3Ns$  is the number of degrees of freedom of the crystal, to a set of systems of equations of the order of  $3s$  where  $s$  is the number of atoms in a unit cell for  $N$  values of the wave vector.

Accordingly, a secular equation of the order of  $3Ns$  which could have been written for the initial system (5.73) is split into  $N$  secular equations of an order which is smaller by  $N$  times. This splitting proved to be possible because we (using the language of group theory) passed on from a coordinate system in which crystal symmetry was not taken into account, to coordinates transforming in accordance with the irreducible representations of a symmetry group -- in the case in question in accordance with irreducible representations of a translation group. The fact that the coordinates  $X_i^{\mu}(q)$  are transformed in accordance with irreducible representation  $\tau_q$  of the translation subgroup can be easily proven by a direct verification.

Thus, the basic property of the crystals common for all of them -- translation symmetry, is automatically taken into account in Born-Karman theory. However, the point symmetry the elements of which will remain for the wave vectors  $q$  at the symmetric points of Brillouin zone, is different for different crystals and different values of  $q$  and it can be taken into account during concrete calculations. Projection operators should be used to determine the symmetry coordinates (see chapter 6). After all of the symmetry coordinates have been found, bearing in mind that normal vibrations which are transformed in accordance with the irreducible representation under consideration, are a linear combination of the respective symmetry coordinates, some conclusions concerning the mode of normal vibrations may be drawn in a number of cases without a calculation.

In particular, if only one normal vibration is transformed in accordance with the irreducible representation in question, its mode will coincide with the respective symmetry coordinate with accuracy to the normalization constant.

If we pass on from the base of the coordinates  $X_i^{\mu}(q)$  to the base of symmetry coordinates which take point symmetry into account, then the secular equation (5.22) of the order of  $3s$  for the determination of vibration frequencies of the crystal with a specified  $q$  may decompose into units. Each unit will be related to a certain irreducible representation, and the order of the unit will be equal to the number  $m_{qp}$  (see [38]) of normal vibrations which are transformed in accordance with the irreducible representation in question. To split the secular equation the matrix  $\tilde{\Phi}(q)$  of the components of the frequency tensor should be subjected to a unitary transformation:

$$\tilde{\Phi}'(q) = \hat{U} \tilde{\Phi}(q) \hat{U}^{\dagger}. \quad (5.75)$$

Here  $\hat{U}$  is a transformation matrix which brings about the transition

to the base of the symmetry coordinates, 1)  $\hat{U}^{-1}$  is a matrix which is transposed and is a complex conjugate with respect to  $\hat{U}$ .

Examples of using symmetry coordinates in the calculation and analysis of vibration spectra of ferroelectrics will be given in paragraph 3 of this chapter. For the time being we will note that, for example, in the calculation of vibration spectrum for a simplified model of  $\text{KH}_2\text{PO}_4$  by means of a transformation of (5.75) it was possible to obtain analytical formulas for vibration frequencies even from a 12th-order secular equation.

### 3. Selection Rules

Selection rules which determine whether a given normal vibration will appear in infrared spectra or Raman spectra are based on a general theorem [39] according to which the integral taken from a function which is transformed in accordance with a non-unit irreducible representation of a group over the entire configuration space is identically equal to zero.

It follows from this theorem that for a function  $F$  relating to a reducible representation  $\tau$ ,  $\int F dV$  will be non-zero only in the case if  $\tau$  contains a unit representation.

We will apply these results to obtain selection rules for infrared absorption the intensity of which in long-wave approximation [40] is defined by the square of the modulus of the matrix element of the dipole moment:

$$[\mu_{00} = \text{vib}] = \langle \psi_{2\text{vib}} | d | \psi_{1\text{vib}} \rangle^2 \quad (5.76)$$

Here  $\psi_{1\text{vib}}$  and  $\psi_{2\text{vib}}$  are the initial and final wave functions of vibratory states. The integrand of the matrix element (5.76) is transformed in accordance with the following representation:

$$\tau = \tau^{(2)} \times V \times \tau^{(1)} \quad (5.77)$$

where  $\tau^{(2)}$  and  $\tau^{(1)}$  are irreducible representations in accordance with which  $\psi_{2\text{vib}}$  and  $\psi_{1\text{vib}}$  respectively are transformed,  $V$  is a vector representation in accordance with which the dipole moment  $d$  is transformed. For the activity of the  $\psi_{1\text{vib}} \rightarrow \psi_{2\text{vib}}$  transition it is necessary that  $\tau$  contain a unit representation or (which, as can be shown, is the same) that  $\tau^{(2)} \times V$  contain  $\tau^{(1)}$ .

1) It is convenient to take as  $\hat{U}$  a rectangular matrix corresponding to symmetry coordinates only for one irreducible representation selected. Then, as a result of transformation of (5.75) we will obtain a unit of secular equation related to the specified irreducible representation [38].

Diagonal matrix elements require special examination. In this case there is only one set of wave functions and their products in pairs realize the so-called symmetric product of the representations  $[(\tau^j)]^2$  [39] and not a direct product of  $\tau^j \times \tau^j$ . Therefore, for the presence of diagonal elements it is necessary that the unit representation be contained in the product of:

$$\tau^j \times [(\tau^j)]^2 \times \tau^j. \quad (5.78)$$

As an example we will examine selection rules for the first-order infrared spectra in which vibrations with a wave vector  $q=0$  appear.

If a transition takes place from the fundamental (completely symmetrical) state, then it follows from (5.77) that the irreducible representation in question is "active" in the infrared spectrum if it is contained in vector representation, i.e. if one or several vector components are transformed in accordance with it.

In a similar manner it can be shown that if, neglecting the absorption, the tensor of polarizability of the crystal is considered to be symmetric, then irreducible representations which are contained in  $[V^j]^2$  will be "active" in the first-order Raman spectrum.

After carrying out a more detailed analysis and determining precisely which component of polarizability tensor is transformed in accordance with a given irreducible representation, it is possible to predict in a number of cases the polarization of scattered radiation by the symmetry of normal vibration and vice versa. In the next paragraph this method will be explained using the Raman spectrum of the ferroelectric  $\text{NaN}_2$  as an example.

#### 4. Group-Theory Analysis of Limit Dipole Vibrations in Ionic Crystals

The standard group-theory analysis does not take into account the dependence of the limit dipole vibrations on the direction of the wave vector  $q \rightarrow 0$ . At the same time, examination of this dependence may materially change the interpretation of the bands of vibration spectra in ionic crystals. To take this dependence into account in group-theory analysis the limit dipole frequencies should be classified according to irreducible representations of the wave-vector group whereas the non-dipole limit vibrations are classified, as before, according to the irreducible representations with  $q=0$  [41].

In order to carry out a group-theory analysis of dipole limit vibrations for a given direction of  $q \rightarrow 0$  it is convenient to carry out first the standard group-theory analysis for  $q=0$  and then make use of compatibility relationships for irreducible representations of the point group that are active in infrared spectra. However, it should be taken

into account that the degree of splitting may prove to be smaller than that predicted by group theory. Thus, in ionic cubic diatomic optically isotropic crystals the thrice degenerated frequency of dipole vibration is split by the macroscopic field into an undegenerated frequency of longitudinal vibration and twice degenerated frequency of the transverse vibration. These frequencies do not depend on the direction of  $q \rightarrow 0$  whereas group theory formally predicts for the whole (nonsymmetric) direction of  $q$  a splitting into three undegenerate vibrations. In addition to this, it does not follow from group-theory considerations that the frequencies of respective vibrations must coincide for wave vectors not belonging to one star. However, in less symmetrical crystals such a classification proves to be more adequate to reality. This is shown, for example, by numerical calculations for crystals of rutile structure [13], which completely fit into the scheme of procedure given above.

More detailed data on normal vibrations can be obtained by determining the symmetry coordinates with the aid of projection operators. To determine symmetry coordinates of dipole vibrations with a specified direction of  $q \neq 0$  symmetry coordinates should first be found with the aid of projection operators for irreducible representations with  $q=0$ , and then a "secondary projection" should be carried out by applying to the symmetry coordinates obtained the projection operators for irreducible representations with a given wave vector  $q$ . The advantage of such an approach consists in that it does not affect at all the symmetry coordinates of nondipole vibrations for which the usual procedure is applicable. With the aid of symmetry coordinates it is possible to determine the character of dipole limit vibrations (longitudinal, transverse or mixed) and also set up transformation matrices and split with their aid the secular equation for determining the vibration frequencies (see subparagraph 2 of this paragraph).

#### 5. Limitations Imposed on Possible Changes in Symmetry in the Case of Phase Transitions of Displacement Type

Landau thermodynamic theory of phase transitions of the second kind limits the class of possible changes in symmetry in the case of a phase transition (see paragraph 2, chapter 3). However, as pointed out in the work [42], in transitions of displacement type when the "order" parameter is connected with the "soft mode" one more limitation should be imposed on the irreducible representation accounting for the phase transition: it must be contained in mechanical representation.

If a phase transition is not connected with the formation of superstructure, i.e. it takes place without a change in the number of atoms in the unit cell, then this mechanical representation corresponds to the wave vector  $q=0$ . We will note that for ferroelectrics in which transition takes place due to instability with respect to the limit dipole vibration the irreducible representation connected with the transition must, con-

sequently, be contained in the vector representation (see subparagraph 3 of this paragraph) and in this manner additional limitations imposed by the "soft mode" on the change in symmetry in the case of phase transition coincide with the limitations imposed by Curie principle.

### Par. 3. Calculations of Vibration Spectra of Actual Ferroelectric Crystals

As already underscored above, calculation of vibration spectra of actual ferroelectric crystals is connected with great difficulties due to which the calculation of a vibration spectrum with the aid of a shell model, for example, one which requires introduction of a large number of parameters is worthwhile chiefly in those cases when experimental dispersion curves  $\omega(q)$  were obtained with the aid of slow-neutron scattering. Then, using models of different degree of complexity it is possible to achieve reliable interpretation of vibration spectra. Unfortunately, it was possible to put such a program into practice only for strontium titanate [26] owing to the fact that it proved to be possible to obtain sufficiently large and pure single crystals and study them with the aid of neutron spectroscopy. For a number of other ferroelectrics (BaTiO<sub>3</sub> [43, 44], KH<sub>2</sub>PO<sub>4</sub> [21, 22], [45-48], NaNO<sub>2</sub>) [23, 49] only a group-theory analysis of the vibration spectrum was made and comparatively simple models for the limit normal vibrations were calculated.

#### 1. Perovskites (BaTiO<sub>3</sub>, SrTiO<sub>3</sub>)

A unit cell of crystals with perovskite structure (SrTiO<sub>3</sub>, BaTiO<sub>3</sub>, etc.) is shown in Figure 5.9a. The space group of the crystal in cubic phase is O<sub>h</sub><sup>F</sup> (Pm3m), in tetragonal phase -- C<sub>4v</sub><sup>F</sup> (P4mm) and in rhombic phase -- C<sub>2v</sub><sup>F</sup> (Pmm2). The results of group-theory analysis for the limit normal vibrations [43, 44, 50] are given in Table 8.

Selection rules indicate that vibrations of the type F<sub>2u</sub> and B<sub>1</sub> (for C<sub>4v</sub>) are forbidden in infrared spectra, and F<sub>1u</sub> and F<sub>2u</sub> -- in Raman spectra. In the case under consideration, analysis of symmetry coordinates makes it possible to determine unambiguously the mode of the vibration F<sub>2u</sub> (Figure 5.9b).

Compatibility relationships for a phase transition from a cubic to tetragonal modification have the following form:

$$F_{1u} \leftrightarrow A_1 + E,$$

$$F_{2u} \leftrightarrow B_1 + E.$$

The dependence of the frequencies of dipole vibrators on the direction of  $q \rightarrow 0$  changes the group-theory classification for the vibrations F<sub>1u</sub> (cubic phase), A<sub>1</sub> and E (tetragonal phase) and A<sub>1</sub>, B<sub>1</sub> and B<sub>2</sub> (rhombic phase). For vibrations of the type F<sub>1u</sub> this dependence will amount to their splitting into a longitudinal (undegenerated) and a transverse (twice degenerated) vibration.

Table 8  
Results of Group-Theory Analysis of the Limit  
Normal Vibrations for Crystals  
With Perovskite Structure

1-Точечная группа . . . . .	$O_h$			$C_{4v}$			$C_{3v}$		
2-Неприводимые представления . . . . .	$F_{1g}$	$F_{2g}$	$F_{3g}$	$A_1$	$B_1$	$E$	$A_1$	$B_1$	$E$
3-Число нормальных колебаний (оптические акустические)	3	1	1	3	1	4	4	4	4
6-Примечание. Неприводимые представления, по которым не преобразуются ни одно из нормальных колебаний кристаллов перовскита, в таблице не приводятся.	1	0	1	0	1	1	1	1	1

- Key: (1) Point group (6) NOTE. Irreducible representations in accordance with which none of the normal vibrations of crystals with perovskite structure are transformed are not given in the table.
- (2) Irreducible representations
- (3) The number of normal vibrations
- (4) Optical
- (5) Acoustic

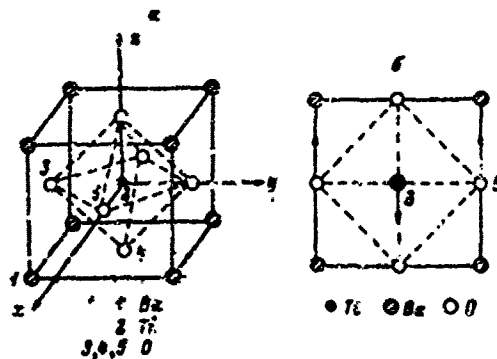


Figure 5.9. Normal vibrations of the type  $F_{2u}$  for crystals with perovskite structure.

a -- a unit cell of crystals with perovskite structure; b -- mode of normal vibration  $F_{2u}$  for crystal lattice of perovskite type.

We will pass on to the results of numerical calculations. Cowley [26] examined six different models for describing lattice vibrations in  $SrTiO_3$ , including a model of "hard" ions. The parameters of the model were determined by means of an adjustment to experimental data using the nonlinear method of least squares. In this process, eight adjustment parameters are used in the model of "hard" ions, and in the simplest of the shell models -- fourteen.

The model of "hard" ions (model 1) leads to considerable divergences with the experiment. Therefore, a number of refinements are suggested: a) the short-range forces are taken into account not only between the neighboring ions but also with the layer of ions following the nearest layer (model 2); b) effective ionic charges are varied (model 3); c) polarizability not only of the negative but also of the positive ions is introduced (models 4, 5, 6).

Each one of these models, 2 and 3 and 4, 5, 6 contains the preceding model and complements it.

As should have been expected, models with the highest numbers in which the largest number of parameters are varied give the best coincidence with the experiment. In this case, when the values of the dielectric and elastic constant approach those of the experiment it is also possible to obtain a fair coincidence for the dispersion curve (Figure 5.10).

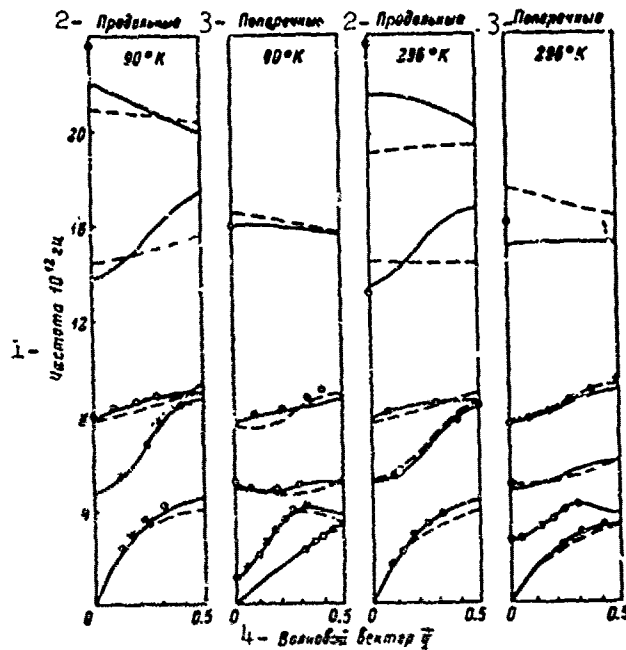


Figure 5.10. Calculated and measured Cowley [26] dispersion curves for  $\text{SrTiO}_3$ .

Solid curves correspond to model 4 and broken curves -- to model 5.

Key: 1 -- Frequency of  $10^{12}$  cps; 2 -- Longitudinal;  
3 -- Transverse; 4 -- Wave vector  $\vec{q}$ .

However, some atomic parameters of the lattice have values which are difficult to explain from physical standpoint. As supposed in [26], this contradiction may be removed if not only the dipole but also the quadrupole moments are taken into account for highly polarizable ions (chiefly negative ions).

An important inference from the results of the calculations on the basis of different models is that merely an insignificant change in the parameters of short-range forces with the charges and polarizabilities of the ions being invariable, greatly affects the results of the calculation. This confirms the supposition following from theory that an insignificant temperature dependence of interaction constants with an exact balance of the short- and long range forces may bring about a high temperature dependence of low-frequency transverse optical vibrations.

We will pass on to a discussion of the results of calculations of the vibration spectrum of barium titanate. Attempts at these calculations were undertaken in the work [44] for a model of "hard" ions. Electron polarizabilities of the ions were also taken into account (phenomenologically, and not within the framework of a shell model) in the calculations. The covalence of the bonds was taken into account by an introduction of effective ionic charges.

Vibrations of ions are described by the following equation:

$$m_i \ddot{x}_i = - \sum_{j,k} (R_{ik}^{xy} + C_{ik}^{xy}) x_j; \quad (q=0).$$

where  $R_{ik}^{xy}$  are constants characterizing the short-range forces of ions and  $C_{ik}^{xy}$  -- structural coefficients, as in (5.50).

The values of  $R_{ik}^{xy}$  are calculated from the known representation of interaction potential [11] (see 4.50).

Substitution of the values of the charges ( $z_{Ti}=4$ ,  $z_{Ba}=2$ ,  $z_O=-2$ ) into these expressions leads to a result that among frequencies which are solutions of dispersion equation, some prove to be imaginary, or in other words, a purely ionic crystal proves to be unstable inasmuch as a strong Coulomb interaction of sublattices is not balanced by short-range forces. Therefore, overlaps of electron shells are introduced:  $z_i' = rz_i$  where  $r$  is an empirical coefficient. However, in this case, solution proves to be stable when  $r \leq 0.1619$ . A value of polarization  $P_s$  understated by more than one half in comparison with the experiment corresponds to this value of  $r$ .

It is, therefore, understandable that in the future it would be of interest to undertake attempts at the calculations of the vibration spectrum of  $BaTiO_3$  for more realistic models.

## 2. Potassium Dihydrogen Phosphate ( $\text{KH}_2\text{PO}_4$ )

Theoretical investigations of the vibration spectrum of  $\text{KH}_2\text{PO}_4$  [22] were undertaken in two directions: 1) group-theory analysis of the entire vibration spectrum and determination and analysis of symmetry coordinates for a value of the wave vector  $q=0$  both for paraelectric and for ferroelectric modification [45, 48]; 2) numerical calculation of the frequencies of normal limit ( $q=0$ ) translation vibrations (a region of comparatively low frequencies of up to  $200 \text{ cm}^{-1}$ ) [21, 46] and calculation of the relative amplitudes of displacement of particles in these modes [47].

A group-theory analysis of vibration spectrum was carried out in the work [45] for paraelectric modification of  $\text{KH}_2\text{PO}_4$ , i.e. the numbers of branches of vibration spectrum and multiplicities of degeneracy of the frequencies of normal vibrations corresponding to different irreducible representations for singular (symmetric) points of Brillouin zone were determined and compatibility relationships making it possible to judge the adhesion or splitting of the branches of vibration spectrum with such a change of the wave vector  $q$  when its group changes were also obtained. A similar calculation was carried out in the work [48] for low-temperature modification.

In accordance with Ginzburg--Andarson--Cochran theory, direct information concerning the micromechanism of a ferroelectric transition can be obtained from spectroscopic studies of limit normal vibrations. This accounts for the special importance of the study and interpretation of Raman spectra and infrared spectra of the first order for ferroelectrics. Therefore, a more detailed analysis was made for the limit normal vibrations of KDP.

In a number of cases, long-wave normal vibrations of a crystal can be approximately divided into external and internal vibrations of molecular or ionic complexes. Although the legitimacy of such a division is not obvious in advance, the fact that in different crystals isomorphous to  $\text{KH}_2\text{PO}_4$  the same bands are observed in Raman spectra in the region of internal vibrations of  $(\text{H}_2\text{PO}_4)^{-1}$  ions indicates that for crystals with the  $\text{KH}_2\text{PO}_4$  structure this approximation is reasonable. In their turn, from the external vibrations of the ions of  $(\text{H}_2\text{PO}_4)^{-1}$  it is possible to separate their orientational and translational motions. The results of a group-theory analysis made on the basis of identification of the limit normal vibrations with the internal, orientational and translational vibrations of  $(\text{H}_2\text{PO}_4)^{-1}$  ions are given in Table 9.

To obtain more detailed data on normal limit vibrations both for ferroelectric [48] and for paraelectric modification [45], symmetry coordinates -- linear combinations of particle displacements, transformed in accordance with a given irreducible representation were obtained with the aid of Malvin [51] projection operators. Analysis of symmetry coordinates indicates that separation of normal vibrations into internal, orientational

Table 9

Results of Group-Theory Analysis of Normal Limit ( $q=0$ ) Vibrations in  $K_2PO_4$  on the Basis of Their Identification With Internal, Orientation<sup>1</sup> and Translational Vibrations of  $(H_2PO_4)^-$  ions

Above curie point						Below curie point					
	$n$	$n_i$	$T_a$	$T_o$	$R$		$n$	$n_i$	$T_a$	$T_o$	$R$
$A_1$	5	3	0	0	1	$A_1$	11	8	1	1	1
$A_2$	5	4	0	0	1	$A_2$	14	8	0	2	1
$B_1$	6	4	0	2	1	$B_1$	13	7	1	3	2
$B_2$	7	5	1	1	0	$B_2$	13	7	1	3	2
$E$	13	7	1	3	2						

NOTE.  $n$  is the total number of vibrations transformed in accordance with a given irreducible representation;  $n_i$ ,  $T_a$ ,  $T_o$  and  $R$  are the numbers of internal vibrations, acoustic and optical translations and orientations respectively.

and translational vibrations is a priori not rigorous although as noted above it can serve as a reasonable approximation for a preliminary interpretation of the spectrum. With the aid of symmetry coordinates it is possible to obtain transformation matrices for splitting the secular equation from which the frequencies of normal vibrations are found similarly to the way this was done in the works [21, 46, 47] for a simplified model. However, an obstacle for a numerical calculation which in principle would make it possible to interpret Raman spectra and infrared spectra of the first order, is the as yet insufficient knowledge of potential function of the crystal.

Group-theory analysis predicts that for a ferroelectric modification, 45 lines must show in the first-order Raman spectrum (34 lines in the infrared spectrum) and for a paraelectric modification -- 28 and 18 lines respectively. But in the experiments on Raman effect [52] 27 well-defined bands were found for paraelectric modification out of which, according to the interpretation of the authors of the work [52], only 18 lines correspond to fundamental frequencies; 36 lines are observed below the point, out of which a portion of the bands also corresponds to composite frequencies. However, if it is assumed that the correlation between protons scarcely splits the frequencies of normal vibrations, then it follows from the analysis of symmetry coordinates that above Curie point 23 lines must show in Raman spectrum and below Curie point -- 36 lines. This agrees better with the experimental data. It is possible that Raman spectrum obtained in the work [52] is not entirely complete and thus the supposition that correlation between protons scarcely splits the frequencies of normal vibrations cannot be considered to have been proven.

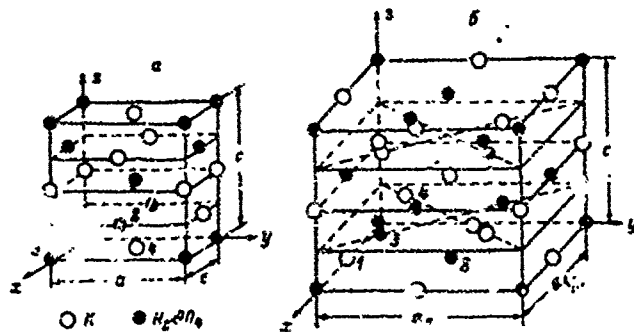


Figure 5.11. Unit cell of  $\text{KH}_2\text{PO}_4$  for a simplified model.

a -- above Curie point; b -- below Curie point. Numerals 1-4 indicate inequivalent structural units.

We will note that (from the standpoint of Ginzburg-Anderson-Cochran theory) ferroelectric vibration in  $\text{KH}_2\text{PO}_4$  corresponds to irreducible representation of  $A_1$  below Curie point and irreducible representation of  $B_2$  above Curie point. This agrees with the schematic mode of ferroelectric vibration assumed by Cochran for  $\text{KH}_2\text{PO}_4$  [7].

A more detailed comparison of results obtained in group-theory analysis, with the experiment requires further experimental studies of Raman spectra and infrared spectra of  $\text{KH}_2\text{PO}_4$ , in particular a study of polarization lines and temperature dependence of intensities and half-widths.

Neutron diffraction analysis shows that the structure of  $\text{KH}_2\text{PO}_4$  crystals may be regarded as consisting of ions of  $\text{K}^+$  and  $\text{H}_2\text{PO}_4$  groups [53]. This also finds a certain confirmation in spectroscopic studies [52]. A unit cell of paraelectric modification of  $\text{KH}_2\text{PO}_4$  for the respective model is shown in Figure 11a and a unit cell of ferroelectric modification -- in Figure 11b.

At the singular points of Brillouin zone, to determine the vibration frequencies, the secular equation may be split into several simpler equations the orders of which are determined from group-theory analysis. For this purpose, transformation matrices are constructed out of the coefficients at the base functions in orthonormalized symmetry coordinates corresponding to the given irreducible representation and then the matrix  $\Phi$  of the components of frequency tensor is transformed in accordance with the following rule [38] (see subparagraph 2, paragraph 2 of this chapter):

$$\Phi' = U \Phi U^\dagger.$$

Here  $\Phi'$  is a transformed secular matrix having a unit form; the transformation matrix  $U^+$  is a transposed matrix complexly conjugate to  $U$ . For the  $\text{KH}_2\text{PO}_4$  model used the splitting of secular equation and numerical calculation [21, 46] were carried out for a  $q \rightarrow 0$  along the tetragonal axis. In doing so, to calculate the long-range Coulomb forces the  $(\text{H}_2\text{PO}_4)^-$  groups were assigned a unit negative charge and repulsive forces were taken into account only between  $\text{K}^+$  ions and the nearest oxygen atoms.

Table 10

Calculation of Frequencies (in  $\text{cm}^{-1}$ ) of Translational Normal Vibrations in  $\text{KH}_2\text{PO}_4$

1 Имя точки Кюри			2 Имя точки Кюри		
ЧИСЛО ПОЯВЛЕНИЯ [52]	ЧИСЛО [21]	СВЯЗЬ С [52]	СВЯЗЬ С [52]	ЧИСЛО [21]	ЧИСЛО ПОЯВЛЕНИЯ [52]
—	5	$B_1'(\tau_1)$	$A_1'(\tau_1)$	—	—
58	66	$E'(\tau_1)$	$B_2'(\tau_1)$	64	60
			$B_3'(\tau_1)$	70	
96	99	$E''(\tau_1)$	$B_1''(\tau_1)$	115	101
			$B_2''(\tau_1)$	95	
116	119	$E'''(\tau_1)$	$B_3''(\tau_1)$	114	115
			$B_1'''(\tau_1)$	130	
135	135	$B_2'''(\tau_1)$	$A_2''(\tau_2)$	147	141
132?			$B_2(\tau_2)$	193	170
186	187	$B_3(\tau_2)$	$A_1(\tau_2)$		214?

NOTE. The 3rd and 4th columns represent compatibility relationships characterizing the behavior of the spectrum during a phase transition. The following relationships exist in addition to those shown in the table:  $A_1(\tau_1) \rightarrow A_1(\tau_1)$ ;  $A_2(\tau_2) \rightarrow A_2(\tau_2)$ .

The results of the calculation are summarized in Table 10 where they are compared with the data on the first-order Raman spectrum [52]. Agreement with experimental data is sufficiently good. The frequency  $A_2$  for ferroelectric modification turns out to be imaginary. This indicates incorrectness of the model of potential used, for describing the respective normal vibration. We will also note that theory predicts unobserved splitting of the frequencies  $E'$ ,  $E''$  and  $E'''$  which could have been clearly detected by means of measurements in polarized light.

Apparently the model used for numerical calculations may be utilized in the calculation of translation spectra both of the crystals isomorphous to  $\text{KH}_2\text{PO}_4$  and of the other crystals consisting of ions of alkaline metals and molecular or ionic complexes approaching in form spherical complexes. Examples of such crystals may be provided by  $\text{Na}_2\text{SO}_4$ ,  $\text{K}_2\text{SO}_4$ ,  $\text{K}_2\text{PO}_4$ , etc.

The calculation which was carried out makes it possible not only to interpret Raman spectra in the region of comparatively low frequencies

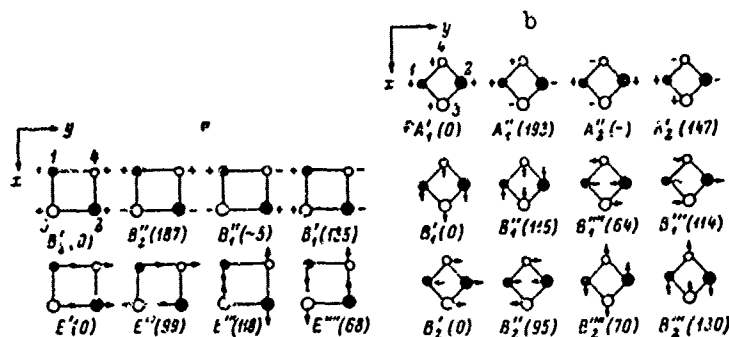


Figure 5.12. Normal Translational Vibrations in  $\text{KH}_2\text{PO}_4$ .

a -- above Curie point; b -- below Curie point. Small circles indicate  $\text{K}^+$  ions and large circles indicate ions of the  $(\text{H}_2\text{PO}_4)$  group; black circles indicate particles lying in  $xy$  plane and white circles -- those at the  $c/4$  level. Displacements along the  $x$ - and  $y$ -axes are indicated by arrowheads; displacements in the positive direction of  $z$ -axis are indicated by plus sign, and in the negative direction -- by minus sign. The numbers in parentheses indicate the respective frequencies in  $\text{cm}^{-1}$ .

but also to find the mode of the respective normal vibrations. For this purpose, frequencies determined from the secular equations obtained should be substituted into equations of motion written for symmetry coordinates of translational vibrations, and these equations should then be solved. Figures 5.12a and 5.12b show normal translational vibrations in  $\text{KH}_2\text{PO}_4$  for paraelectric and ferroelectric modifications respectively and give the frequencies corresponding to them [47]. The character of the change in normal translational vibrations in  $\text{KH}_2\text{PO}_4$  during a phase transition may be graphically seen from a comparison of the figures.

### 3. Sodium Nitrite ( $\text{NaNO}_2$ )

Difficulties of understanding the phenomenon of ferroelectricity at the microscopic level are brought about to a large degree by the complexity of the structure of ferroelectric crystals which represent structures containing complex groups of atoms tightly bound with each other. Because of this, the great interest of researchers in a new ferroelectric  $\text{NaNO}_2$  having a comparatively simple structure is understandable [54].

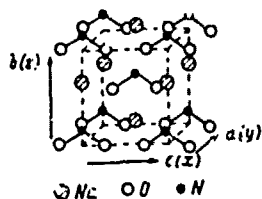


Figure 5.13. The structure of  $\text{NaNO}_2$  below Curie point.

According to the data of x-ray [55] and neutron [56] diffraction studies, at temperatures below Curie point ( $\theta=163^\circ\text{C}$ ) the structure of  $\text{NaNO}_2$  belongs to the group  $C_{2v}^{20}$ . A unit cell is shown in Figure 5.13. The results of a group-theory analysis of vibration spectrum of  $\text{NaNO}_2$  are summarized in Table 11 from which it may be seen that all optical vibrations are active in Raman spectrum. Vibration of the  $A_2$  type is inactive in infrared spectrum.

Table 11

Group-Theory Analysis of Normal Limit Vibrations in  $\text{NaNO}_2$

$\nu$	$n_i$	T	T'	R	$n_i'$	$\alpha_k$
$A_1$	4	1( $T_x$ )	1	0	2	$\alpha_{xx}, \alpha_{yy}, \alpha_{zz}$
$A_2$	1	0	0	1( $R_x$ )	0	$\alpha_{xy}$
$B_1$	4	1( $T_x$ )	1	1( $R_y$ )	1	$\alpha_{xz}$
$B_2$	3	1( $T_y$ )	1	1( $R_x$ )	0	$\alpha_{yz}$

NOTE. The numbers of normal vibrations transformed in accordance with the given irreducible representation:  $n$  -- the total power; T, T', R,  $n_i'$  -- the numbers of acoustic and optical translations, orientations and internal vibrations respectively;  $\alpha_k$  -- tensor components.

A method, described below, which while having a high illuminating power and simplicity in comparison with the usual procedure at the same time makes it possible in the case under consideration to determine unambiguously the symmetry type of vibration lines was used in the works [23, 57] for the interpretation of an experimental vibration spectrum of  $\text{NaNO}_2$  obtained by the method employing Raman effect.

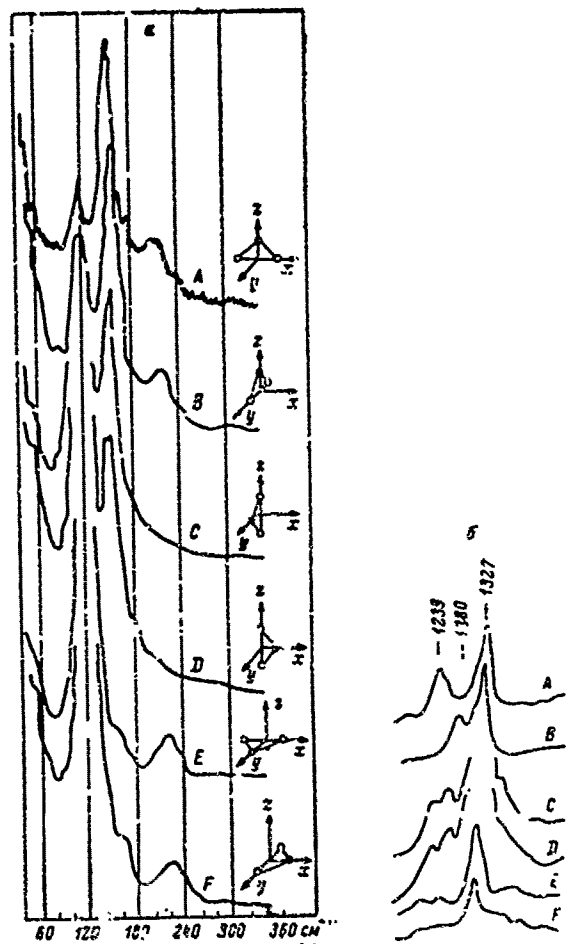


Figure 5.14. Raman spectra of  $\text{NaNO}_2$

a -- the region of low-frequency vibrations of the crystal (y is the direction of observation, z-axis is parallel to the height of the monochromator slit);  
 b -- the region of  $1,000-1,500 \text{ cm}^{-1}$ . Letters indicate different orientations of the crystal in accordance with Figure 5.14b.

A sample of cubic form with edges parallel to crystallographic axes a, b and c was placed on the axis of the lamp and illuminated with natural light. A polaroid passing a component of light with the electric-field E vector parallel to the height of the monochromator slit was installed on the path of scattered light. A coincidence of polarization planes of the polaroid and of the monochromator lattices was achieved with such an arrangement. This permitted a most complete utilization of the monochromator illuminating power. Six spectrograms (Figures 5.14a and 5.14b)

with the orientations of the crystal shown in Figure 5.14a were obtained under these conditions.

The idea of the method consists in the following. The projections  $P_i$  of the dipole moment, which define the intensity of scattered radiation are equal to:

$$P_i = \sum_k \alpha_{ik} E_k. \quad (5.79)$$

Here  $E_k$  are components of electric-field vector,  $\alpha_{ik}$  are components of polarizability tensor. Knowing the irreducible representations to which the components of polarizability tensor correspond (Table 11) and taking (5.79) into account it is possible to determine the polarization of scattered radiation.

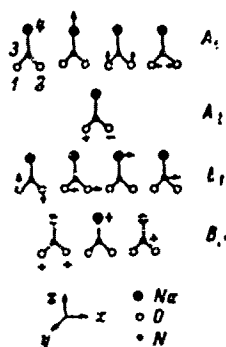


Figure 5.15. Symmetry coordinates of the limit normal vibrations of the ferroelectric  $\text{NaNO}_2$ .

Numerals 1-4 indicate nonequivalent atoms.

Table 12

Intensities of Spectral Lines With Different Orientations of  $\text{NaNO}_2$  Crystal

Ориентация кристалла	$\epsilon_1$	$\epsilon_2$	$\epsilon_3$	$\epsilon_4$	Ориентация кристалла	$A_1$	$A_2$	$B_1$	$E_1$
A	$\epsilon_1$	0	$\epsilon_2$	$\epsilon_3$	D	$\epsilon_1$	$\epsilon_2$	$\epsilon_3$	0
B	$\epsilon_1$	0	$\epsilon_3$	$\epsilon_4$	E	$\epsilon_2$	$\epsilon_3$	0	$\epsilon_4$
C	$\epsilon_2$	$\epsilon_4$	$\epsilon_3$	U	F	$\epsilon_3$	$\epsilon_4$	0	$\epsilon_1$

Key: (1) Orientation of the crystal.

Intensities of spectral lines expected under the conditions of the experiments are given in Table 12. Orientation of the crystal in accordance with Figure 5.13a is shown in the first column of the table. The symbol 0 indicates that with the orientation in question the line must have zero intensity; the symbols  $\epsilon_k$  indicate nonzero intensities. As may be seen from the table, the line of each symmetry type is characterized unambiguously by a certain set of the symbols 0 and  $\epsilon_k$ . The interpretation of the vibration-spectrum bands obtained in this manner is given in Table 13.

Figure 5.15 shows symmetry coordinates obtained with the aid of projection operators. On the basis of their analysis and also on the basis of the study of relative intensities of spectral lines and a comparison of Raman spectra of the crystal and aqueous solution it is possible to draw qualitative conclusions concerning the mode of normal vibrations in  $\text{NaNO}_2$  (Table 13).

It follows from the examination of experimental data and group-theory analysis of the spectrum that apparently a separation of lattice vibrations into internal, orientational and translational vibrations of the  $\text{NO}_2^-$  anion is brought about to a high degree in a crystal of  $\text{NaNO}_2$ . Because of this, it appears possible to calculate the frequencies of translational vibrations for a simple model similar to that used for the calculation of low-frequency vibration spectrum of  $\text{KH}_2\text{PO}_4$ . In this case, to take into account the long-range forces it is only necessary to know the effective charge of the entire  $\text{NO}_2^-$  group. Apparently this charge may be assumed to be equal with good approximation to the electron charge. In such a simplified model the long-range forces are taken into account by a substitution of  $\text{NO}_2^-$  groups with point charges located at a distance of  $\pm b/2$  from sodium cations. The short-range repulsive forces are taken into account only between sodium cations and the nearest oxygen atoms using Pauling formula.

The results of the calculation are given in Table 13 where they are compared with experimental data. It may be seen from the table that the model used is satisfactory for the irreducible representation of  $B_1$ . The considerable intensity of the band of  $220 \text{ cm}^{-1}$  ( $B_2$ ) makes its assignment to the mixed or orientational type of vibrations more probable. It will be possible to form a better-grounded judgement concerning the suitability of the model only after obtaining a more complete scattering spectrum.

An anomalous lowering of the frequency  $\omega(B_1)=153 \text{ cm}^{-1}$  during a phase transition was observed in Raman spectrum of  $\text{NaNO}_2$ . This vibration was interpreted on the basis of group-theory considerations and polarization measurements as an orientational vibration of  $\text{NO}_2^-$  anion about the a-axis, of the  $B_1$  type. This interpretation leads to an inference that the micromechanism of ferroelectric transition in a crystal of  $\text{NaNO}_2$  consists in re-orientation of  $\text{NO}_2^-$  groups about the a-axis [57].

Table 13

Vibration Spectrum of a Ferroelectric  
Crystal of  $\text{NaNO}_2$ 

1		3	Energy of optical translational vibrations
2	критическая		
	от b)		
118	( $A_1$ , оп. б)	--	--
152	( $B_1$ , оп. а)	--	--
177	( $B_1$ , оп. в)	--	174 ( $B_1$ )
229	( $B_1$ , оп. в)	--	224 ( $B_1$ )
?		--	232 ( $A_1$ )
825	( $A_1$ , ин.)	815 ( $A_1$ )	--
1238	( $B_1$ , ин.)	1240 ( $B_1$ )	--
1280		1333 ( $A_1$ )	--

NOTE. Frequencies are expressed in  $\text{cm}^{-1}$ ;  
 op. -- orientational vibration about b-axis;  
 o.t. -- optical translational vibration of  
 $\text{NO}_2^-$  complex with respect to  $\text{Na}^+$  cation along  
 c-axis; in. -- internal vibration of  $\text{NO}_2^-$   
 anion. All bands showing in Raman spectrum  
 of aqueous solution correspond to internal  
 vibrations of  $\text{NO}_2^-$  anion.

Key: (1) Experiment                      (4) Calculation of optical  
 (2) Crystal                                  translational frequen-  
 (3) Aqueous solution                      cies

Results of a group-theory analysis of the vibration spectrum of  $\text{NaNO}_2$  for all symmetric points of Brillouin zone, and also results of a group-theory analysis of the limit dipole frequencies with account taken of their dependence on the direction of  $q \rightarrow 0$  may be found in the work [58].

#### Par. 4. Physical Mechanism of Ferroelectric Transition and Dynamics of Crystal Lattice

Equations obtained in paragraph 1 make it possible to formulate in a sufficiently general form the stability conditions for lattice vibrations and determine relationships connecting dielectric constants  $\epsilon_0$  and  $\epsilon_\infty$  and the frequencies of normal vibrations. However, physical mechanism responsible for the initiation of a phase transition is determined in this case only to the extent to which the initial mode of the crystal has been concretized. Within the framework of the model used in the derivation of the basic relationships the question of why at a certain temperature a disturbance of the condition (5.55), i.e. a phase transition, takes place remains unexplained. Consequently, it is necessary to focus attention on those properties of a shell model which can explain the appearance of

ferroelectric anomalies, i.e., speaking in the language of dynamic representations, it is necessary to determine the possible causes of the loss of dynamic stability of the lattice in a ferroelectric. At the same time, it is of interest to examine certain features of dynamic characteristics of a ferroelectric in the phase transition region in a greater detail and as far as possible on the basis of not excessively complex representations.

### 1. Concept of "Soft Mode" and Anharmonicity of Lattice Vibrations

Proceeding from formulas (5.50)-(5.52) for a shell model we will examine the force constants  $\Phi$  for the simplest case of a diatomic cubic lattice (for example, NaCl, KJ, etc.) [6].

For the limit ( $q \rightarrow 0$ ) transverse waves the field factors  $C_{11} = \frac{4\pi}{3}$ ,  $C_{12} = \frac{4\pi}{3}$  and the force constant  $\Phi_T$  is reduced to the following form:

$$\Phi_T = R - \frac{4\pi (e_m + 2) (ze)^2}{9\epsilon_0} \quad (5.80)$$

In the case of longitudinal waves  $C_{11} = -\frac{8\pi}{3}$ ,  $C_{12} = -\frac{8\pi}{3}$

$$\Phi_L = R + \frac{8\pi (e_m + 2) (ze)^2}{9\epsilon_0} \quad (5.81)$$

The well known relationship between polarization and dipole moments brought about by ionic displacements was used in the derivation of these formulas, i.e.

$$P = \frac{4\pi e_m + 2}{3v} e z x$$

and  $z$  indicates in this case effective dynamic charges.

Thus, examining conditions for one of the principal minors of  $\tilde{\Phi}$  becoming zero, we come to the following condition for transverse vibrations:

$$R - \frac{4\pi (e_m + 2) (ze)^2}{9\epsilon_0} = 0 \quad (5.82)$$

It may be perceived from (5.81) that in principle  $\Phi_L$  does not vanish. The physical sense of the condition (5.82) is obvious and corresponds to the results of Devonshire--Slater theory (see paragraph 4, chapter 4): the sign of the phase transition is the equality of the short-range forces tending to return the displaced ion to the initial position, and long-range electric forces conducive to a displacement of the ion. This relationship is sometimes called ferroelectric-activity criterion [59, 60]. In order that  $\omega_T^2$  become zero and that in accordance with formula (5.40)  $\epsilon_0$  change with temperature according to Curie-

Weiss law, it is sufficient to assume that in the transition region the quantity

$$1 - \frac{4\pi(\epsilon_{\infty} + 2)(ez)^2}{9v^2} \sim (T - \theta), \quad (5.83)$$

where  $\theta$  is Curie temperature.

This relationship (see also paragraph 4, chapter 4) can be obtained by different methods. It is sufficient to assume that any one of the quantities contained in the second term of (5.83) varies as  $1 + \alpha T$  where  $\alpha T$  is a small quantity in comparison with unity. However, Slater [61] showed that temperature coefficients of volume expansion and  $\epsilon_{\infty}$  are too small and that the only reasonable explanation of the relationship (5.83) can be obtained if it is assumed that  $R_0$  depends on the amplitude of ionic displacement, i.e. by assuming that vibrations of at least some of the ions of a ferroelectric have a marked anharmonic character.

The same relationship of the coefficient characterizing the restoring force which acts on the displaced ion is also used in Devonshire--Slater theory [61, 62], and in this subparagraph the model used in dynamic theory hardly differs from the model of anharmonic oscillators. However, the difficulty consists in that the introduction of anharmonicity directly into a dynamic-theory system considerably complicates the problem even if nonlinear terms are regarded as a small perturbation. In this part, such a solution of it proves to be effective and rigorous with which dynamic representations are combined with the methods of statistical physics (see subparagraph 2 of this paragraph).

In doing so, as a result of utilizing thermodynamic perturbation theory (see also chapter 4, paragraph 4, subparagraph 2 and [57]) it is possible to reduce a system of nonlinear oscillators to an equivalent system of harmonic oscillators with a certain new effective force constant which linearly depends on temperature, i.e.  $R_{\text{eff}} = R_0(1 + \alpha T)$ . Substituting these expressions into (5.80) we will obtain the necessary relationship  $\omega_T^2 \sim (T - \theta)$ . At the temperature  $\theta$  when the restoring force  $R_{\text{eff}}$  is equal to Coulomb force the crystal becomes unstable and as a result of a rearrangement of the lattice a new structure is formed which is characterized by the presence of a spontaneous electric moment. A calculation of constants entering the equation (5.82), with the use of atomic parameters of the lattice of NaCl, CsCl, etc. [6, 24] indicates that for alkali haloid crystals the value of  $R$  is approximately twice as large as that of the second addend. In other words, the lattice of halogens proves to be too rigid, the vibrations of ions insufficiently anharmonic and polarizabilities insufficiently high for the start of a mutual compensation of electric and restoring forces, which was discussed above.

For ferroelectrics these relationships prove to be different. In this case, the coefficients of internal field are sufficiently large for the limit ferroelectric transverse vibration and the value of  $R$  is, on

the contrary, small and is characterized by a strong temperature dependence owing to marked anharmonicity. As a result of this, the condition (5.82) is realized. The so-called soft mode of vibrations of a ferroelectric is also reduced to these qualitative representations. It should be noted that these representations cannot be considered to be a specific attribute of dynamic theory. In the language of theory of anharmonic oscillators, stability condition will be written in the following manner:

$$a \left[ 1 + \frac{k_0}{a^2} (3b_1 + 2b_2) \right] - \frac{\beta e^2 z^2 N}{8\pi} = 0 \quad (5.84)$$

(for notations see subparagraph 1, paragraph 4, chapter 4). Apart from the difference in notations this formula coincides with (5.82). The coefficient in front of  $z^2 l^2$  for  $\text{BaTiO}_2$  is several times higher than for halogens whereas the assumption of relative freedom and a marked anharmonicity of displacements of titanium ion makes it possible to consider the force constant "a" to be a small quantity and the ratio  $\frac{3b_1 + 2b_2}{a^2}$  sufficiently large. Therefore, the condition (5.84) can be realized for  $\text{BaTiO}_2$ .

A physical pattern very close to the representations concerning the "soft mode" may be obtained on the basis of thermodynamics.

As far back as 1949, V. L. Ginzburg showed that in the case of a phase transition of the second kind of displacement type (or of the first kind approaching critical point) the frequency of one of vibrations of the crystal lattice must become zero [1] <sup>1)</sup>, namely the frequency of that vibration which is connected with the changes in the order parameter of Landau thermodynamic theory.

Ginzburg proceeded from an interpretation of quadratic term  $\alpha \eta^2$  in the expansion of thermodynamic potential  $\Phi$  with respect to the powers of  $\eta$  (see 3.2) as a generalized elastic energy.

Such an interpretation is confirmed by the circumstance that the equilibrium value of  $\eta = \eta_0$  is determined from the condition  $\frac{\partial \Phi}{\partial \eta} = 0$ , i.e.  $\alpha \eta + \beta \eta^3 = 0$  (see 3.8). This coincides with the equilibrium condition for an anharmonic oscillator:

$$\mu \eta + \nu \eta^3 + \sigma \eta + \beta \eta^3 = 0. \quad (5.85)$$

and must be warranted for transitions of displacement type in the case of which  $\eta$  is simply connected with a displacement of crystal sublattices.

---

1) Only a ferroelectric transition of the second kind was examined in the work [1] (see also [2, 3]) but as noted in the work [3], the approach developed in [1, 2] remains valid for any phase transitions of displacement type.

For small fluctuations of the order parameter  $\Delta\eta = \eta - \eta_0$  we find from (5.85) the following near the equilibrium value of  $\eta_0$ :

$$\frac{d^2}{dt^2}(\Delta\eta) + \nu \frac{d}{dt}(\Delta\eta) + \omega_1^2 \Delta\eta = 0. \quad (5.86)$$

With a  $T > \Theta$

$$\eta_0 = 0; \quad \omega_1^2 = \frac{\alpha}{\mu} = \frac{\alpha_0'(T - \Theta)}{\mu}. \quad (5.87)$$

With a  $T < \Theta$

$$\eta_0 = -\frac{\alpha}{\beta}; \quad \omega_1^2 = \frac{2|\alpha|}{\mu} = \frac{2\alpha_0'(\Theta - T)}{\mu}. \quad (5.88)$$

The linear dependence of the "soft mode"  $\omega_1^2$  on  $\Theta - T$  may be connected with the use of the approximate expansion (3.2) but the fact itself of one of the frequencies of optical vibrations becoming zero (or at least the fact of an anomalous decrease of it) at the point of transition of displacement type apparently does not give rise to doubt.

The parameter  $\mu$  may be expressed in terms of a reduced mass of a vibration with a frequency  $\omega_1$  and effective dynamic charge of the "soft mode":

$$\mu = \frac{m}{2(\epsilon\epsilon)^2 N^2}$$

where  $N$  is the number of particles in a unit of volume.

If the dipole moment of the crystal changes in the case of displacements corresponding to the frequency  $\omega_1$ , then polarization may be selected as the parameter  $\eta$  (we will recall once more that with transitions of displacement type  $\eta \sim$  displacement of sublattices), and the respective phase transition will be a ferroelectric transition.

In this case, the calculation of dielectric constant with (5.86)-(5.88) taken into account, gives:

$$\begin{aligned} T > \Theta & \left\{ \begin{aligned} \epsilon(\omega) &= \epsilon' - i\epsilon'' = \frac{2\pi\mu}{\omega_1^2 - \omega^2 + i\nu\omega}, \\ \omega_1^2 &= \frac{\alpha}{\mu} \end{aligned} \right. \quad (5.89) \\ T < \Theta & \left\{ \begin{aligned} \epsilon(\omega) &= \epsilon'_0 - i\epsilon''_0 = \frac{2\pi\mu}{\omega_1^2 - \omega^2 + i\nu\omega}, \\ \omega_1^2 &= \frac{2|\alpha|}{\mu} \end{aligned} \right. \quad (5.90) \end{aligned}$$

In the derivation of (5.89) and (5.90) it was assumed that a ferroelectric transition from a cubic to tetragonal phase is examined.

Later these considerations were developed by Ginzburg [3,63] for a phase transition of the first kind also. In doing so, it was shown that the following expression remains when  $T > \Theta$ :

$$\omega_1 = \sqrt{\frac{\alpha_0}{\mu}}(T - T_0)^{1/2} \quad (5.91)$$

with the difference that in this case Curie temperature  $T_C$  differs from the temperature of phase transition  $\Theta$ . Therefore, the frequency at the phase-transition point tends to a finite value of

$$\omega_1 = \sqrt{\frac{a_0}{\mu}} (\Theta - T_C)^{1/2} \quad (5.92)$$

for paraelectric phase and to a value of

$$\omega_1 = \gamma \sqrt{\frac{a_1}{\mu}} (\Theta - T_C)^{1/2} \quad (5.93)$$

for ferroelectric phase. Evaluations carried out with the aid of the formulas (5.92) and (5.93) for  $\text{BaTiO}_3$  give a  $\omega_1 \sim 6 \cdot 10^{11}$  hertz and  $\omega_{iz} \sim 1.2 \cdot 10^{12}$  hertz. This corresponds to the wavelengths  $\lambda_1 \sim 3$  mm and  $\lambda_{iz} \sim 1.5$  mm respectively.

## 2. Taking Anharmonicity Into Account by Using the Methods of Perturbation Theory

The possibility of appearance of a situation in which a ferroelectric transition takes place, i.e. a mutual compensation of collective long-range forces conducive to the displacements of ions, and restoring forces brought about chiefly by interaction with the nearest neighbors is determined not only by the balance of these forces but also by their nonlinear character. In other words, explanation of temperature dependences observed in ferroelectrics is possible only with the condition of taking anharmonic effects into account. It was already noted above that solution of dynamic equations (5.22) with account taken of the terms in  $U$  containing powers higher than  $x^2$  is connected with great difficulties even if only because the normalcy (i.e. independence) of different modes of vibrations is then disturbed. In his calculations [6, 7] Cochran circumvented this difficulty by simply postulating the linear dependence of  $R = R_0(1 + \alpha T)$  of the force constant on temperature. However, taking anharmonicity into account in dynamic equations may be achieved by a more correct method.

If it is considered that nonlinear terms are small in comparison with linear terms, then a possibility appears to use the methods of perturbation theory. The assumption concerning the smallness of anharmonic portion of energy being sufficiently correct (at least if the transition point itself is excluded) in the case under consideration, already follows from the fact that as shown in [61] and then in [6], a relatively weak dependence of the quantity  $R$  in the formula (5.80) is required to obtain the necessary relationship of  $\omega_1$ . Thus, the problem in question can now be solved on the basis of thermodynamic perturbation theory, similarly to the way this was done in paragraph 4, chapter 4, but in combination with the use of solutions of differential equations of the vibrations of ions (i.e. of normal coordinates). The question of taking

anharmonicity into account in terms of equations of lattice vibrations and perturbation theory was examined for the first time by Born [11] and then in the works of a number of authors (see [64]). In its application to the problem of ferroelectricity this method was used for the first time by Anderson [4]. The essence of the method is reduced to the following.

The Hamiltonian of an unperturbed system  $\mathcal{H}_0$  is written in the following form:

$$\sum_{\mathbf{q}} \left( \frac{1}{2} \dot{x}^2 + \frac{1}{2} x^2 \right) \quad (5.94)$$

i.e. for simplicity, one acoustical (the superscript "a") and one optical branch (the superscript 0) is taken into account here.

The normal coordinates  $X_{\mathbf{q}}$  are solutions of the system of equations (5.22):  $S_{(\mathbf{q})}^a$  and  $S_{(\mathbf{q})}^0$  are the respective moduli of elasticity.

The anharmonic portion of the Hamiltonian regarded as a perturbation may be represented in the following form:

$$\mathcal{H}_1 = \frac{1}{3!} \sum_{\mathbf{q}_1, \mathbf{q}_2, \mathbf{q}_3} \chi_{\mathbf{q}_1, \mathbf{q}_2, \mathbf{q}_3} X_{\mathbf{q}_1} X_{\mathbf{q}_2} X_{\mathbf{q}_3} + \frac{1}{4!} \sum_{\mathbf{q}_1, \mathbf{q}_2, \mathbf{q}_3, \mathbf{q}_4} \chi_{\mathbf{q}_1, \mathbf{q}_2, \mathbf{q}_3, \mathbf{q}_4} X_{\mathbf{q}_1} X_{\mathbf{q}_2} X_{\mathbf{q}_3} X_{\mathbf{q}_4} \quad (5.95)$$

The fundamental approximation (also used in model theories [59] and [60]) consists in that the distribution functions and the functions of different average  $\exp\left(-\frac{\mathcal{H}_1}{kT}\right)$  are arranged in series with respect to  $\mathcal{H}_1$ :

$$\exp\left(-\frac{\mathcal{H}_1}{kT}\right) \approx \exp\left(-\frac{\mathcal{H}_1}{kT}\right)$$

After this, the problem is actually reduced to the calculation with the aid of an unperturbed Hamiltonian, of the average values of  $\mathcal{H}_1$  additionally multiplied by the polynomials of different powers of  $X_{\mathbf{q}}$ . In doing so, in the lower order with respect to anharmonicity all thermal properties follow from a set of effective Hamiltonians (one for each vibration) which are obtained by the averaging of  $\mathcal{H}_1$  over all normal vibrations with the exception of the one for which an effective Hamiltonian is determined.

In this manner, the free energy is determined in the form of an expansion with respect to the powers of  $\mathcal{H}_1$ :

$$A = -kT \ln \int \exp\left(-\frac{\mathcal{H}_0 + \mathcal{H}_1}{kT}\right) d\mathbf{x} = A_0 + A_1 + \frac{1}{2kT} [A_2 - (A_1)^2] \quad (5.96)$$

Here  $A_0$  is free energy in the absence of perturbation, the first-order term  $A_1$  is a quasi-harmonic average of the perturbation  $\mathcal{H}_1$ , the second-order term is, as usual in perturbation theory, energy fluctuation.

1) Inasmuch as a classical problem is being solved it would be possible to use with equal success not the Hamiltonian function  $\mathcal{H}$  but potential energy  $U$  (see chapter 4, paragraph 4, subparagraph 2).

It is important here that Hamiltonian function  $\mathcal{H}$  is expressed in terms of normal coordinates and makes it possible to determine the temperature dependence of natural vibrations of the lattice. In the work [4], with the aim of simplifying the problem a system of hard ions is examined, i.e. effects brought about by electron polarizability of the ions are not taken into account. Construction of a Hamiltonian function with the displacements of electrons taken into account is not connected with difficulties in principle and at the same time does not introduce qualitative changes into conclusions drawn by Anderson. <sup>1)</sup> As a result of imposition of the condition of minimum of free energy (5.96) in the presence of electric field the value of dielectric constant is defined as  $\epsilon_0 = 1 + \frac{4\pi k^2}{U^2 S_{eff}}$  where  $S_{eff}$  is effective (i.e. taking account of Coulomb forces) value of optical modulus of elasticity connected with vibration mode when  $q=0$ .

The modulus of elasticity  $S^0$  may be written in the following form:

$$S^0(q) = S^0(q) - \frac{1}{2} n e^2 \beta(q), \quad (5.97)$$

where  $\beta(q)$  with  $q=0$  represents Lorentz factor which is equal to  $\frac{4\pi k^2}{3}$  for transverse and  $\frac{8\pi k^2}{3}$  for longitudinal vibrations.

Figure 5.16 shows hypothetical curves of the relationship to  $q$  of two terms of the equation (5.97) and  $S^0$  for transverse branch for Curie temperature. An assumption that (without taking anharmonicity into account) the modulus of elasticity of the transverse optical branch becomes negative at Curie point was taken into account in these relationships.

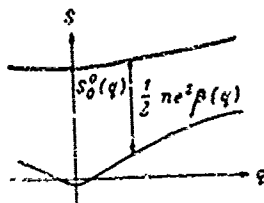


Figure 5.16. Qualitative relationship of elastic modulus to the wave vector  $q$ .

Effective potential energy calculated for such a vibration with the aid of procedure discussed above proves to be equal to:

$$C_{opt} = S^0 |X_{10}|^2 (p+1) |X_{10}|^2.$$

<sup>1)</sup> Anderson's approach was later used in the works [65, 66] in which an expression for the constants of phenomenological theory in terms of microscopic parameters was obtained with the aid perturbation theory. As noted in the work [65], inaccuracies are contained in the respective expressions in the work [66].

Thus, the quantity  $X_{(0)}^0$  (i.e. a transverse optical normal vibration) has a potential with two minima. Taking the value of one of these minima the quantity  $X_{(0)}^0$  receives an increment and this ensures the initiation of ferroelectric polarization.

We will underscore once more that the potential with two minima pertains in Anderson's model not to the entire substance but only to the transverse limit optical vibration. This is the distinction of his theory from the theory corresponding to a case when a potential with two minima acts on ferro-active ions.

Evaluations made by Anderson lead to a conclusion regarding the relative smallness of the effect of anharmonic terms and fluctuations on the character of ion vibrations even in direct proximity to the transition point owing to the fact that anharmonicity has a marked character only for some of the long-wave modes of vibrations and amounts only to a small portion in the total energy balance. In other words, in this subparagraph, dynamic theory agrees well with the conclusions obtained on the basis of a model of anharmonic oscillators and thermodynamic theory of fluctuations in the transition region (see subparagraph 3, paragraph 1, chapter 3 and paragraph 4, chapter 4).

Later, Anderson's approach was developed in a work by Aizu [67] in which dielectric constant was determined not only in a permanent field but in a variable field also. The susceptibility  $\chi$  calculated in [67] for ferroelectric phase near Curie temperature  $\Theta$  proved to be equal to:

$$\chi = \frac{(\nu/\beta)\theta}{s - r - 2\left(\frac{\omega}{\omega_f}\right)^2}. \quad (5.98)$$

For paraelectric phase near  $\Theta$

$$\chi = \frac{2(\nu/\beta)\theta}{r - \theta - 2\left(\frac{\omega}{\omega_f}\right)^2}. \quad (5.99)$$

Here  $f$  is Lorentz factor,  $\alpha = \frac{1}{1 - \frac{\beta e a}{v}}$  where  $\alpha$  is electron polarizability, and  $\omega_f$  is the value of ferroelectric frequency away from Curie point. It is of interest to note that  $\chi$  proves to be maximal not at a  $T = \Theta$  but at

$$r_+ = \theta \left[ 1 + 2\left(\frac{\omega}{\omega_f}\right)^2 \right] \quad (5.100)$$

and at

$$r_- = \theta \left[ 1 - \left(\frac{\omega}{\omega_f}\right)^2 \right].$$

In addition to this, regardless of the dependence on  $\omega$

$$\theta = \frac{r_+ + 2r_-}{3}. \quad (5.101)$$

An attempt at an examination of a ferroelectric the properties of which are determined not by one but by two or more "soft modes" is also reported in the work by Aizu [67]. An analogue of this case in theory of anharmonic oscillators is a crystal in which not one but several sublattices perform anharmonic vibrations (see subparagraph 1, paragraph 4, chapter 4). According to [67] the presence of several "soft modes" leads to a possibility of several successive phase transitions.

Some of the results in [4] were later obtained more rigorously by Wilcox [68] with the aid of diagram technique (see also [69]). Wilcox used a "renormalization of frequencies" in order to obtain Curie-Weiss formula for paraelectric phase.

The physical pattern underlying the calculations examined above is as follows: with the approach to the transition point the frequency of ferroelectric mode drops; directly near the transition point this normal vibration consists in a displacement of ions to a new equilibrium position and vibrations relative to the new equilibrium position. Thus, the potential relief of this vibration is highly anharmonic.

In order to illustrate this pattern in the simplest way it is possible, following Silverman [32, 70] and Blinc [71], to examine it for a model of an equidistant diatomic linear chain of atoms with a mass  $m$  and with interaction between the nearest neighbors (the force constant  $k_1$ ) and those which follow them (the force constant  $k_2$ ). The equations of motion for such a system have the following form:

$$m \frac{d^2 X_i}{dt^2} = -2(k_1 + k_2) X_i + k_1 (X_{i+1} + X_{i-1}) + k_2 (X_{i+2} + X_{i-2}). \quad (5.102)$$

The relationship of the frequencies of the acoustical and optical branch respectively to the wave vector  $q$  is given by the following expressions: 1)

$$\left. \begin{aligned} \omega_1(q) &= \frac{4k_1}{m} \sin^2 \frac{qd}{2} + \frac{4k_2}{m} \sin^2 qd, \\ \omega_2(q) &= \frac{4k_1}{m} \cos^2 \frac{qd}{2} + \frac{4k_2}{m} \sin^2 qd. \end{aligned} \right\} \quad (5.103)$$

Here  $d$  is lattice constant,

$$-\frac{\pi}{2d} < q < \frac{\pi}{2d}.$$

As it follows from (5.103), the frequency  $\omega_1(0)$  is completely determined by the force constant  $k_1$ . Therefore, if  $k_1$  is selected as a small and negative quantity and  $k_2$  -- as a large and positive quantity,

1) We will note that the formulas (5.103) and (5.18 coincide when  $k_2=0$  and  $m_1=m_2=0$ .

then the lattice will be unstable with respect to optical vibrations with small  $q$  but will remain stable for the large values of  $q$ .

Using normal vibrations the Hamiltonian of the system in harmonic approximation may be written in the following form:

$$\mathcal{H}_0 = \frac{1}{2} \sum_q (p_q^2 p_{-q}^2 + \omega_0^2(q) X_q X_{-q}) + \frac{1}{2} \sum_q (p_q^2 p_{-q}^2 + \omega_1^2(q) X_q X_{-q}). \quad (5.104)$$

Next, we will take into account the fourth-order anharmonic term (in the chain under consideration, a third-order term is forbidden owing to the presence of a center of symmetry):

$$\mathcal{H}_1 = \frac{3}{4!} \sum_i (X_{i+1} - X_i)^4. \quad (5.105)$$

$\mathcal{H}_1$  may be expressed in terms of normal coordinates:

$$\mathcal{H}_1 = \frac{48}{Nm^3} \sum_q \left[ \sum_r \sin^2\left(\frac{qr}{2}\right) X_q X_{-q} \right] \cos^2 \frac{qd}{2} X_q^2 X_{-q}^2. \quad (5.106)$$

Effective "quasi-harmonic" Hamiltonian may be obtained by averaging over  $X_q^a$  and  $X_{-q}^a$  using perturbation theory.  $\mathcal{H}_0$  coincides exactly with  $\mathcal{H}_0$  upon substituting  $\omega_0^2(q)$  and  $\omega_a^2(q)$  with  $\bar{\omega}_0^2(q)$  and  $\bar{\omega}_a^2(q)$  where:

$$\omega_j^2 = \left[ \frac{48}{Nm^3} \sum_r \sin^2 \frac{qr}{2} \langle X_q X_{-q} \rangle + \frac{4k_1}{m} \right] \cos^2 \frac{qd}{2} + \frac{4k_2}{m} \sin^2 qd. \quad (5.107)$$

(A similar expression should also be written for  $\bar{\omega}_a^2$  but the frequencies of acoustic vibrations prove to be relatively weakly dependent on temperature).

The average

$$\langle X_q X_{-q} \rangle = \frac{\hbar T}{\omega_0^2(q)} \approx \frac{kT}{\frac{4k_1}{m} \sin^2 \frac{qd}{2}}$$

where  $k$  is Boltzmann constant.

Taking into account that when  $q \sin$  are small  $qd \approx nd$ , we will obtain the following when  $qd \ll 1$ :

$$\omega_j^2(q) = \left[ \frac{4kT}{m k_1} - \frac{4|k_1|}{m} \right] \cos^2 \frac{qd}{2} + \frac{4k_2}{m} \sin^2 qd. \quad (5.108)$$

It may be seen from (5.108) that the presence of anharmonic term stabilizes the system above Curie temperature. With a  $q \rightarrow 0$  the frequency  $\omega_0(0)$  changes with temperature as

$$\omega_0(0) \sim (T - \theta),$$

where

$$\theta = \frac{8|k_1|k_2}{4k_1}.$$

We will now dwell on the attempts at a more detailed examination of ferroelectric vibrations [72]. The properties of excitations for transitions of different types and also problems of attenuation were examined in the work [73] with the aid of the method of self-consistent field. A high anisotropy of ferroelectric mode was observed in noncubic ferroelectrics. This anisotropy connected with the anisotropy of dielectric constant is reduced to a dependence of the frequency  $\omega(q \rightarrow 0)$  on the direction of the wave vector tending to zero (see paragraph 1 of this chapter). It is shown that ferroelectric vibrations have a low attenuation only in the case of applicability of self-consistent-field theory, i.e. precisely in the temperature region where Landau thermodynamic theory is applicable. It is noted that owing to a high attenuation it is difficult to observe ferroelectric vibrations for order-disorder transitions. With the approach to Curie temperature, a slowing-down of relaxation and accordingly an anomalous temperature dependence of dielectric constant are observed.

In the work [65] the semiphenomenological equations in the work [1, 6] were obtained with the aid of temperature diagram technique and a generalization of them is given for a case of  $q \neq 0$ . A strong effect of acoustic mode was noted. It was found that with small  $q$  the spectrum in perovskites is determined by six microscopic constants an experimental determination of which could ensure a verification of theory.

It follows from the foregoing that at the present time dynamic theory describes ferroelectric transitions only qualitatively. As may be seen from paragraph 3 of this chapter, calculations carried out for actual ferroelectric crystals bear a heuristic character and can be utilized chiefly for the interpretation of vibration spectra and only for a qualitative description of their temperature dependence. Difficulties connected first of all with insufficient information on potential function of a crystal apparently do not make it possible to hope for creation in the immediate future of a rigorous anharmonic dynamic theory of concrete ferroelectric transitions. This circumstance explains the interest in the calculation of different approximate and qualitative models and their comparison with the experiments, and as yet extensive work is to be carried out in this direction.

### 3. Transitions of Order-Disorder Type in the Light of Dynamic Theory

Unlike barium titanate and perhaps some of the other crystals in which a ferroelectric transition of displacement type takes place, a transition of order-disorder type takes place in a large number of the other ferroelectrics. The features of such a transition are excellently illustrated by Ising model which was discussed in detail in paragraph 4 of the preceding chapter. Here, however, we would like to draw attention to the fact that lattice vibrations may also play an important part in

transitions of order-disorder type if in these transitions, displacements of sublattices as one whole as, for example, in the case of  $\text{KH}_2\text{PO}_4$  [74], take place along with the disordering of atoms or dipole groups.

As the x-ray data indicate [75], during a phase transition in  $\text{KH}_2\text{PO}_4$  a considerable displacement of the K, P and O ions along the c-axis occurs in comparison with their positions in paraelectric phase. These displacements may explain the magnitude of spontaneous polarization [75]. It is of interest to note that whereas a high isotopic effect is observed for Curie temperature ( $\theta = 122^\circ\text{K}$  for  $\text{KH}_2\text{PO}_4$  and  $213^\circ\text{K}$  for  $\text{KD}_2\text{PO}_4$ ), for spontaneous polarization and Curie constant the isotopic effect is nearly absent. If a change in Curie temperature during deuteronizing points out the paramount role of proton subsystem, then an absence of changes in spontaneous polarization and Curie constant, and also the fact that spontaneous polarization is nearly completely explained by the displacements of ions require taking into account in theory the degrees of freedom corresponding to ionic displacements.

The first such attempt was undertaken in the work [76] using the variational method. However, dynamic aspects of phase transitions were not examined in this theory.

Proceeding from considerations cited above, Kobayashi suggested a new model for describing a phase transition in  $\text{KH}_2\text{PO}_4$ . According to this model, excitation connected with the tunneling of protons (see subparagraph 3, paragraph 3, chapter 4) strongly interacts with the optical vibration of  $\text{K-PO}_4$  along the c-axis with the frequency of the bound mode tending to zero at the transition point. The mode of optical vibration participating in the phase transition is similar to that examined in Cochran's work [7]. Such a model explains the isotopic effect for Curie temperature and its absence for Curie constant and spontaneous polarization.

On the basis of results obtained in the work [74] a conclusion is drawn that  $\text{KH}_2\text{PO}_4$  belongs to a "mixed" type of ferroelectrics since a phase transition in it is connected both with a disordering of the proton system and with instability with respect to the limit optical vibration with this instability appearing at the same time. This point of view was already stated earlier in the works by Blinc and associates [77, 78].

In the light of the foregoing, the results in the work [79] devoted to interconnection of elastic and dielectric properties during a phase transition are of a special interest. As shown in this work, elastic anomalies can also be explained within the framework of dynamic theory (interconnection of elastic and dielectric anomalies was discussed earlier in the work [7] for zinc-blende ( $\text{ZnS}$ ) structure) (see paragraph 2, chapter 3).

The main result in the work [79] is reduced to a discovery that if elastic anomalies are also observed simultaneously with dielectric

anomalies, then a transverse limit optical vibration with a frequency  $\omega_{t0}$  ( $\omega_{t0} \rightarrow 0$  when  $q \rightarrow 0$ ) must participate in the micromechanism of the transition.

The tight bond between optical and acoustical branches may, in particular, lead to a result that with a change in temperature the crystal may become (see paragraph 1, chapter 5) unstable with respect to the transverse acoustic mode even before it becomes unstable in regard to the transverse optical mode. In thermodynamic theory such a situation finds its reflection in that the condition for phase transition is determined not only by the singularity of behavior of dielectric constants  $\sim \epsilon'_0(T - \Theta)$  but also by elastic and piezoelectric constants (see subparagraph 1, paragraph 3, chapter 3).

Thus, although some of the ferroelectric transitions which were formerly regarded as transitions of the order-disorder type and were described by this or other variety of local-minima model, should indeed be regarded as more complex transitions than, for example, those in perovskites, nevertheless they too are closely connected with the singularities of behavior of the optical and acoustic modes of lattice vibrations. Examples of such ferroelectric transitions are transitions in  $\text{KH}_2\text{PO}_4$ ,  $\text{K}_4\text{Fe}(\text{CN})_6 \cdot 3\text{H}_2\text{O}$ , Seignette's salt and in the other ferroelectrics.

In connection with this, it is necessary to note that an anomalous behavior of low-frequency bands of the spectrum was found in the vibration spectrum of  $\text{KH}_2\text{PO}_4$  [80] and  $\text{NaNO}_2$  [49, 57]. In doing so, participation of the limit dipole vibration, the frequency of which decreases at Curie point, in the micromechanism of transition [81] (see in more detail in chapter 15) was proven by direct experiments in the case of  $\text{NaNO}_2$  in which ferroelectric transition is brought about by the ordering of  $\text{NO}_2^-$  groups disordered in the ferroelectric phase.

#### 4. Appearance of "Soft Mode" in Raman Spectra

The question of intensity and spectrum scattered near a phase transition point was examined in the work [82] within the framework of Ginzburg theory.

Spectral density of the intensity of scattered light  $J(\omega)$  is proportional to  $G_\omega$  where  $G_\omega = \frac{1}{2\pi} \int_{-\infty}^{\infty} \eta_q \rightarrow e^{i\omega t} dt$  are Fourier components of the fluctuations of the order parameter. These fluctuations are brought about by thermal motion and can be described in the first approximation by the following equation [82] (see paragraph 4, subparagraph 1):

$$\frac{d}{dt}(\Delta\eta) + \gamma \frac{d}{dt}(\Delta\eta) + \omega_0^2 \Delta\eta = f. \quad (5.109)$$

The equation (5.109) differs from the equation (5.85) by taking into account a random force  $f$  which describes the effect of thermal motion.

It follows from (5.109) that:

$$G_{\omega} = \frac{I_{\omega}}{\omega^2 - \omega_0^2 + i\nu\omega}, \quad (5.110)$$

where

$$I_{\omega} = \frac{1}{2\pi} \int_{-\infty}^{\infty} f(t) e^{-i\omega t} dt.$$

It follows from this that

$$J(\omega) = \frac{\frac{\nu\omega^2}{\pi} I}{(\omega^2 - \omega_0^2)^2 + \nu^2\omega^2},$$

where

$$I = \int_{-\infty}^{\infty} J(\omega) d\omega =$$

is integral intensity of scattered light dependent on the component  $f_{\omega}$  and through it on the temperature [3].

We will note that

$$\left. \begin{aligned} J_0 &= \frac{\nu I}{\pi\omega_0^2}, \\ J(\omega_{max}) &= \frac{I}{\pi\nu(1 - \frac{\omega_0^2}{4\omega_1^2})}, \end{aligned} \right\} \quad (5.111)$$

where the frequencies  $\omega_{max} = \pm \sqrt{\omega_1^2 - \frac{1}{2}\nu^2}$  correspond to the maxima of the function  $J(\omega)$  when  $\omega_1 > \nu\sqrt{2}$ . When  $\omega_1 \leq \nu\sqrt{2}$  the function  $J(\omega)$  has only one maximum, i.e. two satellites in Raman effect -- violet and red merge into one maximum (Figure 5.17) With the approach to the point of a phase transition of the second kind  $\omega_1^2 = \frac{2\alpha_0^2(\theta - T)}{\mu}$  (see 5.88) and changes similar to those shown in Figure 5.10 must occur in the spectrum. These changes should be even sharper in the case of a phase transition approaching critical point.

### 5. Attenuation of Ferroelectric Mode

One of the interesting problems connected with the concept of soft mode is the question concerning its attenuation and, accordingly, concerning the halfwidth of the band corresponding to it in infrared and Raman spectra. In the language of quantum mechanics this is reduced to the question of the lifetime of a quantum of ferroelectric vibration -- ferroelectric phonon.

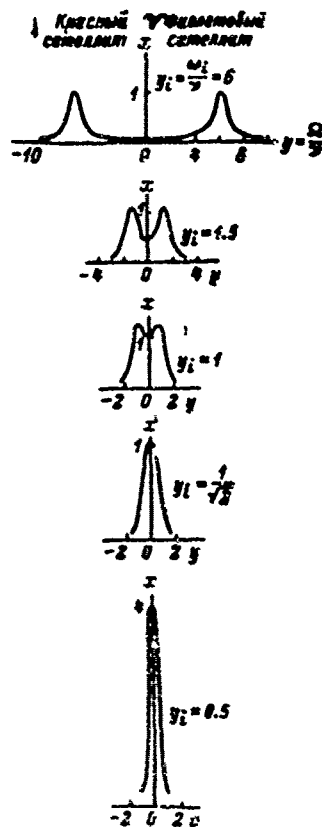


Figure 5.17. Change in the appearance of Raman spectrum according to the ratio of attenuation constant and resonance frequency of vibration.

Key: 1 -- red satellite; 2 -- violet satellite.

In the usual ionic crystals the lifetime of a transverse optical phonon (see, for example, [83]) is determined by the process of its decay into two other phonons weakly dependent on temperature. For a ferroelectric phonon near Curie temperature, owing to the smallness of its frequency it is necessary to take into account not only the process of its decay but also the processes of collision with the other phonons. A respective study for the case of perovskite crystals was carried out in the work [83]. The appearance of phonon spectrum was taken from Cowley's work [26] (Figure 5.18).

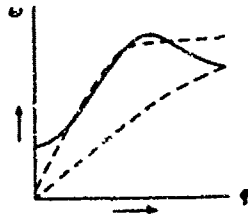


Figure 5.18. The shape of lower branches of phonon spectrum of perovskite crystals.

It may be seen from the figure and laws of conservation that the following processes are possible:

$$\omega_f + a \leftrightarrow o, \quad (5.112)$$

$$\omega_f + a_T \leftrightarrow a_L, \quad (5.113)$$

$$\omega_f \leftrightarrow a + a. \quad (5.114)$$

Here the symbols  $\omega_f$ ,  $a$ ,  $a_T$ ,  $a_L$  and  $o$  belong respectively to a ferroelectric, acoustic, transverse and longitudinal acoustic and optical phonon.

An analysis carried out in [83] indicates that for the case under consideration only the process (5.112) is essential, with the results of the calculations for an isotropic model leading to the following expression for the lifetime of a ferroelectric phonon:

$$\frac{1}{\tau} = \frac{g^2 h v_T \gamma^2 c^2 (n_2 - n_3) \rho \omega_f}{12 \rho c^2 v_T \left( \omega_f + \frac{v_T^2}{c} \right)}. \quad (5.115)$$

Here  $g$  is electrostriction constant,  $h$  -- Planck constant,  $v_T$  -- velocity of transverse sound waves,  $\omega_f = \gamma^2 (T - \Theta)^2$  -- frequency of ferroelectric vibration,  $c$  -- Curie constant,  $\rho$  -- crystal density, the parameter  $\alpha$  characterizes the slope of the ferroelectric branch when  $q$  are small (for  $\text{SrTiO}_3$   $\alpha \sim 10^{-1} \text{ cm}^2/\text{sec}$ ),  $n_i = \frac{1}{e^{\hbar \omega_i / kT} - 1}$  -- the number of quanta of vibrations with the subscripts 2 and 3 corresponding to the transverse acoustic phonons of the ferroelectric branch with  $q \neq 0$  respectively,  $q_0 = \frac{v_T}{\alpha}$ .

We cite the following Dvorak's data [83] on temperature dependence of the lifetime  $1/\tau$  of a ferroelectric phonon for  $\text{SrTiO}_3$ :

$T$ ( $^{\circ}\text{K}$ ).....	50	40	30	20	10	5
$1/\tau$ ( $10^{11}$ 1/sec)...	0.34	0.36	0.38	0.33	0.17	0.05

It may be seen from this that  $\tau$  has an anomalous temperature dependence for ferroelectric mode.

Attenuation time  $\tau$  and attenuation constant  $\Gamma$  defining the width of the band corresponding to the ferroelectric mode in the spectra are connected by the relationship  $\frac{1}{\tau} = \frac{\Gamma}{2}$ . Therefore, investigation of the bandwidth corresponding to  $\omega_1$  may provide a direct way of checking the results set forth above. The results of experimental works [84-87] apparently agree qualitatively with the inferences of theory. However, more exact experimental studies of  $\tau$  are necessary (see also chapter 15).

Attempts at more realistic calculations are also of considerable interest. For example, four-phonon processes the importance of which was pointed out for the first time by Silverman [88] who carried out a respective calculation for a diatomic linear chain, should be taken into account. In the work [89] the attenuation of ferroelectric mode was calculated by more rigorous methods, including taking into account the four-phonon processes for the case of not only low but high temperatures also. The main conclusion of the work is that the relative attenuation of a ferroelectric vibration must be small, with the exception, perhaps, of the near region of transition. Quantities which have to be measured experimentally for a reliable comparison of theoretical results with the experiments are also indicated in [89].

#### 6. Evaluation of Effect of Free Carriers on the Spectrum of Ferroelectrics

Until recently two important sections of solid state physics -- the physics of semiconductors and the physics of ferroelectricity -- had few points of contact with each other. However, after a synthesizing of a number of new ferroelectrics having at the same time semiconductor properties [90, 91], and after the discovery of semiconductor properties in such comparatively well studied ferroelectrics as barium titanate a "border" area of investigations gradually evolved between these two sections and started to develop.

A whole series of physical reasons exist that lead us to expect much that is interesting from this contiguous direction. Indeed, a ferroelectric transition originates as a result of a disturbance of the balance of attractive and repulsive forces which keep the atoms of a crystal lattice in equilibrium positions. But in the usual crystals this balance is preserved up to the melting point or until their mechanical disintegration. Being thus "close" in a certain sense to phase transitions, ferroelectric crystals have an unusually high susceptibility, especially in the transition region, with respect to various kinds of influences and sharply marked nonlinear properties. It is, therefore, natural to expect on one hand the effect of current carriers in ferroelectrics-semiconductors on the phase transitions, and on the other hand -- a sharp change in the semiconductor parameters in the region of a ferroelectric transition, such parameters as the width of forbidden zone, electric conductivity, etc.

As a result, a whole series of new physical effects may appear in ferroelectrics-semiconductors, that are "cross" effects with respect to the physics of semiconductors and the physics of ferroelectricity.

The study of this new area of solid state physics requires a combination of "classical" representations and of the methods of the physics of ferroelectricity and of the physics of semiconductors. This duality is already beginning to show in the first works [92, 93] devoted to a thermodynamic examination of the properties of ferroelectrics-semiconductors. In examining the photo effect in the crystals of SbSJ, V. M. Fridkin [92] postulated the following expression for free energy:

$$A_p = A_0 + \alpha P^2 + \frac{\beta}{2} P^4 + \frac{\gamma}{3} P^6 + \dots + n k_f(P),$$

where  $n$  is the concentration of free or nonequilibrium carriers and  $E_g(P)$  is the width of the forbidden zone. It is then assumed that

$$E_f = E_{g0} + \alpha P^2(T),$$

where  $E_{g0}$  is the width of forbidden zone in paraelectric phase and "a" is a constant not dependent on  $T$  and  $P$ . Such an approximate treatment based on a simple superposition of terms describing the polarization energy of the lattice and of the energy of the carriers in the conduction zone made it possible to make a number of predictions later confirmed by experiments. In particular, the change in Curie temperature with a rise of the concentration [92], the laminar structure in SbSJ [93], etc. were explained on the basis of this theory.

Although at the present time the physics of ferroelectrics-semiconductors is at the stage of initial growth and development, the range of problems that are to be solved has already become outlined sufficiently clearly. Among them are semiconductor properties of ferroelectrics (electric conductivity [94], photoconductivity [95], luminescence, etc.), studies of semiconductor parameters of ferroelectric crystals [91, 94], problems connected with the shielding of spontaneous polarization, distribution of the fields and volume charges in ferroelectrics [96, 97], instabilities in ferroelectrics-semiconductors [98-101], effect of nonequilibrium electronic processes on ferroelectric properties and phase transitions [102], new ferroelectrics-semiconductors [91], superconductivity in ferroelectrics-semiconductors [103-106], etc.

Evaluation of the effect of free carriers on the spectrum of ferroelectrics-semiconductors is also of an unquestionable interest.

A rigorous solution of the problem on infrared spectrum of reflection and absorption in ferroelectrics-semiconductors, i.e. finding the susceptibility of a crystal with account taken of the correlation between normal modes of the lattice and oscillations of an electron plasma is connected with great difficulties. However, by using a simple model it

proves to be possible to evaluate the orders of quantities characterizing the distortion -- brought about by a transfer of free charges -- of the vibration spectrum of the lattice in the phase transition region. A simplified treatment, i.e. a superposition of polarization effects of the lattice vibrations and of the drift of undegenerate electron gas (compare with approximations used in [92]) was successfully used in a number of works [107-109] devoted to the studies of infrared spectra of crystal semiconductors, for example  $Mg_2Sn$ ,  $InSb$ , etc. After a reasonable adjustment of microscopic parameters (effective mass of the carrier  $m^*$  of the effective lattice charges) the theoretical relationships of the real and imaginary parts of the dielectric constant to the frequency in infrared region of the spectrum obtained in these works could be brought into a sufficiently good agreement with the experimental curves even with relatively high concentrations of the free carriers  $N_e \sim 10^{17}$  to  $10^{19} \text{ cm}^{-3}$ .

Conduction current through the crystal is a result of a drift in the direction of the field of undegenerate electron gas. Dissipation losses are defined by the quantity  $\nu = \frac{1}{\tau_e}$  where  $\tau_e$  is electron relaxation time. Complex polarization is a result of combining the electric moments brought about by lattice vibrations and by the carriers of the charges.

The formula for real  $\epsilon'_{\sigma}$  and imaginary  $\epsilon''_{\sigma}$  parts of the dielectric constant of the crystal (the symbol  $\sigma$  indicates the presence of through conductivity) was obtained on the basis of assumption made above similarly to [108]:

$$\epsilon'_{\sigma}(\omega) = \epsilon_{\infty} + \sum_i \frac{s_i^2(\omega_i^2 - \omega^2)}{(\omega_i^2 - \omega^2) + 4\gamma_i\omega^2} - \sum_k \frac{4\pi z_k e_k^2 N_k}{\omega m_k (\omega^2 + \nu_k^2)}, \quad (5.116)$$

$$\epsilon''_{\sigma}(\omega) = \sum_i \frac{2\gamma_i \omega_i s_i^2}{(\omega_i^2 - \omega^2) + 4\gamma_i\omega^2} + \sum_k \frac{4\pi z_k e_k^2 N_k \nu_k}{\omega m_k (\omega^2 + \nu_k^2)}. \quad (5.117)$$

In the expressions (5.116) and (5.117) the first terms represent the spectrum of the lattice, i.e.  $\epsilon'_{\sigma=0}(\omega) = \epsilon'(\omega)$  and  $\epsilon''_{\sigma=0}(\omega) = \epsilon''(\omega)$ , and the second sums represent the spectrum of the current carriers. Summation with respect to  $i$  takes into account the contribution of different lattice vibrations; summation with respect to  $k$  takes into account the contribution of different types of carriers (electrons and holes). In the formulas (5.116) and (5.117)  $z_k e_k$  is effective charge (henceforth  $z_k = \pm 1$ ), and  $N$  is the concentration of free carriers,  $s_i$  is the power of the oscillator.

Next, a number of simplifications are possible. Inasmuch as we are concerned with the soft ferroelectric mode, i.e. with the frequency  $\omega_T$  of the transverse optical vibrations which is considerably lower (at least by 3-10 times) than the other natural frequencies  $\omega_i$  and is characterized by a large value of  $\gamma_T \left( \frac{\gamma_T}{\gamma_i} \right) > 10$ , the effect of all of the

remaining addends in  $\epsilon'$  and  $\epsilon''$  may be neglected both in the region of resonance ( $\omega \rightarrow \omega_T$ ) and away from it ( $\omega \ll \omega_T$ ) without special detriment to later evaluations. In doing so, we have  $s_T^2 = (\epsilon'_s - \epsilon_\infty)\omega_T^2$  where  $\epsilon_s$  is a static ( $\omega \ll \omega_T$ ) dielectric constant of the lattice. If we limit ourselves to taking into account the contribution of free carriers of a certain type (for example, electrons) and if we take into consideration

that with  $\omega \rightarrow 0$   $\frac{e^2 N v}{m^* (\omega^2 - v^2)} \rightarrow \frac{e^2 N}{m^* v} = \sigma_s$  where  $\sigma_s$  is electric conductivity measured with a permanent field,  $m^*$  is effective mass, then (5.116) and (5.117) will be rewritten in the following manner:

$$\epsilon'_s(\omega) = \epsilon_\infty + (\epsilon'_s - \epsilon_\infty) \omega_T^2 \frac{(\omega_T^2 - \omega^2)}{(\omega_T^2 - \omega^2)^2 + 4\gamma_T^2 \omega^2} - \frac{4\pi\sigma_s v}{\omega^2 + v^2} \quad (5.118)$$

$$\epsilon''_s(\omega) = (\epsilon'_s - \epsilon_\infty) \omega_T^2 \frac{2\gamma_T \omega}{(\omega_T^2 - \omega^2)^2 + 4\gamma_T^2 \omega^2} + \frac{4\pi\sigma_s v^2}{\omega(\omega^2 + v^2)} \quad (5.119)$$

We will determine now the effect of the terms  $\sim \sigma_s$  on the character of  $\epsilon'_s(\omega)$  and  $\epsilon''_s(\omega)$  in the region of the frequencies  $\omega_T$  and lower. It is obvious that the position of the maximum of  $\epsilon'_s(\omega)$  (it exists when  $\gamma_T \leq 0.5\omega_T$  are sufficiently small) changes little since the effect of free carriers amounts to an addition of a practically constant quantity even when  $v^2 \ll \omega_T^2$ . This also applies to the position of the center of the absorption line, i.e.  $\epsilon''_s(\omega)_{\max}$ . The position of the point of  $\epsilon'_s(\omega)=0$  defining the frequency of the plasma resonance  $\omega_0$  may change most.

Expanding (5.118) into a series with respect to  $\frac{\Delta\omega}{\omega_T} = \frac{\omega - \omega_T}{\omega_T}$  and determining  $\left(\frac{\Delta\omega}{\omega_T}\right)$  from the condition  $\epsilon'_s(\omega)=0$  we will find:

$$\frac{\Delta\omega}{\omega_T} = \frac{\omega_T - \frac{4\pi\sigma_s v}{\omega_T^2} \frac{1}{1 + \frac{v^2}{\omega_T^2}}}{\frac{(\epsilon'_s - \epsilon_\infty)\omega_T^2}{2\gamma_T^2} - \frac{3\pi\sigma_s v}{\omega_T^2 \left(1 + \frac{v^2}{\omega_T^2}\right)^2}} \quad (5.120)$$

With sufficiently large values of the concentrations  $N_e$ , i.e.  $\sigma_s$ , the value of  $\left(\frac{\Delta\omega}{\omega_T}\right)$  may prove to be large. In this case  $\omega_0$  is determined from the equation

$$\epsilon'_s(\omega) - \frac{4\pi\sigma_s v}{\omega_T^2 + v^2} = 0. \quad (5.121)$$

And if attenuation is sufficiently small ( $\gamma_T < 0.5\omega_T$ ), then from the equation

$$\epsilon'_s - \frac{4\pi\sigma_s v}{\omega_T^2 + v^2} = 0. \quad (5.122)$$

(Condition of low-frequency plasma resonance).

The effect of free carriers on  $\epsilon''(\omega)$  should be characterized by the quantity

$$\epsilon''_{\text{free}} = \epsilon''_0(\nu_T) = \frac{\nu_T}{2\tau} (\epsilon'_0 - \epsilon''_0) + \frac{4\pi N_e}{\nu_T} \frac{\nu_T^2}{1 + \nu_T^2 \tau^2}$$

In the case when the free carriers are electrons, the second terms in (5.118) and (5.119) prove to be commensurable with  $\epsilon'_S$  when the values of  $N_e$  are reasonable, i.e. obtained by experiment. Generally speaking, the value of  $\nu = \frac{1}{\tau}$  changes according to the sign of the carriers [109]. In the case of n-type electric conductivity the relaxation time is relatively long ( $\nu = \frac{1}{\tau} \approx 10^{13} \text{ sec}^{-1}$ ) and in the case of p-type electric conductivity the relaxation time is short ( $\nu = \frac{1}{\tau} = 10^{15} \text{ sec}^{-1}$ ). The former case is of the greatest interest. As regards the effective mass  $m^*$ , according to experimental data this quantity varies in a range of 0.04 to 0.2  $m_e$  in the case of the values of concentration with which we are concerned. Henceforth the larger value of  $m^* = 0.2 m_e$  is used. It is clear that with smaller values of  $m^*$  the effects of the influence of the carriers will be observed in the case of smaller concentrations  $N_e$ . With the assumptions which have been made  $\sigma_S = \frac{e^2 N_e}{m^* \nu} \approx 10^{-4} N_e \text{ sec}^{-1}$  (for p-type semiconductors  $\sigma_S = 10^{-6} N_e \text{ sec}^{-1}$ ).

Coming back to formula (5.121), neglecting unity in comparison with  $\frac{\nu^2}{\omega^2}$  and the second term in the denominator and taking for SrTiO<sub>3</sub>  $\epsilon'_S \approx 230$ ,  $\epsilon''_S \approx 5$ ,  $\nu_T \approx 3000 \text{ K} \approx 0.15 \omega_T$  (see [50]), we have for  $\left(\frac{\Delta\omega}{\omega_T}\right)_{\epsilon=0} \approx 10^{-3}$ . However, already with  $N_e \approx 0.5 \cdot 10^{17} \text{ cm}^{-3}$   $\frac{\Delta\omega}{\omega_T} \approx 0$  and with  $N_e \approx 10^{18} \text{ cm}^{-3}$   $\frac{\Delta\omega}{\omega_T} \approx -2.4 \cdot 10^{-2}$ , and with  $N_e \approx 10^{19} \text{ cm}^{-3}$   $\frac{\Delta\omega}{\omega_T} \approx -0.24$ . In doing so, formula (5.120) becomes incorrect and formula (5.121) or (5.122) should be used. With the approach to Curie  $\frac{\Delta\omega}{\omega_T}$  change little although  $\epsilon'_S$  increases approximately by one order; according to experimental data in [50] the value of  $\nu_T^2/\omega_T^2$  increases approximately by this same magnitude (increase of anharmonicity and, consequently, of the losses).

The curves  $\epsilon'_0(\omega)$  calculated on the basis of (5.118) are shown in Figure 5.19. The second, the low-frequency point of the passage of  $\epsilon'_0(\omega)$  (5.121) through zero has a certain singularity: with a sufficiently high concentration ( $N_e > 10^{18}$ ) away from  $\omega_T$  or with high  $\nu_T$  in the region of the maximum a low-frequency plasma resonance is realized under the conditions of a weak frequency dependence of  $\epsilon'$ . This applies especially to the case described by formula (5.122) when the existence of

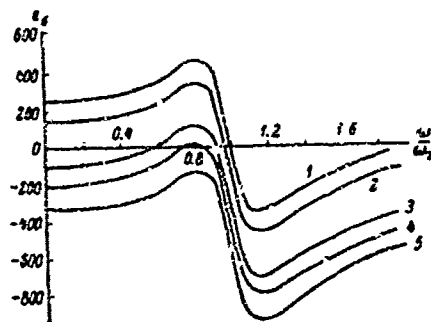


Figure 5.9. Frequency dependence of  $\epsilon'_g$  with  $\frac{T}{\theta} = 7.5$  and  $\gamma_T = 0.15$  for different concentrations of carriers.

$N_e, \text{ cm}^{-3}$ : 1 -- 0; 2 --  $1.5 \cdot 10^{17}$ ; 3 --  $1 \cdot 10^{18}$ ;  
4 --  $3 \cdot 10^{18}$ ; 5 --  $5 \cdot 10^{18}$ .

longitudinal waves is possible in a certain frequency or temperature region (inasmuch as the condition (5.122) can be satisfied by the variation of both variables  $\omega$  and  $T$ ). The width of this region can be determined if the space dispersion of  $\epsilon'_g$  is taken into account.

The relationship  $\epsilon''(\omega)$  with different concentrations is clear from (5.119). With an increase of  $N_e$  the magnitude of the maximum of the absorption line is masked by additional losses brought about by plasma the effect of which decreases with the approach to Curie point  $\theta$  since the value of  $\frac{\epsilon_5 \omega T}{2 \gamma_T}$  increases. The curves of  $\epsilon'_g(T)$  are given in Figure 5.20.

#### 7. Effect of Space Dispersion on Optical Constants

In the examination of electromagnetic waves in different media a local coupling between the induction vector  $D$  and the field  $E$  is usually postulated, i.e.

$$D_i(r) = \epsilon_{ik}(r, \omega) E_k(r). \quad (5.123)$$

In the presence of absorption the tensor of the dielectric constant  $\epsilon_{ik}$  is a complex quantity, i.e.  $D$  is replaced by  $D - i \frac{4\pi}{\omega} j$  where  $j$  is conduction-current density.

In the definition (5.123)  $\epsilon_{ik}$  depends on frequency and no account is taken of the dependence of  $\epsilon_{ik}$  on the wavelength with this dependence taking place if in the period during which the particles move in space (vibrations of the lattice atoms, the range of conduction electron, etc.) the field  $E$  has time to change (see [111, 112]). The magnitude of the space dispersion of  $\epsilon_{ik}$  characterizing the departure beyond the limits of local coupling (5.123) is defined by the parameter  $a/\lambda = \frac{an}{\lambda_0}$  in which "a" is a length (the size of molecules, Debye shielding radius, etc.) characteristic for a given medium,  $\lambda_0 = \frac{2\pi c}{\omega}$  is the wavelength in vacuum,  $\frac{\lambda_0}{n} = \lambda$  is the wavelength in the medium, and  $n$  is refraction index. For the usual condensed media, in the region of optical frequencies  $f=10^{12}$  to  $10^{15}$  hertz, the parameter  $\frac{a}{\lambda_0} = 10^{-7}$  to  $10^{-4}$ , and the effect of space dispersion is negligible. However, near the plasma resonance where  $\epsilon_{ik} \rightarrow 0$ , or in a region where  $\epsilon_{ik}(\omega, T) \rightarrow \infty$  when refractive index anomalously increases and, accordingly, the parameter  $\frac{an}{\lambda_0}$  also, space dispersion may prove to be considerable.

Space dispersion can be taken into account in dynamic equations if the field  $E$  written in the form of a wave propagating in a crystal is introduced into them. However, if the parameter  $\frac{an}{\lambda_0}$  is not very large a phenomenological approach is possible. In this case, unlike (5.123) the relation between  $D$  and  $E$  is written in the form of an expansion with respect to the space derivatives of the field  $E$ , i.e.

$$D_i = \epsilon_{ik}(\omega) E_k + \gamma_{ikl}(\omega) \frac{\partial E_k}{\partial x_l} + \delta_{iklm}(\omega) \frac{\partial^2 E_k}{\partial x_l \partial x_m}. \quad (5.124)$$

As usual, summation is over twice repeated subscripts.

The term with  $\gamma_{ikl}$  is responsible for the appearance of natural optical activity in the crystal 1) (see [111]). It disappears when the body has a center of symmetry. With respect to the order of magnitude  $\gamma_{ikl} \sim a$ . Quadratic term in the expansion (5.124) exists regardless of the presence of the center of symmetry and  $\delta_{iklm}$  is of an order of  $a^2$ . 2)

1) I.e. appearance of a double refraction, and rotation of polarization plane of a linearly polarized wave (see [111, 113]).

2) It can be shown that the value of  $\delta_{iklm}$  from (5.124) is connected with the parameter  $\delta$  contained in the correlation term in the expansion of thermodynamic potential  $\Phi = \alpha P^2 + \frac{1}{2} \beta P^4 + \dots + \delta (\text{grad } P)^2$  (see chapter 1, paragraph 1). In the example examined in chapter 1  $\delta \approx \frac{\pi}{15} d^2$  where  $d$  is lattice constant.

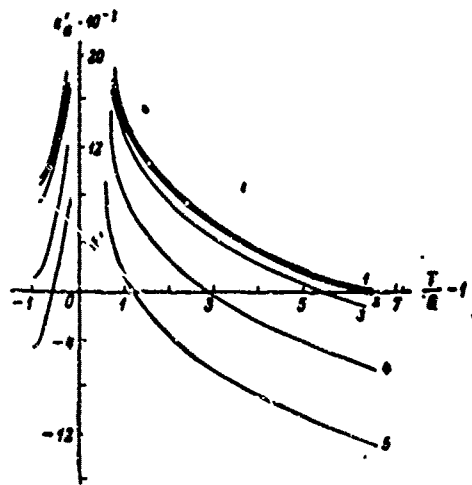


Figure 5.20. Temperature dependence of  $\epsilon'_0$  when  $\frac{\omega}{\omega_T} \approx 0.2$  for different concentrations of the carriers.

$N_e, \text{ cm}^{-3}$ : 1 -- 0; 2 --  $5 \cdot 10^{17}$ ; 3 --  $10^{18}$ ;  
4 --  $3 \cdot 10^{18}$ ; 5 --  $10^{19}$ .

Henceforth a case of an isotropic medium will be examined for simplicity and, consequently, the subscripts in (5.124) will be omitted.

If the medium has a center of symmetry, then after a substitution of

$$E = E_0 \exp(i(\omega t - \omega \mathbf{s} \cdot \mathbf{r})) \quad (5.125)$$

( $\mathbf{s}$  is a unit vector)  
we have:

$$D_i = \epsilon E_i; \quad i = e - a \dot{E}_i; \quad a \approx \left(\frac{\omega}{c}\right)^2 \lambda^2. \quad (5.126)$$

where  $\tilde{n} = n - i\kappa$  is a complex refractive index ( $\kappa$  is absorption index),  
 $\delta \sim a^2, \quad \alpha \sim \left(\frac{a}{\lambda_0}\right)^2.$

The expansion (5.124) and, consequently, (5.126) are used when  $\epsilon$  is a small quantity.

If  $\epsilon \rightarrow \infty$  and  $n$  is correspondingly large, the relationship

$\epsilon_i = \hat{\epsilon}^{-1} D_i$  is inverse dielectric constant

$$\epsilon^{-1} = \epsilon^{-1} + \beta \hat{n}^2, \quad (5.127)$$

with the magnitude of  $\beta$  coinciding with  $\alpha$  with respect to the order of magnitude.

We will examine now the singularity of behavior of electromagnetic waves when  $\epsilon \rightarrow 0$  and  $\epsilon \rightarrow \infty$ .

Propagation of plane waves is defined by Maxwell equations:

$$\mathbf{H} = A(\mathbf{sE}); \quad \mathbf{D} = -A(\mathbf{sH}),$$

whence

$$\nabla = A^2(\mathbf{E} - \mathbf{s}(\mathbf{sE})). \quad (5.128)$$

Substituting into (5.128)  $\mathbf{D} = \hat{\epsilon}\mathbf{E}$  and  $\hat{\epsilon} = \epsilon - \chi n^2$  we will obtain from the equation for  $\hat{n}$  the following multiple solutions for a transverse wave ( $\mathbf{sE} = 0$ ):

$$\hat{n}_{12}^2 = \frac{\epsilon'(\omega)}{1 + \alpha} \quad \text{and if } \alpha \ll 1$$

$$\hat{n}_{12}^2 = \epsilon'.$$

For longitudinal waves

$$\left. \begin{aligned} \mathbf{s}(\mathbf{sE}) &= \mathbf{E}, \\ A_1^2 &= \frac{\epsilon'(\omega)}{\epsilon}. \end{aligned} \right\} \quad (5.129)$$

As is known [112, 113], longitudinal waves exist when  $\epsilon' \rightarrow 0$  otherwise  $n_3 \rightarrow \infty$  and the parameter of expansion  $\frac{an}{\lambda_0}$  becomes anomalously large and, consequently, the entire macroscopic approach  $\left(\frac{\lambda_0}{n} > a\right)$  becomes illegitimate. The condition  $\frac{an}{\lambda_0} \ll 1$  together with (5.129) defines the frequency region of the existence of plasma waves.

For ferroelectric "soft mode" ( $\omega_T \approx 10^{12}$ ) we have  $\alpha \approx 10^{-12}$  and assuming  $\frac{an}{\lambda_0} < 10^{-2}$ , we will obtain  $n_3 \leq 10^3$ .

Taking (5.129) into account we see that the region of existence of plasma waves is limited by the values of  $|\epsilon'| \leq 10^{-6}$ .

It is easy to perceive from formulas (5.129) that this region is very narrow. With the approach to Curie point and taking into account the increase of  $\epsilon'$  and decrease of  $\alpha$  this region becomes even narrower (increase of attenuation  $\gamma$  with  $T \rightarrow \theta$  causes little change in this result).

To determine  $n(\omega)$  of the transverse waves near Curie point it is necessary to make use of formula (5.127) which after a substitution into (5.128) gives the following approximate solutions

$$(5.130)$$

$$n_1 = \epsilon' (1 - \epsilon''\beta + \dots)$$

$$n_2 = -\frac{\beta}{\epsilon''} - \epsilon' + \dots \quad (5.131)$$

with the condition that

$$|\beta| \ll 1. \quad (5.132)$$

Inasmuch as  $\beta \sim 10^{-12}$  the condition (5.132) is satisfied when  $\epsilon \ll 10^3$ . An evaluation indicates that  $n_1^2 \approx \epsilon'$  nearly in the entire range of values of  $\omega$  and  $\tau$  for most ferroelectrics. Space dispersion, i.e. the second term in (5.130) becomes tangible, i.e. of the order of  $10^{-2}$  only in direct proximity to  $\omega_0$ . However, in this case, observation of the usual spectrum is made difficult by dissipations in fluctuations.

The second root of  $n_2^2$  is very large:  $n_2 > 10^3$  away from the resonance. In direct proximity to the point of  $\epsilon''(\omega) = 0$   $n_2^2 \rightarrow \infty$  and then changes the sign  $n_2 \rightarrow -\infty$  (Figure 5.19).

If it is assumed that in this region the value of  $n_2^2$  is finite because of the effect of attenuation and passes through zero, then in a very narrow frequency region  $n_2$  may have reasonable values, i.e. a second transverse wave may exist. With the approach to Curie point the width of both lines narrows owing to an increase in the absolute value of  $\epsilon''$ . With all of the other values of  $\omega$   $n_2^2 > 10^6$  (with  $n_2^2 < 0$   $n_2 = -\infty$ ), i.e. a total internal reflection takes place.

In the absence of a center of symmetry in a crystal and, consequently, for all ferroelectrics in a region where  $P_s \neq 0$ , a first-order term appears in the expression (5.124) and in this case

$$D = \epsilon E - i f [sE].$$

Inasmuch as we are concerned with transverse waves (for plasma waves  $[sE] = 0$ ), when the values of  $\epsilon$  are large we have:

$$\epsilon = \frac{D}{E} + (g[sD])n. \quad (5.133)$$

where  $g$  has an order of  $\frac{a}{\lambda_0} \approx \sqrt{\epsilon}$ .

Substituting (5.133) into (5.128) we will obtain for  $n^2$  a cubic equation

$$\epsilon^2 n^3 - \left(\frac{n^2}{\epsilon} - 1\right)^2 = 0. \quad (5.134)$$

which has the following approximate solutions when  $g\epsilon^{\frac{1}{2}} \ll 1$  [113]:

$$n_{1,2} = (1 \pm g^{1/2}), \quad (5.135)$$

$$n_3 = \frac{1}{\epsilon^{3/2} g}. \quad (5.136)$$

Inasmuch as  $g \sim 10^{-6}$  near  $\omega_1$ , the condition ( $g \epsilon^{3/2} \ll 1$ ) is satisfied when  $\epsilon(\omega, T) \ll 10^3$ . However, for ferroelectrics not having a piezoelectric effect the temperature region above the transition point where approximate solutions (5.135) and (5.136) are valid, may be expanded owing to the circumstance that the value of  $g^2$  must depend on temperature as  $(\Theta - T)^\nu$  where  $\nu \ll 1$  is a quantity dependent on the character of the transition.

It follows from (5.135) and (5.136) that with the approach to Curie point the effect of space dispersion for waves described by the refractive indices  $n_{1,2}$  considerably increases.

Waves defined by  $n_3$  appear owing to space dispersion and their behavior greatly depends on  $\epsilon(\omega, T)$ . However, it should be remembered that the range of values of  $n_{1,2,3}(\omega, T)$  having physical sense is limited by the conditions  $\frac{an}{\lambda_0} \ll 1$  and  $\epsilon^{3/2} g \ll 1$ .

In taking anisotropy of a crystal into account, space dispersion leads to a number of new effects (in particular to a weak optical anisotropy of cubic crystals, see [113]). It may be supposed that for ferroelectrics these effects must be very strongly marked.

We will also note that in the presence of high electric conductivity in a crystal, brought about by electrons the effect of space dispersion considerably increases [107]. With a sufficiently high concentration of free carriers ( $N_e \sim 10^{17}$  and higher) the parameter  $\left(\frac{a}{\lambda_0}\right)^2 \approx \frac{3kT}{\pi \epsilon_0 c^2} \approx 10^{-7}$  to  $10^{-8}$ .

A value close to this one results if it is considered that near  $\omega_0 \approx \omega_D$  where for undegenerate electron gas  $\omega_D = \left(\frac{kT}{8\pi e^2 N_e}\right)^{1/2}$  (see [112]).

Thus, for electron gas

$$\alpha \sim \beta \sim 10^{-7} \text{ to } 10^{-8}; \quad g \sim 10^{-4}.$$

A considerable change in the orders of these values in comparison with the usual crystals and ferroelectrics leads to an appearance of a number of singularities in the relationships  $n(\omega, T)$  [107].

Thus, for ferroelectrics (especially for ferroelectrics-semiconductors) taking space dispersion into account becomes important in the frequency region of "soft mode".

The use of dynamic theory proves to be necessary in describing the micromechanism of ferroelectric transitions in which the frequency of "soft mode" becomes zero or reaches anomalously low values.

Temperature dependence of the halfwidth and intensity of the band corresponding to a ferroelectric vibration in Raman and infrared spectra sharply differs near the transition point from the temperature dependence of the halfwidths and intensities of the other lines of the spectra.

At the present time all theoretical predictions bear only a qualitative character and are made for relatively simple models. Some of them have already received experimental corroboration (see chapter 15).

The further development of dynamic theory may proceed in several directions. Firstly, attempt can be made to do the calculations for more complex models in order to obtain results related to concrete ferroelectric transitions. Secondly, predictions and theory of new physical effects connected with the "soft mode" are of a great interest, for example study of anomalous behavior of Messbauer line at the transition point [114, 115], damping of sound [116], effect of the appearance of a new bound ferroelectric-acoustic mode [117], etc.

Finally, a promising direction is the search for physical mechanisms responsible for the appearance of ferroelectric mode, study of the vibration spectra of ferroelectrics-semiconductors, etc. Thus, the possibilities of dynamic theory of ferroelectricity have not yet, by far, been exhausted.

#### BIBLIOGRAPHY

1. V. L. Ginzburg, ZhETF [Journal of Experimental and Theoretical Physics], Vol 19, p 36 (1949).
2. V. L. Ginzburg, UFN [Achievements of Physical Sciences], Vol 38, p 430 (1949).
3. V. L. Ginzburg, UFN, Vol 77, p 621 (1962).
4. P. Anderson. Fizika Dielektrikov [The Physics of Dielectrics], USSR Academy of Sciences Press, Moscow, p 290 (1960).
5. W. Cochran, Phys. Rev., Lett., Vol 3, p 412 (1959).
6. W. Cochran, Adv. Phys., Vol 9, p 387 (1960).
7. W. Cochran, Adv. Phys., Vol 10, p 401 (1961).
8. W. Ledermann, Proc. Roy. Soc., A182 (1944).

9. R. E. Peiris, Proc. Int. Sci. J. India, Vol 20, p 121 (1954).
10. K. Huang, Proc. Roy. Soc., A208, p 352 (1951).
11. M. Born and K. Huang. Dinamicheskaya Teoriya Kristallicheskih Reshotok [Dynamic Theory of Crystal Lattices]. IL [Foreign Literature Press], Moscow (1956)
12. P. F. Ewald, Ann. Phys., Vol 64, p 253 (1921).
13. M. S. Shur and Yu. N. Tsarev, FTT [Solid State Physics], Vol 10, p 2899 (1968).
14. P. S. Knox. Theory of Excitons. Academic Press, N.Y. (1963).
15. J. S. Scott, L. E. Chesman, S. P. S. Porto, Phys. Rev., Vol. 162, p 834 (1967).
16. R. Ruppin, R. Englman, J. Phys. C (Proc. Phys. Soc.), ser. 2, 1, 614 (1968).
17. A. A. Lucas. Phys. Rev., Vol 162, p 801 (1967).
18. L. D. Landau, Ye. M. Lifshits. Statisticheskaya Fizika [Statistical Physics]. Nauka Publishing House, Moscow (1964).
19. E. W. Kellerman, Phil. Trans. Roy. Soc., Vol 238, p 513 (1940).
20. A. I. Gubanov and M. S. Shur, FTT, Vol 7, p 2626 (1965).
21. M. S. Shur, FTT, Vol 8, p 57 (1966)
22. M. S. Shur, Izv. AN SSSR, ser. fiz. [Bulletin of USSR Academy of Sciences, Physical Series], Vol 31, 1042 (1967).
23. E. V. Chisler, M. S. Shur, Phys. St. Sol., Vol 17, p 163 (1966).
24. A. D. B. Woods, W. Cochran, B. N. Brockhouse, Phys. Rev., Vol 119, p 999 (1960).
25. R. S. Cowley, W. Cochran, B. N. Brockhouse, A. D. B. Woods, Phys. Rev., Vol 131, p 1030 (1963).
26. R. A. Cowley, Phys. Rev., Vol 134, p A981 (1964).
27. K. B. Tolpygo and V. S. Mashkevich, ZhETF, Vol 32, p 520 (1957).
28. R. G. Dick, W. Owerhauser, Phys. Rev., Vol. 112, p 90 (1958).

29. G. Leybfrid. Mikroskopicheskaya Teoriya Teplovykh i Mekhanicheskikh Svoystv Kristallov [Microscopic Theory of Thermal and Mechanical Properties of Crystals]. GIFML [State Publishing House for Physical and Mathematical Literature], Moscow--Leningrad. (1963).
30. R. A. Frazer. Teoriya Matrits i yeyo Prilozheniye k Differentsial'nym Uravneniyam v Dinamike [Matrix Theory and Its Application to Differential Equations in Dynamics]. IL, Moscow (1950).
31. J. H. C. Thompson, Phil. Mag., Vol 44, p 131, (1953).
32. B. D. Silverman, Phys. Rev., Vol 135, p A1596 (1964).
33. R. A. Cowley, Phys. Rev., Lett., Vol 9, p 159 (1962).
34. T. Nagamija, Progr. Theor. Phys. Japan, Vol 1, p 275 (1952).
35. W. Heine. Teoriya Grupp v Kvantovoy Mekhanike [Group Theory]. IL, Moscow (1963).
36. G. Lyubarskiy. Teoriya Grupp i Yeyo Primeneniya v Fizike [Group Theory and Its Application in Physics]. GIFML, Moscow (1963).
37. O. V. Kovalev. Neprivodimyye Predstavleniya Prostravennykh Grupp [Irreducible Representations of Space Groups]. Izd. AN UkSSR [Ukrainian SSR Academy of Sciences Press], Kiev (1961).
38. I. V. V. Raghavacharyulu, Canad. J. Phys., Vol 38, p 1704 (1961).
39. L. D. Landau and Ye. M. Lifshits. Kvantovaya Mekhanika [Quantum Mechanics]. GIFML, Moscow (1963).
40. A. S. Davydov. Kvantovaya Mekhanika [Quantum Mechanics]. GIFML, Moscow (1963).
41. E. V. Chisler and M. S. Shur, Izv. Sib. otd. AN SSSR [Bulletin of Siberian Branch of USSR Academy of Sciences], No 9, Issue 4, p 59 (1967).
42. Yu. I. Sirotin and L. M. Mikhe'ison, FTI, Vol 10, p 1843 (1968).
43. V. Dvorak, Phys. St. Sol., Vol 3, p 2235 (1963).
44. V. Dvorak, V. Janovec, Czechoslovak J. Phys., Vol 12, p 4611 (1962).
45. M. S. Shur, Kristallografiya [Crystallography], Vol 11, p 448 (1966).
46. M. S. Shur, FTI, Vol 8, p 1267 (1966).
47. M. S. Shur, FTI, Vol 8, p 2504 (1966).
48. M. S. Shur, Kristallografiya, Vol 12, p 215 (1967).

49. E. V. Chisler, M. S. Shur, Izv. AN SSSR, ser. fiz., Vol 31, No 7 (1967).
50. V. N. Murzin, R. Ye. Pasynkov, S. L. Solov'yov, UFN [Achievements of Physical Sciences], Vol 92, p 427 (1967).
51. M. A. Melvin, Rev. Mod. Phys., Vol 28, p 18 (1956).
52. A. I. Stekhanov and Ye. A. Popova, FTI, Vol 7, p 3530 (1965).
53. G. E. Bacon, R. S. Pease, Proc. Roy. Soc., Vol A230, p 359 (1955).
54. S. Sawada, S. Nomura, S. Fujii, J. Yoshida, Phys. Rev. Lett., Vol 1, p 320 (1958).
55. G. E. Ziegler, Phys. Rev., Vol 38, p 1040 (1931).
56. M. J. Kay, B. C. Frazer, Acta Cryst., Vol 14, p 56 (1961).
57. E. V. Chisler, M. S. Shur, Phys. St. Sol., Vol 17, p 173 (1966).
58. M. S. Shur. Primeneniye Teorii Grupp dlya Analiza i Rascheta Kolebatel'nykh Spektrov Kristallov [Application of Group Theory for Analysis and Calculation of Vibration Spectra of Crystals]. Candidate's dissertation. FTI [Physical Engineering Institute] imeni A. F. Ioffe, Leningrad (1967).
59. G. A. Smolenskiy, R. Ye. Pasynkov, ZhETF, Vol 25, p 57 (1953).
60. G. A. Smolenskiy, V. Kh. Kozlovskiy, ZhTF [Journal of Technical Physics], Vol 23, p 3 (1956).
61. J. S. Slater, Phys. Rev., Vol 78, p 746 (1950).
62. A. F. Devonshire, Phil. Mag., Vol 40, p 1040 (1949).
63. V. L. Ginzburg, FTI, Vol 2, p 2031 (1960).
64. G. Leybfrid and V. Ludvig. Teoriya Angarmonicheskikh Effektov v Kristallakh [Theory of Anharmonic Effects in Crystals], IL, Moscow (1963).
65. V. G. Vaks, ZhETF, Vol 54, p 910 (1967).
66. P. C. Kwok, P. B. Miller, Phys. Rev., Vol 151, p 387 (1966).
67. K. Aizu, J. Phys. Sec. Japan, Vol 21, p 7 (1966)
68. R. M. Wilcox, Phys. Rev., Vol 139 p A1281 (1965).
69. R. A. Cowley, Adv. Phys., Vol 12, p 421 (1963).

70. B. D. Silverman, R. I. Joseph, Phys. Rev., Vol 129, p 2062 (1963)
71. R. Blinc. Ferroelectricity (in lectures on condensed matter). Trieste (1968).
72. V. G. Vaks. Voprosy Teorii Fazovykh Prevrashcheniy i Spektrov Vozbuzhdeniyy v Sistemakh Mnogikh Tel [Problems of Theory of Phase Transformation and Excitation Spectra in Many-Body Systems]. Author's abstract of doctoral dissertation. IPAN SSSR [USSR Institute of Applied Nuclear Sciences], Leningrad (1967).
73. V. G. Vaks, V. M. Galitskiy, A. I. Larkin, ZhETF, Vol 51, p 1592 (1966).
74. K. K. Kobayshi, J. Phys. Soc. Japan, Vol 24, p 497 (1968)
75. B. C. Frazer, R. Pepinsky, Acta Cryst., Vol 6, p 173 (1953).
76. R. Blinc, M. Ribaric, Phys. Rev., Vol 130, p 1816 (1963).
77. R. Blinc, M. Fintar, J. Zupancic, J. Phys. Chem. Solids, Vol 28, p 407 (1967).
78. R. Blinc, P. Cevc, M. Shara, Phys. Rev., Vol 159, p 411 (1967).
79. J. Lefkowitz, Y. Hazony, Phys. Rev., Vol 169, 441 (1968).
80. I. M. Aref'yev, P. A. Bazhulin, FTT, Vol 7, p 407 (1965).
81. E. V. Chisler, M. S. Shur, FTT, Vol 9, p 1015 (1967).
82. V. L. Ginzburg, A. P. Levanyuk, ZhETF, Vol 39, p 192 (1960).
83. V. Dvorak. Proc. Int. Meet. on Ferroelectricity, Prague, p 61 (1966).
84. W. Spitzer, R. C. Miller, D. A. Kleinman, L. D. Howarth, Phys. Rev., Vol 126, p 1710 (1962).
85. J. M. Ballantyne, Phys. Rev., Vol 136, p A429 (1964)
86. A. S. Barker, Jr., Phys. Rev., Vol 145, p 391 (1965).
87. M. D. Domenico, Jr., S. H. Wemple, S. P. S. Porto, R. P. Bauman, Phys. Rev., Vol 174, p 522 (1968).
88. B. D. Silvermann, Phys. Rev., Vol 125, p 1921 (1962).

89. B. Ya. Bal'gurov, V. G. Vaks, B. I. Shklovskiy. Preprint IAE-1815, Division of Literature, Institute of Atomic Energy imeni I. V. Kurchatov. Moscow (1969).
90. E. Fatuzzo, G. Harbeke, W. J. Merz, R. Nitshe, H. Roetschi, W. Ruppel, Phys. Rev., Vol 127, p 2036 (1962).
91. T. A. Pikka, V. M. Fridkin, FTI, Vol 10, p 2278 (1968).
92. V. M. Fridkin, ZhETF, Letters, Vol 3, p 252 (1966).
93. A. I. Larkin, D. Ye. Khmel'nitskiy, ZhETF, Vol 55, p 2345 (1969).
94. C. N. Berglund, W. S. Baer, Phys. Rev., Vol 157, p 358 (1967).
95. W. Merz, R. Nitshe, Izv. AN SSSR, ser. fiz., Vol 28, p 4 (1964).
96. G. M. Guro, I. I. Ivanchik, I. F. Kovtonyuk, FTI, Vol 10, p 135 (1968).
97. I. I. Ivanchik, FTI, Vol 3, p 373 (1961).
98. M. S. Shur, FTI, Vol 10, p 2652 (1968).
99. M. S. Shur, FTI, Vol 10, p 3560 (1968).
100. M. S. Shur, FTI, Vol 10, p 3684 (1968).
101. M. S. Shur, FTI, Vol 11, No 10 (1969).
102. I. I. Groshik, P. V. Ionov, V. M. Fridkin, FTI, Vol 2, p 1630 (1968).
103. V. L. Gurevich, A. I. Larkin, Yu. A. Firsov, FTI, Vol 4, p 185 (1962).
104. M. L. Cohen, Rev. Mod. Phys., Vol 36, p 240 (1964).
105. J. F. Scholley, W. R. Hostler, M. L. Cohen, Phys. Rev., Vol 12, p 474 (1964).
106. J. F. Scholley, W. R. Hostler, E. Ambler, J. H. Becker, M. L. Cohen, C. S. Koonce, Phys. Rev. Lett., Vol 14, p 305 (1965).
107. R. Ye. Psynkov, Izv. AN SSR, ser. fiz., Vol 81, No 2 (1968).
108. H. Lipson, A. Kohan, Phys. Rev., Vol 158, p 756 (1967).
109. J. Jasperse, A. Kohan, I. Plende, S. Hifra, Phys. Rev., Vol 146, p 526 (1966).
110. R. Sanderson, J. Phys. Chem. Solids, Vol 26, p 803 (1965).

111. L. D. Landau and Ye. M. Lifshits. Elektrodinamika Sploshnykh Sred [Electrodynamics of Continua]. GITL [State Publishing House for Technical and Theoretical Literature], Moscow (1957).

112. V. L. Ginzburg. Rasprostraneniye Elektromagnitnykh Voln v Plazme [Propagation of Electromagnetic Waves in Plasma]. Nauka Publishing House, Moscow (1967).

113. V. L. Ginzburg, ZhETF, Vol 34, p 1593 (1958).

114. C. Muzikar, V. Janovec, V. Dvorak, Phys. St. Sol., Vol. 3, k. 9 (1963).

115. V. G. Vaks, V. M. Galitskiy, A. I. Larkin, ZhETF, Vol 53, (1967).

116. V. Dvorak, Canad. J. Phys., Vol 45, p 3903 (1967).

117. V. Dvorak, Phys. Rev., Vol 167, p 525 (1968).

## CHAPTER 6. ELEMENTS OF SYMMETRY THEORY

### Part. Definition of Group

Any set  $G$  of elements for which the following 4 conditions are satisfied is called a group.

1. For all elements of the set  $G$  there is a defined "multiplication" operation which puts into correspondence to any two elements "a" and b a third element c:

$$c=ab. \quad (6.1)$$

In doing so, generally speaking  $ab \neq ba$ .<sup>1)</sup>

2. Multiplication operation is associative, i.e. for three arbitrary elements a, b and c

$$a(bc)=(ab)c. \quad (6.2)$$

3. A set contains a unit element  $E$  having the property that for any element "a" of the group

$$aE=EA=a. \quad (6.3)$$

4. Together with the element "a" a set contains an element  $a^{-1}$  having the property that

$$aa^{-1}=a^{-1}a=E. \quad (6.4)$$

The simplest examples of groups are: a) all real numbers including zero (addition is a group-multiplication operation), b) all rational positive fractions except zero (multiplication is a group-multiplication operation), c) the aggregate of symmetry operations leaving the energy of a body invariable under specified conditions.

---

1) A group for all elements of which  $ab=ba$  is called Abelian group.

Every subset of a group is called a subgroup if it is a group with respect to the same group-multiplication operation.

The order (i.e. the number of elements) of a finite subgroup containing a finite number of elements is a divisor of the group order.

The simplest example of a subgroup is a subgroup of all integers in a group of all real numbers (group multiplication is addition).

#### Par. Symmetry Transformations. Crystal Symmetry

By symmetry transformations are meant those displacements of a body which superpose it with itself, or those transformations of coordinates which leave the energy of a system invariant. Each one of the possible symmetry transformations may be represented in the form of a combination of a turn of a body by a certain angle, a secular reflection of the body in a certain plane and parallel transfer over a certain distance.

Symmetry transformations of a given body always form a group. For a body of finite dimensions all symmetry axes and planes apparently must have a common point of intersection in order that the application of symmetry operations would not lead to a progressive motion which cannot superpose a body with itself. This restriction also applies to symmetry operations which transform each direction in a crystal into equivalent to it.

Symmetry groups having the property mentioned are called point groups.

Crystals having one and the same point group form a crystal class. Altogether, 32 crystal classes exist.

Two systems of notations of symmetry operations and symmetry groups of the crystals are usually employed. In Schoenflies system  $C_k$  indicates turns by angles that are multiples of  $\frac{2\pi}{k}$ ,  $S_k$  indicates mirror turns by angles that are multiples of  $\frac{2\pi}{k}$ , i.e. turns with a following mirror reflector in a plane perpendicular to the axis of rotation. 1)

The axis with the largest index  $k$  for a given point group is called principal axis. Reflection plane perpendicular to the principal axis is denoted by  $\sigma_h$ , the plane containing the principal axis -- by  $\sigma_v$  or  $\sigma_a$ . Second-order symmetry axis perpendicular to the principal

---

1) The spacing of crystal structure imposes limitations on permissible turns. The point groups of crystals can contain only combinations of reflections and turns by the angles  $\frac{\pi}{2}$ ,  $\frac{\pi}{3}$ ,  $\frac{\pi}{4}$  and  $\frac{\pi}{6}$ .

axis is sometimes denoted by  $U_2$ . A transformation which carries each  $r$  vector into a  $-r$  vector is called inversion and is indicated by  $I$  ( $I = h \cdot C_2$ , i.e. it represents a second-order mirror turn).

In the international system of notations a  $k$ -order axis is denoted by  $k$ , the mirror-rotation axis -- by  $\bar{k}$ , an axis and a reflection plane perpendicular to it -- by  $k/m$  or  $\frac{k}{m}$  (we will recall that here  $k$  is an index equal to 2, 3, 4 and 6 according to the order of the axis, and  $m$  is a letter), an axis and one or more second-order axes perpendicular to it -- by  $k2$ , an axis and one or several reflection planes parallel to it -- by  $km$ , a mirror-rotation axis and one or several twofold axes perpendicular to it -- by  $\bar{k}2$ , a mirror-rotation axis and one or several reflection planes parallel to it -- by  $\bar{k}m$ , an axis and reflection planes perpendicular and parallel to the axis -- by  $(k/m)m$  or  $\frac{k}{m}m$ .

In Table 14 are given Schoenflies notations and international notations of 32 crystal point groups (crystal classes). In addition to the complete international system of notations which was discussed above, Table 14 also gives an often used abbreviated system which differs from the complete system only by that a portion of elements having a relatively low symmetry is omitted from it but in such a way that the symbol retains the basic signs of a given crystallographic class. For example, an abbreviated notation corresponding to a complete notation

$\frac{4}{m} \frac{2}{m} \frac{2}{m}$  is  $4/mmm$  (second-order axes are omitted).

In describing the total symmetry of a crystal (and not of the group of equivalent directions alone) the crystal lattice is considered to be infinite. In doing so, along with the turns and reflections a crystal lattice also has translation symmetry -- a property of being able to coincide with itself in parallel displacements of the lattice vector, and it also may have special symmetry elements -- screw axes which represent a combination of rotation with a subsequent translation along the rotation axis over a portion of the lattice spacing; it may also have glide planes which represent a combination of a specular-reflection plane with a subsequent translation along the direction lying in this plane.

An arbitrary crystal-lattice vector may be represented in the following form:

$$r = n_1 a + n_2 b + n_3 c$$

where  $n_1$ ,  $n_2$  and  $n_3$  are integers and  $a$ ,  $b$  and  $c$  are the base vectors of the translations.

The point group of a crystal imposes certain restrictions on the base vectors of translations. Altogether 14 types of point lattices are possible, which follow from the application of symmetry operations to a point lattice of a general type.

Table 14

## Notations of 32 Point Groups (Crystals Classes)

1	Сингония	9 Обозначение Шюфлиса	10 Международное обозначение	
			11 полное	12 краткое
1	Триклинная. Решетка Браве P. Симметрия $\bar{1}$ .	$C_1$	1	1
		$C_2 (S_2)$	$\bar{1}$	$\bar{1}$
3	Моноклиная. Решетка Браве P, C. Симметрия 2/m.	$C_2 (C_{2h})$	m	m
		$C_2$	2	2
		$C_{2h}$	$\frac{2}{m}$	2/m
4	Ромбическая. Решетка Браве P, C, I, F. Симметрия mmm.	$C_{2v}$	mm2	mm2
		$D_2 (V)$	222	222
		$D_{2h} (V_h)$	$\frac{2}{m} \frac{2}{m} \frac{2}{m}$	mmm
		$S_4$	$\bar{4}$	$\bar{4}$
5	Тетрагональная. Решетка Браве P, I. Симметрия 4/mmm.	$D_{2d} (V_d)$	$\bar{4}2m$	$\bar{4}2m$
		$C_4$	4	4
		$C_{4h}$	$\frac{4}{m}$	4/m
		$C_{4v}$	4mm	4mm
		$D_4$	422	422
		$D_{4h}$	$\frac{4}{m} \frac{2}{m} \frac{2}{m}$	4/mmm
		$C_2$	2	2
		$S_6$	3	3
6	Ромбоэдрическая (тригональная). Решетка Браве R. Симметрия 3m.	$C_{3v}$	3m	3m
		$D_3$	32	32
		$D_{3d}$	$3 \frac{2}{m}$	3m
		$C_3$	3	3
		$S_6$	3	3
7	Гексагональная. Решетка Браве P. Симметрия 6/mmm.	$C_6$	6	6
		$C_{3h}$	$\frac{6}{m}$	6/m
		$C_{2h}$	2	2
		$C_6$	6	6
		$C_{3v}$	3m	3m
		$C_{2v}$	32	32
		$C_3$	3	3
		$C_6$	6	6
8	Кубическая. Решетка Браве P, I, F. Симметрия m3m.	$T$	23	23
		$T_d$	$\frac{2}{m} \bar{3}$	m3
		$O$	432	$\bar{4}3m$
		$O_h$	$\frac{4}{m} \bar{3} \frac{2}{m}$	m3m
		$T$	23	23
		$T_d$	$\frac{2}{m} \bar{3}$	m3

1) Hexagonal syngony may also contain classes of rhombohedral syngony.

- Key: (1) Syngony  
 (2) Triclinic. Bravais lattice P. Symmetry  $\bar{1}$ .  
 (3) Monoclinic. Bravais lattices P, C. Symmetry 2/m.  
 (4) Rhombic. Bravais lattices P, C, I, F. Symmetry mmm.  
 (5) Tetragonal. Bravais lattices P, I. Symmetry 4/mmm.

[Key continued on next page]

Key to Table 14 (continued):

- (6) Rhombohedral (trigonal). Bravais lattice R. Symmetry  $\bar{3}m$ .
- (7) Hexagonal. 1) [See footnote on preceding page]. Bravais lattice P. Symmetry  $6/mmm$ .
- (8) Cubic. Bravais lattices P, I, F. Symmetry  $m\bar{3}m$ .
- (9) Schoenflies notations.
- (10) International notation.
- (11) Complete.
- (12) Abbreviated.

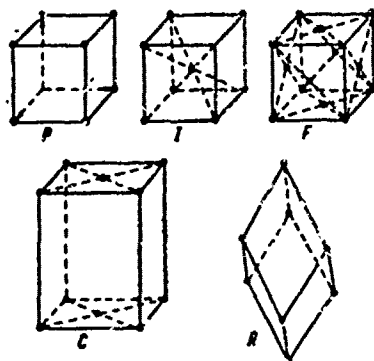


Figure 6.1. Types of Bravais lattice.

Arrowheads indicate the base vectors for primitive lattice P.

These lattices, called Bravais lattices, are classified according to seven syngonies (systems) as shown in Table 15 (several types of Bravais lattices may correspond to one syngony). The types of Bravais lattice are denoted by symbols defining the type of the unit cell (Figure 6.1): P indicates a primitive cell, C -- a centered-base cell, I -- a body-centered cell, F -- a face-centered cell, R -- a primitive cell but only of triclinic syngony.

If a crystal contains only one atom in the unit cell, then its symmetry coincides with the symmetry of syngony to which it belongs. If however, the unit cell contains several atoms, the crystal may have fewer symmetry elements than its syngony, and screw axes and glide planes may be among them.

In the international notations the screw axis is assigned a subscript: for example,  $2_1$  is a second-order screw axis with displacement along the axis following a rotation by half a period, and the glide plane is denoted with the letters a, b, c, n or d according to the type of the glide (see in more detail in the book [1], pp 46, 47).

Altogether 232 space groups exist which describe crystal symmetry. In Schoenflies notations a space group is denoted by a symbol for the crystal class to which a given crystal belongs, with a number corresponding to the given group. International notations are more detailed. They start with a letter describing the type of the lattice (P, C, I, F or R) followed by the notation for the minimal set of symmetry elements, which characterizes the group.

Examples:

A crystal of  $\text{KH}_2\text{PO}_4$  -- a space group in tetragonal phase  $D_{2d}^{12}$ , is in international notations I42d;

barium titanate (above Curie temperature) -- a space group  $O_h$ , is in international notations Pa3m;

a crystal of  $\text{NaNO}_2$  in ferroelectric phase -- a space group  $C_{2v}^{20}$ , is in international notations Im2m.

#### Par. Elements of Representation Theory

We will examine a set  $f$  of linearly independent functions  $\varphi_1, \varphi_2, \varphi_3, \dots, \varphi_f$  having the property that they transform into each other upon the action on them of any group element  $a$ :

$$\varphi_i' = \sum_j a_{ij} \varphi_j \quad (6.5)$$

Here the elements "a" are regarded as operators. Examples of  $\varphi_k$  may be provided, in particular, by the components of some vector, for example, electric-field or polarization vector  $P_x, P_y, P_z$  (in this case  $f=3$ ). Then a third-order matrix  $\alpha$  will correspond to each element of the group  $G$  [see (6.5)].

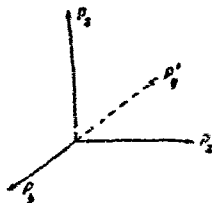


Figure 6.2. Transformation of polarization components  $P_x, P_y, P_z$  with a rotation around a fourth-order axis.

As may be seen from Figure 6.2, with the action, for example, of a rotation by  $\pi/2$  around a fourth-order axis oriented along the z-axis the components  $P_x$ ,  $P_y$  and  $P_z$  are transformed in accordance with the following rules:

$$\begin{aligned} C_4 P_x &= P_y, \\ C_4 P_y &= -P_x \\ C_4 P_z &= P_z \end{aligned}$$

and, consequently, the matrix  $a = (a_{ki})$  has the following form:

$$\begin{pmatrix} 0 & 1 & 0 \\ -1 & 0 & 0 \\ 0 & 0 & 1 \end{pmatrix} \quad (6.6)$$

It is said of a set of matrices  $a_{ki}$  for all elements of a group that they form a representation of the group. The functions  $\varphi_1, \varphi_2, \dots, \varphi_f$  are called the basis of representation and the number  $f$  -- its dimensionality.

If a linear unitary transformation  $S$  is carried out on the functions  $\varphi_1, \varphi_2, \dots, \varphi_f$

$$\varphi'_i = S\varphi_i, \quad (6.7)$$

then the functions  $\varphi'_i$  form the basis of a new representation. The following matrices will have such a representation

$$a' = S^{-1}aS, \quad (6.8)$$

whose traces (the sum of diagonal elements) will be the same as in the former representations.

The traces of representation matrices are called characters of a representation, and representations with the same characters are called equivalent representations.

If an element of a group is mapped by the transformation  $S$ , then  $S^{-1}aS=b$  is also an element of the group. It is said of the totality of all of these elements that they form a class, and it follows from (6.8) that: the characters of all elements of a given class are the same for any representation.

It may turn out that the basis functions can be broken into several sets which with the operation of all elements of the group are transformed only in terms of each other. For example, for the group  $D_{4h}$  the components of polarization vector  $P_x$  and  $P_y$  will be transformed while the component  $P_z$  (oriented along the principal axis) will remain

invariant or will change sign. A representation in accordance with which such a basis is transformed is called reducible. A set of functions which cannot be broken up into such subsets will form the basis of an irreducible representation. An example may be provided by the vector components  $P_x$  and  $P_y$  for the group and  $D_{4h}$  or three vector components  $P_x$ ,  $P_y$  and  $P_z$  for the groups  $O$ ,  $O_h$  or  $T_d$ . And a set of the components  $P_x$ ,  $P_y$  and  $P_z$  for the group  $D_{4h}$  is the basis of a reducible representation.

The number of nonequivalent irreducible representations for a given group is equal to the number of classes in it and the sum of the squares of dimensionalities of irreducible representations is equal to the order of the group.

The matrices of any reducible representation can be reduced by means of linear transformation to a unit form <sup>1)</sup> so that each unit will correspond to an irreducible representation.

Such an operation is called expansion of a reducible representation into irreducible representations. The number of times  $n_\alpha$  which an irreducible representation  $\tau^\alpha$  enters a reducible representation is determined using the following formula:

$$n_\alpha = \frac{1}{N} \sum_a \chi(a) \chi_\alpha^*(a). \quad (6.9)$$

Here  $N$  is the order of the group,  $\chi(a)$  and  $\chi_\alpha(a)$  are the characters of a reducible and irreducible representation respectively, pertaining to the element "a" of the group. Asterisk indicates the sign of a complex conjugate.

The relationships (6.9) are widely used in practice. For example, with their aid it is possible to determine the number of bands in vibration spectra, to determine the splitting and the character of a change in these bands in phase transitions, etc. (see chapter 5).

Standard notations are usually used for irreducible representations of the point groups. One-dimensional representations are denoted with the letters A and B, two-dimensional representations -- with E, three-dimensional representations -- with F (the point groups have no irreducible representations of greater dimensionality). The functions of the bases of the representations A are symmetric, and those of the bases of B -- antisymmetric with respect to the rotations around the principal axis. The subscripts g and u indicate respectively the symmetry and antisymmetry with respect to inversion.  $A_1$  always denotes a unitary (fully symmetric) representation, i.e. such an irreducible representation all characters of which are equal to unity.

1) By a matrix of unit form is meant a matrix in which "units-submatrices" containing nonzero elements are arranged along the main diagonal and all of the remaining elements of the matrix are equal to zero. An example may be provided by the matrix (6.6) in which units  $\begin{pmatrix} 0 & 1 \\ -1 & 0 \end{pmatrix}$  and 1 can be separated.

#### Par. 4. Irreducible Representations of Space Groups

A fundamental property of crystals is translational symmetry. In the language of group theory this means that every space group  $G$  contains an Abelian subgroup of translations  $\mathcal{T}$ . A subgroup of translations has one-dimensional irreducible representations each one of which is connected with a certain value of the wave vector  $q$  so that in an irreducible representation  $\tau_q$  of a translation  $t$  corresponds to  $\exp - iqt$ . Two vectors  $q$  and  $q_1$  are equivalent (i.e. one and the same representation corresponds to them) if they differ by the reciprocal-lattice vector; the base vectors  $b_i$  of the reciprocal lattice are determined from the conditions

$$b_i \cdot a_k = \delta_{ik} \quad (6.10)$$

where  $a_k$  are the base vectors of translations (or, as they are called, "direct"-lattice vectors) (Figure 6.1) and  $\delta_{ik}$  is a Kronecker symbol.

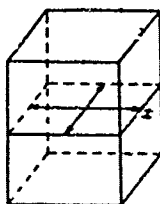


Figure 6.3. The star of wave vectors  $\{q\}$ , connected with the point  $x$  of Brillouin zone of a primitive tetragonal lattice.

The region containing all nonequivalent vectors  $q$  is called Brillouin zone. It can be shown [2] that Brillouin zone always coincides with a unit cell of reciprocal lattice.

Irreducible representations of the space groups are constructed with the aid of small-groups (wave-vector groups) technique. First of all, nonequivalent wave vectors  $q$  are classified according to the "stars"  $\{q\}$  (i.e. according to the aggregates of wave vectors obtained from each other by means of symmetry operations of the point group of the crystal  $G_0$ ). Then irreducible representations of the wave-vector group  $G_q$  are determined (a subgroup of elements of the group  $G$  leaving the wave vector invariant is called wave-vector group  $G_q$  or small group). Each irreducible representation of the group  $G$  is completely determined by the star of wave vectors  $\{q\}$  and by one of the irreducible representations of the group  $G_q$ .

Irreducible representations for the groups  $G_q$  for all space groups are classified in the monograph [12] in the form of so-called loaded representations. Any element of a space group may be represented in the following form:

$$g = tS = tR \quad (6.11)$$

Here  $t$  is translation to which  $\exp - iqt$  corresponds in the irreducible representation of the space group;  $t_\alpha$  is a non-unit translation (i.e. translation over a portion of the lattice spacing);  $r$  is rotation or mirror rotation (i.e. an element of the point group).

The characters of the loaded representations  $\hat{\chi}$  correspond to the elements  $r$  of the point group of a crystal; the characters of the elements are obtained from them using the following rule:

$$\chi(S) = \chi(r) \exp(-iqt). \quad (6.12)$$

As an example we will examine irreducible representations of the space group  $D_{4h}$  for the star  $\{q\}$  connected with the point  $x$  of Brillouin zone (Figure 6.3).

The group elements of the point group  $D_{4h}$  which enter the group  $G_q$ , the characters of loaded representations for the point  $x$  and the values of  $\exp(-iqt_\alpha)$  are given in Table 15. (A line in the column for  $e^{-iqt_\alpha}$  indicates that non-unit translation in the space group does not correspond to the symmetry element in question)

Table 15

Characters of Loaded Representations  
for Point  $x$  of Brillouin Zone

	$\kappa$	$u_0$	$u'_2$	$c_4$	$i$	$\sigma'_2$	$\sigma_2$	$\sigma_4$
$\chi_1$	1	0	0	0	0	0	0	2
$\chi_2$	2	0	0	0	0	0	0	-2
$e^{-iqt_\alpha}$	-	-	-	-	-	-	-	i

It may be seen from the table that in the case under consideration the characters of irreducible representations simply coincide with the characters of the corresponding loaded irreducible representations.

### Par. 5. Miller Indices

Miller indices are usually used to describe the coordinates of the atoms, the lattice vectors and atomic planes in a crystal. These indices are determined in the following manner.

1. Miller indices indicate the coordinates of atoms in units of lattice constants with the origin of coordinates being selected in one of the vertices of a unit cell. For example, Miller indices for a center atom in a body-centered lattice will be  $\frac{1}{2}\frac{1}{2}\frac{1}{2}$ , and the indices of the face centers in a face-centered lattice will be  $\frac{1}{2}\frac{1}{2}0$ ,  $0\frac{1}{2}\frac{1}{2}$  and  $\frac{1}{2}0\frac{1}{2}$ .

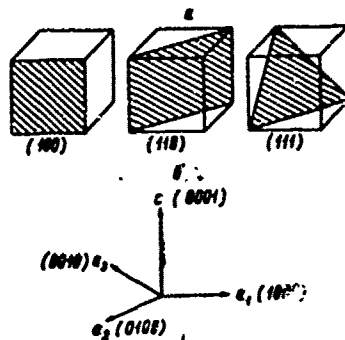


Figure 6.4 Miller Indices

a -- for principal planes of a cubic crystal; b -- for base vectors of a hexagonal crystal.

2. To denote the directions in a crystal, Miller indices represent a set of the smallest integers related to each other as components of a vector parallel to a specified direction. For example, in a cubic crystal, Miller indices for the edges of a cell will be (100), (010) and (001).

3. In order to find Miller indices for atomic planes it is necessary to do the following: write the number of the lattice constants from the origin of coordinates to the points of intersection of a given atomic plane with the axes of coordinates, then take the numbers reciprocal to them and reduce them to the smallest common multiple.

Miller indices for principal planes of a cubic crystal are shown in Figure 6.4a.

The so-called hexagonal Miller indices determined in the same manner as the usual ones are ordinarily used for crystals of hexagonal and trigonal syngony.

Miller indices of the base vectors of a hexagonal crystal are shown in Figure 6.4b as an example.

#### Par. Projection Operators

An arbitrary function  $F$  may be expanded into a series with respect to the orthogonal set of its components ("projections") each one of which is transformed in accordance with a certain row of some irreducible representation of a given group [14]:

$$\gamma = \sum_{j=1}^J \sum_{i=1}^{l_j} f_{ji} \quad (6.13)$$

Here  $J$  is the number of irreducible representations of the group,  $l_j$  is dimensionality of the irreducible representation  $\tau_j$ , and  $f_{ji}$  is a function transformed in accordance with the  $i$ -th row of the irreducible representation  $\tau_j$ .

We will note that any expansion with respect to the complete set of orthonormalized functions is a particular case of the expansion (6.13). For example, expansion into Fourier series

$$F = \sum_{\mathbf{q}} f_{\mathbf{q}} e^{i\mathbf{q}\cdot\mathbf{r}} \quad (6.14)$$

may be regarded as an expansion with respect to the base functions of irreducible representations of a group of translations.

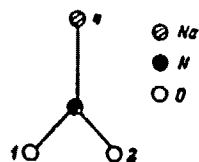


Figure 6.5. The base of a unit cell of the ferroelectric  $\text{NaNO}_2$ .

The use of symmetrized functions  $f_{ji}$  as applied to the vibration spectra -- they are called symmetry coordinates -- makes considerably easier the solution of problems connected with the determination of eigenvalues and eigenfunctions, in particular the calculations of vibration spectra of crystals.

The use of projection operators is a systematic method of determining the symmetry coordinates. It can be proven (see for example [2]) that the operator

$$P_{ji} = \sum_{\mathbf{a}} \tau_{ij}(\mathbf{a}) T(\mathbf{a}), \quad (6.15)$$

where  $\tau_{ik}^j$  is a matrix element  $\tau_j(\mathbf{a})$ ,  $T(\mathbf{a})$  -- an operator corresponding to the symmetry element " $\mathbf{a}$ ", is a projection operator, which means that the function

$$f_{ji} = P_{ji} f \quad (6.16)$$

is transformed in accordance with the  $i$ -th row of irreducible representation of the group  $G$ .

We will explain the application of projection operators by using an example. We will examine the base of a unit cell of the ferroelectric  $\text{NaNO}_2$  (Figure 6.5). It may be seen from (6.15) that projection operator for a unit representation  $A_1$  is reduced simply to a successive application of all elements of a group in any order. To obtain the symmetry coordinates for limit optical vibrations ( $q=0$ ) it is necessary to use only the elements of the point group of a crystal.

Point group of  $\text{NaNO}_2$  is  $C_{2v}$  ( $mm2$ ). As an example we will examine the action of the projection operator on the displacement of atom 1 in the direction of the axis  $x$  ( $x_1$ ). We will use Schoenflies notations for the elements of the group  $C_{2v}$ :  $E$  is a unit element,  $C_2$  -- a second-order axis, and  $\sigma_v$  and  $\sigma'_v$  -- reflection planes containing the axis  $C_2$ . Then we have:

$$\left. \begin{aligned} P_{A_1} &= (E + C_2 + \sigma_v + \sigma'_v) x_1 = \\ &= (E + C_2 + \sigma_v) x_1 + x_1 = \\ &= (E + C_2) x_1 - x_2 + x_1 = \\ &= 2x_1 - 2x_2 + x_1 = 2(x_1 - x_2). \end{aligned} \right\} \quad (6.17)$$

Projection operators determine a symmetry coordinate with accuracy to the normalizing constant. The other symmetry coordinates are found in the same manner.

#### Bibliographical References

An exposition of group theory and a survey of its application in physics may be found in the monographs [2-6]. The books are listed in the order of increasing complexity. (Examination of problems dealing with solid state physics is not correct throughout in the monograph [4]). A review of the earlier books on the application of group theory in physics may be found in the monograph [2].

Mathematical group theory is set forth simply but rigorously in a classical book by Schmidt [7]. A detailed bibliography and a brief exposition of the fundamentals of abstract group theory may be found in the book of problems [8].

The monographs [9, 10] have very clearly written chapters devoted to symmetry theory. A description of the point groups and the characters of their irreducible representations are given in [9], symmetry elements of space groups are examined in [10].

A detailed description of crystal symmetry is given in the monograph [1] and all international notations of symmetry elements are shown.

A detailed description of all space groups may be found in the handbook [11] and in the monograph [12].

Irreducible representations of all of the 230 space groups have been obtained in the monograph [12] using the method set forth in [5] (in this scheme the monograph [12] is unique).

The work [14] sets forth very simply the projection-operators technique for irreducible representations of the point groups. This technique makes it possible to obtain from a given set of functions the linear combinations which are transformed in accordance with a specified irreducible representation of a point group (i.e. combinations which form the basis of representation).

Theory of projection operators for irreducible representations of space groups is set forth in the work [15]. This work also gives projection operators for the space groups of a monoclinic and rhombic symmetry.

Finally, a review of some of the applications of group theory to some of the problems on theory of ferroelectricity may be found in the lectures [16] and in the chapters 3 and 5 of this book.

#### BIBLIOGRAPHY

1. Ch. Kittel'. Vvedeniye v Fiziku Tverdogo Tela [Introduction to Solid State Physics]. Fizmatgiz [State Publishing House for Mathematical and Physical Literature]. Moscow (1963).
2. W. Heine. Teoriya Grupp v Kvantovoy Mekhanike [Group Theory in Quantum Mechanics]. IL [Foreign Literature Press], Moscow (1963).
3. M. I. Petroshe'n' and Ye. N. Trifonov. Primeneniye Teorii Grupp v Kvantovoy Mekhanike [Application of Group Theory in Quantum Mechanics]. Fizmatgiz, Moscow (1967).
4. S. Bagavantam and T. Venkatarayudu [transliterated from Russian]. Teoriya Grupp i Yeyo Primeneniye k Fizicheskim Probleмам [Group Theory and Its Application to Physical Problems]. IL, Moscow (1959).
5. G. Ye. Lyubarskiy. Teoriya Grupp i Yeyo Primeneniye v Fizike [Group Theory and Its Application in Physics]. Fizmatgiz, Moscow (1958).
6. M. Khamermesh. Teoriya Grupp i Yeyo Primeneniye k Fizicheskim Probleмам [Group Theory and Its Application to Physical Problems]. Mir Publishing House, Moscow (1966).
7. O. Yu. Schmidt. Abstraktnaya Teoriya Grupp [Abstract Group Theory]. GITI, Moscow (1933).
8. Ye. S. Lyapin, A. Ya. Ayzenshtadt, M. M. Lesokhin. Uprazhneniya po Teorii Grupp [Exercises in Group Theory]. Nauka Publishing House, Moscow (1967).

9. L. D. Landau and Ye. M. Lifshits. Kvantovaya Mekhanika [Quantum Mechanics]. Fizmatgiz, Moscow (1963).
10. L. D. Landau and Ye. M. Lifshits. Statisticheskaya Fizika [Statistical Physics], Nauka Publishing House, Moscow (1964).
11. International Tables for X-Ray Crystallography, Vol 1. Kynoch Press, Birmingham (1952).
12. O. V. Kovalev. Neprivodimyye Predstavleniya Prostranstvennykh Grupp [Irreducible Representations of Space Groups]. Ukrainian SSR Academy of Sciences Press, Kiev (1961).
13. R. W. Wyckoff. Crystal Structures. N.Y. (1948).
14. M. A. Melvin, Rev. Mod. Phys., Vol 28, p 18 (1956).
15. M. S. Shur. Kristallografiya [Crystallography], Vol 12, p 981 (1967).
16. R. Blinc. Ferroelectricity (in lectures on condensed matter, Trieste). Vienna (1966).

## CHAPTER 7. DOMAIN STRUCTURE OF FERROELECTRICS

### Par. 1. Causes of the Formation of Domains and General Regularities of Domain Structures

Initiation of spontaneous polarization in a crystal takes place along a certain crystallographic direction of paraelectric phase. This direction is usually called ferroelectric axis or axis of spontaneous polarization. In the case of uniaxial ferroelectrics the axis of spontaneous polarization coincides with the single direction and, therefore, is the only axis. In multiaxial ferroelectrics there are several axes of spontaneous polarization and in the paraelectric phase these axes are crystallographically equivalent. Usually the number of possible directions of  $P_s$  is equal to the twofold number of ferroelectric axes. But if spontaneous polarization occurs along polar direction of the paraelectric phase, then there are as many possible directions of  $P_s$  as there are ferroelectric axes [105, 106].

In an ideal crystal, in the absence of external influences the occurrence of spontaneous polarization is equally probable along any one of the possible directions. In transition to ferroelectric state a crystal breaks up into separate regions called domains which are characterized by the direction of spontaneous polarization. It is natural that this process is brought about by a decrease of free energy in the crystal, i.e. free energy of a multidomain state proves to be lower. An examination of this problem can be carried out similarly to the way this is done in the case of ferroelectrics [1, 2]. We will take a crystal of a ferroelectric in the form of a plate with a thickness  $d$  cut out perpendicularly to the axis of spontaneous polarization. For a single-domain crystal, electrostatic energy  $W_{o.d.}$  [o.d.=single-domain] per unit of surface area is expressed as:

$$[o.d.=single-domain] \quad W_{e.l.} = \frac{2\pi P_s^2 d}{4} \quad (7.1)$$

If the crystal breaks up into tabular antiparallel domains as shown in Figure 7.1, then in order to find electrostatic energy it is necessary to solve Laplace equation inside and outside the plate with

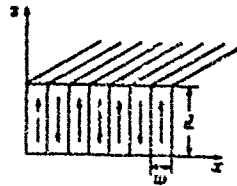


Figure 7.1. Schematic representation of a crystal of a ferroelectric, broken up into antiparallel domains.

appropriate boundary conditions. In this case, energy per unit of area has the following form [3]:

$$W_{\text{m.d.}} = \frac{3.4}{1 + \sqrt{\epsilon_0 \epsilon_r}} w P_s^2 \quad (7.2)$$

[m.d. = m.d. = multidomain]

with the condition that  $w \ll d$  where  $w$  is the width of the domain. Thus, the thinner the domain, the lower the energy of the crystal. However, the process of fragmenting does not take place limitlessly. The fact is that the boundary layers between domains, which are called domain walls or domain boundaries, have a certain energy. Therefore, on one hand a decrease in the dimensions of a domain leads to a decrease of electrostatic energy, but on the other hand the aggregate area of domain boundaries increases and, consequently, their energy also increases. An equilibrium domain structure is determined by the condition of minimum of total energy -- electrostatic energy plus the energy of domain walls, i.e.

$$W = \frac{3.4 w P_s^2}{1 + \sqrt{\epsilon_0 \epsilon_r}} + \frac{\sigma_w d}{w} \quad (7.3)$$

where  $\sigma_w$  is energy per area unit of the domain wall. In such an examination only electrostatic energy of a crystal in the proper depolarizing field and the energy of domain walls are taken into account. In addition to these types of energy, in ferroelectrics a change in elastic energy is also considerable in most cases. Appearance of spontaneous polarization is accompanied by electrostrictive or piezoelectric deformation. Therefore, if there are internal mechanical stresses in a certain region of a crystal, which always exist in an actual crystal, they can be attenuated when the crystal breaks up into domains.

Defects of various kinds must also have a big effect on the formation of domains. When transition to a ferroelectric state is a transition of the first kind, there is a nucleus-formation stage. The defects affect both the position of nuclei in a crystal and the direction of spontaneous polarization in them. Noncoincidence of directions of polarization in separate nuclei must also lead to the formation of domains.

Unlike ferromagnetics, electrostatic depolarizing field of ferroelectrics can be compensated by charges flowing to the surface of the crystal owing to electric conductivity of the crystal itself or of the medium in which it is located. Experiments indicate that even if a crystal of a ferroelectric is in a conductive medium, the domains nevertheless become formed. Thus, apparently in actual crystals, internal mechanical stresses and defects play a very important role in the formation of domain structure. One of the main reasons for this consists in that spontaneous piezoelectric and electrostrictive distortions are very big, they are two or three orders bigger than the magnetostrictive distortions. Therefore, direction in which spontaneous polarization occurs in some specific region of the crystal is determined to a considerable degree by the strain distortions of the crystal lattice in this region.

We will now examine the geometric conditions which must be observed in the formation of domain structure. Neighboring domains have a different direction of spontaneous polarization and, therefore, in the general case not all of the crystallographic axes of neighboring domains coincide. From this point of view, domains are equivalent to twin crystals which appear with reversible polymorphic transformations when the crystal symmetry is impaired. An exception are apparently only domains with an antiparallel orientation of spontaneous polarization in ferroelectrics that are centrosymmetric in paraelectric phase. It is known that twinning takes place in such a manner that elements of the crystal symmetry lost during a phase transition become twinning elements. It could be expected that this rule is observed also in the formation of ferroelectric domains. Then domain walls should coincide only with certain crystallographic planes.

Indeed, Chernyshova [4] noted that the crystals of Seignette's salt break up into domains in such a manner that two second-order axes lost in transition to polar state become twin axes.

Later, Zheludev and Shuvalov [5, 6] showed that the twinning rule is valid for the other ferroelectrics also. Thus, from a crystallographic standpoint, by breaking up into domains a crystal becomes a polysynthetic twin crystal, the domains become the components of this twin crystal, and domain boundaries coincide with the twinning planes. The symmetry elements of nonferroelectric phase lost in phase transition become possible twinning elements. In doing so, as noted in [5, 6] a polydomain crystal regarded as one whole returns to the symmetry of the original nonferroelectric phase. We will note that in actual crystals this rule usually is not satisfied and a slight unipolarity is observed, i.e. domains with one of the possible orientations of spontaneous polarization predominate.

In spite of the seemingly complete analogy between a usual twin crystal and a domain it should not be forgotten that domains possess polarity. Therefore, bound electric charges should be absent at the boundary between them. Otherwise the energy of a domain boundary would increase by the magnitude of energy of electric field set up by these

charges (we consider the crystal to be a sufficiently good dielectric so that the compensation of bound charges by the free charges flowing to the wall owing to the electric conductivity of the crystal does not have to be examined). Thus, the following condition must be satisfied on the wall:

$$\operatorname{div} \mathbf{D} = 0. \quad (7.4)$$

Since  $E=0$ , (7.4) is reduced to

$$\operatorname{div} \mathbf{P} = 0. \quad (7.5)$$

Consequently, the polarization component normal to the boundary must be continuous.

New types of domain structure connected with the possibility of shielding spontaneous polarization by free charges may exist in ferroelectrics-semiconductors. Such a possibility has been examined by Shur [7-10] for a one-dimensional case. The main conclusion of these works is reduced to a prediction of instability in ferroelectrics-semiconductors in the case of fields smaller than a coercive field, i.e. to a propagation of electric-induction waves along the specimen. This instability may be accompanied by fluctuations of current in the external circuit.

## Par. 2. Domain structure of Barium Titanate

Barium titanate is cubic above Curie point. With a transition to ferroelectric phase it becomes tetragonal. In doing so, as already mentioned, the polar axis coincides with the tetragonal  $c$ -axis. Any one of the three mutually perpendicular fourth-order axes of the cubic phase may become a  $c$ -axis and, consequently, spontaneous polarization has six possible directions. Thus, the angle between polarization vectors of the domains may be equal either to  $90^\circ$  or  $180^\circ$ . Domains with a mutually perpendicular direction of spontaneous polarization are called  $90^\circ$ -domains and the boundaries between them --  $90^\circ$ -boundaries or walls. Correspondingly, there may also be  $180^\circ$ -domains and  $180^\circ$ -boundaries (walls) separating them. Domain walls must coincide with the twinning planes which may be planes of the type  $\{110\}$  of the cubic phase and, in addition to this, the condition of continuity of the normal component of spontaneous polarization must be satisfied on them. For  $90^\circ$ -walls these conditions are satisfied by tetragonal planes of the type  $\{011\}$  and  $\{101\}$ . It is obvious that in the case of  $180^\circ$ -walls the normal polarization component must be equal to zero and since spontaneous tetragonal deformation does not depend on the direction of polarization vector, a  $180^\circ$ -wall may be any cylindrical surface with a generatrix of a parallel polar  $c$ -axis.

The basic regularities of domain structure of barium titanate were determined by Kay and Vousden [11], Forsberg [12] and Herz [13, 14] during a study of single crystals in polarized light. In order to understand the possibilities of this method better, we will examine the plates of barium titanate having only  $90^\circ$ -domains (Figure 7.2).

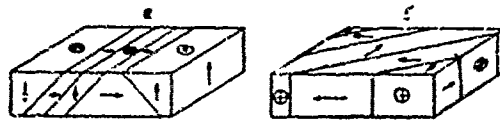


Figure 7.2. Schematic representation of a plate of a single crystal of barium titanate in tetragonal phase with the plate being broken up into  $90^\circ$ -domains. The faces of the plate coincide with pseudocubic planes of the type  $\{001\}$ .

Arrowheads indicate the direction of spontaneous polarization. Circles with a cross indicate the outlet of the negative end of the dipole, a circle with a dot -- that of the positive end of the dipole.

In the cubic nonferroelectric phase the optical indicatrix represents a sphere. Therefore, if a plate is observed in polarized light by placing it on the microscope stage between crossed Nicol prisms it will remain dark in any position of the stage. In tetragonal phase the indicatrix is an ellipsoid of revolution. The axis of rotation is an optical axis and coincides with the crystallographic  $c$ -axis and, consequently, with the polar axis of the crystal also. We will now observe a plate shown in Figure 7.2a in a direction perpendicular to its plane. Through the domains the polar axis of which is oriented normally to the plane of the plate the light passes along the optical axis and, consequently, does not undergo double refraction. Therefore, these domains remain dark during the rotation of the microscope stage. It is usual to call such domains  $c$ -domains.

Domains of the second type in which the polar axis lies in the plane of the plate and through which the light passes along  $a$ -axis are called  $a$ -domains. While passing through  $a$ -domains the light undergoes double refraction. Therefore, in crossed Nicol prisms they will be dark only in those cases when the axes of the indicatrix are parallel to the polarization plane of the analyzer or polarizer. Since in this case the polarization planes of the polarizer and analyzer are perpendicular to the lateral faces of the crystal, the position of extinction is direct. Thus, the  $c$ - and  $a$ -domains are easily differentiated -- during the rotation of the microscope stage  $c$ -domains remain dark whereas  $a$ -domains periodically become translucent and then become dim. In tetragonal phase in barium titanate  $n_a > n_c$ , i.e. the crystal is negative and the position of polar axis in  $a$ -domains can be determined with the aid of compensator. When the compensator is inserted the neighboring  $a$ -domains have dissimilar coloration which they interchange with a turn of the crys-

tal by  $90^\circ$ . In tetragonal region  $c/a > 1$  and therefore the angle between c-axes in  $90^\circ$ -domains is equal not to  $90^\circ$  but to  $89^\circ 24'$ . Consequently, strictly speaking the position of extinction in the neighboring a-domains differs by  $36'$ . The  $180^\circ$ -domains are optically indistinguishable. However, Merz [13, 14] found that if electric field is applied perpendicularly to the direction of spontaneous polarization, then in polarized light the domain appears to consist of light and dark bands parallel to the polar axis. These bands were regarded by Merz as antiparallel domains. It was supposed that under the effect of electric field, spontaneous-polarization vectors in the neighboring domains turn slightly in opposite directions with the indicatrices becoming somewhat distorted in this process. This leads to a result that the positions of extinction of the neighboring domains do not coincide. Later Miller and Savage [15] discovered that the  $180^\circ$  c-domains can be seen in polarized light when the field is applied along the polar axis. Kabayashi et al. [16] made optical and x-ray studies of this effect. They found that  $180^\circ$ -domains are distinguishable in the presence of an electric field in the case when the beam of light passes through the crystal at a certain angle to the normal (Figure 7.3a and b). After shutting off the field the contrast of the pattern gradually becomes weaker and as a result the domains become nearly indistinguishable (Figure 7.3b).

The authors of the work [16] consider that a narrow region (with width of the order of  $10^{-4}$  cm) forms with a slight distortion near the  $180^\circ$ -wall during its motion. In this region, z-axis is inclined approximately by  $1^\circ$  with respect to the polar axis inside the crystal (Figure 7.3c). As may be seen from Figure 7.3c, the regions at the opposite walls are a secular reflection of each other. The optical axes of these regions are also inclined in different directions with respect to the polar axis inside the domain. If polarization planes of the polarizer and analyzer are parallel to the planes (100) and (010), which corresponds to the highest translucence of the regions at the wall, but the light passes through the crystal slightly obliquely at such an angle that its direction coincides with the optical axis of one of the regions, then this region will seem dark whereas the opposite region will appear light. If the beam of light is inclined in the opposite direction, then the dark region becomes light and the light region -- dark.

It was also shown [17] that light and dark regions appear at the  $180^\circ$ -walls upon the application of electric field to an a-domain crystal. Their appearance was also explained by the presence of a monoclinic distortion in the region adjacent to the wall. Since the direction of the axes of the indicatrix in the regions at the walls on two sides of the domain differs approximately by  $1^\circ$ , the position of their extinction is dissimilar. When one region is light, the other one is dark, and vice versa.

Considerable successes in the study of domain structure of the crystals of barium titanate, having both the  $90^\circ$ - and  $180^\circ$ -domains were obtained with the aid of etching method suggested by Hooton and Merz [18]. It was found that those sections of the crystal surface where the positive end of the polar axis comes out are etched twice as fast

in comparison with the sections on which the negative end comes out. The rates of etching of the "lateral" surface and of the positive end of the polar axis have a ratio of 3:4 [19, 20].

Figure 7.4 shows schematically the surface of a crystal of barium titanate before and after the etching. Using this method it was possible to observe antiparallel c-domains and also to detect the "reflection" of c-domains through a-domains.

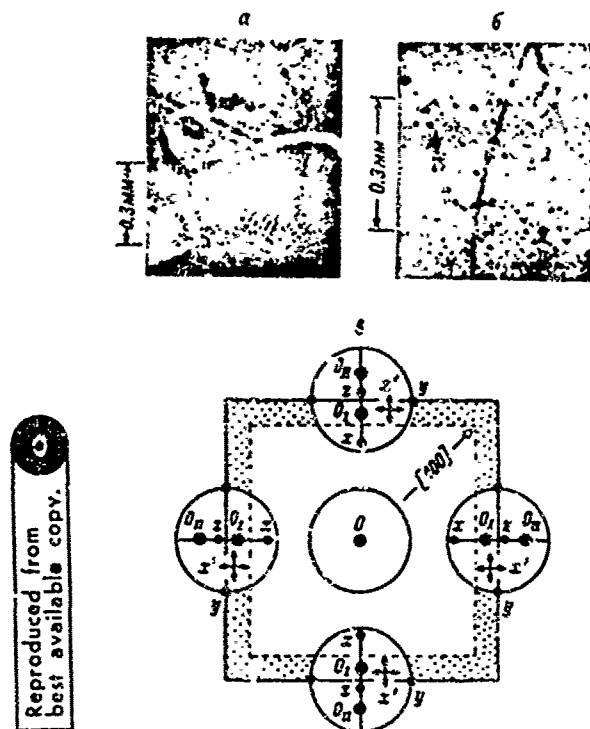


Figure 7.3. Antiparallel domains of barium titanate in polarized light. (After Kabayashi, et al. [16]).

a -- with oblique illumination; b -- with normal illumination; c -- schematic representation of antiparallel domain and stereographic projections showing the orientation of optical axes within the domain and in boundary regions. O -- optical axis of the tetragonal region,  $O_I$  and  $O_{II}$  -- optical axes of low-symmetry regions,  $x'$  -- directions of fluctuations of electric vector in a light wave.

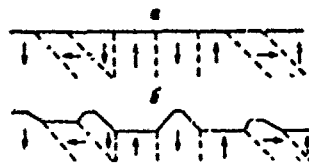


Figure 7.4. Schematic representation of a section of a single crystal of barium titanate. (After Campbell et al. [20]).

a -- before etching; b -- after etching.

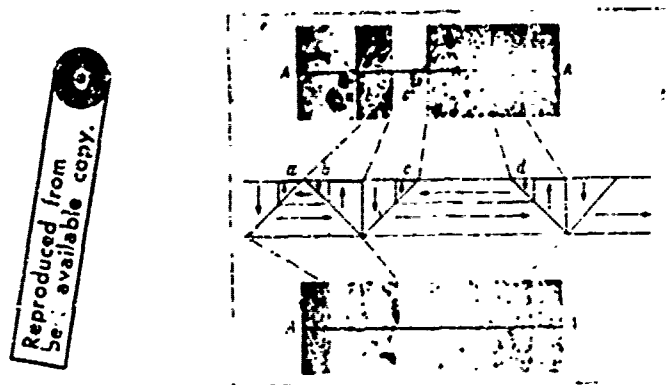


Figure 7.5. Photograph of the upper and lower surface of an etched single crystal of barium titanate and diagram of the domain structure. (After Hooton and Merz [18]).

In Figure 7.5 are shown photographs of two sides of an etched crystal and a diagram of its domain structure constructed on the basis of these photographs. As may be seen from the diagram, c-domains, "a" and b and a so c and d are a mirror image of each other through a-domains. At the  $90^\circ$  boundaries the normal polarization component is continuous. It is usual to say that a "head to tail" arrangement exists. It should be noted that this rule is not always satisfied and "head to head" and "tail to tail" configurations are observed [21, 22]. In this case, the bound charge on the wall is apparently compensated by free charges flowing in owing to electric conductivity of the crystal.

Fousek and Safranová [23] investigated the effect of cooling rate of the crystals when passing through Curie point and also the effect of electric conductivity of the medium on the character of domain structure. The regions of the crystals which had only c-domains were examined in order to exclude the effect of a-domains on the formation of c-domain structure. A sufficiently large size of the regions was selected ( $\sim 250$  microns with a thickness of the crystals of 20-140 microns). With a slow cooling ( $0.1^\circ$  a minute) the aggregate volumes of antiparallel c-domains in a nonconductive medium are equal with accuracy to a few percent. The domains have the form of plates with a thickness of 1-4 microns, perpendicular to one of the a-axes. Apparently such a structure is close to an equilibrium structure. Cooling at any rate in a medium with high conductivity (glycerine with a  $\sigma=10^{-3}$  ohm $^{-1}$ cm $^{-1}$  was used) and also rapid cooling in a nonconductive medium leads to a formation of an irregular domain structure. The emergence of domains on the surface of the crystal has the appearance of chaotically scattered islands with a considerable unipolarity being observed in this process.

Analysis of the results obtained led the authors to a conclusion that at first, with a slight cooling below Curie temperature a nonequilibrium domain structure is formed in either case, with this structure being determined chiefly by the arrangement of the nuclei. Such a structure changes fairly rapidly into an equilibrium structure. However, a nonequilibrium structure may remain either with rapid cooling or, if the crystal is in a conductive medium, owing to the compensation of depolarizing field.

The cause of the formation of  $90^\circ$  domains is rather not a depolarizing field since its energy may be considerably decreased by the appearance of  $180^\circ$  domains, but mechanical stresses. They may appear during the cooling of the crystal in the melt of the solvent or they are connected with different kinds of defects. Fousek and Brezina [24] examined the connection between the size of the crystal, the extent of the defect and its position in the crystal on one hand, and the shape of  $90^\circ$  domain on the other. They selected the simplest model of the defect -- a sphere inside which the condition of a minimum of elastic energy requires a turning of spontaneous polarization by  $90^\circ$  with respect to the encirclement.

Investigation of domain structure of barium titanate in tetragonal phase was conducted not only in polarized light and by etching, other methods were also used. Some of them yielded valuable information on the details of domain configurations.

The method of charged powders [25] was successfully used to study antiparallel c-domains. This method consists in the following: a few drops of hexane which contained fine powder of yellow sulfur and red lead oxide were applied on the surface of the crystal. It was found that sulfur settles better on the positive ends of the dipoles and lead oxide -- on the negative. A sufficiently clear pattern of the domain structure results.

A study of microrelief of the etched surface of single crystals of barium titanate was also conducted with the aid of an electron microscope. Replicas were taken from this surface which were then studied in an electron microscope [20, 26]. The type of the domain, and in the case of c-domains -- the direction of spontaneous polarization, can be determined by the depth of the etching and roughness of the surface.

In Figure 7.6 is given an example of the picture of etched surface on which an antiparallel c-domain was revealed. Visualization of domain structure on the surface of a crystal of barium titanate is possible not only by means of etching but also by the relief of natural face. The fact is that owing to the tetragonality the surfaces of the neighboring a- and c-domains form with each other a small angle  $\arctg \frac{c-a}{a}$  (Figure 7.7). Therefore, the faces of the crystal "wrinkle" and their relief reflects the domain structure.

Study of the natural surface has an advantage over etching since it makes it possible to study the changes in domain structure. Distortions on the faces may be revealed experimentally using the methods of optical interferometry [22, 27] and by studying in an electron microscope the replicas taken from the surface of the crystals [28, 29]. The microrelief can also be revealed by a change in the current of secondary electrons when scanning a finely focused electron beam on the surface of the crystal [30]. Intensity of secondary-electron stream at each point of the surface depends on the angle of incidence of a beam of primary electrons. Therefore, if the intensity of the beam of a cathode-ray tube is modulated by the current of secondary electrons, then an image of the surface can be obtained on the screen.

Another method of visualizing the domains, also making use of the scanning of a finely focused electron beam, was suggested in [31]. The incident electrons bring about a local heating of the crystal and if thin electrodes are applied on the surface, then pyrocurrent can be detected. When gliding on the surface of the crystal the beam shifts from one domain to another, the pyrocurrent changes giving information on the domain pattern.

The use of the electron-mirror method is possible to observe the domains [32-34]. The images of domain structure obtained during the passage of electron beam through a thin crystal are given in a number of works [35-38]. In this case, domain structure becomes "visible" owing to different conditions of electron diffraction both in the domains with a different orientation of the polar axis and in the wall in comparison with the volume of the domains. The data of electron microscopy on the dimensions of the domains and on the thicknesses of the walls are of interest. Thus, domains with a width of 3 to 5  $\cdot 10^{-6}$  cm were observed in [28]. According to the data in [37], 180° domains have a width of 7 to 30  $\cdot 10^{-6}$  cm and 90° domains -- a width of 5 to 300  $\cdot 10^{-6}$  cm. The



Figure 7.6. Electron-microscope photograph of c-domain in barium titanate (magnified 7,000 times) (After Cameron [26]).

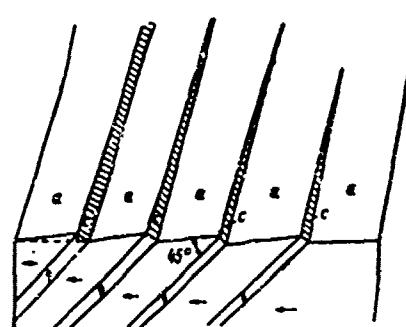


Figure 7.7. Section of a tetragonal crystal of barium titanate, illustrating the distortion of surface on the  $90^\circ$  boundaries between the a- and c-domains (distortions are exaggerated). (After Bhide [22]).

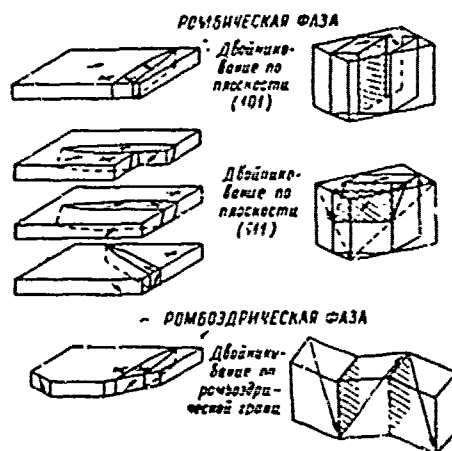


Figure 7.8. Geometry of domains in the rhombic and rhombohedral phases of barium titanate. (After Forsbergh [12]).

- Key:
- |  |  |
|--|--|
| (1) Rhombic phase                            | (4) Rhombohedral phase                             |
| (2) Twinning with respect to the plane (101) | (5) Twinning with respect to the rhombohedral face |
| (3) Twinning with respect to the plane (111) |  |

thickness of the  $90^\circ$  wall between a-domains is less than  $100 \text{ \AA}$  [36, 37]. Studies using the electron-mirror method indicate that on the surface of the crystal there is a layer of about 0.7 microns in thickness with a polarization vector oriented normally to the surface of the crystal, i.e. a layer consisting of c-domains [33].

The works [39-41] show the feasibility of studying the domain structure of barium titanate using the methods of x-ray diffraction topography.

In the rhombic and rhombohedral phases the domain structure of barium titanate was not investigated in such a detail as in the tetragonal phase. Optical studies were conducted here by Kay and Vousden [11] and by Forsbergh [12]. Cameron [26] observed etching patterns in rhombic phase. Figure 7.8 gives the possible domain configurations and indicates the directions of extinction in separate domains.

In the rhombic phase there are  $90^\circ$  and  $60^\circ$  walls. The  $90^\circ$  walls coincide with the pseudocubic planes  $\{001\}$ , i.e. with the rhombic planes  $\{110\}$ , the  $60^\circ$  walls are parallel to the pseudocubic planes  $\{011\}$ , i.e. to the rhombic planes  $\{111\}$ .

In the rhombohedral phase the domain walls are the pseudocubic planes  $\{100\}$ . Naturally, there may also be antiparallel domains in both phases. In the rhombic phase, upon the application of electric field along the polar direction and during an observation in polarized light along this same direction the antiparallel domains become visible, as in the tetragonal phase [42]. The shape of the domains is rectangular with the walls (100) and (110) (the indices are pseudocubic). Walls of the type (110) are visible considerably better.

#### Par. Domain Structure of Triglycine Sulfate

Above Curie temperature, triglycine sulfate belongs to the centrosymmetric point group  $2/m$  of the monoclinic system. Upon transition to polar state the mirror plane disappears and the crystal belongs to the point group 2 of the monoclinic system. Ferroelectric axis is the monoclinic b-axis. Therefore, triglycine sulfate is a uniaxial ferroelectric and only  $180^\circ$  domains can be in it. Since in nonferroelectric phase the crystal does not have piezoelectric effect, spontaneous deformation which accompanies the appearance of spontaneous polarization bears electrostrictive character and does not depend on the direction of polarization. Therefore, antiparallel domains are optically indistinguishable but they rotate the polarization plane in opposite directions, i.e. one domain is a right-hand domain and the other -- a left-hand domain [43, 44].

The use of etching proved to be most successful for visualizing the domain structure. Extensive work on the selection of etching agents and on the study of domain structure using the etching method was carried out by Konstantinova and Sil'vestrova [45-48], by Toyoda [44, 49, 50], by Chynoweth and Feldman [51, 52] and by Meleshina [53]. The powder

method was used in a number of works to reveal the domain structure [44, 49, 50]. When etching the surface of a plate of triglycine sulfate, cut out perpendicularly to the polar axis the positive ends of the domains are etched more strongly than the negative ends, and contain more etching patterns. The domains have an oval form, most often a lenticular form. Large domains pass through the entire thickness of the crystal. The transverse dimensions of separate domains are very diverse. They vary from a few tenths of a millimeter to several millimeters. Chynoweth and Feldman [52] found that domain walls do not always pass through the crystal exactly parallel to the polar axis. There are also needle-shaped domains which do not pass through the entire thickness of the crystal, and even domains which are entirely inside the crystal. It was possible to find such domains on the face parallel to the polar axis using the etching and the powder method [51, 52, 57].

In etching the surface of a crystal the sites of the emergence of dislocations are etched more strongly. Therefore, the problem of identifying small domains and dislocations is important. Etching agents were selected both for revealing the domain structure and dislocations [48, 50, 53, 58]. The biggest successes were achieved apparently in [53] where etching agents which made it possible to reveal the domains and dislocations simultaneously were selected.

Several more methods of revealing the domains were demonstrated using the crystals of triglycine sulfate. Thus, Fousek et al. [59] used the method of condensing the vapors of a polar liquid on the surface of the crystal. Such a method was suggested for the first time by Toshev [60, 61] for visualizing the domain structure of potassium dihydrogen phosphate and ammonium fluoroberyllate. He named it "dew" method. The principle of this method consists in that owing to the presence of strong electric-field gradients along the domain boundaries, a force acts on the polar molecules which tends to draw them into the region of maximum gradient, i.e. to the domain boundary. Owing to this, a more intensive condensation of the vapors takes place along the boundary, and the domain pattern may be seen for a certain length of time.

Distler et al. [62] and also Takagi et al. [63] found that with a condensation of thermally evaporated silver on the surface of triglycine sulfate the formation of nuclei takes place chiefly on the domains of one sign. This makes it possible to reveal the  $180^\circ$  domains with a good contrast. The size of the nuclei is of the order of 100 Å. Therefore, the method has a high resolution and makes it possible to use electron microscopy. Another method of revealing the domains, which is in essence similar to the powder method, was suggested by Distler and Konstantinova [64]. They found that the charged colloidal particles settle with dissimilar density on domains of a different sign. A finely dispersed platinum sol with the size of the particles of 20-100 Å was used. Such small dimensions of the particles ensure high resolution.

## Par. Domain Structure of Seignette's Salt and Potassium Dihydrogen Phosphate

In nonpolar phase the crystals of Seignette's salt belong to the rhombic class 222. Appearance of spontaneous polarization along the rhombic a-axis is accompanied by a monoclinic distortion and the crystals pass into a monoclinic class 2. In doing so, the rhombic a-axis becomes a monoclinic b-axis. However, the notations of the axes are usually not changed and the polar axis is called a-axis. The a-axis forms angles of  $90^\circ$  with the b- and c-axes. The angle between the b- and c-axes becomes a non- $90^\circ$  angle. Seignette's salt is a uniaxial ferroelectric and, consequently, only  $180^\circ$  domains can be in it. However, the situation is here completely different in comparison with the case of triglycine sulfate.

The fact is that in nonferroelectric phase, Seignette's salt is noncentrosymmetric and has a piezoelectric effect. Therefore, spontaneous deformation [displacement in the plane (100)] is linearly connected with spontaneous polarization and, thus, depends on its direction. Antiparallel domains may be obtained by means of a  $180^\circ$  turn around the b-axis (the so-called b-domains) or around c-axis (c-domains) (Figure 7.9). The b- and c-axes which were second-order axes in nonferroelectric phase become twin axes and the twinning takes place with respect to the planes (001) and (010) respectively. Thus, b-domains have walls parallel to the plane (001), and c-domains -- those parallel to the plane (010). We will note here an important difference between the  $180^\circ$  walls of a tetragonal barium titanate and triglycine sulfate on one hand and of Seignette's salt -- on the other. While in the former case a wall could be any cylindrical surface with a generatrix parallel to the polar axis, in the latter case the  $180^\circ$  walls are only certain crystallographic planes.

Although breaking up of Seignette's salt into domains was supposed a long time ago, domain structure was not observed directly for a long time, and there were only indirect experimental facts which confirmed its existence. Observations of Barkhause electric jumps [65-66] belong here, i.e. observations of jumps in the process of polarization, and detection of pyroelectric effect by means of electrostatic charged powders [67, 68]. In the latter case, pyroelectric effect would have been equal to zero if the regions of spontaneous polarization had been very small and had been uniformly distributed along opposite directions. In addition to this, the effect of electric field and mechanical stresses on the intensity of x-ray reflexes was discovered later [69-72]. This phenomenon was explained by a change in domain structure in the presence of external influences.

Direct observation of domains in crystals of Seignette's salt was carried out only in 1948 when Klassen-Neklyudova et al. [73] discovered that twinning may be seen well in polarized light on the x-cut. The feasibility of optical observation of antiparallel domains is not so obvious and, as already noted above, in barium titanate and triglycine sulfate domains of this kind are optically indistinguishable without an applica-

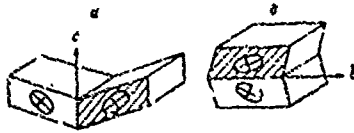


Figure 7.9. Schematic representation of domains in Seignette's salt and the position of indicatrices in them.

a -- a-domains; b -- b-domains.

tion of external influences to the crystal. The fact is that in unpolarized phase Seignette's salt is noncentrosymmetric. Therefore, appearance of spontaneous polarization is accompanied by a spontaneous linear electrooptical effect which consists in a turn of the indicatrix around the polar axis (see chapter 11 for more details on electrooptical effect). The angle of rotation  $\alpha$  is determined from the following relationship [74]:

$$\lg 2\alpha = \frac{2a_{22}}{a_{22} - a_{23}} \quad (7.6)$$

where  $a_{ik}$  are coefficients in the equation of the indicatrix

$$a_{11}x_1^2 + a_{22}x_2^2 = 1,$$

i.e.

$$a_{22} = \frac{1}{n_2^2}, \quad a_{23} = \frac{1}{n_2^2} \pi \quad a_{23} = \alpha_{21} E_1,$$

Here  $\alpha_{21}$  is a coefficient describing the aggregate electrooptical effect. According to the calculations the angle  $2\alpha$  should amount to  $1-2^\circ$  and can be completely detected by experiments. In antiparallel domains the indicatrix is turned in different directions as shown in Figure 7.9. Therefore, in an observation of a plate of seignette's salt along the polar axis in crossed Nicol prisms the  $180^\circ$  domains have different positions of extinction the angle between which is equal to  $2\alpha$ . In accordance with formula (7.6) the angle  $2\alpha$  has the same temperature dependence as spontaneous polarization [74-76] and Indenbom [74, 77] showed that it can be used as an order factor in the expansion of thermodynamic potential.

A thorough study of domain structure of Seignette's salt in polarized light was carried out by Chernysheva [4, 73, 74, 78-80] and also by Furuichi and Mitsui [3, 81]. Figure 7.10 shows a photograph of the pattern of x-cut observed in microscope when domains of one polarity are in the position of extinction. Both the b- and c-domains form bands with a



Figure 7.10. Domain structure of Seignette's salt taken in polarized light. (After Klassen-Neklyudova et al. [73]).

width of from 1 to 500 microns. Configurations consisting both of the b- and c-domains in the form of mutually perpendicular systems of bands are usually observed. Some domains have a wedge-like form and do not come out to the surface of the crystal. The wedge may be oriented not only along the b- and c-axes but along the polar a-axis also [80, 82].

Mitsui and Furuichi [3] showed that the width of a domain is proportional to the square root of the crystal thickness  $d$  and that the following relationship is satisfied fairly well:

$$w = 1.1 \cdot 10^{-2} \sqrt{d}. \quad (7.7)$$

Mueser and Flunkert [83] noted that Curie point of the regions with b-domain is somewhat higher than that of the regions with c-domains. It is of interest that crystals grown at a temperature corresponding to polar state prove to be broken up into domains although the solution has a sufficiently good electric conductivity and the surface charges are compensated [75]. This experiment shows that elastic energy, and not electrostatic energy, is determinative in the formation of domains.

Indenbom and Chernysheva [84] and Nakamura and Ohi [75, 85, 86] noted a correlation between the domain pattern and arrangement of screw dislocations. Nakamura and Ohi observed domains fixed on screw dislocations and not disappearing even upon an application of strong electric fields. Calculations of the form of such domains were undertaken in [87]. Unlike barium titanate the domain structure of Seignette's salt was studied almost exclusively optically although the feasibility of using electron microscopy [28] and etching with water [88] had been shown.

Domain structure of potassium dihydrogen phosphate has been little studied. Above Curie point  $\text{KH}_2\text{PO}_4$  belongs to the noncentrosymmetric tetragonal class  $\bar{4}2m$ . Spontaneous polarization appears along the fourth-

order axis. Thus, this is a uniaxial ferroelectric and only  $180^\circ$  domains can be in it. Spontaneous deformation consists in a displacement in the base plane. In doing so, tetragonal unit cell becomes monoclinic (the true symmetry is rhombic). Tetragonal planes (100) and (010) may be the twinning planes. This leads to a domain structure which is completely analogous to the domain structure of Seignette's salt. Owing to a small turn of the indicatrix in the neighboring domains they can be differentiated in polarized light [3, 89, 90]. Toshev [61, 91] successfully used the "dev" method to reveal the domains.

#### Par. 5. Domain Walls

Until now, when examining the domain structure of ferroelectrics we did not touch upon the question of what the domain walls are, and their thickness and energy. We will recall that in the case of ferromagnetics domain walls are a wide transition region in which magnetization vector gradually turns from one direction to another. The case of a  $180^\circ$  wall is shown schematically in Figure 7.11a. The thickness of a wall is determined from the condition of a minimum of the sum of exchange energy and anisotropy energy. A portion of the wall energy connected with exchange interaction decreases with an increase in wall thickness since a parallel orientation of magnetic moments is most favorable for this interaction. At the same time, the portion of wall energy which is connected with anisotropy increases with the wall thickness since the volume in which intensity of magnetization does not coincide with the easy direction increases. Exchange energy considerably exceeds anisotropy energy. Therefore, domain walls in ferromagnetics are sufficiently thick.

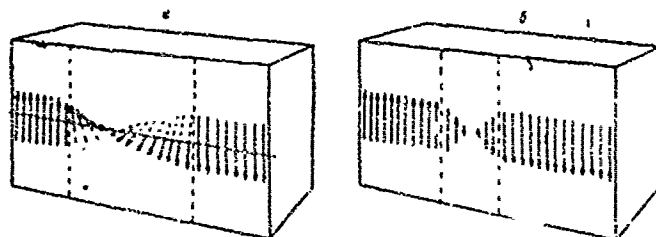


Figure 7.11. Schematic representation of  $180^\circ$  domain wall in a ferromagnetic (a) and in a ferroelectric (b).

In ferroelectrics the electrostatic-interaction energies of dipoles oriented in parallel and in antiparallel do not differ very markedly. At the same time, anisotropy is high. Therefore, it should be expected from general considerations alone that domain walls in ferroelectrics are considerably thinner than in ferromagnetics. The second important distinc-

tion of domain walls of ferroelectrics consists in the behavior of polarization vector inside the wall. In ferromagnetics the modulus of magnetization-intensity vector in the wall does not change. In the case of ferroelectrics, owing to a high anisotropy it is difficult to expect rotation of the polarization vector, rather its modulus changes. Therefore, for example in the case of a  $180^\circ$  wall, a pattern shown schematically in Figure 7.11b may be expected.

In the greater portion of works devoted to a theoretical examination of energy and thickness of domain walls in ferroelectrics the crystal together with the wall is regarded as a continuum. Calculations are performed similarly to the way this is done in the case of ferromagnetics. Thus, Merz [92] examined the energy of a  $180^\circ$  wall of barium titanate in the form of a sum of dipole-interaction energy and anisotropy energy. He determined from the condition of a minimum of aggregate energy the thickness of the wall and its energy. The thickness proved to be equal to one lattice constant, and energy -- to 7 ergs/cm<sup>2</sup>.

The first phenomenological calculations for a domain wall of Seignette's salt were carried out by Mitsui and Furrichi [81]. However, they did not take into account the energy of piezoelectric deformation, electrostriction was taken into account inconsistently, and deformations did not satisfy Saint-Venant continuity conditions. An exact phenomenological theory of domain walls in tetragonal titanate and Seignette's salt was developed by Zhirnov [93]. He used a method suggested by Landau and Lifshits [94] for the study of domain structure of ferromagnetics. Using thermodynamic-equilibrium condition in the absence of an external electric field the course of the change in polarization in the wall was determined, and explicit expressions for the thickness of the wall and its energy were also obtained. Examination was carried out with the condition of  $\text{div}P=0$ , i.e. with the condition of absence of bound charges on the wall.

The following types of energy were taken into account in writing the expression for thermodynamic potential: 1) anisotropy energy brought about by a deflection of polarization vector from the easy direction; 2) elastic energy; 3) energy connected with electrostriction and if the crystal was above Curie temperature -- piezoelectric with piezoeffect; 4) energy connected with nonuniform distribution of polarization vector. Zhirnov determined that polarization vector in the wall does not rotate but that its modulus changes. Numerical evaluations of the thicknesses and energies of walls in barium titanate and Seignette's salt are given in Table 16.

A similar examination was carried out by Ivanchik [95] and Bulayevskiy [96] for barium titanate and by Fousek [97] for triglycine sulfate. In doing so, unlike [93], in [95, 96] a ferroelectric phase transition in barium titanate was considered to be a transition of the first kind and in the expansion for thermodynamic potential the sixth-order term for polarization was taken into account. In addition to this, Ivanchik [95] showed that periodicity in the arrangement of antiparallel domains

Table 16

Width (h) and Energy ( $\epsilon_w$ ) of Domain Walls in Barium Titanate and Seignette's Salt According to the Data of Different Authors

1 Титанат бария				6 Триглицин сульфат		7 Сеignetтоса соль		8 Автор
2 180° стена		3 90° с. стена		4 А, см	5 $\epsilon_w$ , эрг/см <sup>2</sup>	А, см	$\epsilon_w$ , эрг/см <sup>2</sup>	
А, см	$\epsilon_w$ , эрг/см <sup>2</sup>	А, см	$\epsilon_w$ , эрг/см <sup>2</sup>					
4	7	--	--	--	--	--	--	9 Мерц [92]
5	20	10	50-100	2-4	--	12; $T = 0^\circ C$ 220; $T = 20^\circ C$	6 · 10 <sup>-2</sup> ; $T = 0^\circ C$ 1.2 · 10 <sup>-2</sup> ; $T = 20^\circ C$	Жирнов [93] 10
7-20	10-30	--	--	--	--	--	--	Иванчик [95] 11
7	10.5	11	3.4	--	--	--	--	Булаевский [96] 12
--	--	100	35	--	--	--	--	Холоденко [98] 13
--	--	--	--	--	--	24; $T = 0^\circ C$ 23; $T = 20^\circ C$	5.7 · 10 <sup>-2</sup> ; $T = 0^\circ C$ 1.0 · 10 <sup>-2</sup> ; $T = 20^\circ C$	Митсуи и Фуруичи [91] 14
4	1.4	4000	--	--	--	--	--	Литтл [21] 15
--	--	--	--	--	--	--	--	Кинасе и Такашаси [102] 16
--	--	--	--	100	4-12	--	--	Фусек [97] 17

- key: (1) Barium titanate (10) Zhirnov [93]  
 (2) 180° wall (11) Ivanchik [95]  
 (3) 90° wall (12) Bulayevskiy [96]  
 (4) cm=centimeter (13) Kholodenko [98]  
 (5) ergs/cm<sup>2</sup> (14) Mitsui and Furuichi [91]  
 (6) Triglycine sulfate (15) Little [21]  
 (7) Seignette's salt (16) Kinase and Takalashi [102]  
 (8) Author (17) Fousek [97]  
 (9) Merz [92]

follows from thermodynamic theory. As in [93], it was determined that owing to high anisotropy in quadratic terms for polarization in the expression for free energy the rotation of polarization vector in the wall proves to be impossible. In the case of Seignette's salt anisotropy is determined chiefly by the rhombic symmetry of the crystal in paraelectric phase. Barium titanate is cubic in paraelectric phase and, therefore, anisotropy in quadratic terms for polarization appears only owing to electrostriction. The thicknesses and energies of the boundaries according to the calculations in [95] and [96] are given in Table 16.

A detailed examination of a 90° wall in barium titanate was carried out by Kholodenko [98] for the case when the condition  $\text{div } P=0$  on the boundary is not satisfied and there are bound charges whose density

is equal to the density of the free charges which compensate them. Calculated data for this case are also given in Table 16.

The case of a  $180^\circ$  domain wall in barium titanate when the wall is a plane parallel to the c-axis was examined in the works [93, 95-98]. Owing to the anisotropy of elastic energy it may be expected that the energy of such a wall will depend on its orientation with respect to the a-axis. Using the method similar to that used in [93] Dvořák and Janovec [99] calculated the relationship of the energy of a  $180^\circ$  wall to the angle  $\varphi$  between the wall and a-axis. They found that the energy of the wall is a periodic function of  $\varphi$  with minima at  $\varphi = \frac{\pi}{2} n$  and maxima at  $\varphi = \frac{\pi}{2} \left( n + \frac{1}{2} \right)$  ( $n$  is an integer or a null). This result agrees with the tendency -- discovered in [23] -- of  $180^\circ$  walls to become oriented along the a-axis. However, as the calculations showed, the difference between the maximum and minimum energies of the walls amounts only to 0.01 percent. It is difficult to suppose that such a small difference in energy may be the cause of the orientation of domain walls along the a-axis.

As we have already underscored, phenomenological theories regard a wall as a continuum. Generally speaking such an approach is correct only when the thickness of the wall is  $\pi$  : greater than the interatomic distances but when it amounts only to a few lattice constants, as in the case of  $180^\circ$  walls, the validity of such a consideration is problematic. In particular, as noted in [39], possibly it is precisely because of this that the inference of phenomenological theory concerning weak angular dependence of the wall energy does not correspond to reality.

Creation of microscopic theory of domain walls encounters great difficulties. Kaenzig and Sommerhalder [100] examined a simple model of a ferroelectric -- a body-centered cubic lattice of point dipoles. The energy of the wall was defined as the difference between the energies of the crystal with a wall and without a wall. Naturally, in such an examination the dipole-interaction energy alone is taken into account. The authors of the work [100] obtained the following formula for wall energy:

$$\sigma_w = 0.88P^2a$$

where  $P$  is polarization within the domain and " $a$ " is lattice constant.

Two models were proposed for domain walls in  $\text{KH}_2\text{PO}_4$  [101]. In one of them the rotation of polarization vector takes place by means of two successive turns by  $90^\circ$  and in the second model polarization is absent in the wall since the dipole moments are completely compensated. Kinase and Takahashi [102] made an attempt to create a microscopic theory of a  $180^\circ$  domain wall in barium titanate. An assumption that no rotation of polarization vector takes place in the wall but that its modulus changes was laid down as the basis of the model. Next, the results of a calcul -

tion by Kinase [103] for local fields at the sites of titanium ions were used for a parallel and antiparallel arrangement of dipole moments of the unit cells. In doing so, it was considered that only titanium ions are displaced. Using a method of calculation for lattice distortion in a one-domain crystal suggested by them earlier, Kinase and Takahashi [104] determined these distortions in domain wall. They found that a  $180^\circ$  boundary has practically a zero thickness. According to their calculations the energy of the boundary is  $1.40 \text{ ergs/cm}^2$ . If the displacement not of titanium ions alone but of the oxygen ions  $O_I$  (Figure 1.3b) is also taken into account, then a thickness of the boundary equal to two lattice parameters results.

#### BIBLIOGRAPHY

1. L. D. Landau, Ye. M. Lifshits. Electrokinamika Sploshnykh Sred [Electrodynamics of Continua]. Izd.FML [Publishing House for Physical and Mathematical Literature], Moscow (1959).
2. Ch. Kittel, Rev. Mod. Phys., Vol 21, p 541 (1949). (Translation in the collection: Fizika Ferromagnitnykh Oblastey [Physics of Ferromagnetic Regions], IIL [Foreign Literature Press], Moscow (1951)].
3. T. Mitsui, J. Furuichi, Phys. Rev., Vol 90, p 193 (1953).
4. M. A. Chernysheva, DAN SSSR [Proceedings of USSR Academy of Sciences], Vol 74, p 247 (1950).
5. I. S. Zheludev, L. A. Shuvalov, Kristallografiya [Crystallography], Vol 1, p 681 (1956).
6. I. S. Zheludev, L. A. Shuvalov, Izv. AN SSSR, ser. fiz. [Bulletin of USSR Academy of Sciences, Physical Series], Vol 21, p 264 (1957).
7. M. S. Shur, FTT [Solid State Physics], Vol 10, p 2652 (1968).
8. M. S. Shur, FTT, Vol 10, p 3560 (1968).
9. M. S. Shur, FTT, Vol 10, p 3684 (1968).
10. M. S. Shur, Izv. AN SSSR, ser. fiz., Vol 33, p 207 (1969).
11. H. F. Kay, P. Vouse, Phil. Mag., Vol 40, p 1019 (1949).
12. P. W. Forsbergh, Phys. Rev., Vol 76, p 1187 (1949).
13. W. J. Merz, Phys. Rev., Vol 88, p 421 (1952).
14. W. J. Merz, J. Appl. Phys., Vol 25, p 1346 (1954).
15. R. C. Miller, A. Savage, Phys. Rev. Lett., Vol 2, p 294 (1959).

16. J. Kabayashi, N. Yamada, T. Nakamura, Phys. Rev. Lett., Vol 11, p 410 (1963).
17. T. Nakamura, D. Ogihara, J. Kabayashi, J. Phys. Soc. Japan, Vol 18, p 1716 (1963).
18. J. A. Hooton, W. J. Merz, Phys. Rev., Vol 98, p 409 (1955).
19. D. S. Campbell, Phil. Mag., Vol 46, p 1261 (1955).
20. D. S. Campbell, D. J. Stirling, Brit. J. Appl. Phys., Vol 7, p 62 (1956).
21. E. A. Little, Phys. Rev., Vol 98, p 978 (1955).
22. V. G. Bhide, N. J. Bapat, J. Appl. Phys., Vol 34, p 181 (1963).
23. J. Fousek, M. Safrankova, Japan J. Appl. Phys., Vol 4, p 403, (1965).
24. J. Fousek, B. Brezina, Czechosl. J. Phys., Vol B11, p 261 (19610).
25. G. J. Pearson, W. L. Feldman, J. Phys. Chem. Solids, Vol 9, p 28 (1959).
26. D. P. Cameron, IBM J. Res. Developm., Vol 1, p 2, (1957).
27. V. G. Bhide, N. J. Bapat, Physica, Vol 27, p 531 (1961).
28. G. V. Spivak, E. Igras, I. S. Zheludev, DAN SSSR, Vol 122, p 54 (1958).
29. E. Igras, G. V. Spivak, I. S. Zheludev, Kristallografiya, Vol 4, p 121 (1959).
30. G. Y. Robinson, R. M. White, Appl. Phys. Lett., Vol 10, p 320, (1967).
31. I. C. Burfcot, R. V. Latham, Brit. J. Appl. Phys., Vol 14, p 933 (1963).
32. G. V. Spivak, E. Igras, I. A. Pryamkova, I. S. Zheludev, Kristallografiya, Vol 4, p 123 (1959).
33. F. L. English, J. Appl. Phys., Vol 39, p 128 (1968); Vol 39, p 3231 (1968).
34. K. V. Moffitt, J. Appl. Phys., Vol 39, p 3878 (1968).
35. M. Tanaka, N. Kitamura, G. Hehjo, J. Phys. Soc. Japan, Vol 17, p 1197 (1962).
36. H. Blank, S. Amelinckx, Appl. Phys. Lett., Vol 2, p 140 (1953).

37. E. Fuchs, W. Liesk, J. Phys. Chem. Solids, Vol 25, p 845, (1964).
38. E. V. Shmakov, G. V. Spivak, FTT, Vol 10, p 1016 (1968).
39. C. Bousquet, M. Lambert, A. M. Quttet, A. Guinier, Acta Cryst., Vol 16, p 989 (1963).
40. N. Mizeki, M. Hasegawa, J. Phys. Soc. Japan, Vol 19, p 550 (1964).
41. J. Caslavsky, Czechosl. J. Phys., Vol B14, p 454 (1964).
42. D. R. Callaby, J. Appl. Phys., Vol 36, 2751 (1965).
43. L. A. Shuvalov, K. S. Aleksandrov, I. S. Zheludev, Kristallografiya, Vol 4, P 130 (1959).
44. H. Toyoda, S. Waku, H. Hirabayashi, J. Phys. Soc. Japan, Vol 14, P 1003 (1959).
45. V. P. Konstantinova, I. M. Sil'vestrova, V. A. Yurin, Kristallografiya, Vol 4, p 125 (1959).
46. V. P. Konstantinova, I. M. Sil'vestrova, K. S. Aleksandrov. In the collection: Fizika Dielektrikov [Physics of Dielectrics], Izd. AN SSSR [USSR Academy of Sciences Press], Moscow, p 351 (1960).
47. V. P. Konstantinova, Izv. AN SSSR, ser. fiz., Vol 24, p 1324 (1960).
48. V. P. Konstantinova, Kristallografiya, Vol 7, p 748 (1962).
49. H. Toyoda, J. Phys. Soc. Japan, Vol 14, p 376 (1959).
50. H. Toyoda, J. Phys. Soc. Japan, Vol 15, p 1539 (1960).
51. A. G. Chynoweth, Phys. Rev., Vol 117, p 1235 (1960).
52. A. G. Chynoweth, W. L. Feldman, J. Phys. Chem. Sol., Vol 15, p 225 (1960).
53. V. A. Meleshina, Kristallografiya, Vol 9, p 381 (1964).
54. A. G. Chynoweth, J. L. Abel, J. Appl. Phys., Vol 30, p 1073 (1959).
55. A. G. Chynoweth, J. L. Abel, J. Appl. Phys., Vol 30, p 1515 (1959).
56. V. A. Meleshina, I. S. Zheludev, I. S. Rez. Kristallografiya, Vol 5, p 322 (1960).
57. L. Taurel, M. Eimer. Compt. rend., Vol 256. p 642 (1963).
58. T. Nakamura, H. Nakamura, Japan J. Appl. Phys., Vol 1, p 253 (1962).

59. J. Fousek, M. Safrankova, I. Kaczer, Appl. Phys. Lett., Vol 8, p 192 (1966).
60. S. D. Toshev, Kristallografiya, Vol 8, p 114 (1963).
61. S. D. Toshev, Kristallografiya, Vol 8, p 680 (1963).
62. G. I. Distler, V. P. Konstantinova, Yu. M. Gerasimov, G. A. Tolmacheva, ZhETF [Journal of Experimental and Theoretical Physics], Letters, Vol 6, p 868 (1967).
63. M. Takagi, S. Suzuki, K. Tanaka, J. Phys. Soc. Japan, Vol 23, p 134 (1967).
64. G. I. Distler, V. P. Konstantinova, Kristallografiya, Vol 13, p 631 (1968).
65. M. Kluge, H. Schoenfeld, Naturwiss., Vol 21, p 194 (1933).
66. H. Mueller, Phys. Rev., Vol 47, p 175 (1935).
67. W. G. Cady, Piezoelectricity. N. Y., 1946 (Translation into Russian: W. Cady. Piezoelectricity and Its Practical Application. II [Foreign Literature Press], Moscow, 1949).
68. H. Mueller, Ann. N.Y. Acad. Sci., Vol 40, p 321 (1940).
69. S. Miyake, J. Phys. Soc. Japan, Vol 2, p 98 (1947).
70. S. Miyake, Proc. Phys. Math. Soc. Japan, Vol 23, pp 371, 810 (1941).
71. S. Miyake, Acta Cryst., Vol 2, p 192 (1949).
72. A. R. Ubbelohde, I. Woodward, Proc. Roy. Soc., Vol A165, p 448 (1946).
73. M. V. Klassen-Neklyudova, M. A. Chernysheva, A. A. Shternberg, DAN SSSR, Vol 63, p 527 (1948).
74. V. L. Indenbom, M. A. Chernysheva, Kristallografiya, Vol 2, p 526 (1957).
75. T. Nakamura, J. Phys. Soc. Japan, Vol 11, p 624 (1956).
76. R. Abe, J. Phys. Soc. Japan, Vol 13, p 244 (1958).
77. V. L. Indenbom, M. A. Chernysheva, ZhETF, Vol 32, p 697 (1957).
78. M. A. Chernysheva, DAN SSSR, Vol 81, p 1065 (1951).
79. M. A. Chernysheva, DAN SSSR, Vol 91, p 87 (1953).

80. M. A. Chernysheva, Izv. AN SSSR, ser. fiz., Vol 21, p 289 (1957).
81. I. Furuichi, T. Mitsui, Phys. Rev., Vol 80, p 93 (1950).
82. M. Marutake, J. Phys. Soc. Japan, Vol 7, p 25 (1952).
83. H. E. Mueser, H. Flunkert, Z. Phys., Vol 150, p 21 (1958).
84. V. A. Indenbom, M. A. Chernysheva, Izv. AN SSSR, ser. fiz., Vol 22, p 1459 (1958).
85. T. Nakamura K. Ohi, J. Phys. Soc. Japan, Vol 16, p 209 (1961).
86. K. Ohi, T. Nakamura, J. Phys. Soc. Japan, Vol 17, p 1195 (1962).
87. H. Takahasi, T. Nakamura, Y. Ishibashi, J. Phys. Soc. Japan, Vol 15, p 853 (1960).
88. E. Straubel-Fischer, Naturwiss., Vol 44, p 230 (1957).
89. N. N. Fomichev, izv. AN SSSR, ser. fiz., Vol 29, p 962 (1965).
90. A. Fouskova, P. Bayon, J. Lajzerowics, Compt. rend., Vol 262, p 907 (1966).
91. V. A. Koptshik, S. D. Toshev, Izv. AN SSSR, ser. fiz., Vol 29, p 956 (1965).
92. W. J. Merz, Phys. Rev., Vol 95, p 690 (1954).
93. V. A. Zhirnov, ZhETF, Vol 35, p 1175 (1958).
94. L. D. Landau, Ye. M. Lifshits, Phys. Zs. Sowjetunion, Vol 8, p 153 (1935).
95. I. I. Ivanchik, FTI, Vol 3, p 3731 (1961).
96. L. N. Bulayevskiy, FTI, Vol 5, p 3183 (1963).
97. J. Fousek, Japan J. Appl. Phys., Vol 6, p 950 (1967).
98. L. P. Kholodenko, FTI, Vol 3, p 3142 (1961).
99. V. Dvořák, V. Janovec, Japan J. Appl. Phys., Vol 4, p 400 (1965).
100. W. Känzing, R. Sommerhølder, Helv. Phys. Acta, Vol 26, p 603 (1953).
101. H. M. Barkla, D. M. Finlayson, Phil. Mag., Vol 44, p 109 (1953).
102. W. Kinase, H. Takahashi, J. Phys. Soc. Japan, Vol 12, p 464 (1957).

103. W. Kinase, Progr. Theor. Phys. (Kyoto), Vol 13, p 529 (1955).
104. W. Kinase, H. Takahashi, J. Phys. Soc. Japan, Vol 10, p 942 (1955).
105. L. A. Shuvalov, Kristallografiya, Vol 8 p 617 (1963);  
J. Phys. Soc. Japan, Vol 28, Suppl., 38 (1970): Proc. of the 2nd Intern.  
Meet. Ferroelectr., Kyoto (1969).
106. K. Aizu, J. Phys. Soc. Japan, Vol 23, p 794 (1967).

## CHAPTER 8. SPONTANEOUS POLARIZATION AND REPOLARIZATION PROCESSES

### §1. Spontaneous Polarization and Dielectric Hysteresis

One of the most remarkable properties of ferroelectrics is their ability to change the direction of spontaneous polarization by an external electric field. This process is known as repolarization, and it can be observed on an oscillograph scope with the aid of the circuit proposed by Sawyer and Tauer [1] (Figure 8.1). Here vertical deflection of the beam is proportional to the charge on the specimen and horizontal deflection is proportional to the voltage on it. The process of periodic repolarization with alternating current of industrial frequency is usually observed with the aid of this diagram. The Sawyer-Tauer method can be used only if the electrical conductivity of the specimen is low. Otherwise the loop will be distorted by the active component of the current. For this reason more sophisticated schemes have been proposed to compensate for the current of conductivity [2, 3].

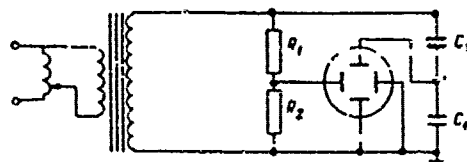


Figure 8.1. Circuit for observing dielectric hysteresis loops.  $C_x$  -- ferroelectric specimen;  $C_i$  -- integrating capacitor;  $R_1$  and  $R_2$  -- voltage divider.

The dependence of polarization on electric field strength is of the hysteresis loop form and is depicted schematically in Figure 1.2 (see Chapter 1). If perfect saturation is achieved, i.e., the direction of spontaneous polarization coincides in the entire crystal with the direction of the external electric field, then important information concerning the ferroelectric can be derived from the hysteresis loop. The growth of polarization with increasing electric field strength after saturation is

caused only by the processes of electron and ion displacement (induced polarization), and not by a reversal of spontaneous polarization. Therefore the permittivity of a crystal along the polar axis can be found from the slope of the saturation branch, and spontaneous polarization can be determined by extrapolating the saturation branch to  $E = 0$ . (Figure 1.2). The electric field strength at which polarization vanishes is called the coercive field ( $E_c$ ). Theoretical calculations of the coercive field as the field in which the spontaneous polarization vector in a single-domain crystal jumps suddenly from the position of the antiparallel to the parallel field yield for barium titanate fields of the order  $10^5$ - $10^6$  V/cm [4, 5]. The experimentally observed coercive fields are three orders of magnitude smaller than the theoretical values. This discrepancy is explained by the fact that the change of direction of spontaneous polarization is not abrupt in the entire domain, but is a result of movement of the domain walls. This subject is examined at length in the ensuing sections of this chapter.

There is considerable difference between repolarization of ferroelectrics and remagnetization of ferromagnetics, despite the seemingly perfect analogy of these processes. When a magnetic field whose direction does not coincide with the axis of easy magnetization is applied to a ferromagnetic, the processes of displacement of the domain walls are followed by the processes of rotation, during which time the spontaneous magnetization vector rotates, asymptotically approaching the direction of the field. In the case of ferroelectrics anisotropy is so great that there is practically no rotation of the spontaneous polarization vector in tolerable electric fields, i.e., this vector can lie only on the ferroelectric axes (they correspond to the axes of easy magnetization of ferromagnetics).

We will examine now the temperature dependence of spontaneous polarization. In the case of the first order phase transition spontaneous polarization occurs abruptly at the Curie point, while in the case of the second order phase transition it changes continuously. Both cases are depicted schematically in Figure 1.1. Barium titanate, whose spontaneous polarization temperature dependence is illustrated in Figure 8.2, is an example of a ferroelectric with the first order phase transition. Polarization in pseudocubic direction [100] was determined experimentally. Since in the rhombic phase spontaneous polarization is aimed in pseudocubic direction [110] the experimental value must be multiplied by  $\sqrt{2}$  to find the true value. Spontaneous polarization in the rhombohedral phase coincides with pseudocubic axis [111]. Here, therefore, the experimental values must be multiplied by  $\sqrt{3}$ . Spontaneous polarization occurs abruptly at the Curie point [7, 8]. The coercive field at room temperature varies for different crystals from 500-2,000 V/cm. Its temperature dependence is shown in Figure 8.3. In the rhombohedral phase the coercive field grows rapidly as the temperature approaches the helium temperatures [10].

The temperature dependence of spontaneous polarization of triglycine sulfate is characteristic of second order phase transitions (Figure 8.4).

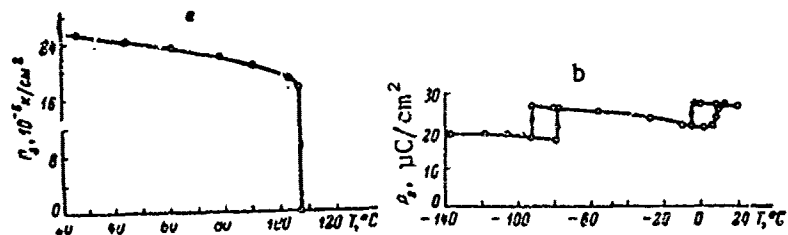


Figure 8.2. Spontaneous polarization temperature dependence of barium titanate: a -- in tetragonal phase (Merz [6]); b -- in orthorhombic and rhombohedral phases (Wieder [7]). The component of spontaneous polarization on pseudocubic axis [ $10^\wedge$ ] was determined in the orthorhombic and rhombohedral phases.

The value of  $P_s$  according to the data of different authors varies in a rather broad range [11-15]. The coercive field at room temperature is approximately 400 V/cm [12].

According to thermodynamic theory, if in the expansion of the thermodynamic potential we are limited to the terms  $P^4$ , we find the temperature dependence of spontaneous polarization from equation (3.9a). If the term with  $P^6$  is considered, as in (3.12), then it is easy to show that

$$P_s^2 = \frac{\alpha_0'}{\beta} (\theta - T) - 2 \frac{\gamma}{\beta} (\theta - T)^2 \quad (8.1)$$

if  $\alpha_0'$  is known, then coefficients  $\beta$  and  $\gamma$  can be found by the method of least squares from the experimental dependence of  $P_s^2$  on  $(\theta - T)$  near the Curie point.

In the case of triglycine sulfate  $\beta = 4 \cdot 10^{-10}$  (el. st. un./ $\text{cm}^2$ ) $^{-2}$  and  $\gamma = 5 \cdot 10^{-18}$  (el. st. un./ $\text{cm}^2$ ) $^{-4}$  [16]. In the extremely narrow temperature range just below the Curie point somewhat different values were obtained for these coefficients [17]. Using experimental values of  $\beta$  and  $\gamma$  it is possible to estimate the values of the first three terms in the expansion of the thermodynamic potential (3.12). This estimate shows that the term with  $P^4$  is extremely small. Therefore the second term in (8.1) can be discarded, whereupon we find that  $P_s^2$  is a nearly linear function of  $(\theta - T)$ . The investigations of Strukov [18] and Gonzalo [19] show that this function is linear at least to  $(\theta - T) \sim 0.1^\circ$ .

For ferroelectrics isomorphic to potassium dihydrophosphate the second term in (8.1) is most important, and near the Curie point spontaneous polarization is a linear function of temperature, and here  $P_s$  increases

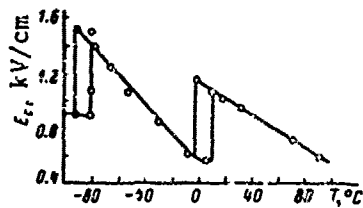


Figure 8.3. Temperature dependence of coercive field ( $E_c$ ) of barium titanate crystal (according to Winder [9]).

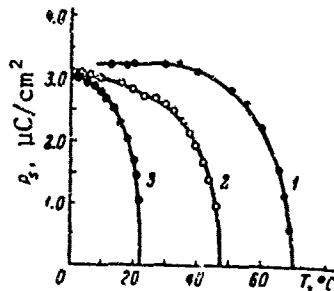


Figure 8.4. Temperature dependence of spontaneous polarization of triglycine fluoberyllate (1), triglycine sulfate (2) and triglycine selenate (3) (according to Hoshino, et al [11]).

very rapidly as the temperature falls. This shows that the phase transition of potassium dihydrophosphate is by nature close to the critical point (see Chapter 12).

The temperature dependence of spontaneous polarization of Seignette's salt is illustrated in Figure 8.5.  $P_s$  changes smoothly at the Curie points. The coercive field intensity has a maximum value of  $\sim 200$  V/cm between 5 and 15°C.

If a ferroelectric crystal is single-domain or domains of one of the possible orientations prevail in it (unipolar), then a change of its temperature will lead to the pyroelectric effect, i.e., to the appearance of charges on the surface of the crystal. By analyzing the pyroelectric effect it is possible to determine the pyroelectric coefficient

$$p = \frac{dP_s}{dT} . \quad (8.2)$$

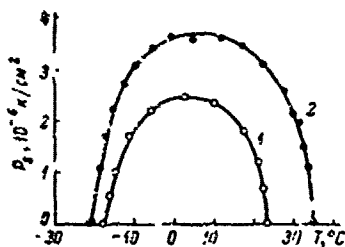


Figure 8.5. Temperature dependence of spontaneous polarization of Seignette salt: ordinary (1) and deuterated (2) (according to Hablutzel [20]).

If the temperature dependence of the pyroelectric coefficient is known it is theoretically possible, starting at the Curie point, to determine by integration of (8.2) the magnitude of spontaneous polarization. The compensation method, by which it is possible to avoid leaks of the pyroelectric charge, is most often used for analysis of the pyroelectric effect. Zheludev and Gladkiy [21] used this method to analyze Seignette's salt crystals polarized with the aid of mechanical stresses, and Koptsik and Gavrilova [22, 23] used it to analyze unipolar crystals of barium titanate, triglycine sulfate and Seignette's salt. Polycrystalline barium titanate was also analyzed [24, 25]. It is noteworthy that measurement of the pyroelectric effect near the Curie point involves great difficulties, since the observed effect becomes partially the result of change of the domain structure, which amounts either to breakdown into domains or reduction of unipolarity. This feature becomes the determining factor near the Curie point and the coefficient passes through the maximum considerably below the Curie point [22, 23].

Chynoweth [26] used the dynamic method to analyze the pyroelectric effect. In this method the part of the crystal to which the electrode is attached is periodically heated by infrared pulses and the resulting pulses of pyroelectricity are measured. For pyrocurrent density, obviously, we have:

$$i = \frac{dP_s}{dt} = \left[ \frac{dP_s}{dT} \cdot \frac{dT}{dt} \right]. \quad (8.3)$$

At a constant rate of change of temperature  $\left(\frac{dT}{dt}\right)$  the pyrocurrent is proportional to  $\frac{dP_s}{dT}$ . Therefore by integrating (8.3) it is possible to find in relative units the temperature dependence of spontaneous polarization. This method was used for analysis of monocrystals [26, 27] and ceramics [28, 29] of barium titanate, and also triglycine sulfate monocrystals [30].

## §2. Elementary Processes of 180° Repolarization

Repolarization of ferroelectrics in an electric field occurs as a result of change in their domain structure. In order to understand this phenomenon, therefore, it is necessary first of all to know the individual elementary processes that occur and the laws that govern them. The most direct information concerning this can be obtained from direct observations of the domains. If, however, we are interested in the integral characteristics of change of polarization of the entire crystal, to which all the mechanisms contribute, or we want to know which one of them is the most important, then the answers to these questions can be found by analyzing the change of summary polarization. These measurements can be taken by purely electrical methods.

There are two ways to solve the problem of repolarization. The best results are obtained by analyzing the simplest case -- 180° repolarization,

when the field is applied along the axis of spontaneous polarization and its direction changes  $180^\circ$ . These are c-domain crystals of barium titanate, uniaxial pyroelectrics -- triglycine sulfate, guanidine, aluminum sulfate hexahydrate, etc. In this case repolarization may be the result of the following mechanisms:

1) formation of  $180^\circ$  domains with spontaneous polarization parallel to the field;

2) growth of nuclei in the direction of spontaneous polarization to the electrodes without substantial change of the cross section of these domains;

3) expansion of new domains formed, i.e., movement of  $180^\circ$  walls to the side, perpendicular to the direction of spontaneous polarization.

Merz's analyses in polarized light [31] of the repolarization of c-domain barium titanate monocrystals revealed that on application of an electric field opposite spontaneous polarization nuclei of antiparallel domains form near the electrodes. These nuclei grow like thin needles in the direction of the polar axis from one electrode to the other. Notable lateral expansion was not observed. Numerous observations of various researchers show that in not very strong fields, up to a few kilovolts per centimeter, antiparallel domains form chiefly in the same places.

Chynoweth and Abel [32] tried to create artificially on triglycine sulfate centers at which nuclei would be formed. For this purpose they created, first of all, places with high field intensity, for which holes were made on one of the surfaces, and secondly, defects by local irradiation with x-rays [33]. Despite, however, the seemingly favorable conditions at these places for the formation of antiparallel domains, the location of their formation could not be predetermined.

Thus it is still not known what local features of a crystal facilitate the formation of nuclei. It should be pointed out that Miller and Savage [34] were able to create antiparallel domains at a given point on barium titanate crystals with the aid of a hole. If the nuclei formed at the same places in weak fields then, according to Stadler and Zachmanidis [35], in strong fields of approximately 20 kV/cm the nuclei form at different places every time, in most cases. The fraction of domains that form at repeated places increases as the field intensity decreases and in the presence of sudden mechanical and thermal actions.

Merz [31, 36, 37] states that the formation of nuclei in not very strong fields is a statistical process and its probability is an exponential function of field intensity

$$R = R_0 e^{-\frac{U}{kT}} \quad (8.4)$$

where  $\alpha$  plays the part of the activation field. It has also been theorized that the nuclei are generated by heat fluctuations. Lardner [38] later showed that the probability of such a mechanism of formation of new domains is infinitesimally small. Stadler and Zachmanidis nevertheless point out [35] that if the domain wall energy is  $\sigma_w = 0.4 \text{ erg/cm}^2$ , then in fields exceeding 10 kV/cm the formation of nuclei as a result of thermal fluctuations may become a reality. Their experimental rate of formation of nuclei in strong fields (2-450) kV/cm is proportional to  $E^{1.4}$ . For Seignette's salt Mitsui and Furuichi [39] found that the rate of formation of new domains is an exponential function of the field.

If for strong fields the formation of nuclei can be regarded as experimentally proved, then for weak fields the question remains unanswered. The appearance of antiparallel domains in different cycles of repolarization at the same places may correspond not only to the formation there of nuclei. It is not ruled out that there were already tiny antiparallel domains at these places, which grow when the field is applied and can be detected experimentally only when they reach a certain size. It is also held that the surface layers of a crystal play an important part in nucleation processes [40, 41]. Janovec [41] also proceeded from the presence of a space charge on the surface of the barium titanate crystal, gives a possible explanation of this phenomenon. In this case a strong electric field forms in the surface layer perpendicular to the surface. On one of the surfaces this field will always be aimed opposite the spontaneous polarization of the crystal volume, regardless of the direction of the field, and the formation of tiny antiparallel domains is favorable here from the standpoint of energy.

The nuclei of the new domains formed develop primarily in the direction of spontaneous polarization, growing from one electrode to the other. This stage of development of nuclei precedes their lateral expansion. Stadler [42] measured the forward growth rate of domains for barium titanate by the stroboscopic illumination method. He derived the following equation for the dependence of the growth rate on the field:

$$v = (5,500 \text{ cm/sec}) \exp (-1.8 \text{ kV/cm/E}). \quad (2.5)$$

In their first observations of the repolarization of barium titanate Merz [31, 36] and Little [43] did not detect notable lateral expansion of the domains. Soon afterwards Miller and Savage [34, 44-47] conducted a series of tests, in which they used liquid electrodes of concentrated lithium fluoride solution. They found that in fields up to 1 kV/cm repolarization is chiefly the result of the lateral motion of the  $180^\circ$  walls. In some cases the entire region of the crystal beneath the electrode was repolarized by the growth of a single domain. Further studies revealed that there is also lateral growth of the domains with metallic electrodes [48].

Tests conducted later by Stadler and Zachmanidis [49, 50] in strong fields up to 450 kV/cm and in a broad temperature range showed that in this case too there is lateral motion of the 180° walls. It is noteworthy that the expanding domains have a rather regular shape, which depends on the temperature and field intensity [34, 45, 50, 51]. The results of these observations are summarized in Figure 8.6. Nakamura [52] developed a purely kinematic theory of lateral growth of antiparallel c-domains. The domain forms which he obtained coincide with the observed forms.

For the dependence of boundary velocity ( $v$ ) on the field, Miller and Savage derived the exponential law

$$v = v_{\infty} e^{-\frac{\delta}{E}} \quad (8.6)$$

Here  $\delta$  signifies the activation field and  $v_{\infty}$  the wall velocity for  $E \rightarrow \infty$ . The value  $\delta$  is sensitive to impurities and increases somewhat with the field. As seen in Figure 8.7, however,  $\delta$  varies only between 2 and 5 kV/cm as the velocity changes eight orders of magnitude. The tendency of  $\delta$  to increase with the field apparently explains the high values  $\delta = 7.8$  kV/cm (for  $v_{\infty} = 2.8 \cdot 10^4$  cm/sec) obtained by Taylor [53] with the fields of 2.5-6 kV/cm. The rate of lateral movement is extremely sensitive to temperature, and when the temperature is increased from 25 to 100°C it increases approximately four orders of magnitude. The temperature dependence is determined chiefly by the diminution of  $\delta$  with temperature [54].

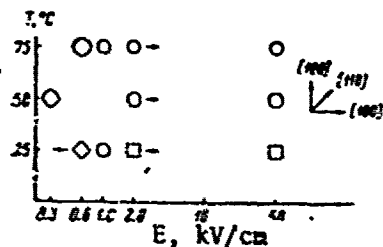


Figure 8.6. Diagram illustrating form of 180° domain in barium titanate as function of external electric field strength and temperature. To the right are directions [100] and [110]. (According to Stadler and Zachmanidis [50]).

It is noteworthy that at constant voltage wall velocity decreases approximately five-fold through the first 2,000 Å, and then remains constant [55]. Miller and Savage explained this phenomenon with the aid of the surface layer model proposed by Drougard and Landauer [56]. In the strong electric fields of 2-250 kV/cm, as demonstrated by Stadler and Zachmanidis [49], the rate of lateral motion is proportional to  $E^{1.4}$ . The effect of impurities and electrode material on the speed of the 180° domain wall was investigated [55, 48]. It was also discovered that if the field is eliminated after total repolarization a certain number of small domains may be formed with polarization antiparallel to the polarization of the crystal. This phenomenon became known as reverse switching.

The 90° domains should have an effect on the motion of the 180° walls in barium titanate monocrystals, since because of the great anisotropy of

permittivity considerable heterogeneity of the field can be expected at the point of the crystal where the a-domain intersects it. Callaby's investigations [57] showed that the a-domains can have a notable effect on the movement of the  $180^\circ$  walls only when they have sufficiently great width.

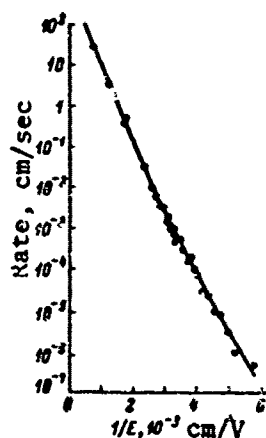


Figure 8.7. Rate of lateral motion of  $180^\circ$  wall in barium titanate as function of inverse electric field strength (according to Miller and Savage [45]).

at 550 V/cm. The reduction of velocity also depends on the field. It is greater for weak fields and smaller for strong. These results were interpreted by Callaby on the basis of his surface layer model.

The lateral motion of the  $180^\circ$  walls was observed in triglycine sulfate by Chynoweth and Abel [59] in weak electric fields of 30-35 V/cm. In these experiments liquid electrodes were used, and the domain structure after each partial repolarization was analyzed by the charged powders method. Mitsui and Furuichi observed the motion of the walls in Seignette's salt, and according to their data wall velocity  $v \sim (E - E_0)$  [39, 60].

Considerable difficulties are encountered in explaining the mechanism of lateral movement of the  $180^\circ$  walls. Since the  $180^\circ$  wall is extremely thin, its displacement parallel to itself, as indicated by estimates, is improbable [36, 15]. Therefore it is theorized that the lateral movement is apparent. In reality the nucleus of the antiparallel domain, which grows from one electrode to the other, leading to the displacement of the wall, forms near the actual  $180^\circ$  wall. It can be expected that it is easier for such nuclei to form than new domains, which are completely surrounded by the medium with antiparallel polarization, if only because the summary area of the walls of the nucleus adjacent to the old domain is less than that of the nucleus of the isolated domain.

The laws of motion of the  $180^\circ$  walls in the rhombic phase of barium titanate, as established by Callaby [58], are generally the same as in the tetragonal phase. The antiparallel domains in the rhombic phase are rectangular with walls corresponding to planes (100) and (110) (a section of the (110) type was analyzed). The dependence of the velocity of these walls on the field obeys the law (8.6) with  $v_0 = 3 \cdot 10^3$  cm/sec and  $\delta = 5.7 \cdot 10^3$  V/cm for wall (100) and with  $v_0 = 5.5 \cdot 10^2$  cm/sec and  $\delta = 4.1 \cdot 10^3$  V/cm for wall (110). As in the tetragonal phase, velocity is maximal at the initial moment and diminishes by measure of travel of the wall, reaching a constant value after passing a certain distance. The length of this path depends on the field; 70 Å at 160 V/cm and 70,000 Å

One of the first investigations of such a model was done by Drougard [61], who advanced the theory that the probability of formation of a nucleus as a protuberance on the wall of the existing antiparallel domain is proportional to the perimeter of the wall and that the nucleus, although once formed, spreads rapidly on the wall through the thickness of the crystal. This model leads to a repolarization rate proportional to domain area. It follows from the tests of Miller and Savage [45], however, that the rate of repolarization is not proportional to the area, but to the perimeter of the expanding domain, since according to their data wall velocity is not a function of domain area.

To reach agreement with the experimental data Miller and Weinreich [62] used a somewhat different model. They surmised that many nuclei form simultaneously on the wall in the form of protuberances and that their probability of formation is proportional to wall perimeter. Since many nuclei form simultaneously, each of them expands on a small portion of the wall until it reaches its neighbor. Therefore the process of repolarization is determined only by the mechanism of formation of the nuclei, which prefer the shape of plane triangles, facing the domain (Figure 8.8). With this shape the additional energy attributed to the greater total area of the domain walls is slight. Miller and Weinreich analyzed the change of energy ( $\Delta U$ ) of a crystal associated with the formation of a nucleus. They took into account the energy of spontaneous polarization of the nucleus in the electric field, the energy of newly formed domain walls and the energy of the depolarizing field. Since wall velocity ( $v$ ) is determined by the rate of formation of the nuclei due to heat fluctuations, then

$$v \sim \exp\left(-\frac{\Delta U}{kT}\right). \quad (8.7)$$

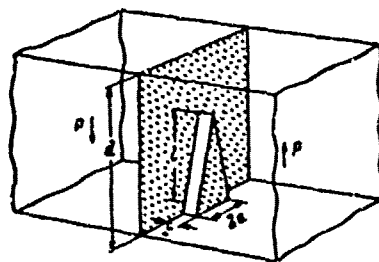


Figure 8.8. Schematic diagram of triangular nucleus on  $180^\circ$  domain wall. (According to Miller and Weinreich [62]).

The optimal nucleus dimensions  $a^*$  and  $z^*$  and activation energy  $\Delta U^*$  corresponding to them can be determined from the conditions  $\partial \Delta U / \partial a = 0$  and  $\partial \Delta U / \partial z = 0$ . Assuming nucleus thickness ( $c$ ) to be equal to one lattice constant, then when  $E = 300$  V/cm  $a^* = 3.6 \cdot 10^{-6}$  cm and  $z^* = 16 \cdot 10^{-5}$  cm.  $\Delta U^*$  depends on the thickness of the nucleus, and here the relation

$$\Delta U_n^* = n^2 \Delta U_1^* \quad (8.8)$$

is valid, where  $\Delta U_1^*$  and  $\Delta U_n^*$  are the activation energies for nuclei that are one and  $n$  lattice constants thick. Wall movement is governed in principle by the formation of nuclei of different thickness, and therefore wall velocity can be written in the form of a series:

$$v = \text{const} \sum_n \exp\left(-\frac{\Delta U_n^*}{kT} n^{3/2}\right). \quad (8.9a)$$

Since  $\Delta U_n^*$  is inversely proportional to  $E$ , then (8.9a) can be written in the form:

$$v = v_0 \sum_n \exp\left(-\frac{1}{E} n^{3/2}\right). \quad (8.9b)$$

The first term plays the principal part in weak fields, which corresponds to the formation of nuclei of one lattice constant thickness. Then the experimental exponential dependence of  $v$  on  $E$  (8.6) is obtained. The experimental  $\delta$  coincides with the theoretical if wall energy is assumed to be  $0.4 \text{ erg/cm}^2$ . Using this model it is also possible to explain the change in domain shape as a function of the field.

The formation of nuclei with  $n > 1$ , having a great energy of activation, becomes increasingly probable as the field strengthens. Possibly related to this is the experimentally observed slight increase of  $\delta$  with the field. Stadler and Zachmanidis [49] showed that when  $E > 2 \text{ kV/cm}$  series (8.9b) changes as  $E^x$ . For  $E \sim 2 \text{ kV/cm}$   $x = 1.45-1.40$ , and when  $E$  ranges from  $3 \text{ kV/cm}$  to  $450 \text{ kV/cm}$   $x = 1.36-1.34$ . This dependence of wall velocity on the field coincides satisfactorily with their experimental dependence.

Other models of the growth of antiparallel domains in barium titanate were proposed by Burfoot [63, 64], Abe [65], Nakamura [66]. Helical dislocation, spreading perpendicular to the wall, plays an important role in the  $180^\circ$  wall movement in Nakamura's model [66]. Dislocation leads to the appearance of a step on the wall, which grows in a spiral under the influence of the field, with the result that the wall shifts, remaining parallel. As shown by Miller and Weinreich [62], however, it is improbable that this mechanism operates in fields up to  $\sim 10^3 \text{ V/cm}$ .

The theory of movement of domain walls in  $\text{KH}_2\text{PO}_4$  was advanced by Schmidt [67].

### §3. Integral Characteristics of $180^\circ$ Repolarization

Now that we have become familiar with individual processes of  $180^\circ$  repolarization and their principles, established by direct observation of the change of domain structure, we will proceed to the general principles of repolarization. The pulse method proposed by Merz [36] turned out to be very fruitful in this regard.

A crystal is subjected to rectangular pulses of alternating polarity. The growth time of the pulses ( $\sim 10 \text{ nsec}$ ) is much shorter than the repolarization time, so that it may be assumed that the entire process of repolarization proceeds at constant voltage. Pulse amplitude and duration must be such as to ensure complete repolarization of the specimen. Consequently

the specimen is hooked up to a resistor, the voltage on which, proportional to the repolarization current, also known as the switching current, is observed on the oscillograph scope.

The voltage pulse and switching current pulses are depicted schematically in Figure 8.9 for voltage pulses of alternating and of the same polarity. It is obvious that if the electric field is directed along the axis of spontaneous polarization and  $180^\circ$  repolarization takes place, then the area beneath the current pulse is  $2P_s$ , converted to unit of area of the electrode. Switching time  $t_s$  and maximum switching current  $i_{\max}$  are clear from Figure 8.9. In his first investigations of barium titanate monocrystals by this method Merz obtained important results [36, 37, 68].

The dependences of  $i_{\max}$  and  $t_s$  on voltage are of the form illustrated in Figure 8.10. In fields up to 5 kV/cm the exponential law

$$i_{\max} \sim \frac{1}{t_s} - \frac{1}{t_m} e^{-\frac{t_s}{t_m}}, \quad (8.10)$$

where  $\alpha$  represents the activation field, is satisfied. According to Merz's data [36, 37]  $\alpha$  is of the order of  $10^4$  V/cm and depends on crystal thickness. Subsequent investigations yielded lower values of  $\alpha$ . Thus Drougard [61] obtained  $\alpha$  values varying from 5-10 kV/cm for various crystals of thickness  $10^{-2}$  cm; Taylor [53] obtained  $\alpha = 8.2$  kV/cm for  $10^{-1}$  cm thickness in fields of 2.5-6 kV/cm. Stadler [66] verified Merz's dependence [36] of  $\alpha$  on crystal thickness, and according to his data  $\alpha \approx 4$  kV/cm for a thickness of  $5 \cdot 10^{-2}$  cm and reaches 28 kV/cm at a thickness of  $10^{-3}$  cm, satisfying the exponential law for  $t_s$  to the field strength determined according to equation (1.4),  $(1 + \frac{0.007}{d})$  kV/cm, where  $d$  is the thickness of the crystal in cm. For thicknesses of the order of  $10^{-2}$  cm this field is approximately 2 kV/cm, which is considerably less than the 5 kV/cm found by Merz.

Drougard [61] analyzed on barium titanate crystals the dependence of the instantaneous switching current on effective polarization  $P$ , changing from  $-P_s$  to  $+P_s$ . In moderate fields the experimental results agree satisfactorily with the equation

$$i_s = Q_s \left[ 1 - \left( \frac{P}{P_s} \right)^2 \right]^{-\frac{1}{2}}, \quad (8.11)$$

where  $i_s$  is the switching current,  $P$  is polarization at any moment of time,  $Q_s$  is the total switching charge and  $\beta$  is the coefficient  $(0.4-2.3) \cdot 10^7 \text{ sec}^{-1}$

The character of the switching time as a function of the field differs in stronger fields. Merz [37] discovered in the first investigations of

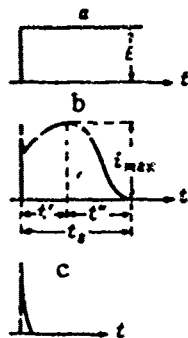


Figure 8.9. Schematic diagram of voltage and current pulses: a -- voltage pulse; b -- repolarization current pulse with voltage pulses of alternating polarity; c -- current pulse with voltage pulses of the same polarity.

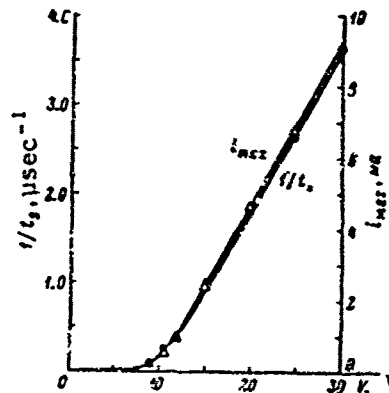


Figure 8.10. Maximum repolarization current  $i_{max}$  and inverse switching time  $1/t_s$  as functions of applied field for barium titanate mono-crystal. Specimen thickness  $(2.5-35) \cdot 10^{-3}$  cm. (Merz [36]).

repolarization that barium titanate crystals behave in strong fields like resistors, i.e., the repolarization current is linearly related to the field:

$$i_{max} \sim \frac{1}{i_{max}} = \frac{E - E_0}{\beta d} \quad (8.12)$$

where  $E_0$  is the threshold field,  $\beta$  is a constant,  $d$  is crystal thickness. In this formula  $\frac{1}{\beta} = u$  may be thought of as domain wall mobility. Hence Merz concluded that repolarization in strong fields is determined by the advance of  $180^\circ$  domains through the thickness of the crystal. Later, however, Stadler [70, 69] discovered in analogous investigations that the law

$$t_s = 9E^{-1.4}, \quad (8.13)$$

where  $E$  is given in kV/cm and  $t_s$  in sec, and where  $t_s$  is not a function of crystal thickness, is satisfactorily satisfied for the repolarization time in strong fields.

The processes of repolarization on bipolar pulses were also investigated on the crystals of other ferroelectrics: triglycine sulfate [15, 71-79], Seignette's salt [80],  $KH_2PO_4$  [81], guanidine aluminum sulfate hexahydrate [82-86], colemanite [87],  $LiH_3(SeO_3)_2$  [88, 89],  $(NH_4)HSO_4$  [90], thiourea [91], tetraethyl ammonium trichloromercurate [92]. The switching

time of all these ferroelectrics, like that of barium titanate, is an exponential function of field strength (8.10) in moderate fields, and for triglycine sulfate  $\alpha$  depends on crystal thickness according to the law  $\alpha = \alpha_0 d^{-3/2}$  [93, 94]. In strong fields the repolarization time of Seignette's salt, guanidine aluminum sulfate, colemanite and  $(\text{NH}_4)\text{HSO}_4$  depends on the field according to the law (8.12). In fields between 20 and 50 kV/cm (at room temperature) the repolarization time of triglycine sulfate is inversely proportional to the field [73] (Figure 8.11a):

$$t_s = \text{const } E^{-1} \quad (8.14)$$

and mobility increases with crystal thickness [75]. In the case of  $\text{LiH}_3(\text{SeO}_3)_2$  [89] in fields from 5 to 50 kV/cm

$$t_s = \text{const } E^{-5/2}. \quad (8.15)$$

For the area  $t_s = \text{const } E^{-3/2}$  [91] from 100 V/cm to 3 kV/cm.

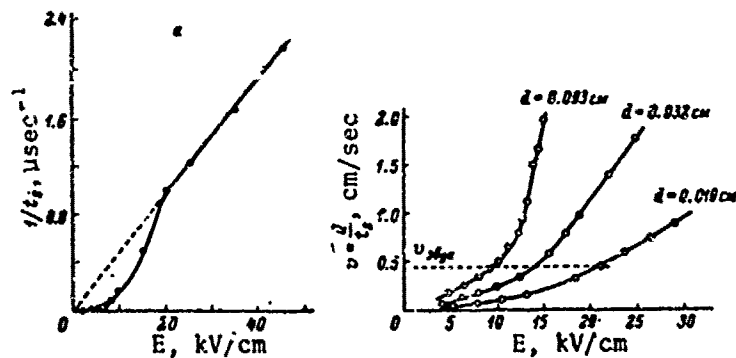


Figure 8.11. Dependences characterizing repolarization of triglycine sulfate crystals: a -- dependence of inverse repolarization time  $1/t_s$  for triglycine sulfate at room temperature (Fatuzzo and Merz [73]); b -- dependence of growth rate of domains  $v = d/t_s$  on direction of electric field at 45°C for triglycine sulfate crystals of different thickness (Binggeli and Fatuzzo [75]).

The first explanation of laws (8.10) and (8.12) of repolarization was offered by Merz [36, 37, 68], who hypothesized that the repolarization time in weak fields is determined by the time of formation of the nuclei of new antiparallel domains, and that  $t_s$  is therefore an exponential function of  $E$ , and in strong fields, by the growth time of antiparallel domains through

the crystal, hence a linear relation between  $t_s$  and the field. Later studies, particularly the discovery of lateral movement of  $180^\circ$  walls, forced re-examination of these first concepts.

The identical character of the dependence of the inverse switching time and rate of lateral wall movement on the field [formulas (8.6) and (8.7)] indicated that repolarization in moderate fields occurs chiefly by means of lateral expansion of  $180^\circ$  domains. The values of  $\alpha$  and  $\delta$  in the first experiments of Merz and Miller, of course, differed substantially, but even the  $\alpha$ -values obtained by Stadler [69] are close to the  $\delta$ -values. Taylor [53], analyzing the repolarization of barium titanate crystals with liquid electrodes in fields of 1.5-6 kV/cm, obtained practically identical values for  $\alpha$  and  $\delta$ .

Fatuzzo and Merz [73], Wieder [87], Fatuzzo [94], Wite [95] developed a model of repolarization. Fatuzzo [94] did a theoretical model calculation of current pulses during repolarization in the most general and regular form, and we will discuss the basic concepts of his model, a special case of which is the Wieder model [87]. It is theorized that the nuclei of anti-parallel domains are formed randomly on the crystal surface, as in a static process. The time  $t_n$  required for the formation of all nuclei is an exponential function of the field:

$$\frac{1}{t_n} = \frac{1}{t_0} \exp\left(-\frac{\alpha}{E}\right). \quad (8.16)$$

Each nucleus grows in the direction of the field during time  $t_d$ . The developing domain expands laterally. At the same time new nuclei are formed, grow ahead, expand, etc. The lateral movement can be real (i.e., the wall moves as a whole, parallel to itself) or apparent, but in either case the velocity of the wall is assumed to be isotropic and the domain circular in cross section. Proceeding from these assumptions Fatuzzo calculated the dependence of repolarization current on time and of repolarization time on the field. The character of both these dependences is determined by the magnitude of the parameter  $k$ . For actual lateral movement

$$k = \frac{\mu E}{R r_c}, \quad (8.17)$$

where  $\mu$  is wall mobility,  $R$  is the probability of formation of nuclei, and  $r_c$  is the radius of the nucleus.

For apparent lateral motion

$$k = 2 \frac{R^*}{R}, \quad R \sim \exp\left(-\frac{\alpha'}{E}\right), \quad R^* \sim \exp\left(-\frac{\alpha''}{E}\right), \quad (8.18)$$

where  $R$  is the probability of formation of an isolated nucleus,  $R^*$  is the probability of the formation of a nucleus next to an existing domain. In both cases the greater  $k$  the greater should be the role of lateral movement of the walls. The physical sense of  $k$  is particularly clear in the case of apparent lateral movement. Here  $k$  shows how much more readily a nucleus forms next to an existing domain than does an isolated nucleus, i.e., as if to characterize "nucleus-domain interaction." In the case  $k \gg 1$  lateral wall movement plays the chief role in the repolarization process (Wieder's conclusions [87] are valid, specifically, for this case). Fatuzzo found that when  $k \gg 1$  and the movement is real,

$$t_s \sim R^* \exp(\alpha'/E), \quad (8.19)$$

where  $\alpha' = 5\alpha''/3$ . In the case of apparent lateral movement

$$t_s \sim \exp(\bar{\alpha}/E), \quad (8.20)$$

where  $\bar{\alpha} = 2\alpha''/3 + \alpha'/3$ .

In strong fields the dependence of  $t_s$  on  $E$  according to (8.19) can be regarded as a power function, and it is close to the one observed experimentally for barium titanate and thiourea. It cannot be ruled out, therefore, that apparent lateral wall movement changes into real lateral wall movement in these crystals in a strong field. The repolarization current pulse is symmetrical for  $k \gg 1$ , i.e.,  $t' \approx t''$ . (The meaning of  $t'$  and  $t''$  is clear from Figure 8.7). This is understandable from simple qualitative considerations. If repolarization by means of lateral movement predominates, then the repolarization current is proportional to the perimeter  $l$  of the domains. When  $t = 0$ ,  $l \neq 0$  and  $i_s = 0$ , then  $i_s$  increases and passes through a maximum. Comparison of the experimental shape of pulse  $i_s$  with theoretical indicates that barium titanate and colemanite relate to the case  $k \gg 1$ . When  $k$  is not too great compared to unity and does not depend on the field, then the probabilities of formation of nuclei, both isolated and adjacent to a domain, are similar and  $\alpha' \approx \alpha''$ . In this case the dependence of  $t_s$  on the field is of exponential character:

$$t_s = \text{const} \exp \alpha'/E. \quad (8.21)$$

For  $k \approx 0$ , when the mechanism of lateral movement has practically no influence, the shape of pulse  $i_s$  is markedly asymmetrical and  $t' \approx 0$ . In this case the formation of isolated nuclei and their forward growth are the prime factors in repolarization. Consequently  $i_s$  is proportional to the rate of formation of the nuclei, and it is maximal at the beginning of the process. This obviously corresponds to guanidine aluminum sulfate

hexahydrate. Triglycine sulfate, tetramethyl ammonium trichloromercurate occupy an intermediate position, and for these compounds the best agreement between the experimental and theoretical current forms occurs respectively for  $k = 1$  and  $k = 5$ .

Judging by Strukov's data [90],  $(\text{NH}_4)\text{HSO}_4$  crystals also belong to this group. Wieder [74] noted that for triglycine sulfate Fatuzzo's model does not agree with the experiment in the case of great crystal thickness of the order of 0.5-1.0 cm. This is possibly related to the fact that in this case defects within the crystal, not taken into account in the model, have a considerable effect on the apparent lateral movement of the  $180^\circ$  walls.

The Fatuzzo and Wieder models pertain to the region of weak fields; thus, as regards strong fields, the generally accepted point of view at this time is that the repolarization time of ferroelectrics, for which the relation between the inverse repolarization time and the field is linear, is determined by the growth time of domains from one electrode to the other. The reasons for the exponential relation between  $t_s$  and the field in some of the ferroelectrics are not yet clear. In a sufficiently strong field the rate of domain wall travel may be so great as to exceed the speed of sound. Stačler [96, 49] pointed this out with respect to barium titanate, but this problem was investigated most thoroughly by Binggeli and Fatuzzo [75] on triglycine sulfate crystals.

The forward growth time of domains of triglycine sulfate at room temperature in fields greater than 20 kV/cm is greater than the time of nucleus formation. It is nearly equivalent to repolarization time, and therefore the growth rate can be determined from electric measurements. At higher temperature the field strength above which the situation occurs diminishes. The dependences of growth rate on the field, obtained by Binggeli and Fatuzzo for crystals of various thickness are presented in Figure 8.11b. It is clear from this figure, first of all, that each curve has two linear segments, corresponding to different mobilities and, secondly, the mobilities on both segments increase as crystal thickness increases. The discontinuity on the experimental curves occurs at a velocity close to the velocity of propagation of longitudinal sound waves. The authors feel that since during movement of a wall there is some deformed region near it, displacement of this region along with the wall due to internal friction causes additional energy losses, and consequently increases the "friction" for the wall itself. In the case of wall travel at supersonic velocity deformation cannot follow, i.e., the wall travels without creating distortions of the crystal lattice near it, and therefore its mobility increases. As regards the dependence of mobility on crystal thickness, then in the case of triglycine sulfate it obviously cannot be attributed to a particular surface layer, as is usually done for barium titanate. The fact is, perhaps, that as the domain grows its length increases without substantial changes in lateral dimensions, and therefore the depolarizing field, which opposes the external field, diminishes. This

leads to wall movement with acceleration. Then, the thicker the crystal the greater the average velocity and mobility determined by it.

During repolarization of ferroelectrics there are small abrupt changes in polarization, which by analogy with the same abrupt changes in magnetization of ferromagnetics, have come to be known as Barkhausen jumps. Barkhausen jumps are detected experimentally as small bursts of repolarization current. Barkhausen pulses have been analyzed chiefly during repolarization of barium titanate crystals [97-101, 44]. There are several reasons for the appearance of such pulses: a) the formation of the nucleus of an antiparallel domain; b) initial jump in the growth of such domain; c) merging of two  $180^\circ$  domain walls. Negative Barkhausen pulses correspond to the formation of small domains with polarization opposite to the direction of the field.

The history of the specimen has a considerable effect on the repolarization process. The investigations of Fatuzzo [71], Shuvalov [76-78], Tambovtsev [79] of triglycine sulfate crystals showed that if bipolar voltage pulses are applied to the specimen at different intervals i.e., one interval between pulses is greater than another, then  $i_{\max}$  and  $t_s$  for pulses of different polarity do not coincide. This phenomenon takes place in fields where the exponential law for the switching time is satisfied. Apparently the conditions of the formation of nuclei change within the interval between pulses. The greater the time between pulses, the worse the conditions become for the formation of nuclei. One of the factors that prevent the application of ferroelectrics as matrix memory elements of digital computers is the fatigue effect.

This phenomenon was discovered on barium titanate crystals [102] and amounts to a gradual reduction of the repolarized volume after several millions of repolarizations. The repolarized volume can be restored to its initial value by repolarizing the crystal after a few minutes with industrial alternating current. The investigations of Hayashi, et al [103] showed that the higher the temperature and frequency of the pulses the faster fatigue sets in. Tiny a-domains ( $\sim 10^{-4}$  cm wide) were observed on the surface of "fatigued" crystals. Hayashi and coauthors, on the basis of these experimental data, concluded that the fatigue effect is related to heating during repolarization of the region of the crystal located between the electrodes (in such experiments electrode covers part of the crystal). As a result mechanical stresses build up here, chiefly due to reduction of tetragonality compared to the surrounding parts of the crystal, and these stresses are the cause of small wedge-shaped a-domains. These domains prevent the movement of the  $180^\circ$  walls, which leads to incomplete repolarization. It should be pointed out that this explanation does not coincide with the results of Callaby's investigation [57] of the influence of a-domains on the motion of  $180^\circ$  walls. According to his estimates, a-domains of such narrow width should have no significant effect. It is noteworthy that fatigue does not occur at  $77^\circ\text{K}$  [104]. The reason for this is not known, but in any case it is not that the barium titanate crystal is

in the rhombohedral phase, since fatigue occurs at 173°K in some crystals, whereas in others it does not occur at 250°K.

Seignette's salt crystals, as a general rule, do not hold residual polarization very well, and this indicates the exceptional stability of the natural non-monodomain state. The longer the field is applied during polarization and the stronger this field, the more slowly depolarization takes place in them.

Investigation of partial repolarization produced interesting results [73, 108]. It seems that if a pulse of less duration than some critical time  $t^*$  is applied to a crystal, then it leaves behind practically no residual polarization. This phenomenon was investigated most thoroughly by Taylor [108] on triglycine sulfate crystals. He showed that time  $t^*$  decreases as field strength and temperature increase, and increases as crystal thickness increases. If a crystal can be completely repolarized by the successive discharge to the crystal of a small number of pulses of duration greater than  $t^*$ , then with pulses of duration less than  $t^*$  this can be done only by discharging a large number of pulses. When pulse duration, for example, is 6 microsec and the number of pulses is  $10^4$ , repolarization comprises only 10%, but when the number of pulses is  $10^8$  it increases to 90%. Thus there is some amount of residual polarization even with durations less than  $t^*$ , but very little. A possible explanation of the observed phenomenon consists in the fact that if the time of application of the field is less than the time required for the growth of a nucleus through the crystal, the antiparallel domain disappears after completion of the pulse under the influence of the depolarizing field.

The absence of a threshold field at which the process begins represents a considerable difference between the repolarization of ferroelectrics and remagnetization of ferromagnetics. This is evident even by the character of the dependence of repolarization time on the field in weak fields (8.10). The slow repolarization of barium titanate crystals was analyzed by Wieder [109], who established that in fields of 100-600 V/cm the amount of polarization is satisfactorily described by the equation:

$$P = 2P_s \frac{-1 \exp \frac{t}{\tau}}{1 - \exp \frac{t}{\tau}} \quad (8.22)$$

Nakamura [110] and Romanyuk and Zheidev [106] also found the dependence of polarization on time to be exponential for Seignette's salt.

Landauer, et al [4], starting with law (8.10) of repolarization, determined that the coercive field depends on the rate of increase of voltage, i.e., on its amplitude and frequency. Actually, the frequency dependence of the coercive field is observed experimentally [111-116]. Herc Borodin, et al [116] found that at frequencies of several Hertz the coercive field diminishes as the frequency increases, and then, even at higher frequencies, in accordance with theory, increases. It is noteworthy

that the coercive field of barium titanate increases as crystal thickness diminishes. The reasons for the dependence on thickness are obviously the same as for  $\alpha$  in (8.10). These dependences are usually related to the presence of surface layers.

#### §4. Repolarization of Barium Titanate Crystals in the Presence of 90° Domains

Ferroelectric crystals with not only 180° domains also become repolarized through the formation of new domains and the movement of domain boundaries, but not only 180°. The great variety of processes that occur during repolarization, their influence on each other, the dependence of the development of some of them on the initial domain structure, make it practically impossible to formulate any general theory of repolarization for this case. Analyses amount only to determination of integral characteristics of repolarization, such, for instance, as repolarization time, without any sort of model interpretation, or to a detailed experimental and theoretical analysis of individual processes and their interactions. Of all ferroelectric crystals in which may occur more than 180° repolarization, only barium titanate crystals have been analyzed. The inverse repolarization time of barium titanate in the orthorhombic and rhombohedral phases in fields of 5-12 kV/cm is a linear function of the field according to law (8.12) [7] (the field is applied in direction [100]). On transition from the tetragonal phase to the orthorhombic and from the orthorhombic to the rhombohedral the repolarization time with the same voltage jump decreases [7]. This is evidence that the more asymmetric the phase is, the easier it is for repolarization to occur. The abrupt change of repolarization time during phase transitions conforms with the abrupt reduction of the coercive field (see §1).

Of the individual aspects of repolarization the 90° motion of the walls in tetragonal barium titanate has been analyzed most thoroughly. This subject is discussed in Little's work [43], a series of works by Fousek and Brezina [117-121], and also Borodin et al [116]. Fousek and Brezina [118] examined a model of a crystal with one 90° wall, dividing two domains with spontaneous polarization parallel and perpendicular to the field. In contrast to reality, in order to simplify the calculations the wall was assumed to be parallel to the electrodes, and it was assumed that connected charges on it prior to application of the field are compensated by free charges. For a crystal with such a domain wall and lacking internal stresses the change of energy after application of an external field can be written as follows:

$$U_1 = \frac{1}{2\epsilon_0} \int_V \epsilon E^2 dV - \int_V (EP_x) dV. \quad (8.23)$$

This is valid in the assumption that the time of influence of the field is much shorter than the time required for compensation of connected charges occurring on the wall. Energy  $U_1$  depends on the location of the

domain wall in the crystal, and therefore pressure acts upon the wall. The part of the pressure caused by the presence of the second term in (8.23) changes direction in accordance with the direction of the field. The first term in (8.23) depends on the position of the wall by virtue of the fact that permittivity in the domains differs by more than one order of magnitude. The pressure attributed to this term is applied from the direction of the domain with the least permittivity, regardless of the direction of the field. Thus, when sinusoidal voltage is applied to a crystal the pressure acting on the  $90^\circ$  wall is asymmetric.

"Regenerative forces" prevent movement of the wall under the influence of pressure. They are attributed first of all to the fact that the energy of the wall, by virtue of the presence of defects, is some non-monotonic function of its location in the crystal, and secondly by the fact that during movement of the wall, on the lateral faces of the crystal, to which the spontaneous polarization of one of the domains is normal, there will occur a surface charge and the field created by it, and the energy of the crystal will increase [121]. Because of the asymmetry of the external pressure the bias loop, i.e., change of the position of the wall during the period, is also asymmetric. Actually, as borne out by observations, deviations from the equilibrium position are always greater in the direction of the domain with spontaneous polarization perpendicular to the field. Furthermore, in the same direction there is usually continuous displacement of the neutral position of the wall, around which it vibrates [118].

In the opinion of Fousek and Brezina [121], this may be related to the fact that during the time of movement of the wall the charges on the lateral facets of the crystal are compensated, and therefore the "regenerative force" is diminished. The movement of the wall is of a relaxation character and as the frequency increases its deviation decreases rapidly (Figure 8.12a). A characteristic feature is the presence of a threshold field, at which wall movement becomes notable, i.e., when its deviation exceeds  $0.5 \mu$ . As the frequency increases, the threshold field strengthens (Figure 8.12b).

When an electric field, perpendicular to spontaneous polarization, is applied to a single-domain barium titanate crystal, wedge-shaped  $90^\circ$  domains appear in the crystal, growing through the crystal, and in the case of an alternating field, oscillating within it. Analysis of the formation and growth of these domains, and also of their interaction with  $180^\circ$  domains, was conducted by Little [43] and by Fousek and Brezina [122].

As the wedge-shaped domains grow the Barkhausen jumps appear, corresponding to rotation of spontaneous polarization in volumes of  $10^{-9}$ - $10^{-7}$  cm<sup>3</sup> [123]. It has been shown experimentally that some of the jumps correspond to sudden movements of a wedge, following some lag in its growth. The Barkhausen jump also occurs when the wedge reaches the opposite boundary of the crystal and is converted into a parallelepiped. Analysis of the change in the thickness of a single a-domain in an alternating field as a function of its amplitude and frequency was conducted by Borodin, et al [116].

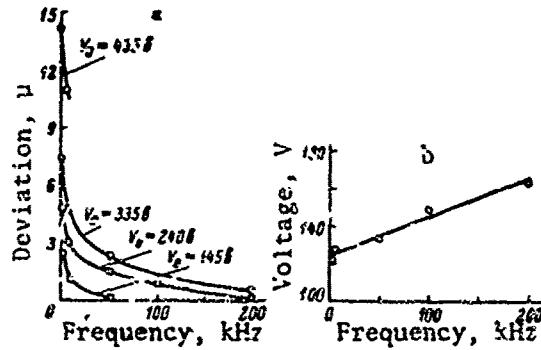


Figure 8.12. Dependences characterizing motion of  $90^\circ$  walls in barium titanate: a -- dependence of maximum deviation of wall from frequency of applied voltage at various amplitudes ( $V_0$ ); b -- frequency dependence of threshold voltage, at which wall movement becomes notable (deviation  $>0.5 \mu$ ). (According to Fousek and Brezina [121]).

### §5. Repolarization of Polycrystalline Ferroelectrics

A polycrystal consists of a set of crystals oriented in various fashion, each of which has a complex domain structure. Therefore repolarization of polycrystalline ferroelectrics is a complex process and formulation of its theory involves insurmountable difficulties. Statistical examination, of course, is possible. It is analogous to the examination made for polycrystalline ferromagnetics. Such calculations were done by Turik [124-126], who proposed distribution of domains according to coercive and internal fields and considered the chaotic distribution of the crystallographic axes of individual crystals, examining only  $180^\circ$  repolarization of the domains.

The maximum polarizations of polycrystalline ferroelectrics can be achieved when the spontaneous polarization in each crystallite acquires one of the possible directions that is closest of all to the direction of the field. These polarization values can be calculated with consideration of the symmetry of the crystal [127-133].

The experimental polarizations of ceramics, obtained from hysteresis loops, are always considerably smaller than the theoretical values. This indicates that complete recrystallization is not achieved and it is wise to assume here that the primary processes are those of  $180^\circ$  repolarization, since these processes do not involve deformation of the individual crystallites.  $90^\circ$  rotations nevertheless occur, as indicated by the character of deformation of specimens during quasistatic polarization and repolarization. According to Mason's data [134], only 10% of the possible  $90^\circ$  reorientations of tetragonal barium titanate occur in a field of 30 kV/cm. According to the data of Subbarao, et al [135], the figure is

12%, and 17% according to Beriincourt and Krueger [136], and after removal of the field the fraction of 90° reorientations decreases to 12%. In tetragonal solid solutions of  $\text{Pb}(\text{Ti}, \text{Zr})\text{O}_3$  up to 53% of the 90° reorientations are achieved, but on removal of the field the number decreases 44% [136].

Uchida and Ikeda [137] also conducted similar investigations. These researchers calculated the deformation and polarization of ferroelectric ceramics in the assumption that all domains whose direction of spontaneous polarization after reorientation makes with the direction of the field angles smaller than  $\phi_{180}$  and  $\phi_{90}$ , respectively, become repolarized in a given polarizing field. The dependences of  $\phi_{180}$  and  $\phi_{90}$  on the field were calculated according to the experimental dependences of deformation and polarization on the field. For barium titanate in a field of 20 kV/cm (30°C)  $\phi_{90} \approx 16^\circ$  and  $\phi_{180} \approx 75^\circ$ .

The amount of polarization achieved with a given electric field strength diminishes with time. So-called aging occurs, which consists in the fact that as time passes the domain walls become attached in those places where their energy is minimum. Aging also occurs in monocrystals. Specimens can be "rejuvenated," by heating them above the Curie point or by subjecting them to a strong variable electric field. The effect is strongest in the latter case, since the so-called aftereffect takes place, attributed, according to Rzhaznov [138], to the formation of some texture due to the fact that the fraction of the domains reoriented by 90° during the first cycles of field alternation, is eventually more easily repolarized 180°.

El'gard's investigations [139] verify this point of view and show that the processing of a specimen with a field parallel to the measurement field produces a substantially greater effect compared to processing in the perpendicular direction. Despite the fact that total polarization is not reached in polycrystals, the change of the parameters of the hysteresis loop (coercive field and total polarization) with temperature reflects the temperature dependence of domain wall stability. As in monocrystals, the coercive field decreases in polycrystalline barium titanate on transition to a less symmetric phase [140-143].

The repolarization of polycrystalline specimens in the pulse mode has been analyzed very little [144, 145], but there are numerous works pertaining to analysis of nonlinear electric properties. It is obvious that a ferroelectric capacitor in an electric circuit under sufficient voltage behaves like a nonlinear component. The concept of capacitance can be used to describe it, assuming capacitance to be that of a linear capacitor which has the same charge on its plates at the same voltage or, let us say, charge amplitude at the same sinusoidal voltage, equal to the amplitude of the first harmonic of the charge on the ferroelectric capacitor, etc. Capacitances will obviously differ under different conditions of equivalence. Some effective permittivities can be calculated on the basis of these

capacitances and the geometric dimensions of the ferroelectric capacitor.

Extensive investigations of this type have been carried out especially on polycrystalline perovskite. These include the works of Vul [146], Bokov [147, 142], Verbitskaya [148-150], Khodakov [151], Sinyakov, et al [153], El'gard [153-157, 139].

Usually two types of permittivity are measured -- the so-called total or normal permittivity ( $\epsilon_t$ ) and first harmonic permittivity ( $\epsilon_I$ ). The total permittivity may be defined as the permittivity of the linear capacitor ( $C_t$ ) with the geometry of the ferroelectric capacitor which at a given voltage has on its plates the same charge as the ferroelectric capacitor.  $C_t$  can be found from the hysteresis loop for any of its branches. Usually  $\epsilon_t$  is defined as the total permittivity for the main branch of the hysteresis loop.  $\epsilon_I$  can be defined as the permittivity of the linear capacitor ( $C_I$ )<sup>1</sup> with the geometry of the ferroelectric capacitor which, when sinusoidal voltage is applied to it, has on its plates a charge equal to the first harmonic component of the charge of the ferroelectric capacitor under the same voltage.

At the same electric field intensity in the case when saturation has an effect  $\epsilon_t < \epsilon_I$ . This is related to the fact that with sinusoidal voltage the change of the charge in a half-period due to saturation is of "flattened" form, and therefore the maximum charge is less than the amplitude of its first harmonic [147]. The curves of the dependence of  $\epsilon_t$  and  $\epsilon_I$  on electric field strength pass through a maximum (Figure 8.13). The path of the curves depends here on the history of the specimen. Aging plays a very important role. The highest values of  $\epsilon_t$  and  $\epsilon_I$  can be obtained after processing the specimen in a strong variable electric field, when the aftereffect has an influence. The application of a stationary field, which impedes repolarization, therefore leading to a reduction of  $\epsilon_t$  and  $\epsilon_I$ , has the greatest effect on  $\epsilon_t$  and  $\epsilon_I$  (Figure 8.14). Since  $\epsilon_t$  and  $\epsilon_I$  are determined in rather strong fields principally by repolarization processes, then, as demonstrated by Bokov [142, 147], their temperature dependence reflects the change of domain wall mobility with temperature.

Maximum  $\epsilon_t$  and  $\epsilon_I$  occur in barium titanate and solid solutions based on barium titanate after low-temperature phase transitions in the ferroelectric phase. These maxima are explained by the fact that on transition to a less symmetric phase domain wall mobility, which monotonically diminishes within each phase at low temperature, increases

---

<sup>1</sup> $C_I$  is measured on ordinary bridge instruments.

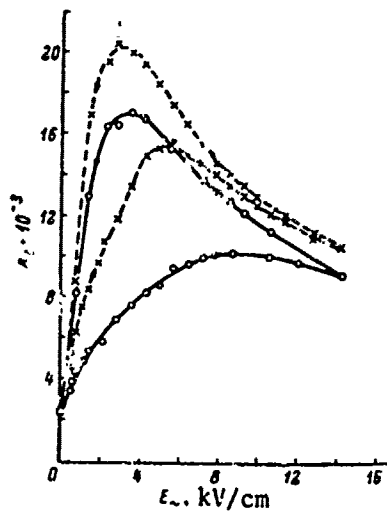


Figure 8.13. Dependence of  $\epsilon_I$  of solid solution of  $\text{Ba}_{0.9}\text{Sr}_{0.1}\text{TiO}_3$  on strength of variable electric field. Frequency 70 Hz. Electric field strength calculated according to effective voltage. Room temperature. Continuous curves correspond to measurements after aging and broken curves -- after heating above Curie point. (According to Bokov [147]).

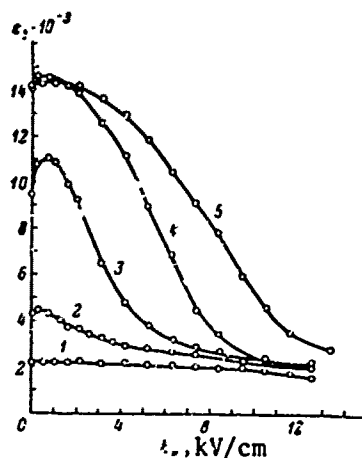


Figure 8.14. Dependence of  $\epsilon_I$  of polycrystalline barium titanate on strength of stationary biasing field for different variable field strengths. Frequency 70 Hz. Room temperature (According to Bokov [158]). 1 --  $E_{\sim} = 0.1$ ; 2 --  $E_{\sim} = 2.1$ ; 3 --  $E_{\sim} = 4.0$ ; 4 --  $E_{\sim} = 6.8$ ; 5 --  $E_{\sim} = 9.5$  kW/cm.

sharply. As the strength of the electric field increases,  $\epsilon_t$  and  $\epsilon_I$  increase quite sharply near the Curie point, where wall mobility is especially high. Here the maximum permittivity increases and is displaced toward low temperatures. Especially great displacements occur in solid solutions with "eroded" phase transition.

The displacement of maximum permittivity in this case is not related to the displacement of the Curie point. In a weak electric field, after cooling below the Curie point, the permittivity drops rapidly due to the saturation effect, related to the appearance and growth of spontaneous polarization. In a strong field repolarization processes take place and the permittivity is determined by the magnitude of spontaneous polarization and the volume within which it changes its direction. At low temperature, below the Curie point, on the one hand, spontaneous polarization increases, which should lead to an increase in the permittivity in a strong field, and on the other hand, movement of the domain walls becomes more and more difficult and, consequently, the volume within which spontaneous polarization changes direction steadily shrinks. Just below the Curie point the former process prevails and permittivity increases. As the temperature

continues to drop, reduction of the repolarizing volume begins to prevail, and this leads to lower permittivity. The stronger the field the lower the temperature at which reduction of the repolarizing volume prevails over higher spontaneous polarization. In an electric field of sufficient strength, when almost total saturation is achieved in the entire ferroelectric temperature range, the temperature dependences of  $\epsilon_t$  and  $\epsilon_y$  smooth off, the maxima during phase transitions vanish and these dependences actually follow the curve of change of spontaneous polarization with temperature.

Great nonlinearity was discovered by Smolenskiy and Isupov [159] in several solid solutions of  $\text{Ba}(\text{Ti}, \text{Sn})\text{O}_3$  and  $\text{Ba}(\text{Ti}, \text{Zr})\text{O}_3$ . The high domain wall mobility in specimens of these systems is apparently related to the small distortion of the elementary cell [159], rhombohedral symmetry of the ferroelectric phase and, for certain compounds, similarity of the two structural phase transitions and Curie points [142]. Also advanced is the viewpoint that the nonlinearity of this type of solid solutions with "eroded" phase transition near maximum  $\epsilon$  is caused by the transition of some of the crystallites under the influence of the field into the ferroelectric state [160]. Vertitskaya [148-150, 161] developed perovskite ceramics with an especially high nonlinearity. These compounds are known as varicaps.

#### BIBLIOGRAPHY

1. Sawyer, C. B. and C. H. Tauer, Phys. Rev., 35, p. 269, 1930.
2. Diamant, H., Rev. Sci. Instrum., 28, p. 30, 1957.
3. Roetschi, H., Rev. Sci. Instrum., 39, p. 152, 1962.
4. Landauer, R., D. R. Young and M. E. Drougard, J. Appl. Phys., Vol. 27, p. 752, 1956.
5. Kinase, W. and H. Takahashi, J. Phys. Soc. Japan, Vol. 12, p. 464, 1957.
6. Merz, W. J., Phys. Rev., Vol. 91, p. 513, 1953.
7. Wieder, H. H., Phys. Rev., Vol. 99, p. 1161, 1955.
8. Kanzig, W. and R. Meier, Helv. Phys. Acta, Vol. 21, p. 585, 1949.
9. Wieder, H. H., J. Appl. Phys., Vol. 26, p. 1479, 1955.
10. Merz, W. J., Phys. Rev., Vol. 81, p. 1064, 1951.
11. Hoshino, S., T. Mitsui, F. Jona and R. Pepinsky, Phys. Rev., Vol. 107, p. 1255, 1957.
12. Domanski, S., Proc. Phys. Soc., Vol. B 72, p. 306, 1958.

13. Taurel, L., *Compt. rend.*, Vol. 246, p. 70, 1958.
14. Kiyasu, Z., K. Hushimi and K. Kataoka, *J. Phys. Soc. Japan*, Vol. 13, p. 661, 1958.
15. Toyoda, H., S. Waku, H. Shibata and Y. Tanaka, *J. Phys. Soc. Japan*, Vol. 14, p. 109, 1959.
16. Triebwasser, S., *IBM J. Res. Developm.*, Vol. 2, p. 212, 1958.
17. Gonzalo, J. A., *Phys. Rev.*, Vol. 144, p. 662, 1966.
18. Strukov, B. A., *Phys. St. Sol.*, Vol. 14, K 135, 1966.
19. J. A. Gonzalo, *Phys. Rev. Lett.*, Vol. 21, p. 749, 1968.
20. Hablutzel, J., *Helv. Phys. Acta*, Vol. 12, p. 439, 1939.
21. Zheludev, I. S. and V. V. Gladkiy, *Kristallografiya* (Crystallography), Vol. 11, p. 415, 1966.
22. Koptsik, V. A. and N. D. Gavrilova, *Izv. AN S.S.R., ser. fiz.* (News of USSR Academy of Sciences, Physics Series), Vol. 79, p. 1969, 1965.
23. Gavrilova, N. D., *Kristallografiya*, Vol. 10, p. 346, 1965.
24. Cook, W. R., D. A. Berlincourt and F. Scholz, *J. Appl. Phys.*, Vol. 34, p. 1392, 1963.
25. Borodin, V. Z., L. M. Berberova, S. G. Gakh, O. P. Kramarov, L. S. Kremenchugskiy, A. F. Mal'nev, V. B. Samoylov and M. L. Sholokhovich, *Izv. AN SSSR, ser. fiz.*, Vol. 31, p. 1818, 1967.
26. Chynoweth, A. G., *J. Appl. Phys.*, Vol. 27, p. 78, 1956.
27. Miller, R. C. and A. Savage, *J. Appl. Phys.*, Vol. 30, p. 808, 1959.
28. Perls, T. A., T. J. Diesel and W. I. Dobrov, *Phys. Rev.*, Vol. 29, p. 1297, 1958.
29. Lur'ye, M. S. and I. V. Ignat'yeva, *Fizika Tverdogo Tela* (Solid State Physics), No. 1, USSR Academy of Sciences Publishing House, Moscow, p. 190, 1959.
30. Chynoweth, A. G., *Phys. Rev.*, Vol. 117, p. 1235, 1960.
31. Merz, W. J., *Phys. Rev.*, Vol. 88, p. 421, 1952.
32. Chynoweth, A. G. and J. L. Abel, *J. Appl. Phys.*, Vol. 30, p. 1615, 1959.
33. Chynoweth, A. G., *Phys. Rev.*, Vol. 113, p. 159, 1959.

34. Miller, R. C. and A. Savage, Phys. Rev., Vol. 112, p. 755, 1958.
35. Stadler, H. L. and P. J. Zachmanidis, J. Appl. Phys., Vol. 35, p. 2625, 1964.
36. Merz, W. J., Phys. Rev., Vol. 95, p. 690, 1954.
37. Merz, W. J., J. Appl. Phys., Vol. 27, p. 938, 1956.
38. Landauer, R., J. Appl. Phys., Vol. 28, p. 227, 1957.
39. Mitsui, T. and J. Furuichi, Phys. Rev., Vol. 90, p. 193, 1953.
40. Prutton, M., Proc. Phys. Soc., Vol. 72, p. 307, 1958.
41. Janovec, V., Czechosl. J. Phys., Vol. 9, p. 468, 1959.
42. Stadler, H. L., J. Appl. Phys., Vol. 37, p. 1947, 1966.
43. Little, E. A., Phys. Rev., Vol. 98, p. 978, 1955.
44. Miller, R. C., Phys. Rev., Vol. 111, p. 736, 1958.
45. Miller, R. C. and A. Savage, Phys. Rev., Vol. 115, p. 1176, 1959.
46. Miller, R., Fizika Dielektrikov (Physics of Dielectrics), USSR Academy of Sciences Publishing House, Moscow, p. 329, 1960.
47. Miller, R. C. and A. Savage, Phys. Rev. Lett., Vol. 2, p. 294, 1959.
48. Miller, R. C. and A. Savage, Phys. Rev., Vol. 31, p. 662, 1960.
49. Stadler, H. L. and P. J. Zachmanidis, J. Appl. Phys., Vol. 34, p. 3255, 1963.
50. Stadler, H. L. and P. J. Zachmanidis, J. Appl. Phys., Vol. 35, p. 2395, 1964.
51. Hisimi, K., J. Phys. Soc. Japan, Vol. 15, p. 731, 1960.
52. Nakamura, T., J. Phys. Soc. Japan, Vol. 15, p. 1579, 1960.
53. Taylor, G. W., Austral. J. Phys., Vol. 15, p. 549, 1962.
54. Savage, A. and R. C. Miller, J. Appl. Phys., Vol. 31, p. 1546, 1960.
55. Miller, R. C. and A. Savage, J. Appl. Phys., Vol. 32, p. 714, 1961.
56. Drougard, M. E. and R. Landauer, J. Appl. Phys., Vol. 30, p. 1663, 1959.

57. Callaby, D. R., J. Appl. Phys., Vol. 38, p. 431, 1967; Proc. Internat. Meet. Ferroelectr., II, Prague, p. 105, 1966.
58. Callaby, D. R., J. Appl. Phys., Vol. 36, p. 2751, 1965.
59. Chynoweth, A. G. and J. L. Abel, J. Appl. Phys., Vol. 30, p. 1073, 1959.
60. Mitsui, T. and I. Furuichi, Phys. Rev., Vol. 95, p. 558, 1954.
61. Drougard, M. E., J. Appl. Phys., Vol. 31, p. 352, 1960.
62. Miller, R. C. and G. Weinreich, Phys. Rev., Vol. 117, p. 1460, 1960.
63. Burfoot, J. C., Proc. Phys. Soc., Vol. 73, p. 641, 1959.
64. Burfoot, J. C. and R. V. Peacock, Proc. Phys. Soc., Vol. 73, p. 973, 1959.
65. Abe, R., J. Phys. Soc. Japan, Vol. 14, p. 633, 1959.
66. Nakamura, T., J. Phys. Soc. Japan, Vol. 9, p. 425, 1954.
67. Schmidt, V. H., Proc. Intern. Meet. Ferroelectr., II, Prague, p. 97, 1966.
68. Merz, W., Fizika Dielektrikov (Physics of Dielectrics), USSR Academy of Sciences Publishing House, Moscow, p. 286, 1960.
69. Stadler, H. L., J. Appl. Phys., Vol. 33, p. 3487, 1962.
70. Stadler, H. L., J. Appl. Phys., Vol. 29, p. 1485, 1958.
71. Fatuzzo, E., Helv. Phys. Acta, Vol. 31, p. 309, 1958.
72. Pulvary, C. F. and W. Kuebler, J. Appl. Phys., Vol. 29, p. 1742, 1958.
73. Fatuzzo, E. and W. J. Merz, Phys. Rev., Vol. 116, p. 61, 1959.
74. Wieder, H. H., J. Appl. Phys., Vol. 35, p. 1224, 1964.
75. Bingeli, B. and E. Fatuzzo, J. Appl. Phys., Vol. 36, p. 1431, 1965.
76. Shuvalov, L. A., Kristallografiya, Vol. 5, p. 282, 1960.
77. Shuvalov, L. A., Kristallografiya, Vol. 5, p. 409, 1960.
78. Shuvalov, L. A., Izv. AN SSSR, ser. fiz., Vol. 24, p. 1416, 1960.
79. Tambovtsev, D. A., Kristallografiya, Vol. 9, p. 511, 1964.
80. Wieder, H. H., Phys. Rev., Vol. 110, p. 29, 1958.

81. Bornarel, P., A. Fouskova, P. Guyon and J. Lajzerowica, Proc. Intern. Meet. Ferroelectr., II, Prague, p. 81, 1966.
82. Wieder, H. H., Proc. IRE, Vol. 45, p. 1094, 1957.
83. Prutton, M., Proc. Phys. Soc., Vol. B 70, p. 702, 1957.
84. Prutton, M., Proc. Phys. Soc., Vol. B 70, p. 1064, 1957.
85. Fatuzzo, E., Helv. Phys. Acta, Vol. 33, p. 429, 1960.
86. Holden, A. N., W. J. Merz, J. P. Remeika and B. T. Matthias, Phys. Rev., Vol. 101, p. 962, 1956.
87. Wieder, H. H., J. Appl. Phys., Vol. 31, p. 180, 1960.
88. Fatuzzo, E., Helv. Phys. Acta, Vol. 32, p. 302, 1959.
89. Fatuzzo, E., Helv. Phys. Acta, Vol. 33, p. 21, 1960.
90. Strukov, B. A., K. A. Mityayeva and Ye. N. Rodicheva, FTT [Fizika tverdogo tela; Solid State Physics], Vol. 6, p. 76, 1964.
91. Goldsmith, G. J. and J. G. White, J. Chem. Phys., Vol. 31, p. 1175, 1959.
92. Fatuzzo, E., Proc. Phys. Soc., Vol. 76, p. 797, 1960.
93. Sonin, A. S. and V. V. Gladkiy, Kristallografiya, Vol. 5, p. 145, 1960.
94. Fatuzzo, E., Phys. Rev., Vol. 127, p. 1999, 1962.
95. Wite, D. J., J. Appl. Phys., Vol. 32, p. 1169, 1961.
96. Stadler, H. L., J. Appl. Phys., Vol. 29, p. 1485, 1958.
97. Newton, R. P., A. I. Ahearn and L. G. McKay, Phys. Rev., Vol. 75, p. 103, 1949.
98. Kibblewhite, A. C., Proc. IEE, B 102, p. 59, 1955.
99. Chynoweth, A. G., Phys. Rev., Vol. 110, p. 1316, 1958.
100. Chynoweth, A. G., J. Appl. Phys., Vol. 30, p. 280, 1959.
101. Miller, R. C., J. Phys. Chem. Sol., Vol. 17, p. 93, 1960.
102. Merz, W. J. and J. R. Anderson, Bell. Lab. Record, Vol. 33, p. 535, 1955.

103. Hayashi, M., S. Imaizumi and R. Abe, Japan J. Appl. Phys., Vol. 3, p. 637, 1964.
104. Stadler, H. L., J. Appl. Phys., Vol. 29, p. 743, 1958.
105. Abe, R., J. Phys. Soc. Japan, Vol. 13, p. 244, 1958.
106. Romanyuk, N. A. and I. S. Zheludev, Kristallografiya, Vol. 5, p. 403, 1960.
107. Romanyuk, N. A. and I. S. Zheludev, Kristallografiya, Vol. 5, p. 904, 1960.
108. Taylor, C. W., J. Appl. Phys., Vol. 37, p. 593, 1966.
109. Wieder, H. H., J. Appl. Phys., Vol. 27, p. 413, 1956.
110. Nakamura, T., J. Phys. Soc. Japan, Vol. 12, p. 477, 1957.
111. Wieder, H. H., J. Appl. Phys., Vol. 28, p. 367, 1957.
112. Campbell, D. S., J. Electron. Contr., Vol. 3, p. 330, 1957.
113. Gurevich, V. M., I. S. Zheludev and I. S. Rez, Kristallografiya, Vol. 5, p. 802, 1960.
114. Gurevich, V. M. and I. S. Zheludev, Izv. AN SSSR, ser. fiz., Vol. 24, p. 342, 1960.
115. Brandt, A. A. and V. Ya. Shevchenko, Kristallografiya, Vol. 9, p. 292, 1964.
116. Borodin, V. Z., V. G. Kuznetsov and T. N. Lezgintseva, Izv. AN SSSR, ser. fiz., Vol. 29, p. 1982, 1968.
117. Fousek, J. and B. Brezina, Czechosl. J. Phys., Vol. 9, p. 265, 1959.
118. Fousek, J. and B. Brezina, Czechosl. J. Phys., Vol. 10, p. 511, 1960.
119. Brezina, B. and J. Fousek, FTT, Vol. 4, p. 1400, 1962.
120. Fousek, J. and B. Brezina, Izv. AN SSSR, ser. fiz., Vol. 28, p. 717, 1964.
121. Fousek, J. and B. Brezina, J. Phys. Soc. Japan, Vol. 19, p. 830, 1964.
122. Fousek, J. and B. Brezina, Czechosl. J. Phys., Vol. B 1', p. 344, 1961.
123. Brezina, N., J. Fousek and A. Glanc, Czechosl. J. Phys., Vol. B 11, p. 595, 1961.

124. Turik, A. V., FTT, Vol. 5, p. 1213, 1963.
125. Turik, A. V., FTT, Vol. 9, p. 2406, 1963.
126. Turik, A. V., FTT, Vol. 9, p. 2922, 1963.
127. Rzhhanov, A. V., Usp. Fiz. Nauk (Advances in Physical Sciences), Vol. 38, p. 486, 1949.
128. Bogdanov, S. V., B. M. Vul and M. M. Timonin, Izv. AN SSSR, ser. fiz., Vol. 21, p. 374, 1957.
129. Bogdanov, S. V., B. M. Vul and R. Ya. Razbash, Kristallografiya, Vol. 2, p. 115, 1957.
130. Shuvalov, L. A., Kristallografiya, Vol. 2, p. 119, 1957.
131. Marutake, M., J. Phys. Soc. Japan, Vol. 11, p. 807, 1956.
132. Redin, R. D., G. W. Marks and C. E. Antoniak, J. Appl. Phys., Vol. 34, p. 600, 1963.
133. Isupov, V. A., Izv. AN SSSR, ser. fiz., Vol. 31, p. 1793, 1957.
134. Mason, W. P., Phys. Rev., Vol. 74, p. 1134, 1948.
135. Subbarao, E. C., M. C. McQuarrie and W. R. Buessem, J. Appl. Phys., Vol. 28, p. 1194, 1957.
136. Berlincourt, D. and H. H. A. Krueger, J. Appl. Phys., Vol. 30, p. 1804, 1959.
137. Uchida, N. and T. Ikeda, Japan J. Appl. Phys., Vol. 6, p. 1079, 1967.
138. Rzhhanov, D. V., ZhETF [Zhurnal eksperimental'noy i teoreticheskoy fiziki; Journal of Experimental and Theoretical Physics], Vol. 19, p. 335, 1949.
139. El'gard, A. M., FTT, Vol. 4, p. 1329, 1962.
140. Smolenskiy, G. A. and K. I. Rozgachev, ZhTF [Zhurnal tekhnicheskoy fiziki; Journal of Technical Physics], Vol. 24, p. 1751, 1954.
141. Marks, G. W., D. L. Waidelich and L. A. Meuson, Communication and Electronics, No. 26 (No. 25), p. 469, 1956.
142. Bokov, V. A., Izv. AN SSSR, ser. fiz., Vol. 21, p. 382, 1957.
143. Bokov, V. A., ZhTF, Vol. 28, p. 77, 1958.

144. Verbitskaya, T. N., L. M. Aleksandrova, A. S. Sokolova, N. I. Zhuravleva, E. B. Rayevskaya, Ye. I. Shirobokova and V. V. Filippov, Izv. AN SSSR, ser. fiz., Vol. 31, p. 1853, 1967.
145. Taylor, G. W., J. Appl. Phys., Vol. 38, p. 697, 1967.
146. Vul, B. M. and I. M. Gol'dman, DAN SSSR (Reports of USSR Academy of Sciences), Vol. 49, p. 179, 1945.
147. Bokov, V. A., ZhT, Vol. 26, p. 1902, 1956.
148. Verbitskaya, T. N., DAN SSSR, Vol. 100, p. 29, 1955.
149. Verbitskaya, T. N., Izv. AN SSSR, ser. fiz., Vol. 20, p. 185, 1956.
150. Verbitskaya, T. N., Elektrichestvo (Electricity), No. 6, p. 90, 1956.
151. Khodakov, A. L., ZhTF, Vol. 26, p. 51, 1956.
152. Sinyakov, Ye. V. and V. V. Gal'perin, ZhETF, Vol. 30, p. 675, 1956.
153. El'gard, A. M., FTT, Vol. 3, p. 1485, 1961.
154. El'gard, A. M., FTT, Vol. 3, p. 1515, 1961.
155. El'gard, A. M., FTT, Vol. 4, p. 1312, 1962.
156. El'gard, A. M., Izv. AN SSSR, ser. fiz., Vol. 29, p. 2076, 1965.
157. El'gard, A. M., Izv. AN SSSR, ser. fiz., Vol. 29, p. 2079, 1965.
158. Bokov, V. A., Candidate Dissertation, Institute of Crystallography, USSR Academy of Science, Moscow, 1958.
159. Smolenskiy, G. A. and V. A. Isupov, ZhTF, Vol. 24, p. 1375, 1954.
160. Diamond, H., J. Appl. Phys., Vol. 32, p. 909, 1961.
161. Verbitskaya, T. N., Segnetoelektriki (Ferroelectrics), Rostov State University Publishing House, p. 209, 1968.

## CHAPTER 9. PERMITTIVITY

### §1. Dependence of Permittivity on Temperature

Examination of the behavior of ferroelectrics in the phase transition region from the point of view of thermodynamics indicates that permittivity above the Curie point, measured in a weak electric field along the ferroelectric axis, i.e., the axis on which may occur spontaneous polarization, should obey the Curie-Weiss law:

$$\epsilon = \frac{C/4\pi}{T - \theta}. \quad (9.1)$$

Since usually  $\epsilon \gg 1$  and, thus,  $\epsilon \approx 4\pi\chi$ , then

$$\chi = \frac{C}{T - \theta}. \quad (9.2)$$

The temperature dependences of inverse susceptibility for first and second order transitions are presented in Figure 1.1. For the first order transition  $\theta < T_c$  and permittivity is discontinuous at the point of transition. In the case of the second order transition  $\theta = T_c$  and permittivity is theoretically infinite at the Curie point. The inverse permittivity ( $1/\epsilon$ ) below  $T_c$  in this case is a linear function of temperature with an angular coefficient two times greater in absolute value than in the paraelectric phase (the so-called "pair law"). These derivations of thermodynamic theory are valid for the case of a mechanically free crystal ( $\sigma = 0$ ) and for isothermic permittivity  $\chi^T(\epsilon^T)$ , i.e., for susceptibility, the magnitude of which is determined in such a way that the temperature of the crystal remains constant during the measurement process. In many cases the latter condition is very important, since measurements are usually made at such frequencies that changes in the temperature of the crystal, which are usually the result of the electrocaloric effect, cannot be compensated by heat transfer from the ambient medium and, thus, the adiabatic dielectric susceptibility  $\chi^S(\epsilon^S)$  is measured.

Following [1-4], we will calculate the difference between  $\chi^T$  and  $\chi^T$  for ferroelectrics with the second order phase transition. Assuming  $E = E(T, S, P)$  we may express  $dE$  through the partial derivatives and, assuming  $dS = 0$ , readily obtain

$$\left(\frac{\partial E}{\partial P}\right)_S = \left(\frac{\partial E}{\partial P}\right)_T + \left(\frac{\partial E}{\partial T}\right)_P \cdot \left(\frac{\partial T}{\partial P}\right)_S. \quad (9.3)$$

For the differential of elastic enthalpy  $H = U + \sigma u$  in the case of a mechanically free crystal we have

$$dH = T dS + E dP. \quad (9.4)$$

Hence

$$\begin{aligned} T &= \left(\frac{\partial H}{\partial S}\right)_P, \quad E = \left(\frac{\partial H}{\partial P}\right)_S \\ \left(\frac{\partial T}{\partial P}\right)_S &= \left(\frac{\partial E}{\partial S}\right)_P. \end{aligned} \quad (9.5)$$

The right hand side of (9.5) can be written in the form

$$\left(\frac{\partial E}{\partial S}\right)_P = \frac{\left(\frac{\partial E}{\partial T}\right)_P}{\left(\frac{\partial S}{\partial T}\right)_P}. \quad (9.6)$$

Recalling (9.5) and (9.6), (9.3) acquires the form

$$\left(\frac{\partial E}{\partial P}\right)_S = \left(\frac{\partial E}{\partial P}\right)_T + \frac{\left(\frac{\partial E}{\partial T}\right)_P}{\left(\frac{\partial S}{\partial T}\right)_P} \quad (9.7)$$

or

$$\frac{1}{\epsilon^0} = \frac{1}{\epsilon^T} + \frac{T}{c_p} \left(\frac{\partial \epsilon}{\partial T}\right)_P, \quad (9.8)$$

where  $c_p$  is heat capacity at constant polarization. Now we will turn to equation (3.8a) and recall that  $\alpha = \alpha_0(T - \theta) = \frac{2\pi}{C}(T - \theta)$ . Differentiating (3.8a) with respect to  $T$ , we obtain

$$\left(\frac{\partial \epsilon}{\partial T}\right)_P = \frac{4\pi}{C} P. \quad (9.9)$$

Substituting (9.9) into (9.8), we obtain:

$$\frac{1}{\chi^2} = \frac{1}{\chi^2} + \frac{16\pi^2}{C^2} \cdot \frac{T}{c_p} P_s^2. \quad (9.10)$$

Differentiating (3.8a) with respect we P, we obtain

$$\frac{1}{\chi^2} = \left(\frac{\partial \chi}{\partial P}\right)_T = \frac{4\pi(T-\theta)}{C} + 6\pi P_s. \quad (9.11)$$

Substituting this expression for  $1/\chi T$  into (9.10), we have:

$$\frac{1}{\chi^2} = \frac{4\pi(T-\theta)}{C} + 6\pi P_s + \frac{16\pi^2 T}{C^2 c_p} P_s^2. \quad (9.12)$$

Since  $\epsilon \approx 4\pi\chi$ , then

$$\frac{1}{\epsilon^2} = \frac{T-\theta}{C} + \left(\frac{6\pi}{4\pi} + \frac{4\pi}{C^2} \cdot \frac{T}{c_p}\right) P_s^2. \quad (9.13)$$

If the measurements are made in the same field, then above the Curie point polarization will be extremely small and the terms that are functions of polarization in (9.10), (9.11) and (9.13) can be discarded. Therefore

$$\frac{1}{\epsilon^2} = \frac{1}{\epsilon^2} = \frac{T-\theta}{C}. \quad (9.14)$$

Thus, the difference between the adiabatic and isothermic permittivity is negligible and both obey the Curie-Weiss law. Below the Curie point, thanks to spontaneous polarization  $P_s$ , the correction for adiabaticity in (9.10) may become substantial. We will examine the deviation of angular coefficients of the dependence  $\frac{1}{\epsilon^2}(T)$  above and below the Curie point. Expression (3.9a) for  $P_s^2$  after substitution of  $\alpha_0'$  by  $\frac{2\pi}{C}$  acquires the form

$$P_s^2 = \frac{2\pi(\theta-T)}{C^2}. \quad (9.15)$$

Substituting this expression for  $P_s^2$  into (9.13) we obtain:

$$\frac{1}{\epsilon^2} = \frac{2(T-\theta)}{C} \left(1 + \frac{4\pi^2}{C^2} \cdot \frac{T}{c_p}\right). \quad (9.16)$$

Differentiating (9.16) with respect to T:

$$\frac{\partial}{\partial T} \left( \frac{1}{\epsilon} \right)_{T < T_c} = -\frac{2}{C} \left[ 1 + \frac{4\pi T}{C\epsilon_0 \epsilon} (2 - \frac{0}{T}) \right]. \quad (9.17)$$

From (9.17), recalling (9.14), we obtain for the ratio of the slopes of inverse susceptibilities for  $T \approx \theta$ :

$$\frac{\frac{\partial}{\partial T} \left( \frac{1}{\epsilon} \right)_{T < T_c}}{\frac{\partial}{\partial T} \left( \frac{1}{\epsilon} \right)_{T > T_c}} = -2 \left( 1 + \frac{4\pi T}{C\epsilon_0 \epsilon} \right). \quad (9.18)$$

Consideration of the correction for adiabaticity gives, for instance, for triglycine sulfate, a theoretical ratio of angular coefficients equal to 2.4, which agrees satisfactorily with experimental values [4, 5]. The adiabatic correction is also large in the case of calcite, where it is of the order of 38% [3].

It must be emphasized once again that it follows from thermodynamic theory that permittivity is maximum only on the axis of spontaneous polarization, i.e., the axis of the paraelectric phase on which spontaneous polarization can occur. All the relations which we derived above for dielectric susceptibility and permittivity are valid for a mechanically free crystal ( $\sigma = 0$ ). Since crystals in the ferroelectric phase (more precise, each domain) always display the piezoelectric effect, and some ferroelectrics are piezoelectrics even above the Curie point, it must be borne in mind that for piezoelectrics the difference between permittivities measured at constant voltages and constant deformation may be very great.

If a crystal is freely deformed during measurements, then at electric field frequencies less than the frequency of mechanical resonance, the free permittivity ( $\epsilon_0$ ) will be measured. At frequencies above the frequency of mechanical resonance deformation of the crystal due to inertia will not be able to follow the field, and therefore the clamped permittivity ( $\epsilon''$ ) will be measured. The difference between these permittivities will depend on the piezoelectric-moduli and elastic rigidity constants:

$$\epsilon''_j - \epsilon_0^j = -4\pi d_{ik} d_{jmn} \frac{E_i E_n}{c_{klmn}} \quad (9.19)$$

where  $d_{ikl}$  and  $d_{jmn}$  are the tensor components of the piezoelectric-moduli and  $c_{klmn}^E$  are the tensor components of the elastic rigidity constants.

One of the most characteristic representatives of ferroelectrics with the second order phase transition is triglycine sulfate. The

<sup>1</sup>The derivation of this relation is given, for example, in [6].

temperature dependence of the permittivity of triglycine sulfate, measured in three crystallographic directions, is presented in Figure 9.1, and the temperature dependence of  $1/\epsilon_b$  is shown in Figure 9.2. As seen in

Figure 9.1, permittivity is low on the a and c axes and has no anomaly at the Curie point. Permittivity on the axis of spontaneous polarization ( $\epsilon_b$ ) strictly obeys the Curie-Weiss law. The extremely rigorous investigations of Gonzaio [5] and Craig [8] of the behavior of  $\epsilon$  near the Curie point showed that in the paraelectric region deviations from this law occur only when there are only a few hundredths of a degree to the Curie point. No temperature hysteresis is noted. The Curie constant is  $3.56 \cdot 10^3$  [5]. The maximum permittivity of triglycine sulfate is of the order of  $10^5$ , and Sekido and Mitsui [9] found that  $\epsilon_b \text{ max}$  increases as crystal thickness increases. They explained this dependence by the presence of a surface layer  $1.5 \cdot 10^{-6}$  cm thick with a low permittivity.

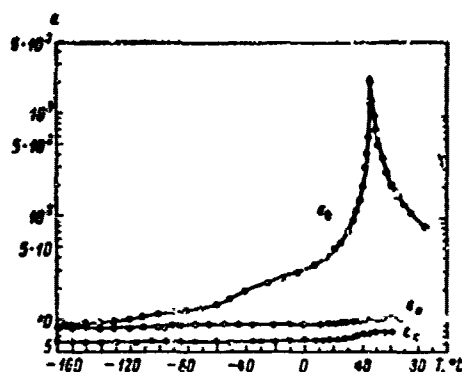


Figure 9.1. Temperature dependence of permittivity of triglycine sulfate crystal (According to Hoshino, et al [7]).

The permittivity of  $\text{KH}_2\text{PO}_4$  on the axis of spontaneous polarization ( $\epsilon_c$ ) reaches  $10^5$  (Figure 9.3), but the spontaneous polarization of this compound is also reflected by permittivity in the nonpolar direction ( $\epsilon_a$ ). Starting at the Curie point,  $\epsilon_a$  diminishes rapidly as the temperature falls. For  $\epsilon_c$  in the interval  $50^\circ$  above the Curie point the Curie-Weiss law (9.1) is satisfied with  $C = 3.25 \cdot 10^3 \text{ deg}$  [11]. Potassium dihydrophosphate is also a piezoelectric material above the Curie point, and therefore the behavior of the clamped permittivity can be studied during measurements on frequencies above the piezoelectric frequency in the paraelectric region. In this case the Curie-Weiss law is also valid with the same Curie constant, but with  $\theta$   $4^\circ$  lower than that of the free crystal [11]. The fact that the Curie constant does not change indicates that the difference between the inverse free and clamped permittivities is independent of temperature.

Seignette's salt occupies a special position among ferroelectrics with the second order phase transition, since it has two Curie points, one

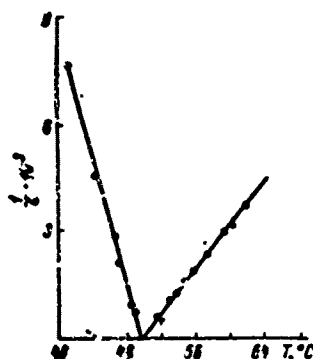


Figure 9.2. Temperature dependence of  $1/\epsilon_b$  of triglycine sulfate crystal (According to Triebwasser [4]).

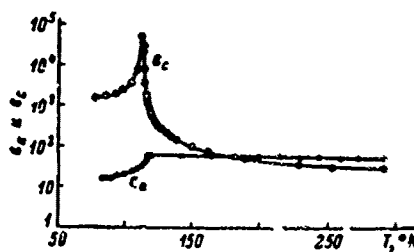


Figure 9.3. Temperature dependence of permittivity of  $\text{KH}_2\text{PO}_4$  crystal. Frequency 800 Hz,  $E_{\sim} = 200$  W/cm. (According to Busch [10]).

at  $+24^\circ$  and one at  $-18^\circ\text{C}$ . Permittivity has an anomaly only on the ferroelectric axis  $a$  ( $\epsilon_a$ ) (Figure 9.4).  $\epsilon_b$  and  $\epsilon_c$  are small and depend little on temperature. Between 25 and  $32^\circ\text{C}$   $\epsilon_a$  obeys the Curie-Weiss law with  $C = 2.24 \cdot 10^3$  deg and  $\theta = 23.0 \pm 0.5^\circ\text{C}$ , but between 34 and  $50^\circ\text{C}$  the constants are different:  $C = 1.71 \cdot 10^3$  deg and  $\theta = 25.3 \pm 0.05^\circ\text{C}$ . Below the lower Curie point in the  $-18$  to  $-28^\circ\text{C}$  interval the Curie-Weiss law is satisfied less precisely [8]. At frequencies above the piezoelectric resonance frequency in the ferroelectric regions the Curie-Weiss law is also satisfied with the same Curie constants as in the case of a mechanically free crystal.

Thus, as in the case of  $\text{KH}_2\text{PO}_4$ , the difference between the inverse permittivities of mechanically clamped and free crystals does not depend on temperature. In the case of the clamped crystal  $\theta$  decreases for the upper transition and increases for the lower. Here the transition points nearly coincide. This is evidence that spontaneous polarization would not occur in an absolutely clamped crystal [13]. In deuterated Seignette's salt convergence of the Curie points leads simply to a narrowing of the temperature range in which spontaneous polarization exists.

Of the ferroelectrics with the first order phase transition, we will examine here only the behavior of the permittivity of barium titanate. Above the Curie point barium titanate is cubic, and consequently isotropic. Therefore the anomaly of permittivity at the Curie point occurs in any direction. Above the transition temperature the Curie-Weiss law is satisfactorily obeyed. The Curie constant, according to various researchers [14-18], varies in rather broad limits. Apparently the most correct data were obtained on monocrystals by Merz [17] and Drougard and Young [18]. According to Merz  $C = 1.56 \cdot 10^5$  deg, and according to Drougard and Young  $C = 1.73 \cdot 10^5$  deg.  $\theta$  in the Curie-Weiss law is approximately  $10^\circ$  below the Curie point [18].

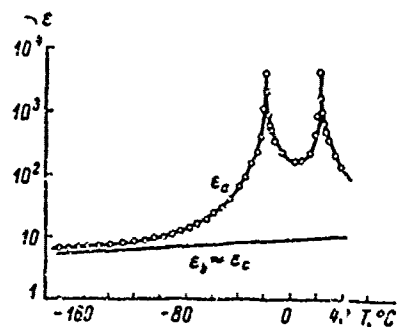


Figure 9.4. Temperature dependence of permittivity of Seignette's salt crystal. Frequency 1 kHz.  $\epsilon_a$  from  $-40^\circ\text{C}$  to  $+45^\circ\text{C}$  measured for  $E = 4$  V/cm. (According to Hablutzel [12]).

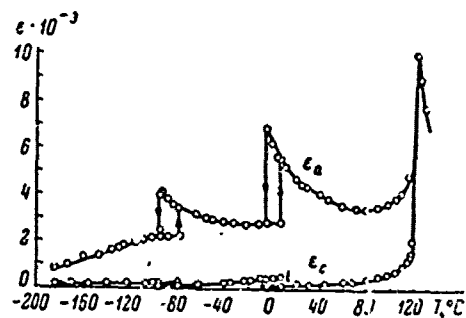


Figure 9.5. Temperature dependence of permittivity of barium titanate crystal (according to Merz [21]).

Permittivity drops sharply at the Curie point ( $120^\circ\text{C}$ ), and here temperature hysteresis is observed [18-20], which amounts to about  $2^\circ$  in monocrystals [18]. The sharp drop of permittivity at the Curie point, presence of temperature hysteresis and the fact that  $\theta < T_c$ , all agree with the derivations of thermodynamic theory for the first order phase transition. In the tetragonal phase of the ferroelectric region, as seen in Figure 9.5, permittivity is very anisotropic, and in contrast to triglycine sulfate,  $\text{KH}_2\text{PO}_4$  and Seignette's salt, the permittivity on the polar axis is much smaller than in the perpendicular directions. Drougard and Young [22] demonstrated that  $\epsilon_c$  at frequencies below the piezoelectric resonance frequency depend substantially on whether or not the crystal is single-domain or is divided into antiparallel domains. In the former case the free permittivity is measured and  $\epsilon_c \approx 200$ . In the latter case the piezoelectric deformation of adjacent antiparallel domains has different signs, which inhibits their deformation in the direction of the thickness of the crystal. Therefore the permittivity of a crystal "clamped with respect to thickness" is actually measured and  $\epsilon_c \approx 160$ .

The curves in Figure 9.5 were plotted for crystals, one of which in the tetragonal phase was a-domain, and the other c-domain. On transition to the rhombic and rhombohedral phases the domain structure becomes more complex and the reduced permittivities in no way correspond to definite crystallographic directions. The fact that different values of  $\epsilon$  are obtained in the rhombic phase for different crystals is attributed to the substantial difference in their domain structures. In the rhombohedral phase the character of the domain structure should have no effect on  $\epsilon$ , and for this reason it was long unclear why  $\epsilon$  varies from crystal to crystal. Doubts were even expressed concerning the rhombohedral symmetry of this phase [23]. The investigations of Sawaguchi and Charters [24],

however, proved that the scattering of permittivity values is a result of the effect of squeezing of domains [25].

In the ferroelectric region, even in a very weak electric field, the domain walls may be shifted somewhat, and therefore polarization of the crystal may change as a result of reorientation of spontaneous polarization in some small volume. This part of polarization is known as orientation polarization ( $P_{or}$ ), and the orientation not related to movement of the domain walls and attributed only to the processes of elastic electron and ion displacements, can be called induced polarization ( $P_i$ ). Thus, for summary polarization  $P$  we have

$$P = P_i + P_{or}. \quad (9.20)$$

Since usually  $\epsilon \gg 1$ , permittivity may be written in the form of the sum

$$\epsilon = \epsilon_i + \epsilon_{or}. \quad (9.21)$$

$P_{or}$  can be reduced to zero if a sufficiently strong stationary field is applied and the crystal is made single-domain. The greater the summary area of the domain walls, other conditions being equal, the greater  $\epsilon_{or}$  should be. Therefore, for instance, one might expect that in the case of polycrystalline barium titanate  $\epsilon_{or}$  will comprise a very large part of the summary permittivity.

Several facts indicate that this is the case: 1) dielectric losses in the ferroelectric phase are much greater than in the paraelectric phase; 2) when a strong constant field is applied the permittivity and losses drop sharply; 3) permittivity and losses diminish with time and aging occurs. In order to determine experimentally  $\epsilon_{or}$  of a polycrystal the orientation processes would have to be excluded and  $\epsilon_i$  measured rather accurately. This is difficult to do, however, since in the case of the application of a constant field  $\epsilon_i$  may also diminish as a result of 90° reorientation of the domains in the biasing field (see §2). It is very difficult to calculate  $\epsilon_i$  of a polycrystal with sufficient accuracy.

Marutake [26], using Bruggeman's equation [27] for the permittivity of a polycrystal consisting of piezoelectric crystallites, calculated  $\epsilon$  for ceramic barium titanate according to data for a monocystal. He obtained  $\epsilon = 2,500$ . This is substantially higher than the values usually obtained at room temperature ( $\epsilon = 1,500-2,000$ ). Therefore the calculation was also done with consideration of the piezoelectric effect, and each crystallite was assumed to be single-domain and spherical [26]. In this

case the answer was  $\epsilon = 1,500$ . The assumptions made during the calculation are so coarse that serious attention cannot be accorded the agreement with the experimental value.

Turik [28], who used a crystallite with a regular  $90^\circ$  domain structure and employed the permittivity tensors calculated by Lezgintseva [29] for a crystal with the same domain structure, also calculated  $\epsilon$ . Generalizing Odelevskiy's equation for the permittivity of a double-phase heterogeneous mixture for a multiphase system and assuming the distribution of crystallites with respect to position in the space of their crystalline axes to be equally probable, Turik obtained satisfactory agreement between the theoretical and experimental permittivities for the tetragonal phase.

Orientation polarization was completely ignored in both these calculations, although judging by the reduced permittivity as a result of aging, its contribution amounts to 10-20%. Analysis of the dependence of the permittivity of polycrystalline barium titanate on the amplitude of a variable field shows that from 100 V/cm and below the permittivity and losses are practically independent of field strength [31]. This indicates that certain reversible displacements of the domain walls take place. The question arises concerning the mechanisms of depolarization in weak fields. No definite answer has been found, although there is an opinion that movement of the  $90^\circ$  walls is the chief contributor [32].

Estimates made on the basis of experimental data on the movement of  $90^\circ$  walls in monocrystals indicated that their reversible displacements may produce an additive to permittivity not exceeding 200 [33]. Since the losses are governed chiefly by movement of the domain walls, the change of their mobility with temperature within the limits of a single phase and during low-temperature phase transitions should be reflected substantially on the temperature curve of losses. Actually, Bokov [34] showed that the experimental temperature dependences of  $\tan \delta$  of polycrystalline barium titanate in solid solutions based on it can be explained qualitatively proceeding from the temperature dependence of domain wall mobility. On transition from the paraelectric phase to the ferroelectric phase  $\tan \delta$  increases sharply due to the appearance of  $P_{or}$  and great losses associated with it. As the temperature falls the part of the volume of the crystal in which the direction of spontaneous polarization changes diminishes and  $\tan \delta$  decreases.

On transition from the tetragonal phase to rhombic and from rhombic to rhombohedral domain wall mobility increases (this is valid not only for monocrystals, but also for ceramics [35-38]), and consequently  $P_{or}$  increases. The increase of  $P_{or}$  leads to a sharp increase in  $\tan \delta$ , which then decreases as the temperature drops and as  $P_{or}$  decreases. Thus,  $\tan \delta$  passes through maxima in all phase transitions (Figure 9.6). In the rhombohedral phase, as a rule,  $\tan \delta$  has a broad maximum, which is displaced toward high temperatures when the frequency is increased [39]. There is no doubt that this maximum is also attributable to orientation

polarization. As a result of the larger share of orientation polarization during transition from the tetragonal phase to rhombic and from rhombic to rhombohedral, none of the sudden changes in permittivity that might be expected judging by the behavior of the permittivity of the monocrystal (Figure 9.5) occur in ceramics during these transitions. The application of a strong stationary field considerably reduces losses, and there are no anomalies in  $\tan \delta$  during the phase transitions (Figure 9.6). In the rhombohedral phase, of course, losses remain high, and this apparently indicates that in this case too there are some oscillations of the domain walls.

It should be pointed out that polycrystalline barium titanate with granularity less than 1 micron displays an exceptionally high permittivity of 3,000-3,500 [40-43]. Two explanations have been offered for such high values of  $\epsilon$ . The authors proceed from the fact that at such small crystallite dimensions each of them should be single-domain. The first explanation, advanced by Kniekamp and Heywang [40-42], and later examined in greater detail by Goswami et al [44], is based on the fact that due to the absence of domain structure a depolarizing field acts on the crystallites, diminishing the effect of saturation, which leads to higher permittivity.

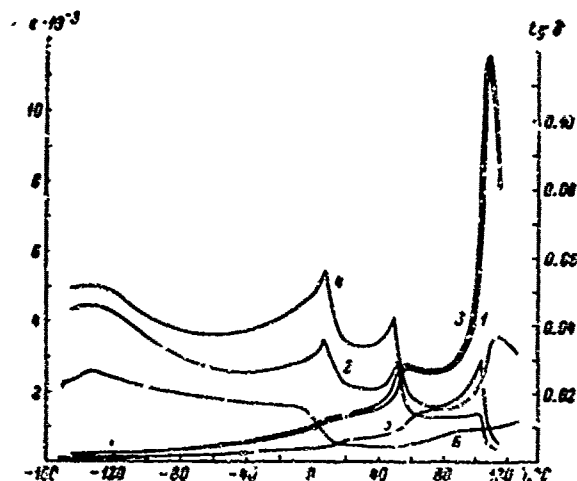


Figure 9.6. Temperature dependence of permittivity and  $\tan \delta$  of solid solution of  $\text{BaTi}_{0.95}\text{Zr}_{0.05}\text{O}_3$  in variable and stationary fields of different strengths. Frequency 1 kHz. (Bokov [39]). 1 --  $\epsilon$  for  $E_{\parallel} = 3$  V/cm,  $E_{\perp} = 0$ ; 2 --  $\tan \delta$  for  $E_{\parallel} = 3$  V/cm,  $E_{\perp} = 0$ ; 3 --  $\epsilon$  for  $E_{\parallel} = 24$  V/cm,  $E_{\perp} = 0$ ; 4 --  $\tan \delta$  for  $E_{\parallel} = 24$  V/cm,  $E_{\perp} = 0$ ; 5 --  $\epsilon$  for  $E_{\parallel} = 24$  V/cm,  $E_{\perp} = 18$  kV/cm; 6 --  $\tan \delta$  for  $E_{\parallel} = 24$  V/cm,  $E_{\perp} = 18$  kV/cm.

The most serious objection against such interpretation is: why is the depolarizing field not compensated by free charges that can migrate to

boundaries of the crystallites due to the electrical conductivity of the matter itself? In the second explanation, advanced by Buessem et al [45], it is assumed that because of the absence of 90° domain walls in the tetragonal phase strong mechanical stresses from the environment act on each crystallite: compressive stresses on the c axis and tensile stresses on the a axis. According to thermodynamic theory, such stresses lead to an increase in permittivity.

The contribution of orientation polarization to permittivity and losses can also be substantial in the case of triglycine sulfate mono-crystals [46]. Fousek and Janousek [47] analyzed the dependence of  $\epsilon$  and losses on the summary polarization of a crystal, which changed by degrees from  $+P_s$  to  $-P_s$ . The permittivity and losses were maximum in the region  $P = 0$ , where one might expect maximum summary area of domain walls. The value of  $\epsilon_{or}$  here is extremely high, amounting to 70-80 at a frequency of 1 kHz. Hence the great scattering of the values of  $\epsilon$  obtained by various researchers [7, 48, 49] is understandable.  $\epsilon_{or}$  and losses in triglycine sulfate depend strongly on frequency. Here there are two regions of dispersion: one up to  $\sim 10^4$  Hz and the other at approximately  $10^6$  Hz. It is assumed that the high-frequency component of  $\epsilon_{or}$  is related to vibration of the domain walls attached to defects, and the low-frequency component is attributed to vibrations of the walls that continually migrate during the aging process, and diminishes with the passing of time.  $\epsilon_{or}$  of triglycine sulfate varies with temperature. It is noteworthy here that at  $-80^\circ\text{C}$  there is a maximum, the position of which depends on frequency [50].

Bornarel et al [51] noted the important contribution of orientation processes to the permittivity and losses of  $\text{KH}_2\text{PO}_4$  crystals.

## 52. Nonlinear Properties in Paraelectric Region

Polarization of ferroelectrics in a weak electric field was examined in the preceding section. We will now examine the effect of strong electric fields on the polarization of ferroelectrics. The dependence of the polarization of all dielectric materials on the field is, generally speaking, nonlinear and can be written in the form of an expansion in terms of the powers of E. If the field is applied in the direction of the principal axis, so that polarization is parallel to the field, then for centrosymmetric crystals

$$P = \epsilon E + cE^3 + \dots \quad (9.22)$$

and for non-centrosymmetric

$$P = aE + bE^2 + cE^3 + \dots \quad (9.23)$$

Hence, for permittivity we have, respectively:

$$\epsilon = 1 + 4\pi(\alpha + 3\epsilon E^2 + \dots), \quad (9.24a)$$

$$\epsilon = 1 + 4\pi(\alpha + 2\beta E + 3\gamma E^2 + \dots), \quad (9.24b)$$

The nonlinearity of the dependence of polarization on field strength of practically all dielectric materials is impossible to detect all the way up to break-through fields, but the fact that it does exist is shown by the electro-optic effect. Most ferroelectrics have high permittivity. Consequently, roughly speaking, ions in the crystal lattice are displaced under the influence of the electric field for such comparatively great distances that the nonlinear dependence of displacement and consequently of polarization on electric field strength, becomes substantial. We are speaking here, of course, of induced polarization, not involving displacement of domain walls.

We will examine the nonlinear properties of ferroelectric materials in the paraelectric and ferroelectric phases individually.

In the paraelectric phase the relation between polarization and field strength is expressed by formula (3.20), whence coefficient  $\beta$  in the expansion of thermodynamic potential (3.7) can be determined on the basis of experimental data.  $\beta$  should be positive for second order phase transitions and negative for first order phase transitions.

Joseph and Silverman [52], proceeding from the Born-Karman dynamic theory of the crystal lattice, theoretically analyzed problems of nonlinearity in the paraelectric region and derived the relations between the field and polarization, analogous to (3.8a). As demonstrated, with consideration of only the first two terms in (3.7) the dependences of isothermic and adiabatic susceptibilities on polarization are determined by relations (9.11) and (9.12), respectively. The experimental determination of these dependences makes it possible to determine coefficient  $\beta$ . It should be pointed out that equations (9.11), (9.12) and (9.13) are valid for differential dielectric susceptibility and permittivity. In the paraelectric region, in the frequency range where is no dispersion, differential dielectric permittivity coincides with the reverse dielectric permittivity, i.e., with the permittivity measured in a weak high-frequency field with the simultaneous application of a strong constant field to the specimen, usually called the biasing field.

The reverse permittivity can be measured both under static conditions, when the biasing field is constant, and under dynamic conditions, when the biasing field is variable, but its frequency is much lower than that on which the measurements are made. The procedure for measuring the reverse permittivity under dynamic conditions was developed by Drougard, et al [53], and also by Kaczmarek [54]. Since the adiabatic permittivity is measured and the polarization created by the biasing field is substantial, it is necessary in the general case to consider the correction for adiabaticity

and  $\epsilon^S$  is given by expression (9.13). The first term in the parentheses gives the saturation effect and the second the adiabatic correction. In the case of barium titanate the latter is insignificant [53], and therefore (9.13) can be rewritten in the form

$$\frac{1}{\epsilon(E)} - \frac{1}{\epsilon(0)} = \frac{3\beta}{2\pi} P^2. \quad (9.25)$$

Thus the difference between the reverse susceptibilities is a linear function of  $P^2$ , and the angular coefficient is determined only by  $\beta$ , which is a simple method for determining it. Expression (9.25) can be reduced to another form, in which the dependence of the difference of permittivities on biasing field strength is given in explicit form. If the biasing field is not very strong we may assume  $P = \chi E$  and by substituting this expression for polarization into (9.25) we readily obtain:

$$\epsilon(E) - \epsilon(0) = -\frac{6\beta[\epsilon(0)]^4}{(4\pi)^2} E^2. \quad (9.26)$$

Analyses of this type of dependences for triglycine sulfate were done in the dynamic state by Triebwasser [4]. The experimental values of the difference between the reverse susceptibilities as a function of  $P^2$  lie approximately on a straight line, the slope of which yields  $\beta = 4.6 \cdot 10^{-10}$  (el. stat. un./cm<sup>2</sup>)<sup>-2</sup>. When the adiabatic correction, which is large for triglycine sulfate, is taken into account,  $\beta = 3.8 \cdot 10^{-10}$  (el. stat. un./cm<sup>2</sup>)<sup>-2</sup>. The latter value agrees satisfactorily with the value found from the temperature dependence of spontaneous polarization (see §1, Chapter 8). Chapelle and Taurel [55], who discovered some change of  $\beta$  with temperature, measured the dependence of permittivity of triglycine sulfate on polarization under static conditions. When polarization increases, i.e., when biasing field strength increases, permittivity of triglycine sulfate decreases, which corresponds to  $\beta > 0$ , as should be expected for the second order phase transition. The theoretical dependences of  $\frac{\epsilon(E)}{\epsilon(0)}$  are shown in Figure 9.7 for three temperatures.

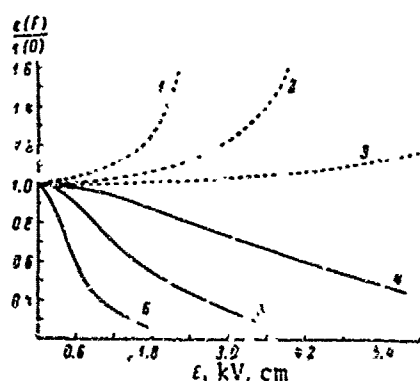


Figure 9.7. Theoretical dependences of ratio  $\frac{\epsilon(E)}{\epsilon(0)}$  for triglycine sulfate crystal (continuous curves) and barium titanate crystal (broken curves) on biasing field strength. (According to Triebwasser [4]).  
 1 --  $T = T_c$ ; 2 --  $T - T_c = 5^\circ\text{C}$ ;  
 3 --  $T - T_c = 18^\circ\text{C}$ ; 4 --  $T - \theta = 2^\circ\text{C}$ ; 5 --  $T - \theta = 1^\circ\text{C}$ ; 6 --  $T - \theta = 0.5^\circ\text{C}$ .

Somewhat different investigations were undertaken by Baumgartner [1] on potassium dihydrophosphate crystals. First the dependence of permittivity on field strength under static conditions was found. These measurements yielded the adiabatic permittivity. Secondly, using a ballistic galvanometer, the dependence of polarization on field strength was obtained, differentiation of which makes it possible to determine isothermal permittivity. In the case of adiabatic permittivity the dependence on polarization is determined both by the saturation effect [first term in the parentheses in (9.13)], and by the adiabatic correction [second term in the parentheses in (9.13)]. Knowledge of both permittivities makes it possible to estimate both corrections. It seems that the adiabatic correction prevails first to a polarization of  $2 \cdot 10^{-6} \text{C/cm}^2$ , but then the correction for saturation becomes greater and increases rapidly with polarization.

After application of the biasing field in the case of the second order phase transition the temperature dependence of polarization in the general case has the form illustrated in Figure 3.10a. The dependence of permittivity on temperature, as before, has a maximum, but as field strength increases it is displaced toward higher temperatures, and its magnitude diminishes.

The first order phase transition takes place in barium titanate. Consequently  $\beta < 0$  and as the biasing field strengthens permittivity should increase. The theoretical curves are illustrated in Figure 9.7. The investigations of Drougard, et al [53], and also of Kaczmarek and Pietrzak [54] of barium titanate monocrystals in the dynamic state showed that in accordance with theory the experimental values of  $\beta$  are less than 0. Immediately below the Curie point, according to data [53],  $\beta = -0.5 \cdot 10^{-12} (\text{el. stat. un./cm}^2)^{-2}$  and at  $144^\circ\text{C}$   $\beta = -0.3 \cdot 10^{-12} (\text{el. stat. un./cm}^2)^{-2}$ , and according to data [54], at  $144^\circ\text{C}$   $\beta = -0.57 \cdot 10^{-12} (\text{el. stat. un./cm}^2)^{-2}$ . The temperature dependence of  $\beta$  was investigated in both works. Drougard, et al [53] did their investigation in the  $120$ - $150^\circ\text{C}$  temperature range and found that  $\beta$  diminishes linearly as temperature increases. Extrapolation of this dependence to temperatures above  $150^\circ\text{C}$  shows that  $\beta$  passes through zero at  $175^\circ\text{C}$ . According to the data of Kaczmarek and Pietrzak [53], the temperature dependence of  $\beta$  is substantially nonlinear, and from extrapolation of this dependence it can be expected that  $\beta$  vanishes in the  $130^\circ\text{C}$  region.

Triebwasser [56] analyzed the effect of the electric field on the permittivity of barium titanate monocrystals in the paraelectric region under static conditions. The results of these measurements are given in Figure 9.8, where the broken curves show the theoretical dependence derived from thermodynamic theory. The theory and experiment coincide only in a comparatively narrow interval of fields. Triebwasser attributes this discrepancy to the formation of near-electrode layers of a space charge under the influence of a constant field, leading to reduced apparent permittivity. This explanation is confirmed by the fact that at the initial moment after application of a constant electric field permittivity increases to the value predicted by theory, but as time goes by it

diminishes. At the same time the electric field strength within the crystal diminishes, as can be judged by observing the electro-optic effect. It is assumed that the permittivity of the surface layers is less than that of the mass. The crystal represents a triple-layer dielectric material, and its apparent permittivity is determined by the permittivities of all three layers. The thickness of the surface layer depends on the voltage applied, and therefore the apparent permittivity is a function of voltage.

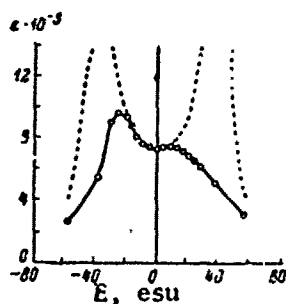


Figure 9.8. Dependence of permittivity of barium titanate monocrystal on biasing field strength at temperature  $10^\circ$  higher than Curie point. Broken curves show theoretical dependence. (According to Triebwasser [56]).

Investigations of polycrystalline barium titanate, both under static [54, 57, 58] and under dynamic [54] conditions, revealed that the biasing field reduces permittivity in both cases, i.e.,  $\beta > 0$ . Kirillov and Isupov [58] offer a possible explanation for this. It is based on the assumption that the space charged layer is formed not only on the electric, but also on the boundary of the crystallites comprising the polycrystalline specimen. When the ferroelectric phase transition is a first order phase transition, according to thermodynamic theory, the dependence of polarization on field strength in the region of the

Curie point has the form illustrated in Figure 13.1. To the paraelectric phase correspond the curves with  $t > 1$ . In the case when  $dP/dt < 0$  the crystal will be in an unstable state, and therefore there will an abrupt transition to a new state.

Proceeding from the null field toward increasing values, then at some field strength polarization increases abruptly, which corresponds to induced transition to the ferroelectric state. In the reverse direction the transition is back to the paraelectric state. The so-called double hysteresis loops will occur in a variable field. The problem of induced phase transition is examined in greater detail in Chapter 13. Here we will point out simply that as shown by the curves in Figure 13.2, the increase of polarization slows down in the ferroelectric state as the field increases, i.e., permittivity decreases. To this region of fields correspond the extreme left and right sections of the broken curve in Figure 9.8.

### §3. Reverse Permittivity in the Ferroelectric Region

The dependence of polarization on electric field strength in the ferroelectric region is determined principally by repolarization processes. The nonlinear electric properties of ferroelectric materials attributed to repolarization are discussed in Chapter 8. We will discuss here the

dependence of reverse permittivity, i.e., of dielectric permittivity, measured in a weak variable field, on the strength of a biasing electric field.

A phenomenological analysis of the dependence of polarization of a single-domain crystal on the strength of an electric field applied along the polar axis was done in the works of Lyagin and Geyvashovich [59], Bogdanov [60], Pasyukov [61]. By virtue of spontaneous polarization the result of the electric field will differ in the direction of spontaneous polarization and against it. Therefore it is necessary to consider in the expansion of polarization in terms of the powers of electric field strength, terms with even powers of E. The expansion has the form:

$$P = P_s + aE + bE^2 + cE^3 + \dots \quad (9.27)$$

and equation (9.24b) is valid for the differential permittivity along the polar axis.

We will note that in (9.27)  $|bE^2| \gg |cE^3|$  in tolerable fields. The expressions for b through the coefficients of expansion (3.7) and  $P_s$  were found in [59].  $b < 0$ , and therefore if field strength coincides with the direction of spontaneous polarization, permittivity diminishes as field strength increases, but increases when the field is in the opposite direction. The reverse and differential permittivities coincide for a single-domain crystal at moderate frequencies (if, of course, the amplitude of the variable field is low). Therefore (9.24b) can be regarded also as the expression for reverse permittivity, in which E is biasing field strength. If the crystal is not single-domain, then the situation is more complex.

In the case of triglycine sulfate, as mentioned in §1, permittivity in a weak field, according to Fousek and Janousek [47], depends substantially on the summary area of domain walls. The application of a biasing field causes the domain structure to change, and therefore influences the orientation part of permittivity. The curve of the dependence of permittivity on biasing field strength is obviously governed by the initial state of the crystal. In a rather strong field, when the crystal becomes practically single-domain, reverse permittivity will equal differential permittivity, corresponding to the slope of the saturation branch.

In the case of the c-domain barium titanate crystal the presence of  $180^\circ$  domains, as demonstrated by Drougard and Young [22], leads to a reduction of permittivity on the polar axis by the virtue of the "clamping" effect (sec 21). The dependences of reverse permittivity on field strength in the quasistatic regime (the complete cycle of change of the field takes 3 hours) are shown in Figure 9.9. By tracing the curve of change of permittivity we see that  $\epsilon_c$  decreases substantially when field strength is in the coercive region, and when many antiparallel domains are formed. The

dependence of reverse permittivity on the biasing field for polycrystalline barium titanate is illustrated in Figure 8.14 (curve 1). The drop of permittivity in this case is a result of reduction both of the orientation and induction components of polarization.

Orientation polarization may decrease by virtue of considerable reduction of the summary area of domain walls, chiefly the  $180^\circ$  walls, and "clamping" of the remaining walls.

As regards induced polarization, its change may be related to the fact that processes of  $90^\circ$  repolarization take place in the biasing field. In this case, because  $\epsilon_c < \epsilon_a$ , permittivity measured in the same direction in which the biasing field ( $\epsilon_{||}$ ) is applied, will be less than the permittivity measured in the perpendicular direction ( $\epsilon_{\perp}$ ). This effect could be detected experimentally on the basis of the anisotropy of  $\epsilon$ . It is simply impossible to make measurements in crossed fields. Therefore the anisotropy of polarized ceramics was analyzed [62-66]. The difference between  $\epsilon_{||}$  and  $\epsilon_{\perp}$  is small, amounting only to a few percent.

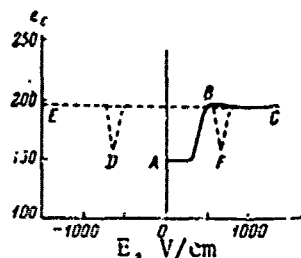


Figure 9.9. Dependence of reverse permittivity ( $\epsilon_c$ ) of barium titanate monocrystal on biasing field strength. The sequence is ABCDEBFC. The complete cycle of change takes 3 hours. (According to Drougard and Young [22]).

This result agrees with the data of [67, 68], in which it was established that the fraction of  $90^\circ$  reorientations is small and decreases considerably after the field is removed. Although all these investigations do not afford a direct answer to the question concerning the importance of  $90^\circ$  repolarization in the reduction of reverse permittivity, they nevertheless show that it does not have a great effect. This is also verified by the fact that according to Poplavko's data [69], the permittivity of ceramics is practically independent of the biasing field at frequencies of  $10^{10}$  Hz, when the orientation part of polarization is absent.

The effect of the biasing field which we have examined on permittivity in the ferroelectric range pertains to the case when a constant or very slowly variable field is applied (for instance, one cycle in 3 hours, as in [22]). It is noteworthy that during change of the biasing field by stages the measurements are made each time beginning at some specific time, so as to avoid nonstationary phenomena, which we will examine later.

Drougard, et al [70] detected on barium titanate crystals a sharp increase in permittivity and losses during the time of the repolarization process. This phenomenon was later analyzed by Prutton [71], Husimi [72],

Fatuzzo [73, 74], Fouskova and Janousek [75, 76, 78-80], Stadler, et al [77]. The investigations were conducted on monocrystals of barium titanate [70, 72, 74, 76, 78], triglycine sulfate [73-76, 79], Seignette's salt [80], guanidine aluminum sulfate [71], lithium selenate [73], triglycine fluorberyllate [79]. The measurements were conducted in a weak alternating field at frequencies of  $10^5$  Hz and above. The repolarizing field was applied either as a low-frequency sinusoidal field or as rectangular bipolar pulses.

The dependence of increments of permittivity and conductivity on time (starting at the front of the repolarizing pulse) is illustrated in

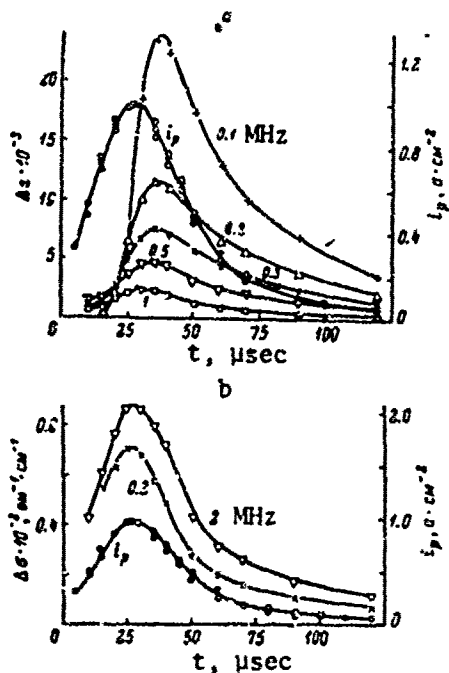


Figure 9.10. Time dependence (Fouskova and Janousek [76]). a -- polarization current  $i_p$  and current of change of permittivity ( $\Delta\epsilon$ ); b -- change of equivalent parallel conductivity ( $\Delta\sigma$ ) during repolarization of barium titanate monocrystal by rectangular pulses  $E = 784$  W/cm.

than capacitive character of resistance of the specimen. Allowance for the effect of the alternating field on the formation of nuclei, adjacent to existing domain walls, according to Fouskova's calculations [82], yields qualitative agreement between the theoretical and experimental time dependences of the changes of permittivity and conductivity. The effect,

Figure 9.10 for the barium titanate crystal. Here we see that permittivity is ambiguously related to the repolarization current and has a strong frequency dependence. According to Fatuzzo's data [74], triglycine sulfate and barium titanate have two regions of relaxation dispersion: low-frequency and high-frequency. For barium titanate one relaxation frequency is 29 kHz and the other lies above  $2 \cdot 10^9$  Hz. In the case of triglycine sulfate, in contrast to barium titanate, the experimental data for low-frequency relaxation indicate that there is a set of relaxation times. The center of their distribution corresponds to 6.8 kHz. The high-frequency dispersion region is located at a frequency of 100 MHz. It is noteworthy that for the given  $i_{p \max}$  the maximum relative increase in permittivity is independent of temperature [77].

The reasons for the increase in permittivity during repolarization are discussed in a number of works. Assuming that the high-frequency electric field has an effect on the number of nuclei and new domains formed, then, as demonstrated by Landauer and coworkers [81], this model leads to an inductive rather

however, of a variable field on the development of isolated nuclei leads to time dependences absolutely different from the experimental. This indicates, in accordance with [81], that these processes are of minor importance. In Fatuzzo's interpretation [73, 74], the increase in the combined permittivity is attributed to strongly damped oscillations in the high-frequency field of traveling domain walls of the growing  $180^\circ$  domains. Here low-frequency dispersion is related to vibrations of the leading front of the acicular domain, and high-frequency dispersion to vibrations of its side walls.

Permittivity, after passage of the sharp maximum at the moment of repolarization, if the latter is not complete, remains for a long time above its initial value, gradually approaching it. If constant voltage is changed step-by-step, even in small steps, permittivity increases with each abrupt increase of the field and then, over a period of tens of minutes, gradually drops. It is noteworthy that a burst of permittivity is observed both during a sharp increase and reduction of the field. This phenomenon was investigated experimentally on polycrystals by Piekara and Fajak [83], Lur'ye [84], Koch [85], and on barium titanate monocrystals by Borodin [86]. The higher the rate of change of the field, the greater the increase in permittivity [86, 87]. For barium titanate monocrystals when the biasing field is changed in the frequency range of 0.5-0.1 Hz, transition occurs from an increase of permittivity during repolarization to a reduction, when the effect of piezoelectric clamping is manifested [86]. The prolonged retention of high permittivity after partial repolarization is related to the fact that domain boundaries removed from the positions in which they had minimal energy and were clamped to some extent, can now vibrate in the weak field, thereby leading to an increase in the orientation component of permittivity. As time passes the migrating domain walls "find" new locations, in which they have rather low energy, where they are also clamped. The fields of space charges perhaps play an important part in stabilization of the domain walls. At a low rate of change of the biasing field these charges move together with the wall, continuously stabilizing its position. When the rate of change of the biasing field is great, the charges cannot follow the wall, and its mobility in the high-frequency field and its contribution to permittivity are thereby increased [86].

#### 54. Dispersion of Permittivity

The dispersion dependences of the permittivity of ferroelectrics of the "bias" and "order-disorder" types differ substantially. Of the first type of ferroelectrics, we will examine here the properties of practically the only well investigated representative -- barium titanate.

In the investigations of Benedict and Durand [88] ( $2.4 \cdot 10^{10}$  Hz), Nakamura and Furuichi [89] ( $3.3 \cdot 10^9$  Hz), Stern and Lurio [90] (up to  $2 \cdot 10^9$  Hz), Ballantyne [91] ( $2.4 \cdot 10^{10}$  Hz), dispersion was not observed in barium titanate monocrystals in the paraelectric region. Ballantyne [91] analyzed the reflection spectra in a wide range of wavelengths and used them to calculate the frequency dependence of permittivity (Figure 9.11).

On the basis of these data, dispersion begins only at  $1.5 \cdot 10^{11}$  Hz ( $5 \text{ cm}^{-1}$ ) and the frequency of the "soft" mode, responsible for the high values of permittivity, lies in the  $6-13 \text{ cm}^{-1}$  range (the spectrum is discussed in greater detail in Chapter 14).

The investigations of Schmitt [92], Poplavko [93], Nekrasov, et al [94] of polycrystalline barium titanate showed that there is no dispersion in the paraelectric phase, at least up to  $2 \cdot 10^{10}$  Hz. There is a notable reduction of  $\epsilon$ , according to the data of Poplavko, et al [95], starting at  $5 \cdot 10^{10}$  Hz. In this frequency region, naturally, where there is no dispersion, even nonlinear properties are retained. Losses increase in the paraelectric phase with increasing frequency by measure of approach to the dispersion region. As regards the temperature dependence of losses, at frequencies above  $10^8$  Hz it is quite strong. At the Curie point  $\tan \delta$  passes through a maximum and drops sharply on transition to the ferroelectric phase [90]. The curve of losses is determined by the temperature dependence of the frequency of the low-frequency mode of vibrations of the crystal lattice. The frequency and temperature dependences of dielectric losses were analyzed most thoroughly on  $\text{SrTiO}_3$  in the works of Rupprecht and Bell [96, 97] and Barker and Tinham [98]. According to [97], for  $\text{SrTiO}_3$

$$\lg \delta = (T - T_c)^{-1} \cdot (\alpha + \beta T + \gamma T^2). \quad (9.28)$$

where  $\alpha$  is determined by crystal defectiveness and  $\beta$  and  $\gamma$  by the anharmonicity of vibrations of the crystal lattice. All three parameters are functions of frequency. This temperature dependence of losses is satisfactorily described from the viewpoint of dynamic theory [99].

Barium titanate is a piezoelectric material in the ferroelectric phase. Therefore strong dispersion of permittivity occurs in the frequency range of resonance mechanical vibrations of the crystal and at higher frequencies clamped permittivity is measured. The investigations of Benedict and Durand [88] and Ballantyne [91] of single-domain crystals showed that  $\epsilon_a$  on a frequency of  $2.4 \cdot 10^{10}$  Hz is approximately one-half its value on low frequencies, but dielectric dispersion is still not observed. The results of these measurements are presented in Figure 9.12. According to Ballantyne's data [91], notable dispersion begins only at frequencies of  $10^{11}$  Hz, i.e., of the same order as in the paraelectric region. These frequency dependences of  $\epsilon'_a$  and  $\epsilon''_a$  are presented in Figure 9.13.  $\epsilon_c$  at high frequencies was analyzed by Turik and Chernyshev [100], who obtained  $\epsilon_c \sim 60-80$  at  $3 \cdot 10^9$  Hz, i.e., close to the clamped permittivity.

Historically the first investigations of barium titanate at high frequencies were conducted on polycrystalline specimens. In the works of Vul [101], Novosil'tsev and Khodakov [102], measurements were made up to  $10^8$  Hz and notable dispersion was not detected. Mash [103] observed some reduction of permittivity at a frequency of  $1.27 \cdot 10^9$  Hz. Later on Powles

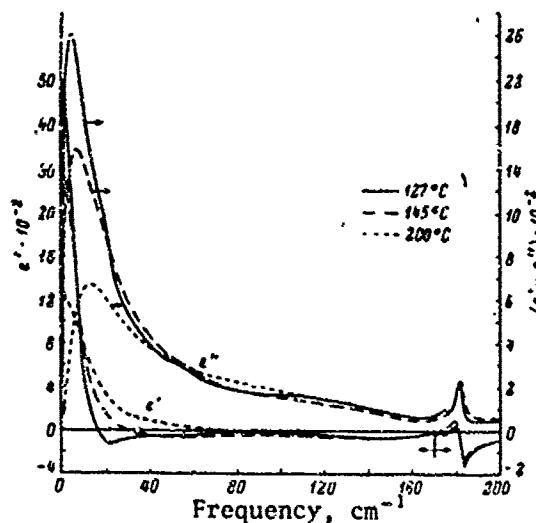


Figure 9.11. Frequency dependence of real ( $\epsilon'$ ) and imaginary ( $\epsilon''$ ) components of permittivity of barium titanate monocrystal in paraelectric region.  $\epsilon'$  and  $\epsilon''$  were computed by the Kramers-Kroenig method from data on reflection spectrum. (According to Ballantyne [91]).

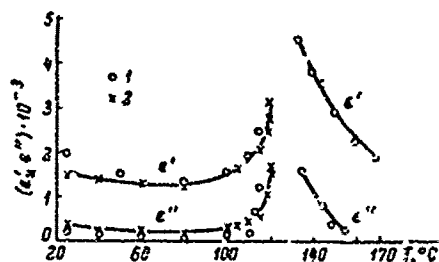


Figure 9.12. Temperature dependence of real ( $\epsilon'_a$ ) and imaginary ( $\epsilon''_a$ ) components of permittivity of single-domain barium titanate monocrystal at  $2.4 \cdot 10^{10}$  Hz. The electric vector is perpendicular to the c axis. 1 -- according to Benedict and Durand [88]; 2 -- according to Ballantyne [91].

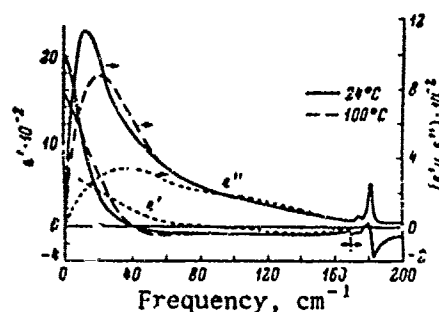


Figure 9.13. Frequency dependence of real ( $\epsilon'$ ) and imaginary ( $\epsilon''$ ) components of permittivity of single-domain barium titanate monocrystal in ferroelectric region. Electric vector perpendicular to c axis.  $\epsilon'$  and  $\epsilon''$  computed by the Kramers-Kroenig method from data on reflection spectra. (According to Ballantyne [91]).

and Jackson [104, 105] detected strong dispersion in the  $10^9$ - $10^{10}$  Hz range. The presence of dispersion in this frequency range was later verified by all the numerous investigations [69, 92-95, 106-108]. Here dispersion is

observed in all three ferroelectric phases [94, 109, 110]. At room temperature permittivity from 1,200-1,500 decreases on low frequencies, according to the latest data, to 500-600 at  $10^{10}$  Hz (Figure 9.14).

The studies of Murzin and Demeshina [111] of the reflection spectra showed that strong dispersion resumes on  $10^{11}$  Hz, which agrees with data obtained on monocrystals. It is noteworthy that a substantial reduction of permittivity of polydomain monocrystals was observed in a number of works in the  $10^8$ - $10^{10}$  Hz frequency range [112, 113, 89, 94]. The nature of dispersion of the permittivity of ceramics in the  $10^9$ - $10^{10}$  Hz range as yet remains uncertain. Since a single-domain crystal does not display dispersion in this frequency range, the features of the macroscopic structure, i.e., granularity of the material or presence of domains, are obviously the reason.

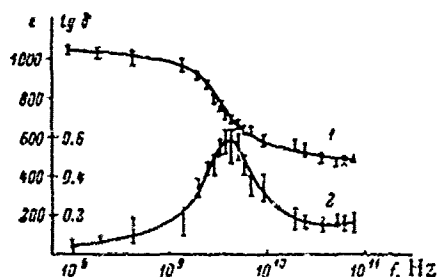


Figure 9.14. Frequency dependence of permittivity (1) and  $\tan \delta$  (2) of polycrystalline barium titanate. Room temperature.  $\epsilon = 1,350$  at a frequency of 1 kHz. (According to Poplavko, et al [95]).

Essentially two dispersion mechanisms have been advanced: one relates the reduction of permittivity with transition at high frequencies to the condition of piezoelectric clamping [114, 115], and the second states that much of the permittivity is caused by orientation polarization and dispersion is attributed to the inertia of the domain walls [116]. According to Devonshire [114], the piezoelectric, mechanical vibrations of individual domains must be examined. There is also a transition to the condition of complete piezoelectric clamping at frequencies higher than the resonance frequency of these vibrations. Approximation of the resonance frequency on the basis of a domain dimension of several microns yields the required order of magnitude. This mechanism of dispersion is also discussed in [117-119].

Hippel [115], in contrast to Devonshire, feels that the resonance vibrations of entire crystallites, rather than of individual domains, should be examined. Apparently this mechanism is improbable, since direct observations show that crystallites have complex domain structure and it is improbable that each of them as a whole would possess considerable piezoelectric activity.

Kittel [116], who analyzed the equation of motion of  $180^\circ$  walls without consideration of damping, offered an explanation for the dispersion of inertia of the domain walls. The solution of the equation with very approximate coefficients yields a resonance frequency of  $2 \cdot 10^9$  Hz. The

fact that dispersion is of a relaxation rather than resonance character can easily be explained by strong attenuation.

This mechanism was examined in greater detail and more rigorously by Sannikov [120]. In his model the domain wall vibrates within the limits of its potential depression with an amplitude considerably smaller than the effective wall thickness. In contrast to the Kittel-Sannikov model, Nettleton [121, 122] examined, rather than the motion of the 180° domain wall as a whole, the vibration of local protuberances adjacent to the wall, with a thickness of one lattice constant. His numerical estimates showed that this model can also explain microwave dispersion in polycrystalline barium titanate. Thus, several mechanisms of dispersion have been offered, but so far there are no sufficiently convincing data in favor of any one of them.

Thus, the "clamped" type of ferroelectrics is characterized by the absence of dielectric dispersion in the paraelectric phase, and in the case of the single-domain crystal, in the ferroelectric phase as well, all the way up to the frequencies of vibrations of the crystal lattice; dispersion on UHF frequencies occurs only in the presence of the domain structure.

We will turn now to ferroelectric materials with the order-disorder type phase transition. The dielectric properties of triglycine sulfate in the microwave region have been analyzed in a number of works [123-130]. It has been established that strongest dispersion occurs in the region of the phase transition, and only on the ferroelectric axis (b) (Figure 9).  $\epsilon_b$  decreases at the Curie point even at frequencies of  $10^7$ - $10^8$  Hz.  $\epsilon_b$  inversely proportional to frequency in the dispersion region at a fixed temperature. Hill and Ichiki [127], analyzing experimental data from the viewpoint of the classic Debye theory of dipole relaxation, concluded that there is Gauss distribution of relaxation times. Here the most probable relaxation time is  $\tau_0 \sim \frac{1}{T - T_c}$ . In the ferroelectric region at frequencies of  $10^5$ - $10^6$  Hz there is a reduction of permittivity in all three crystallographic directions, related to transition to the condition of piezoelectric clamping [130]. The frequency of dielectric dispersion on the polar axis increases rapidly by measure of distance from the Curie point. At room temperature there is no reduction of  $\epsilon_a$  until  $2 \cdot 10^{10}$  Hz [130].

Several works [130-137] pertain to analysis of the permittivity of Seignette's salt at high frequencies. Seignette's salt possesses the piezoelectric effect in the paraelectric region, and therefore at frequencies above the frequency of piezoelectric resonance the mechanically clamped permittivity is measured. As already mentioned, the Curie-Weiss law is satisfied here and the difference between the inverse susceptibilities is independent of temperature. At frequencies of  $10^9$  Hz the permittivity measured in the direction of the ferroelectric axis experiences dispersion, particularly strong in the regions of the Curie temperatures [133-135, 130, 137]. The temperature dependences of permittivity at various frequencies

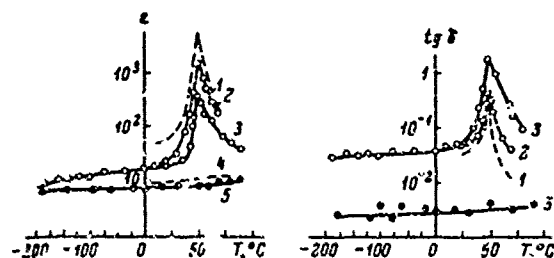


Figure 9.15. Dependence of permittivity and  $\tan \delta$  of triglycine sulfate crystal on temperature at different frequencies (According to Poplavko and Solomonova [130]). 1 --  $\epsilon_b$  and  $\tan \delta_b$  at  $4.7 \cdot 10^4$  Hz; 2 --  $\epsilon_b$  and  $\tan \delta_b$  at  $5 \cdot 10^6$  Hz; 3 --  $\epsilon_b$  and  $\tan \delta_b$  at  $8.4 \cdot 10^9$  Hz; 4 --  $\epsilon_a$  at  $4.7 \cdot 10^4$  Hz; 5 --  $\epsilon_a$  and  $\tan \delta_a$  at  $2 \cdot 10^{10}$  Hz.

all the way up to  $1.3 \cdot 10^{10}$  Hz, obtained by Sandy and Jones [137], are presented in Figure 9.16. Here we see that at rather high frequencies permittivity has maxima at the phase transition temperatures. Relaxation is of a Debye character with one relaxation time. It is assumed that dispersion in Seignette's salt is related to rotation of dipolar hydroxyl groups. Dispersion was not observed on the nonferroelectric axes measurements up to  $2 \cdot 10^{10}$  Hz [130].

The dielectric properties of  $\text{KH}_2\text{PO}_4$  crystals at high frequencies have been analyzed in a number of works [138-141]. It has already been mentioned in §1 that this ferroelectric possesses the piezoelectric effect in the paraelectric phase and at frequencies higher than the frequency of mechanical resonance, as in the case of Seignette's salt, the Curie-Weiss law is satisfied. Here transition to the condition of piezoelectric clamping does not lead to a change in the Curie constant. Dispersion of a relaxation character was observed in [139] during measurements at frequencies up to  $3.5 \cdot 10^{10}$  Hz in deuterated crystals. The temperature dependence of  $\tan \delta$  in the paraelectric region obeys law (9.28) and can be explained within the frameworks of dynamic theory [140], and not by dipole relaxation [142]. Dispersion of permittivity in  $\text{KH}_2\text{PO}_4$  above the Curie point was also analyzed from the point of view of tunnel transition of a proton along the hydrogen bond [143].

Another characteristic representative of ferroelectrics of the order-disorder type is  $\text{NaNbO}_3$ . This ferroelectric material displays strong dispersion of permittivity [144-146] (Figure 9.17) on the ferroelectric axis in the vicinity of the Curie point. According to Hata [145, 146], who did measurements up to  $2.4 \cdot 10^{10}$  Hz, minimum permittivity is observed on high frequencies at the ferroelectric phase transition temperature, and its dispersion dependence corresponds to one relaxation time. Near

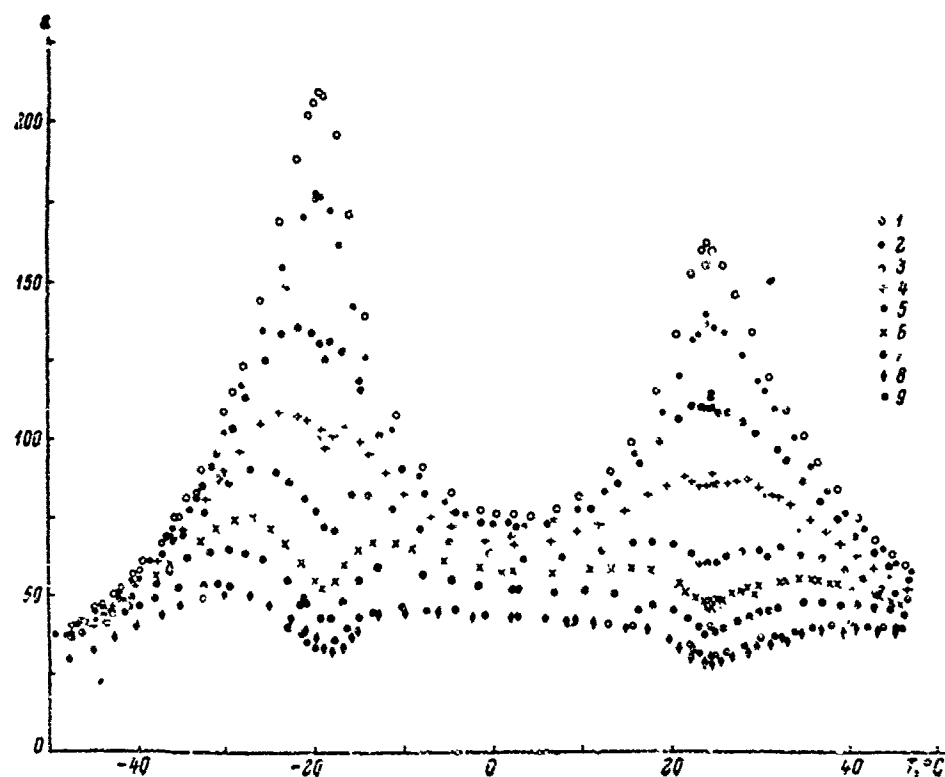


Figure 9.16. Temperature dependence of permittivity of Seignette's salt crystal at various frequencies (according to Sandy and Jones [157]): 1 --  $2.5 \cdot 10^9$  Hz; 2 --  $3 \cdot 10^9$  Hz; 3 --  $3.9 \cdot 10^9$  Hz; 4 --  $5.1 \cdot 10^9$  Hz; 5 --  $7.05 \cdot 10^9$  Hz; 6 --  $8.25 \cdot 10^9$  Hz; 7 --  $9.45 \cdot 10^9$  Hz; 8 --  $11.96 \cdot 10^9$  Hz; 9 --  $12.95 \cdot 10^9$  Hz.

the transition temperature the relaxation frequency is proportional to  $(T - T_0)$ , where  $T_0 \approx 162^\circ\text{C}$ . No notable changes of permittivity were noted in a wide frequency range on the a and c axes. It is presumed that the dispersion in  $\text{NaNO}_2$  is related to rotation of dipolar groups  $\text{NO}_2^-$  around the a axis. Theoretical works [147, 148] are devoted to explanation of dielectric dispersion in this compound.

#### §5. Effect of Irradiation

Irradiation has a considerable influence on the properties of ferroelectrics, as observed by Zheludev, et al [149] on Seignette's salt crystals. It turned out that after irradiation with  $\gamma$ -rays the permittivity maxima at the Curie points become smaller and are displaced with respect to temperature toward each other. In addition the so-called double loop is observed instead of the normal hysteresis loop, and after large doses of irradiation hysteresis loops are not observed at all.

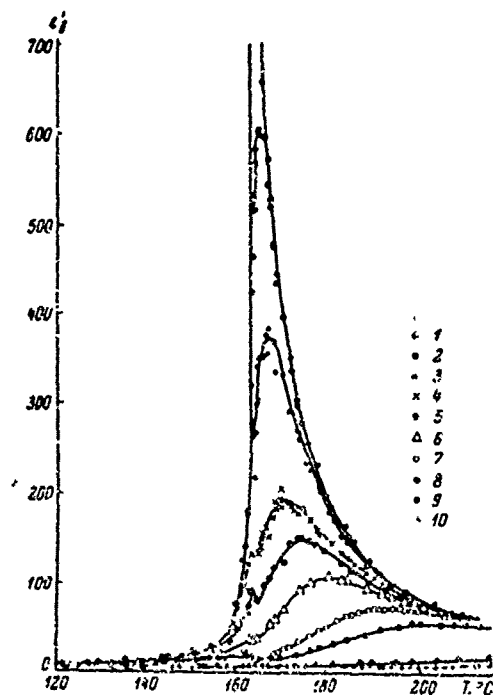


Figure 9.17. Temperature dependence of permittivity of  $\text{NaNO}_2$  crystal on b axis at various frequencies.

(According to Hatta [146]). 1 -- 5 MHz; 2 -- 32 MHz; 3 -- 64 MHz; 4 -- 130 MHz; 5 -- 160 MHz; 6 -- 350 MHz; 7 -- 600 MHz; 8 -- 1,000 MHz; 9 -- 9,000 MHz; 10 -- 24,000 MHz.

Subsequent investigations showed that irradiation with x-rays and ultraviolet rays lead to the analogous effect. The effect of irradiation on the properties of ferroelectrics has been analyzed chiefly on crystals of Seignette's salt and triglycine sulfate. These include the works of Yurin, et al [149-154], Eisner [155, 156], Chynoweth [157], Okada [158-160], Starodubtsev and Peshikov [161-165], among other investigators [166-176].

The results of the investigations show that irradiation stabilizes the domain structure that exists at the moment of irradiation. If during irradiation a crystal is in the single-domain state, then the loop is asymmetric and displaced (Figure 9.18c); if it is in the polydomain state it is a double loop (Figure 9.18b). In the case when irradiation occurs above the Curie point the loop is normal (Figure 9.18a). The form of the hysteresis loop changes if the crystal is held for a long time in the state in which the domain structure differs from that at the moment of irradiation. If, for example, a crystal with a double hysteresis loop is held for a long time at a temperature above the Curie point, then its loop becomes normal. If, however, the same crystal is then held for a long time in the polydomain state, the loop again becomes double.

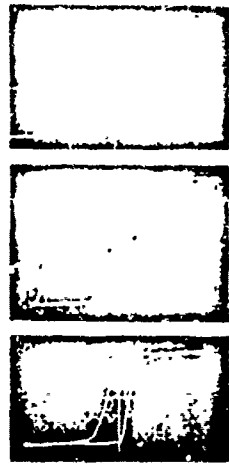


Figure 9.18. Oscillograms of hysteresis loops of triglycine sulfate crystal, illustrating the effect of  $\gamma$ -irradiation. (According to Yurin, et al [154]). a -- before irradiation; b -- after dose of  $2 \cdot 10^6$  r; c -- after dose of  $2 \cdot 10^6$  r; irradiation in this case in the presence of constant field  $+E = E_{sat}$ . Maximum field strength  $E_{sat} = 2$  kV/cm, frequency 50 Hz, temperature  $20^\circ\text{C}$ .

rivalry of these two factors, acting in opposite directions: weakening of the forces of interaction leads to reduction of the Curie point, and the appearance of an internal field, to displacement of maximum  $\epsilon$  toward higher temperatures, and here maximum  $\epsilon$  is diminished. This notion of the effect of defects is verified by experiments on compensation of the internal field by a constant electric field [162-165]. A directional electric field increases maximum  $\epsilon$  in the corresponding manner and simultaneously displaces the maximum toward lower temperatures, thereby compensating the action of the internal field.

Radiation effects have also been analyzed in barium titanate [180-192], and all works, with the exception of [191, 192], pertain to analysis of the effect of irradiation with neutrons. When the dose of irradiation is increased to  $10^{18}$  neutron/cm<sup>2</sup> the processes of repolarization proceed with greater difficulty, the Curie point drops and receptivity at the Curie point also decreases. As a result of irradiation with a dose exceeding  $10^{20}$  neutron/cm<sup>2</sup>, permittivity has no maximum and the crystal lattice remains cubic. Here the elementary cell becomes larger. The mechanism of the effect of radiation defects on the ferroelectric properties of barium titanate is unknown at the present time.

Quite the same pattern holds true for Seignette's salt crystals containing copper atoms as impurity, introduced to the crystals during the growth process [153, 177-179]. The action of radiation defects has the equivalent effect of some internal effective bias field, the direction of which coincides in each domain with spontaneous polarization. In other words, unidirectional anisotropy occurs. If the stabilizing state is the single-domain state the internal biasing field may be compensated by a constant electric field. It is assumed that impurity ions or radiolysis products, as a result of directional diffusion, occupy the positions in the crystal lattice that stabilize the direction of spontaneous polarization [153].

The effect of radiation defects however, cannot be reduced simply to the creation of an internal biasing field. Defects, moreover, weaken the forces of interaction, leading to the appearance of spontaneous polarization. The position of the peak on the curve of the temperature dependence of  $\epsilon$  is determined by the

#### BIBLIOGRAPHY

1. Baumgartner, H., *Helv. Phys. Acta*, Vol. 23, p. 651, 1950.
2. Devonshire, A. F., *Phil. Mag. Suppl.*, Vol. 3, p. 85, 1954.
3. Wieder, H. H., *J. Appl. Phys.*, Vol. 30, p. 1010, 1954.
4. Triebwasser, S., *IBM J. Res. Developm.*, Vol. 2, p. 212, 1958.
5. Gonzalo, J. A., *Phys. Rev.*, Vol. 144, p. 662, 1966.
6. Nay, J., Fizicheskiye Svoystva Kristallov (Physical Properties of Crystals), IL [Foreign Literature] Publishing House, Moscow, 1960.
7. Hoshino, S., T. Mitsui, F. Jona and R. Pepinsky, *Phys. Rev.*, Vol. 107, p. 1255, 1957.
8. Craig, P. P., *Phys. Lett.*, Vol. 20, p. 140, 1966.
9. Sekido, T. and T. Mitsui, *J. Phys. Chem. Sol.*, Vol. 28, p. 967, 1967.
10. Busch, C., *Helv. Phys. Acta*, Vol. 11, p. 269, 1938.
11. Baumgartner, H., *Helv. Phys. Acta*, Vol. 24, p. 326, 1951.
12. Hablutzel, J., *Helv. Phys. Acta*, Vol. 12, p. 489, 1939.
13. Kanzig, W., *Sol. St. Phys.*, Vol. 4, Acad. Press Inc. Publ., New York (1957). [Translated into Russian. Translator: V. Kentsig. Segnetoelektriki i Antisegetoelektriki (Ferroelectrics and Antiferroelectrics), IL Publishing House, Moscow, 1960].
14. Roberts, S., *Phys. Rev.*, Vol. 75, p. 989, 1949.
15. Granicher, H., *Helv. Phys. Acta*, Vol. 22, p. 395, 1949.
16. Kanzig, W. and N. Maikoff, *Helv. Phys. Acta*, Vol. 24, p. 343, 1951.
17. Merz, W. J., *Phys. Rev.*, Vol. 91, p. 513, 1953.
18. Drougard, M. E. and D. K. Young, *Phys. Rev.*, Vol. 95, p. 1152, 1954.
19. Roy, N. A., DAN SSSR (Reports of USSR Academy of Sciences), Vol. 81, p. 545, 1951.
20. Misareva, A., *Czechosl. J. Phys.*, Vol. 6, p. 527, 1956.
21. Merz, W. J., *Phys. Rev.*, Vol. 76, p. 1221, 1949.

22. Demgard, M. E. and D. P. Young, Phys. Rev., Vol. 94, p. 1561, 1954.
23. Jona, F. and R. Pepinsky, Phys. Rev., Vol. 105, p. 861, 1957.
24. Sawaguchi, E. and M. L. Charters, Phys. Rev., Vol. 117, p. 465, 1960.
25. Huibregtse, E. I. and D. R. Young, Phys. Rev., Vol. 103, p. 1705, 1956.
26. Marutake, M., J. Phys. Soc. Japan, Vol. 11, p. 807, 1956.
27. Bruggeman, D. A., Z. Phys., Vol. 92, p. 561, 1934.
28. Turik, A. V., Izv. AN SSSR, ser. fiz. (News of USSR Academy of Sciences, Physics Series), Vol. 29, p. 2072, 1965.
29. Lezgintseva, T. N., FTT [Fizika tverdogo tela; Solid State Physics], Vol. 6, p. 2401, 1964.
30. Odelevskiy, V. I., ZhTF [Zhurnal tekhnicheskoy fiziki; Journal of Technical Physics], Vol. 21, p. 678, 1951.
31. Lewis, B., Proc. Phys. Soc., Vol. 73, p. 17, 1959.
32. McQuarrie, M., J. Amer. Ceram. Soc., Vol. 39, p. 54, 1956.
33. Fousek, J. and B. Brezina, Czechosl. J. Phys., Vol. B11, p. 344, 1961.
34. Bokov, V. A., ZhTF, Vol. 27, p. 1784, 1957.
35. Smoienskiy, G. A. and K. I. Rozgachev, ZhTF, Vol. 24, p. 1751, 1954.
36. Marks, G. W., D. L. Waidelech and L. A. Mouson, Communication and Electronics, Vol. 26, p. 469, 1956.
37. Bokov, V. A., Izv. AN SSSR, ser. fiz., Vol. 21, p. 382, 1957.
38. Bokov, V. A., ZhTF, Vol. 28, p. 77, 1956.
39. Bokov, V. A., Candidate dissertation, Institute of Crystallography, USSR Academy of Sciences, Moscow, 1958.
40. Kniekamp, H. and W. Heywang, Z. angew. Phys., Vol. 6, p. 385, 1954.
41. Kniekamp, H. and W. Heywang, Naturwissenschaften, Vol. 41, p. 172, 1954.
42. Kniekamp, H. and W. Heywang, Naturwissenschaften, Vol. 41, p. 61, 1954.
43. Egerton, L. and S. E. Koonce, J. Amer. Ceram. Soc., Vol. 38, p. 412, 1955.

44. Goswami, A. K., L. E. Cross and W. R. Buessem, *J. Phys. Soc. Japan*, Vol. 24, p. 279, 1968.
45. Buessem, W. R., L. E. Cross and A. K. Goswami, *J. Amer. Ceram. Soc.*, Vol. 49, p. 33, 1966.
46. Sonin, A. S. and S. S. Gorbach, *Izv. AN SSSR, ser. fiz.*, Vol. 29, p. 1996, 1965.
47. Fousek, J. and V. Janousek, *Phys. St. Sol.*, Vol. 13, p. 195, 1966.
48. Konstantinova, V. P., I. M. Sil'bestrova and K. S. Aleksandrov, *Kristallografiya* (Crystallography), Vol. 4, p. 691, 1959.
49. Petrov, V. M., *Kristallografiya*, Vol. 6, p. 632, 1961.
50. Itoh, K. and T. Mitsui, *J. Appl. Phys.*, Vol. 23, p. 334, 1967.
51. Bornarel, P., A. Fouskova, P. Guyon and I. Laizerowicz, *Proc. Intern. Meet. Ferroelectr.*, 2, Prague, p. 81, 1966.
52. Joseph, R. I. and B. D. Silverman, *Phys. Rev.*, Vol. 133, A207, 1964.
53. Drougard, M. E., R. Landauer and D. R. Young, *Phys. Rev.*, Vol. 98, p. 1010, 1955.
54. Kaczmarek, F. and I. Pietrzak, *Acta Phys. Polonica*, Vol. 27, p. 335, 1965.
55. Chappelle, I. and L. Taurel, *Compt. rend.*, Vol. 249, p. 378, 1959.
56. Triebwasser, S., *Phys. Rev.*, Vol. 118, p. 100, 1960.
57. Vul, B. M., *Izv. AN SSSR, Ser. Fiz.*, Vol. 21, p. 379, 1957.
58. Kirillov, V. V. and V. A. Isupov, *Izv. AN SSSR, ser. fiz.*, Vol. 31, p. 1835, 1967.
59. Lyagin, I. V. and Ya. I. Geyvashovich, *Izv. AN SSSR, ser. fiz.*, Vol. 22, p. 1424, 1958.
60. Bogdanov, S. V., *FTT*, Vol. 5, p. 807, 1963.
61. Pasynkov, P. Ye., *FTT*, Vol. 3, p. 1587, 1961.
62. Moseley, D. S., *J. Acoust. Soc. Am.*, Vol. 27, p. 947, 1955.
63. Bechmann, R., *J. Acoust. Soc. Am.*, Vol. 28, p. 347, 1956.
64. Marutake, M. and T. Ikeda, *J. Phys. Soc. Japan*, Vol. 12, p. 233, 1957.

65. Bogdanov, S. V., Izv. AN SSSR, ser. fiz., Vol. 24, p. 1353, 1960.
66. El'gard, A. M., Izv. AN SSSR, ser. fiz., Vol. 29, p. 2079, 1965.
67. Berlincourt, D. and H. H. A. Krueger, *J. Appl. Phys.*, Vol. 30, p. 1804, 1959.
68. Uchida, N. and T. Ikeda, *Japan J. Appl. Phys.*, Vol. 6, p. 1079, 1967.
69. Poplavko, Yu. M., FTT, Vol. 6, p. 58, 1964.
70. Drougard, M. E., H. L. Funk and D. R. Young, *J. Appl. Phys.*, Vol. 25, p. 1166, 1954.
71. Prutton, M., *Proc. Phys. Soc.*, Vol. 70, p. 702, 1957.
72. Huzimi, K., *J. Appl. Phys.*, Vol. 30, p. 978, 1959.
73. Fatuzzo, E., *J. Appl. Phys.*, Vol. 32, p. 1571, 1961.
74. Fatuzzo, E., *J. Appl. Phys.*, Vol. 33, p. 2588, 1962.
75. Misarova, A. and V. Janousek, *Czechosl. J. Phys.*, Vol. 10, p. 687, 1960.
76. Fouskova, A. and V. Janousek, *J. Phys. Soc. Japan*, Vol. 20, p. 1619, 1965.
77. Stadler, H. L., T. Nakamura, Y. Ishibashi and H. Kuroki, *Proc. Intern. Meet. Ferroelectr.*, Vol. 2, Prague, p. 138, 1966.
78. Misarova, A. and V. Janousek, *Czechosl. J. Phys.*, Vol. 11, p. 465, 1961.
79. Janousek, V. and A. Fouskova, *Czechosl. J. Phys.*, Vol. 13, p. 549, 1963.
80. Fouskova, A. and V. Janousek, *Czechosl. J. Phys.*, Vol. 12, p. 413, 1962.
81. Landauer, P., D. R. Young and M. E. Drougard, *J. Appl. Phys.*, Vol. 27, p. 752, 1956.
82. Fouskova, A., *J. Phys. Soc. Japan*, Vol. 20, p. 1625, 1965.
83. Fiekara, A. and Z. Pajak, *Acta Phys. Polonica*, Vol. 12, p. 170, 1953.
84. Lar'ye, M. S., Izv. AN SSSR, ser. fiz., Vol. 21, p. 439, 1957.
85. Koch, W., *Z. Naturforschung*, Vol. 13a, p. 303, 1958.
86. Borodin, V. Z., Izv. AN SSSR, ser. fiz., Vol. 29, p. 1986, 1965.
87. Fousek, J., Z. Malek, A. J. Salim and N. S. Al Ali, *Proc. Phys. Soc.*, Vol. 80, p. 1199, 1962.

88. Benedict, T. S. and J. L. Durand, Phys. Rev., Vol. 109, p. 1091, 1958.
89. Nakamura, E. and J. Furuichi, J. Phys. Soc. Japan, Vol. 15, p. 1955, 1960.
90. Stern, E. and A. Lurio, Phys. Rev., Vol. 123, p. 117, 1961.
91. Ballantyne, J. M., Phys. Rev., Vol. 136, A429, 1964.
92. Schmitt, H. J., Z. angew. Phys., Vol. 9, p. 107, 1957.
93. Poplavko, Yu. M., FTT, Vol. 4, p. 2606, 1962.
94. Nekrasov, M. M., Yu. M. Poplavko, B. Ya. Yazytskiy, V. G. Tsykalov and L. P. Solomonova, Izv. AN SSSR, ser. fiz., Vol. 31, p. 1882, 1967.
95. Poplavko, Yu. M., V. G. Tsykalov and V. I. Molchanov, FTT, Vol. 10, p. 3425, 1968.
96. Rupprecht, G., R. O. Bell and B. D. Silverman, Phys. Rev., Vol. 123, p. 97, 1961.
97. Rupprecht, G. and R. O. Bell, Phys. Rev., Vol. 125, p. 1915, 1962.
98. Barker, A. S. and N. Tinkham, Phys. Rev., Vol. 125, p. 1527, 1962.
99. Silverman, B. D., Phys. Rev., Vol. 125, p. 1921, 1962; Vol. 135, A1596, 1964.
100. Turik, A. V. and K. R. Chernyshev, Izv. AN SSSR, ser. fiz., Vol. 31, p. 1775, 1967.
101. Vol, B. M., Elektrichestvo (Electricity), No. 3, p. 12, 1946.
102. Novosil'tsev, N. S. and A. L. Khodakov, ZhTF, Vol. 27, p. 651, 1947.
103. Mash, D. I., ZhETF [Zhurnal eksperimental'noy i teoreticheskoy fiziki; Journal of Experimental and Theoretical Physics], Vol. 17, p. 537, 1947.
104. Powles, I. G., Nature, Vol. 162, p. 614, 1948.
105. Powles, I. G. and W. Jackson, Proc. Inst. Electr. Eng., Vol. 96, p. 383, 1949.
106. Hippel, A., Rev. Mod. Phys., Vol. 22, p. 221, 1950.
107. Linayeva, G. A. and G. I. Skanavi, FTT, Vol. 2, p. 506, 1960.
108. Poplavko, Yu. M., FTT, Vol. 4, p. 1069, 1962.

109. Rabenhorst, H. and I. Melichercik, *Ann. Phys.*, Vol. 1, p. 261, 1958.
110. Petrov, V. M. and A. Yu. Teverovskiy, *Izv. AN SSSR, ser. fiz.*, Vol. 31, p. 1879, 1967.
111. Murzin, V. N. and A. I. Demeshina, *FTT*, Vol. 6, p. 182, 1964; *Izv. AN SSSR, ser. fiz.*, Vol. 28, p. 695, 1964.
112. Fousek, J., *Czechosl. J. Phys.*, Vol. 8, p. 254, 1958; Vol. 9, p. 172, 1959.
113. Petrov, V. M., *FTT*, Vol. 2, p. 997, 1960.
114. Devonshire, A. F., *Phil. Mag.*, Vol. 42, p. 1065, 1951.
115. Hippel, A., *Z. phys.*, Vol. 133, p. 158, 1952.
116. Kittel, C., *Phys. Rev.*, Vol. 83, p. 458, 1951.
117. Ikegami, S., *J. Phys. Soc. Japan*, Vol. 18, p. 1203, 1963.
118. Gerson, R., I. M. Peterson and D. R. Rote, *J. Appl. Phys.*, Vol. 34, p. 3142, 1963.
119. Turik, A. V., *Izv. AN SSSR, ser. fiz.*, Vol. 31, p. 1861, 1967.
120. Sannikov, D. G., *ZhETF*, Vol. 41, p. 133, 1961; *Izv. AN SSSR, ser. fiz.*, Vol. 28, p. 703, 1964.
121. Nettleton, R. E., *J. Phys. Soc. Japan*, Vol. 21, p. 1633, 1966.
122. Nettleton, R. E., *J. Phys. Soc. Japan*, Vol. 22, p. 1375, 1967.
123. Lurio, A. and E. Stern, *J. Appl. Phys.*, Vol. 31, p. 1125, 1960.
124. Nakamura, E. and J. Furuichi, *J. Phys. Soc. Japan*, Vol. 15, p. 2101, 1960.
125. Petrov, V. M., *Kristallografiya*, Vol. 6, p. 632, 1961.
126. Nakamura, E., *J. Phys. Soc. Japan*, Vol. 17, p. 961, 1962.
127. Hill, R. M. and S. K. Ichiki, *Phys. Rev.*, Vol. 128, p. 1140, 1962.
128. Hill, R. M. and S. K. Ichiki, *Phys. Rev.*, Vol. 132, p. 1603, 1963.
129. Sonin, A. S. and S. S. Gorbach, *Izv. AN SSSR, ser. fiz.*, Vol. 29, p. 1996, 1965.
130. Poplavko, Yu. M. and L. P. Solomonova, *FTT*, Vol. 8, p. 2455, 1966; *Izv. AN SSSR, ser. fiz.*, Vol. 31, p. 1771, 1967.

131. Bantle, W. and G. Busch, *Helv. Phys. Acta*, Vol. 10, p. 262, 1937.
132. Mueller, H., *Phys. Rev.*, Vol. 58, p. 565, 1940.
133. Akao, H., T. Tanakura and T. Sasaki, *J. Phys. Soc. Japan*, Vol. 7, p. 361, 1952.
134. Akao, H. and T. Sasaki, *J. Chem. Phys.*, Vol. 23, p. 2710, 1955.
135. Iackle, W., *Z. angew. Phys.*, Vol. 12, p. 148, 1960.
136. Petrov, V. M., *Kristallografiya*, Vol. 7, p. 403, 1962.
137. Sandy, F. and R. V. Jones, *Phys. Rev.*, Vol. 168, p. 481, 1968.
138. Granicher, H. and W. Shurter, *Z. angew. Math. Phys.*, Vol. 8, p. 382, 1957.
139. Hill, R. M. and S. K. Ickiki, *Phys. Rev.*, Vol. 130, p. 150, 1963.
140. Kaminow, I. P. and G. O. Harding, *Phys. Rev.*, Vol. 129, p. 1562, 1963.
141. Kaminow, I. P., *Phys. Rev.*, Vol. 138, p. A1539, 1965.
142. Mason, W. P., *Phys. Rev.*, Vol. 72, p. 854, 1947.
143. Silvermar, B. D., *Phys. Rev. Lett.*, Vol. 20, p. 443, 1968.
144. Nakamura, E., *J. Phys. Soc. Japan*, Vol. 17, p. 961, 1962.
145. Hatta, I., T. Sakudo and S. Sawada, *J. Phys. Soc. Japan*, Vol. 21, p. 1612, 1966.
146. Hatta, I., *J. Phys. Soc. Japan*, Vol. 24, p. 1045, 1968.
147. Yamadam, I. and Y. Fujii, *J. Phys. Soc. Japan*, Vol. 21, p. 1613, 1966.
148. Yamada, Y. and Y. Fujii, *J. Phys. Soc. Japan*, Vol. 24, p. 1053, 1968.
149. Zheludev, I. S., M. A. Proskurin, V. A. Yurin and A. S. Baberkin, *DAN SSSR*, Vol. 103, p. 207, 1955.
150. Yurin, V. A., *Kristallografiya*, Vol. 1, p. 734, 1956.
151. Zheludev, I. S. and V. A. Yurin, *Izv. AN SSSR, ser. fiz.*, Vol. 20, p. 211, 1956.
152. Yurin, V. A., *Izv. AN SSSR, ser. fiz.*, Vol. 21, p. 329, 1957.
153. Yurin, V. A., *Izv. AN SSSR, ser. fiz.*, Vol. 24, p. 1329, 1960.

154. Yurin, V. A., A. S. Baberkin, E. N. Korniyenko and I. V. Gavrilova, Izv. AN SSSR, ser. fiz., Vol. 24, p. 1334, 1960.
155. Eisner, I. Ya., Kristallografiya, Vol. 2, p. 296, 1957.
156. Eisner, I. Ya., Kristallografiya, Vol. 9, p. 111, 1964.
157. Chyncweth, A. G., Phys. Rev., Vol. 113, p. 159, 1959.
158. Okada, K., J. Phys. Soc. Japan, Vol. 16, p. 414, 1961.
159. Okada, K., J. Phys. Soc. Japan, Vol. 16, p. 1647, 1961.
160. Okada, K., Japan J. Appl. Phys., Vol. 2, p. 613, 1963.
161. Peshikov, Ye. V. and S. V. Starodubtsev, FTT, Vol. 4, p. 239, 1962.
162. Starodubtsev, S. V. and Ye. V. Peshikov, Radiatsionnyye Effekty v Tverdykh Telakh (Radiation Effects in Solids), Academy of Sciences UzSSR Publishing House, Tashkent, p. 126, 1963.
163. Starodubtsev, S. V. and Ye. V. Peshikov, Radiatsionnyye Effekty v Tverdykh Telakh, Academy of Sciences UzSSR Publishing House, Tashkent, p. 129, 1963.
164. Starodubtsev, S. V. and Ye. V. Peshikov, FTT, Vol. 7, p. 3175, 1965.
165. Peshikov, E. V. and S. V. Starodubtsev, Proc. Intern. Meet. Ferroelectr., Vol. 2, Prague, p. 267, 1966.
166. Karmen, K. N., FTT, Vol. 2, p. 679, 1960.
167. Toyoda, K., A. Shimada and T. Tanaka, J. Phys. Soc. Japan, Vol. 15, p. 536, 1960.
168. Sil'vestrova, I. M. and V. A. Yurin, FTT, Vol. 4, p. 2319, 1962.
169. Rewai, T., Phys. St. Sol., Vol. 2, p. 1151, 1962.
170. Krueger, H. A., W. R. Cook, C. C. Sartain and H. P. Yockey, J. Appl. Phys., Vol. 34, p. 218, 1963.
171. Boutin, H., B. C. Frazer and H. F. Jona, J. Phys. Chem. Sol., Vol. 24, p. 1341, 1963.
172. Toyoda, K., A. Kawabata and T. Tanaka, Japan J. Appl. Phys., Vol. 2, p. 311, 1963.
173. Romanyuk, N. A. and N. S. Pidzyraylo, Kristallografiya, Vol. 9, p. 870, 1964.

174. Romanyuk, N. A. and I. S. Zheludev, Kristallografiya Vol. 9, p. 876, 1964.
175. Tuktarova, L. S., Kristallografiya, Vol. 10, p. 432, 1965.
176. Asch, G. and R. Michel, Japan J. Appl. Phys., Vol. 6, p. 1008, 1967.
177. Eisner, I. Ya., Izv. AN SSSR, ser. fiz., Vol. 21, p. 334, 1957.
178. Konstantinova, V. P. and V. A. Yurin, Kristallografiya, Vol. 2, p. 294, 1957.
179. Yurin, V. A. and I. S. Zheludev, Kristallografiya, Vol. 4, p. 253, 1959.
180. Rogers, F. T., J. Appl. Phys., Vol. 27, p. 1066, 1956.
181. Wittels, M. C. and F. A. Sherrill, J. Appl. Phys., Vol. 28, p. 606, 1957.
182. Lefkowitz, I. and T. Mitsu, J. Appl. Phys., Vol. 30, p. 269, 1959.
183. Lefkowitz, I., J. Phys. Chem. Sol., Vol. 10, p. 169, 1959.
184. Vodop'yanov, L. K. and G. I. Skanavi, Izv. AN SSSR, ser. fiz., Vol. 24, p. 253, 1960.
185. Hilczer, B., Bull. Acad. Polon. Sci., Vol. 10, p. 353, 1967.
186. Hilczer, B., Phys. St. Sol., Vol. 2, p. 447, 1962.
187. Schenk, M., Phys. St. Sol., Vol. 4, K25, 1964.
188. Hilczer, B., Phys. St. Sol., Vol. 5, K113, 1965.
189. Glower, D. D. and D. L. Hester, J. Appl. Phys., Vol. 36, p. 2175, 1965.
190. Weik, H. and J. Schneider, J. Phys. Lett., Vol. 19, p. 619, 1966.
191. Solovev, S. P., I. I. Kuzmin and V. A. Harchenko, Proc. Intern. Meet. Ferroelectr., Vol. 2, Prague, p. 277, 1966.
192. Peshikov, Ye. V. and S. V. Starodubtsev, Radiatsionnyye Narusheniya v Tverdykh Telakh i Zhidkostyakh (Radiation Damage in Solids and Liquids), FAN [Branch of the Academy of Sciences, USSR] Publishing House, Tashkent, p. 60, 1967.

## CHAPTER 10. ELECTROMECHANICAL PROPERTIES OF FERROELECTRICS

### §1. Ferroelectrics That Are Not Piezoelectrics in Paraelectric Phase

By examining the thermodynamic potential of a piezoelectric crystal successively: as a function of deformations and polarization ( $u, P$ ), mechanical stresses and polarization ( $\sigma, P$ ), deformation and electric field strength ( $u, E$ ), mechanical stresses and field strength ( $\sigma, E$ ) and discarding terms of higher orders, we may derive the following equations:

$$u_{ij} = -c_{ijkl}^0 u_{kl} + q_{ijkl} P_k P_l \quad (10.1)$$

$$u_{ij} = -e_{ijk}^0 u_{kl} - v_{ijkl} P_k P_l \quad (10.2)$$

$$u_{ij} = -c_{ijkl}^0 u_{kl} + \lambda_{ijkl} E_k E_l \quad (10.3)$$

$$u_{ij} = -e_{ijk}^0 u_{kl} + \lambda_{ijkl} E_k E_l \quad (10.4)$$

From these equations, by substituting (10.2) into (10.1) and (10.4) into (10.3), we obtain relations that give the relationship between the coefficients of electrostriction, or inverse piezoelectric effect,  $q$  and  $\tilde{e}$ ,  $v$  and  $\lambda$ :

$$v_{ijkl} = e_{ijk}^0 q_{lmn} \delta_{lm} \delta_{kn} \quad (10.5)$$

$$q_{ijkl} = c_{jkmn}^0 \delta_{kn} \delta_{lm} \quad (10.6)$$

$$\lambda_{ijkl} = e_{ijk}^0 v_{lmn} \delta_{lm} \delta_{kn} \quad (10.7)$$

$$v_{ijkl} = c_{jkmn}^0 \lambda_{lmn} \delta_{lm} \delta_{kn} \quad (10.8)$$

After replacing in (10.1) and (10.2) the polarization component by their expression through susceptibility and field strength ( $P_i = \chi_{ij} E_j$ ) and comparing (10.1) with (10.3), and also (10.2) with (10.4), we obtain

$$v_{ijkl} = q_{ijmn} \chi_{mk} \chi_{nl} \quad (10.9)$$

$$\lambda_{ijkl} = v_{ijmn} \chi_{mk} \chi_{nl} \quad (10.10)$$

Devonshire [1] demonstrated that the electrostrictional coefficients also have another physical meaning. By differentiating (10.2) two times with respect to the polarization components, we find:

$$\frac{\partial^2 u_{ij}}{\partial P_k \partial P_l} = \delta_{ijkl} + \delta_{ijlk} = 2\delta_{ijkl}. \quad (10.11)$$

On the other hand, the relations

$$\left(\frac{\partial u_{ij}}{\partial P_k}\right)_c = \left(\frac{\partial E_k}{\partial \sigma_{ij}}\right)_P. \quad (10.12)$$

are valid. Hence

$$2\delta_{ijkl} = \frac{\partial^2 E_k}{\partial \sigma_{ij} \partial P_l} = \left[ \frac{\partial \left( \frac{1}{\lambda_{kl}} \right)}{\partial \sigma_{ij}} \right]_P. \quad (10.13)$$

Analogously we may derive

$$2\lambda_{ijkl} = \left( \frac{\partial \lambda_{kl}}{\partial \sigma_{ij}} \right)_P. \quad (10.14)$$

Thus, coefficients  $\lambda$  and  $\delta$  mean the rate of change of susceptibility and its inverse value, respectively, with pressure.

We will now find out what will be the result at the Curie point of spontaneous polarization, which can be treated as a unique type of "action," leading to a reduction of symmetry of the crystal. Then, according to the Curie principle, a crystal (more accurately, domain) in the ferroelectric phase will possess elements of symmetry, which are common to the crystal in the paraelectric phase and to the polar vector. Here the inversion center will be lost and the crystal will become a piezoelectric. Thus the piezoelectric effect in such ferroelectrics may be considered a morphic effect. Strictly speaking, these considerations are valid only for second order phase transitions, since in the case of the first order transition the symmetries of both phases are unrelated. But since during ferroelectric phase transitions there is no fundamental rearrangement of the crystal and the distortions of the crystal lattice that do occur are very small, treatment of spontaneous polarization as an "action" is always valid. From this standpoint it might be expected that equations (10.1) and (10.2) will also be valid for the ferroelectric phase, with the same electrostrictional coefficients  $\delta$  and  $q$ , and polarization will be defined as the sum of spontaneous and induced polarization. Then equation (10.2), for the case of a mechanically free crystal ( $\sigma = 0$ ), will acquire the form:

$$[u_{ij}] = \delta_{ijkl} (P_{ik} + P_{ki}) (E_{jl} + E_{lj}) = \delta_{ijkl} P_{ik} P_{jl} + \delta_{ijlk} P_{ik} P_{jl} + \delta_{ijkl} P_{ik} P_{jl} + \delta_{ijlk} P_{ik} P_{jl}. \quad (10.15)$$

The first term in (10.15) corresponds to spontaneous  $(u_{ij})_s$ , the second and third to piezoelectric  $(u_{ij})_p$ , and the fourth to electrostrictional deformations:

[n=p]

$$(u_{ij})_0 = \delta_{ij} P_{ik} P_{kl} \quad (10.16)$$

$$(u_{ij})_0 = 2\delta_{ijk} P_{kl} P_{lm} + g_{ij} P_{kl} \quad (10.17)$$

where

$$g_{ij} = 2\delta_{ijk} P_{kl} \quad (10.18)$$

On the other hand

$$(u_{ij})_0 = d_{ij} E_i \quad (10.19)$$

Comparing (10.19) and (10.17), and recalling (10.18), we obtain:

$$d_{ij} = g_{kij} \lambda_{kl} = 2\delta_{ijk} P_{lm} \lambda_{kl} \quad (10.20)$$

It is clear from (10.17) that the piezoelectric effect in the ferroelectric phase can be regarded in this case as electrostriction, linearized by spontaneous polarization. We will note that (10.18) may be derived through differentiation of (10.2) with respect to  $P_j$ . Knowing the electrostrictional coefficients  $\delta$  for the paraelectric phase and the magnitude and direction of spontaneous polarization, we can determine from (10.15) all tensor components of spontaneous deformation, and from (10.18) the piezoelectric coefficients  $g$ . In consideration of the terms of higher orders in (10.2) in the expansion of free energy, there will be terms of the fourth, sixth, etc. orders in terms of polarization. Consequently each term in (10.15) will have an additive, although a small one from the practical point of view. Moreover, in (10.15), in addition to quadratic terms for  $P_{in}$ , with coefficients  $\delta$ , there will be other new quadratic terms. The coefficients of these terms will correspond to the tensor components of the electrostriction coefficients of the ferroelectric phase, which were the result of reduction of crystal symmetry.

The coefficient of elastic pliancy and rigidity in the ferroelectric phase, determined under conditions of constant polarization and constant electric field, can differ substantially. In the general case we have for deformation tensor components:

$$u_{ij} = -\delta_{ijk} P_{kl}^2 + g_{kij} P_{kl} \quad (10.21)$$

When :

$$P_i = -d_{ijk} E_j \quad (10.22)$$

Substituting (10.22) into (10.21) and separating the terms with the same mechanical stress tensor components, we obtain [1]:

$$s_{ijkl}^p = s_{ijkl}^r + \epsilon_{mij} d_{pkl}. \quad (10.23)$$

It follows from (10.23), recalling (10.20), that the behavior of certain elastic pliabilities  $s_{ijkl}^E$  is determined by the behavior of dielectric susceptibility.

The examination presented here, naturally, is valid only for a single-domain crystal. When a crystal is broken down into domains, as pointed out in Chapter 7, according to the rule formulated by Zheludev and Shuvalov [2, 3], the elements of symmetry of the initial nonferroelectric phase that are lost on transition into the ferroelectric phase become elements of twinning. Therefore a multidomain crystal (not unipolar) displays macro-symmetry in the nonferroelectric phase. Hence, if the latter is centrosymmetric it should not display the piezoelectric effect.

We will now examine the electrostriction, piezoelectric and elastic properties of the two best known ferroelectrics that are centrosymmetric in the paraelectric phase.

### 1. Barium Titanate

The matrix of electrostriction coefficients  $\delta$  for cubic barium titanate has the form

$$\begin{array}{cccccc} \delta_{11} & \delta_{12} & \delta_{12} & 0 & 0 & 0 \\ \delta_{12} & \delta_{21} & \delta_{12} & 0 & 0 & 0 \\ \delta_{12} & \delta_{12} & \delta_{11} & 0 & 0 & 0 \\ 0 & 0 & 0 & \delta_{44} & 0 & 0 \\ 0 & 0 & 0 & 0 & \delta_{44} & 0 \\ 0 & 0 & 0 & 0 & 0 & \delta_{44} \end{array} \quad (10.24)$$

Coefficients  $\lambda$  also have the analogous matrix. In the case of a mechanically free crystal ( $\sigma = 0$ ) equations (10.2) and (10.4) are written as follows:

$$u_{ij} = \delta_{ijkl} E_k E_l, \quad (10.25)$$

$$u_{ij} = \lambda_{ijkl} E_k E_l. \quad (10.26)$$

If in the paraelectric phase, for instance, a field is applied along axis  $x_1$ , then (10.25) and (10.26) in matrix notation will acquire the form:

$$\left. \begin{array}{l} u_1 = \delta_{11} E_1^2 \\ u_2 = \delta_{12} E_1^2 \end{array} \right\} \quad (10.27)$$

$$\left. \begin{array}{l} u_1 = \lambda_{11} E_1^2 \\ u_2 = \lambda_{12} E_1^2 \end{array} \right\} \quad (10.28)$$

Hence coefficients  $\delta_{11}$ ,  $\delta_{12}$ ,  $\lambda_{11}$  and  $\lambda_{12}$  may be determined according to the experimental values of  $u_1$  and  $u_2$ . Schmidt [4] conducted such experiments. Relation (10.16) may also be used and, if the magnitude of spontaneous polarization and spontaneous deformations are known coefficients  $\delta_{11}$ ,  $\delta_{12}$  and  $\delta_{44}$  can be calculated. At room temperature, when symmetry is tetragonal, using  $P_S = P_3 = 2.6 \cdot 10^{-6}$  C/cm<sup>2</sup> [5],  $u_1 = u_2 = -3.4 \cdot 10^{-3}$  and  $u_3 = 7.5 \cdot 10^{-3}$  [6], we obtain [7]:

$$\left. \begin{aligned} \delta_{11} &= 1.25 \cdot 10^{-12} \text{ esu.} \\ \delta_{12} &= -0.56 \cdot 10^{-12} \text{ esu.} \end{aligned} \right\} \quad (10.29)$$

In order to determine the coefficient  $\delta_{44}$  it is necessary to take the values  $u_4$  and  $P_S$  for the rhombic phase. At 0°C  $u_4 = 2.9 \cdot 10^{-3}$ ,  $P_S = 51 \cdot 10^{-6}$  C/cm<sup>2</sup> [8] or  $P_S = 29.4 \cdot 10^{-6}$  C/cm<sup>2</sup> [9], and for  $\delta_{44}$  we obtain [7]:

$$\delta_{44} = \begin{cases} 0.67 \cdot 10^{-12} \text{ esu.} \\ 0.73 \cdot 10^{-12} \text{ esu.} \end{cases} \quad (10.30)$$

Investigations of the effect of mechanical stresses on the ferroelectric phase transition and the behavior of dielectric susceptibility in the paraelectric region show (see Chapter 13, §2) that when mechanical stresses are applied the Curie-Weiss law (9.1) and (9.2) continues to be valid, and here the Curie constant remains the same, while only  $\chi$  changes. In other words, the slope of the straight line  $\frac{1}{\chi}(T)$  remains the same. The straight line is simply displaced on the temperature axis parallel to itself. This means that  $\frac{\partial(\frac{1}{\chi})}{\partial T}$ , in view of (10.13) and  $\delta$ , is independent of temperature. Thus, coefficients  $\delta$  in the paraelectric phase are the "true" crystal constants. Since relations (10.9) and (10.10) are valid, the electrostriction coefficients  $\lambda$  and  $\nu$ , by virtue of the strong temperature dependence of susceptibility, increase rapidly as the Curie point is approached.

The matrix of the piezoelectric moduli for the tetragonal phase corresponds to the point group of this phase (4mm) and has the form:

$$\begin{pmatrix} 0 & 0 & 0 & 0 & d_{13} & 0 \\ 0 & 0 & e & d_{13} & 0 & 0 \\ d_{31} & d_{31} & d_{33} & 0 & 0 & 0 \end{pmatrix} \quad (10.31)$$

Expressions (10.18) for piezoelectric coefficients  $g$  and (10.20) for the piezoelectric moduli in the case when spontaneous polarization is directed on the  $z$  axis, are written in the form [10]:

$$g_{21} = 2\theta_{12}P_s \quad (10.32)$$

$$g_{33} = 2\theta_{11}P_s \quad (10.33)$$

$$g_{13} = \theta_{14}P_s \quad (10.34)$$

$$d_{21} = 2\theta_{12}P_s\alpha_2^0 \quad (10.35)$$

$$d_{33} = 2\theta_{11}P_s\alpha_3^0 \quad (10.36)$$

$$d_{13} = \theta_{14}P_s\alpha_1^0 \quad (10.37)$$

Using relations (10.32-10.37), we may determine on the basis of piezoelectric measurements the electrostriction coefficients  $\delta$ . Caspari and Merz [11], Berlincourt and Jaffe [7], Huibregtse, et al [12] investigated the piezoelectric properties of single-domain barium titanate monocrystals. The coefficients  $g$  and  $d$  at 25°C, according to [7], are listed in Table 17. Calculation of coefficients  $\delta$  on the basis of experimental values of the piezoelectric coefficients  $g$  using equations (10.32-10.34) yields:

$$\left. \begin{aligned} \theta_{11} &= 1.23 \cdot 10^{-12} \text{ esu} \\ \theta_{12} &= -0.49 \cdot 10^{-12} \text{ esu} \\ \theta_{14} &= 0.65 \cdot 10^{-12} \text{ esu} \end{aligned} \right\} \quad (10.38)$$

which agrees quite well with (10.29) and (10.30).

Table 17. Elastic and Piezoelectric Coefficients of Barium Titanate (Berlincourt and Jaffe [7])

1) Упругие податливости (при 25° С), $10^{-13}$ см <sup>2</sup> /дин				2) Пьезоэлектрические коэффициенты (при 25° С), эд. стат. ед.								
	3) монокристалл		4) керамика			3) монокристалл		4) керамика				
	3)	4)	3)	4)		3)	4)	3)	4)			
$k_{11}$	8.05	8.55	$d_{12} \cdot 10^6$	11.76	8.10	$d_{21} \cdot 10^6$	-1.04	-2.37				
$k_{33}$	15.7	8.93	$d_{33} \cdot 10^6$	2.57	5.73	$g_{12} \cdot 10^6$	5.07	6.27				
$k_{12}$	-2.35	-2.61	$g_{21} \cdot 10^6$	-7.67	-1.57	$g_{33} \cdot 10^6$	19.17	3.89				
$k_{13}$	-5.24	-2.85	5) Упругие податливости монокристаллов (при 150° С), $10^{-13}$ см <sup>2</sup> /дин									
$k_{14}$	18.4	23.3									$\delta_{11}$	8.33
$k_{15}$	8.8	22.3									$\delta_{12}$	-2.68
$D_{11}$	1.25	8.18									$\delta_{13}$	9.24
$D_{33}$	10.8	6.78										
$\delta_{11}$	-3.45	-2.88										
$\delta_{12}$	-3.28	-1.95										
$\delta_{13}$	12.4	18.3										

- KEY: 1. Pliances at 25°C,  $10^{-13}$  cm<sup>2</sup>/dyne  
 2. Piezoelectric coefficients at 25°C, esu  
 3. Monocrystals  
 4. Ceramics  
 5. Elastic pliances of monocrystals at 150°C,  $10^{-13}$  cm<sup>2</sup>/dyne

Calculations by both methods yield similar values of  $d_{31}^0$  up to the Curie point. On transition to the paraelectric phase the electrostriction coefficients  $\delta$  remain practically constant (Figure 10.1a). This most convincingly shows that the coefficients  $\delta$  are the "true" crystal constants. The temperature dependences of the piezoelectric moduli  $d_{31}$  and  $d_{33}$ , according to (10.35) and (10.36), are determined by the dependence of  $\chi_3^0$  (or  $\epsilon_c^0$ ) on temperature, and therefore increase sharply in absolute value as the Curie point is approached. The dependence of  $d_{31}$  on temperature is illustrated in Figure 10.1b.

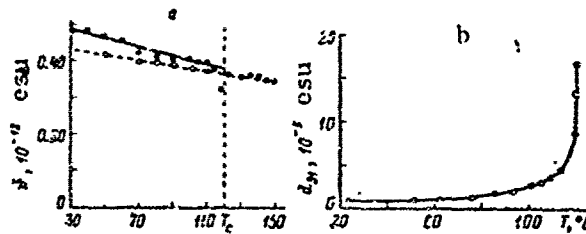


Figure 10.1. Electrostriction and piezoelectric properties of barium titanate monocrystal (Huibregtse, et al [12]). a -- temperature dependence of electrostriction coefficient  $\delta_{12}^0$ , determined as  $u_1/P_3^2$  (broken curve),  $2nd_{31}/\epsilon_3^0 P_3$  (continuous curve); b -- temperature dependence of piezoelectric modulus  $d_{31}$ .

The entire discussion so far has concerned the single-domain monocrystal. If  $180^\circ$  repolarization processes, which occur under the influence of a sufficiently strong electric field, are taken into account, the deformation pattern of a crystal becomes much more complex. The dielectric hysteresis loop is illustrated schematically in Figure 10.2a, and also shown in Figure 10.2b and c is the corresponding curve of change of crystal deformation.

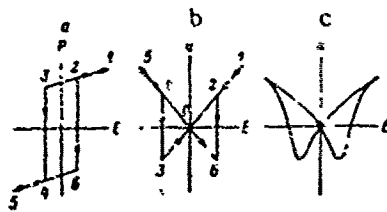


Figure 10.2. Schematic diagrams of: a -- dielectric hysteresis loop; b -- hysteresis quadratic dependence of deformation on electric field strength (ideal); c -- actual dependence of deformation on electric field strength.

It is assumed that only  $180^\circ$  repolarization takes place. Piezoelectric deformation takes place on segment 1-2-3. The transition from 3-4 is related to repolarization and the sign of piezoelectric deformation changes. On segment 4-5, where the crystal is again single-domain, deformation once again becomes a linear function of the field. When the field has the opposite direction deformation changes in the sequence 5-4-6-2-1. Thus, the dependence of deformation on field strength resembles a butterfly.

The elastic properties of barium titanate monocrystals in the cubic and tetragonal phases were analyzed by Berlincourt and Jaffe [7] and Huibregtse, et al [12, 15]. The values of  $s_{ij}^E$  and  $s_{ij}^P$  at 25 and 150°C [7] are presented in Table 17, and the temperature dependences of  $s_{11}^P$ ,  $s_{11}^E$  and  $(2s_{12} + s_{66})^P$  are shown in Figure 10.3). For the tetragonal phase, when  $P_s$  is directed along the  $z$  axis, after substitution of coefficients  $g$  and  $d$  according to (10.32-10.37), (10.23) yields [10]:

$$\left. \begin{aligned} s_{11}^E &= s_{11}^P = s_{11}^E + 4s_{11}^E P_s^2 \chi_3^E \\ s_{12}^E &= s_{12}^P + 4s_{12}^E P_s^2 \chi_3^E \\ s_{13}^E &= s_{13}^P + 4s_{13}^E P_s^2 \chi_3^E \\ s_{14}^E &= s_{14}^P = s_{14}^E + 16s_{14}^E P_s^2 \chi_3^E \\ s_{15}^E &= s_{15}^P = s_{15}^E + 8s_{15}^E P_s^2 \chi_3^E \\ s_{22}^E &= s_{22}^P \end{aligned} \right\} \quad (10.39)$$

It follows from (10.39) that the temperature dependences of  $s_{11}^E$  and  $(2s_{12}^E + s_{66}^E)$  in the tetragonal phase should reflect the change of  $\chi_3^E$  with the susceptibility temperature, which is observed experimentally (Figure 10.2). For elastic pliancies, determined for  $P = \text{const}$ , we should expect a weak temperature dependence. This is true for  $(2s_{12} + s_{66})^P$ . The increase of  $s_{11}^P$  in the tetragonal phase, observed experimentally, as the Curie point is approached, is not understood. The reason is perhaps the fact that near the Curie point, despite the polarizing field applied during the measurements, domains appear. Elastic pliancies in the cubic phase are identical during constant polarization and constant field, since here there is no piezoelectric effect.



Figure 10.5. Temperature dependence of elastic properties of barium titanate monocrystal (Huibregtse, et al [12]).  
a -- temperature dependence of elastic pliancies  $s_{11}^P$  and  $s_{11}^E$ ; b -- temperature dependence of  $(2s_{12} + s_{66})^P$  (broken curve) and  $(2s_{12} + s_{66})^E$  (continuous curve).

Roberts [14] and Rzhhanov [15, 16] independently discovered that polycrystalline barium titanate, after polarization in a sufficiently strong constant electric field, displays great piezoelectric activity. Processes of repolarization occur in individual crystallites under the influence of the polarizing field, with the result that a polar axis appears in a ceramic specimen, coinciding in direction with the field. Such a ceramic is a special case of piezoelectric textures, examined by Shubnikov [17, 18], and belongs to the point group  $\infty m$ , i.e., has a rotation axis of infinite order and an infinite number of planes of symmetry parallel to it. When the polarizing field is applied along the z axis the matrix of piezoelectric moduli of this ceramic has the form (10.31).

Bogdanov, et al [19, 20], Shuvalov [21], Kholodenko and Shirobokov [22], by averaging, derived the expressions for the piezoelectric moduli of ceramics through the piezoelectric moduli of a monocrystal. In these calculations a certain distribution of orientations  $P_g$  after polarization was assumed. For simplicity the interaction between individual grains was not taken into account and it was assumed that the electric field was homogeneous in the entire specimen and equal to the average macroscopic field, i.e., the anisotropy of permittivity in the domains was not taken into account. The question of orientations  $P_g$  after polarization was examined in §5, Chapter 8. We will recall simply that mainly  $180^\circ$  repolarization takes place.

Marutake and Ikeda [23, 24], who assumed that a ceramic consists of unidomain spherical crystallites, used a somewhat different method to determine the physical properties of ceramics through the properties of a monocrystal. In their calculations they considered the anisotropy of the permittivity of the crystallites and their piezoelectric interaction. The average piezoelectric moduli of ceramics calculated by both methods are quite close to the experimental values, taking into account also that the latter have greater scattering, since they depend on porosity, industrial technology, etc.

Mason [25], who examined nonpolarized ceramics as a homogeneous medium possessing electrostriction, in which polarization occurs under the influence of a constant field, took a totally different approach to the problem of determining the physical properties of ceramics. These notions are also developed by Baerwald [26]. The piezoelectric properties of polycrystalline barium titanate have been analyzed experimentally by numerous investigators [14-16, 24, 25, 27-42]. The influence of the porosity of specimens [37] and of the conditions of polarization [34, 38, 43] on piezoelectric properties has been investigated. In addition to the most easily measured piezoelectric moduli  $d_{31}$  and  $d_{33}$ , Bogdanov, et al [36, 44] determined piezoelectric modulus  $d_{15}$ . The values of the piezoelectric moduli are presented in Table 18. Polarized ceramics also displays a volumetric piezoelectric effect, and under the influence of hydrostatic pressure p polarization appears:

$$P_3 = (2d_{31} + d_{33}) E$$

(16.46)

This effect is investigated by Jaffe [45], and also by Perls, et al [46].

It was pointed out above that the character of deformation of a monocrystal under the influence of an electric field is determined not only by the piezoelectric effect, but also by  $180^\circ$  repolarization, with the result that the sign of deformation is changed. The same is true for ceramics, but here, as in the case of monocrystals with  $90^\circ$  domains, there is also the process of partial  $90^\circ$  repolarization (for example displacement of  $90^\circ$  walls) under the influence of an electric field. By virtue of the tetragonality of the elementary cell, rotation of spontaneous polarization by  $90^\circ$ , even in a small volume, leads to substantial deformation of the entire specimen.

The dependence of the deformation of ceramics on the electric field strength was investigated by several authors [47-49]. It is of quadratic character (Figure 10.2c), and therefore this effect is usually called electrostriction. The dependence is quadratic by virtue both of the fact that  $180^\circ$  repolarization changes the sign of piezoelectric deformation and of the fact that  $90^\circ$  repolarization occurs chiefly from a position nearly perpendicular to the field to a position nearly parallel to the field. The fraction of reorientations from the direction antiparallel to the field to perpendicular is apparently small, since the processes are primarily those of  $180^\circ$  reorientation. The fraction of  $90^\circ$  reorientations is determined on the basis of the magnitude of deformation during polarization [48, 49].

$90^\circ$  reorientation may occur, apparently the result chiefly of the motion of  $90^\circ$  domain walls between domains with spontaneous polarization directed, roughly speaking, perpendicular and parallel to polarization, can also occur in polarized ceramics in a field that is weak enough so as not to reduce residual polarization. Such wall movement results in deformations with the same sign as piezoelectric deformations. The contribution of these deformations to the overall effective piezoelectric deformation in barium titanate is apparently large only near the Curie point. In all likelihood it is specifically  $90^\circ$  reorientations that are responsible for the maximum experimentally observed piezoelectric modulus  $|d_{31}|$  near the Curie point.

During measurements in a rather strong polarizing field the temperature dependence of  $|d_{31}|$  in the tetragonal phase, as is to be expected, according to calculation formulas [19-22], is close to the temperature dependence of  $d_{15}$  of the monocrystal [10] and practically no maximum is observed near the Curie point [50].

$180^\circ$  reorientation should not be expected to contribute greatly to the effective piezoelectric deformation in the case of solid solutions of  $\text{Ba}(\text{Ti}, \text{Sn})\text{O}_3$  and  $\text{Ba}(\text{Ti}, \text{Zr})\text{O}_3$ , in which domain wall mobility is great.

Roy [51] and Bokov [50] found that in certain of these solid solutions the

dependence of piezoelectric moduli  $d_{33}$  and  $|d_{31}|$  on polarizing field intensity passes through a maximum. This anomalous dependence can be explained on the basis of the large contribution of processes other than  $180^\circ$  reorientation to the effective piezoelectric effect. The question of the dependence of the piezoelectric modulus and losses on the strength of a variable stimulating electric field, important for the practical application of piezoceramics, was investigated in several works [52-56].

The piezoelectric moduli of polarized ceramics, like dielectric polarization, diminish as time passes, and aging occurs. The most notable drop occurs during the first hours after polarization, then it levels off gradually [35, 53, 57]. At the same time the Q-factor of the ceramic piezoelectric element increases [57]. Reduction of the piezoelectric moduli is apparently related to slight depolarization as a result of reverse  $90^\circ$  reorientations.

The piezoelectric properties of ceramic barium titanate have been investigated in a number of works in the static mode in a strong electric field or in the presence of large mechanical stresses. If piezoelectric deformations, according to Kovalenko [58], increase linearly, at least up to 5 kV/cm as the strength of a stationary electric field increases, then the dependence of polarization on mechanical stresses is nonlinear. The direct piezoelectric effect has been investigated in numerous works [44, 48, 59-66]. Under compression in the direction of polarization, the dependence of the induced charge on mechanical stresses has a maximum [62, 66]. If a specimen is compressed in the direction perpendicular to polarization, this dependence also has a maximum, and with stresses of 400-660 kg/cm<sup>2</sup> the sign of the induced charge changes [62, 63, 65, 66]. It is noteworthy here that the sign of change of polarization remains unchanged after the removal of a small load [65]. The dependence of polarization on hydrostatic pressure is linear, at least up to 1,000 kg/cm<sup>2</sup> [65].

The unusual dependences of polarization on mechanical stresses can be explained qualitatively by the  $90^\circ$  reorientations that occur under the influence of pressure. Here, as shown by tests, rather strong mechanical stresses can lead even to depolarization. That pressure actually causes  $90^\circ$  reorientation is verified by the results of Subbarao, et al [67], Berlincourt and Krueger [48], Belyukhanova, et al [68], Syrkin and El'gard [69]. It was shown in these works that deformation in the ferroelectric phase, occurring under the influence of mechanical stresses, is established over a long period of time, reaching tens of minutes, which can be explained only by rearrangement of domain structure.

These same processes explain mechanical nonlinearity in the presence of dynamic stresses, observed in the tests of Verlyukhanova, et al [68]. The elastic properties of ceramics under small loads depend substantially on the polarizing intensity. Young's modulus increases as the field increases (this effect is analogous to the so-called  $\Delta E$ -effect in ferromagnetics), and the forward and reverse curves do not coincide, which leads during cyclic change of the field to a "butterfly" type dependence [24, 25, 70].

At the Curie temperature and at the temperatures of transition from a ferroelectric phase with one symmetry to a ferroelectric phase with another symmetry Young's modulus has minima [29, 31, 32, 50, 57, 70]. The dependence of the elastic constants of barium titanate ceramics on porosity was investigated by Marutake and Ikeda [71].

## 2. Triglycine Sulfate

The matrix of electrostriction coefficients  $d^c$  of triglycine sulfate in the paraelectric phase has the form:

$$\begin{array}{cccccc}
 d_{11} & d_{12} & d_{13} & 0 & d_{15} & 0 \\
 d_{21} & d_{22} & d_{23} & 0 & d_{25} & 0 \\
 d_{31} & d_{32} & d_{33} & 0 & d_{35} & 0 \\
 0 & 0 & 0 & d_{41} & 0 & d_{44} \\
 d_{51} & d_{52} & d_{53} & 0 & d_{55} & 0 \\
 0 & 0 & 0 & d_{61} & 0 & d_{66}
 \end{array} \quad (10.41)$$

Spontaneous polarization on the y axis leads to linearization of electrostriction, i.e., the appearance of the piezoelectric effect. The piezoelectric coefficients  $g$  can be determined according to (10.18), whence in the specific case:

$$\left. \begin{array}{l}
 g_{1i} = 2d_{1i}P_y \quad (i = 1, 2, 3 \neq 5), \\
 g_{11} = d_{11}P_x, \\
 g_{24} = d_{24}P_x, \\
 g_{24} = d_{44}P_x, \\
 g_{12} = d_{42}P_x.
 \end{array} \right\} \quad (10.42)$$

The corresponding piezoelectric moduli  $d$  will be nonzero values. Here, according to (10.20), only piezoelectric moduli  $d_{2i}$  should display anomalies at the Curie point, since only they are related to anomalously increasing susceptibility  $\chi_2^c$ .

The electrostriction and piezoelectric properties of triglycine sulfate crystals have been investigated by many researchers, although measurement results do not coincide satisfactorily. Konstantinova, et al [72, 73], and also Hussimi and Kataoka [74], were the first to derive the complete matrices of piezoelectric moduli, and also of the coefficients of elastic pliancy and rigidity. The results of these investigations do not agree. Data [72, 73] were subjected to critical review in [75]. Later on Ikeda and coauthors [76] measured piezoelectric moduli  $d_{21}$ ,  $d_{22}$ ,  $d_{23}$ ,  $d_{25}$ , and Fotchenkov and Zaytseva [77] measured piezoelectric modulus  $d_{22}$ , but even in this case the values of  $d_{22}$  do not coincide satisfactorily. The basic cause of the discrepancy between the experimental data is apparently the different degree of monodomianization of the crystals in the various tests.

The relations between the coefficients are readily found by substitution. Thus, by substituting (10.49) into (10.48) and comparing with (10.50) we have:

$$d_{ijk} = -\epsilon_{ilm} \delta_{lmjk} \quad (10.51)$$

$$\chi_{ij}^u = \chi_{ij}^u + \epsilon_{ilm} d_{jlm} \quad (10.52)$$

Analogously, we obtain:

$$g_{ijk} = h_{ilm} \delta_{lmjk} \quad (10.53)$$

$$d_{ijk} = g_{ijk} \chi_{ij}^u \quad (10.54)$$

$$e_{ijk} = \delta_{ilm} \chi_{ij}^u \quad (10.55)$$

$$\chi_{ij}^u = \chi_{ij}^u - h_{ilm} g_{jlm} \quad (10.56)$$

$$d_{ijkl}^E = d_{ijkl}^E + g_{kmn} d_{mkl} \quad (10.57)$$

$$c_{ijkl}^E = c_{ijkl}^E + h_{kmn} e_{mkl} \quad (10.58)$$

All coefficients are related, which is particularly important for crystals with the ferroelectric phase transition.

At least one of the tensor components of dielectric susceptibilities  $\chi^u$  and  $\chi^G$  has an anomaly at the Curie point. Therefore it follows from (10.54) that either the piezoelectric moduli  $d$  related to them, or piezoelectric coefficients  $g$  also have an anomaly. On the basis of (10.55) the same can be said of coefficients  $e$  and  $h$ . As we will see later on, experiments show that coefficients  $d$  and  $e$  are anomalous, and piezoelectric coefficients  $g$  remain practically constant during the phase transition. This indicates that the spontaneous polarization that occurs is not reflected on the relation between such crystal parameters as deformation and polarization. Therefore spontaneous deformation can be regarded as a manifestation of the inverse piezoelectric effect.

It follows from (10.57) and (10.58) that by virtue of the anomalous behavior of piezoelectric coefficients  $d$  and  $e$  in the region of the ferroelectric phase transition, the coefficients that describe elastic properties should also be anomalous. Tests have shown that  $s^E$  and  $c^E$  also display an anomaly. Thus, by way of summary we will note that coefficients  $d$ ,  $e$ ,  $s^E$  and  $c^E$  behave anomalously during the ferroelectric phase transition as a consequence of an increase of  $\chi^u$  and  $\chi^G$ .

In equations (10.43)-(10.50) we considered only the terms that are linear with respect to  $P$  and  $E$ . Quadratic terms could also be considered. Then, for example, instead of equation (10.45) for a mechanically free crystal we will have

$$u_i = \epsilon_{ij} P_j + \delta_{ijk} P_k P_j \quad (10.59)$$

If polarization in the ferroelectric phase is regarded as the sum of spontaneous and induced polarizations, then equation (10.59) will become:

$$[N=in] \quad u_{ij} = \epsilon_{kij} P_{sk} + \epsilon_{kij} P_{sk} + \delta_{ijkl} P_{sk} P_{sl} + 2\delta_{ijkl} P_{sk} P_{sl} + \delta_{ijkl} P_{sk} P_{sl} \quad (10.60)$$

hence

$$(u_{ij})_s = \epsilon_{kij} P_{sk} + \delta_{ijkl} P_{sk} P_{sl} \quad (10.61)$$

$$g_{kij} = \epsilon_{kij} + 2\delta_{ijkl} P_{sl} \quad (10.62)$$

Thus, spontaneous deformation should depend, strictly speaking, on  $P_s$ . It follows from (10.62) that piezoelectric coefficients  $g$  acquire some correction. This means in practice, first of all, that piezoelectric coefficients  $g$ , and consequently the corresponding piezoelectric moduli  $d$ , which were equal in the paraelectric phase, become unequal and, secondly, new piezoelectric coefficients appear. Both the former and the latter, naturally, correspond to the reduction of symmetry of the crystal. All this pertains to a single-domain crystal.

A crystal, breaking down into domains in the ferroelectric phase, thereby reverts, with respect to its macrosymmetry, to the symmetry of the paraelectric phase, and since the paraelectric phase is piezoelectric, then a polydomain crystal will display the piezoelectric effect [2, 3]. This is the chief difference between polydomain crystals of ferroelectrics that display and do not display the piezoelectric effect in the paraelectric phase.

We will now discuss the piezoelectric and elastic properties of two of the most thoroughly analyzed ferroelectrics that are acentrosymmetric in the paraelectric phase -- potassium dihydrophosphate and Seignette's salt.

### 1. Potassium Dihydrophosphate

$KH_2PO_4$  crystals are tetragonal in the paraelectric phase (point group  $\overline{4}2m$ ). The matrix of piezoelectric moduli for this phase is of the form:

$$\begin{matrix} 0 & 0 & 0 & d_{31} & 0 & 0 \\ 0 & 0 & 0 & 0 & d_{11} & 0 \\ 0 & 0 & 0 & 0 & 0 & d_{33} \end{matrix} \quad (10.63)$$

Spontaneous polarization occurs on the  $z$  axis. Susceptibility  $\chi_3^j$  on this axis obeys the Curie-Weiss law. Therefore, according to (10.54), we can expect that piezoelectric modulus  $d_{36}$ , relating polarization on the  $z$  axis to mechanical shear stresses, acting in plane  $xy$ , will have an

anomaly at the Curie point. As shown by the investigation of Bantle and Caflish [88] of the direct and of Arx and Bantle [89] of inverse piezoelectric effect, piezoelectric modulus  $d_{36}$  increases anomalously as it approaches the Curie point (Figure 10.4). The temperature dependence obeys the Curie-Weiss law:

$$d_{36} = d_{36}^0 + \frac{A}{T - T_0} \quad (10.64)$$

where  $A = 1.26 \cdot 10^{-7}$  esu and  $d_{36}^0 = -8 \cdot 10^{-8}$  esu. Since dielectric susceptibility  $\chi_3^\sigma$  also obeys the Curie-Weiss law, then, according to (10.54), piezoelectric coefficient  $g_{36}$ , which is equal to the ratio of shearing deformation  $u_6$  for  $\sigma = 0$  to polarization  $P_3$ , is not anomalous at the Curie point. It turns out, furthermore, that extrapolation of the temperature dependence of  $g_{36}$  to the ferroelectric phase agrees satisfactorily with the value obtained as the ratio of spontaneous deformation  $u_6$  to spontaneous polarization [90]. This is illustrated in Figure 10.5, where the temperature dependence of  $\frac{1}{g_{36}} = \frac{P_3}{u_6}$  is given. It is noteworthy that the ratio  $\frac{P_3}{u_6}$  is of the same order of magnitude as that of other piezoelectric crystals.

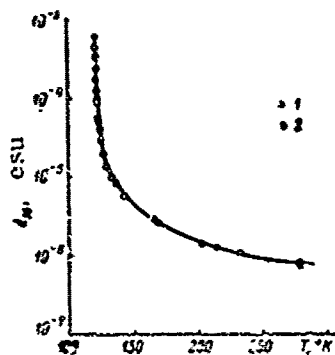


Figure 10.4. Temperature dependence of piezoelectric modulus  $d_{36}$  of potassium dihydrophosphate crystal. 1 -- values obtained by Bantle and Caflish [88] during measurement of direct piezoelectric effect; 2 -- values obtained by Arx and Bantle [89] during measurements of inverse piezoelectric effect.

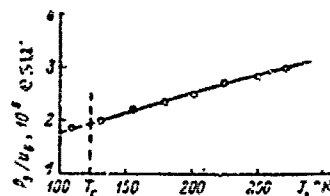


Figure 10.5. Temperature dependence of  $\frac{1}{g_{36}} = \frac{P_3}{u_6}$  for mechanically free potassium dihydrophosphate crystal.  $1/g_{36}$  in the paraelectric phase are calculated from  $\frac{1}{g_{36}} = \frac{\chi_3^\sigma}{d_{36}^\sigma}$  according to experimental values of  $\chi_3^\sigma$  and  $d_{36}^\sigma$ . The point in the ferroelectric phase was found as the ratio of spontaneous polarization to spontaneous deformation (De Quervain [90]).

Thus, we are convinced by example of potassium dihydrophosphate that piezoelectric coefficient  $g$  has no anomaly at the Curie point, and the anomaly of the piezoelectric modulus is a consequence of an anomaly of the corresponding dielectric susceptibility, and that spontaneous deformations can be viewed as the result of the inverse piezoelectric effect in the presence of spontaneous polarization. It was mentioned in Chapter 9 that the difference between inverse susceptibilities ( $\eta_3^u - \eta_3^\sigma$ ) in the paraelectric phase is independent of temperature. Therefore, it follows from (10.56), recalling the weak temperature dependence of  $g_{36}$ , that coefficient  $h_{36}$  also changes little with temperature. In other words, coefficients  $g$  and  $h$  are the "true" crystal constants.

For the mechanically free crystal, according to (10.45)  $u_6 = g_{36} P_3$ . Hence it is clear that near the Curie point, where polarization is a nonlinear function of field strength, the dependence of deformation on the field should also be nonlinear. Furthermore, nonlinearity can also be caused by electrostriction, as seen in (10.61). Nonlinearity of the dependence of deformation on electric field strength has been actually observed experimentally [83]. Potassium dihydrophosphate at the Curie point displays a rather large change of susceptibilities perpendicular to the axis of spontaneous polarization (Figure 9.5). Hence, according to (10.54), piezoelectric modulus  $d_{14}$  should also change. Such change was actually observed experimentally both in  $\text{KH}_2\text{PO}_4$  [91] and in crystals of isomorphic compounds  $\text{KD}_2\text{PO}_4$  and  $\text{RbH}_2\text{PO}_4$  [92].

Spontaneous deformation in potassium dihydrophosphate, as already mentioned, consists in displacement in the base plane, with the result that symmetry becomes rhombic. I. the new coordinate system corresponding to this symmetry orthogonal axes  $x'$  and  $y'$  extend along the diagonals of the square face of the elementary tetragonal cell, and the direction of the  $z$  axis remains the same. The matrix of piezoelectric moduli of the paraelectric phase in the new coordinate system has the form:

$$\begin{pmatrix} 0 & 0 & 0 & 0 & d'_{15} & 0 \\ 0 & 0 & 0 & -d'_{15} & 0 & 0 \\ d'_{31} & -d'_{31} & 0 & 0 & 0 & 0 \end{pmatrix} \quad (10.65)$$

It can be shown that  $d'_{31} = d_{36}/2$  and  $u'_1 + u'_2 = 2u'_1 = u'_c$ . Piezoelectric modulus  $d'_{31}$  is anomalous at the Curie point. In the ferroelectric phase potassium dihydrophosphate belongs to point group  $mm$  with the following matrix of piezoelectric moduli:

$$\begin{pmatrix} 0 & 0 & 0 & 0 & d'_{15} & 0 \\ 0 & 0 & 0 & d'_{15} & 0 & 0 \\ d'_{31} & d'_{31} & d'_{33} & 0 & 0 & 0 \end{pmatrix} \quad (10.66)$$

Due to the reduction of symmetry, equality of the absolute values in two pairs of piezoelectric moduli vanished and a new modulus  $d_{33}''$  appeared.

These changes can be interpreted as the result of electrostriction and spontaneous polarization, and they follow directly from the general examination presented at the beginning of this section. The polydomain crystal of potassium dihydrophosphate, as a ferroelectric crystal in the paraelectric phase, retains piezoelectric properties. Only piezoelectric modulus  $d_{33}''$  is lost.

The elastic properties of potassium dihydrophosphate are a good illustration of the features that should be observed at the Curie point in the behavior of certain elastic coefficients of ferroelectrics. The matrix of the coefficients of elastic pliancy of potassium dihydrophosphate in the paraelectric phase has the form:

$$\begin{array}{ccccccc}
 s_{11} & s_{12} & s_{13} & 0 & 0 & 0 & \\
 s_{12} & s_{11} & s_{13} & 0 & 0 & 0 & \\
 s_{13} & s_{13} & s_{33} & 0 & 0 & 0 & \\
 0 & 0 & 0 & \gamma_{44} & 0 & 0 & \\
 0 & 0 & 0 & 0 & \gamma_{44} & 0 & \\
 0 & 0 & 0 & 0 & 0 & 0 & s_{66}
 \end{array} \tag{10.67}$$

Piezoelectric modulus  $d_{36}$  has an anomaly in the paraelectric phase near the Curie point. Hence, according to (10.57) and (10.58), coefficients  $s_{66}^E$  and  $c_{66}^E$  should change anomalously with temperature. The cause of the anomaly is the following. The condition  $E = \text{const}$  is realized in the experiment as  $E = 0$ . On the facet perpendicular to the  $z$  axis are attached electrodes, which are shorted, and therefore a crystal investigated under these conditions is often a "shorted" crystal. If a shorted crystal is acted upon by shearing stress  $\sigma_6$ , then polarization occurs on the  $z$  axis. By virtue of the inverse piezoelectric effect, this leads to an increase in shearing deformation  $u_6$ . This effect will be particularly great near the Curie point, where piezoelectric modulus  $d_{36}$  increases anomalously. Hence the pliancy of the crystal to shearing stresses  $\sigma_6$ , i.e.,  $s_{66}^E$ , should increase anomalously as the Curie point is approached. The picture should be quite different for  $E \neq \text{const}$  (the so-called "isolated" crystal). Now polarization  $P_3$ , caused by stresses  $\sigma_6$ , should create depolarizing field  $E_3 = -4\pi P_3$ , which reduces polarization almost to zero. Thus, conditions  $P = 0$ , a special case of  $P = \text{const}$ , are satisfied. Since polarization does not occur, there is no reason for deformation  $u_6$  to increase, and the coefficients  $s_{66}^P$  and  $c_{66}^P$  display no anomalies at the Curie point, i.e., they are the true crystal constants.

The elastic properties of potassium dihydrophosphate and the thermodynamic conditions under which measurements were made by one method

or another, are discussed in the works of Zwicker [93], Mason [94], Jona [95], Baumgartner [96]. Experimental results showed that the elastic coefficients measured for  $E = 0$  actually behave anomalously at the Curie point (Figure 10.6). The Curie-Weiss law

$$s_{66}^E - s_{66}^P = \frac{D}{T - T_c}, \quad (10.68)$$

where  $D = 4.5 \cdot 10^{-11}$  cm<sup>2</sup>·deg/dyne, is satisfied for  $(s_{66}^E - s_{66}^P)$ . This is not surprising, recalling (10.15) and (10.12). The coefficients of elasticity, not related to shear in the xy plane, display no anomalies at the Curie point [93].

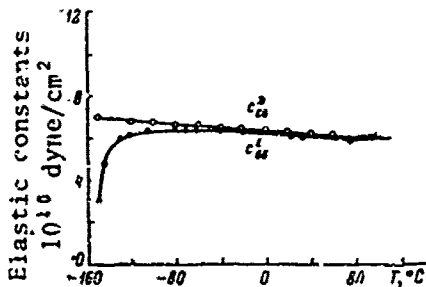


Figure 10.6. Temperature dependence of coefficients of elastic rigidity  $c_{66}^E$  and  $c_{66}^D$  ( $\sim c_{66}^P$ ) of potassium dihydrophosphate crystal (Mason [94]).

As in the case of measurement of permittivity, during investigation of elastic properties it is necessary to distinguish to what conditions the experimental data correspond - isothermic or adiabatic [96].

## 2. Seignette's Salt

In nonpolar phases (above 24°C and below -18°C) Seignette's salt belongs to rhombic acentrosymmetric class 222. The matrix of piezoelectric moduli for these phases appears as follows:

$$\begin{pmatrix} 0 & 0 & 0 & d_{14} & 0 & 0 \\ 0 & 0 & 0 & 0 & d_{25} & 0 \\ 0 & 0 & 0 & 0 & 0 & d_{36} \end{pmatrix} \quad (10.69)$$

Spontaneous polarization occurs on the x axis. Therefore only piezoelectric modulus  $d_{14}$ , which relates polarization on the ferroelectric axis to shearing stress, should be anomalous at the Curie points. Piezoelectric moduli  $d_{25}$  and  $d_{36}$ , like susceptibilities, are not anomalous on the y and z axes, and are only slightly dependent on temperature. At 25°C [97]  $d_{25} = -1.69 \cdot 10^{-6}$  esu and  $d_{36} = 0.355 \cdot 10^{-6}$  esu. New piezoelectric moduli appear in the ferroelectric phase, which has monoclinic symmetry by virtue of linearization of electrostriction, and the matrix has the form:

$$\begin{pmatrix} d_{11} & d_{12} & d_{13} & d_{14} & 0 & 0 \\ 0 & 0 & 0 & 0 & d_{25} & d_{26} \\ 0 & 0 & 0 & 0 & d_{35} & d_{36} \end{pmatrix} \quad (10.70)$$

The piezoelectric properties of Seignette's salt have been investigated throughout the years by many researchers [97-111]. The first efforts did not take into account the fact that during measurements of piezoelectric modulus  $d_{14}$  motion of domain walls may play an important part. When an electric field is applied on the x axis movement of the walls can lead to shearing deformation in the yz plane, i.e., coinciding with piezoelectric deformation. Shearing stresses in the yz plane, in turn, change the domain structure and if of sufficient magnitude, can make the crystal single-domain.

The process of polarization and repolarization of Seignette's salt crystals under the influence of mechanical stresses was thoroughly investigated by Zheludev and Romanvuk [112]. If for piezoelectric measurements the experiment is set up so that domain wall motion occurs, this may lead to values of piezoelectric modulus  $d_{14}$  so overstated that anomalies will not be observed near the Curie points [98]. Many investigators have managed to a considerable degree to avoid domain wall movement, finding maxima on the temperature dependence [97, 100, 101, 107]. In the paraelectric phase above the upper Curie point modulus  $d_{14}$  behaves like dielectric susceptibility  $\chi_a$  (or  $\epsilon_a$ ). The temperature dependence of  $d_{14}$  obeys the Curie-Weiss law

$$d_{14} = \frac{B}{T - T_c} \quad (10.71)$$

where  $B = 8.67 \cdot 10^{-5}$  esu in the 25-34°C temperature range.  $B = 5.17 \cdot 10^{-5}$  esu above 34°C. The analogous reduction of the Curie constant also occurs in the Curie-Weiss law for permittivity (see §1, Chapter 9). The ratio of deformation to polarization (i.e., piezoelectric coefficient  $g_{14}$ ) depends little on temperature [107] and is about equal to the ratio of spontaneous deformation to spontaneous polarization. Piezoelectric deformation, particularly near the Curie points, like polarization, displays saturation. There is also dispersion of modulus  $d_{14}$ . It is noteworthy here that the ratio  $d_{14}/\epsilon_a$  does not depend on frequency [108].

Fotchenkov [110] and Schmidt [111] recently investigated monoclinic piezoelectric moduli  $d_{11}$ ,  $d_{12}$  and  $d_{13}$ . Electrostriction coefficients  $\hat{c}_{11}$ ,  $\hat{c}_{21}$  and  $\hat{c}_{31}$  were determined from measurements in paraelectric phases [113], and were computed as the ratio of spontaneous deformations  $u_1$ ,  $u_2$  and  $u_3$  to the square of spontaneous polarization [114], or were calculated on the basis of experimental values of  $P_s$  and corresponding coefficients  $g$  [111].

In the polydomain state, not being unipolar, a Seignette's salt crystal, according to the general rule [2, 3], has the symmetry of the paraelectric phase, and therefore retains the corresponding piezoelectric moduli. The application of a sufficiently strong field on the x axis leads

to repolarization, and in this case deformations  $u_1$ ,  $u_2$  and  $u_3$  are quadratic functions of the field. This phenomenon can be regarded as electrostriction [115], although the quadratic dependence is a result only of repolarization.

The investigations of the elastic properties of Seignette's salt are rather numerous [97, '09, 116-124]. All coefficients of elastic pliancy  $s$  and rigidity  $c$ , with the exception of  $s_{44} = 1/c_{44}$ , have a very weak temperature dependence [123]. Coefficient  $s_{44}^P$  is practically independent of temperature and mechanical stresses, whereas  $s_{44}^E$  is anomalous at the Curie point and depends substantially on mechanical stresses. According to Mueller's data [117], at temperatures above the top Curie point the difference  $s_{44}^E - s_{44}^P$  obeys the Curie-Weiss law

$$s_{44}^E - s_{44}^P = \frac{D}{T - T_0}, \quad (10.72)$$

where  $D = 6.7 \cdot 10^{-11} \text{ cm}^2 \cdot \text{deg}/\text{dyne}$ . Application of a biasing field on the ferroelectric axis leads to an increase in the coefficient of elastic rigidity  $c_{44}^E$  [118, 120, 122]. In the paraelectric phase this can be the consequence of reduction of dielectric susceptibility under the influence of a biasing field. The fact that adiabatic coefficients of elasticity, which differ from the isometric coefficients in the presence of a biasing field [96], are measured when dynamic methods are used may also be important. In the ferroelectric phase the biasing field will have an effect on elastic properties, chiefly by virtue of change of the part played by domain wall movements in shearing deformations.

### §3. Absorption of Ultrasound and Internal Friction in Ferroelectrics

In the region of the Curie point ferroelectrics display anomalously large scattering of energy during elastic vibrations at sonic and ultrasonic frequencies. This phenomenon is usually investigated by measuring the absorption of ultrasound or by investigating the attenuation of free vibrations of the mechanical resonators made of ferroelectric crystals. These methods were used to investigate Seignette's salt crystals [85, 120, 122, 125-132], triethylamine sulfate and compounds isomorphic to it [87, 127, 133-136];  $\text{KH}_2\text{PO}_4$  [137], and also certain ceramic ferroelectrics [138-141]. All experimental works indicate that at the Curie point the coefficient of absorption of ultrasound has an anomalously high peak (Figure 10.7).

The decrement of attenuation of free vibrations of mechanical resonators made of ferroelectric crystals behaves similarly. The anomalous absorption of sound in the region of the Curie point in Seignette's salt crystals is manifested most strongly during shearing vibrations in the plane perpendicular to the ferroelectric axis, i.e., when the character of deformation during vibrations is the same as during spontaneous

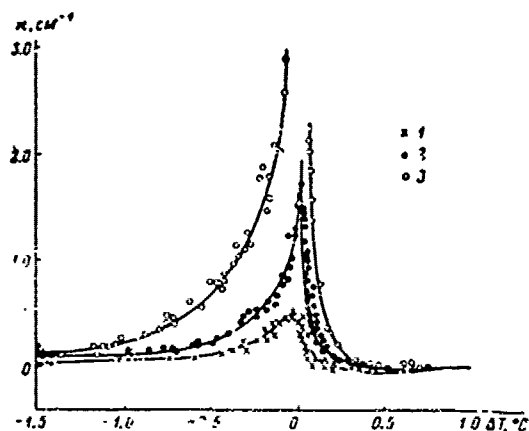


Figure 10.7. Temperature dependence of ultrasound absorption coefficient ( $\kappa$ ) of triglycine sulfate crystal,  $\Delta T = T - T_c$ . Ultrasonic wave longitudinal, propagating on  $z$  axis (Minayeva, et al [1361]). 1 -- 5 MHz; 2 -- 10 MHz; 3 -- 15 MHz.

polarization. The ultrasound absorption coefficient in the paraelectric phase near the Curie point in the ferroelectric phase also depends substantially on the biasing field on the ferroelectric axis. In the ferroelectric phase the absorption coefficient first increases when the shearing stress is increased, and then diminishes. During cyclic change of the field the absorption coefficient describes a butterfly-like curve. The nature of great absorption in the ferroelectric phase is doubtless. It is displacement of the domain walls.

The analogous phenomenon occurs also in ferromagnetics, where the absorption of sound is also great. The absorption coefficient peaks at the Curie point and depends on the constant magnetic field applied to the specimen. The dependences of the absorption coefficient on temperature and biasing field, experimentally observed in the ferroelectric phase, can be easily interpreted, qualitatively, as the domain mechanism. In this case it is difficult to formulate any theory. Of greatest importance, obviously, are investigations of ferroelectrics with the second order phase transition in the immediate vicinity of the Curie point.

The question of sound absorption near the second order phase transition was examined theoretically by Landau and Khalatnikov [142]. They used for the case of the second order phase transition the general theory of relaxation absorption of sound [143] and demonstrated that the temperature dependence of the sound absorption coefficient is governed by the increased relaxation time of the transition parameter. For ferroelectrics the parameter is spontaneous polarization. As a sound wave propagates it becomes absorbed as a result of the relaxation mechanism, by virtue of the fact that the deformations that occur alter the equilibrium value of

polarization. The investigations of Kessenikh, et al [132] on frequencies of 10-200 kHz show that Scignette's salt has at least two mechanisms of sound absorption. One is described by the Landau-Khalatnikov theory, where relaxation time is approximately  $10^{-9}/\Delta T$  ( $\Delta T$  is the distance from the Curie point). The second mechanism is frequency-independent, and its nature is not clear.

When a linear relationship exists between the transition parameter and deformation, anomalous absorption cannot be explained from the standpoint of the Landau-Khalatnikov theory. This pertains to the paraelectric phase of all crystals which are centrosymmetric in this phase, and also to centrosymmetric crystals in the case when the nature of the vibration is such that due to the absence of the corresponding piezoelectric coefficient there is no linear relationship between deformation and polarization. Some consider that anomalous absorption in this case is the result of the interaction of the sound wave with thermal fluctuations of the transition parameter [144, 145].

The fluctuation mechanism of absorption is discussed by Levanyuk, et al [136, 145, 146]. Also noteworthy among the theoretical investigations pertaining to the problem of the propagation and absorption of sound waves in ferroelectrics is Sannikov's work [147], who conducted a phenomenological examination of the relationship between electromagnetic and acoustic waves, and also the work of Tani and Tsuda [148]. It is shown in the latter work that the anomalous behavior of one of the transverse optical modes near the Curie point in ferroelectrics of the displacement type may also lead through phonon-phonon interaction to anomalous behavior of sound waves.

In the single-domain state and far from the Curie point there is apparently no mechanism characteristic of ferroelectrics, which would lead to great absorption. This is supported by investigations of the propagation of longitudinal hypersonic waves in single-domain  $\text{LiNbO}_3$  crystals.

It seems that these crystals display attenuation of elastic waves in the UHF range by one order of magnitude less than in quartz, and the effectiveness of the conversion of electromagnetic vibrations into elastic vibrations is greater [149-152]. It is noteworthy that elastic waves of such high frequencies can be rather easily excited in a crystal by the method proposed by Baranskiy [153]. One of the ends of the specimen is placed in the loop of the electric field of a coaxial resonator or in the loop of the electric field at the end of a closed coaxial line, and elastic vibrations are excited with the aid of the piezoeffect. As shown by the investigations of Lemanov, et al [152], attenuation in the 200-2,000 MHz range has a quadratic frequency dependence, which is in accord with the general theory of attenuation of elastic waves, advanced by Akhiezer [154, 155].

## BIBLIOGRAPHY

1. Devonshire, A. F., *Phil. Mag. Suppl.*, Vol. 3, p. 85, 1954.
2. Zheludev, I. S. and L. A. Shuvalov, *Kristallografiya (Crystallography)*, Vol. 1, p. 681, 1956.
3. Zheludev, I. S. and L. A. Shuvalov, *Izv. AN SSSR, ser. fiz.*, (News of USSR Academy of Sciences, Physics Series), Vol. 21, p. 264, 1957.
4. Schmidt, G., *Naturwissenschaften*, Vol. 45, p. 8, 1958.
5. Merz, W. J., *Phys. Rev.*, Vol. 91, p. 513, 1953.
6. Kay, H. F. and P. Vousden, *Phil. Mag.*, Vol. 40, p. 1019, 1949.
7. Berlincourt, D. and H. Jaffe, *Phys. Rev.*, Vol. 111, p. 143, 1958.
8. Meyerhofer, D., *Phys. Rev.*, Vol. 112, p. 413, 1958.
9. Huibregtse, E. J. and D. R. Young, *Phys. Rev.*, Vol. 103, p. 1705, 1956.
10. Devonshire, A. F., *Phil. Mag.*, Vol. 42, p. 1065, 1951.
11. Caspari, M. E. and W. J. Merz, *Phys. Rev.*, Vol. 80, p. 1082, 1950.
12. Huibregtse, E. J., W. H. Bessey and M. E. Drougard, *J. Appl. Phys.*, Vol. 30, p. 899, 1959.
13. Huibregtse, E. J., M. E. Drougard and D. R. Young, *Phys. Rev.*, Vol. 93, p. 1562, 1956.
14. Roberts, S., *Phys. Rev.*, Vol. 71, p. 890, 1947.
15. Rzhanov, D. V., *ZhETF [Zhurnal eksperimental'noy i teoreticheskoy fiziki; Journal of Experimental and Theoretical Physics]*, Vol. 19, p. 502, 1949.
16. Rzhanov, D. V., *UFN [Uspekhi fizicheskikh nauk; Progress of Physical Sciences]*, Vol. 38, p. 486, 1949.
17. Shubnikov, A. V., *P'yezoelektricheskiye Tekstury (Piezoelectric Textures)*, USSR Academy of Sciences Publishing House, Moscow, 1946.
18. Shubnikov, A. V., I. S. Zheludev, V. P. Konstantinova and I. M. Sil'bestrova, *Issledovaniye P'yezoelektricheskikh Tekstur (Analysis of Piezoelectric Textures)*, USSR Academy of Sciences Publishing House, Moscow, 1955.
19. Bogdanov, S. V., B. M. Vul and R. Ya. Razbesh, *Kristallografiya*, Vol. 2, p. 115, 1957.

20. Bogdanov, S. V., B. M. Vul and A. M. Timenin, Izv. AN SSSR, ser. fiz., Vol. 21, p. 374, 1957.
21. Shuvalov, L. A., Kristallografiya, Vol. 2, p. 119, 1957.
22. Kholodenko, L. P. and M. Ya. Shirobokov, ZhTF [Zhurnal tekhnicheskoy fiziki; Journal of Technical Physics], Vol. 27, p. 929, 1957.
23. Marutake, M., J. Phys. Soc. Japan, Vol. 11, p. 807, 1956.
24. Marutake, M. and T. Ikeda, J. Phys. Soc. Japan, Vol. 12, p. 253, 1957.
25. Mason, W., P'yezoelektricheskiye Kristally i ikh Primeneniya v Ul'traakustike (Piezoelectric Crystals and Their Application in Ultra-acoustics), II. [Foreign Literature] Publishing House, Moscow, 1952.
26. Baerwald, H. G., Phys. Rev., Vol. 105, p. 480, 1957.
27. Mason, W. P., Phys. Rev., Vol. 74, p. 1134, 1948.
28. Roy, N. A., DAN SSSR (Reports of USSR Academy of Sciences), Vol. 73, p. 937, 1950.
29. Roy, N. A., Akustich. Zhurn. (Acoustics Journal), Vol. 1, n. 264, 1955.
30. Pipes, L. A., J. Appl. Phys., Vol. 23, p. 818, 1952.
31. Smolenskiy, G. A. and V. A. Isupov, ZhTF, Vol. 24, p. 1575, 1954.
32. Smolenskiy, G. A., N. P. Tarutin and N. P. Grudtsin, ZhTF, Vol. 24, p. 1584, 1954.
33. Mesnard, G. and L. Eyraud, J. Phys. Rad., Vol. 16, p. 928, 1955.
34. Bogdanov, S. V., B. M. Vul and R. Ya. Razbash, ZhTF, Vol. 26, p. 958, 1956.
35. Koelobayev, I. P., Izv. AN SSSR, ser. fiz., Vol. 20, p. 195, 1956.
36. Bogdanov, S. V., B. M. Vul and R. Ya. Razbash, Kristallografiya, Vol. 2, p. 115, 1957.
37. Berlincourt, D. and H. H. A. Krueger, Phys. Rev., Vol. 105, p. 56, 1957.
38. Shuvalov, L. A., M. M. Kachkacheva, L. Z. Rusakov and I. S. Zheludev, Izv. AN SSSR, ser. fiz., Vol. 22, p. 1516, 1958.
39. Koch, W., Zs. Naturforsch., Vol. 13a, p. 303, 1958.
40. Allsopp, A. L. and D. F. Gibbs, Phil. Mag., Vol. 4, p. 359, 1958.

41. Bullinger, G., *Z. angew. Phys.*, Vol. 12, p. 410, 1960.
42. Jankiewicz, A. and J. Terpilowski, *Act. Phys. Polon.*, Vol. 23, p. 407, 1963.
43. Zheludev, I. S., T. V. Legintseva and N. V. Feldman, *Izv. AN SSSR, ser. fiz.*, Vol. 31, p. 1009, 1967.
44. Bogdanov, S. V., P. M. Gal and I. Ya. Razbash, *Kristallografiya*, Vol. 6, p. 271, 1961.
45. Jaffe, H., *Phys. Rev.*, Vol. 73, p. 1251, 1948.
46. Perls, T. A., T. J. Diesel and W. J. Dobrov, *Phys. Rev.*, Vol. 29, p. 1297, 1958.
47. Verbitskaya, T. N., *DAN SSSR*, Vol. 14, p. 555, 1957.
48. Berlincourt, D. and H. H. A. Krueger, *J. Appl. Phys.*, Vol. 50, p. 1804, 1959.
49. Uchida, N. and T. Ikeda, *Japan J. Appl. Phys.*, Vol. 6, p. 1079, 1967.
50. Bokov, V. A., *Akustich. Zhurn.*, Vol. 5, p. 104, 1957.
51. Roy, N. A., *Akustich. Zhurn.*, Vol. 2, p. 62, 1956.
52. Hueter, T. E., D. P. Neuhaus and J. Kolb, *J. Acoust. Soc. Am.*, Vol. 26, p. 696, 1954.
53. Lewis, B., *Proc. Phys. Soc.*, Vol. 73, p. 17, 1959.
54. Gerson, R., *J. Acoust. Soc. Am.*, Vol. 32, p. 1297, 1960.
55. Velyukhanova, G. A., R. Ye. Pasynkov, V. I. Pozern and I. M. Fl'gard, *Izv. AN SSSR, ser. fiz.*, Vol. 24, p. 1362, 1960.
56. Velyukhanova, G. A., V. I. Pozern, R. Ye. Pasynkov and V. P. Popov, *FTT [Fizika tverdego tela; Solid State Physics]*, Vol. 5, p. 506, 1963.
57. Mason, W. P. and R. F. Wick, *Proc. IRE*, Vol. 42, p. 1606, 1954.
58. Kovalevko, G. M., *Izv. AN SSSR, ser. fiz.*, Vol. 21, p. 594, 1957.
59. Mason, W. P., *J. Acoust. Soc. Am.*, Vol. 27, p. 73, 1955.
60. Bogdanov, S. V., *Izv. AN SSSR, ser. fiz.*, Vol. 21, p. 390, 1957.
61. Vul, B. M. and S. V. Bogdanov, *Fizika Dielektrikov (Physics of Dielectrics)*, USSR Academy of Sciences Publishing House, Moscow, p. 281, 1960.

62. Bogdanov, S. V., B. M. Vul and R. Ya. Razbash, Kristallografiya, Vol. 6, p. 72, 1961.
63. Dobrer, Ye. K. and K. N. Karmen, ZhTF, Vol. 27, p. 508, 1957.
64. Izhak, I. A. and O. A. Shugurov, ZhTF, Vol. 28, p. 518, 1958.
65. Rotenberg, B. A., FTT, Vol. 1, p. 1777, 1959.
66. Kozlobayev, I. P., Izv. AN SSSR, ser. fiz., Vol. 24, p. 1366, 1960.
67. Subbarao, E. C., M. C. McQuarrie and W. R. Buessem, J. Appl. Phys., Vol. 28, p. 1194, 1957.
68. Velyukhanova, G. A., R. Ye. Pasyukov, V. I. Pozern, V. P. Popov, FTT, Vol. 5, p. 506, 1963.
69. Syrkin, L. N. and A. M. El'gard, FTI, Vol. 7, p. 1206, 1965.
70. Fedotov, I. I., FTT, Vol. 6, p. 602, 1964.
71. Marutake, M. and T. Ikeda, J. Phys. Soc. Japan, Vol. 11, p. 814, 1956.
72. Konstantinova, V. P., I. M. Sil'vestrova and K. S. Aleksandrov, Kristallografiya, Vol. 4, p. 69, 1959.
73. Konstantinova, V. P., I. M. Sil'vestrova and K. S. Aleksandrov, Fizika Dielektrikov, USSR Academy of Sciences Publishing House, Moscow, p. 351, 1960.
74. Hussimi, K. and K. Kataoka, J. Phys. Soc. Japan, Vol. 14, p. 105, 1959.
75. Balato, A. D., Acta cryst., Vol. 14, p. 78, 1961.
76. Ikeda, T., Y. Tanaka and H. Toyoda, J. Phys. Soc. Japan, Vol. 16, p. 2593, 1961.
77. Fotchenkov, A. A. and M. P. Zaytseva, Kristallografiya, Vol. 7, p. 934, 1962.
78. Schmidt, G. and P. Pfannschmidt, Phys. St. Sol., Vol. 3, p. 2215, 1963.
79. Ikeda, T., Y. Tanaka and H. Toyoda, Japan J. Appl. Phys., Vol. 2, p. 199, 1963.
80. Telle, F. and J. Chapelle, Proc. Intern. Meet. Ferroelectr., Vol. 1, Prague, p. 448, 1966.
81. Jona, F. and G. Schirane, Phys. Rev., Vol. 117, p. 139, 1960.

82. Fotchenkov, A. A., M. P. Zaytseva and L. I. Zherebtsova, Kristallografiya, Vol. 8, p. 724, 1963.
83. Sil'vestrova, I. M., Izv. AN SSSR, ser. fiz., Vol. 24, p. 1337, 1960.
84. Letta, F., compt. rend., Vol. 250, p. 3162, 1966; Vol. 253, p. 1556, 1961.
85. Minayeva, K. A., Kristallografiya, Vol. 7, p. 425, 1962.
86. Vasilescu, D., R. Cornillon and G. Mallet, Compt. rend., Vol. 265, p. 631, 1967.
87. Shuvaiov, L. A. and K. A. Pluzhnikov, Kristallografiya, Vol. 6, p. 632, 1961.
88. Bantle, W. and C. Caflish, Helv. Phys. Acta, Vol. 16, p. 235, 1943.
89. Arx, A. and W. Bantle, Helv. Phys. Acta, Vol. 16, p. 211, 1943; Vol. 17, p. 298, 1944.
90. De Quervain, M., Helv. Phys. Acta, Vol. 17, p. 509, 1944.
91. Ess, H., Thesis, Eidy Techn. Hochschule, Zurich, 1946.
92. Shuvalov, L. A., I. S. Zheludev, A. V. Mnatsakanyan, Ts. Zh. Ludupov and I. Fiala, Izv. AN SSSR, ser. fiz., Vol. 31, p. 1919, 1967
93. Zwicker, B., Helv. Phys. Acta, Vol. 19, p. 523, 1946.
94. Mason, W. P. Phys. Rev., Vol. 69, p. 173, 1946.
95. Jona, F., Helv. Phys. Acta, Vol. 23, p. 795, 1956.
96. Baumgartner, H., Helv. Phys. Acta, Vol. 23, p. 651, 1950.
97. Mason, W. P., Phys. Rev., Vol. 55, p. 115, 1939.
98. Valasek, J., Phys. Rev., Vol. 17, p. 475, 1921; Vol. 19, p. 478, 1922; Vol. 20, p. 639, 1922; Vol. 24, p. 560, 1924; Science, Vol. 65, p. 235, 1927.
99. Sawyer, C. B. and C. H. Tower, Phys. Rev., Vol. 35, p. 267, 1930.
100. Shul'vas-Sorokina, E. D., Z. Phys., Vol. 73, p. 700, 1932; Vol. 77, p. 541, 1932.
101. Schwartz, E., Elektr. Nachr. Techn., Vol. 9, p. 481, 1932.
102. Bloomenthal, S., Physics, Vol. 4, p. 172, 1933.

103. Vigness, J., Phys. Rev., Vol. 46, p. 255, 1934; Vol. 48, p. 198, 1935.
104. Norgorden, O., Phys. Rev., Vol. 49, p. 820, 1936; Vol. 50, p. 782, 1936.
105. Hinz, H., Z. Phys., Vol. 111, p. 617, 1939.
106. Lichtenstein, R. M., Phys. Rev., Vol. 72, p. 492, 1947.
107. Kawai, H., J. Phys. Soc. Japan, Vol. 2, p. 131, 1947; Vol. 3, p. 111, 1948.
108. Kawai, H. and M. Marutake, J. Phys. Soc. Japan, Vol. 5, p. 8, 1948; Vol. 4, p. 91, 1949.
109. Muser H. E., Z. Phys., Vol. 145, p. 621, 1956.
110. Fotchenkov, A. A., Kristallografiya, Vol. 5, p. 415, 1960.
111. Schmidt, G., Z. Phys., Vol. 161, p. 579, 1961.
112. Zheludev, I. S. and N. A. Romanyuk, Kristallografiya, Vol. 4, p. 710, 1959.
113. Mueller, H., Phys. Rev., Vol. 58, p. 805, 1940.
114. Mason, W. P., Bell Syst. Techn. J., Vol. 26, p. 89, 1947.
115. Fotchenkov, A. A., I. S. Zheludev and V. P. Zaytseva, Kristallografiya, Vol. 7, p. 576, 1961.
116. Hinz, H., Z. Phys., Vol. 111, p. 617, 1939.
117. Mueller, H., Phys. Rev., Vol. 57, p. 829, 1940.
118. Mueller, H., Phys. Rev., Vol. 58, p. 565, 1940.
119. Ludy, W., Helv. Phys. Acta, Vol. 15, p. 527, 1942.
120. Matthias, R., Helv. Phys. Acta, Vol. 16, p. 89, 1943.
121. Huntington, H. B., Phys. Rev., Vol. 72, p. 321, 1947.
122. Price, W. I., Phys. Rev., Vol. 75, p. 946, 1949.
123. Jona, F., Helv. Phys. Acta, Vol. 23, p. 795, 1950.
124. Rewaj, T., Acta Phys. Polon., Vol. 21, p. 45, 1963.
125. Yakovlev, I. A., T. S. Velichkina and K. N. Baranskiy, ZhETF, Vol. 52, p. 35, 1957; Vol. 53, p. 1075, 1957.

126. Yakovlev, I. A. and T. S. Velichkina, UFN, Vol. 63, p. 411, 1957.
127. Shuvalov, L. A. and Yu. S. Likhacheva, Izv. AN SSSR, ser. fiz., Vol. 24, p. 1216, 1960.
128. Merkulov, L. G. and Ye. S. Sokolova, Akustich. Zhurn., Vol. 7, p. 495, 1961.
129. Shustin, O. A., T. S. Velichkina, K. N. Baranskiy and I. A. Yakovlev, ZhETF, Vol. 40, p. 979, 1961.
130. Baranskiy, K. N., O. A. Shustin, T. S. Velichkina and I. A. Yakovlev, ZhETF, Vol. 43, p. 750, 1967.
131. Shirokov, A. M. and L. A. Shuvalov, Kristallografiya, Vol. 8, p. 753, 1965.
132. Kessenikh, G. G., A. M. Shirokov and L. A. Shuvalov, Kristallografiya, Vol. 15, p. 452, 1968.
133. O'Brien, E. J. and T. A. Litovitz, J. Appl. Phys., Vol. 35, p. 180, 1964.
134. Minayeva, K. A. and A. P. Levanyuk, Izv. AN SSSR, ser. fiz., Vol. 29, p. 978, 1965.
135. Minayeva, K. A. and B. A. Strukov, FTT, Vol. 8, p. 32, 1966.
136. Minayeva, K. A., A. P. Levanyuk, B. A. Strukov and V. A. Koptsik, FTT, Vol. 9, p. 1229, 1967.
137. Litov, E. and E. A. Behring, Phys. Rev. Lett., Vol. 21, p. 809, 1968.
138. Hueter, T. and D. Neuhaus, J. Acoust. Soc. Am., Vol. 27, p. 292, 1955.
139. Takuro, I., J. Phys. Soc. Japan, Vol. 15, p. 809, 1958.
140. Postnikov, V. S., V. S. Pavlov, G. A. Gridnev, S. K. Turkov, B. M. Darinskiy and I. A. Gluzman, Izv. AN SSSR, ser. fiz., Vol. 31, p. 1845, 1967.
141. Grinval'd, G. Sh. and V. Ya. Fritsberg, Izv. AN SSSR, ser. fiz., Vol. 31, p. 1850, 1967.
142. Landau, L. D. and I. S. Khalatnikov, DAN SSSR, Vol. 96, p. 469, 1954.
143. Mandel'shtam, L. I. and M. A. Leontovich, ZhETF, Vol. 7, p. 438, 1957.
144. Fixman, M., J. Chem. Phys., Vol. 36, p. 1961, 1962.
145. Levanyuk, A. P., ZhETF, Vol. 49, p. 1504, 1965.

146. Levanyuk, A. P., K. A. Minayeva and B. A. Strukov, FTT, Vol. 10, p. 2443, 1968.
147. Sannikov, D. G., FTT, Vol. 4, p. 1619, 1962.
148. Tani, K. and N. Tsuda, Phys. Lett., Vol. 25A, p. 529, 1967.
149. Wen, C. P. and R. F. Mago, Appl. Phys. Lett., Vol. 9, p. 135, 1966.
150. Grace, M. J., R. W. Kedzie, M. Kestigian and A. B. Smith, Appl. Phys. Lett., Vol. 9, p. 155, 1966.
151. Spenser, E. G. and T. V. Lenzo, J. Appl. Phys., Vol. 38, p. 423, 1967.
152. Lemanov, V. V., A. B. Sherman, G. A. Smolenskiy, N. B. Angert and V. P. Klyuyev, FTT, Vol. 10, p. 1720, 1968.
153. Baranskiy, K. N., DAN SSSR, Vol. 114, p. 517, 1957.
154. Akhiezer, A. A., ZhETF, Vol. 8, p. 1518, 1938.
155. Woodruff, T. O. and H. Ehrenreich, Phys. Rev., Vol. 113, p. 1553, 1961.

## CHAPTER 11. ELECTROOPTIC AND CERTAIN OTHER NONLINEAR OPTICAL PHENOMENA IN FERROELECTRICS

Nonlinear optical phenomena -- generation of optical harmonics, the electrooptic effect, optical detection and other phenomena are related to the dependence of the refraction coefficient of a medium on the electric field strength. They occur as a result of the nonlinear dependence of polarization of the medium on the electric field.

It is clear from general considerations that ferro- and antiferroelectrics, which are characterized by high polarization capacities, should also display substantial dependence of polarization capacity on the field and also great nonlinearity. The time-averaged free energy of unit of volume  $\bar{F}$  of the medium on which acts a light field with amplitude  $E$  and low-frequency field (static field in the particular case) with amplitude  $E_0$ , can be represented, according to [1], in the form:

$$\begin{aligned} \bar{F} = & \chi_1 : EE^* + \chi_2 : E_0 E_0^* + \dots + X_1 : EEE^* + X_2 : EE^* E_0 + \dots \\ & \dots + X_3 : EEEE^* + X_4 : EE E_0 E_0^* + \dots \end{aligned} \quad (11.1)$$

The coefficients  $\chi_1$  and  $\chi_2$  are linear susceptibilities for fields of the corresponding frequencies. Coefficients of the type  $X_1$  and  $X_3$  are nonlinear susceptibilities, which describe the generation of optical harmonics. Coefficients of the type  $X_2$  and  $X_4$  are nonlinear susceptibilities, which describe linear and quadratic electrooptic effects, respectively (Pockels' effect and Kerr's effect).  $\chi$  and  $X$  are tensors, the order of which correspond to the number of points. The letter  $E$  conditionally denotes the amplitudes of the light fields of the various frequencies which are written in the form:

$$E = E_r^{(\omega, k)} + E_0^{(\omega_0, k_0)} \quad (11.2)$$

(here  $k$  is the wave vector,  $r$  is the radius vector,  $\omega$  is the frequency of the light fields).

Not all terms are written in this expression, even in the examined orders of the expansion, and the processes of excitation of acoustical and optical phonons, diffusion of light on acoustical and optical phonons, Faraday's effect, etc., are not taken into account. We will turn now to the electrooptic effect.

### §1. General Concept of the Electrooptic Effect in Ferroelectrics

Under the conditions of investigation of the electrooptic effect ( $E$  is small,  $E_0$  is large) polarization of the medium will have the form:

$$P = \frac{\partial F}{\partial E} = \chi : E_0 + \chi : EE_0 + \chi : EE_0 E_0 + \dots \quad (11.3)$$

The electrooptic effect is manifested in the dependence of birefringence of crystals on a strong stationary or variable field applied to the specimen. Reviews [2-4] examine the electrooptic effect in ferroelectrics.

We will examine the generally accepted description of the electrooptic effect in crystals using the optic indicatrix, and then show how the coefficients of the electrooptic effect are related to the corresponding nonlinear susceptibilities. The optic indicatrix or ellipsoid of refraction indices describes the dependence of the refraction coefficients of a crystal on direction. Its equation has the form

$$a_{ij}x_i x_j = 1. \quad (11.4)$$

where  $a_{ij}$  are the polarization constants,  $x_i, x_j$  are coordinates,  $\epsilon = 1/c = 1/n^2$ ,  $\epsilon$  is permittivity,  $n$  is the refraction index. On the principal axes  $a_{11} = 1/\epsilon_{11} = 1/n_1^2$ ,  $a_{22} = 1/\epsilon_{22} = 1/n_2^2$ ,  $a_{33} = 1/\epsilon_{33} = 1/n_3^2$  where  $n_1, n_2, n_3$  are the principal refraction indices. The electrooptic effect is described by the change of polarization constants when an electric field is applied (the frequency of which is below the frequency of the light), which can be represented graphically as distortion of the ellipsoid of refraction indices (optic indicatrix), reduced to deformation and rotation:

$$\Delta a_{ij} = r_{ijk} E_k + R_{ijkl} E_l + \dots \quad (11.5)$$

where  $\Delta a_{ij} = a_{ij}(E) - a_{ij}(0)$  is the increment of polarization constants;  $E_k, E_l$  are the vector components of electric field strength. The terms containing three and more high field strength powers are usually ignored. The first term characterizes the linear electrooptic effect, and the second -- quadratic electrooptic effect;  $r_{ijk}$  are the coefficients of the linear electrooptic effect, being third class tensor components;  $R_{ijkl}$  are the coefficients of the quadratic electrooptic effect, being fourth class

tensor components. The coefficients of linear electrooptic effect  $r$  are related to nonlinear susceptibilities  $X$ , which describe the linear electrooptic effect. This relationship can be proved for the isotropic case by the following simple method: without a field  $n^2 = 1 + 4\pi X$ , and when a strong field is applied

$$n^2 = \frac{1}{\mu} = 1 + 4\pi X + 4\pi X E + \dots \quad (11.6)$$

On the other hand, from equation (11.5)

$$\Delta n^2 = r E = \frac{1}{n^2} - \frac{1}{n^2_0} = -\frac{4\pi X E}{n^4} \quad (11.7)$$

Consequently there exists between  $r$  and  $X$  a relation of the type

$$r = -\frac{4\pi}{n^4} X \quad (11.8)$$

The analogous relation exists between the coefficients of the quadratic electrooptic effect and the coefficients of nonlinear susceptibilities.

We will write the matrix form of the coefficients of the linear effect in two-index notation:

		$E_1$	$E_2$	$E_3$
$a_{11} - a_{11}^0$	...	$r_{11}$	$r_{12}$	$r_{13}$
$a_{21} - a_{21}^0$	...	$r_{21}$	$r_{22}$	$r_{23}$
$a_{31} - a_{31}^0$	...	$r_{31}$	$r_{32}$	$r_{33}$
$a_{23}$	...	$r_{41}$	$r_{42}$	$r_{43}$
$a_{31}$	...	$r_{51}$	$r_{52}$	$r_{53}$
$a_{12}$	...	$r_{61}$	$r_{62}$	$r_{63}$

Here  $a_{11}^0, a_{22}^0, a_{33}^0$  are the principal polarization constants in the absence of an electric field ( $a_{23}^0 = a_{31}^0 = a_{12}^0 = 0$ );  $a_{11}, a_{22}, a_{33}, a_{23}, a_{31}, a_{12}$  are the polarization constants in the presence of an electric field, the components of which on the axes are  $E_1, E_2, E_3$ .

The matrices of the coefficients of the linear optic effect are quite analogous to the matrices of piezoelectric coefficients, and the matrices of the coefficients of the quadratic effect -- to the matrices of electrostriction coefficients.

The matrix notation of the coefficients of the quadratic electrooptic effect has the form:

	$E_1^2$	$E_2^2$	$E_3^2$	$E_1 E_2$	$E_1 E_3$	$E_2 E_3$
$\Delta a_1$	...	$R_{11}$	$R_{12}$	$R_{13}$	$R_{14}$	$R_{15}$
$\Delta a_2$	...	$R_{21}$	$R_{22}$	$R_{23}$	$R_{24}$	$R_{25}$
$\Delta a_3$	...	$R_{31}$	$R_{32}$	$R_{33}$	$R_{34}$	$R_{35}$
$\Delta a_4$	...	$R_{41}$	$R_{42}$	$R_{43}$	$R_{44}$	$R_{45}$
$\Delta a_5$	...	$R_{51}$	$R_{52}$	$R_{53}$	$R_{54}$	$R_{55}$
$\Delta a_6$	...	$R_{61}$	$R_{62}$	$R_{63}$	$R_{64}$	$R_{65}$

Here two-index symbols are used for the fourth class tensor and the following definitions are introduced:  $E_1 E_1^2 = E_1^3$ ,  $E_2 E_2^2 = E_2^3$ ,  $E_3 E_3^2 = E_3^3$ ,  $E_3 E_2 = E_2 E_3 = E_4^2$ ,  $E_1 E_3 = E_3 E_1 = E_5^2$ ,  $E_1 E_2 = E_2 E_1 = E_6^2$ ;  $\Delta a_1 = a_{11} - a_{11}^0$ ,  $\Delta a_2 = a_{22} - a_{22}^0$ ,  $\Delta a_3 = a_{33} - a_{33}^0$ ,  $\Delta a_4 = a_{23}$ ,  $\Delta a_5 = a_{31}$ ,  $\Delta a_6 = a_{12}$ .

The linear electrooptic effect coexists with the inverse piezoelectric effect in a mechanically free crystal. As a result of the inverse piezoelectric effect the electric field will cause deformation of the crystal, which will lead, by virtue of the piezooptic effect, to a change in polarization constants. A change in polarization constants not related to the inverse piezoelectric effect when a field is applied to a crystal is called the true linear electrooptic effect. A change in polarization constants caused by the inverse piezoelectric effect is called a false electrooptic effect. The summary electrooptic effect is measured experimentally. The first term of equation (11.5) can be written in the form:

$$\Delta \epsilon_{ij} = (r_{ijk}^* + P_{ijlm} d_{klm}) E_k, \quad (11.9)$$

where  $r_{ijk}^*$  are the coefficients of the true electrooptic effect,  $P_{ijlm}$  are the tensor components of the elasto-optic coefficients and  $d_{klm}$  are the piezoelectric coefficients.

The quadratic electrooptic effect is also divided into true and false. The true quadratic electrooptic effect is not related to deformation of a crystal by electrostriction when a field is applied, and a false quadratic electrooptic effect is determined by such deformation.

To exclude a false electrooptic effect measurements must be made in a variable electric field, the frequency of which is greater than the resonance frequencies of the specimen, so that the specimen can be regarded as "clamped." Measurements may also be done by the static method and the summary effect measured, after which the false one is excluded from it by calculating it from measurement data of elasto-optic and piezoelectric or electrostriction coefficients.

The equations of the electrooptic effect can also be written through crystal polarization vector components instead of field strength. Such notation is quite convenient for ferroelectric crystals. Actually, using the coefficients  $m_{ij}$  or  $M_{ij}$ , from relations

$$\Delta \epsilon_{ij} = m_{ijk} P_k + M_{ijkl} P_k P_l, \quad (11.10)$$

where  $m_{ijk}$  are linear and  $M_{ijkl}$  are quadratic electrooptic coefficients, and  $P_j$  are components of complete polarization of a crystal, we exclude the effect of the temperature dependence of permittivity entering in  $P_j$ . In

many cases, therefore, coefficients  $m_{ijk}$  and  $M_{ijk}$  display an extremely weak temperature dependence.

The electrooptic coefficients are usually determined by measuring the intensity of the light passing through a crystal placed between crossed polarizers, depending on the strength of the field applied to the crystal. The birefringence of the crystal is determined from intensity measurements. When the difference between the paths of the ordinary and extraordinary rays of some intensity is equal to  $\lambda/2$ , then intensity is maximal. This intensity  $V_{\lambda/2}$  is called the half-wave intensity. It is related by means of simple relations to the electrooptic coefficients.

All ferroelectrics display the linear electrooptic effect below the Curie point, since they lack a center of symmetry. The quadratic electrooptic effect is observed both in the para- and in the ferroelectric phases, regardless of the presence or absence of a center of symmetry. If a center of symmetry exists in the paraelectric phase, there are only even electrooptic effects in it. If such a crystal is separated into domains in the ferroelectric phase, then too only even effects can be observed, since odd effects are compensated in various domains (unipolarity is not considered). If a crystal broken down into domains lacks a center of symmetry in the paraelectric phase, odd effects may occur, since the macrosymmetry of the crystal when broken down into domains corresponds to the symmetry of the paraelectric phase [5]. A crystal broken down into domains will lack the components of odd effects that appeared as a result of linearization of the even effects (see below).

The magnitude of the refraction coefficients of crystals depends largely on the electron energy levels -- their positions and probability of transition between them. Therefore one of the most important mechanisms of the electrooptic effect and other optic nonlinear effects is related to displacement of these levels in an electric field.

Several attempts have been made to tie in zonal structure with the polarization of a crystal. The zonal structure of strontium titanate was analyzed [6] and it was found that displacements of ions has a notable influence on the magnitude of the smallest energy slot between the valence zone formed by the 2p-electrons of oxygen, and the conductance zone formed by the 3d-electrons of titanium. The change in the width of the slot changes the electron polarization capacity. The electrooptic effect is examined in [7] and more completely in [8] on the basis of the results of [6] as a result of change of zonal structure during polarization of the perovskite type lattice.

It can be concluded on the basis of investigations of the dispersion of electrooptic coefficients and electroreflection in crystals of the perovskite type that the strong absorption bands in the ultraviolet region, corresponding to 4-6 eV [9-12] are the largest contributors to the refraction coefficients and electrooptic effect in the visible region of the spectrum.

The electrooptic effect can be described with the aid of the phenomenological model proposed in [13]. Examination of the motion of an anharmonic oscillator, used by Blombergen [14] to describe optical non-linear properties, is based on this model. To an electric field of optical frequency is added a stationary local field. The equation of motion of an electron in the unidimensional case with consideration of anharmonic perturbation then acquires the form:

$$x + \Gamma \dot{x} + \omega_0^2 x + bx^3 = \frac{e}{m} (E(\omega, t) + \beta E(0)), \quad (11.11)$$

where  $\Gamma$  is the attenuation constant,  $\omega_0$  is the resonance frequency,  $b$  is the anharmonic force constant,  $e$  is charge,  $m$  is electron mass,  $E(\omega, t)$  is the electric field of a light wave with frequency  $\omega$ ,  $E(0)$  is an external stationary electric field,  $\beta$  is a parameter of the local field.

This model yields an expression for linear electrooptic coefficient  $r$ :

$$r = \frac{(n^2 - 1)^2 b}{2n^4 N_0 e m \omega_0^3}, \quad (11.12)$$

where  $N_0$  is the number of oscillators per unit volume. After replacing the term  $bx^2$  with  $cx^3$  we obtain an expression for the quadratic electrooptic coefficient. In either case the dependence of the electrooptic coefficients on frequency contains the factor  $(n^2 - 1)^2/n^4$ . This agrees very well with experimental data on the dispersion of electrooptic coefficients in crystals with the perovskite structure [15], and in lithium niobate [16].

On transition to the ferroelectric state the quadratic effect becomes linearized in a manner analogous to the linearization of electrostriction and the appearance of the piezoelectric effect. Actually, if birefringence is proportional to the square of polarization, in the ferroelectric phase, where induced polarization  $P_{in}$  is much less than spontaneous  $P_s$  ( $P_{in} \ll P_s$ )

$$[\mu = in] \quad \Delta n = k(P_s + P_{in})^2 \approx kP_s^2 + 2kP_s P_{in} = A + BP_{in}, \quad (11.13)$$

and  $A$  and  $B$  are certain constants, i.e., the linear electrooptic effect will be observed. Its magnitude is proportional to spontaneous polarization. It is this very phenomenon that takes place in ferroelectrics of the perovskite structure, which do not display the linear electrooptic effect in the paraelectric phase. If the linear effect occurs in the paraelectric phase, then on transition to the ferroelectric state new components of the linear effect will appear as a result of linearization of the quadratic effect [17, 18]. The new tensor components of the linear electrooptic coefficients  $r_{ij}$  appear to be proportional to the product of  $\epsilon$  (more accurately, induced polarization) and spontaneous polarization. The new

tensor components  $m_{ij}$  will be proportional to spontaneous polarization. Components  $m_{ij}$ , not being the result of linearization, depend little on temperature.

## §2. Spontaneous Electrooptic Effect

Birefringence in barium titanate, as shown in [19, 20], is proportional to the square of total polarization of a crystal. Analysis of birefringence of barium titanate in the region of the Curie point during the application of strong electric fields, carried out in [19], verified the quadratic dependence of birefringence on polarization during field-induced (or forced) ferroelectric transitions. At the Curie point there is a sharp change in birefringence. The temperature dependence of the birefringence of barium titanate according to [19] and of lead titanate according to [20] is shown in Figures 11.1 and 11.2.

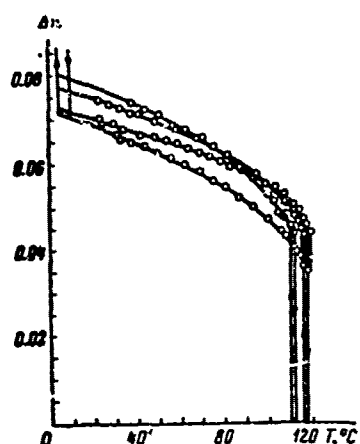


Figure 11.1. Temperature dependence of birefringence of four barium titanate crystals (Meyerhofer [19]).

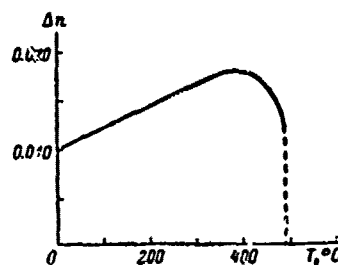


Figure 11.2. Temperature dependence of birefringence of lead titanate (Shirane [20]).

The change of birefringence at the Curie point can be regarded as a spontaneous electrooptic effect caused by spontaneous polarization. Therefore, in crystals of the perovskite type, for instance, the relation  $\Delta n = \text{const } P^2$ , where  $P$  is total polarization, including spontaneous and induced polarization, is satisfied in some temperature range near the Curie point, for both birefringence in the absence of a field (natural birefringence) and application of external electric fields [19, 21]. In particular, the magnitude of linear coefficient  $m_{33}$  in barium titanate, determined by measuring the natural birefringence and spontaneous polarization [22], agrees satisfactorily with that obtained from analysis of an induced electrooptic effect in tetragonal barium titanate [23].

The temperature dependence of the birefringence of lithium niobate

was recently analyzed [24, 25]. This crystal is optically negative at room temperature. As the temperature rises, negative birefringence diminishes, vanishes near 880°C and then becomes positive, increasing almost up to the Curie point itself. In the vicinity of the Curie point the increase of  $\Delta(n_e - n_o)$  slows down ( $n_e$  is the index of extraordinary refraction and  $n_o$  is the index of the ordinary ray), related to the disappearance of spontaneous polarization.

Repeated attempts have been made to compute the birefringence of barium titanate and certain other ferroelectrics with the perovskite structure, resulting from the spontaneous electrooptic effect, on the basis of a model of point polarized ions in the assumption of isotropic polarization [26-30]. The results of these works disagree with each other and with experimental data. According to experimental data [19, 31, 32], barium titanate is an optically negative crystal. Certain calculations, however, have produced a positive value. In the latest works [27, 30] a value close to zero has been found. This discrepancy between theoretical and experimental data is usually explained at the present time by the need to take into account the anisotropy of the polarization of oxygen ions.

Polarization anisotropy should be the result of large internal fields that act in ferroelectrics, which can lead to saturation of electron polarization due to overlapping of electron shells during large displacements of ions. The complex temperature dependence of the birefringence of  $\text{PbTiO}_3$  (Figure 11.2) is perhaps related to the influence of the polarization anisotropy of oxygen. This explains the failure of attempts to correlate the temperature dependence of the birefringence of perovskite type ferroelectrics far from the Curie point with only the temperature dependence of lattice distortions which, in turn, are presumably proportional to the square of spontaneous polarization. The effects of saturation of optic dielectric permittivity in the direction of spontaneous polarization possibly play a lesser role in ferroelectrics of the groups potassium dihydrophosphate, Seignette's salt, triglycine sulfate and others, than in ferroelectrics of the perovskite type, due to the smaller refraction indices and complex configuration of internal fields, not parallel, to the resulting polarization [33].

### §3. Electrooptic Properties of Certain Ferroelectrics

We will now examine the electrooptic properties of certain ferroelectrics in greater detail.

The matrix of quadratic electrooptic coefficients for the cubic phase of perovskite type crystals (point group of symmetry  $m\bar{3}m$ ) has the form:

	$E_1^2$	$E_2^2$	$E_3^2$	$E_1 E_2$	$E_1 E_3$	$E_2 E_3$
$a_{11} - a_{12}^2$ . . . . .	$R_{11}$	$R_{12}$	$R_{13}$	0	0	0
$a_{22} - a_{12}^2$ . . . . .	$R_{12}$	$R_{11}$	$R_{13}$	0	0	0
$a_{33} - a_{12}^2$ . . . . .	$R_{13}$	$R_{13}$	$R_{11}$	0	0	0
$a_{23}$ . . . . .	0	0	0	$R_{44}$	0	0
$a_{31}$ . . . . .	0	0	0	0	$R_{44}$	0
$a_{12}$ . . . . .	0	0	0	0	0	$R_{44}$

Thus there are three different, nonzero electrooptic coefficients  $R_{11}$ ,  $R_{12}$  and  $R_{44}$ .

The optic indicatrix for such crystals in the absence of an external field is described by the equation

$$a^0(x^2 + y^2 + z^2) = 1, \quad (11.14)$$

where  $a^0 = 1/n^2$ .

When a field is applied in direction  $\langle 100 \rangle$  the optic indicatrix deforms and its equation acquires the form

$$(a^0 + R_{11}E_1^2)x^2 + (a^0 + R_{12}E_1^2)(y^2 + z^2) = 1, \quad (11.15)$$

The crystal becomes uniaxial. The principal axes of the deformed indicatrix coincide with the principal axes of the nondeformed indicatrix.

Induced birefringence during propagation of light in direction  $\langle 001 \rangle$  is related in this case to field intensity by the equation

$$\Delta n = n_o - n_e \approx -\frac{1}{2}n^2(R_{11} - R_{12})E_1^2. \quad (11.16)$$

For determination of  $R_{44}$  the field must be applied in direction  $\langle 110 \rangle$ , and the light should propagate in direction  $\langle 001 \rangle$ . Then birefringence will be

$$\Delta n = n^2 R_{44} E_1^2. \quad (11.17)$$

The analogous relations are also derived for coefficients  $M_{ij}$ .

The magnitude of electrooptic coefficients  $R_{ij}$  of barium titanate in the paraelectric phase diminishes as temperature rises approximately in correspondence with the reduction of permittivity [34].

Coefficients  $M_{ij}$  for many compounds of the perovskite class, on the other hand, are practically independent of temperature. Here  $M_{ij}$  for such crystals as  $\text{BaTiO}_3$ ,  $\text{KTaO}_3$ ,  $\text{SrTiO}_3$ ,  $\text{KTa}_{0.75}\text{Nb}_{0.25}\text{O}_3$  (KTN) differ very little from each other [10] (Table 13). This is an argument in favor of a general mechanism of the electrooptic effect in these crystals, related to the effect of the field on interzone transitions between the 2p-valence zone and the nd-conductance zone ( $n = 3, 4, 5$  for titanium, niobium and tantalum ions) [9-12].

Electrooptic analyses in a wide range of wavelengths are very

important for investigations of the relationship between electron zonal structure of crystals and the magnitude of the electrooptic effect. Coefficients  $M_{ij}$  in crystals of the perovskite type have recently been found to increase as wavelength decreases, starting with wavelengths of  $\sim 0.4 \mu$  [10]. Here the experimental data conform with the dispersion theory in single-oscillator approximation.

It was recently shown that certain perovskite type crystals of complex composition, in particular  $\text{PbMg}_{1/3}\text{Nb}_{2/3}\text{O}_3$  [35-38], display a large electrooptic effect and low half-wave intensities. The temperature dependence of  $R_{11} - R_{12}$  in the  $\text{PbMg}_{1/3}\text{Nb}_{2/3}\text{O}_3$  crystal [36] is illustrated in Figure 11.3. This great magnitude of coefficients  $R_{ij}$  is related [36] to features of eroded phase transitions, by virtue of which domain orientation and induction of the ferroelectric phase contribute to the electrooptic effect in a broad temperature range.

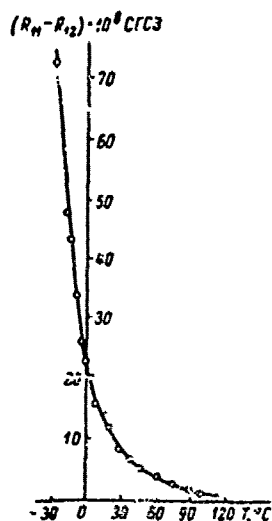


Figure 11.3. Temperature dependence of  $(R_{11} - R_{12})$  for lead magnesium niobate (Smolenskiy, et al [36]).

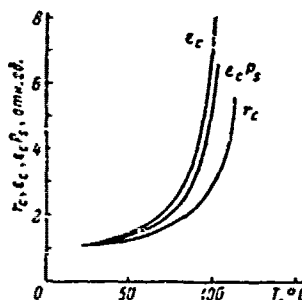


Figure 11.4. Temperature dependence of linear electrooptic coefficient  $r_c$  compared to  $\epsilon_c$  and product  $\epsilon_c P_s$  in relative units for tetragonal barium titanate (Johnston and Weingart [25]).

The temperature dependence of the electrooptic effect in tetragonal barium titanate in the ferroelectric phase was analyzed [25]. The temperature dependence of linear electrooptic coefficients  $r_{ij}$  in barium titanate is illustrated in Figure 11.4 [25]. It is clear from the figure that the character of the temperature dependence of  $r_{ij}$  corresponds approximately to the temperature dependence of the product of dielectric permittivity and polarization. This satisfactorily agrees with the concepts of linearization of the quadratic electrooptic effect in the ferroelectric phase.

Above the Curie point triglycine sulfate (TGS) belongs to the centrosymmetric point group 2/m. In the paraelectric phase, therefore, it does not display a linear electrooptic effect, and the linear effect in the ferroelectric phase is not the result of linearization of the quadratic effect. The electrooptic properties of TGS were analyzed in [39-45], and in [39, 40, 2-44] only the electrooptic coefficients that determined deformation of the indicatrix were investigated, while in [41, 45] rotation of the indicatrix was analyzed. Data are presented in [41] concerning the temperature dependence of indicatrix rotation, occurring as a result of thermo-optic and spontaneous electrooptic and elasto-optic effects. The effect of the application of a field along ferroelectric axis b on indicatrix orientation was investigated in [45].

Analysis of the temperature dependence of certain electrooptic coefficients of TGS [39] showed that a linear effect still occurs 2-3° above the Curie point, although coefficients  $r_{ij}$  decrease, which may be explained by the "erosion" of the second order phase transition in the electric field. Here minimal nonlinearity is observed on ferroelectric axis b, whereas permittivity, measured on radio frequencies, is maximal in this direction. It is theorized in this connection [39] that polarization on optical frequencies is caused basically by other structural elements of the crystal lattice than on lower frequencies. Such components may be groups of  $SO_4^{2-}$  ions, which agrees with the results of [46].

The linear effect in TGS in the ferroelectric phase, as in barium titanate, is by its nature a linearized quadratic effect. Therefore the temperature dependence of  $r_{ij}$  is governed by the product  $\epsilon P_s$ . In particular, according to [45], the temperature dependence of coefficient  $r_{52}$  is proportional to  $\epsilon_2 \cdot P_s \sim \frac{A}{(T_c - T)^{1/2}}$ . The temperature dependence of linear coefficients  $m_{ij}$  is analogous to the temperature dependence of polarization [44], as should be the case for the linearized quadratic effect. In the paraelectric phase TGS displays a quadratic electrooptic effect, and the quadratic electrooptic coefficients diminish as temperature increases according to the Curie-Weiss law, analogously to  $\epsilon$  [39] (Figure 11.5).

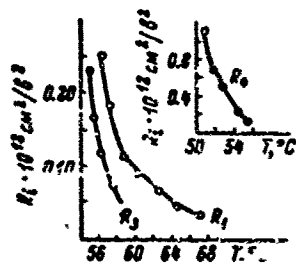


Figure 11.5. Temperature dependence of quadratic electrooptic coefficients in triglycine sulfate (Vasilevskaya, et al [39]).

$$R_1 = n_1^2 R_{22} - n_2^2 R_{11}; \quad R_2 = n_1^2 R_{12} - n_2^2 R_{21};$$

$$R_3 = (n_1^2 R_{13} - n_2^2 R_{31}) + (n_1^2 R_{11} - n_2^2 R_{21});$$

Table 19. Quadratic Electrooptic Coefficients of Several Ferro- and Antiferroelectrics at Room Temperature

Name of crystal	$R_{ij} \cdot 10^4$ CGS				$M_{ij} \cdot 10^4$ CGS
	$R_2 = n^2 R_{22} - n^4 R_{11}$	$R_3 = n^2 R_{31} - n^4 R_{11}$	$R_4 = n^2 (R_{12} - R_{11})$	$R_4 = n^2 R_{44}$	
$KH_2PO_4$	2.8	1.2	0.8	0.3	$M_{33} = -2.86$ [1]
$KD_2PO_4$	4.2	1.1	0.9	0.5	—
$RbH_2PO_4$	4.6	1.0	0.8	0.4	—
$NH_4H_2PO_4$	2.2	1.5	0.5	0.2	—
$ND_4D_2PO_4$	5.2	2.1	0.8	0.4	—
$BaTiO_3$	—	—	—	—	$M_{11} = M_{12} = 1.44$ [19] $M_{44} = 1.88$ —
$SrTiO_3$	—	—	—	—	$M_{11} = M_{12} = 1.55$ [19] $M_{11} = M_{12} = 1.77$ [19]
$KTaO_3$	—	—	—	—	$M_{44} = 1.33$ $M_{11} = M_{12} = 1.83$ [19] $M_{11} = 1.5$
$KTa_{0.9}Nb_{0.1}O_3$	—	—	—	—	$M_{12} = 0.43$ $M_{44} = 1.83$
$PbMg_{1/2}Nb_{1/2}O_3$	—	$R_{11} = R_{12} = 13.4$	—	—	$M_{11} = M_{12} = 0.183$
$PbZn_{1/2}Nb_{1/2}O_3$	—	$R_{44} = 2.3$ [24]	—	—	$M_{44} = 0.03$ [24]
$KNaC_4H_4O_6 \cdot 4H_2O$	—	$n^2 (M_{11} - R_{11}) = 200$ [21]	—	—	$n^2 (M_{11} - M_{12}) = 1.72$ [21] $M_{31} = M_{11} = 1.5$ $M_{11} = M_{12} = -36$ [19] $M_{11} = M_{12} = 33$

[CGS = Cgs (centimeter-gram-second) electrostatic system].

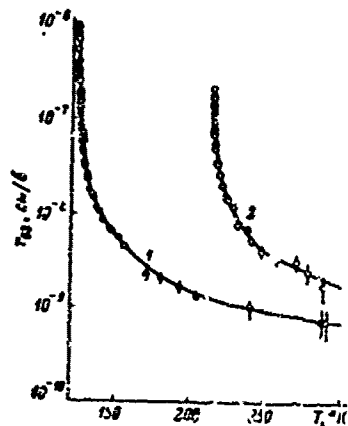


Figure 11.6. Temperature dependence of coefficient  $r_{63}$  for  $\text{KH}_2\text{PO}_4$  (1) and  $\text{KD}_2\text{PO}_4$  (2) in paraelectric phase (Zwicker and Scherrer [47]).

Potassium dihydrophosphate (KDP) in the paraelectric phase displays a linear electrooptic effect. It was the first ferroelectric crystal in which electrooptic properties were carefully investigated [47].

The equation of the indicatrix of KDP, according to [47], has the form:

$$\frac{x^2 + y^2}{n_1^2} + \frac{z^2}{n_2^2} + 2r_{11}(yE_1 + xE_2)z + 2r_{63}xyE_3 = 1 \quad (11.18)$$

(the variables pertain to the principal axes  $a_1, a_2, c$  of the crystal).

In the case of application of an electric field on the tetragonal axis  $c$  and use of a coordinate system connected to a nonprimitive tetragonal nucleus, the edges of which are  $a_1' = \sqrt{2}a_1$ , where  $a_1$  is the edge of the primitive tetragonal nucleus, the indicatrix is described by the equation:

$$\frac{x'^2}{n_1^2}(1 + r_{63}E_3) + \frac{y'^2}{n_1^2}(1 - r_{63}E_3) + \frac{z'^2}{n_2^2} = 1. \quad (11.19)$$

It follows from this equation that when light propagates parallel to electric field  $E_3$ , induced birefringence (longitudinal electrooptic effect) is equal to.

$$n_1' - n_2' \approx n_1^2 r_{63} E_3. \quad (11.20)$$

When light propagates along  $a_1'$  and  $a_2'$  perpendicular to  $E_3$  (lateral effect) the following relations are satisfied:

$$n_2 - n_1' \approx (n_2 - n_1) + \frac{1}{2} n_1^2 r_{63} E_3. \quad (11.21)$$

$$n_1 - n_2' \approx (n_2 - n_1) - \frac{1}{2} n_1^2 r_{63} E_3. \quad (11.22)$$

In this case the linear lateral electrooptic effect is superimposed on natural birefringence, equal to  $n_2 - n_1$ .

Thus the coefficient  $r_{63}$  can be determined by several methods. The

temperature dependence of the electrooptic coefficient  $r_{63}$  is shown in Figure 11.6 for KDP. For coefficient  $r_{63}$ , as for permittivity, the Curie-Weiss law is satisfied. Coefficient  $m_{63}$ , as might be expected, is practically independent of temperature. The linear electrooptic effect in KDP was also investigated in [48, 49]. The spontaneous electrooptic effect in KDP was examined in [47, 50, 51]. The results of investigation of the quadratic electrooptic effect in KDP are summarized in [52].

When the electric field and light are oriented in certain directions KDP does not display a linear electrooptic effect and only the quadratic effect occurs [53]. These directions are:

Direction of field	Direction of light
$\langle 100 \rangle$	$\langle 001 \rangle$
$\langle 100 \rangle$	$\langle 010 \rangle$
$\langle 110 \rangle$	$\langle 001 \rangle$
$\langle 001 \rangle$	$\langle 010 \rangle$

The optical indicatrix for the case when the field is applied in direction  $\langle 001 \rangle$  has the form

$$\left(\frac{1}{n_o^2} + R_{12}E^2\right)(x^2 + y^2) + \left(\frac{1}{n_e^2} + R_{33}E^2\right)z^2 = 1. \quad (11.23)$$

For the case of a field applied along axis  $\langle 100 \rangle$  the optical indicatrix can be expressed as follows:

$$\left(\frac{1}{n_o^2} + R_{11}E^2\right)x^2 + \left(\frac{1}{n_o^2} + R_{12}E^2\right)y^2 + \left(\frac{1}{n_e^2} + R_{33}E^2\right)z^2 = 1. \quad (11.24)$$

During investigation of induced birefringence in directions not characterized by the linear effect it is possible to determine the following quadratic electrooptic coefficients:

$$\left. \begin{aligned} R_a &= n_o^2 R_{33} - n_e^2 R_{12}, & R_b &= n_o^2 R_{31} - n_e^2 R_{11}; \\ R_c &= n_o^2 (R_{12} - R_{11}), & R_d &= n_e^2 R_{33}. \end{aligned} \right\} \quad (11.25)$$

The quadratic electrooptic effect of the KDP group of ferroelectrics in the paraelectric phase has the usual maximum when the field is applied along optical axis  $c$  (the indicatrix is described by equation (11.23); see coefficients  $k_a$  in Table 19).

Works appeared recently [54, 55] on the investigation of the electrooptic effect in Seignette's salt. The results of investigation in the temperature range including both phase transitions are presented in [54].

The electrooptic properties of lithium niobate crystals are investigated in [56-59]. Nonlinearity was found to increase as wavelength decreases, analogous to the case of ferroelectrics with the perovskite structure [10].

Solid solutions of the system  $(\text{Sr}_x\text{Ba}_{1-x})\text{Nb}_2\text{O}_6$  with the structure of tetragonal potassium-tungsten bronze [60], the ferroelectric properties of which are discussed in [61], display extremely high electrooptic coefficients. Several new promising electrooptic crystals with this structure have been grown recently, which also possess ferroelectric properties --  $\text{KSr}_2\text{Nb}_5\text{O}_{15}$  [62],  $\text{K}_6\text{Li}_4\text{Nb}_{10}\text{O}_{30}$  [63],  $\text{Ba}_2\text{NaNb}_5\text{O}_{15}$  [64]. The electrooptic effect in  $\text{Ba}_2\text{NaNb}_5\text{O}_{15}$ , in particular, is about twice as great as that of lithium niobate. The electrooptic effect in crystals with this structure in the tetragonal ferroelectric phase (point group 4mm) is characterized by three independent electrooptic coefficients:  $r_{13} = r_{23}$ ,  $r_{42} = r_{51}$ ,  $r_{33}$ , and in the rhombic phase (mm2) -- by five ( $r_{13}$ ,  $r_{23}$ ,  $r_{42}$ ,  $r_{51}$ ,  $r_{33}$ ).

The magnitudes of some electrooptic coefficients of a number of ferroelectrics are listed in Tables 19 and 20.

Table 20. Linear Electrooptic Coefficients of Certain Ferroelectrics and Antiferroelectrics at Room Temperature

Name of crystal	$r_{ij} \cdot 10^6$ crco	$m_{ij} \cdot 10^6$ crco
$\text{KH}_2\text{PO}_4$	$r_{33} = -30$ ; $r_{31} = 26$ [66]	$m_{33} = -24.3$ [2]
$\text{KD}_2\text{PO}_4$	$r_{33} = -79$ ; $r_{31} = 26.4$ [67, 68]	
$\text{KH}_2\text{AsO}_4$	$r_{33} = -39$ [3]	
$\text{RbH}_2\text{PO}_4$	$r_{33} = -39$ [69]	
$\text{RbH}_2\text{AsO}_4$	$r_{33} = -35$ [70]	
$\text{CsH}_2\text{AsO}_4$	$r_{33} = -50$ [70]	
$\text{NH}_4\text{H}_2\text{PO}_4$	$r_{33} = -25$ ; $r_{31} = 61$ [66]	
$\text{NH}_4\text{H}_2\text{AsO}_4$	$r_{33} = -19$ [3]	
$\text{ND}_4\text{H}_2\text{PO}_4$	$r_{33} = 3$ [71]	
$\text{BaTiO}_3$	$r_{33} = r_{32} = r_{31} = 324$ ; $r_{13} = 4930$ [22]	$m_{33} = 25$ [23]
$\text{KNaC}_4\text{H}_4\text{O}_6 \cdot 4\text{H}_2\text{O}$	$r_{41} = -6$ ; $r_{32} = -3.1$ ; $r_{33} = 0.93$ [2, 21]	$m_{41} = 2.21$ [2, 2]
$\text{LiNbO}_3$	$r_{22} = 20.4$ ; $r_{33} = 36.6$ ; $r_{13} = 30$ ; $r_{24} = 5.6$ [22]	
$\text{LiTaO}_3$	$r_{13} = 20.1$ ; $r_{33} = 91.2$ [65]	
$\text{Sr}_{0.75}\text{Ba}_{0.25}\text{Nb}_2\text{O}_6$	$r_{33} = 402$ ; $r_{13} = 300$	
$\text{KSr}_2\text{Nb}_5\text{O}_{15}$	$r_{33} = 270$ [62]	
$\text{K}_6\text{Li}_4\text{Nb}_{10}\text{O}_{30}$	$r_{33} = 391$ [63]	
$\text{Ba}_2\text{NaNb}_5\text{O}_{15}$	$r_{33} = 220$ ; $r_{13} = 315$ [64]	
	$r_{42} = 9$ ; $r_{51} = 650$ ; $r_{33} = 210$ [64]	

#### §4. Optic Activity

Investigations of the optic activity of ferroelectrics (rotation of plane of polarization), in particular, detection of change of the sign of optic activity in an electric field, are closely related to investigations of the electrooptic properties of ferroelectrics. The change in the direction of rotation of the plane of polarization of light (change of the sign of optical activity) was found in [72] by applying a field in lithium hydroselenite  $\text{LiH}_3(\text{SeO}_2)_2$ . Lithium hydroselenite is an optically biaxial

crystal, characterized by high optic activity. The directions of rotation of the two optic axes have different signs, while the forces of rotation are equal in absolute value. The crystal is a uniaxial ferroelectric and in the absence of a field breaks down into  $180^\circ$  domains. When the crystal is repolarized by an electric field the optic axes interact and therefore the sign of rotation of the plane of polarization of light propagating on the optic axes changes.

More complete and accurate data were obtained in [73] concerning the optic activity of lithium hydroselenite; in particular, the rotation of the plane of polarization due to the electrooptic effect, occurring with the application of an electric field, was taken into account.

Crystallographic examination of the possibility of change of the sign and magnitude of optic activity during electrical and mechanical repolarization of ferroelectrics, carried out by Shuvalov and Ivanov [74], showed that optic activity and change of sign are possible in enantiomorphic classes 1, 2, 3, 4, 6 and in planal classes m and  $2mm$ .

### §5. Ferroelectric Materials in Nonlinear Optics

We will proceed now to examine certain optic properties of ferroelectrics in strong light fields.

During the years following the discovery of lasers by Basov, Prokhorov and Townes it became possible to produce powerful light beams in which the intensity of the electric field of the light wave reached  $\sim 10^5$  V/cm and more. In our discussion of electrooptic phenomena we assumed that the electron polarization of a medium does not depend on the light field intensity. With respect to the propagation of a laser beam it is essential to consider the nonlinearity of a medium in relation to the light wave, since the intensity of the light field becomes comparable with internal fields in the substance. As a result of nonlinearity of the medium the light waves become distorted, the superposition principle is violated, the generation of higher harmonics, sum and difference frequencies become possible during the interaction of strong light and radio waves and stationary polarization may occur in the crystal due to the action of a strong electric field of optic frequency (optic detection), etc. [14, 75, 76].

Generation of the second harmonic, development of stationary polarization in a crystal during the action of a strong electric field of optical frequency, and the linear electrooptic effect can be described with the aid of the analogous relations, derived from differentiation of the expression for free energy with respect to the fields (11.1): generation of the second harmonic:

$$P_i^{(2)} = \chi_{ijkl} E_j E_k \quad (11.26)$$

onset of stationary polarization

$$P_i^{\omega} = X_{ijk}^{\omega} E_j^{\omega} E_k^{\omega}; \quad (11.27)$$

linear electrooptic effect

$$P_i^{\omega} = \chi_{ijk}^{\omega} E_j^{\omega} E_k^{\omega}, \quad (11.28)$$

where  $P_i$  are polarization components,  $E_j$ ,  $E_k$  are components of the electric field,  $X_{ijk}$  are components of the coefficient of nonlinear susceptibility, being third class tensors. The superscripts denote the frequency of the electric field [9].

All three of these effects, by considerations of symmetry, are possible only in noncentrosymmetric crystals. The tensor  $X_{ijk}$  may have 18 independent components. In the case of generation of the second harmonic, however, according to Kleinman [77], for crystals in which dispersion and losses can be ignored the additional conditions of symmetry

$$X_{ijk}^{2\omega} = X_{kij}^{2\omega} = X_{jki}^{2\omega}, \quad (11.29)$$

are satisfied.

Consequently the number of independent components decreases to 10. In this case the matrix of the coefficients of nonlinear susceptibility in two-index notation acquires the following form:

	$E_1$	$E_2$	$E_3$	$2E_1, E_2$	$2E_1, E_3$	$2E_2, E_3$
$P_1$ . . . .	$X_{11}^{\omega}$	$X_{12}^{\omega}$	$X_{13}^{\omega}$	$X_{14}^{\omega}$	$X_{15}^{\omega}$	$X_{16}^{\omega}$
$P_2$ . . . .	$X_{21}^{\omega}$	$X_{22}^{\omega}$	$X_{23}^{\omega}$	$X_{24}^{\omega}$	$X_{25}^{\omega}$	$X_{26}^{\omega}$
$P_3$ . . . .	$X_{31}^{\omega}$	$X_{32}^{\omega}$	$X_{33}^{\omega}$	$X_{34}^{\omega}$	$X_{35}^{\omega}$	$X_{36}^{\omega}$

Kleinman's conditions (equation (11.29)) are valid within the limits of error for all investigated crystals [78-82].

The generation of the second harmonic and linear electrooptic effect should obviously be related to each other. In the simplest case, when assumption [77] is satisfied and the tensor components are related to the principal axes of the tensor of inverse permittivities, the following relation will exist between these effects (cf. equation (11.8)):

$$r_{ij} = -4\pi A_j X_{ij}^{2\omega}, \quad (11.30)$$

where  $A_1 = \frac{1}{\epsilon_{11}^{\omega}}$ , . . . ,  $A_6 = \frac{1}{\epsilon_{11}^{\omega} \epsilon_{22}^{\omega}}$ .

This relation, strictly speaking, should be valid in the case when the frequency of the electric field in which the electrooptic effect is measured is sufficiently close to the frequency of the light field generating the second harmonic.

The coefficients of nonlinear susceptibility  $\chi_{ijk}$  differ among the various crystals by more than two orders of magnitude. Miller [78] introduced another coefficient ( $\delta$ ), characterizing the nonlinearity of the crystals. From the expression for free energy, describing the generation of the second harmonic through polarization, he derived an expression that relates the coefficients of nonlinear susceptibility to the product of the corresponding linear susceptibilities:

$$\chi_{ijk}^{\alpha\beta\gamma} = \chi_{ii}^{\alpha} \chi_{jj}^{\beta} \chi_{kk}^{\gamma} \delta_{ijk}. \quad (11.31)$$

Here  $\alpha, \beta, \gamma$  correspond to frequencies  $\omega_{\alpha}, \omega_{\beta}, \omega_{\gamma}, \omega_{\alpha} = \omega_{\beta} \pm \omega_{\gamma}$ ;  $\chi_{ii}^{\alpha}$  is linear susceptibility on frequency  $\omega_{\alpha}$  on the principal axis  $i$ , etc. (polarization  $P_i^{\alpha} = \chi_{ii}^{\alpha} E_i^{\alpha}$ ).

For generation of the second harmonic this relation acquires the form:

$$\chi_{ijk}^{\alpha\beta\gamma} = \chi_{ii}^{\alpha} \chi_{jj}^{\beta} \chi_{kk}^{\gamma} \delta_{ijk}. \quad (11.32)$$

Coefficient of nonlinearity  $\delta_{ijk}$  differs little for the various nonlinear effects in the same crystal and for various crystals (Table 21). This is evidence that formulation of the laws of optic nonlinear phenomena through polarization is preferable to field strength, since the parameters obtained better characterize the crystal. Coefficient of nonlinearity  $\delta$  for the electrooptic effect is proportional to the electrooptic coefficient  $m$ . As already pointed out, electrooptic coefficients  $m_{ij}$  and  $M_{ij}$  are characterized by great constancy compared to coefficients  $r_{ij}$  and  $R_{ij}$ . Coefficients  $\delta_{ij}$  are the standard nonlinear susceptibilities and can be regarded as a measure of nonlinearity due to electron processes. The determination of these coefficients from anharmonic oscillator model [14] indicated that they are proportional to anharmonic force constant  $b$  [13] (cf. equation (11.11)). An attempt was made [83] to determine these coefficients on the basis of the change of zonal structure in the electric field, using the results of [6-9]. As in [7], it is assumed that

$$\Delta W''(k) = \sum_{ij} \sigma''_{ij}(k) P_i P_j, \quad (11.33)$$

where  $\Delta W''(k)$  is the energy displacement of the  $n$ -zone at the  $k$ -point of the Brillouin zone,  $\sigma''(k)$  is the tensor of the polarization potential,

$P_i, P_j$  are lattice polarization components. The effective polarization potential  $\zeta$  is introduced. It is found by averaging the coefficients  $\sigma_{ij}^n$  for various directions of light polarization. As a result of the calculation it is possible to derive an expression that relates the electrooptic coefficients with  $\zeta$ , and consequently expressions for  $\delta_{ij}$  through  $\zeta$ . It is assumed here that  $\zeta$  are the same for all frequencies, i.e., zonal displacement is identical with respect to ion and electron polarization. Calculation of  $\sigma$  for a number of crystals, presented in [83], gives overstated values compared to the experimental. Consequently, as indicated in [83],  $\zeta$  is indeed smaller on optical frequencies than in the static case.

Table 21. Nonlinear Susceptibility during Generation of Second Harmonic  $X_{ij}^{2\omega}$  and Nonlinear Coefficients  $\delta$  for Certain Nonlinear Effects in a Number of Ferro- and Antiferroelectrics ( $\delta_{ij}^{2\omega}$  for the Generation of Second Harmonic,  $\delta_{ij}^0$  for Stationary Polarization and  $\delta_{ij}^{\omega}$  for Electrooptic Effect)

Crystal	$X_{ij}^{2\omega}$	$\delta_{ij}^{2\omega}/(4\pi)^9$	$\delta_{ij}^0/(4\pi)^9$	$\delta_{ij}^{\omega}/(4\pi)^9$
$\text{KH}_2\text{PO}_4$	$X_{36} = 1.00$ } [82]	0.55 } [81]	0.26 [81]	0.15 } [81]
	$X_{31} = 0.86$ }			
$\text{KD}_2\text{PO}_4$	$X_{36} = 0.99$ } [82]	0.51 } [81]	—	0.39 [81]
	$X_{31} = 0.85$ }			
$\text{RbH}_2\text{PO}_4$	$X_{36} = 0.75$ [80]	0.50 } [81]	—	—
$\text{RbH}_2\text{AsO}_4$	$X_{36} = 1.04$ [80]	0.51 [87]	—	—
$\text{KH}_2\text{AsO}_4$	$X_{36} = 1.01$ [82]	0.23 [87]	—	—
	$X_{31} = 0.86$ [80]	—	—	0.22 [81]
	$X_{36} = 0.70$ [80]	—	—	—
$\text{RbH}_2\text{AsO}_4$	$X_{36} = 0.64$ [82]	0.23 [87]	—	—
$\text{CaH}_2\text{AsO}_4$	$X_{36} = 0.53$ [80]	0.17 [87]	—	—
$\text{NH}_4\text{H}_2\text{PO}_4$	$X_{36} = 0.93$ } [80]	0.55 [87]	—	0.24 } [81]
	$X_{31} = 0.89$ }			
$\text{ND}_2\text{D}_2\text{PO}_4$	$X_{36} = 1.10$ [80]	0.54 [87]	—	—
$\text{LiNbO}_3$	$X_{32} = 6.3; \lambda = 1.058 \mu\text{m}$	—	—	—
	$X_{31} = 11.9$ [100]	0.18 } [81]	—	—
	$X_{33} = 83; \lambda = 1.15 \mu\text{m}$ [100]	1.6 }	—	—
$\text{LiTeO}_3$	$X_{32} = 4.3$ } [100]	0.06 } [81]	—	—
	$X_{31} = 2.6$ }			
	$X_{33} = 40$ [81]			
$\text{BaTiO}_3$	$X_{32} = 10$ } [80, 100]	0.52 } [81]	—	0.24 [81]
	$X_{31} = 37$ }			
	$X_{33} = 15$ }			
$\text{K}_2\text{Li}_4\text{Nb}_5\text{O}_{30}$	$X_{32} = 14.8$ } [80]	0.64 } [80]	—	—
	$X_{31} = 11.5$ }			
$\text{Ba}_2\text{NaNb}_5\text{O}_{15}$	$X_{32} = 23.0$ } [80]	0.77 } [80]	—	—
	$X_{33} = 16.4$ }			
	$X_{31} = 18.9$ }			

Comment. For  $\text{KH}_2\text{PO}_4$  the value  $X_{36}^{2\omega}$  is used as the unit  $X_{ij}^{2\omega}$ . The absolute value of  $X = 3 \cdot 10^{-9}$  Cgs electrostatic system [96]. For quartz  $X_{11}^{2\omega}$  and  $\delta_{11}^{2\omega}/(4\pi)^9$  are used [81].

In order to determine the large nonlinear effects in addition to great nonlinearity it is necessary that the conditions of synchronism be satisfied. The essence of these conditions consists in the following. A powerful light wave modulates the permittivity of a medium according to the traveling wave law. If within the medium waves of three frequencies  $\omega_1, \omega_2, \omega_3$  interact (for instance,  $\omega_1 + \omega_2 = \omega_3$ ), the strong nonlinear interaction among the waves and accumulation of the energy of the waves by measure of their propagation within the medium are possible only if the phase relations among the propagating waves remain constant over the entire distance, i.e.,

$$k_1^{(1)} + k_2^{(1)} = k_3^{(1)} \quad (11.34)$$

where  $k$  is the wave vector.

For second harmonic generation the condition of synchronism has the form

$$2k_1 = k_2,$$

or

$$\Delta_2 = 0, \text{ or } \Delta_2 = 2k_1 - k_2. \quad (11.35)$$

For a bounded medium the accumulation of energy is possible also when  $\Delta_2 \neq 0$ , but  $\Delta_2$  should not be exceedingly large. The length of specimens for which accumulation of energy during second harmonic generation is still possible is determined by the relation

$$L_2 \Delta_2 \approx \frac{\pi}{2}. \quad (11.36)$$

The condition of synchronism may be satisfied if the coefficients of refraction of the wave of initial frequency and of the second harmonic for the corresponding direction of propagation of the waves are equal (we will recall that  $|k| = \frac{n\omega}{c}$ , where  $n$  is the refraction index,  $\omega$  is frequency,  $c$  is the speed of light). The conditions of synchronism can be satisfied only for various combinations of waves of different polarization; for instance, two ordinary incident waves in combination with an extraordinary wave of the second harmonic, the condition of synchronism has the form

$$k_1^o + k_1^e = k_2^e. \quad (11.37)$$

This case is realized in  $\text{NH}_2\text{PO}_4$ , since here  $n_1^o > n_1^e$ , and even  $n_1^o > n_2^e$ .

Angle  $\theta_0$  between the direction in which the condition of synchronism

is satisfied and the optic axis is called the angle of synchronism. The direction of synchronism  $Oz$  in a KDP crystal is shown schematically in Figure 11.7. For the ordinary and extraordinary waves of the original radiation and extraordinary wave of the second harmonic the condition of synchronism has the form

$$k_1^o + k_1^e = k_2^e. \quad (11.38)$$

This case may also be satisfied in a uniaxial negative crystal.

An extremely important value characterizing the nonlinear properties of a crystal is the so-called mismatch gradient. The mismatch gradient determines the rate of change of mismatch  $\Delta$  during deviation from angle of synchronism  $\theta_0$ , i.e., is equal to  $d\Delta/d\theta$  in the vicinity of  $\theta_0$ .

A great advantage of crystals when used in nonlinear optics is the possibility of noncritical generation of the second harmonic, i.e., they satisfy the conditions of synchronism for angle of synchronism  $\theta_0 = 90^\circ$ . Here the velocities of the waves of polarization of the second order and the emissions which they produce are different, birefringence does not occur and the coherent path of the specimen on which energy can accumulate during second harmonic generation is determined only by the divergence of the laser beam.

The conditions of synchronism are of analogous form for various versions of parametric amplification (for instance, amplification of two weak waves with frequencies  $\omega_1$  and  $\omega_2$  using high-frequency pumping  $\omega_p = \omega_1 + \omega_2$  or parametric frequency conversion  $\omega_1 + \omega_p = \omega_2$ , where  $\omega_p$  is the pumping frequency).

If a mirror is used to return to a crystal operating as a parametric amplifier the required part of the energy of waves of the required frequency, the parametric amplifier may become a generator.

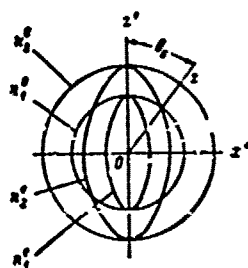


Figure 11.7. Indicatrix of refraction indices  $n_1^o, n_2^o, n_1^e, n_2^e$  of  $\text{KH}_2\text{PO}_4$  crystal for two optical frequencies  $\omega$  and  $2\omega$  in plane  $z'x'$ , where  $z'$  is the optic axis,  $\theta_0$  is the angle for which the condition of synchronism is satisfied.

The most effective crystals used at the present time in nonlinear optics are ferro- and antiferroelectrics, in particular ferroelectrics with the  $\text{KH}_2\text{PO}_4$ , tetragonal potassium-tungsten bronze and lithium niobate structures (Table 21). These crystals can satisfy the conditions of

synchronism, and in certain cases (at certain temperatures and with certain electric fields) noncritical second harmonic generation is possible.

In the case of the  $\text{RbH}_2\text{PO}_4$  crystal, noncritical second harmonic generation is possible due to temperature adjustment of dispersion characteristics [84]. In the case of  $\text{KH}_2\text{PO}_4$  noncritical second harmonic generation can be achieved through adjustment of dispersion characteristics with the aid of an electric field near the Curie point [85]. The condition of noncritical second harmonic generation for lithium niobate is the relation:

$$n_1^0 - n_2^0 = (n_1^0 - n_2^0) - (n_1^0 - n_2^0) = 0. \quad (11.39)$$

This relation may be satisfied by varying wavelength and temperature (temperature adjustment of dispersion characteristics). The temperatures at which it is possible to obtain in lithium niobate summary frequencies of various lasers under conditions of noncritical phase matching, and also frequencies one-half the original frequency, were calculated in [24]. The temperature adjustment of dispersion characteristics for obtaining noncritical phase matching is easily accomplished in crystals with the potassium-tungsten bronze structure [62-64]. The directions of synchronism and magnitudes of mismatch gradients are calculated in [87] for KDP, ADP and lithium niobate crystals.

Great stability with respect to large light flux pulse capacities (up to several hundred  $\text{MWt/cm}^2$ ) is noted in crystals of the KDP group. Certain crystals, however, cannot operate under conditions of irradiation with laser beams of considerable power. Fluctuations of the refraction index occur in lithium niobate, for instance, during irradiation (optical aging). This phenomenon occurs to a lesser extent in lithium tantalate crystals [88]. It occurs in KTN crystals under the simultaneous effect of a laser beam and stationary biasing field [89]. The causes of this phenomenon are not completely clear. Presumably, in particular [89], it is related to the formation of a space charge as a result of photoexcitation of current carriers from traps. This charge, in turn, leads to irregularities in the refraction coefficient due to a great electrooptic effect. It is possible that the magnitude of this charge is related to the number of free lattice nodes capable of serving as traps for current carriers and, consequently, are sources of photoelectrons [63]. Attempts are being made to create new materials in which fluctuations of the refraction index will not take place. In particular, analysis of the optical nonlinear properties of niobium compounds with the tetragonal potassium-tungsten bronze structure with filled cation positions in the lattice showed that some of them display less optical aging than lithium niobate. These include  $\text{K}_6\text{Li}_4\text{Nb}_{10}\text{O}_{30}$  with filled positions in the pentagonal, tetragonal and triangular lattice channels [63],  $\text{K}_2\text{Sr}_4\text{Nb}_{10}\text{O}_{30}$  [62] and  $\text{Na}_2\text{Ba}_4\text{Nb}_{10}\text{O}_{30}$  [64] crystals with filled positions in the pentagonal and tetragonal channels.

The results of the estimate of nonlinear optic properties with the aid of the powder method, not requiring good crystals, are presented for several materials in [90]. The following ferroelectrics are characterized [90] by great optic nonlinearity in combination with the possibility of phase matching:  $\text{KIO}_3$ ,  $\text{PbTiO}_3$ ,  $\text{KNbO}_3$ , etc.  $\text{BaTiO}_3$ ,  $\text{Gd}_2(\text{MoO}_4)_3$ , etc. are characterized by great optic nonlinearity, but without phase matching.

Noteworthy are attempts to create sources of coherent emission on the basis of ferroelectric matrices, since the direct action of the electric field on the laser beam is possible in such sources.

The generation of coherent light emission using the ferroelectric  $\text{Gd}_2(\text{MoO}_4)_3$ , containing a mixture of neodymium, was reported in [91].

Induced emission of lithium niobate crystals with neodymium impurity was achieved in [92].

For the parameters of nonlinear optic materials the reader is referred to overviews [14, 93, 94] and Table 21.

#### BIBLIOGRAPHY

1. Akhmanov, S. A. and R. V. Khokhlov, Introduction to Russian edition of N. Blombergen's monograph Nelineynaya Optika (Nonlinear Optics), "Mir" Publishing House, Moscow, 1966.
2. Zheludev, I. S., UFN [Uspekhi fizicheskikh nauk; Progress of Physical Sciences], Vol. 88, p. 253, 1966.
3. Vlokh, O. G. and I. S. Zheludev, Kristallografiya (Crystallography), Vol. 5, p. 389, 1960; O. G. Vlokh, Ukr. fiz. Zh. (Ukrainian Physics Journal), Vol. 10, p. 1001, 1965; V. A. Shamburov and O. G. Vlokh, Radioelektronika i Elektronika (Radio Engineering and Electronics), Vol. 9, p. 505, 1964.
4. Rez, I. S., UFN, Vol. 93, p. 633, 1967.
5. Zheludev, I. S. and L. A. Shuvalov, Kristallografiya, Vol. 1, p. 681, 1956.
6. Kahn, H. A. and A. J. Leyendecker, Phys. Rev., Vol. 135, A1324, 1964.
7. Zook, J. D. and T. N. Casselman, Phys. Rev. Lett., Vol. 17, p. 960, 1966.
8. Brews, J. R., Phys. Rev. Lett., Vol. 18, p. 662, 1967.
9. Ward, J. F. and P. A. Franken, Phys. Rev., Vol. 133, A183, 1964.
10. Geusic, J. E., S. K. Kurtz, L. G. van Uitert and S. H. Wemple, Appl. Phys. Lett., Vol. 4, p. 141, 1964.

11. Kurtz, S. K., Proc. Intern. Meet. Ferroelectr., Vol. 1, Prague, p. 413, 1966.
12. Frova, A. and P. J. Boddy, Phys. Rev., Vol. 153, p. 605, 1967.
13. Kurtz, S. K. and F. N. H. Robinson, Appl. Phys. Lett., Vol. 10, p. 62, 1967.
14. Blombergen, N., Nelineynaya Optika, "Mir" Publishing House, Moscow, 1966.
15. Chen, F. S., J. F. Geusic, S. K. Kurtz, J. G. Skinner and S. H. Wemple, J. Appl. Phys., Vol. 37, p. 588, 1966.
16. Jwasaki, H. H. Toyoda and N. Niizeki, Japan J. Appl. Phys., Vol. 6, p. 1419, 1967.
17. Anistratov, A. G. and K. S. Aleksandrov, Izv. AN SSSR, ser. fiz. (News of USSR Academy of Sciences, Physics Series), Vol. 31, p. 1129, 1967.
18. Sonin, A. S., V. E. Perfilova and A. S. Vasilevskaya. Izv. AN SSSR, ser. fiz., Vol. 31, p. 1125, 1967.
19. Meyerhofer, D., Phys. Rev., Vol. 112, p. 413, 1958.
20. Shirane, G., R. Pepinsky and B. C. Frazer, Acta Cryst., Vol. 9, p. i31, 1959.
21. Merz, W. J., Phys. Rev., Vol. 91, p. 513, 1953.
22. Zheludev, I. S., Ye. V. Sidnenko and S. I. Teplyakova, Kristallografiya, Vol. 12, p. 604, 1967.
23. Johnston, A. K. and J. M. Weingart, J. Opt. Soc. Am., Vol. 55, p. 828, 1965.
24. Hobden, M. V. and J. Warner, Phys. Lett., Vol. 22, p. 243, 1966.
25. Miller, R. C. and A. Savage, Proc. Intern. Meet. Ferroelectr., Vol. 1, Prague, p. 405, 1966.
26. Kinase, W., J. Kobayashi and Y. Yamada, Phys. Rev., Vol. 128, p. 348, 1959.
27. Kinase, W., Y. Ichikoshi and S. Hyakubu, J. Phys. Soc. Japan, Vol. 20, p. 1438, 1965.
28. Lawless, W. N., Phys. Rev., Vol. 138 A, p. 1751, 1965.
29. Meysner, L. B. and A. S. Sonin, FTT [Fizika tverdogo tela; Solid State Physics], "Fizmatgiz", p. 3657, 1965.

30. Scnin, A. S. and L. B. Meysner, Izv. AN SSSR, ser. fiz., Vol. 31, p. 1122, 1967.
31. Forsbergh, P. W., Phys. Rev., Vol. 76, p. 1187, 1949.
32. Lawless, W. N. and R. C. DeVries, J. Appl. Phys., Vol. 35, p. 2638, 1964.
33. Kentsig, V., Segnetoelektriki i Antisegetoelektriki (Ferroelectrics and Antiferroelectrics), IL [Foreign Literature] Publishing House, Moscow, 1960.
34. Perfilova, V. E. and A. S. Sonin, FTT, Vol. 8, p. 107, 1966.
35. Berezhnoy, A. A., Izv. AN SSSR, ser. fiz., Vol. 31, p. 1154, 1967.
36. Smolenskiy, G. A., N. N. Kraynik, A. A. Berezhnoy and I. Ye. Myl'nikova, FTT, Vol. 10, p. 457, 1967.
37. Berezhnoy, A. A. V. N. Bukhman, L. T. Kudinova and I. Ye. Myl'nikova, FTT, Vol. 10, p. 255, 1968.
38. Bonner, W. A., E. F. Dearborn, J. E. Geusic, H. M. Marcos and L. C. van Uitert, Appl. Phys. Lett., Vol. 10, p. 163, 1967.
39. Vasilevskaya, A. S. V. E. Perfilova and A. S. Sonin, Izv. AN SSSR, ser. fiz., Vol. 31, p. 1132, 1967.
40. Sonin, A. S., V. E. Perfilova and A. S. Vasilevskaya, Izv. AN SSSR, ser. fiz., Vol. 29, p. 969, 1965.
41. Ivanov, N. R. and L. A. Shuvalov, Kristallografiya, Vol. 11, p. 614, 1966.
42. Vasilevskaya, A. S., A. S. Sonin and I. A. Slep'kov, Kristallografiya, Vol. 11, p. 749, 1966.
43. Vasilevskaya, A. S. and A. S. Sonin, Kristallografiya, Vol. 12, p. 303, 1967.
44. Sonin, A. S. and A. S. Vasilevskaya, FTT, Vol. 9, p. 1951, 1967.
45. Ivanov, N. R. and L. A. Shuvalov, Kristallografiya, Vol. 11, p. 760, 1966.
46. Kislovskii, I. D., L. A. Shuvalov, N. R. Ivanov and E. K. Galanov, Proc. Intern. Meet. Ferroelectr., Vol. 1, Prague, p. 205, 1966.
47. Zwicker, B. and P. Scherrer, Helv. Phys. Acta, Vol. 17, p. 346, 1944.
48. Vlokh, O. G., Kristallografiya, Vol. 7, p. 632, 1962.

49. Vlokh, O. G. and L. F. Lutsiv-Shumskiy, Ukr. Fiz. Zh., Vol. 10, p. 1119, 1965.
50. Vlokh, O. G. and L. F. Lutsiv-Shumskiy, Izv. AN SSSR, ser. fiz., Vol. 31, p. 1139, 1967.
51. Vishnevskiy, V. I. and I. V. Speranskiy, Opt. i Spektrosk. (Optics and Spectroscopy), Vol. 22, p. 357, 1966.
52. Perfilova, V. E. and A. S. Sonin, Izv. AN SSSR, ser. fiz., Vol. 31, p. 1136, 1967.
53. Perfilova, V. E. and A. S. Sonin, Kristallografiya, Vol. 10, p. 427, 1965.
54. Anistratov, A. T. and K. S. Aleksandrov, Kristallografiya, Vol. 12, p. 459, 1967.
55. Vlokh, O. G. and L. F. Lutsiv-Shumskiy, Kristallografiya, Vol. 12, p. 455, 1967.
56. Turner, E. H., Appl. Phys. Lett., Vol. 8, p. 303, 1966.
57. Lenzo, P. V., E. G. Spencer and K. Nassau, J. Opt. Soc. Am., Vol. 56, p. 633, 1966.
58. Zook, J. D., D. Chen and G. N. Otto, Appl. Phys. Lett., Vol. 11, p. 159, 1967.
59. Vasilevskaya, A. S., A. S. Sonin, I. S. Rez and G. A. Plotinskiy, Izv. AN SSSR, ser. fiz., Vol. 31, p. 1159, 1967.
60. Lenzo, P. V., E. G. Spencer and A. A. Ballman, Appl. Phys. Lett., Vol. 11, p. 23, 1967.
61. Smolenskiy, G. A., Ya. M. Ksendzov, A. I. Agranovskaya and S. N. Popov, Fizika Dielektrikov (Physics of Dielectrics), Vol. II, USSR Academy of Sciences Publishing House, Moscow-Leningrad, p. 244, 1959.
62. Giess, E. A., G. Burns, D. F. O'Kane and A. W. Smith, Appl. Phys. Lett., Vol. 11, p. 233, 1967.
63. van Uitert, L. G., S. Singh, H. J. Levinstein, J. E. Geusic and W. A. Bonner, Appl. Phys. Lett., Vol. 11, p. 161, 1967.
64. Geusic, J. E., H. J. Levinstein, J. J. Rubin, S. Singh and L. G. van Uitert, Appl. Phys. Lett., Vol. 11, p. 269, 1967.
65. Turner, E. H., E. G. Spencer and A. A. Ballman, Appl. Phys. Lett., Vol. 8, p. 81, 1966.

66. Carpenter, R. O. B., J. Opt. Soc. Am., Vol. 40, p. 225, 1950.
67. Sliker, T. R. and S. R. Barlage, J. Appl. Phys., Vol. 34, p. 1037, 1963.
68. Ott, J. H. and T. R. Sliker, J. Opt. Soc. Am., Vol. 54, p. 1442, 1964.
69. Vasilevskaya, A. S., M. S. Koldobskaya, L. G. Lomova, V. P. Popova, G. A. Regul'skaya, I. S. Rez, Yu. P. Sobeskiy, A. S. Sonin and V. S. Suvorov, Kristallografiya, Vol. 12, p. 447, 1967.
70. Vasilevskaya, A. S., Candidate dissertation, Moscow, 1967.
71. Vasilevskaya, A. S., Ye. I. Volkova, V. A. Koptsik, L. N. Rashkovich, T. A. Regul'skaya, I. S. Rez, A. S. Sonin and V. S. Suvorov, Kristallografiya, Vol. 12, p. 518, 1967.
72. Futama, H. and R. Pepinsky, J. Phys. Soc. Japan, Vol. 17, p. 725, 1962.
73. Ivanov, N. R., L. A. Shuvalov, A. V. Mirenskiy and T. D. Shnyrev, Kristallografiya, Vol. 12, p. 307, 1967.
74. Shuvalov, I. A. and N. R. Ivanov, Kristallografiya, Vol. 9, p. 363, 1964.
75. Akhmanov, S. A. and R. V. Khokhlov, Problemy Nelineynoy Optiki (Problems of Nonlinear Optics), ser. "Itogi Nauki" (Advances of Science), VINITI [All-Union Institute of Scientific and Technical Information (of the State Committee of the Council of Ministers, USSR, for Science and Technology and of the Academy of Sciences, USSR)] Publishing House, Moscow, 1964.
76. Akhmanov, S. A. and R. V. Khokhlov, UFN, Vol. 88, p. 439, 1966.
77. Kleinman, D. A., Phys. Rev., Vol. 126, p. 1977, 1962.
78. Miller, R. C., Phys. Rev., Vol. 131, p. 95, 1963.
79. Savage, A. and R. C. Miller, Appl. Opt., Vol. 1, p. 661, 1962.
80. Miller, R. C., Phys. Rev., Vol. 134, A1513, 1964.
81. Miller, R. C., Appl. Phys. Lett., Vol. 5, p. 17, 1964.
82. Van derZill, J. P. and N. Bloembergen, Phys. Rev., Vol. 135, A1662, 1964.
83. Domenico, M. and S. H. Wemple, Appl. Phys. Lett., Vol. 12, p. 352, 1968.
84. Suvorov, V. S. and A. A. Filimonov, FTT, Vol. 9, p. 2131, 1967.

85. Adams, N. I. and J. J. Barret, IEEE, J. Quant. Electron., Vol. 2, p. 430, 1966.
86. Miller, R. C., G. D. Boyd and A. Savage, Appl. Phys. Lett., Vol. 6, p. 77, 1965.
87. Weber, H. P., E. Mathieu and K. P. Meyer, J. Appl. Phys., Vol. 37, p. 3584, 1966.
88. Ashkin, A., G. D. Boyd, J. M. Dziedzic, K. G. Smith, A. A. Ballman, H. J. Levinstein and K. Nassau, Appl. Phys. Lett., Vol. 9, p. 72, 1966.
89. Caen, F. S., J. Appl. Phys., Vol. 38, p. 3418, 1967.
90. Kurtz, S. K. and T. T. Perry, J. Appl. Phys., Vol. 39, p. 3798, 1968.
91. Borshardt, H. J. and P. E. Bierstedt, Appl. Phys. Lett., Vol. 8, p. 50, 1966.
92. Yevlanova, N. F., A. S. Kovalev, V. A. Koptsik, L. S. Kopinenko, A. M. Prokhorov and L. N. Rashkevich, ZhETF [Zhurnal eksperimental'noy i teoreticheskoy fiziki; Journal of Experimental and Theoretical Physics], Letters, Vol. 5, p. 351, 1967.
93. Suvorov, V. S. and A. S. Sonin, Kristallografiya, Vol. 11, p. 832, 1966.
94. Robinson, F. H. H., Bell. System. Tech. J., Vol. 46, p. 913, 1967.
95. Ashkin, A., G. D. Boyd and J. M. Dziedzic, Phys. Rev. Lett., Vol. 11, p. 14, 1963.
96. Suvorov, V. S., A. S. Sonin and I. S. Rez, ZhETF, Vol. 53, p. 49, 1967.
97. Suvorov, V. S., Candidate dissertation, Moscow, 1968.
98. Pershan, N., Progress in Optics, Vol. 5, p. 134, 1966.
99. Miller, R. C., D. A. Kleinman and A. Savage, Phys. Rev. Lett., Vol. 11, p. 146, 1963.
100. Boyd, G. D., R. C. Miller, K. Nassau, W. L. Bond and A. Savage, Appl. Phys. Lett., Vol. 5, p. 234, 1964.
101. Miller, R. C. and A. Savage, Appl. Phys. Lett., Vol. 9, p. 169, 1966.
102. Miller, R. C. and A. Savage, Proc. Intern. Meet. Ferroelectr., Vol. 1, Prague, p. 105, 1966.
103. Miller, R. C., Phys. Rev., Vol. 131, p. 95, 1963.

## CHAPTER 12. THERMAL PROPERTIES OF FERROELECTRICS

### §1. Thermal Capacity

In order to understand the nature and character of the ferroelectric phase transition it is particularly important to know the dependence of thermal capacity on temperature in the region of the transition.

According to thermodynamic theory, as we know, first order phase transitions occur with latent heat of transition, and for second order phase transitions thermal capacity must change abruptly. Ferroelectric phase transitions are exceptions in this sense and, as shown in Chapter 3, the expressions for the thermal anomalies can be derived by using the expansion of the thermodynamic potential in terms of degrees of polarization. Equation (3.5) can be written for entropy change ( $\Delta S$ ) in the form:

$$\Delta S = -P_s^2 \frac{2\pi}{C}. \quad (12.1)$$

In the case of the first order phase transition we have for latent heat of transition  $\Delta Q$ :

$$\Delta Q = -\frac{2\pi}{C} T_s P_s^2, \quad (12.2)$$

where  $P_s$  is the jump of spontaneous polarization at the Curie point. The jump of thermal capacity for the second order phase transition can also be determined from (12.1):

$$\Delta c = -\frac{2\pi}{C} T_s \frac{dP_s^2}{dT_s}. \quad (12.3)$$

Recalling (3.9a), or making the corresponding substitution in (3.10), we can find another, often more convenient formula for  $\Delta c$ :

$$\Delta c = \left(\frac{2\pi}{C}\right)^2 \frac{T_s}{P_s}. \quad (12.4)$$

The thermal anomalies at the Curie point have been analyzed most thoroughly for ferroelectrics with the second order phase transition. Hoshino, et al [1] and Strukov, et al [2-5] analyzed the temperature dependences of thermal capacity of triglycine sulfate and isomorphous compounds. The curve plotted by Strukov, et al [2] for the triglycine sulfate crystal is illustrated in Figure 12.1. The experimental values of entropy change ( $\Delta S$ ) of this group of ferroelectrics are presented in Table 23. The discrepancy between the theory and experiment has the form of the curve  $c(T)$  in the region of transition. The theoretical dependence of thermal capacity on temperature can be calculated according to equation (12.3). This dependence has an abrupt change at the point of transition, but it does not have a sharp peak [1]. The peak of thermal capacity at the Curie point is observed in triglycine selenate [4], triglycine fluorberyllate [5], and  $\text{NH}_4\text{HSO}_4$  [6] crystals. The reasons for the discrepancy between the theoretical and experimental dependences are not known at this time.

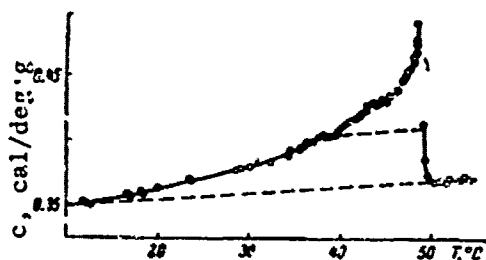


Figure 12.1. Temperature dependence of thermal capacity of shorted triglycine sulfate crystal (Strukov [2]).

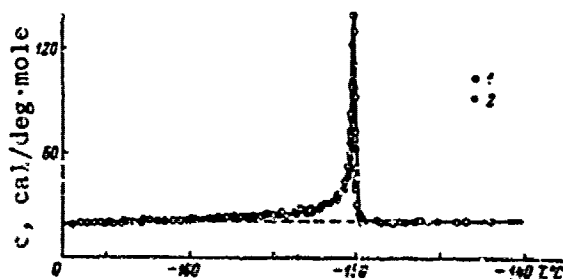


Figure 12.2. Temperature-dependence of thermal capacity of shorted potassium dihydrophosphate crystal. 1 -- according to Strukov, et al [13]; 2 -- according to Stephenson and Hooley [11].

It should be pointed out that if terms that take into account the fluctuating heterogeneity of polarization are introduced in the expression for the thermodynamic potential, then near the Curie point  $c \sim |\ln|T - \theta||$  for axial ferroelectrics and  $c \sim (T - \theta)^{-1/2}$  for ferroelectrics with two

and three ferroelectric axes [7]. The experimental results for triglycine sulfate [8, 3] and triglycine fluorberyllate [3] in a narrow temperature range near the Curie point, in the opinion of the authors of these works, satisfy the logarithmic function. Thus, it has been found theoretically and by processing experimental data that the thermal capacity at the Curie point has a logarithmic feature.

This coincidence, however, apparently cannot be regarded as the complete theoretical explanation of the anomaly. The fact is that consideration of fluctuations may yield only a very narrow peak of thermal capacity, whereas the experimentally observed maximum is asymmetric and quite broad. Strukov, et al [9] and also Baumberger, et al [10], analyzed the influence of a stationary field on the anomalous change of thermal capacity of triglycine sulfate crystals. On application of an electric field the thermal capacity peak vanishes and no abrupt jump is noted. The greater the strength of the field the more "eroded" the thermal capacity anomaly becomes. This transformation is not surprising. The change of thermal capacity caused by a change of polarization is determined, as before, by relation (12.3), but now  $P$  is not spontaneous polarization, but the equilibrium polarization in the external field. Temperature dependences of polarization in the presence of an electric field for the case of the second order phase transition are given in Figure 3.10b. The character of these dependences is such that  $dP/dT$  and the product  $P(dP/dT)$ , which determines the behavior of thermal capacity, change monotonically with temperature, without abrupt jumps. Thus, the electric field leads to smoothing of the thermal capacity peak.

The thermal capacity anomaly at the Curie point was quite carefully analyzed on potassium dihydrophosphate crystals. These studies were conducted by Stephenson and Hooley [11], Reese and May [12], Strukov, et al [19]. The peak of thermal capacity of potassium dihydrophosphate is narrow and high (Figure 12.12). In the paraelectric phase, just  $0.5^\circ$  above the Curie point, thermal capacity is again normal [13]. This all indicates that the phase transition in potassium dihydrophosphate is a second order phase transition, and possibly first order near the critical point.

The analytical form of the function  $c(T_c - T)$  apparently cannot be regarded accurately established. In the ferroelectric phase, according to the data of Strukov, et al [13, 14],  $c \sim (T_c - T)^{-\delta}$ , where  $\delta \approx 0.5$ . The results of Reese and May [12] are in better agreement with the logarithmic law, although they also satisfy the power function, albeit at somewhat greater distance from the maximum. Here  $\delta = 0.5$  below the transition and  $\delta = 1.0$  above the transition. Even the same experimental results of Stephenson and Hooley [11], according to Teaney's calculations [14], satisfy the power law with  $\delta = 0.5$ , and according to Grindlay's calculations [15], are in better accord with the logarithmic dependence. The application of an electric field, just as in the case of triglycine sulfate, leads to a reduction and erosion of the thermal capacity anomaly [13]. The

thermal capacity peak at the Curie point is also displayed by  $\text{RbH}_2\text{PO}_4$  [16]. In contrast to the preceding two phosphates, the thermal capacity peak of  $\text{KD}_2\text{PO}_4$ , isomorphic to them, is so high and narrow that experimental data can be explained only in the assumption of latent heat of transition [13, 17, 18].

Table 22. Heat ( $\Delta Q$ ) and Entropy ( $\Delta S$ ) of Transition of Several Ferroelectrics

Compound	$\Delta Q$ , cal/ /mole	$\Delta S$ , cal/mole·g	Source
Triglycine sulfate	150	0.48	[1]
Triglycine selenate	342	—	[2]
Triglycine fluoro-	—	0.57	[3]
beryllate	400	1.17	[4]
$\text{KH}_2\text{PO}_4$	—	0.74	[5]
$\text{KD}_2\text{PO}_4$	105.2	$0.838 \pm 0.02A$ $0.69 \pm 0.02$ Forr, $0.2790 \pm 0.0032$ or r. to $0^\circ\text{K}$ $0.843 \pm 0.014$	[6]
$\text{RbH}_2\text{PO}_4$	—	0.684	[7]
from cubic to	7	0.12	[8]
tetragonal	$50 \pm 5$	0.125	[9]
phase	47	0.12	[10]
from tetragonal	16	0.058	[11]
to rhombic	$22 \pm 4$	0.076	[12]
	15.3	0.054	[13]
	28	0.091	[14]
from rhombic	$8 \pm 2$	0.04	[15]
to tetragonal	14.3	0.07	[16]
	12	0.06	[17]
from cubic to	$190 \pm 15$	0.28	[18]
tetragonal	$134 \pm 5$	0.19	[19]
from tetragonal	$85 \pm 10$	0.17	[20]
to rhombic			
from rhombic to	$32 \pm 5$	0.12	[21]
rhombohedra			

The thermal capacity of Seignette's salt has been investigated by numerous researchers [19-23], but these works are comparatively old and their results differ greatly from each other. It can be said only that the heats of transition at the Curie points are low. According to Wilson's data [22], the thermal capacity anomaly at the top Curie point is positive and at the bottom Curie point it is negative.

The ferroelectric phase transition of barium titanate, in contrast to the preceding ferroelectrics, is a second order transition and should take place with latent heat. During calorimetric measurements, however, by virtue of defects, internal stresses, etc., only a thermal capacity peak is observed (Figure 12.3). The heat of transition can be determined by integrating  $\Delta Q = \int \Delta c dT$ .  $\Delta Q$  and  $\Delta S$ , obtained by various authors [24-27], are listed in Table 22. Presented here also are  $\Delta Q$  and  $\Delta S$  for low-temperature phase transitions of barium titanate, and also for all three phase transitions of  $\text{KNbO}_3$ , which by its properties is the analog to barium titanate.

It is noteworthy that relation (12.2) is satisfied with good accuracy for barium titanate.

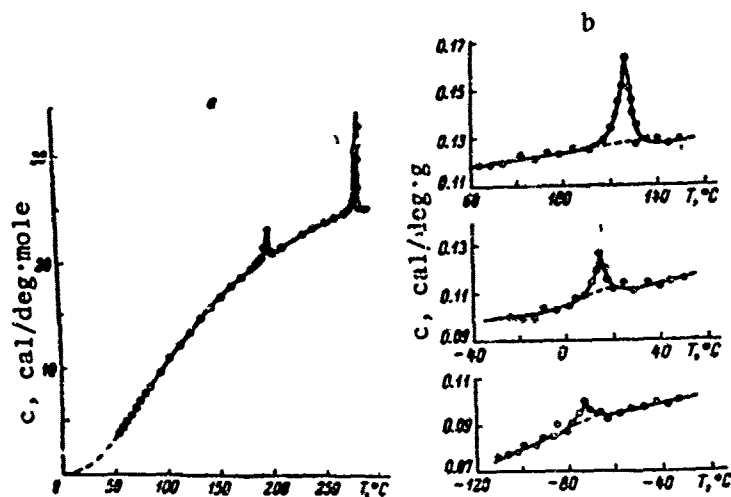


Figure 12.3. Temperature dependence of thermal capacity of polycrystalline barium titanate. a -- according to Todd and Lorenson [27]; b -- according to Shirane and Takeda [25].

## 52. Thermal Conductivity

The thermal conductivity of ferroelectrics has not yet been analyzed to an extent sufficient to permit discussion of any general principles. Data are available only for phosphates and certain perovskites.

The thermal conductivity of phosphate crystals was analyzed by Suemune [30, 31], who detected in all isomorphous compounds strong anomaly at the Curie point (Figure 12.4). In ordinary crystalline dielectrics at moderately low temperatures the dependence of thermal conductivity on  $T$  at high temperatures is a power function of  $T^{-1}$ , and at lower temperatures it is exponential. In the case of ferroelectrics with hydrogen bonds, in Suemune's opinion [31], the unordered position of hydrogen in the paraelectric phase leads to limitation of the mean free path of the phonon by the dimensions of the elementary nucleus and the temperature dependence of thermal conductivity is determined by the temperature curve of thermal capacity, which drops with temperature. Thus, there is presumably a formal analogy with glass, where the mean free phonon path is limited by the dimensions of the crystallite.

Below the Curie point the hydrogen becomes ordered and thermal conductivity increases sharply. The height of the thermal conductivity peak at temperatures below  $10^{\circ}\text{K}$  is proportional in a number of phosphates to  $T_C^2$ . The experimental data for the thermal conductivity of ferroelectrics with

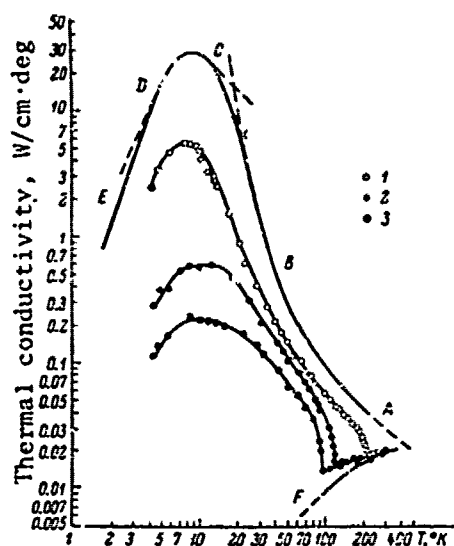


Figure 12.4. Temperature dependence of thermal conductivity of  $\text{KH}_2\text{PO}_4$ ,  $\text{KD}_2\text{PO}_4$  and  $\text{KH}_2\text{AsO}_4$  crystals (Suemune [31]). Theoretical curve: in regions A and B the thermal resistance is attributed to scatter processes, in range C to point defects, in D to dislocations and in E to the crystal surface. The drop of thermal capacity in region F is related to the unordered distribution of hydrogen atoms. 1 --  $\text{KD}_2\text{PO}_4$ ; 2 --  $\text{KH}_2\text{PO}_4$ ; 3 --  $\text{KH}_2\text{AsO}_4$ .

the perovskite type structure, obtained by different authors, disagree considerably. Thus, polycrystalline specimens of barium titanate, lead titanate and certain solid solutions based on barium titanate display at the Curie point small thermal conductivity peaks [32-36]. Barium titanate monocrystals, according to some data [37] display no anomalies at all during phase transition, whereas according to other investigators [38], thermal conductivity passes through minima at the Curie point during low-temperature phase transitions.

The latter results may be explained from the viewpoint of dynamic theory, according to which the energies of the acoustic and lateral optic branches of oscillation converge near phase transitions for low wave numbers. By virtue of the closeness of the energies of two types of vibrations the number of scattering events in which optical phonons participate may increase, and consequently thermal conductivity may decrease [38, 39]. That such a scattering mechanism actually occurs is verified by Steigmeier's studies [40] of  $\text{SrTiO}_3$  monocrystals. He discovered that the application of a stationary electric field in the direction perpendicular to the temperature gradient results in a substantial increase in thermal conductivity at temperatures below 50°K. The effect of the electric field on thermal conductivity, in Steigmeier's opinion, is related to displacement of the optical branch with respect to frequency.

### §3. Electrocaloric Effect

The electrocaloric effect is an effect connected with the pyroelectric effect, consisting in a change of entropy of a system when placed in an electric field. In the general case

$$dS = \left(\frac{\partial S}{\partial E}\right)_T dE + \left(\frac{\partial S}{\partial T}\right)_E dT. \quad (12.5)$$

Recalling that

$$\left(\frac{\partial S}{\partial T}\right)_E = \frac{c_E}{T} \quad (12.6)$$

and

$$\left(\frac{\partial S}{\partial E}\right)_T = \left(\frac{\partial P}{\partial T}\right)_E \quad (12.7)$$

we obtain from (12.5) with the condition  $dS = 0$ :

$$dT = -\frac{T}{c_E} \left(\frac{\partial P}{\partial T}\right)_E dE. \quad (12.8)$$

Thus, under adiabatic conditions a change in electric field strength leads to a change in temperature of the body. Since the change of temperature is proportional to  $(\partial P/\partial T)$ , we should expect the effect to be strongest specifically in ferroelectrics, and near the phase transition, where the dependence of spontaneous polarization and dielectric susceptibility on temperature is especially strong. For comparison with the experiment it is often convenient to use another expression for the electrocaloric effect, which can be derived by regarding entropy as a function of  $P$  rather than of  $E$ . Then

$$dS = \left(\frac{\partial S}{\partial P}\right)_T dP + \left(\frac{\partial S}{\partial T}\right)_P dT. \quad (12.9)$$

Recalling that

$$\left(\frac{\partial S}{\partial T}\right)_P = \frac{c_P}{T} \quad (12.10)$$

and the relation of the Maxwell type

$$\left(\frac{\partial S}{\partial P}\right)_T = -\left(\frac{\partial E}{\partial T}\right)_P, \quad (12.11)$$

we have for adiabatic conditions from (12.9)

$$dT = \frac{T}{c_P} \left(\frac{\partial E}{\partial T}\right)_P dP. \quad (12.12)$$

Then, using the equation of state (3.8a), (12.12) can be reduced to the form

$$dT = \frac{2\pi}{c} \cdot \frac{T}{c_P} P dP. \quad (12.13)$$

After integration of (12.13) we obtain

$$\Delta T = \frac{2\pi T}{C\epsilon_p} (P_1^2 - P_2^2). \quad (12.14)$$

Thus, in the case of the second order phase transition the change of temperature is directly proportional to the change of the square of polarization.

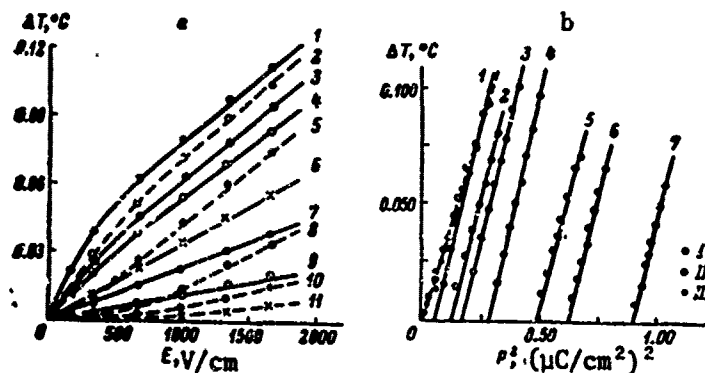


Figure 12.5. Dependences illustrating electrocaloric effect on triglycine sulfate crystals (Strukov [43]). a -- dependence of change of temperature of crystal on electric field strength at various distances from Curie point ( $T - T_c$ ). 1 --  $-0.041^\circ\text{C}$ ; 2 --  $+0.147^\circ\text{C}$ ; 3 --  $-0.289^\circ\text{C}$ ; 4 --  $-0.535^\circ\text{C}$ ; 5 --  $+0.0412^\circ\text{C}$ ; 6 --  $-1.375^\circ\text{C}$ ; 7 --  $-2.637^\circ\text{C}$ ; 8 --  $+1.240^\circ\text{C}$ ; 9 --  $-8.004^\circ\text{C}$ ; 10 --  $+1.784^\circ\text{C}$ ; 11 --  $+3.176^\circ\text{C}$ . b -- dependence of change of temperature of crystal on  $P^2$  at various distances from Curie point ( $T - T_c$ ). I --  $+0.147^\circ\text{C}$ ; II --  $+0.412^\circ\text{C}$ ; III --  $+1.240^\circ\text{C}$ ; 1 --  $0.005^\circ\text{C}$ ; 2 --  $-0.290^\circ\text{C}$ ; 3 --  $-0.387^\circ\text{C}$ ; 4 --  $-0.663^\circ\text{C}$ ; 5 --  $-1.190^\circ\text{C}$ ; 6 --  $-1.570^\circ\text{C}$ ; 7 --  $-2.188^\circ\text{C}$ .

The electrocaloric effect of ferroelectrics was first discovered experimentally by Kobeko and Kurchatov [41] on Seignette's salt crystals. Later on Seignette's salt [42], triglycine sulfate [43, 44, 10], triglycine selenate [45, 46], triglycine fluorberyllate [46] crystals, polycrystalline barium titanate [47], strontium titanate [48, 49], were analyzed. The experimental data for the first four ferroelectrics agree satisfactorily with equation (12.14). The dependences of  $\Delta T$  on  $E$  and  $P^2$  are shown in Figure 12.5 for triglycine sulfate crystals. Above the Curie point the straight line  $\Delta T = f(P^2)$  passes through the origin of the coordinate system. Below the Curie point the straight lines cut on the abscissa segments equal to  $P_S^2$ . Thus, electrocaloric measurements make it possible to determine the magnitude of spontaneous polarization, and more accurately, apparently, near the Curie point than from the hysteresis loops.

Measurements of the electrocaloric effect on strontium titanate were aimed at investigating the possibility of reaching low temperatures through adiabatic depolarization. Hegenbarth [48] brought about maximum change of temperature of polycrystalline specimens in the 16-18°K range, where  $\Delta T \sim 0.1^\circ\text{K}$  for  $E = 10 \text{ kV/cm}$ . Kikuchi and Sawaguchi [49] produced the maximum effect of  $\Delta T = 0.28^\circ\text{K}$  ( $E = 7 \text{ kV/cm}$ ) at 11.5°K on monocrystals.  $\Delta T$  rapidly diminishes as the temperature approaches the liquid helium temperature [48].

#### BIBLIOGRAPHY

1. Hoshino, S., T. Mitsui, F. Jona and R. Pepinsky, *Phys. Rev.*, Vol. 107, p. 1255, 1957.
2. Strukov, B. A., FTT [Fizika tverdogo tela; Solid State Physics], Vol. 6, p. 2862, 1964.
3. Strukov, B. A., *Proc. Intern. Meet. Ferroelectr.*, Vol. 1, Prague, p. 191, 1966.
4. Strukov, B. A., S. A. Taraskin, V. A. Koptsik and V. M. Varikash, Kristallografiya (Crystallography), Vol. 13, p. 541, 1968.
5. Strukov, B. A., S. A. Taraskin and V. A. Koptsik, ZhETF [Zhurnal Eksperimental'noy i Teoreticheskoy Fiziki; Journal of Experimental and Theoretical Physics], Vol. 51, p. 1037, 1966.
6. Strukov, B. A. and M. N. Danilycheva, FTT, Vol. 5, p. 1724, 1963.
7. Levanyuk, A. P., Izv. AN SSSR. ser. fiz. (News of USSR Academy of Sciences, Physics Series), Vol. 29, p. 879, 1965.
8. Grindley, I., *Phys. Lett.*, Vol. 18, p. 239, 1965.
9. Strukov, B. A., S. A. Taraskin, T. L. Skomorokhova and K. A. Minayeva, Izv. AN SSSR, ser. fiz., Vol. 29, p. 982, 1965.
10. Baumberger, C., J. P. Duraire and L. Godefroy, *Proc. Intern. Meet. Ferroelectr.*, Vol. 1, Prague, p. 199, 1966.
11. Stephenson, C. C. and J. G. Hooley, *J. Am. Chem. Soc.*, Vol. 66, p. 1397, 1944.
12. Reese, W. and L. F. May, *Phys. Rev.*, Vol. 162, p. 510, 1967.
13. Strukov, B. A., M. Amin and V. A. Kopzik, *Phys. St. Sol.*, Vol. 27, p. 741, 1968.
14. Teaney, D. T., *Sol. St. Comm.*, Vol. 5, p. 207, 1967.
15. Grindlay, J., *Phys. Rev.*, Vol. 139, A 1603, 1965.

16. Amin, M. and B. A. Strukov, FTT, Vol. 10, p. 3158, 1968.
17. Strukov, B. A., M. Amin and A. S. Sonin, FTT, Vol. 9, p. 2421, 1967.
18. Reese, W. and L. F. May, Phys. Rev., Vol. 167, p. 504, 1968.
19. Kobeko, P. P. and I. G. Nelidov, Sow. Phys., Vol. 1, p. 382, 1932.
20. Rusterholz, A. A., Helv. Phys. Acta, Vol. 7, p. 643, 1934; Vol. 8, p. 39, 1935.
21. Hicks, J. F. G. and J. G. Hooley, J. Am. Chem. Soc., Vol. 60, p. 2994, 1938.
22. Wilson, A. J. C., Phys. Rev., Vol. 54, p. 1103, 1938.
23. Bantle, W., Helv. Phys. Acta, Vol. 15, p. 375, 1942.
24. Blattner, H., W. Kanzig and W. Merz, Helv. Phys. Acta, Vol. 22, p. 35, 1949.
25. Shirane, G. and A. Takeda, J. Phys. Soc. Japan, Vol. 7, p. 1, 1952.
26. Volger, J., Philips Res. Rep., Vol. 7, p. 21, 1952.
27. Todd, S. S. and R. E. Lorenson, J. Am. Chem. Soc., Vol. 74, p. 2043, 1952.
28. Shirane, G., H. Danner, A. Pavlovic and R. Pepinsky, Phys. Rev., Vol. 93, p. 672, 1954.
29. Triebwasser, S. and J. Halpern, Phys. Rev., Vol. 98, p. 1562, 1955.
30. Suemune, Y., J. Phys. Soc. Japan, Vol. 21, p. 802, 1966.
31. Suemune, Y., J. Phys. Soc. Japan, Vol. 22, p. 735, 1967.
32. Yoshida, J., S. Nomura and S. Sawada, J. Phys. Soc. Japan, Vol. 13, p. 1550, 1958.
33. Yoshida, J., J. Phys. Soc. Japan, Vol. 15, p. 2211, 1960.
34. Kodzherspirov, F. F., FTT, Vol. 3, p. 781, 1961.
35. Dimarova, Ye. N. and Yu. M. Poplavko, Izv. AN SSSR, ser. fiz., Vol. 29, p. 985, 1965.
36. Dimarova, Ye. N. and Yu. M. Poplavko, Izv. AN SSSR, ser. fiz., Vol. 31, p. 1842, 1967.
37. Suemune, Y., J. Phys. Soc. Japan, Vol. 20, p. 174, 1965.

38. Mante, A. J. and J. Volger, Phys. Lett., Vol. 24A, p. 139, 1967.
39. Jnoue, M., J. Phys. Soc. Japan, Vol. 25, p. 288, 1968.
40. Steigmeier, E. F., Phys. Rev., Vol. 168, p. 523, 1968.
41. Kobeko, P. P. and I. V. Kurchatov, Z. f. Phys., Vol. 66, p. 192, 1930.
42. Wieseman, G. G. and J. K. Kuebler, Phys. Rev., Vol. 131, p. 2023, 1963.
43. Strukov, B. A., Kristallografiya, Vol. 11, p. 892, 1966.
44. Strukov, B. A., Phys. St. Sol., Vol. 14, K 135, 1966.
45. Strukov, B. A., S. A. Taraskin and V. M. Varikash, FTT, Vol. 10, p. 1836, 1968.
46. Remoissenet, M. and L. Godefroy, Compt. rend., Vol. 266, p. 948, 1968.
47. Karchevskiy, A. I., FTT, Vol. 3, p. 3092, 1961.
48. Hegenbarth, E., Cryogenics, Vol. 1, p. 242, 1961; Phys. St. Sol., Vol. 2, p. 1544, 1962; Vol. 8, p. 59, 1965.
49. Kikuchi, A. and E. Sawaguchi, J. Phys. Soc. Japan, Vol. 19, p. 1497, 1964.

## CHAPTER 13. EFFECT OF ELECTRIC FIELD AND MECHANICAL STRESSES ON THE FERROELECTRIC PHASE TRANSITION

### §1. Effect of Electric Field

The effect of an electric field on the ferroelectric phase transition can be examined on the basis of thermodynamic theory [1-3]. We will assume that an electric field is applied on the ferroelectric axis and we will examine the equation  $\partial\Phi/\partial P = 0$ , which considering terms  $P^6$  in the expansion of the thermodynamic potential, has the form

$$E = 2\alpha P + 2\beta P^3 + \gamma P^5. \quad (13.1)$$

In the case of the second order phase transition only coefficient  $\alpha$  can be negative. Therefore, when  $E > 0$  there is only one positive solution for  $P$ . When  $E = \text{const}$ ,  $P$  is a continuous function of temperature and is a nonzero value at all temperatures (Figure 3.10a). Thus the result of the application of the electric is that there is no phase transition as such. The temperature dependence of permittivity, however, has, as before, a peak. As biasing field intensity increases, the peak decreases and is displaced toward higher temperatures. Wieder [4] demonstrated that the shift ( $\Delta T$ ) of the peak, according to thermodynamic theory, should obey the law

$$\Delta T = \frac{3}{4} \cdot \frac{\beta^{1/2}}{\alpha} E^{1/2}. \quad (13.2)$$

Investigations of colemanite [4] and triglycine sulfate (normal and deuterated) [5] showed that the experimental values of  $\Delta T$  agree satisfactorily with equation (13.2).

For the first order phase transition  $\beta < 0$ . In examining the dependence of polarization on the field it is convenient to introduce standard values of polarization ( $p$ ), electric field strength ( $e$ ) and temperature ( $t$ ), related linearly through the coefficients of the expansion of (3.12) with  $P$ ,  $E$  and  $T$ , respectively [2]. Equation (13.1) is written in new variables in the form [2]:

$$\epsilon = 2p^2 - 4p^3 + 2pt. \quad (13.3)$$

The theoretical dependences of polarization on field  $e$  for various temperatures  $t$  are given in Figure 13.1. Only those segments on the curves, where  $dp/de > 0$ , correspond to stable states. Therefore, when  $dp/de$  becomes negative an abrupt transition takes place on the vertical line into the stable state. The transition occurs at the points where

$$\frac{d\epsilon}{dp} = 2t - 6p^2 + 5p^3 = 0. \quad (13.4)$$

Equation (13.4) has two real roots for  $p^2$ , when

$$36p^2 - 40t > 0. \quad (13.5)$$

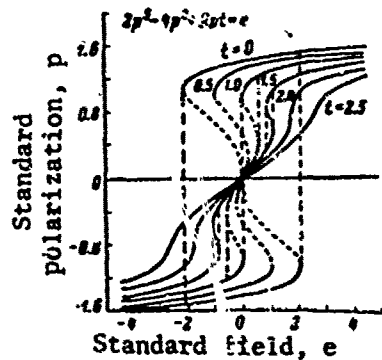


Figure 13.1. Dependence of standard polarization ( $p$ ) on standard electric field strength ( $e$ ) for several standard temperatures ( $t$ ) near the Curie point (Merz [2]).

If  $\alpha < 0$ , then one root is positive and the other is negative. If  $\alpha > 0$ , then both roots are positive. The temperature range above the Curie point ( $t > 1$  in Figure 13.1) corresponds to the latter case. As seen from the curves in Figure 13.1, in some interval of values  $t > 1$  an abrupt change in polarization should occur as field strength changes. When change is cyclic the field will be described as the so-called double hysteresis loops. An abrupt increase in polarization corresponds to a transition from the paraelectric to the ferroelectric state, induced by the electric field. The temperature dependence of polarization for  $E = \text{const}$  are illustrated in Figure 3.10b. The temperature above which the induced phase transition will not occur can be determined from condition

(13.5), since equation (13.4) will not have real roots. The displacement of the transition temperature with electric field strength is related to the size of the jump of polarization ( $\Delta P$ ) and change of entropy ( $\Delta S$ ) by an equation of the Clapeyron-Clausius type [1]:

$$\frac{\partial T_c}{\partial E} = -\frac{\Delta P}{\Delta S}. \quad (13.6)$$

The dependence of polarization on electric field strength is conveniently observed on an oscillograph scope with the aid of the same circuit used for observing dielectric hysteresis (see §1, Chapter 8). Such investigations were conducted by Merz [2], Cross [6], Drougard [7] on barium titanate crystals with the field applied in direction [100].

According to theory, directly above the Curie point in the temperature interval of approximately  $8^\circ$  the dependence of polarization on electric field strength has the form of a double hysteresis loop (Figure 13.2).

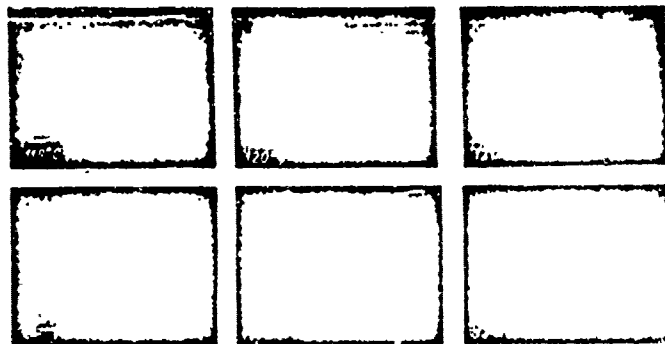


Figure 13.2. Double hysteresis loops observed on barium titanate monocrystals in some temperature range immediately above the Curie point. The electric field is applied in direction [100]. (According to Drougard and Huibregtse [8]).

The abrupt, field induced transition from the paraelectric state to the ferroelectric state can also be observed by investigating the pyroelectric effect by the dynamic method. Chynoweth [9] discovered that in some temperature range above the Curie point pyroelectric current, depending on the stationary field applied, first increases rapidly, and then drops abruptly, and slowly diminishes as the field continues to increase. The jump corresponds to transition to the ferroelectric state. At great distances from the Curie point the pyroelectric current peaks smoothly without abrupt changes. The observed dependence of pyroelectric current on electric field strength agrees with the theoretical dependence.

Polarization jumps lead to jumps in birefringence. Investigation of the electrooptic effect in the vicinity of the Curie point was done by Meyerhofer [10]. His dependences of  $\Delta n$  on the strength of the field, applied in directions [100] and [110], are shown in Figure 13.3. The phases, induced in this case, are tetragonal and rhombic, respectively. If the electric field is applied in direction [110], then near the Curie point there is a mixture of tetragonal and rhombic domains. At higher temperatures the induced phase is completely rhombic. There is less birefringence in this phase than in the tetragonal phase.

The ratio  $P^2/\Delta n$  is considerably greater in the induced rhombic phase than in the rhombic phase stable below  $5^\circ\text{C}$ . This shows that these phases are not identical. In certain crystals with the field applied in direction [110] Meyerhofer [10] observed a transition first into rhombic and then, in a stronger field, into a new phase with greater polarization on [110], but with less birefringence. What phase this was could not be established on the basis of electrical and optic measurements. In the presence of two

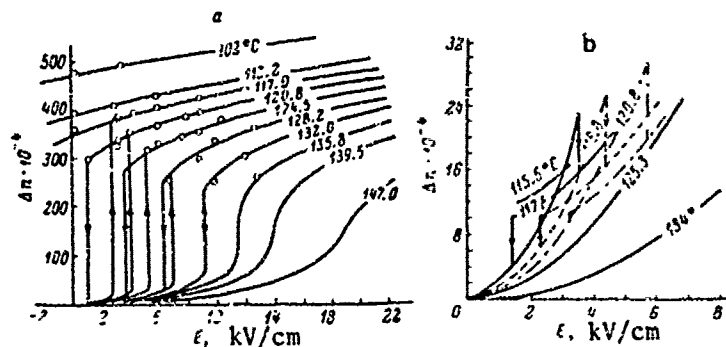


Figure 13.3. Dependence of birefringence of barium titanate crystal on electric field strength in vicinity of Curie point. a -- field applied in direction [100]; b -- field applied in direction [110]. (According to Meyerhofer [10]).

consecutive induced transitions the dependence of polarization on field strength has the form of the so-called quadrupole hysteresis loop (Figure 13.4a). In barium titanate crystals the transition to the induced phase occurs through the formation of nuclei of the new phase, i.e., the same as in the case of the absence of a field.

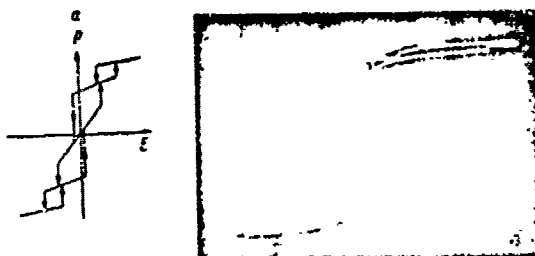


Figure 13.4. Hysteresis loops observed in barium titanate crystals at temperatures close to the points of phase transitions: a -- quadrupole hysteresis loop obtained in barium titanate crystal near Curie point. Electric field applied in direction [110] (Meyerhofer [10]); b -- triple hysteresis loop in barium titanate crystal in rhombic phase at temperature close to temperature of transition into tetragonal phase. Electric field applied in pseudo-cubic direction [100] (Dreugard and Huibregtse [8]).

An electric field also has an effect on the phase transition between two ferroelectric phases with different directions of spontaneous polarization. Thus, Huibregtse and Young [11], investigating the effect of an electric field on the transition from the tetragonal to the orthorhombic

phase, observed that a field in the direction [100] lowers the transition temperature. Thus, the range of the tetragonal phase is expanded. This is natural, since an external electric field on [100] favors the direction of polarization corresponding to the tetragonal phase. The dependence of polarization on the strength of an electric field applied in direction [100] at a temperature somewhat below the transition temperature (range of thermal hysteresis) has the form of a triple hysteresis loop (Figure 13.4b). This is related to the fact that the component of spontaneous polarization in direction [100] is smaller in the rhombic phase than in the tetragonal phase.

Triple hysteresis loops can be observed only at frequencies below 5 Hz. At higher frequencies the crystal is destroyed. Huibregtse and Young [11] showed that the presence of the triple hysteresis loop follows from thermodynamic theory. Comparison of thermodynamic theory with the results of dielectric measurements makes it possible to determine many coefficients in the expansion of the thermodynamic potential by degrees of polarization. If this expansion is written in the form

$$\Phi = \Phi_0 + A(P_x^2 + P_y^2 + P_z^2) + B(P_x^4 + P_y^4 + P_z^4) + D(P_x^2 P_y^2 + P_x^2 P_z^2 + P_y^2 P_z^2) + C(P_x^2 + P_y^2 + P_z^2) + G(P_x^2 P_y^2 + P_x^2 P_z^2 + \dots), \quad (13.7)$$

then coefficient A can be determined from Curie-Weiss law (9.1), B and C from measurements of the dielectric constant and spontaneous polarization in the tetragonal phase, and D and G from comparison of theoretical and experimental triple hysteresis loops [11]. These methods yielded the following coefficients in the expansion of thermodynamic potential (13.7) for barium titanate (according to Drougard and Huibregtse [8]):

Coefficient	Values (in esu)
A . . .	$3.7 \cdot 10^{-6} (T - T_0)$ , rAe $T_0 = 110^\circ \text{C}$
B . . .	$4.5 \cdot 10^{-15} (T - T_0)$ , rAe $T_0 = 175^\circ \text{C}$
C . . .	$9 \cdot 10^{-22}$
D . . .	$6 \cdot 10^{-13}$
G . . .	$4 \cdot 10^{-22}$

Coefficient B is a linear function of temperature. That the value of B for  $8^\circ \text{C}$  lies on the same straight line with values obtained from measurements of dielectric nonlinearity in the paraelectric phase [12] is a remarkable fact (see §2, Chapter 9).

## §2. Effect of Mechanical Stresses

All mechanical stress tensor components can, in principle, have an effect on the ferroelectric phase transition. In practice, however, investigations with large stresses, yielding a substantial effect, can be done only with hydrostatic compression. In this section, therefore, we will examine almost exclusively the action of such a type of pressure.

In the case of the first order phase transition the change of transition temperature with pressure (p) is determined by the Clapeyron-Clausius two-phase equilibrium equation:

$$\frac{dT_c}{dp} = T_c \frac{\Delta V}{\Delta Q}, \quad (13.8)$$

where  $\Delta V$  is the change in volume during phase transition and  $\Delta Q$  is latent heat of transition.

For the second order phase transition displacement of the Curie point with pressure can be determined from the Ehrenfest relation:

$$\frac{dT_c}{dp} = \frac{\alpha - \alpha'}{c_p - c'_p} \cdot \frac{T_c}{\rho}, \quad (13.9)$$

where  $\alpha$  and  $\alpha'$  are the coefficients of volumetric expansion of the top and bottom transitions, respectively,  $c_p$  and  $c'_p$  are the corresponding thermal capacities at constant pressure and  $\rho$  is density. Thermodynamic investigation of the effect of hydrostatic pressure on the second order ferroelectric phase transition in the centrosymmetric nonpolar phase was conducted by Kholodenko and Shirobokov [13], Smolenskiy and Pasynkov [14], Devonshire [1].

For  $dT_c/dp$  the following expression was obtained:

$$\frac{dT_c}{dp} = - \frac{\beta_{1i} + \beta_{2i} + \beta_{3i}}{\frac{\beta_{ii}}{T_c}}, \quad (13.10)$$

where it is assumed that spontaneous polarization occurs on the  $i$ -th axis;  $(\beta_{1i} + \beta_{2i} + \beta_{3i})$  is the same as the coefficient of volumetric electrostriction. We will note that it is easy to derive (13.8) from (13.10) by multiplying the numerator and the denominator of the right hand side by  $T_c$  and  $P_s$  at the transition point and by using (12.2).

Equations (13.9) and (13.10) show that if in the presence of spontaneous polarization the volume of the ferroelectric increases, the Curie point decreases as pressure increases and conversely.

The effect of pressure on the ferroelectric phase transition has been most thoroughly analyzed for barium titanate. These investigations were done by Merz [15], Klimovski [16-19], Minomura, et al [20], Leonidova and Volk [21], Samara [22], Polandov, et al [23]. The data of several researchers are presented in Figure 13.5. Most results coincide quite well. The value of  $dT_c/dp$  lies within the range  $(4.8-6.3) \cdot 10^{-3} \text{ deg} \cdot \text{atm}^{-1}$ , which is close to  $7 \cdot 10^{-3} \text{ deg} \cdot \text{atm}^{-1}$ , computed according to (13.8). Reduction of the transition temperature leads to a reduction of spontaneous polarization at room temperature and of tetragonality of the elementary nucleus [24].

The coefficient  $\alpha'_0$  in the expansion of the thermodynamic potential and, consequently, Curie constant  $C$  depend little on pressure. The

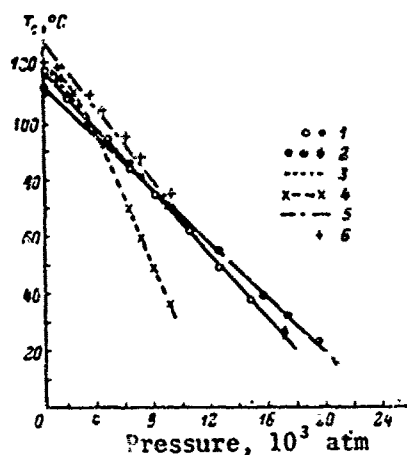
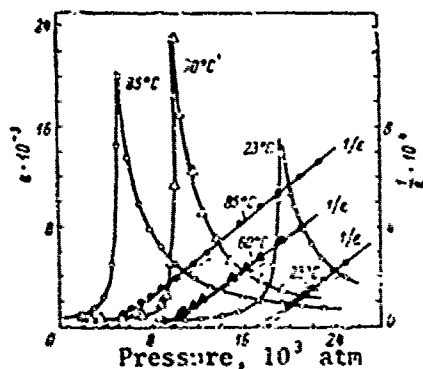


Figure 13.5. Dependence of Curie point of barium titanate on hydrostatic pressure according to the data of several researchers: 1 and 2 -- Samara [22] (1 -- monocrystals; 2 -- ceramics); 3 -- Merz [15]; 4 -- Klimovski [17]; 5 -- Minomura, et al [20]; 6 -- Leonidova and Volk [21].

point with increasing pressure. The reasons for this are not known. How the low-temperature phase transitions will behave when pressure is increased can be predicted on the basis of Clapeyron-Clausius equation (13.8). As pressure increases, the temperature of transition from the tetragonal phase to rhombic should decrease with the coefficient  $2.6 \cdot 10^{-3} \text{ deg} \cdot \text{atm}^{-1}$ , and the temperature of transition from the rhombic phase to rhombohedral should increase with the coefficient  $2 \cdot 10^{-3} \text{ deg} \cdot \text{atm}^{-1}$ . Only the first transition has been investigated experimentally, for which Minomura, et al [20] found a linear decrease of the transition temperature with the coefficient  $2.8 \cdot 10^{-3} \text{ deg} \cdot \text{atm}^{-1}$ .



Curie-Weiss temperature  $\theta$  drops with pressure, and more slowly than  $T_c$  in monocrystals [22, 23]. This indicates that the phase transition by its nature is close to the critical point. Accordingly the permittivity at the Curie point increases [22], and the jump in polarization diminishes [23]. In the paraelectric phase the dependence of permittivity on pressure obeys some form of the Curie-Weiss law [22] (Figure 13.6):

$$\epsilon = \frac{C^*}{p - p_0} \quad (13.11)$$

where  $C^* \sim (1.8-2.9) \cdot 10^6 \text{ atm}$ , and  $p_0$  varies from crystal to crystal. Values from  $1.8 \cdot 10^3$  to  $5 \cdot 10^3 \text{ atm}$  have been determined. In contrast to monocrystals, ceramic specimens of barium titanate display a decreasing value of permittivity at the Curie

Figure 13.6. Dependence of permittivity of barium titanate monocrystal on hydrostatic pressure for three temperatures. Measurements made on axis c. (According to Samara [22]).

The effect of hydrostatic pressure on the dielectric properties of certain polycrystalline solid solutions based on barium titanate ( $\text{Ba, Sr})\text{TiO}_3$  [25],  $\text{Ba}(\text{Ti, Sn})\text{O}_3$  [26, 27] and  $\text{Ba}(\text{Ti, Zr})\text{O}_3$  [28, 29], has been investigated in several works. The temperature of the peak permittivity decreases with increasing pressure in all these systems, and  $\epsilon$  at the peak, as in polycrystalline barium titanate, decreases. The decrease is quite substantial in the case of the last two systems.

In contrast to hydrostatic pressure, two-dimensional [30, 31] and unidimensional [32-35] mechanical compression of monocrystals and ceramics of barium titanate, causing distortion of the elementary nucleus, increase the temperature of the ferroelectric phase transition. As shown by Sinyakov, et al [35], unidimensional pressure has an effect on the field induced (in direction [100]) transition from the paraelectric to the ferroelectric state. If the field and the pressure coincide in direction, then the field of transition increases with pressure, and if the pressure is perpendicular to the field, then it decreases. Uniaxial pressure also changes the temperatures of transition from the tetragonal to the rhombic and from the rhombic to rhombohedral phases. As pressure increases, the temperature of the first transition increases, and that of the second decreases [35], i.e., the temperature range in which the rhombic phase is stable is expanded.

The effect of hydrostatic pressure on the ferroelectric phase transition in triglycine sulfate was investigated by Jona and Shirane [36], Zheludev, et al [37], Leonidova, et al [38-40]. The coefficient of volumetric electrostriction in triglycine sulfate is negative and in accordance with (13.10) the transition temperature increases with pressure. This increase is linear up to  $3 \cdot 10^3$  atm with the coefficient  $2.6 \cdot 10^3 \text{ deg} \cdot \text{atm}^{-1}$  [36, 38]. If the coefficients  $\alpha_0'$  and  $\beta$  in the expansion of thermodynamic potential (3.7) are independent of pressure, then  $P_s^2$  should be a linear function of temperature and pressure. Experimental results for triglycine sulfate in the range of temperatures close to the Curie point show that  $P_s^2$  is actually a linear function of  $T$  and  $p$  [36]. The linear dependence of  $P_s^2$  on temperature at various pressures was also observed in the case of triglycine fluorberyllate [41].

It was reported [42] that at pressures up to  $23 \cdot 10^3$  atm two phase transitions occur in triglycine sulfate. The nature of the new phases is presently unknown. Perhaps the behavior of triglycine sulfate at such pressures is analogous to that of triglycine selenate. Polandov, et al [43] noted that triglycine selenate crystals under sufficiently high pressures change into a nonferroelectric phase, different from the paraelectric phase, stable at atmospheric pressure.

The effect of hydrostatic pressure on the Curie temperature of

$\text{KH}_2\text{PO}_4$  and  $\text{KD}_2\text{PO}_4$  was investigated by Uneyashi, et al [44]. The Curie point decreases with increasing pressure in both compounds with the coefficient  $(-4.52 \pm 0.06) \cdot 10^{-3} \text{ deg} \cdot \text{atm}^{-1}$  for  $\text{KH}_2\text{PO}_4$  and  $(-2.63 \pm 0.05) \cdot 10^{-3} \text{ deg} \cdot \text{atm}^{-1}$  for  $\text{KD}_2\text{PO}_4$ . In the opinion of the authors [44], such dependence of the phase transition temperature on pressure is substantiation of the tunnel model of these ferroelectrics. According to this model the transition temperature is determined by the distance between two potential minimas of the hydrogen bond and correlation energy of the four protons (or deuterons) surrounding each  $\text{PO}_4$ -group [45]. It can be expected that both these factors decrease with pressure. Therefore the Curie point decreases as the pressure increases. The probability of tunneling is greater for protons than for a deuteron, hence the effect of pressure is greater in the case of  $\text{KH}_2\text{PO}_4$ . Novakovic [46] established that the tunnel model agrees not only qualitatively, but also quantitatively with experimental results on the effect of pressure on the transition temperature.

Seignette's salt crystal under hydrostatic pressure were first investigated by Yeremeyev [47] who established that when pressure is increased the upper Curie point is displaced toward higher temperatures. Then Bancroft [48] performed detailed analyses up to a pressure of  $10 \cdot 10^3 \text{ atm}$  and Samara [49] up to  $20 \cdot 10^3 \text{ atm}$ . According to the data of these authors, the top Curie point increases linearly with pressure with the coefficient  $11 \cdot 10^{-3} \text{ deg} \cdot \text{atm}^{-1}$ . This dependence can be measured only up to  $5 \cdot 10^3 \text{ atm}$ , since at higher pressures the Curie point becomes higher than the decomposition temperature. The lower Curie point also increases with increasing pressure up to  $10 \cdot 10^3 \text{ atm}$  with the coefficient  $3.8 \cdot 10^{-3} \text{ deg} \cdot \text{atm}^{-1}$ , and from  $10 \cdot 10^3$  to  $20 \cdot 10^3 \text{ atm}$  with the coefficient  $4.4 \cdot 10^{-3} \text{ deg} \cdot \text{atm}^{-1}$ . Since the bottom Curie point increases with pressure more slowly than the top, the temperature range in which spontaneous polarization exists is expanded, but the maximum spontaneous polarization remains practically unchanged [49]. The Curie constants  $C$  in the Curie-Weiss law (9.1) for the top and bottom Curie points increase approximately 1% per 1 atm increase of pressure. The isotherms for  $\epsilon_a$ , as in the case of barium titanate, obey a law of the type (13.11) in the paraelectric phase. Spontaneous polarization increases and decreases with pressure near the phase transitions in accordance with thermodynamic theory, and  $P_s^2$  is a linear function of pressure.

#### BIBLIOGRAPHY

1. Devonshire, A. F., *Advances in Phys.*, Vol. 3, p. 86, 1954.
2. Merz, W. J., *Phys. Rev.*, Vol. 91, p. 513, 1953.
3. Kholodenko, L. P., *Kristallografiya (Crystallography)*, Vol. 1, p. 393, 1956.
4. Wieder, H. H., *J. Appl. Phys.*, Vol. 30, p. 1010, 1959.

5. Sil'vestrova, I. M., Kristallografiya, Vol. 6, p. 582, 1961.
6. Cross, L. E., Phil. Mag., Vol. 44, p. 1161, 1953.
7. Drougard, M. E., J. Appl. Phys., Vol. 27, p. 1559, 1956.
8. Drougard, M. E. and E. J. Huibregtse, IBM J. Res. Developm., Vol. 1, p. 318, 1957.
9. Chynoweth, A. G., J. Appl. Phys., Vol. 27, p. 78, 1956.
10. Meyerhofer, D., Phys. Rev., Vol. 112, p. 413, 1958.
11. Huibregtse, E. J. and D. R. Young, Phys. Rev., Vol. 103, p. 1705, 1956.
12. Drougard, M. E., R. Landauer and D. R. Young, Phys. Rev., Vol. 98, p. 1010, 1955.
13. Kholodenko, L. P. and M. Ya. Shirobokov, ZhETF [Zhurnal eksperimental'noy i teoreticheskoy fiziki; Journal of Experimental and Theoretical Physics], Vol. 21, p. 1250, 1951.
14. Smolenskiy, G. A. and R. Ye. Pasyukov, ZhETF, Vol. 24, p. 69, 1953.
15. Merz, W. J., Phys. Rev., Vol. 78, p. 52, 1950.
16. Klimovski, J. and J. Pietrzak, Proc. Phys. Soc., Vol. 75, p. 456, 1960.
17. Klimovski, J. and J. Pietrzak, Acta Phys. Polon., Vol. 19, p. 369, 1960.
18. Klimovski, J., Phys. St. Soi., Vol. 2, p. 456, 1962.
19. Klimovski, J., Bull. Soc. Amis. siet. lettres, Posnana, B, No. 17, p. 59, 1964.
20. Minomura, S., T. Kawakubo, T. Nakagawa and S. Sawada, Japan J. Appl. Phys., Vol. 3, p. 562, 1964.
21. Leonidova, G. G. and T. R. Volk, FTT [Fizika tverdogo tela; Solid State Physics], Vol. 7, p. 3344, 1965.
22. Samara, G. A., Phys. Rev., Vol. 151, p. 378, 1966.
23. Poiandov, I. N., B. A. Strukov and V. P. Mylov, FTT, Vol. 9, p. 1477, 1967.
24. Kabalkina, S. S., B. M. Shulenin and L. F. Vereshchagin, DAN SSSR (Reports of USSR Academy of Sciences), Vol. 144, p. 1019, 1962.
25. Shirane, G. and K. Sato, J. Phys. Soc. Japan, Vol. 6, p. 20, 1951.

26. Polandov, I. N., DAN SSSR, Vol. 150, p. 779, 1963.
27. Polandov, I. N. and V. P. Mylov, FTT, Vol. 9, p. 2319, 1967.
28. Polandov, I. N. and V. P. Mylov, FTT, Vol. 6, p. 499, 1964.
29. Polandov, I. N., FTT, Vol. 7, p. 1874, 1965.
30. Forsbergh, P. W., Phys. Rev., Vol. 93, p. 686, 1954.
31. Jaffe, H., D. Berlincourt and J. M. McKee, Phys. Rev., Vol. 105, p. 57, 1957.
32. Takagi, Y., E. Sawaguchi and T. Akioka, J. Phys. Soc. Japan, Vol. 3, p. 270, 1948.
33. Sinyakov, Ye. V. and I. A. Izhak, DAN SSSR, Vol. 100, p. 243, 1955.
34. Sinyakov, Ye. V., Ye. F. Dudnik and S. A. Flerova, FTT, Vol. 8, p. 2848, 1966.
35. Sinyakov, Ye. V., S. A. Flerova and O. A. Kubyshkin, Izv. AN SSSR, ser. fiz. (News of USSR Academy of Sciences, Physics Series), Vol. 31, p. 1768, 1967.
36. Jona, F. and G. Shirane, Phys. Rev., Vol. 117, p. 139, 1960.
37. Zheludev, I. S., N. A. Tikhomirova and V. M. Fridkin, Kristallografiya, Vol. 7, p. 795, 1962.
38. Leonidova, G. G., I. N. Polandov and I. P. Galentovskaya, FTT, Vol. 4, p. 3337, 1962.
39. Leonidova, G. G., N. P. Netesova and T. R. Volk, FTT, Vol. 9, p. 593, 1967.
40. Leonidova, G. G. and N. P. Netesova, FTT, Vol. 10, p. 2526, 1968.
41. Mylov, V. P., I. N. Polandov and B. A. Strukov, FTT, Vol. 9, p. 3012, 1967.
42. Suchan, H. L. and H. G. Drickamer, J. Chem. Phys., Vol. 31, p. 856, 1959.
43. Polandov, I. N., V. P. Mylov, B. A. Strukov and V. M. Varikash, FTT, Vol. 10, p. 1377, 1968.
44. Umebayashi, H., B. C. Frazer and G. Shirane, Sol. St. Comm., Vol. 5, p. 591, 1967.

45. Imry, Y., I. Pelah and E. Wiener, J. Chem. Phys., Vol. 43, p. 2332, 1965.
46. Novakovic, L., J. Phys. Chem. Sol., Vol. 29, p. 963, 1968.
47. Kurchatov, I. V., Segnetoelektriki (Ferroelectrics), Gostekhizdat [State Publishing House of Technical and Theoretical Literature], Moscow-Leningrad, 1933.
48. Bancroft, D., Phys. Rev., Vol. 53, p. 587, 1938.
49. Samara, G. A., J. Phys. Chem. Sol., Vol. 26, p. 121, 1965.

## CHAPTER 14. RADIOSPECTROSCOPIC ANALYSES AND INVESTIGATIONS OF THE MESSBAUER EFFECT IN FERROELECTRICS

Radiospectroscopic methods yield valuable information concerning the symmetry of the crystal lattice, local magnetic and electric fields of the lattice, character of the chemical bond, lattice dynamics, etc. Therefore these models are used extensively in the study of ferroelectrics.

Analyses of the spectra of the resonance absorption of gamma-rays (the Messbauer effect) yield information physically similar to the information extracted by radiospectroscopic methods. In this chapter, therefore, we will examine also the results of studies of the Messbauer effect in ferroelectrics.

Analyses of the electroparamagnetic resonance (EPR) and nuclear magnetic resonance (NMR) are usually done in the presence of an external stationary magnetic field. In NMR it also largely determines the resonance frequency  $\omega$ . In the simplest case of free spin:  $\omega = \gamma H_0$  ( $H_0$  is the external magnetic field,  $\gamma$  is the gyromagnetic ratio). The EPR spectrum is determined both by the external magnetic field and by the internal crystal fields of the lattice. Analyses of nuclear quadrupole resonance do not require the application of a magnetic field, and the spectrum is determined entirely by intracrystalline fields.

### §1. Electron Paramagnetic Resonance

In the EPR method the magnetic dipole moments of electrons of the shell of paramagnetic ions are used as probes that yield information concerning the crystal lattice. This method is extremely sensitive to details of the structure and changes in it. It yields information concerning the character of phase transitions and related changes in symmetry, motion of ions and reorientation of dipole groups, etc. [1].

EPR spectra are interpreted with the aid of the concepts of static intracrystalline field, acting on the electrons. The theory of point charges and dipoles and perturbation theory are usually employed here for comparison of theory with experiment. The phenomenological method of the

so-called spin Hamiltonian, which is the energy operator, is used most frequently for describing the EPR spectrum. The Hamiltonian usually consists of a Zeemann term, describing the separation of energy levels in a magnetic field, and terms that describe the interaction of the electron spin of an ion with the intracrystalline field acting upon it. The EPR spectrum can be described if the parameters entering in the Hamiltonian are known.

The fine structure of EPR spectra is determined basically by the local symmetry of the crystalline field at the point where the paramagnetic ion is located. One or another form of spin Hamiltonian is used for describing the spectrum in accordance with the character of symmetry of the surroundings, since the spin Hamiltonian should be invariant in relation to all elements of symmetry of a given point group.

For example, for the case of an ion in the S-state with spin  $S = 5/2$  and tetragonal symmetry (groups  $C_4$ ,  $S_4$ ,  $C_{4v}$ ,  $C_{4h}$ ,  $D_4$ ,  $D_{2d}$ , and  $D_{4h}$ ), the spin Hamiltonian can be represented in the form:

$$\mathcal{H} = g_1 \beta H_x S_x + g_2 \beta (H_y S_y + H_z S_z) + B_2^0 O_2^0 + B_4^0 O_4^0 + B_4^2 O_4^2; \quad (14.1)$$

for trigonal symmetry (groups  $C_3$ ,  $C_{3v}$ ,  $D_3$ ,  $D_{3d}$ ,  $S_6$ )

$$\mathcal{H} = g_1 \beta H_x S_x + g_2 \beta (H_y S_y + H_z S_z) + B_2^0 O_2^0 + B_4^0 O_4^0 + B_4^2 O_4^2; \quad (14.2)$$

for rhombic and other cases of symmetry, lower than axial

$$\mathcal{H} = g_x \beta H_x S_x + g_y \beta H_y S_y + g_z \beta H_z S_z + B_2^0 O_2^0 + B_2^2 O_2^2 + B_4^0 O_4^0 + B_4^2 O_4^2 + B_4^4 O_4^4. \quad (14.3)$$

Here the following symbols are used:  $\mathcal{H}$  -- energy operator (spin Hamiltonian); first two terms in equations (14.1) and (14.2) and the first three terms in equation (14.3) describe the Zeemann separation of the basic state in magnetic field H with consideration of the anisotropy of the g-factor;  $\beta$  is the Bohr magneton; S is the electron spin operator of the ion. The other terms describe the interaction of ion spin with the crystalline field.

The indices  $B_i^k$  denote the Hamiltonian constants, determination of which is the purpose of the experiment. The symbols  $O_i^k$  denote the operators of the spin variables of the corresponding orders, specifically:

$$O_2^0 = 3S_z^2 - S(S+1),$$

$$O_2^2 = \frac{1}{2}(S_x^2 - S_y^2),$$

$$O_4^0 = 35S_z^4 - [30S(S+1) - 25]S_z^2 - 6S(S+1) + 35^2(S+1)^2,$$

$$O_4^2 = \frac{1}{4}([7S_z^2 - S(S+1) - 5](S_x^2 + S_y^2) + (S_x^2 + S_y^2)[7S_z^2 - S(S+1) - 5]),$$

$$O_4^4 = \frac{1}{8}(S_x(S_x^2 + S_y^2) + (S_x^2 + S_y^2)S_x),$$

$$O_4^4 = \frac{1}{8}(S_x^4 + S_y^4).$$

where

$$S_x = S_y \pm iS_z$$

If the spin of the paramagnetic ion differs from 5/2, then the number of terms in the spin-Hamiltonian may change. For  $S = 7/2$ , for instance, operators of the 6th order should be taken into account. In the case of tetragonal symmetry terms  $B_6^0 O_6^0 + B_6^4 O_6^4$  should be added to Hamiltonian (14.1), where

$$O_6^0 = 231S_x^2 - 105[3S(S+1) - 7]S_x^4 + [105S^2(S+1)^2 - 525S(S+1) + 294]S_x^6 - \\ - 5S^2(S+1)^2 + 40S^2(S+1)^2 - 60S(S+1), \\ O_6^4 = \frac{1}{4} \{ [11S_x^2 - S(S+1) - 38] (S_x^4 + S_x^2) + (S_x^4 + S_x^2) [11S_x^2 - S(S+1) - 38] \}.$$

In addition to the examined terms, the Hamiltonian should include those that describe the superfine interaction between spins of nucleus I and electron shell S of the paramagnetic ion. These terms, which should be added to (14.1)-(14.3), have the form:

$$AS_x^2 I_x + B(S_x^2 I_x + S_y^2 I_y) \quad (14.4)$$

for axial symmetry and

$$AS_x I_x + BS_x I_x + CS_y I_y \quad (14.5)$$

for rhombic symmetry. To determine the character of symmetry of the surroundings of a paramagnetic ion it is necessary to analyze the angular dependence of the EPR spectrum. The spin-Hamiltonian constants are found from data concerning the positions of the EPR lines at certain angles between the axes of the crystal and external magnetic field (see, for instance, [1-3] on general EPR problems). Such an EPR dependence in lithium niobate is given by way of example of the angular dependence of the EPR spectrum in Figure 14.1 according to data [4]. The five observed lines per-

tain to transitions between states with spin projections:  $\frac{5}{2} \leftrightarrow \frac{3}{2}$ ,  $\frac{3}{2} \leftrightarrow \frac{1}{2}$ ,

$\frac{1}{2} \leftrightarrow -\frac{1}{2}$ ,  $-\frac{1}{2} \leftrightarrow -\frac{3}{2}$  and  $-\frac{3}{2} \leftrightarrow -\frac{5}{2}$ . The spectrum is described by the following

Hamiltonian parameters for the case of the trigonal symmetry which lithium niobate possesses (see expressions (14.2) and (14.4)):  $c$   
 $= 3B_2^0 = 760$  e,  $b_4^0 = 60B_4^0 = -9$  e,  $A = B = 87 \pm 7$  e. It is assumed that  $Mn^{2+}$  ions replace  $Nb^{5+}$  ions.

EPR investigations are conducted in ferroelectrics on impurities of certain paramagnetic ions found in the crystal lattice (the impurity concentration is usually a fraction of a percent) just like analyses of

paramagnetic defects of the crystal lattice, occurring, for instance, during irradiation of ferroelectrics, and also during reduction of a number of oxygen-containing ferroelectrics.

Ions with a half-filled d- or f-shell, in the S-state are most often used as the paramagnetic impurity, since the electron resonance spectra of these ions can be detected even at high temperatures by virtue of the weak interaction of their electron shells with the crystal lattice and, consequently, rather long time of spin-lattice relaxation and relatively narrow line width. These ions are most often  $\text{Fe}^{+++}$  or  $\text{Mn}^{++}$ , the basic state of which is  ${}^6S_{5/2}$ , or  $\text{Gd}^{+++}$  or  $\text{Eu}^{++}$  ions in the  ${}^8S_{7/2}$  state.

The EPR has been analyzed most thoroughly in ferroelectrics with the perovskite structure. We will illustrate, therefore, the capability of the EPR method by way of example of barium titanate. Hornig, et al [5] first observed the EPR spectrum in barium titanate crystals. It was found that the spectrum is caused by impurity ions  $\text{Fe}^{+++}$  in the basic state  ${}^6S_{5/2}$ , substituting  $\text{Ti}^{++++}$  ions. The EPR in the tetragonal and cubic phases on  $\text{Fe}^{+++}$  was investigated in [5, 6].

The following form of Hamiltonian was used in [5] for describing the EPR in the tetragonal phase:

$$\mathcal{H} = g\beta HS + DS_z^2 + aS_x^2 + b(S_x^2 + S_y^2). \quad (14.6)$$

The parameter D is the axial field parameter. In the cubic phase  $a = b$ ,  $D = 0$ .

It was shown [5, 6] that the crystalline field in the positions occupied by  $\text{Fe}^{+++}$  ions possesses axial symmetry and the z axis of the axial field coincides with the tetragonal axis of the crystal.

Thus the symmetry of the immediate surroundings of  $\text{Fe}^{+++}$  ions and, consequently, presumably of  $\text{Ti}^{++++}$  ions, coincides with the tetragonal symmetry of the lattice. Anisotropy of the g-factor was not noted.

The spin Hamiltonian parameters for  $\text{Fe}^{+++}$  according to [5], in the cubic phase (+160°C) are:  $g = 2.0036 \pm 0.002$ ,  $a = 0.0102 \pm 0.001 \text{ cm}^{-1}$ ,  $D = 0$ ; in the tetragonal phase (+27°C):  $g = 2.0036 \pm 0.002$ ;  $a = 0.0091 \pm 0.002$ ,  $D = 0.0929 \text{ cm}^{-1}$ .

The EPR spectrum on  $\text{Fe}^{+++}$  in the rhombic and rhombohedral phases of barium titanate is investigated in [7]. It turned out in the rhombic phase that the axial axis is perpendicular to spontaneous polarization.

The EPR spectrum of barium titanate crystals doped with  $\text{Gd}^{+++}$  ions was investigated [8, 9].  $\text{Gd}^{+++}$  ions replace chiefly  $\text{Ba}^{++}$  ions in the lattice, and therefore, naturally, the crystalline field in the tetragonal

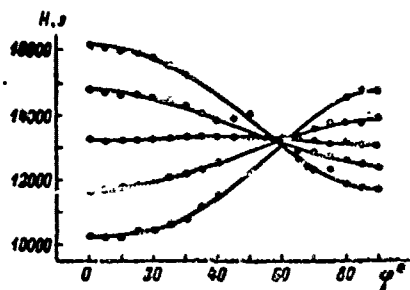


Figure 14.1. Angular dependence of EPR spectrum of  $Mn^{2+}$  in  $LiNbO_3$  at room temperature ( $\lambda \approx 8$  mm) [4].  $\phi$  -- angle between trigonal axis and external magnetic field  $H$ .

phase, acting on  $Gd^{3+}$ , possesses axial symmetry and the axial axis coincides with the tetragonal axis  $c$ . It should be pointed out, however, that in addition to the lines of  $Gd^{3+}$  in the positions of  $Ba^{2+}$ , there is also a cubic spectrum, which in [9] is ascribed to  $Gd^{3+}$  in the positions of  $Ti^{4+}$ , since the larger  $Gd^{3+}$  ions, extending into the octahedron, should move oxygen ions apart, and therefore the axial component of the field may vanish.

Analyses of EPR on  $Mn^{2+}$  ions were done in [10-12]. The crystalline field in the tetragonal phase, acting on  $Mn^{2+}$ , has axial symmetry. It is proposed [12] that  $Mn^{2+}$  ions replace  $Ba^{2+}$  faster than  $Ti^{4+}$ , but this can hardly be considered conclusively proved.

Many works contain an analysis of the temperature dependence of the EPR spectrum [6-8]. Shown in Figure 14.2, for example, is the temperature dependence of the resonance magnetic fields of  $BaTiO_3$ , doped with  $Gd^{3+}$ , in the tetragonal phase [18]. The greatest temperature dependence is observed for the axial field  $D$  or  $b_{2.0}$ .

Of great importance are attempts to connect the spin Hamiltonian parameters with the coefficients of the crystalline field potential, which can be represented, as we know, in the form of expansion in terms of spherical harmonics:

$$V_{cr} = A_2^0 Y_2^0 + A_4^0 \left[ Y_4^0 + \left(\frac{5}{14}\right)^{1/2} (Y_4^4 + Y_4^{-4}) \right] + \dots \quad (14.7)$$

The first term describes the axial field and is denoted through  $V_{ax}$ , and the second term describes the cubic field and is denoted through  $V_{cu}$ .

The problem of determining the amount of separation of the basic S-state under the influence of the crystalline field is quite complex. The S-state should be separated neither by the crystalline field nor by spin-orbital interaction, and the separation observed in tests is evidence of the need to take into account the admixture of various perturbed states. The problem of separation of the  ${}^6S_{5/2}$ -state was first examined by

Van Vleck and Penney [13]. The problem was also discussed later [14-17]. Various schemes of perturbation of the basic state of  $Gd^{4f7}$  have been considered [18].

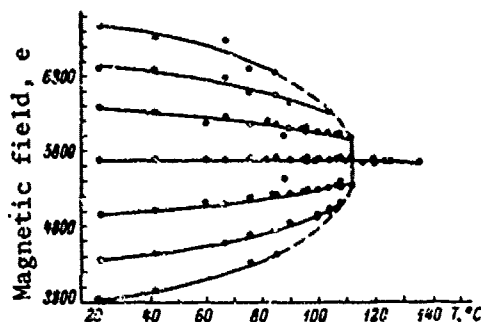


Figure 14.2. Temperature dependence of resonance magnetic fields in tetragonal phase of  $BaTiO_3$  doped with  $Gd^{4f7}$ . (According to Rimai and De Mars [8]).

The contributions of the various mechanisms of axial separation are proportional either to the first or second power of the axial potential of the crystalline field. According to [15]

$$D = \alpha V_{ax} + \beta V_{ax}^2 \quad (14.8)$$

Calculation on the basis of a model of point charges and dipoles [8] shows that the change of axial potential  $V_{ax}$  in position  $Ba^{2+}$  or  $Ti^{4+}$  on transition to the tetragonal phase depends in the case of the barium titanate lattice on distortion of the cubic lattice  $\delta a/a$ , where  $a$  is the lattice constant, and also on

terms of the type  $(\delta z_i/a)^2$ , where  $\delta z_i$  is displacement of "i" type ions from positions in the cubic phase. Here the amount of deformation  $\delta a/a$  of the lattice is proportional to the square spontaneous polarization, since the deformation of the lattice in barium titanate is by its nature the result of electrostriction (barium titanate lacks the piezoelectric effect in the paraelectric phase). The terms  $(\delta z_i/a)^2$  are also proportional to  $P_s^2$ .

An experiment for tetragonal barium titanate yielded a linear dependence between axial field parameter  $D$  or  $b_{2,0}$  and square spontaneous polarization, and also  $\delta a/a$  (Figure 14.3) which, apparently, testifies to the small contribution of the quadratic term of the axial potential to axial field parameter  $D$  or  $b_{2,0}$  (see equation (14.8)) (the symbol  $D$  is usually employed in the Hamiltonian for  $Fe^{4f7}$ , and  $b_{2,0}$  for  $Gd^{4f7}$ ). In the case at hand, consequently, axial parameter ( $D$  or  $b_{2,0}$ ) is proportional to the electric field gradient, since the field gradient is proportional to the coefficient of the axial crystalline field potential  $A_2^0$  (see equation (14.7)).

Quadrupole separation in several compounds was measured on  $Fe^{57}$  [16] with the aid of the Messbauer effect and the field gradient obtained from separation was compared with the axial field parameter  $D$  known from EPR analyses. In other words, an attempt was made to measure experimentally the relationship between  $D$  and  $V_{ax}$  in several compounds. The great scattering of points, however, hardly permits the reaching of any general conclusions concerning the validity of present theories.

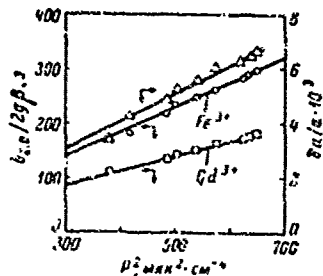


Figure 14.3. Dependence of axial field parameter  $b_{2,0}/2g\beta$  and also of  $\delta a/a$  on  $P_s^2$  in  $\text{BaTiO}_3$  doped with  $\text{Gd}^{+++}$  and  $\text{Fe}^{+++}$ . (According to Rimai and De Mars [8]). a -- cubic lattice parameter,  $P_s$  -- spontaneous polarization.

Another interesting direction of the EPR analyses of ferroelectrics is investigation of crystal lattice defects. Many attempts have been made to analyze crystal lattice defects of barium titanate by means of EPR. EPR signals in reduced barium titanate containing certain impurities, ascribed to F-centers (negative ion vacancies of the crystal lattice, capturing one electron), have been detected in a number of works [21-23]. No signals corresponding to single-charge vacancies were observed, however in [24-26]. Therefore the question of the existence of such vacancies in barium titanate remains unanswered.

It has also been shown through EPR analyses that finely dispersed barium titanate powder with granularity reduced to  $1,000 \text{ \AA}$  does not show a change in the intracrystalline field, i.e., spontaneous polarization is not reduced under these conditions [27].

EPR analyses are less developed in ferroelectrics with lower symmetry than in the case of perovskites. This is apparently the result of the difficulty in deciphering the spectra. Development of analyses of perovskites was also facilitated by the ability to observe the clearly distinct temperature dependence of separation after eliminating degeneration as the result of phase transition from the cubic phase to a phase with lower symmetry, making it possible to determine small deviations in cubic symmetry. In the case, however, of phase transition between phases with lower symmetry, there is much less change in separation.

The free radicals that appear as a result of irradiation in many ferroelectrics with lower symmetry have been analyzed with the aid of EPR.

An attempt was made [19] to correlate theoretically the temperature dependence of separation of the crystalline field in  $\text{SrTiO}_3$  on  $\text{Gd}^{+++}$  with the presence of the "soft" ferroactive mode, which, according to [19], should apparently contribute to the temperature dependence of parameter  $b_{4,0}$  ( $b_{4,0} = 60B_4^0$ ) (see equations (14.1)-(14.3)). EPR analyses on  $\text{Gd}^{+++}$  in  $\text{KTaO}_3$  [20], however, did not reveal much change in the parameter  $b_{4,0}$ , although  $\text{SrTiO}_3$  and  $\text{KTaO}_3$  are similar from the point of view of crystal lattice dynamics. Therefore the question of the influence of the ferroactive mode on the temperature dependence of  $b_{4,0}$  remains unanswered.

These analyses established the number of nonequivalent free radical positions, and consequently the number of groups of atoms associated with them in the elementary nucleus, change of this number on transition to the Curie point, form and dynamics of free radical formation, etc. EPR analyses were conducted [28, 29] in irradiated Seignette's salt in which, as it turned out, three types of free radicals formed. They were identified and their behavior was investigated as a function of time and temperature. EPR analyses on impurity ions  $\text{Cu}^{++}$  in triglycine sulfate and Seignette's salt [30, 31] yields some information concerning the causes of "fixing" of spontaneous polarization in these ferroelectrics by the introduction of  $\text{Cu}^{++}$ , which is manifested in the appearance of double hysteresis loops, increased coercive force, etc. [32-35]. It turned out that glycine groups related to various elementary nuclei are bonded to each other by the copper ion. This also impedes repolarization of the crystal.

It should be pointed out in conclusion that EPR analyses in ferroelectrics yield valuable information concerning lattice symmetry at the location of paramagnetic impurity and concerning changes in symmetry during phase transitions, aid in determining the character of impurity substitution (its location in the lattice), etc.

## §2. Nuclear Magnetic Resonance (NMR)

The greatest successes in NMR analyses in ferroelectrics have been achieved as a result of investigating ferroelectrics with hydrogen bonds, to which are devoted most work. Analyses have also been done on other nuclei. NMR analyses made it possible in many cases to clarify crystalline structure, determine the positions of resonating nuclei, analyze the character of ferroelectric phase transition, etc.

We will discuss briefly the parameters that are determined with the aid of NMR. The position of resonance lines and chemical displacement yield information concerning the chemical bond and its changes at the Curie point. We will recall that chemical displacement is  $\Delta H_0/H_0 \cdot 100$ , where  $\Delta H_0$  is the difference between the resonance magnetic fields of a given nucleus for the investigated crystal and the corresponding standard at some fixed frequency of the NMR signal.  $H_0$  is the resonance field on the same frequency for the corresponding standard. The chemical displacement is related to change in electron density near the nucleus and distortion of spherical symmetry of the closed electron shell, leading to a change in the screening effect of the electron cloud in relation to the nucleus.

Valuable information concerning crystalline structure and molecular motion is also derived from analysis of the second moment of the resonance line. The second moment  $S_2$  of the absorption line, the contour of which is some function of the external magnetic field  $f(H - H_0)$ , is

$$S_2 = \frac{\int_{-\infty}^{\infty} (H - H_0)^2 f(H - H_0) dH}{\int_{-\infty}^{\infty} f(H - H_0) dH} \quad (14.9)$$

where  $H$  is the external field,  $H_0$  is some fixed external field, in particular, corresponding to the center of the line. This value depends on the mutual location and mobility of nuclei, on which resonance is observed. In particular, according to Van Vleck [36], for a polycrystal containing identical nuclei, without consideration of molecular motion

$$S_2 = \frac{8}{3} I(I+1) g^2 \mu_{\text{nu}}^2 N^{-1} \sum_{i>j} r_{ij}^{-6} \quad (14.10)$$

where  $I$  is the spin of resonating nucleus,  $g$  is the spectroscopic separation factor,  $\mu_{\text{nu}}$  is the nuclear magneton,  $N$  is the total number of nuclei in the crystal,  $r_{ij}$  is the vector connecting nuclei  $i$  and  $j$ . Comparison of the experimental and theoretical values of the second moment makes it possible to clarify the position of resonating nuclei in the crystal lattice, and also to make conclusions concerning the mobility of certain groups of atoms. Analysis of spin lattice relaxation time  $T_1$  yields information concerning the motion dynamics of nuclei. The temperature dependence of the spectrum in the vicinity of the Curie point yields information concerning the nature and character of the phase transition. Finally, analysis of the quadrupole separation of the spectrum and especially analysis of the purely quadrupole resonance makes it possible to measure the electric field gradient tensor and to determine with great accuracy the structure and character of the internal motion. Nuclear quadrupole resonance will be discussed at length below. We will illustrate the capabilities of the NMR method by way of several examples.

The first to measure the second moment in the ferroelectric phase transition was Losche [37] at the upper Curie point of Seignette's salt. It was shown later [38] that Seignette's salt displays no notable change of the second moment at the bottom Curie point, which indicates that these two phase transitions have a different character. Analyses of changes of the second moments made it possible to refine the nature of the ferroelectric transition in many ferroelectrics. Lundin, et al [39], for example, reported about a change of the second moment in potassium ferrocyanide and showed that its ferroelectric properties are closely related to the ordering of dipolar molecules of the water of crystallization [40-42]. NMR analyses in dicalcium strontium propionate [43] led to the conclusion that spontaneous polarization in this compound is related to the disruption of the plane structure of the propionic acid ion ( $\text{CH}_3\text{CH}_2\text{COO}$ ), which is, to some degree, analogous to the mechanism of spontaneous polarization in triglycine sulfate.

In certain cases it is very useful to do NMR analyses in deuterated crystals. The mechanism of ferroelectric transition related to the ordering of  $\text{NH}_4^+$  groups was proposed as a result of NMR analyses in ammonium sulfate  $(\text{NH}_4)_2\text{SO}_4$  and deuterated ammonium sulfate [44]. Particularly interesting

results were obtained from analysis of deuterated crystals of the potassium dihydrophosphate and triglycine sulfate groups. Analysis of proton resonance in potassium dihydrophosphate [44], as is well known, did not turn up substantial changes of the second moment at the Curie point. Analogous results were obtained from analysis of the form of NMR lines on protons and nuclei of fluorine in ferroelectrics of the triglycine sulfate group [46-48]. These results contradict present notions concerning the great role of hydrogen bonds in spontaneous polarization in these compounds.

NMR analyses on deuterons with quadrupole moments yield much information concerning the character of motion of hydrogen ions and changes in crystal structure and also produce information concerning change in the character of motion of hydrogen. A sudden change was noted [50] in quadrupole distribution of NMR lines on deuterons in deuterated potassium dihydrophosphate at the Curie point. Above the Curie point was observed a spectrum corresponding to one value of the electric field gradient tensor, and below the Curie point, to two different tensor values. The reason for this could be that above the Curie point the deuterons "jump" back and forth on the O-D...O bond at a higher frequency than the frequency of quadrupole separation (see below), and the electric field gradient tensor corresponding to two equilibrium positions is moderated. As the temperature falls below the Curie point the time between jumps increases sharply, and therefore, instead of one line there will be two lines corresponding to two electric field gradients in two different equilibrium positions. In a narrow temperature range near the Curie point coexist a high-temperature spectrum and a low-temperature spectrum, indicating that a first order phase transition takes place. It turned out here that the electric field gradient tensor does not experience considerable change on transition through the Curie point.

Data concerning the electric field gradient tensor in two equilibrium positions of deuterons [50] in combination with data concerning the temperature dependence of spin-lattice relaxation time [52] made it possible to evaluate the temperature dependence of the time between the skips of deuterons on the O-D...O bond [49] (Figure 14.4). It is clear from Figure 14.4 that when a potassium dihydrophosphate crystal is cooled the time between skips of deuterons increases at the Curie point by at least 8 orders of magnitude. Whether the motion of deuterons on the line above the Curie point is truly a tunnel effect or represents thermally activated jumps through a barrier has not yet been established.

Interesting results were also obtained from analysis of NMR in deuterated triglycine sulfate [49, 50]. Analysis of the spectrum of  $\text{ND}_3^+$  groups [50], and also of the total spectrum of the deuterons of triglycine sulfate, including the spectra of deuterons forming the bond O-D...O [49], made it possible to clarify the role of each of the three glycine groups found in the triglycine sulfate molecule during the ferroelectric phase transition. As was shown in [51], the planar glycine group GIII and non-planar group GII are connected by a short hydrogen bond. The proton is located in planar group GIII. If the proton jumps into group GII, the

nitrogen of this group returns to the plane and the nitrogen in the previously planar group leaves the plane. Thus groups GII and GIII change roles. NMR analyses [49] made it possible to establish that the deuterons of groups GII and GIII in the paraelectric phase jump back and forth on the bond at a frequency greater than the frequency of quadrupole separation, and "freeze" in group GII below the Curie point.

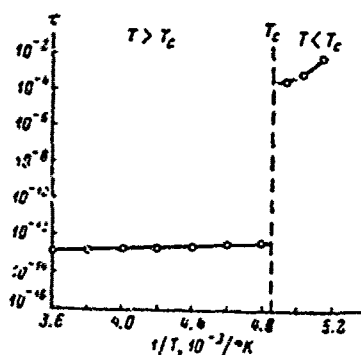


Figure 14.4. Temperature dependence of deuteron skipping time on hydrogen bond in  $KD_2PO_4$  according to Bjorkstam (figure taken from [49]).

Investigations [50] show, furthermore, that GI glycine groups in the paraelectric phase are statistically not distributed above and below the mirror plane, as was proposed in [51], but lie in this plane [49, 50]. Large, but gradual changes in the field gradient tensor at the location of the deuteron of group GI on cooling below the Curie point are evidence of a gradual displacement of the GI group from the mirror plane into its low-temperature position, found in [51]. Thus, NMR data show that the ferroelectric transition in triglycine sulfate should be regarded as a combination of the order-disorder transition of protons OIII-H-OII and glycine

groups GII and GIII and transition of the displacement type for group GI.

Analogous results were recently obtained from analysis of deuteron resonance in the antiferroelectric  $ND_4D_2PO_4$  [53]. The extra separation of the NMR lines in the ferroelectric phase is interpreted as the result of ordering of deuterons in the hydrogen bonds between the phosphate ions.

One of the interesting questions of the physics of ferroelectricity is that of the influence of the character of the chemical bond on spontaneous polarization. It is important to determine, in particular, whether there is a change in the degree of covalence of the bond at the point of transition in a number of ferroelectrics and antiferroelectrics of the perovskite type. The magnitude of the chemical displacement (~1.2%) observed in compounds of the perovskite type on  $Pb^{207}$  nuclei is evidence for substantial covalent character of the chemical bond of the lead ions in these compounds [54]. Lead zirconate and one of its solid solutions do not display change in chemical displacement at the Curie point. This indicates that the ferro- or antiferroelectric phase transition is not related to substantial change in the covalence of the bonds of lead ions.

Noteworthy of the works on NMR analyses for various nuclei are [55, 56]. The NMR of Seignette's salt on  $Na^{23}$  ions was analyzed in [55]. Work [56] pertains to analysis of quadrupole separation of NMR on  $Li^7$

nuclei in several ferroelectrics containing lithium ions (lithium ammonium and lithium potassium tartrates, lithium niobate and lithium tantalate). We will examine briefly NMR analyses in lithium niobate and lithium tantalate. NMR on  $\text{Li}^7$  nuclei in lithium niobate was examined in [56-59]. It was shown that the asymmetry parameter  $\eta = 0$  in lithium niobate and lithium tantalate (determination of the various parameters describing the interaction between the quadrupole moment of the nuclei and the crystalline field of the lattice is described in the following section).

NMR analyses substantiate x-ray and neutronographic data concerning the rhombohedral symmetry of these crystals, to which correspond  $\eta = 0$ . The quadrupole bond constants in lithium tantalate increase in the vicinity of  $300^\circ\text{C}$ . The quadrupole bond constant of  $\text{Li}^7$  in lithium niobate, according to [59], is 53 kHz. The second moment of the resonance curve was determined in [58]. The mechanism of spin-lattice relaxation is discussed in [58, 59], but a universally accepted point of view has not yet been developed. The opinion that the mechanism of relaxation in the investigated crystals is primarily quadrupole is propounded in [59]. Comparison of the results of experimental and theoretical determination of the electric field gradients with the aid of the point ion model suggests that there is substantial covalence of the chemical bonds of Li in these compounds.

Some interesting results were obtained from NMR analysis on  $\text{Na}^{23}$  nuclei in sodium nitrate. Anomalies in the temperature dependence of quadrupole separation were discovered at the ferroelectric Curie point near  $163^\circ\text{C}$  and also at  $178^\circ\text{C}$ , corresponding to phase transitions [60-62]. According to [62], there are two different electric field gradients in the range of the antiferroelectric phase ( $\sim 1^\circ\text{C}$  above the ferroelectric region). This is not in accord with the model of the sinusoidal antiferroelectric phase (see Chapter 17). Analysis of the orientation and temperature dependences of the second moment of the central component of the spectrum [63] revealed a plateau in the temperature dependence at  $165\text{-}180^\circ\text{C}$  with the magnetic field oriented parallel to the a axis, which is possibly related to the retention of a certain amount of ordering at these temperatures in the paraelectric region.

The NMR on  $\text{Nb}^{93}$  nuclei in potassium niobate was analyzed [64], but since the basic results of this work were obtained from analysis of the quadrupole separation of NMR lines and from investigation of the quadrupole resonance, this work is discussed below.

A report appeared recently concerning observation of the NMR spectra on  $\text{Nb}^{93}$  nuclei in lithium niobate [65]. The quadrupole bond constant at room temperature was  $22.02 \pm 0.04$  MHz and the asymmetry parameter  $\eta = 0$ .

### §3. Nuclear Quadrupole Resonance

Nuclear quadrupole resonance (NQR) may occur in the absence of a stationary magnetic field. The magnetic vector of a variable field interacts with the magnetic moment of the nucleus, which is "rigidly" attached to

the electric quadrupole moment of the nucleus. The electric quadrupole moment interacts, in turn, with the internal crystalline field gradient of the lattice. There are also transitions between the energy levels corresponding to this latter interaction under NQR conditions.

The Hamiltonian describing the interaction of the electric quadrupole moment of the nucleus with the field gradient at the location of the nucleus, disregarding terms of higher order according to [66, 67] has the form

$$H_Q = QVE = \sum_{\mu=-2}^2 Q_{\mu} \nabla E_{-\mu} \quad (14.11)$$

where  $Q$  is the tensor operator describing the quadrupole distribution of charge in the nucleus,  $\nabla E$  is the electric field gradient in the position of the nucleus.

The tensor components of the quadrupole charge have the form:

$$\left. \begin{aligned} Q^0 &= \frac{eQ}{2I(2I-1)} (3I_z^2 - I^2), \\ Q^{21} &= \frac{eQ}{2I(2I-1)} \frac{\sqrt{6}}{2} (I_x(I_x \pm I_y) + (I_x \pm I_y)I_x), \\ Q^{22} &= \frac{\sqrt{6}eQ}{4I(I-1)} (I_x \pm I_y)^2. \end{aligned} \right\} \quad (14.12)$$

where  $e$  is electron charge,  $I$  is nucleus spin operator,  $Q$  is the scalar quadrupole moment of the nucleus. Here  $Q$  is found from the relation:

$$eQ = \int \rho_i r_i^2 (3 \cos^2 \theta_{i1} - 1) d\tau_i.$$

where  $\rho_i$  is charge density in volume  $d\tau_i$  in the nucleus at distance  $r_i$  from the center and  $\theta_{i1}$  is the angle between radius  $r_i$  and the axis of nuclear spin  $I$ .

The tensor components of the internal field gradient have the form:

$$\left. \begin{aligned} \nabla E^0 &= \frac{1}{2} \frac{\partial E_x}{\partial x}, \\ \nabla E^{21} &= \frac{1}{\sqrt{6}} \left( \frac{\partial E_x}{\partial x} \pm i \frac{\partial E_y}{\partial y} \right), \\ \nabla E^{22} &= \frac{1}{2\sqrt{6}} \left( \frac{\partial E_x}{\partial x} - \frac{\partial E_y}{\partial y} \pm 2i \frac{\partial E_z}{\partial y} \right). \end{aligned} \right\} \quad (14.13)$$

where  $E$  is the crystalline field at the location of the nucleus due to the charges surrounding the nucleus.

for the principal coordinate axes X, Y, Z of the symmetric field gradient tensor, assuming the Laplace relation

$$\frac{\partial^2 V}{\partial X^2} + \frac{\partial^2 V}{\partial Y^2} + \frac{\partial^2 V}{\partial Z^2} = 0.$$

to be valid, where V is the crystalline field potential, the Hamiltonian of quadrupole interaction will have the form:

$$\mathcal{H}_Q = \frac{e^2 q Q}{4I(2I-1)} \left\{ 3I_z^2 - I(I+1) + \frac{1}{2} \eta (I_x^2 - I_y^2) \right\}. \quad (14.14)$$

Here

$$\frac{\partial E_E}{\partial Z} = eq, \quad \eta = \frac{\left( \frac{\partial^2 V}{\partial X^2} - \frac{\partial^2 V}{\partial Y^2} \right)}{\frac{\partial^2 V}{\partial Z^2}} = \frac{\partial^2 V}{\partial X^2} < \frac{\partial^2 V}{\partial Y^2} < \frac{\partial^2 V}{\partial Z^2}.$$

The value  $\eta$  is called the asymmetry parameter. For the case of axial symmetry ( $\eta = 0$ ) the matrix elements have the form:

$$\langle m | \mathcal{H}_Q | m \rangle = \frac{e^2 q Q}{4I(2I-1)} [3m^2 - I(I+1)] \delta_{mm}, \quad (14.15)$$

where  $m$  and  $m'$  are the magnetic quantum numbers of nuclear spin corresponding to the different states,  $\delta_{mm'}$  are Kronecker's indices ( $\delta_{mm'} = 0$ , when  $m \neq m'$  and  $\delta_{mm'} = 1$ , when  $m = m'$ ). Then the energy levels of quadrupole interaction  $W_m$  are determined by the expression:

$$W_m = \frac{e^2 q Q}{4I(2I-1)} [3m^2 - I(I+1)]. \quad (14.16)$$

The quadrupole resonance frequency is determined by the difference between the energy levels, between which there is a transition,  $h\nu = W_{m'} - W_m$ . The sampling rule  $|\Delta m| = 1$  is valid here. When  $\eta \neq 0$ , however, transitions become possible between states with  $m$  differing by more than one. The value  $\frac{e^2 q Q}{h}$  is called the quadrupole bond constant.

In the case of  $\eta$  different from 0, the quadrupole interaction energy levels depend on  $\eta$ , and when field gradient asymmetry is great they are calculated by solving graphically the scalar equations for the energy or by tables of their numerical values found with the aid of computers.

Knowledge of the quadrupole resonance frequencies, along with analysis of the orientation dependences of line intensity and Zeemann

separation of quadrupole levels with a weak external magnetic field makes it possible to determine the electric field gradient tensor in the position of the nuclei (magnitude and orientation of its components) and asymmetry parameter  $\eta$ .

Due to deviation in the distribution of charges of the electron shell of the ions from spherical symmetry, however, the field gradient in the positions of the nuclei is not equal to the field gradient due to all other ions of the crystal lattice. In order to convert from the field gradient on the nucleus to the "external" gradient  $q_{ex}$  the following relation is often used:

$$q = q_{ex}(1 - \gamma_{\infty}), \quad (14.17)$$

where  $\gamma_{\infty}$  is the so-called Sternheimer's antiscreening factor [68]. It reaches  $\sim 10^2$  for heavy nuclei. It is obvious that  $\gamma_{\infty}$ , generally speaking, is not constant and may depend on the character of chemical bond, distance between ions, etc.

NMR analysis of nuclei with quadrupole moments makes it possible to determine the quadrupole separation of NMR lines, from which the asymmetry parameter and field gradient can be found [56]. Some of the findings of analysis of the quadrupole separation of NMR were given in the preceding section.

NQR analyses and analysis of quadrupole separation yield information on the symmetry of the crystal structure, presence of nonequivalent positions of atoms, their mutual distribution, form of chemical bond, etc. Analysis of NQR relaxation times makes it possible to judge the character of internal motion in crystals. By virtue of the fact that NQR frequencies are determined by the electric field gradient, this method is particularly sensitive to any type of change of crystalline fields and therefore yields valuable information concerning the conditions of occurrence of the ferroelectric state and character of ferroelectric phase transitions. The reader is referred to [66, 67, 69, 70] concerning general questions of NQR.

Very little work has been done on NQR in ferroelectrics. The chief reason for this is difficulty in growing large crystals of quality good enough to ensure NQR signals. Quadrupole separation of NMR and NQR in  $\text{KNbO}_3$  on  $\text{Nb}^{93}$  nuclei was studied in [64]. The temperature dependence of the NQR spectrum in potassium niobate was analyzed in detail in [71]. The quadrupole bond constant at  $-40^\circ\text{C}$  (rhombic phase) was  $e^2qQ/h = 23.1$  MHz, the asymmetry parameter  $\eta = 0.806$ . In the rhombic phase the asymmetry parameter  $\eta = 0$  and the quadrupole bond constant  $e^2qQ/h = 16$  MHz. The principal axis of the electric field gradient in the rhombic phase was not accurately determined. It was shown only that it is oriented at an angle about  $20^\circ$  to the polar axis of the crystal. One interesting result of the work was the conclusion that the phase transitions between the cubic,

tetragonal, rhombic and rhombohedral phases are first order phase transitions, but the different regions of the crystal display phase transitions at several different temperatures, and here the higher the transition temperature the narrower the range of the transition.

The temperature dependence of the quadrupole bond constant of  $\text{KNbO}_3$  in different phases is shown according to [71] in Figure 14.5.

The temperature dependence of NQR frequencies, as we know, is related to moderation of the electric field gradient as a result of thermal motion (as occurs, for instance, in deuterated potassium dihydrophosphate and triglycine sulfate, as mentioned above), and also to strictly the temperature dependence of the electric field gradient due to change in the distances between atoms as the temperature is changed. These contributions can be distinguished by measuring the dependence of the gradient determined from NQR frequencies not only on temperature, but also on pressure. Evaluation of the various possible contributions to the temperature dependence of frequencies for  $\text{KNbO}_3$  [71] showed that the temperature dependence can be disregarded due to moderation of the gradient and the observed temperature dependence is related chiefly to the "true" change of the gradient.

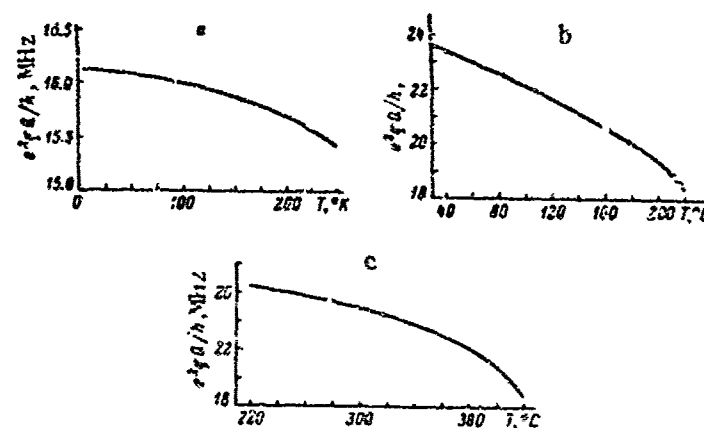


Figure 14.5. Temperature dependence of quadrupole bond constant of  $\text{KNbO}_3$  in three phases (according to Hewitt [71]). a -- rhombohedral; b -- rhombic; c -- tetragonal.

Comparison of the computed electric field gradient for various temperatures in the tetragonal phase using the point ion lattice model and experimental value showed that the temperature dependence of NQR frequencies is explained satisfactorily when the temperature dependence of the lattice parameters and ion displacements is taken into account.

Satisfactory agreement between the theoretical and experimental data may mean that the ion model is valid for  $\text{KNbO}_3$ , although the roughness of this type of calculation should be borne in mind.

The temperature dependence of the NQR spectrum on  $\text{As}^{75}$  nuclei in crystals of the  $\text{KH}_2\text{AsO}_4$  group were analyzed in [72, 73]. A sharp increase of frequencies was noted during phase transition to the spontaneous-polarized state. One of the reasons for this may be localization of protons in one of the potential minima near the "top" or "bottom" oxygen, leading to an increase in the measured field gradient on  $\text{As}^{75}$  nuclei. There is such a great expansion of the lines in the region of the transition that resonance could not be detected. In  $\text{CsH}_2\text{AsO}_4$  crystals, furthermore, the signal vanished at temperatures somewhat lower than the Curie point, possibly because the temperatures of the frequencies of proton transfer and investigated quadrupole resonance coincide in this region. The temperature dependence of NQR frequencies in the paraelectric phase favors the rotation of the  $\text{AsO}_4$  groups in this phase.

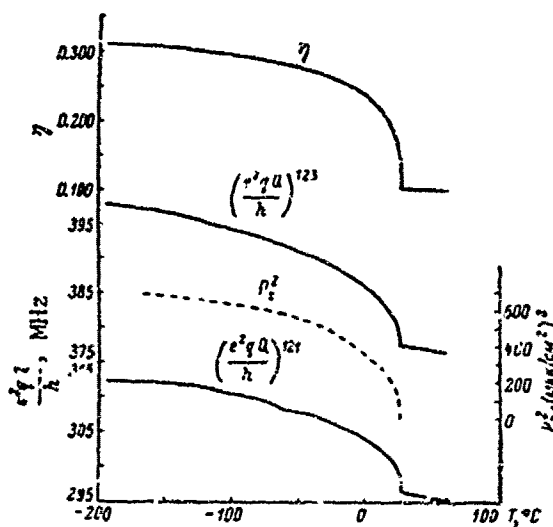


Figure 14.6. Temperature dependence of quadrupole bond constants of  $\text{Sb}^{121}$  and  $\text{Sb}^{123}$ , asymmetry parameter  $\eta$  and  $P_s^2$  in antimony sulfidite (according to Popov, et al [76]).

NQR signals were recently discovered with the aid of a pulsed spectrometer [74] and their temperature dependence was examined in antimony sulfidite and sulfbromide [75, 76]. The temperature dependence of the quadrupole bond constants of  $\text{Sb}^{123}$  and  $\text{Sb}^{121}$  nuclei and asymmetry parameter  $\eta$  in antimony sulfidite  $\text{SbSI}$  according to [76] is illustrated in Figure 14.6. The ferroelectrics of this group are characterized by a phase transition of the displacement type. The electric field gradient in the vicinity of the Curie point of antimony sulfidite changes as the square of spontaneous polarization, analogous to the results obtained for barium titanate by EPR methods [8] and Messbauer's results (see below). In addition to anomalies

of the field gradient and asymmetry parameter at the Curie point, slight anomalies were detected, corresponding to low-temperature phase transitions.

#### §4. Messbauer's Method of Analyzing Ferroelectrics

Analysis of the gamma-ray resonance absorption spectrum (Messbauer effect) can yield interesting information concerning crystal lattice dynamics, electric field gradients, character of chemical bond, etc.

The essence of the Messbauer effect, as we know, consists in the following. The nucleus of some element emits  $\gamma$ -quantum with the energy  $h\nu$ . Other nuclei of this element, located in a lower energy state, may absorb this quantum. Part of the energy of the quantum, however, both during emission and during absorption, may be consumed in the recoil of the emitting and absorbing nuclei. In view of the fact that atoms are firmly bonded in a solid, the entire lattice as a whole, and not individual nuclei, experiences recoil during the emission and absorption of a  $\gamma$ -quantum. Because of the great mass of the lattice its recoil energy is infinitesimal and energy losses during the emission and absorption of  $\gamma$ -quanta are so small that they can be made up by the relative head-on mechanical motion of the source of  $\gamma$ -quanta and absorber. Then, due to the Doppler effect, the frequency of the  $\gamma$ -quanta will change and the resonance conditions can be satisfied through a change of relative velocity.

The probability of energy loss by nuclei to recoil increases as a result of vibrations of the lattice, since phonons can be excited in the lattice during emission and absorption of  $\gamma$ -quanta.

The probability of the Messbauer effect occurring at the ferroelectric Curie point, as theoretically predicted [77], should diminish due to the excitation of low-energy phonons corresponding to the soft "ferro-active" mode of vibrations. This was verified experimentally [78-83].

The temperature dependence of the Messbauer effect was investigated [78-81] in solid solutions of  $\text{Ba}(\text{Ti}_{1-x}\text{Sn}_x)_3$  enriched with  $\text{Sn}^{119}$  isotopes. It was shown that the probability of the Messbauer effect actually passes through a minimum at the Curie point. It was also shown that in solid solutions with a rather high concentration of  $\text{BaSnO}_3$  the minimum of the Messbauer effect lies at a lower temperature than maximum permittivity. This was explained in [78-80] on the basis of the theory that as a result of erosion of the phase transition at these solid solution concentrations the Curie temperatures of the microregions enriched with  $\text{Sn}^{119}$  are lower than the mean Curie temperature of the solid solution.

The minimum probability of the Messbauer effect at the Curie point was observed on  $\text{Fe}^{57}$  nuclei in  $\text{BaTiO}_3$  [82] and in  $\text{PbFe}_{1/2}\text{Mn}_{1/2}\text{O}_3$  [83].

Thus, these investigations of the Messbauer effect also speak in behalf of the validity of the concepts of the dynamic theory of ferroelectricity. It should be pointed out, however, that no changes in the line width of

$\text{Sn}^{119}$  in solid solutions of  $\text{Ba}(\text{Ti}, \text{Sn})\text{O}_3$  were detected in [34] during transition through the Curie point.

A study of the Messbauer effect on  $\text{Sn}^{119}$  and  $\text{Fe}^{57}$  nuclei in  $\text{BiFeO}_3$  and its solid solutions with  $\text{Sr}(\text{Sn}_{1/3}\text{Mn}_{2/3})\text{O}_3$ , combining electric and magnetic ordering, was reported in [84, 85] (see Chapter 18). The effective magnetic field on iron nuclei which, extrapolated to  $0^\circ\text{K}$ , was approximately 550 ke, was estimated from the temperature dependence of Zeemann separation in the antiferromagnetic region. The appearance of an effective magnetic field on  $\text{Sn}^{119}$  nuclei below the Neel point, explained by the exchange reaction  $\text{Sn}^{4+} - \text{O}^{2-} - \text{Fe}^{3+}$ , was also noted in these investigations. The presence of a quadrupole moment in the  $\text{Fe}^{57}$  nucleus makes it possible to estimate the gradient of the electric field acting on this nucleus. The magnitude of the field gradient in  $\text{BiFeO}_3$  [84, 85],  $\text{PbFe}_{1/2}\text{Ta}_{1/2}\text{O}_3$  [85], and  $\text{BaTiO}_3$  [82], was investigated and it agreed satisfactorily with the theoretical value obtained on the basis of the model of point charges and point dipoles.

The temperature dependences of quadrupole separation  $\Delta E$  and square spontaneous polarization in  $\text{BaTiO}_3$  are shown in Figure 14.7 [82]. The satisfactory coincidence of these dependences indicates that in the tetragonal phase of barium titanate the gradient of the electric field acting on the  $\text{Fe}^{57}$  nucleus (to which quadrupole separation is directly proportional) is proportional to the square spontaneous polarization. The value estimated from the model of point charges and point dipoles with consideration of displacement of ions in the assumption that the effective charge is 60% of the ion charge, agreed satisfactorily with the experimental value.

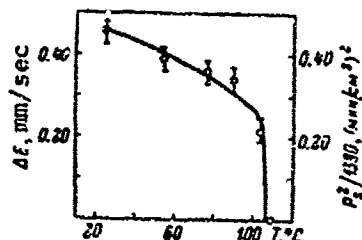


Figure 14.7. Temperature change of quadrupole separation  $\Delta E$  and square of spontaneous polarization in barium titanate (according to Bhide and Multani [82]).

distortion of the lattice of perovskites in the ferroelectric phase is a result of electrostriction and is proportional to the square of spontaneous polarization). Thus, investigations of the Messbauer effect confirm that the axial field parameter in spin Hamiltonian D or  $b_{2.0}$  is related

The proportionality of the field gradient, and consequently of coefficient  $A_2^0$  in the axial potential of the crystalline field (equation (14.7)) to the square of spontaneous polarization should be compared with the results of analysis of the EPR in  $\text{BaTiO}_3$  [8]. It was found in these studies that the axial field parameter in spin Hamiltonian D or  $b_{2.0}$  changes as  $P_s^2$  or is linear in relation to tetragonal distortion of the lattice (we will recall that

linearly to axial potential  $V_{\omega}$ , (cf. (14.8)) and with the field gradient.

Moreover, the temperature dependence of isomeric displacement (determined according to the position of the doublet center) was measured [82] and a jump was found in isomeric displacement at the Curie point, which is ascribed to the change in the degree of covalence of the chemical bond with the onset of spontaneous polarization.

Investigation of the Messbauer effect on barium titanate crystals treated by different methods [82, 86] showed a change in the surrounding of  $Fe^{57}$  impurity in the barium titanate lattice, depending on the heat treatment of the crystal.

Investigations of the Messbauer effect in boracites [87] revealed a new phase transition between the rhombic and trigonal phases. At the Curie point corresponding to the phase transition from the cubic to the rhombic phase, an abrupt increase was noted in the area of the resonance curve. A brief report appeared in [88] concerning investigation of the Messbauer effect in potassium ferrocyanide.

Investigations of the Messbauer effect in ferroelectrics have only begun. The data obtained already suggest the effectiveness of this method in application to ferroelectrics. Certain questions, however, still require further investigation. In particular, further investigation of the probability of the effect in the region of the Curie point of different types of ferroelectrics and more rigorous theoretical interpretation of the results are very important.

#### BIBLIOGRAPHY

1. Al'tshuler, S. A. and V. B. Koz'yev, Elektronnyy Paramagnitnyy Rezonans (Electron Paramagnetic Resonance), Fizmatgiz [State Publishing House of Literature on Physics and Mathematics], 1961.
2. Lou, V., Paramagnitnyy Rezonans v Tverdykh Telakh (Paramagnetic Resonance in Solids), IL [Foreign Literature] Publishing House, Moscow, 1962.
3. Zaripov, M. M. and L. Ya. Shekun, Paramagnitnyy Rezonans (Paramagnetic Resonance), Kazan' University Publishing House, p. 5, 1964.
4. Petrov, M. P., FTT [Fizika tverdogo tela; Solid State Physics], Vol. 10, p. 3254, 1968.
5. Hornig, A. W., E. T. Jaynes and H. E. Weaver, Phys. Rev., Vol. 96, p. 1703, 1954.
6. Hornig, A. W., R. C. Rempel and H. F. Weaver, Phys. Rev. Lett., Vol. 1, p. 284, 1958; J. Phys. Chem. Sol., Vol. 10, p. 1, 1959.

7. Sakudo, T., J. Phys. Soc. Japan, Vol. 18, p. 1626, 1963; T. Sakudo and H. Unoki, J. Phys. Soc. Japan, Vol. 19, p. 2109, 1964.
8. Rimai, L. and G. A. De Mars, Phys. Rev., Vol. 127, p. 702, 1962.
9. Takeda, T. and A. Watanabe, J. Phys. Soc. Japan, Vol. 19, p. 1742, 1964.
10. Odehnal, M., Czechosl. J. Phys., Vol. 13, p. 566, 1963.
11. Ikushima, H. and S. Hayakawa, J. Phys. Soc. Japan, Vol. 19, p. 1986, 1964.
12. Ikushima, H., J. Phys. Soc. Japan, Vol. 21, p. 1866, 1966.
13. Van Vleck, J. H. and W. G. Penney, Phil. Mag., Vol. 17, p. 961, 1934.
14. Pryse, M. N. L., Phys. Rev., Vol. 80, p. 1107, 1950.
15. Watanabe, H., Progr. Theor. Phys., Vol. 18, p. 405, 1957.
16. Nicholson, W. Y. and G. Burns, Phys. Rev., Vol. 129, p. 2490, 1963.
17. Germanier, M. M., D. Gainon and R. Lacroix, Phys. Lett., Vol. 2, p. 105, 1962.
18. Hutchison, C. A., B. R. Judd and D. F. O. Pope, Proc. Phys. Soc., Vol. B70, p. 514, 1957.
19. Rimai, L., T. Deutsch and B. D. Silverman, Phys. Rev., Vol. 133, A1123, 1964.
20. Unoki, H. and T. Sakudo, J. Phys. Soc. Japan, Vol. 21, p. 1730, 1966.
21. Sroubek, Z. and K. Zdansky, Czechosl. J. Phys., Vol. 13, p. 309, 1963.
22. Ikushima, H. and S. Hayakawa, Japan J. Appl. Phys., Vol. 4, p. 328, 1965.
23. Takeda, T. and A. Watanabe, J. Phys. Soc. Japan, Vol. 21, p. 1132, 1966.
24. Ikegami, S. and J. Ueda, J. Phys. Soc. Japan, Vol. 19, p. 195, 1964.
25. Roteberg, B. A., Yu. L. Danilyuk, Ye. I. Gindin and V. G. Prokhvatilov, FTT, Vol. 7, p. 3048, 1965.
26. Shapkin, V. V., Candidate Dissertation, Leningrad. 1967.
27. Bursian, E. V. and V. V. Shapkin, FTT, Vol. 9, p. 285, 1967.
28. Souldon, G. C. and W. C. Souldon, J. Chem. Phys., Vol. 35, p. 208, 1961.

29. Abe, R. and J. Suzuki, Proc. Intern. Meet. Ferroelectr., Vol. 2, Prague, p. 358, 1966.
30. Losche, A. and W. Windsch, Phys. St. Sol., Vol. 11, K55, 1965.
31. Stankowski, J., Proc. Intern. Meet. Ferroelectr., Vol. 2, Prague, p. 364, 1966.
32. Yurin, V. A., Izv. AN SSSR, ser. fiz. (News of USSR Academy of Sciences, Physics Series), Vol. 21, p. 329, 1957.
33. Eisner, I. Ya., Izv. AN SSSR, ser. fiz., Vol. 21, p. 334, 1957.
34. Yurin, V. A. and I. S. Zheludev, Kristallogr.fiya (Crystallography), Vol. 4, p. 255, 1959.
35. Yurin, V. A., Candidate Dissertation, Moscow, 1963.
36. Van Vleck, J. H., Phys. Rev., Vol. 74, p. 1168, 1948.
37. Losche, A., Exp. Techn. Phys., Vol. 3, p. 18, 1955.
38. Bjorkstam, J. L. and E. A. Uehling, Phys. Rev., Vol. 114, p. 961, 1959.
39. Lundin, A. G., K. S. Aleksandrov, G. M. Mikhaylov and S. P. Gabuda, Izv. AN SSSR, ser. fiz., Vol. 24, p. 1195, 1960.
40. Lundin, A. G. and E. P. Zeyer, Izv. AN SSSR, ser. fiz., Vol. 29, p. 910, 1965.
41. Lundin, A. G., G. M. Mikhaylov and S. P. Gabuda, DAN SSSR (Reports of USSR Academy of Sciences), Vol. 136, p. 864, 1961.
42. Aleksandrov, K. S., S. P. Gabuda, A. G. Lundin and G. M. Mikhaylov, Acta Cryst. Suppl., Vol. 16, No. 13, p. 190, 1963.
43. Aleksandrov, K. S., S. P. Gabuda and A. G. Lundin, Izv. AN SSSR, ser. fiz., Vol. 29, p. 907, 1965.
44. O'Reilly, D. E. and I. Tsang, J. Chem. Phys., Vol. 46, p. 1291, 1967.
45. Bjorkstam, J. L., E. D. Jones, H. B. Silsbec and E. A. Uehling, J. Chem. Phys., Vol. 37, p. 469, 1962.
46. Blinc, R., S. Detoni and M. Pintar, Phys. Rev., Vol. 24, p. 1036, 1961.
47. Blinc, R. and I. Zupancic, J. Phys. Chem. Sol., Vol. 24, p. 1379, 1963.
48. Blinc, R., G. Lanajner, M. Pintar and I. Zupancic, J. Chem. Phys., Vol. 44, p. 1784, 1966.

49. Blinc, R., Proc. Intern. Meet. Ferroelectr., Vol. 2, Prague, p. 333, 1966.
50. Bjorkstam, J. L., Phys. Rev., Vol. 153, p. 599, 1967.
51. Hoshino, S., Y. Okaya and R. Pepinsky, Phys. Rev., Vol. 115, p. 323, 1959.
52. Schmidt, V. H. and E. A. Uehling, Phys. Rev., Vol. 126, p. 447, 1962.
53. Soest, J. F. and E. A. Uehling, Bull. Am. Phys. Soc., Vol. 12, p. 290, 1967.
54. Anderson, D. H., J. Chem. Phys., Vol. 40, p. 1168, 1964.
55. Blinc, R., J. Petkovsek and I. Zupancic, Phys. Rev., Vol. 136, A1684, 1964.
56. Burns, G., Phys. Rev., Vol. 127, p. 1193, 1962.
57. Peterson, G. E., P. M. Bridenbaugh and P. Green, J. Chem. Phys., Vol. 46, p. 4009, 1967.
58. Golenishchev-Kutuzov, V. A., U. K. Kopvillem, L. N. Rashkovich and N. F. Yevlanova, FTT, Vol. 10, p. 759, 1968.
59. Vogdanov, V. L., V. P. Klyuyev, V. V. Lemanov and S. A. Fedulev, FTT, Vol. 10, p. 1118, 1968.
60. Weiss, A. and D. Diedenkapp, Zs. Naturforsch., Vol. 17a, p. 794, 1962.
61. Lundin, A. G. and S. P. Gabuda, FTT, Vol. 5, p. 2009, 1963.
62. Betsuyaku, H., J. Phys. Soc. Japan, Vol. 21, p. 137, 1966.
63. Vinogradova, I. S. and A. G. Lundin, FTT, Vol. 10, p. 769, 1968.
64. Cotts, R. M. and W. D. Knight, Phys. Rev., Vol. 96, p. 1285, 1954.
65. Kind, R., H. Granicher, B. Derighett, F. Waldner and E. Brun, Sol. St. Comm., Vol. 6, p. 439, 1968.
66. Cohen, M. H. and F. Reif, Sol. St. Phys., Vol. 5, p. 321, 1957.
67. Das, T. P. and E. L. Hahn, Sol. St. Phys. Suppl., Vol. 1, 1958.
68. Sternheimer, R. M., Phys. Rev., Vol. 80, p. 102, 1950; R. M. Sternheimer and H. M. Folly, Phys. Rev., Vol. 102, p. 731, 1956.

69. Grechishkin, V. S. UFN [Uspekhi fizicheskikh nauk; Progress of Physical Science], Vol. 69, p. 189, 1959; V. S. Grechishkin and G. B. Soyfer, PTE, No. 1, p. 5, 1964.
70. Semin, G. K. and E. I. Fedin, Zh. Strukt. Khim. (Journal of Structural Chemistry), Vol. 1, p. 252, 464, 1960.
71. Hewitt, R. R., Phys. Rev., Vol. 121, p. 45, 1961.
72. Zhukov, A. P., I. S. Rez, V. I. Pakhomov and G. K. Semin, Phys. St. Sol., Vol. 27, K129, 1968.
73. Zhukov, A. P., I. S. Rez, V. I. Pakhomov and G. K. Semin, Izv. AN SSSR, ser. fiz., Vol. 33, p. 274, 1969.
74. Safin, I. A., B. N. Pavlov and D. Ya. Shtern, Zav. Lab. (Plant Laboratory), Vol. 30, p. 676, 1964.
75. Kraynik, N. N., S. N. Popov and I. Ye. Myl'nikova, FTT, Vol. 8, p. 3664, 1966.
76. Popov, S. N., H. H. Kraynik and I. Ye. Myl'nikova, Izv. AN SSSR, ser. fiz., Vol. 33, p. 271, 1969.
77. Muzikar, C., V. Janovec and V. Dvorak, Phys. St. Sol., Vol. 3, K9, 1963.
78. Bokov, V. A., V. P. Romanov and V. V. Chekin, FTT, Vol. 7, p. 1886, 1965.
79. Chekin, V. V., V. P. Romanov, B. I. Verkin and V. A. Bokov, ZhETF [Zhurnal eksperimental'noy i teoreticheskoy fiziki; Journal of Experimental and Theoretical Physics], Letters, Vol. 2, p. 186, 1965.
80. Bokov, V. A., V. P. Romanov, B. I. Verkin, L. I. Kasakevich and V. V. Chekin, Proc. Intern. Meet. Ferroelectr., Vol. 1, Prague, p. 80, 1966.
81. Belov, V. F. and I. S. Zheludev, ZhETF, Letters, Vol. 6, p. 843, 1967.
82. Bhide, V. G. and M. S. Multani, Phys. Rev., Vol. 139, p. 1983, 1965.
83. Sklyarevskiy, V. V., I. I. Lukashevich, V. P. Romanov, I. Filippov, Yu. N. Venevtsev and A. S. Viskov, ZhETF, Letters, Vol. 5, p. 212, 1966.
84. Mitrophanov, K. P., M. V. Plotnikova, A. S. Viskov, Ju. Ja. Tomashpolskii, Ju. N. Venevtsev, V. S. Shpinel, Proc. Intern. Meet. Ferroelectr., Vol. 1, Prague, p. 87, 1966.
85. Mitrofanov, K. P., A. S. Viskov, M. V. Plotnikova, Yu. N. Venevtsev and V. S. Shpinel', Izv. AN SSSR, ser. fiz., Vol. 28, p. 2029, 1965.
86. Bhide, V. G. and M. S. Multani, Phys. Rev., Vol. 149, p. 239, 1966.

87. Schmid, H. and J. M. Trooster, *Sol. St Comm.*, Vol. 5, p. 31, 1967.

88. Hazong, Y., C. Earls and J. Lefkowitz, *bull. Am. Phys. Soc.*, GD8,  
Vol. 11, p. 268, 1966.

## CHAPTER 15. EXPERIMENTAL INVESTIGATIONS OF LATTICE VIBRATIONS OF FERROELECTRICS NEAR CURIE TEMPERATURE

As follows from the dynamic theory of ferroelectricity [1-6] (see Chapter 5), a limiting dipole transverse optical vibration with wave vector  $k$ , approaching zero, should be seen in the vibration spectrum of ferroelectric crystals. The frequency of this mode diminishes substantially near the Curie point, and it is characterized by great anharmonicity.

The reduction of frequency is explained within the framework of these concepts by the fact that short-acting rotational forces of this mode are compensated in harmonic approximation near the Curie point by farther-reaching electrostatic forces. The frequency of the ferroactive mode in the range of small  $k$  does not vanish, but remains positive due to the contribution of an anharmonic action, the magnitude of which depends strongly on temperature. And this explains the strong temperature dependence of frequency for small  $k$  [7].

We will examine existing experimental results of the analysis of optical spectra, inelastic scattering neutrons and thermal diffusion of x-rays and electrons, in which are obtained data concerning these "ferroactive" low-frequency lattice vibrations. Here we will more or less ignore the investigations of other regions of the spectra. In particular, we will not discuss the vibrations of protons in the hydrogen bond. Certain information concerning the vibrations of protons in hydrogen-containing ferroelectrics is found in Chapter 14. A more thorough review of a number of studies of the lattice dynamics of ferroelectrics is given in [8, 9].

### 51. Infrared Spectra

No anomalies in the region of the ferroelectric phase transition were noted in the first analyses of the infrared spectra of perovskite type ferroelectrics, conducted with the aid of measurements of transmission spectra in the  $300-1,000 \text{ cm}^{-1}$  range [10, 11]. The reason for this is that the "ferroactive" mode of vibrations is characterized by an extremely low frequency of  $\sim 10^{11}$  Hz near the Curie point, lies in the far infrared region and its detection involves great experimental difficulties. Moreover, due

to strong absorption in this frequency range, even the finest specimens that can be made are opaque. Therefore it was necessary to resort to the reflection method, whereby it was possible to detect the "ferroactive" mode in a number of ferroelectrics and to analyze the temperature dependence of its frequency [12-17]. In the reflection method the dependence of the coefficient of reflection on frequency is measured and then the frequency dependence of the phase angle of the reflected coefficient is determined with the aid of the Kramers-Kroenig relation, after which the real and imaginary parts of permittivity  $\epsilon'(\omega)$  and  $\epsilon''(\omega)$  (or refraction coefficient) are computed.

By way of example we will examine in greater detail crystals with the perovskite structure. According to the dynamic theory of the crystal lattice, the total number of normal vibrations is  $3n$  (where  $n$  is the number of atoms in the elemental nucleus). In crystals with the  $ABO_3$  structure this number is 15, of which 12 are optical vibrations<sup>1</sup>. Considering, however, symmetry for the wave vector  $k = 0$  in the infrared spectrum of cubic crystals with the perovskite structure, only three normal vibrations of the type  $F_{1u}(xyz)$  should be observed. On conversion to the tetragonal phase these three bands should expand into doublets and, moreover, yet another band should appear, corresponding to one of the separation components of vibration of the type  $F_{2u}(xyz)$ . In the rhombic phase there should be 12 absorption bands. Considering the direction of  $k$ , the vibrations are separated into  $n$  longitudinal and  $2n$  transverse vibrations, the frequencies of which differ. Therefore there should be extra lines in the combination scatter spectra, corresponding to longitudinal vibrations.

The infrared spectra of ferroelectrics of the perovskite type were analyzed [10-21]. The reflection spectra of monocrystals and polycrystalline specimens of  $BaTiO_3$ ,  $SrTiO_3$  and certain other compounds were analyzed [13, 15, 18] on the basis of the Kramers-Kroenig relations and dispersion theory, and satisfactory agreement was obtained between the theoretical and experimental results. The anomalous temperature dependence of the lowest frequency vibration was first discovered during analysis of the reflection spectra of  $SrTiO_3$  [12]. At room temperature it lies in the  $100\text{ cm}^{-1}$  region, and at  $93^\circ\text{K}$  in the  $50\text{ cm}^{-1}$  region. This vibration is a ferroactive mode, predicted by theory, and the two-fold reduction of temperature corresponds to a four-fold increase in permittivity, so that the relation  $\omega_{T0} = A(T - \theta)^{1/2}$  is satisfied.

$BaTiO_3$  at a low temperature in the paraelectric phase also displays a change of frequency of ferroactive vibration, satisfying this relation, and there is an increase in the force of the oscillator and degree of

---

<sup>1</sup>This analysis does not take into account the separation of dipole frequencies by the macroscopic field. See Chapter 6 for more thorough analysis.

anharmonicity [15, 16]. The frequency dependence of  $\epsilon'$  and  $\epsilon''$  of  $\text{BaTiO}_3$  monocrystals is illustrated in Figure 9.11 for various temperatures [16]. However, quantitative estimates of  $\omega_{\text{TO}}$  depend on the assumptions made in the calculation and differ about three-fold in [13, 16, 17]. We will note that from analyses of infrared spectra of barium titanate [13, 16, 17] it follows that the ferroactive mode is damped due to great attenuation.

The temperature dependence of the frequency of the ferroactive mode in  $\text{KTaO}_3$  was recently measured [21] by means of determining the total conductivity from infrared reflection spectra. Its frequency changes from  $106 \text{ cm}^{-1}$  at  $463^\circ\text{K}$  to  $26 \text{ cm}^{-1}$  at  $12^\circ\text{K}$ . The temperature dependence of the square frequency of this transverse optic mode and  $1/\epsilon$  were found to be in satisfactory quantitative agreement.

The estimate for  $\text{BaTiO}_3$  showed that ferroactive vibration governs more than 90% of the entire polarization of the crystal and the biggest contribution to overall polarization comes from the electron polarization of ions. Thus, ferroactive vibration in crystals of the perovskite type is of complex electron-ion character. Theories on the dependence of zonal electron structure of crystals on the displacements of atoms are now developed [22, 23]. In titanates with the perovskite structure the size of the slot between the 2p-zone of oxygen ions and 3d-zone of titanium ions for the most part should depend on the displacements of ions, and vibrations of ions change the overlapping of p-orbits of oxygen with the 3d-orbits of titanium, which is adiabatically adjusted to the vibration of the lattice. In accordance with theoretical concepts of the nature of antiferroelectricity a low-frequency vibration, governing about 90% of all polarization, was also discovered during analysis of the infrared spectrum of the antiferroelectric  $\text{PbZrO}_3$ . Until recently, however, the temperature dependence of the vibration spectra of antiferroelectrics was not analyzed, even though such analyses are unquestionably of great importance.

Several works pertain to analyses of the infrared spectra of ferroelectrics with hydrogen bonds, in particular  $\text{KH}_2\text{PO}_4$  and triglycine sulfate [25-27]. The reflection spectra of  $\text{KH}_2\text{PO}_4$  [25], like the transmission spectra in the  $10\text{-}100 \text{ cm}^{-1}$  range, show an eroded band, shifting as the temperature drops toward the Curie point in the direction of lower frequencies. This low-frequency vibration is apparently related to the ferroelectric properties of  $\text{KH}_2\text{PO}_4$ . Triglycine sulfate [25] does not display this low-frequency vibration.

Analyses of the infrared spectra of ferroelectrics with the order-disorder phase transition yield information concerning the character of motion of polar groups. It was concluded [28], in particular, that the  $\text{NO}_2$  anion in sodium nitrate revolves around the a axis, but has extreme difficulty in rotating around the c axis.

## §2. Combination Scatter Spectra

In the combination scatter spectra of crystals with the perovskite structure the first order spectrum is forbidden in the cubic phase by the rules of selection. Analyses of the combination scattering in ferroelectrics are very difficult due to the proximity of the lines of ferroactive vibrations to the exciting line and their blurring, which conforms with the theoretical predictions [29-31]. Analyses of combination scattering of barium titanate were carried out in [32-37]. BaTiO<sub>3</sub> monocrystals were analyzed [34] in the 4-475°K temperature range. The appearance of several lines, depending on temperature in the vicinities of the phase transition, is noted, related, perhaps, to the increase of domains.

It can be assumed that certain lines found in early works on combination scattering can also be attributed to the presence of domains. One of the vibrations that strongly depends on temperature is interpreted in [34] as a longitudinal mode.

A ferroactive mode was recently observed in barium titanate crystals by means of Raman scattering, in the form of a broad nonresonance band [35, 36]. Careful analyses [36] were done rather good single-domain crystals. The attenuation and frequency of this mode, corresponding to low attenuation [36] were calculated and found to be in good agreement with the results of infrared spectral analyses [17].

Presented below are frequency  $\omega_{TO}$  and attenuation  $\Gamma$  of the ferroactive mode in barium titanate at difference temperatures [36]:

T, °C	$\omega_{TO}$ , cm <sup>-1</sup>	$\Gamma$
10	34 ± 3	1 ± 0.1
30	39 ± 4	1.2 ± 0.2
60	50 ± 8	1.8 ± 0.3

These results, along with the results of infrared spectral analyses, show that the ferroactive mode is damped in barium titanate [13, 16, 17]. However, the question of its attenuation is not conclusively settled. In [37] there is considerably less attenuation of this mode and no damping at all. The analogous conclusion concerning the relatively slight attenuation in the paraelectric phase was made on the basis of neutron radiography (see below). There is great divergence between the frequencies found in various works for this mode (about three-fold in [36] and [37]).

Investigations of combination scattering in the presence of an electric field were undertaken recently. The application of an electric field to perovskite crystals in the cubic phase leads to the disappearance of the center of symmetry and consequently makes it possible to observe the first order spectrum. The combination scattering in SrTiO<sub>3</sub> and KTaO<sub>3</sub> crystals in the paraelectric phase was investigated in [38] as a function of field strength. The temperature dependence of the frequency of the

ferroactive mode of  $\text{KTaO}_3$  in different fields is illustrated in Figure 15.1. Strengthening of the electric field leads to an increase in the frequency of the ferroactive mode, which is related to the nonlinearity of permittivity: reduction of  $\epsilon$  in the presence of a field agrees with the observed increase in the frequency of the ferroactive mode.

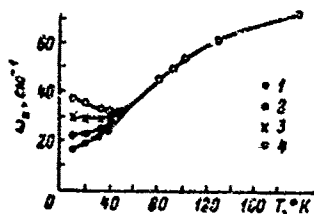


Figure 15.1. Temperature dependence of frequency of parallel component of ferroactive mode at different electric field strengths (field in direction  $[001]$ ) in  $\text{KTaO}_3$  crystals (according to Fleury and Worlock [38]). Electric field: 1 -- 1,000 V/cm; 2 -- 5,000 V/cm; 3 -- 10,000 V/cm; 4 -- 15,000 V/cm.

to strong anharmonism and unordering of the lattice in the paraelectric phase. The bands corresponding to frequencies 155 and 188  $\text{cm}^{-1}$  are shifted near the Curie point 19 and 11  $\text{cm}^{-1}$ , respectively, toward the low-frequency region. An attempt is made in Chapter 6 to interpret the vibration spectrum of  $\text{KH}_2\text{PO}_4$  in the low-frequency range [41].

The results of combination spectral analyses [42-44] and infrared spectral analyses [28] of  $\text{NaNO}_2$  indicate that inversion of  $\text{NO}_2^-$  anions into the mirror configuration on transition to the disordered state is improbable, and also are evidence for their rotation around the a axis. Actually, rotation of the  $\text{NO}_2^-$  ion around the a axis should lead to substantial change in line component intensity corresponding to perfectly symmetric vibration of the anion with field vector  $E \parallel b$  and  $E \parallel c$ . Reduction of the intensity of the component with  $E \parallel c$  and increase of intensity with  $E \parallel b$  were actually observed experimentally [43].

Also observed in [42-44] were an anomalous reduction of frequency and increase in the half-width of one of the lines in the region of the Curie point (Figure 15.2). This line lies in the vicinity of 153  $\text{cm}^{-1}$  and corresponds to orientation vibration of the  $\text{NO}_2^-$  anion around the a axis. Orientation vibration of anions around the a axis is presumably ferroactive vibration. The amount of reduction of the frequency of this vibration,

Analysis of the combination scatter spectra of  $\text{KH}_2\text{PO}_4$  and  $\text{NH}_4\text{H}_2\text{PO}_4$  crystals [39] revealed a line in the 34  $\text{cm}^{-1}$  region at room temperature, shifted toward the exciting line by approximately 2  $\text{cm}^{-1}$  near the Curie point. Analyses of the combination spectrum of  $\text{KH}_2\text{PO}_4$

at various temperatures are described in [40]. A frequency shift, narrowing and separation of lines were noted on transition through the Curie point. A wide band of the continuous spectrum was observed near 120  $\text{cm}^{-1}$ . When the crystal cools, the band narrows and its intensity decreases, and at 100°K the band disappears. The authors consider [40] that the great width of the band is related

however, is not enough to explain the high value of  $\epsilon$  near the Curie point.

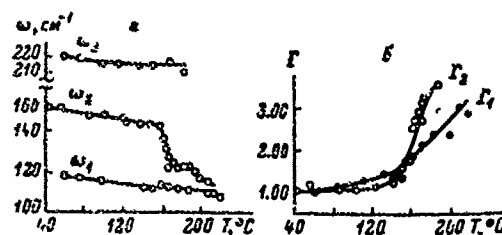


Figure 15.2. Temperature dependence (Chisler and Shur [44]). a -- frequencies of combination scatter spectrum of NaNO<sub>2</sub> in low-frequency range ( $\omega_1$  is orientation vibration of NO<sub>2</sub><sup>-</sup> around "b" axis,  $\omega_2$  is orientation vibration of NO<sub>2</sub><sup>-</sup> around "a" axis,  $\omega_3$  is orientation vibration of NO<sub>2</sub><sup>-</sup> around "c" axis): b -- half-widths of bands  $\omega_1 - \Gamma_1$ ,  $\omega_2 - \Gamma_2$ .

Ferroactive modes of vibrations in the investigated crystals were not observed in analyses of the combination spectra of NH<sub>4</sub>SO<sub>4</sub>, NH<sub>4</sub>HSO<sub>4</sub>, RbHSO<sub>4</sub>, TGS and NaNO<sub>2</sub> [45-48].

### §3. Inelastic Scattering of Slow Neutrons

Extremely interesting results concerning the investigation of crystal lattice dynamics are obtained with the aid of inelastic scattering of slow neutrons. The change of neutron energy in inelastic scattering yields information concerning the vibration spectrum of a diffusing crystal, where the neutrons are "active" in relation to all vibrations with any  $k$ , both optic and acoustic.

During coherent scattering of neutrons on monocrystals in each given direction and with given wave vector  $k$ , a discrete spectrum is obtained on the background of the continuous spectrum from incoherent and multiphonon scattering. Dispersion curves  $\omega(k)$  can be plotted from these data when the spectra are recorded under various conditions.

During incoherent scattering of neutrons by polycrystals a continuous spectrum is obtained, from which the actual frequency distribution function  $G(\omega)$  can be obtained.

The "flat" segments of the optic and acoustic branches, where many vibrations with various  $k$  fall into a rather narrow frequency range, contribute substantially to scattering. Therefore the contribution to the spectrum by the low-frequency optical branch will be distributed through a rather wide frequency interval and its separation poses substantial difficulties.

Thus, the most valuable information concerning ferroactive vibrations is acquired by analyzing monocrystals (see [49, 50] concerning the interaction of slow neutrons with a substance and experimental procedures).

Inelastic scattering of neutrons on polycrystalline specimens of  $\text{BaTiO}_3$  [51, 52] and also  $\text{PbTiO}_3$  and  $\text{SrTiO}_3$  [52], does not display substantial anomalies on transition through the Curie point. The peaks in the frequency region below  $100 \text{ cm}^{-1}$  are apparently related to acoustic vibrations of the lattice.

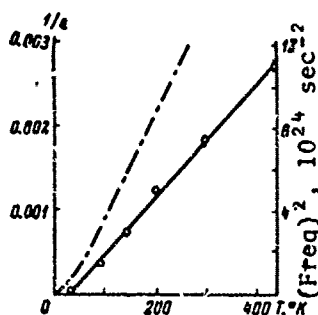


Figure 15.3. Temperature dependences of square of the frequency of soft transverse optic mode and  $1/\epsilon$  (dot-dash curve) in strontium titanate (Cowley [53]).

Cowley [53], with the aid of inelastic coherent scattering of neutrons, analyzed monocrystals and plotted the dispersion curves for certain normal vibrations in  $\text{SrTiO}_3$ , propagating in direction [001]. He found a peak of inelastic scattering of neutrons in this crystal, related to low-frequency coherent optic vibration for  $k \rightarrow 0$ . The temperature dependences of the square of the frequency of this mode and  $1/\epsilon$  are illustrated in Figure 15.3 ( $\epsilon$  is taken from [54, 55]).

As seen in Figure 15.3, the square of the frequency of the ferroactive mode is a linear function of temperature  $\omega_{\text{TO}}^2 = K(T - \theta)$ , which verifies the validity of Cochran's assumption [6]. An interesting hypothesis was also propounded concerning the nature of the phase transition in  $\text{SrTiO}_3$  at  $110^\circ\text{K}$ , which in Cowley's opinion [53] is a result of random degeneration of the ferroactive branch of the transverse optic vibrations and longitudinal acoustic branch. Such degeneration should lead to an anomalous temperature dependence of elastic constants and velocity of ultrasound, as observed experimentally [56].

The soft optic mode was analyzed [57] with the aid of the inelastic scattering of neutrons in  $\text{KTaO}_3$  monocrystal. The soft optic mode was also recently detected with the aid of inelastic scattering of neutrons in  $\text{BaTiO}_3$  monocrystal in the paraelectric phase [58]. The soft transverse optic mode in  $\text{BaTiO}_3$  has a lower frequency than even the transverse acoustic mode, aside from the region of small  $k$  [58]. Identification of the modes in the region of "intersection" of the acoustic and optic branches is apparently inconclusive. The energy of the soft mode decreases as the temperature drops from 1.4 MeV at  $430^\circ\text{C}$  to 0.8 MeV at  $230^\circ\text{C}$ , and here the relation  $\hbar^2 \omega_{\text{TO}}^2 = A \cdot 10^4 / \epsilon = B(T - \theta)$  is valid.

11 MeV is equal to  $8.07 \text{ cm}^{-1}$

In  $\text{BaTiO}_3$   $A \sim 0.11 \text{ MeV}^2$ , whereas in  $\text{SrTiO}_3$   $A \sim 3.7 \text{ MeV}^2$  [12, 53] and in  $\text{KTaO}_3$   $A \sim 2.8 \text{ MeV}^2$  [21, 57].

Analysis of inelastic incoherent scattering of neutrons was done on polycrystalline specimens of a number of hydrogen- and deuterium-containing ferroelectrics. The results the investigation of  $\text{KH}_2\text{PO}_4$  and  $\text{KD}_2\text{PO}_4$  are discussed in [59-61];  $(\text{NH}_4)_2\text{SO}_4$ ,  $\text{NH}_4\text{HSO}_4$ ,  $(\text{NH}_4)_2\text{ReF}_4$  and  $\text{K}_4\text{Fe}(\text{CN})_6 \cdot 5\text{H}_2\text{O}$  are discussed in [62]. However, no notable changes that could be related to ferroactive low-frequency modes, were observed in the neutron spectra at the Curie point. This is a result primarily of the structural complexity of these ferroelectrics and of the fact that the investigations were conducted on polycrystalline specimens.

It should be pointed out that the study of low-frequency vibrations in ferroelectrics with the order-disorder type of phase transition is very important. New proof is being found at this time that these transitions are not of purely relaxation character and are related not only to the ordering of "ready" dipole moments, but also to displacements of ions, leading to rearrangement of the lattice. Therefore, experimental determination of the modes of vibrations that cause the ferroelectric phase transition will help to solve the problem of the nature of spontaneous polarization in these crystals.

#### §4. Thermal Diffusive Scattering of X-rays and Electrons

New data were obtained recently concerning the vibrations of the barium titanate lattice through analyses of the thermal diffusive scattering of x-rays [63, 64] and electrons [65]. In the diffraction pattern for barium titanate monocrystals, in addition to the diffraction spots near the reciprocal lattice points and diffraction bands, which are the result of acoustic vibrations of the lattice, there are also diffraction bands caused by ferroactive low-frequency transverse optic vibrations. Here the ferroactive vibrations have low frequency all the way to short wavelengths.

The frequency was estimated with the aid of the known dependence -- of inverse proportionality of the intensity of thermal diffusive scattering to the square of the frequency of the vibrations causing it. It turned out that in the region  $k/k_{\text{max}} \approx 0.4$ , the frequency was  $\sim 10^{12} \text{ sec}^{-1}$ .

The experimentally observed modulation of band intensity in the space of the reciprocal lattice can be explained on the basis of the assumption that the ferroactive vibration corresponds to displacements of the cations of barium and titanium to one side and of oxygen atoms OI and OII to the opposite side. This configuration of displacements "freezes" on transition to the tetragonal ferroelectric phase. The concept of "freezing" of the ferroactive vibration in the ferroelectric phase is also encountered in Cochran's work [4]. The configuration of displacements of ions in the ferroactive mode according to [63, 64] agrees with certain structural data

or the displacements of ions in tetragonal barium titanate, obtained with the aid of x-ray and neutron radiography, specifically with Evans' first model of displacements [65] and the model of Frazer, et al [67].

Efforts have been made in a number of works to determine the form of normal vibrations by relating them to vibrations of certain groups of atoms. Thus, it was assumed [10-12, 15] that two high-frequency vibrations of the  $F_{1u}$  type correspond to internal vibrations of the  $TiO_6$  octahedron, and the low-frequency vibration to vibration of cation A relative to the octahedron. It is now clear however, that in this vibration there are very substantial relative displacements of Ti and O atoms [18, 53, 63, 64], which is in better agreement with model theories and crystallochemical concepts of the nature of ferroelectricity in barium titanate.

Another important result of analyses of the diffusive scattering of x-ray [64] was the discovery of anisotropy of the frequency of ferroactive vibrations in the tetragonal phase: the frequency of vibration on the a axis was lower than on the c axis. This agrees satisfactorily with the fact that permittivity is greater on the a axis than on the c axis. According to Cochran's theory, indeed,  $\epsilon/\epsilon_\infty = \prod_i (v_i^{LO}(0)/v_i^{TO}(0))$ , where  $v_i^{LO}(0)$  and  $v_i^{TO}(0)$  are the frequencies of longitudinal and transverse optic vibrations with zero wave vector. Consequently the frequency of the transverse optic vibration on the a axis should be lower than on the c axis, which is observed experimentally.

Thus, experimental analyses of the vibrations of the crystal lattice of ferroelectric crystals have verified the validity of the basic concepts of dynamic theory [1-6]. The presence of the low-frequency ferroactive mode is also substantiated by investigations of the Mossbauer effect (see Chapter 14) and by investigations of the dielectric properties of ferroelectrics in the UHF range (see Chapter 9). The approach to the ferroelectric phase transition from the point of view of the instability of the crystal lattice in relation to the transverse optic mode with a low wave vector is very fruitful and has stimulated the extensive development of research in various branches of solid state physics.

Experimental dispersion relations between the frequency and wave vector of certain modes make it possible to determine a number of constants of dynamic theory. Thus, on the basis of the dispersion curve of the ferroactive mode in strontium titanate, obtained from neutron radiography, a model of rigid ions and a shell model were calculated for various parameters in a harmonic approximation [53]. The use of harmonic approximation, however, involves a number of difficulties: negative values of short-term polarization, overstated values of polarization of positive ions, etc. The chief difficulty is the inability to explain the temperature dependence of the frequency of the ferroactive mode. This temperature dependence is attributed to anharmonic interaction between modes.

Several attempts have been made recently to take anharmonicity into account by introducing to the theory the parameters of interaction between modes, determined from experimental data [68, 69]. A model with two parameters of anharmonic interaction between titanium and oxygen, determined from experimental data on the basis of thermal expansion and the temperature dependence of the frequency of the ferroactive mode, is proposed in [69]. This made it possible to bring the theoretical results and experimental data on infrared reflection, neutron scattering, etc. into better agreement. As regards further development of the theory that takes into account anharmonic effects, experimental data on the dispersion relations for normal modes of vibrations in the different crystallographic directions are important.

The state of dynamic theory is described in detail in Chapter 5.

#### BIBLIOGRAPHY

1. Ginzburg, V. L., UFN [Usp'ekhi fizicheskikh nauk; Progress of Physical Sciences], Vol. 38, p. 430, 1949; ZhETF [Zhurnal eksperimental'noy teoreticheskoy fiziki; Journal of Experimental and Theoretical Physics], Vol. 19, p. 36, 1949.
2. Ginzburg, V. L., FTT [Fizika tverdogo tela; Solid State Physics], Vol. 2, p. 2031, 1960.
3. Ginzburg, V. L., UFN, Vol. 77, p. 621, 1962.
4. Ginzburg, V. L., ZhETF, Vol. 39, p. 192, 1960.
5. Anderson, P., Fizika Dielektrikov (Physics of Dielectrics), USSR Academy of Sciences Publishing House, Moscow, p. 290, 1960.
6. Cochran, W., Adv. Phys., Vol. 9, p. 387, 1960; Vol. 10, p. 401, 1961.
7. Silverman, B. D., Phys. Rev., Vol. 135, A1596, 1964.
8. Murzin, V. N., P. Ye. Pasyukov and S. P. Solob'yev, UFN, Vol. 92, p. 427, 1967.
9. Silverman, B. D., Proc. intern. Meet. Ferroelectr., Vol. 1, Prague, p. 3, 1966.
10. Last, J. T., Phys. Rev., Vol. 105, p. 1740, 1957.
11. Yatsenko, A. F., AN SSSR, ser. fiz. (News of USSR Academy of Sciences, Physics Series), Vol. 22, p. 1456, 1958.
12. Barker, A. S. and M. Tinkham, Phys. Rev., Vol. 125, p. 1527, 1962.

13. Spitzer, W. G., K. C. Miller, D. A. Kleinman and L. E. Howarth, *Phys. Rev.*, Vol. 126, p. 1710, 1962.
14. Ikegami, S., J. Ueda and S. Kisaka, *J. Phys. Soc. Japan*, Vol. 17, p. 1210, 1962.
15. Murzin, V. N. and A. I. Demeshina, *FTT*, Vol. 5, p. 2359, 1963; Vol. 6, p. 182, 1964; *Izv. AN SSSR, ser. fiz.*, Vol. 28, p. 695, 1964.
16. Ballantyne, J. M., *Phys. Rev.*, Vol. 136, A429, 1964.
17. Barker, A. S., *Phys. Rev.*, Vol. 145, p. 391, 1966.
18. Murzin, V. N., A. I. Demeshina and S. V. Bogdanov, *FTT*, Vol. 6, p. 3372, 1964.
19. Murzin, V. N., A. I. Demeshina and S. V. Bogdanov, *Izv. AN SSSR, ser. fiz.*, Vol. 29, p. 290, 1965.
20. Stekhanov, A. I., A. A. Karamyan and N. I. Astaf'yev, *FTT*, Vol. 7, p. 157, 1965.
21. Perry, C. H. and T. F. McNelly, *Phys. Rev.*, Vol. 154, p. 456, 1967.
22. Kahn, A. H. and A. J. Leyendecker, *Phys. Rev.*, Vol. 135, A1324, 1964.
23. Brews, J. R., *Phys. Rev. Lett.*, Vol. 18, p. 662, 1967.
24. Perry, C. H., D. J. Carthy and G. Rupprecht, *Phys. Rev.*, Vol. 138, A1537, 1965.
25. Barker, A. S. and M. Tinkham, *J. Chem. Phys.*, Vol. 38, p. 2257, 1963.
26. Aref'yev, I. M., P. A. Bazhulin and T. V. Mikhal'tseva, *FTT*, Vol. 7, p. 2412, 1965; I. M. Aref'yev and P. A. Bazhulin, *FTT*, Vol. 7, p. 401, 1965.
27. Aref'yev, I. M., P. A. Bazhulin and I. S. Zhefudev, *FTT*, Vol. 7, p. 2834, 1965.
28. Sato, Y., K. Gesi and Y. Takagi, *J. Phys. Soc. Japan*, Vol. 16, p. 2172, 1961.
29. Ginzburg, V. L. and A. P. Levanyuk, *ZhETF*, Vol. 39, p. 112, 1960.
30. Ginzburg, V. L., *UFN*, Vol. 77, p. 621, 1962.
31. Ginzburg, V. L. and A. P. Levanyuk, *Pamyati G. S. Landsberga (Memoirs of G. S. Landsberg)*, USSR Academy of Sciences Publishing House, Moscow, p. 104, 1959.

32. Bobovich, L. S. and E. V. Bursian, Opt. i Spektrosk. (Optics and Spectroscopy), Vol. 11, p. 131, 1961.
33. Ikegami, S., J. Phys. Soc. Japan, Vol. 19, p. 46, 1964.
34. Perry, C. H., D. B. Hall, Phys. Rev. Lett., Vol. 15, p. 700, 1965.
35. Pinczuk, A., W. Taylor, E. Burstein and I. Lefkowitz, Sol. St. Comm., Vol. 5, p. 429, 1967.
36. DiDomenico, M., S. P. S. Porto, and S. H. Wemple, Phys. Rev. Lett. Vol. 19, p. 855, 1967; M. DiDomenico, S. H. Wemple, S. P. S. Porto and R. P. Bauman, Phys. Rev., Vol. 174, p. 522, 1968.
37. Rimai, L., J. L. Parsons, J. T. Hickmott and T. Nakamura, Phys. Rev., Vol. 168, p. 623, 1968.
38. Fleury, P. A. and J. M. Worlock, Phys. Rev., Vol. 174, p. 613, 1968.
39. Aref'yev, I. M. and P. A. Bazhulin, FTT, Vol. 7, p. 407, 1965.
40. Stekhanov, A. I. and Ye. A. Popova, FTT, Vol. 10, p. 415, 1968.
41. Shur, M. S., Izv. AN SSSR, ser. fiz., Vol. 31, p. 1042, 1967.
42. Chisler, E. V. and M. S. Shur, Phys. St. Sol., Vol. 17, p. 163, 1966; Vol. 17, p. 173, 1966.
43. Chisler, E. V. and M. S. Shur, FTT, Vol. 9, p. 1015, 1967.
44. Chisler, E. V. and M. S. Shur, Izv. AN SSSR, ser. fiz., Vol. 31, p. 1098, 1967.
45. Bazhulin, P. A., T. P. Myasnikova and A. V. Rakov, FTT, Vol. 5, p. 1783, 1963.
46. Stekhanov, A. I. and V. A. Gabrichidze, FTT, Vol. 5, p. 3105, 1963.
47. Gorelik, V. S., I. S. Zheludev and M. M. Sushchinskiy, Kristallografiya (Crystallography), Vol. 11, p. 604, 1966.
48. Arbatskaya, A. N., I. S. Zheludev, U. A. Zirnin and M. M. Sushchinskiy, Kristallografiya, Vol. 10, p. 335, 1965.
49. Gurevich, I. I. and L. V. Tarasov, Fizika Neytronov Nizkikh Energiy (Physics of Low-Energy Neutrons), "Nauka" Publishing House, Moscow, 1965.
50. Frockhouse, B. N., D. B. Woods, G. Dolling and J. M. Thorson, Proc. Third Conf. Peace Employment Atom. Energy, Geneva, 1960.

51. Pelah, I. and I. I. Lefkowitz, Inelastic Scattering of Neutrons, IAEA, Vienna, p. 601, 1961.
52. Solov'yev, S. P., O. L. Kukhto, N. A. Chernoplakov and I. G. Zemlyanov, FTT, Vol. 8, p. 2699, 1965.
53. Cowley, R. A., Phys. Rev., Vol. 134, A981, 1964.
54. Mitsui, T. and W. B. Westphal, Phys. Rev., Vol. 124, p. 354, 1961.
55. Weaver, H. E., J. Phys. Chem. Sol., Vol. 11, p. 274, 1959.
56. Bell, R. C. and G. Rupprecht, Phys. Rev., Vol. 129, p. 90, 1963.
57. Shirane, G., R. Nathans and V. J. Minkiewicz, Phys. Rev., Vol. 157, p. 396, 1967.
58. Shirane, G., B. C. Frazer, V. J. Minkiewicz, J. A. Leake and A. Linz, Phys. Rev. Lett., Vol. 19, p. 234, 1967.
59. Palevsky, H., K. Otens and Y. Wakuta, Inelastic Scattering of Neutrons, IAEA, Vienna, Vol. 2, p. 273, 1964.
60. Wakuta, Y., J. Phys. Soc. Japan, Vol. 18, p. 672, 1963.
61. Pelah, I., E. Wiener and J. Imry, Inelastic Scattering of Neutrons, IAEA, Vienna, p. 325, 1965.
62. Rush, J. J. and T. J. Taylor, Inelastic Scattering of Neutrons, IAEA, Vienna, p. 333, 1965.
63. Harada, J., M. Watanabe, S. Kodera and G. Honjo, J. Phys. Soc. Japan, Vol. 20, p. 630, 1965.
64. Harada, J. and G. Honjo, J. Phys. Soc. Japan, Vol. 22, p. 45, 1967.
65. Harada, J., M. Tanaka and G. Honjo, J. Phys. Soc. Japan, Vol. 21, p. 968, 1966.
66. Evans, H. T., Acta Cryst., Vol. 14 p. 1019, 1961.
67. Frazer, B. C., H. R. Danner and R. Pepinsky, Phys. Rev., Vol. 100, p. 745, 1955.
68. Barker, A. S. and J. J. Hopfield, Phys. Rev., Vol. 135, A1732, 1964.
69. Cowley, R. A., Phil. Mag., Vol. 11, p. 673, 1965.

## CHAPTER 16. FERROELECTRICS WITH BLURRED PHASE TRANSITION

### §1. Fundamental Properties

Analysis of the physical properties of polycrystalline specimens of solid solutions  $\text{Ba}(\text{Ti}, \text{Sn})\text{O}_3$  [1, 2] revealed strong blurring of  $\epsilon$  peaks in the ferroelectric phase transitions of solid solutions with a high concentration of  $\text{BaSnO}_3$  (Figure 16.1). The existence of piezoelectric vibrations in prepolarized specimens at temperatures considerably higher (tens of degrees) than the temperature of the  $\epsilon$  peaks, was also brought to attention there. In these respects the given solid solutions differed substantially from barium titanate, where the piezoelectric vibrations ceased on approaching maximum  $\epsilon$ . The theory of noncurrent passage of the ferroelectric phase transition in different parts of a crystal when heated, due to internal stresses and fluctuations of composition, was advanced in [2]. By fluctuations of composition we mean deviations of the concentration of  $\text{BaSnO}_3$  in microregions from the average concentration, which inevitably occur in the statistical distribution of Ti and Sn ions in the octahedral nodes of the perovskite lattice. These composition fluctuations are presumably in the "frozen" state at room temperature. Because of the dependence of the Curie point on composition, various microregions of the crystal experience the phase transition at different temperatures.

The analogous phenomena were also observed in solid solutions of  $\text{Ba}(\text{Ti}, \text{Zr})\text{O}_3$  [3]. It was found that in the case of solid solutions of  $(\text{Ba}, \text{Sr})\text{TiO}_3$  (at high  $\text{SrTiO}_3$  concentrations), piezoelectric vibrations of prepolarized polycrystalline specimens may also occur at temperatures above the temperature of peak permittivity [4, 5], although the  $\epsilon$  peaks remain rather sharp [6].

Somewhat later unusual dielectric properties were discovered in  $\text{PbMg}_{1/3}\text{Nb}_{2/3}\text{O}_3$  and  $\text{PbNi}_{1/3}\text{Nb}_{2/3}\text{O}_3$  [7]. The permittivities of both compounds were high and passed through peaks: in the case of  $\text{PbNi}_{1/3}\text{Nb}_{2/3}\text{O}_3$  -- through a rather fat one, and in the case of  $\text{PbMg}_{1/3}\text{Nb}_{2/3}\text{O}_3$  through a sharper peak

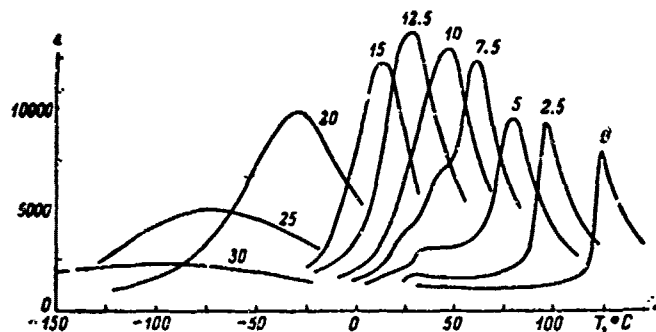


Figure 16.1. Temperature dependence of permittivity of solid solutions  $\text{BaTiO}_3\text{-BaSnO}_3$  in weak fields: at frequency of 1 kHz. The numbers near the curves indicate the concentration of  $\text{BaSnO}_3$  in mole %. (According to Smolenskiy and Isupov [2]).

(Figure 16.2). At lower temperatures  $\text{PbMg}_{1/3}\text{Nb}_{2/3}\text{O}_3$  did not display a dielectric hysteresis loop (Figure 16.3), and  $\text{PbNi}_{1/3}\text{Nb}_{2/3}\text{O}_3$  displayed a strong displacement of the  $\epsilon$  peak (and the  $\tan \delta$  peak corresponding to it) toward higher temperatures as the frequency of the measurement field was increased (Figure 16.2). Later on [8] dielectric hysteresis loops were found in  $\text{PbNi}_{1/3}\text{Nb}_{2/3}\text{O}_3$  (Figure 16.4) and also displacement of the temperature of the  $\epsilon$  peak with increasing field frequency in  $\text{PbMg}_{1/3}\text{Nb}_{2/3}\text{O}_3$  (Figure 16.5). Thus, both compounds are ferroelectrics, but they also manifest properties that are unusual for previously known ferroelectrics, since the position of the peak on the curve  $\epsilon = f(T)$  depends on their frequency.

The properties of polycrystalline  $\text{PbMg}_{1/3}\text{Nb}_{2/3}\text{O}_3$  and  $\text{PbNi}_{1/3}\text{Nb}_{2/3}\text{O}_3$  are analyzed in detail in [8] for the purpose of proving their ferroelectric state. As proof of the ferroelectric state of these compounds is examined [8] not only the dielectric hysteresis loop, but also the basic curve  $P = f(E)$ , formed in Figures 16.3 and 16.4 by the vertices of the hysteresis loops. On the basis of the curve in the region of relatively low fields is a discontinuity (i.e., a sort of detached field), characteristic of ferroelectrics. It was determined from the hysteresis loops that spontaneous polarization of  $\text{PbMg}_{1/3}\text{Nb}_{2/3}\text{O}_3$  reaches a high value ( $\sim 14 \cdot 10^{-6} \text{ C/cm}^2$  at  $120^\circ\text{C}$ ) and is nonzero at temperatures higher than the temperature of the  $\epsilon$  peaks. When a stationary field is applied to specimens of both compounds the permittivity measured in the weak field diminishes and the peaks of  $\epsilon$  and  $\tan \delta$  are displaced toward higher temperatures.

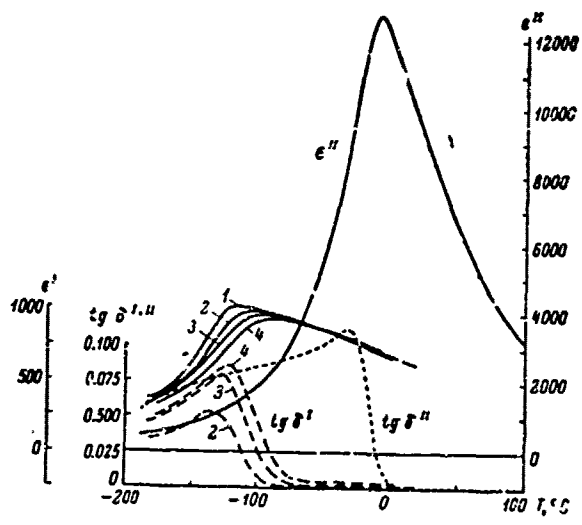


Figure 16.2. Temperature dependences of  $\epsilon$  and  $\tan \delta$  of  $\text{PbNi}_{1/3}\text{Nb}_{2/3}\text{O}_3$  at 1 (1), 45 (2), 450 (3) and 1,500 (4) kHz and of  $\text{PbMg}_{1/3}\text{Nb}_{2/3}\text{O}_3$  at 1 kHz (Smolenskiy and Agranovskaya [7]).

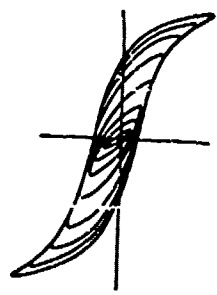


Figure 16.3. Dielectric hysteresis loops of polycrystalline  $\text{PbMg}_{1/3}\text{Nb}_{2/3}\text{O}_3$  at  $-90^\circ\text{C}$  and various electric field intensities ( $E_{\text{max}} = 20 \text{ kV/cm}$ ) (Smolenskiy, et al [8]).

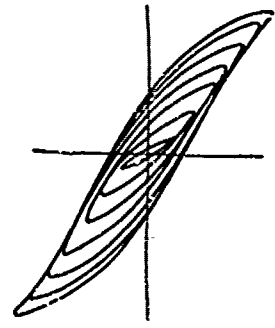


Figure 16.4. Hysteresis loops of polycrystalline  $\text{PbNi}_{1/3}\text{Nb}_{2/3}\text{O}_3$  at  $-196^\circ\text{C}$  at different field intensities ( $E_{\text{max}} = 60 \text{ kV/cm}$ ) (Smolenskiy, et al [8]).

It was possible to excite piezoelectric vibrations in  $\text{PbMg}_{1/3}\text{Nb}_{2/3}\text{O}_3$  specimens placed in a stationary field  $E = 15 \text{ kV/cm}$ . Piezoelectric modulus  $d_{31}$  peaks near  $-20^\circ\text{C}$ , reaching  $-2.5 \cdot 10^{-6} \text{ CGSE}$ . At the very same temperature the coefficient of electromechanical coupling  $k_T$  peaks and the resonance and antiresonance frequencies pass through a minimum. The piezoelectric

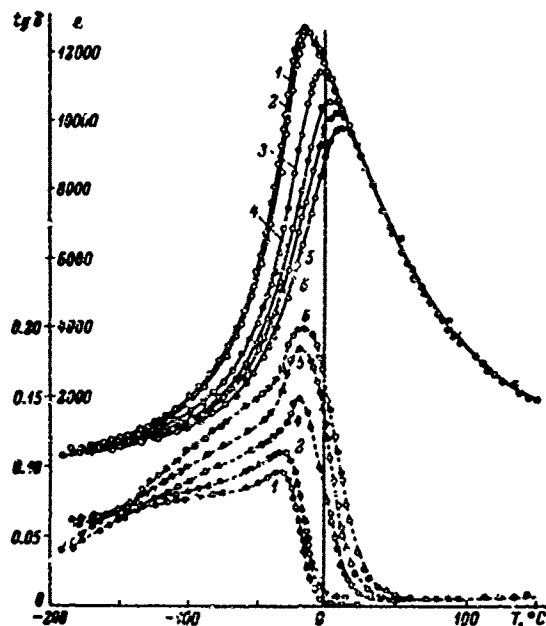


Figure 16.5. Temperature dependence of permittivity (continuous curves) and  $\tan \delta$  (broken curves) of polycrystalline  $\text{PbMg}_{1/3}\text{Nb}_{2/3}\text{O}_3$  in weak fields at different frequencies. (According to Smolenskiy, et al [8]).  
 1 -- 0 kHz; 2 -- 1; 3 -- 45; 4 -- 450; 5 -- 1,500; 6 -- 4,500 kHz.

vibrations exist in a rather broad temperature range above the temperatures of the  $\epsilon$  peaks. In prepolarized (at  $-190^\circ\text{C}$ ) specimens, however, the piezoelectric vibrations at  $E = 0$  vanished, even after heating to  $-60^\circ\text{C}$ . A similar dependence was also noted for  $\text{PbNi}_{1/3}\text{Nb}_{2/3}\text{O}_3$ .

On the curves that depict the temperature dependences of the coefficients of linear expansion there are flat peaks in the temperature range corresponding to the peaks of low-frequency  $\epsilon$ . All this is regarded as verification of the ferroelectric phase transitions in the investigated compounds.

The growth of  $\text{PbMg}_{1/3}\text{Nb}_{2/3}\text{O}_3$  and  $\text{PbNi}_{1/3}\text{Nb}_{2/3}\text{O}_3$  monocrystals and analysis of their properties are described in [9]. The character of the temperature dependence of  $\epsilon$  and  $\tan \delta$  of the monocrystals was the same as for polycrystalline specimens. There was also a displacement of maximum  $\epsilon$  and  $\tan \delta$  toward higher temperatures with increasing frequency.

The temperature dependence of spontaneous polarization and coercive field of  $\text{PbMg}_{1/3}\text{Nb}_{2/3}\text{O}_3$  monocrystals, determined from hysteresis loops, is

illustrated in Figure 16.6. It is clear from the figure that there is no perceptible jump of  $P_s$  in the region of the  $\epsilon$  maxima. Saturation of the loops is not achieved at high temperatures.

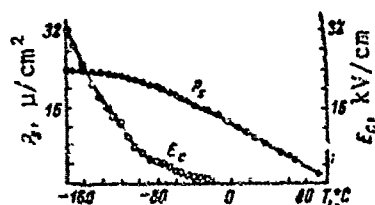


Figure 16.6. Temperature dependence of spontaneous polarization and coercive field of  $\text{PbMg}_{1/3}\text{Nb}_{2/3}\text{O}_3$  monocrystal (according to Bokov and Myl'nikova [9]).

boundaries, however, are indistinct and apparently have great thickness. If the process of repolarization takes place at a sufficiently low temperature, then, by removing the field it is possible to "freeze" the corresponding domain structure. If then, in the absence of a field, the crystal is heated, the visibility of the domains gradually worsens. The boundaries become less distinct. At approximately  $-60^\circ\text{C}$  the entire visible domain structure vanishes and the crystal becomes optically isotropic.

We see in Figure 16.7, where the temperature dependence of the birefringence of a polarized  $\text{PbMg}_{1/3}\text{Nb}_{2/3}\text{O}_3$  crystal in the absence of a field is represented, that when heated up to  $-60^\circ\text{C}$  the crystal is almost entirely depolarized.

Analysis of polycrystalline specimens and monocrystals of  $\text{PbMg}_{1/3}\text{Nb}_{2/3}\text{O}_3$  in a broad frequency range [10] showed that the displacement of the peak on the curve  $\epsilon = f(T)$  with increasing frequency, which occurs at radio frequencies, ceases in the UHF range (Figure 16.8).

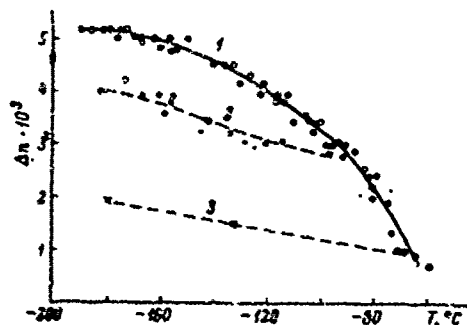


Figure 16.7. Temperature dependence of birefringence of field-cooled  $\text{PbMg}_{1/3}\text{Nb}_{2/3}\text{O}_3$  monocrystal (Bokov and Myl'nikova [9]). Curve 1 plotted for heating without field, curves 2 and 3 for cooling from  $-90$  and  $-60^\circ\text{C}$ .

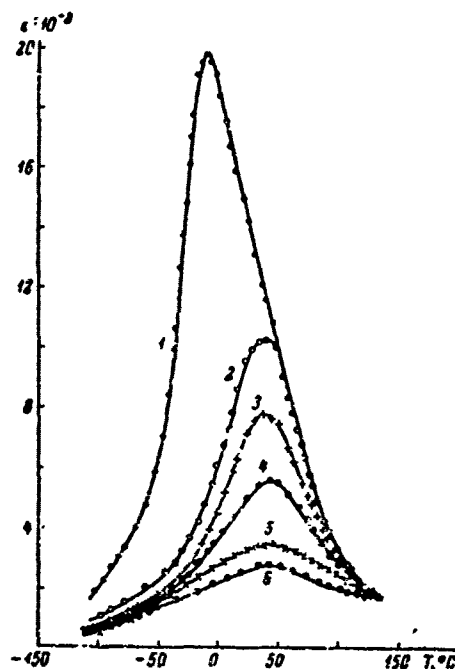


Figure 16.8. Temperature dependence of permittivity of  $\text{PbMg}_{1/3}\text{Nb}_{2/3}\text{O}_3$  monocrystal at different frequencies (according to Khuchua [10]). 1 --  $10^3$ ; 2 --  $10^8$ ; 3 --  $6.6 \cdot 10^8$ ; 4 --  $10^9$ ; 5 --  $1.5 \cdot 10^9$ ; 6 --  $2 \cdot 10^9$  Hz.

It is noteworthy that interesting dielectric properties of strontium-bismuth titanates (SBT) have been known for a long time [11, 12]. The permittivity of SBT is high ( $\sim 10^3$ ) and increases with cooling, passing through a flat peak, the position of which depends on the frequency of the probing field. Skanavi [13] classified SBT as nonferroelectric compounds and theorized that the relaxation dielectric polarization of SBT is caused by thermal ionic polarization. Investigations in rather strong electric fields have established, however, that SBT have dielectric hysteresis loops at low temperatures, although by no means saturated, which suggests that the ferroelectric mechanism contributes to some degree to the dielectric polarization of these compounds [4].

Bogdanov disputes the validity of this assumption [15]. He points to the lack of dielectric hysteresis loop saturation and to the failure of attempts to detect the phase transition by the x-ray diffraction method. He also points to the nonlinear dependence of the temperature of the  $\epsilon$  peak on the bismuth titanate concentration, and to the fact that the dependence of the temperature of the  $\epsilon$  peak is strong only at low bismuth titanate concentrations (which makes it difficult to explain the strong blurring of the phase transition at high concentrations). It is emphasized here that

37. E. Fuchs, W. Liesk, J. Phys. Chem. Solids, Vol 25, p 845, (1964).
38. E. V. Shmakov, G. V. Spivak, FTT, Vol 10, p 1016 (1968).
39. C. Bousquet, M. Lambert, A. M. Quittet, A. Guinier, Acta Cryst., Vol 16, p 989 (1963).
40. N. Niizeki, M. Hasegawa, J. Phys. Soc. Japan, Vol 19, p 550 (1964).
41. J. Caslavsky, Czechosl. J. Phys., Vol B14, p 454 (1964).
42. D. R. Callaby, J. Appl. Phys., Vol 36, 2751 (1965).
43. L. A. Shuvalov, K. S. Aleksandrov, I. S. Zheludev, Kristallografiya, Vol 4, P 130 (1959).
44. H. Toyoda, S. Waku, H. Hirabayashi, J. Phys. Soc. Japan, Vol 14, P 1003 (1959).
45. V. P. Konstantinova, I. M. Sil'vestrova, V. A. Yurin, Kristallografiya, Vol 4, p 125 (1959).
46. V. P. Konstantinova, I. M. Sil'vestrova, K. S. Aleksandrov. In the collection: Fizika Dielektrikov [Physics of Dielectrics], Izd. AN SSSR [USSR Academy of Sciences Press, Moscow, p 351 (1960).
47. V. P. Konstantinova, Izv. AN SSSR, ser. fi ., Vol 24, p 1324 (1960).
48. V. P. Konstantinova, Kristallografiya, Vol 7, p 748 (1962).
49. H. Toyoda, J. Phys. Soc. Japan, Vol 14, p 376 (1959).
50. H. Toyoda, J. Phys. Soc. Japan, Vol 15, p 1539 (1960).
51. A. G. Chynoweth, Phys. Rev., Vol 117, p 1235 (1960).
52. A. G. Chynoweth, V. L. Feldman, J. Phys. Chem. Sol., Vol 15, p 225 (1960).
53. V. A. Meleshina, Kristallografiya, Vol 9, p 381 (1964).
54. A. G. Chynoweth, J. L. Abel, J. Appl. Phys., Vol 30, p 1073 (1959).
55. A. G. Chynoweth, J. L. Abel, J. Appl. Phys., Vol 30, p 1515 (1959).
56. V. A. Meleshina, I. S. Zheludev, I. S. Rez. Kristallografiya, Vol 5, p 322 (1960).
57. L. Turel, M. Eimer. Compt. rend., Vol 256, p 642 (1963).
58. T. Nakamura, H. Nakamura, Japan J. Appl. Phys., Vol 1, p 253 (1962).

strontium titanate is not a ferroelectric (not a classic ferroelectric in any case). His arguments, however, are not sufficiently convincing. Actually, not only SBT, but also many other compounds generally recognized to be ferroelectrics, do not display hysteresis loop saturation.

The x-ray diffraction method in the case of ferroelectrics with a blurred phase transition very often does not detect changes in symmetry. The nonlinearity of the dependence of the  $\epsilon$  peak temperature on concentration may be only apparent in connection with the limited range of solubility of bismuth titanate in strontium titanate. (A strong increase in the concentration of bismuth titanate in a specimen may result in only a weak increase of its concentration in solid solution, which leads to termination of the dependence of the  $\epsilon$  peak temperature on concentration). Strontium titanate is actually not a common ferroelectric, but with small additives of  $\text{BaTiO}_3$  (1-2 mole %) to  $\text{SrTiO}_3$ , the ferroelectric properties of the resulting solid solution are unquestionable. Finally, the fact that SBT displays the discontinuity characteristic of ferroelectrics on the initial polarization curve [8] is convincing proof of the ferroelectric properties of SBT. Furthermore, Fritsberg's work [16], pertaining to analysis of solid solutions of  $\text{SrTiO}_3$ - $\text{Bi}_{2/3}\text{TiO}_3$ - $\text{PbTiO}_3$  clearly shows a smooth transition of the  $\epsilon$  maximum in SBT with increasing  $\text{PbTiO}_3$  concentration to what is certainly a ferroelectric  $\epsilon$  peak in solid solutions enriched with lead titanate.

The analogous phenomena were observed in [14] (level peak on the curve  $\epsilon = f(T)$ , displacement of the peak toward higher temperatures with increasing frequency, far from saturated hysteresis loops), in solid solutions of  $(\text{Ba}, \text{Sr})(\text{Ta}, \text{Nb})_2\text{O}_6$ .

Goodman [17] described the properties of barium zirconate-niobate, to which can be ascribed the formula  $\text{Ba}_6(\text{Nb}_8\text{Zr}_2)\text{O}_{30}$  and structure of the tetragonal bronze potasso-tungstate type. The permittivity  $\epsilon_c$  of this compound also peaks as the temperature changes, shifting toward higher temperatures as frequency is increased. On the c axis there are dielectric hysteresis loops. Spontaneous polarization decreases smoothly with heating, but does not vanish in the temperature range where the  $\epsilon$  peak occurs, but retains a high value, continuing to diminish gradually with heating at even higher temperatures. Goodman classifies the phase transition in this compound as a third order ferroelectric phase transition, during which the second derivative of spontaneous polarization with respect to temperature should experience a jump at the point of transition. It is clear from the preceding that there is a far reaching analogy in the properties of the above-described compounds. It would be erroneous, however, to speak of third order transitions in these cases. Here the temperature of transition cannot be related to maximum  $\epsilon$  at any frequency, since spontaneous polarization itself is not equal to zero on any frequency in this temperature range. If the transition occurs at a very high temperature, where  $P_s = 0$ , then the occurrence of  $\epsilon$  peaks and the dependence of their temperature on frequency are inconceivable.

## §2. Principles of Phase Transition Blurring

The great number of various ferroelectrics with the same character of dielectric polarization is reminiscent of the nature of phenomena that occur in these crystals. The general structural features of all these compounds -- different ions in the same crystallographic positions, can be distinguished by careful examination. The assumption of the possibility of statistical distribution of different ions in these positions led to assumptions concerning the presence of composition fluctuations resulting in the blurring of the ferroelectric phase transition and relaxation character of dielectric polarization. Hence it stood to reason that dielectric polarization will also be of relaxation character if one starts with classical ferroelectrics but achieves phase transition blurring. Measurements of the  $\epsilon$  of solid solutions  $\text{Ba}(\text{Ti}, \text{Sn})\text{O}_3$  with a strongly blurred  $\epsilon$  maximum on various frequencies supported this conclusion [8]. Thus, the relationship between the relaxation character of dielectric polarization and blurring of the ferroelectric phase transition became obvious.

Internal stresses and fluctuations in composition are regarded in [2] as the causes of blurring of the ferroelectric phase transition. Internal stresses, however, occurring in domains of a monocrystal or in the grains of polycrystalline specimens due to spontaneous deformation during phase transition, obviously cannot be a deciding factor. Actually, if we examine solid solutions  $\text{BaTiO}_3$ - $\text{BaSnO}_3$ , we find that barium titanate displays the most spontaneous deformation, and here the internal stresses should be correspondingly maximal. In this series of compounds nevertheless, it is precisely  $\text{BaTiO}_3$  that has the most distinct phase transition.

It should be pointed out that the phase transition can also be blurred as a result of macroscopic nonequilibrium heterogeneity in composition (caused, for instance, by incomplete mutual dissolving of the components of the solid solutions). However, prolonged annealing of a number of ferroelectric solid solutions with the blurred phase transition, carried out at high temperatures [8], did not eliminate the blurring of the transition. In the case of  $\text{PbMg}_{1/3}\text{Nb}_{2/3}\text{O}_3$ , which is not a solid solution, but a compound, one cannot speak at all of incomplete dissolving. It may be assumed, then, that macroscopic composition heterogeneities in most of the examined cases are not the main factor in blurring of the transition, although generally speaking their effect should be taken into account whenever they are possible.

Quantitative evaluation of the effect of fluctuations in composition on the blurring of phase transitions was done in [18]. The investigation was done on a solid solution of two compounds with the perovskite structure  $\text{AB}'\text{O}_3 + \text{AB}''\text{O}_3$ , where the A ions are located in cubic octahedrons and the B' and B'' ions in the octahedral positions. Presumably there is no such ordering of B' and B'' ions in the octahedral nodes. Suppose the concentration of  $\text{AB}''\text{O}_3$  in the solid solution is  $p$ . In the solid solution there is a

small space containing  $n$  "molecules" of  $ABO_3$ , where  $B = B'$  or  $B''$ . Events, consisting in the detection of each "molecule" in the space set aside (which is infinitesimally small compared to the volume of the specimen), are regarded as independent events. Then the probability of finding  $m$  molecules of  $AB''O_3$  in this space is:

$$P(m) = C_2^m p^m (1-p)^{n-m} = \frac{n!}{m!(n-m)!} p^m (1-p)^{n-m}. \quad (16.1)$$

Using Sterling's equation, taking the logarithm and introducing the symbol for  $AB''O_3$  concentration in the examined small volume  $q = m/n$ , we obtain

$$\lg P(q) = n \left[ q \lg \frac{p(1-q)}{(1-p)q} + \lg \frac{1-p}{1-q} \right] - \frac{1}{2} \lg [2\pi q(1-q)n]. \quad (16.2)$$

In order to use this equation we must know the value of  $n$ . For this purpose it is necessary to select the volume in which spontaneous polarization takes place simultaneously in all its parts, i.e., which polarizes spontaneously as a whole. Some indications of the size of this space are given by Kanzig [19] (but only for pure barium titanate).

Kanzig, as we know, on the basis of x-ray diffraction data, concluded that near the temperature of the phase transition from the paraelectric state to the ferroelectric state barium titanate crystals break up into tiny regions, in which, due to thermal fluctuations, the spontaneously polarized state occurs at one moment and vanishes at another. These regions exist in  $BaTiO_3$  in a narrow temperature range; they cannot be detected in the crystal very far from the transition temperature. Spontaneous polarization occurs in each of these regions (we will call them "Kanzig regions") whether or not it takes place in the analogous adjacent regions.

It is obvious that a similar phenomenon, that of the breaking down of a crystal in the phase transition region into polar and nonpolar regions, should occur also in ferroelectric solid solutions, where the temperature at which spontaneous polarization takes place in each Kanzig region will be determined by the concentration  $q = m/n$  in this region. It is natural to assume the dimensions of the volume which we have set aside to coincide with the dimensions of the Kanzig regions. Kanzig estimates the upper bound of linear dimensions of these regions to be  $10^{-5}$  cm and the lower bound to be  $10^{-6}$  cm. The elemental nucleus ("molecule") of the examined solid solutions measures  $\sim 4 \text{ \AA}$ , so that the upper bound for  $n$  is 16 million and the lower is 16,000. If  $n$  is close to the lower bound, then according to [2], deviations in the concentration of  $AB''O_3$  in the Kanzig region from the average concentration should be rather substantial.

Calculation by equation (16.2) using a value of  $n$  close to the lower

bound ( $n = 27,000$ ) yields curves of distribution of Kanzig regions in terms of composition, shown in Figure 16.9. The width of the interval of perceptible concentrations is conditionally the same as the width of the peak at height  $0.2P_{\max}$ . The width of the interval of these concentrations with constant  $n$  clearly depends on macroscopic concentration  $p$ , and

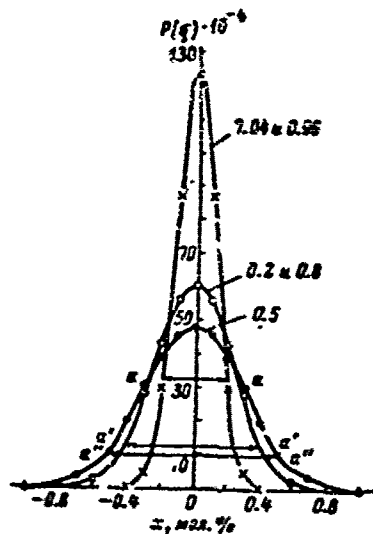


Figure 16.9. Curves of distribution of Kanzig regions in terms of composition for  $n = 27,000$  and  $p$  equal to 0.04, 0.2, 0.5, 0.8 and 0.9 (Isupov [18]).  $x$  -- deviation of component concentrations in Kanzig region from macroscopic (in mole %),  $aa$ ,  $a'a''$ ,  $a''a'''$  -- conditional concentration intervals.

it is clearly equal to zero when  $p$  is 0 and 1. When  $p$  is 0.5 it is maximal. The Curie point of the Kanzig region will be determined by the concentrations of the components in this region. The more the Curie point (average) depends on component concentration, naturally, the greater will be the width of the temperature range in which the phase transition occurs (the Curie region) with the given  $n$ . For  $Ba(Ti, Sn)O_3$ , for example, the change of the Curie point is about  $8^\circ C$  per 1 mole % of  $BaSnO_3$ . When  $n = 27,000$  and  $p = 0.2$  the width of the conditional interval of concentrations is 0.008 or 0.8 mole %, which yields a Curie region width of  $6.4^\circ C$ . Evaluation of the width of the Curie region for the compound  $PbMg_{1/3}Nb_{2/3}O_3$  yields about  $150^\circ C$  [20].

Thus, quantitative estimates of the blurring of phase transitions due to fluctuations of composition yield values that agree satisfactorily with experimental data.

As shown by Rolov [21], it is easy to find from relation (16.1) the expression for the distribution of Kanzig regions with respect to Curie points  $T_c$ :

$$[cp=me] \quad P(T_c) = \frac{1}{\sqrt{2\pi p(1-p)}} e^{-\frac{n(T_c - T_c^{me})^2}{2n^2 p(1-p)}} \quad (16.3)$$

where  $\gamma = (T_c - T_c^{me}) / (q - p)$  is the coefficient that determines the rate of change of the Curie point as component concentration changes, and  $T_c^{me}$  is the mean transition temperature. This expression is more convenient for calculations.

Various factors that can influence the degree of blurring of ferroelectric phase transitions are discussed in [20]. Also examined is a crystal  $A(B'_{1-x}B''_x)O_3$  with a perovskite structure, in which each of the elemental nuclei has the composition  $AB'O_3$  or  $AB''O_3$ . If the charges of  $B'$  and  $B''$  are not equal, obviously, the nuclei will have some positive or negative charge, even though the crystal as a whole is electroneutral.

If the energies of reaction between nuclei  $AB'O_3$  and  $AB''O_3$ ,  $AB'O_3$  and  $AB''O_3$ ,  $AB'O_3$  and  $AB''O_3$  are equal, then the distribution of ions  $B'$  and  $B''$  will be statistical, and the parameters of long-range and short-range order will be equal to zero. One of the conditions for this is (assuming a heterovalent bond) equality of the charges of ions  $B'$  and  $B''$ . Another condition will be equality of the geometrical dimensions of these ions. Otherwise nuclei  $AB'O_3$  tend to surround themselves with oppositely charged  $AB''O_3$  nuclei, and the nuclei with the larger  $B'$  ions tend to surround themselves with nuclei with smaller  $B''$  ions (in the latter case the  $AO_{12}$  polyhedron is deformed, but the ordering of large and small octahedrons leads to reduction of the overall (summary) elastic energy). The result will be either long-range order (as, for example, in the case of  $PbMg_{0.5}^{2+}W_{0.5}^{6+}O_3$ ) or simply short-range order (as, obviously, in  $PbFe_{0.5}^{3+}Nb_{0.5}^{5+}O_3$ ). In the presence of long-range order there are no fluctuations in composition. In the presence of short-range order the fluctuations are smaller than in statistical distribution. Deviation of the ratio of the number of ions  $B'$  to the number of ions  $B''$  from 1:1 also weakens the ordering tendency and the distribution of  $B'$  and  $B''$  ions will be close to statistical (as, for example, in  $PbMg_{1/3}Nb_{2/3}O_3$ ).

In the case of solid solutions with limited solubility in those compositions that are close to the solubility limit, segregation of atoms can be expected, i.e., enrichment of some microscopic sections of the crystal with  $B'$  ions and of others with  $B''$  ions (a sort of predissociated state). This should lead to a sharp increase in the blurring of the phase transition.

Regardless of the character of distribution of ions, it must be taken into account that the electrostatic and elastic energies of the Kanzig region -- spontaneously polarized region, surrounded by a medium without spontaneous polarization, are proportional to the squares of spontaneous polarization ( $P_s$ ) and spontaneous deformation, respectively. For large  $P_s$  and great spontaneous deformation, therefore, the simultaneous onset of spontaneous polarization in a large volume of the crystal, with the formation of domain structure, is preferable from the energy standpoint to the gradual transition of individual segments of the crystal into the ferroelectric state while the surrounding space remains in the unpolarized state. This apparently explains the absence of a notable Curie region in solid

solutions  $\text{BaTiO}_3\text{-PbTiO}_3$  and  $\text{SrTiO}_3\text{-PbTiO}_3$ , where spontaneous deformation and polarization increase sharply as the concentration of lead titanate, which of the perovskite ferroelectrics has a 6 times greater maximum spontaneous polarization and spontaneous deformation than barium titanate, increases. It has been shown experimentally that in solid solutions  $\text{Na}_{0.5}\text{Bi}_{0.5}\text{TiO}_3\text{-PbTiO}_3$ , by measure of increasing concentration of lead titanate, accompanied by an increase in deformation and electrostatic energies, phase transition blurring, which is great in  $\text{Na}_{0.5}\text{Bi}_{0.5}\text{TiO}_3$ , actually decreases [22].

It is noteworthy that a different explanation of the blurring of ferroelectric phase transitions is found in several works [23-26]. Here, as in [18], the concept of the separation of a crystal near the Curie point into a set of regions, in which spontaneous polarization occurs at one moment and vanishes another under the influence of thermal fluctuations. The term "Kanzig regions," introduced in [18], is used in [23, 24] for these regions.

The authors of [23, 24], examining the phase transition of the crystal from the spontaneously polarized state to the unpolarized state, write the change of thermal capacity during the phase transition in the form:

$$c_p(T) = \frac{dQ}{dT} = Q_0 \frac{d}{dT} \left( \frac{V_1}{V} \right), \quad (16.4)$$

where  $Q_0$  is the energy of transition per unit volume of the crystal into the nonpolar state,  $V_1/V$  is the relative volume of the substance experiencing the phase transition. If the unit volume of the crystal is divided near the transition point into  $N$  Kanzig regions with volume  $V_0$ , of which  $N_1$  are in the nonpolar state, then the entropy  $S$  of the system is determined through the number of possible locations of the nonpolar regions among the total number of regions  $N$ . Ignoring spontaneous deformation, it follows from the minimum free energy that

$$\frac{V_1}{V} = \frac{N_1}{N} = \frac{1}{1 + \exp\left(-\frac{V_0 \Delta\phi}{kT}\right)}, \quad (16.5)$$

where  $\Delta\phi$  is the change in the thermodynamic potential and  $V_0$  is the volume of an individual region. For the first order transition

$$\Delta\phi = Q_0 \frac{T_0 - T}{T_0} = Q_0 \frac{\Delta T}{T_0}. \quad (16.6)$$

Considering the relation

$$Q_0 = \frac{1}{2} \frac{T_0}{T} P_S^2. \quad (16.7)$$

where  $C$  is the Curie-Weiss constant, we obtain from (16.4)-(16.7):

$$c_p(T) = \nu \frac{1}{\operatorname{ch} x + 1}. \quad (16.8)$$

where

$$x = \frac{V_0 P_S^2}{2kC} \cdot \frac{\Delta T}{T}; \quad \nu = \frac{1}{8} \frac{V_0 P_S^4}{kC^2} \left( \frac{T_0}{T} \right)^2. \quad (16.9)$$

It follows from (16.8) that the thermal capacity curve is "blurred" in some temperature interval. Introducing the temperature interval  $T_1$  for the blurring characteristic, in which thermal capacity is one-half the value compared to its maximum, the authors obtain:

$$T_1 = 3.52 \frac{kCT_0}{V_0 P_S^2}. \quad (16.10)$$

The correlation between individual regions leads to a reduction of the degree of blurring of the phase transition.

It follows from expression (16.10) that the principal factors governing the degree of blurring, in the case of examination of heterophasal fluctuations, are  $V_0$  and the ratio  $CT_0/P_S^2$ . Thus, the higher the transition temperature, the larger  $C$  and the smaller  $P_S$ , the greater will be the degree of blurring for the same  $V_0$ .

Thus, the blurring of phase transitions in [23, 24] is explained without involving theories of fluctuations in composition with a favorable ratio of the values  $V_0$ ,  $C$ ,  $T_0$ ,  $P_S$ . The problems of the quantitative character of the phenomenon, however, are by no means solved. The fact is that there are distinct phase transitions in all simple perovskite compounds in which there are no fluctuations in composition. The blurring of phase transitions occurs only in the solid solutions and complex perovskite compounds (such as  $\text{PbMg}_{1/3}\text{Nb}_{2/3}\text{O}_3$ ) that have fluctuations in composition. Therefore fluctuations of composition are a more important cause of blurring of phase transitions than thermal fluctuations in ferroelectrics of complex composition.

Examination of thermal heterophasal fluctuations in ferroelectrics is useful, in particular because the explanation of the properties of

ferroelectrics with a blurred phase transition with the aid of fluctuations in composition embodies examination of thermal heterophasal fluctuations (see below).

Noteworthy in this regard are the works of Rolov [21, 26], pertaining to examination of several properties of ferroelectrics with a blurred phase transition (blurring of  $\epsilon$  peak, temperature curve of  $P_s$ , thermal conductivity, etc.), the conclusions of which are valid, regardless of the causes of blurring.

### §3. Kinetics of Transitions

We will now examine, on the basis of concepts of compositional fluctuations as the chief cause of transition blurring, the kinetics of the blurred ferroelectric phase transition [20, 27]. Here, as before, we will discuss the first order transition, close to the second order transition. We will define the mean Curie temperature of the crystal  $T_c^{me}$  as the temperature that corresponds to the transition of one-half the volume of the crystal to the ferroelectric state. This temperature can be determined by different methods (in particular, by dilatometric measurements).

We will examine a ferroelectric with a blurred phase transition during cooling from high temperatures. Let the temperature of the crystal be considerably higher than  $T_c^{me}$ , but lower than the Curie point of individual parts of the crystal, which have the maximum local Curie temperature  $T_c^{lo}$ .

Then under these conditions there will be regions of spontaneous polarization, surrounded on all sides by a nonpolar phase (isolated polar regions). The term "domainoids" is used in [27] for such regions. In contrast to domains, which we define as spontaneously polarized regions (in which the electric moments of all elemental nuclei have the same direction), surrounded by spontaneously polarized regions with a different direction of spontaneous polarization, domainoids are spontaneously polarized regions (in which the electric moments of all elemental nuclei also have the same direction), surrounded on all sides by parts without spontaneous polarization. The Kanzig regions are defined here as the minimal spontaneously polarized regions in the nonpolar environment, i.e., nuclei of a new phase of critical dimensions.

While the temperature is relatively high there will be few isolated polar regions and they will be separated from each other by very great distances compared to the dimensions of these regions, so that the forces of interaction between them can be ignored. Two important processes take place during cooling: growth of existing isolated polar regions due to their combining with adjacent parts of the paraelectric phase, and appearance of new isolated polar regions. As the distance between these regions diminishes, the interaction between them is strengthened.

At some stage the polar regions begin to join together. This may lead either to the formation of domain walls between them or to their fusion and formation of large isolated polar regions.

When  $T = T_c^{me}$ , where the volume of the ferroelectric phase is identical to that of the paraelectric phase, the crystal can be imagined as some complex combination of two mutually penetrating phases.

On cooling below  $T_c^{me}$  the domain structure gradually spreads through the entire crystal. However, in connection with the fact that the crystal has a large number of segments with a low local Curie temperature, the domains that form (in contrast to the domains in ordinary ferroelectrics) are not continuous, and they contain a large number of nonpolar "islands." The number of these islands diminishes by measure of cooling of the crystal and distance from  $T_c^{me}$ .

In examining this domain structure we may obviously assume that the position of the boundary between domains, in which it passes through the maximum number of nonpolar islands is the most stable position. In other words, the planes with the maximum density of nonpolar islands are the natural boundaries between adjacent domains. A high concentration of nonpolar islands on domain boundaries may lead to great average wall thickness and to uneven domain edges. This conclusion agrees with experimental results [9] on optical analysis of  $PbMg_{1/3}Nb_{2/3}O_3$  crystals.

In such an examination of a blurred transition we must deal with the important role of thermal heterophasal fluctuations. If the temperature of the specimen  $T$  is higher than the local Curie temperature of any section of the crystal, then spontaneous polarization will occur in this section from time to time under the influence of thermal fluctuations. The spontaneously polarized state will be metastable here. If  $T < T_c^{lo}$ , then spontaneous polarization in this section will be stable, but will disappear from time to time under the influence of thermal fluctuations. Here, the greater  $T_c^{lo} - T$  the less often thermal fluctuation will be of sufficient magnitude and the shorter the lifetime of the polar region in the nonpolar state. However, in a sufficiently wide range of temperatures adjacent to  $T_c^{lo}$ , the possibility of disappearance of spontaneous polarization in the polar region cannot be ignored.

From the given examination of the kinetics of the blurred phase transition we may explain several properties of  $PbMg_{1/3}Nb_{2/3}O_3$  and  $PbNi_{1/3}Nb_{2/3}O_3$ , investigated in [8, 9]: features of piezoelectric vibrations, birefringence and domain structure.

As the crystal is cooled in the absence of a field the joining of isolated regions leads to very small domain dimensions, with the result that the domain structure is not visible under the microscope. When an electric field is applied individual domains enlarge at the expense of others. Here the nonpolar islands previously located on the boundaries of the small domains find themselves within the enlarged domains. By measure

of reorientation and enlargement of domains visible birefringence appears in monocrystals and polycrystalline specimens display piezoelectric properties, which may last at low temperatures even after termination of the field. If, however, the field is terminated and the temperature does not differ very much from  $T_C^{pc}$ , then depolarization will occur from time to time in individual parts of domains as a result of thermal fluctuations. With the reappearance of spontaneous polarization in these parts its direction may not coincide with the initial direction. Consequently large domains will break down into small domains (the formation of small domains within the initial large domains, where the contours of the original large domains are preserved), visible birefringence and piezoelectric properties will diminish. At low temperatures this process proceeds slowly, and speeds up on heating (and by the time the temperature of  $PbMg_{1/3}Nb_{2/3}O_3$  reaches  $-60^\circ C$  the process is complete). The existence of piezoelectric vibrations in the presence of a stationary field at very high temperatures (up to  $90^\circ C$  in  $PbMg_{1/3}Nb_{2/3}O_3$ ) is easily explained by the presence of isolated polar regions at these temperatures.

It also becomes understandable why many ferroelectrics with the blurred phase transition, possessing a relatively low coercive field, do not have dielectric hysteresis loop saturation, even with very high fields. Apparently, the increase of polarization does not conclude with the reorientation of all existing domains and isolated polar regions, but continues due to the gradual transition of the nonpolar parts of the crystal into the polar state under the influence of the electric field.

#### §4. Dielectric Polarization

In view of a number of features of ferroelectrics with the blurred phase transition, there may be other mechanisms of polarization in addition to the polarization mechanisms characteristic of ordinary ferroelectrics [20, 27]. One such mechanism is relaxation of isolated polar regions and their boundaries.

Spontaneous polarization of an isolated polar region can have six different directions  $[100]$ ,  $[\bar{1}00]$ ,  $[010]$ ,  $[0\bar{1}0]$ ,  $[001]$  and  $[00\bar{1}]$  in the case of tetragonal symmetry of the ferroelectric phase, 12 in the case of rhombic symmetry and eight in the case of rhombohedral symmetry. It can be assumed that an isolated polar region possessing spontaneous polarization in one of these directions will be located in a potential hole. At temperatures lower than  $T_C^{lo}$ , but close to  $T_C^{lo}$ , the central potential hole corresponds to the state with zero polarization. When  $T \ll T_C^{lo}$  the central hole does not exist. As the case may be, in describing the state of an isolated polar region we may examine several potential holes, symmetric with respect to the state with  $P = 0$ . Thermal motion may cause the polarization vector to jump from one direction to another through the state with zero polarization, i.e., may lead to depolarization of the

region with subsequent polarization in any of the possible directions. The application of an electric field greatly increases the residence time of the region in one of the potential holes. Thus, we will have relaxation polarization, similar to thermal ionic polarization. The number of relaxation elements here, however, will be strongly dependent on temperature.

The boundaries between the polar and nonpolar phases are in continuous motion under the influence of thermal motion. We will examine the growth of a new layer of cells of the polar phase on such a boundary. We will recall that our discussion concerns first order phase transitions. As the number of cells in the growing "step" increases, the energy of this step will increase at first (unstable nucleus), peak (critical nucleus), and then diminish when the step reaches sufficiently large dimensions. In view of the finite dimensions of an isolated polar region, however, the size of the step and the reduction of its energy are also limited. Thus, we can talk of two potential holes, one of which is related to the dipole moment, equal to zero and the other to some dipole moment  $p$ . The expansion or disappearance of an isolated polar region of a new layer of elemental nuclei on a facet is related to the transition of this layer from one potential hole to another and is equivalent to relaxation of a dipole with the energy  $p^2/2$ . Apparently it is also necessary to consider the resonance of the boundaries between the polar and nonpolar phases, as suggested in [28].

The formulation of a theory of dielectric polarization of ferroelectrics with blurred phase transition is obviously a very complex problem in statistical physics. The first task toward the development of such a theory is to determine the critical dimensions of spontaneously polarized regions in a nonpolar environment. The energy of such regions will obviously be the sum of change of free energy  $\phi = A(T - T_c)P^2 + BP^4 + CP^6 + \dots$  during the phase transition, and also of the electrostatic, deformation and surface energies. Jaskiewicz [29] did such a calculation for nuclei in ellipsoidal form. He arrived at dimensions corresponding to the estimate of the dimensions of the Kanzig regions. However, the surface energy in this calculation is very roughly approximated, and presumably it is equal to one-half the energy of the  $180^\circ$  domain wall. The existence of frontal boundaries (perpendicular to  $P_s$ ) along with flank boundaries (parallel to  $P_s$ ) was completely disregarded.

In addition to the need to formulate a theory of dielectric polarization of ferroelectrics with blurred phase transition, it is still important to continue experimental research on these ferroelectrics and to determine accurately those values with which the theory will operate.

#### BIBLIOGRAPHY

1. Smolenskiy, G. A. and V. A. Isupov, DAN SSSR (Reports of USSR Academy of Sciences), Vol. 9, p. 653, 1954.
2. Smolenskiy, G. A. and V. A. Isupov, ZhTF [Zhurnal tekhnicheskoy fiziki;

- Journal of Technical Physics], Vol. 21, p. 1375, 1954.
3. Smolenskiy, G. A., N. P. Tarutin and N. P. Grudtsin, ZhTF, Vol. 24, p. 1584, 1954.
  4. Bokov, V. A., ZhTF, Vol. 27, p. 1784, 1957.
  5. Bokov, V. A., Akust. Zh. (Acoustics Journal), Vol. 3, p. 194, 1957.
  6. Smolenskiy, G. A. and K. I. Rozgachev. ZhTF, Vol. 24, p. 175, 1954.
  7. Smolenskiy, G. A. and A. I. Agranovskaya, ZhTF, Vol. 28, p. 1491, 1958.
  8. Smolenskiy, G. A., V. A. Isupov, A. I. Agranovskaya and S. N. Popov, FTT [Fizika tverdogo tela; Solid State Physics], Vol. 2, p. 2906, 1960.
  9. Bokov, V. A. and I. Ye. Myl'nikova, FTT, Vol. 3, p. 841, 1961.
  10. Khuchua, N. P., Proc. Intern. Meet. on Ferroelectr., Prague, Vol. 2, p. 161, 1966.
  11. Skanavi, G. I. and Ye. N. Matveyeva, ZhETF [Zhurnal eksperimental'noy i teoreticheskoy fiziki; Journal of Experimental and Theoretical Physics], Vol. 30, p. 1047, 1956.
  12. Skanavi, G. I., Ya. M. Ksendzov, V. A. Trigubenko and V. G. Prokhvatilov, ZhETF, Vol. 33, p. 320, 1957.
  13. Skanavi, G. I., Izv. AN SSSR, ser. fiz. (News of USSR Academy of Sciences, Physics Series), Vol. 24, p. 124, 1960.
  14. Smolenskiy, G. A., V. A. Isupov and A. I. Agranovskaya, FTT, Vol. 1, p. 992, 1959.
  15. Bogdanov, S. V., FTT, Vol. 5, p. 3390, 1963.
  16. Fritsberg, V. Ya., Izv. AN Latv. SSR (News of Academy of Sciences Latvian SSR), No. 5, p. 166, 1961.
  17. Goodman, G., J. Am. Ceram. Soc., Vol. 43, p. 105, 1960.
  18. Isupov, V. A., ZhTF, Vol. 26, p. 1912, 1956.
  19. Kanzig, W., Helv. Phys. Acta, Vol. 24, p. 175, 1951.
  20. Isupov, V. A., FTT, Vol. 5, p. 187, 1963.
  21. Rolov, B. N., FTT, Vol. 6, p. 2128, 1964.
  22. Isupov, V. A., P. L. Strelets, I. A. Serova, N. D. Yatsenko and T. M. Shirobolskiy, FTT, Vol. 6, p. 790, 1964.

23. Fritsberg, V. Ya. and B. N. Rolov, Izv. AN SSSR, ser. fiz., Vol. 28, p. 649, 1964.
24. Fritsberg, W. J., Proc. Intern. Meet. on Ferroelectr., Vol. 1, Prague, p. 163, 1966.
25. Rolov, B. N. and O. V. Dumbrays, Izv. AN SSSR, ser. fiz., Vol. 31, p. 1051, 1967.
26. Rolov, B. N., Izv. AN Latv. SSR, ser. fiz. i tekhn. n. (News of Academy of Sciences Latvian SSR, Physics and Technical Sciences Series), No. 6, p. 14, 1966
27. Isupov, V. A., Izv. AN SSSR, ser. fiz., Vol. 28, p. 653, 1964.
28. Khuchua, N. P., Candidate dissertation, Institute of Semiconductors, USSR Academy of Sciences, Leningrad, 1967.
29. Jaskiewicz, A., Acta Phys. Polon., Vol. 22, p. 489. 1962.

## CHAPTER 17 ANTIFERROELECTRICS

The properties of antiferroelectric compounds and some of their solid solutions are discussed in this chapter. Chief attention is focused on antiferroelectrics with the perovskite structure, since they have been investigated most thoroughly.

The term "antiferroelectric" was first introduced by Kittel [1]. An antiferroelectric is defined [1] as a crystal with spontaneously polarized ion chains, where adjacent ion chains of a given type are polarized in opposite directions. It is usually assumed that the nature of antiferroelectricity is analogous to that of ferroelectricity.

The first compound to be classified as an antiferroelectric was lead zirconate [2]. It should be recalled, however, that the possibility of transitions between phases with different orientation of dipole atom groups was examined by Frenkel [3], who also predicted the possibility of antiparallel ordering of dipole moments parallel to hydrogen halide crystals [4]. As already stated, antiferroelectrics, like ferroelectrics, can be divided into two groups -- one with a phase transition into the displacement type antiferroelectric state, the other with a phase transition into the order-disorder type of antiferroelectric state.

We will proceed to the specific examples of antiferroelectrics.

### 51. Antiferroelectrics with the Perovskite Type Structure

#### 1. Lead Zirconate

##### Structure of Lead Zirconate

X-ray diffraction analyses [5] have shown that at temperatures above the antiferroelectric Curie point, equal to 230°C, lead zirconate has a perovskite type cubic structure. Superstructural lines have been detected [6], however, indicating that the true nucleus in the paraelectric phase is distorted and is a multiplet nucleus. According to x-ray diffraction and neutron radiographic analyses [7, 8] and also optical analyses in polarized light [9], rhombic distortion occurs at temperatures below 230°C.

The elemental nucleus contains 8 formula units of  $\text{PbZrO}_3$ . The three-dimensional group is  $C_{2v}^3 - Pba2$  [8].

Lead ions are displaced by pairs from positions in the ideal cubic lattice in plane (001) to the opposite side, approximately diagonally to the facet (cubic direction  $\langle 110 \rangle$ , rhombic axis  $a$ ). Zirconium ions are displaced in the same manner. There are also small components of displacements on axis  $b$ .

Oxygen ions are also displaced in antiparallel in plane (001). Thus plane (001) is nonpolar. The magnitudes of the displacements on the  $a$  axis are:  $0.26 \text{ \AA}$  for lead ions,  $0.04 \text{ \AA}$  for zirconium ions; on the  $b$  axis --  $0.01 \text{ \AA}$  for lead ions and  $0.066 \text{ \AA}$  for zirconium ions.

The displacements of lead ions are shown schematically in Figure 17.1 in projection onto plane (001) [7], verified in [8]. There are simultaneously uncompensated components of displacements of oxygen ions on the  $c$  axis,

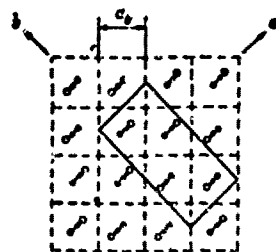


Figure 17.1. Projection of anti-ferroelectric structure of  $\text{PbZrO}_3$  on plane (001) (according to Sawaguchi [7]). The arrows indicate the direction of displacement of lead ions. Each square corresponds to an elemental nucleus with parameter  $a_0$ , containing one  $\text{PbZrO}_3$  unit. The solid line denotes the projection of a rhombic elemental nucleus.

which should have produced spontaneous polarization of  $\sim 25 \mu\text{C}/\text{cm}^2$ , assuming the ion charge of oxygen to be two and spontaneous polarization to be equal to the product of the ion charge and its displacement from the position in the center of the octahedron. The parameters of the rhombic elemental nucleus at room temperature are:  $a = 5.884 \text{ \AA}$ ,  $b = 11.768 \text{ \AA}$ ,  $c = 8.220 \text{ \AA}$ .

There is no notable displacement in plane (001) and the relation  $b = 2a$  is satisfied, with the result that the structure is pseudotetragonal. The distances O-O at room temperature vary from  $2.52$  to  $3.28 \text{ \AA}$ . The shortest distance between zirconium ions and oxygen ions is  $1.92 \text{ \AA}$ . Examination of the arrangement of lead ions and oxygen ions, between which the distances are shortest, shows that two different configurations of shortest distances are

realized in lead zirconate, and consequently there are two possible types of systems of partially homeopolar bonds between lead and oxygen [8, 10].

At a higher temperature there is a phase transition in pure lead zirconate near  $230^\circ$  into the rhombohedral ferroelectric phase, existing in a narrow temperature range, and then into the paraelectric phase [6, 11, 12]. Here the transition to the ferroelectric phase is accompanied by an increase in the volume of the specimen, and into the paraelectric phase, by a decrease in volume (Figure 17 2a).

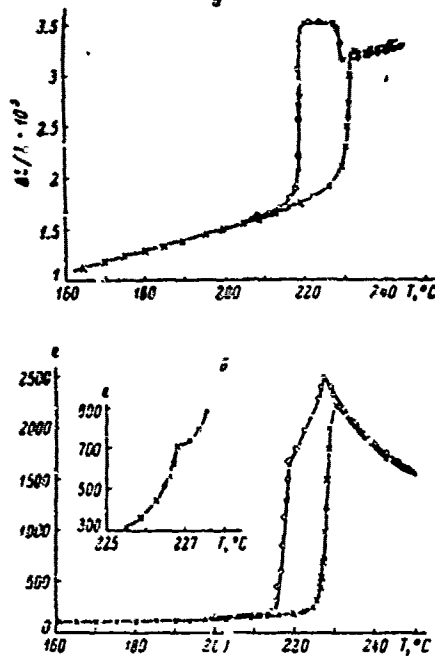


Figure 17.2. Temperature dependence of thermal expansion  $\Delta l/l$  (a) and permittivity (b) of highly pure  $\text{PbZrO}_3$  (according to Gul'po [11]).

#### Dielectric Properties of Weak and Strong Fields

The temperature dependence of permittivity, measured in a weak field, of pure lead zirconate is represented in Figure 17.2b [11]. The anomaly in permittivity and relative elongation in lead zirconate was discovered independently by Smolenskiy [13-15] and Roberts [16]. In the paraelectric phase the law  $\epsilon = \epsilon_0 + \frac{C}{T - \theta}$  is obeyed, where  $C = 1.55 \cdot 10^5 \text{K}$ ,  $\theta = 455^\circ\text{K}$  and  $\epsilon_0 < 50$  [21]. In specimens in which there is no ferroelectric phase [17], apparently related to impurities, in particular hafnium, the dependence of polarization on the intensity of a variable field is practically linear with the exception of a narrow region near the phase transition. The phase transition temperature drops as electric field strength increases (approximately  $1.5^\circ$  at a field strength of 20 kV/cm), and the permittivity at temperatures somewhat lower than the phase transition temperature increases. In stronger electric fields, however, there is induced phase transition into the rhombohedral ferroelectric phase. The critical field decreases linearly with increasing temperature at a rate  $dE_c/dT = 1.7 \text{ kV/cm} \cdot \text{deg}$  [17].

Measurements of the permittivity of lead zirconate in a wide frequency range of  $10^3$ - $4 \cdot 10^{10}$  [18-21] showed the absence of dispersion of  $\epsilon$  in the paraelectric and antiferroelectric phases and notable dispersion

of  $\epsilon$  and an increase of  $\tan \delta$  near the Curie point in the range of the ferroelectric phase. Dispersion in the ferroelectric phase is related to the presence of domain boundaries, mobile in an electric field, which are absent in the antiferro- and paraelectric phases (see Chapter 9). At higher frequencies, close to the natural vibration frequencies of the crystal lattice, a new dispersion mechanism, common to polar and nonpolar phases, goes into effect. This mechanism of dispersion has not yet been analyzed in antiferroelectrics. An increase of  $\tan \delta$  is noted [21] in lead zirconate at frequencies above  $10^{10}$  Hz, apparently related to the long-wave mode of vibrations.

#### Piezoelectric Effect, Effect of Pressure, Heat Capacity

It follows from structural data concerning the presence of an uncompensated polarization component that lead zirconate may display the piezoelectric effect, which is substantiated by Robert's data for ceramic specimens [16]. A qualitative conclusion has been reached as a result of analysis of the temperature dependence of the elastic properties of lead zirconate ceramics [22] to the effect that the anomaly of elastic properties is partially the result of an abrupt change in the pliancy coefficient in the presence of stationary polarization  $s^p$  and partially because of piezoelectric activity. It should be pointed out, however, that a firm conclusion concerning piezoelectric activity of lead zirconate in the antiferroelectric phase can be made only after examination of little-detwinned monocystals.

The application of hydrostatic pressure [23] increases the temperature of the phase transition between the antiferro- and paraelectric phases  $dT_c/dp \approx 4.1^\circ\text{C/kbar}$ , which is in agreement with thermodynamic theory. No data were obtained [23] about an intermediate ferroelectric phase. Perhaps the range of existence of this phase narrows when pressure is applied and vanishes altogether as pressure is increased (we will recall that subnucleus volume is greater in this phase than in the paraelectric phase and much greater than in the antiferroelectric phase). At a pressure of 6.4 kbar the phase transition line has a discontinuity and the new slope is  $dT_c/dp \approx 1.1^\circ\text{C/kbar}$ . This discontinuity possibly corresponds to a new phase boundary.

Heat capacity measurements [24, 25] showed that a latent heat of transition equal to 440 cal/mole [24] corresponds to the antiferroelectric phase transition (in specimens without a ferroelectric phase).

#### Optical Properties

The birefringence of small, strongly detwinned  $\text{PbZrO}_3$  crystals was analyzed in [9]. The refraction coefficient has a minimal value on the  $a$  axis, on which occur chiefly antiparallel displacements of lead and zirconium ions. Barium titanate, as we know, also has a minimal refraction coefficient in the direction of spontaneous polarization. Analysis in

polarized light revealed the existence of planes of twinning of the type  $(hk0)$  where  $h, k \neq 1$ . This is regarded [9] as experimental proof of the nonpolarity of plane  $(001)$ , since planes  $(hk0)$  with  $h, k \neq 1$  cannot be domain boundaries in a ferroelectric due to the requirement of zero charge on a boundary, which is generally true only when electrical conductivity is quite low.

It was shown [9] that birefringence in  $\text{PbZrO}_3$  cannot be regarded simply as a result of the elasto-optic effect with the assumption of proportionality between the difference of refraction coefficients and deformation of the nucleus without additional contrived theories concerning the magnitude of the elasto-optic constants.

## 2. Lead Hafnate

Lead hafnate,  $\text{PbHfO}_3$ , was first synthesized and analyzed in [26]. At room temperature there is rhombic distortion, analogous to the distortion in lead zirconate. Comparison of the positions and intensities of superstructural lines suggests that the configuration of ion displacements is also analogous to lead zirconate. Elemental nucleus parameters at room temperature, assuming tetragonal symmetry, are:  $a = 4.136 (\pm 0.001) \text{ \AA}$ ,  $c/a = 0.991 (\pm 0.001)$ . The Curie-Weiss law with  $C = 0.95 \cdot 10^5 \text{ cK}$  and  $\theta = 50^\circ \text{K}$ , is valid in the paraelectric phase. The Curie point is around  $200^\circ \text{C}$  [26, 27], and also there is a phase transition at about  $160^\circ \text{C}$  between two different antiferroelectric phases.

The symmetry of the intermediate phase is pseudotetragonal, as in solid solutions  $(\text{Pb}, \text{Sr})\text{ZrO}_3$  (see below). At  $200^\circ \text{C}$   $a = 4.134 (\pm 0.001) \text{ \AA}$  and  $c/a = 0.997$ . A sharp increase in volume with increasing temperature corresponds to both phase transitions.

The application of a stationary biasing electric field causes a slight increase in reverse permittivity and lowering of the Curie point (about  $2^\circ \text{C}$  in a field of  $10 \text{ kV/cm}$ ). The dependence of polarization on stationary field intensity is linear in all three phases all the way up to fields of  $40 \text{ kV/cm}$ , with the exception of a narrow region near the Curie point, where slight upward turns were noted on the curves  $P = f(E)$ .

## 3. Solid Solutions of $\text{PbZrO}_3$ and $\text{PbHfO}_3$ . Concept of Phase Transitions of "Buckling"

Solid solutions of  $\text{PbZrO}_3$  and  $\text{PbHfO}_3$  can be divided into two groups: solutions in which the domain of the ferroelectric rhombic phase expands as the concentration of the second component is increased, and solutions in which this domain narrows and even disappears. In solid solutions of the first group, as a rule, the second component has a higher structural factor  $t$  (see Chapter 2) than lead zirconate. If the second component has a lower structural factor the ferroelectric phase usually vanishes. It is noteworthy in general that antiferroelectrics of the perovskite class have a

structural factor  $t$  less than unity. This experimental rule was formulated by Zhdanov and Venetsev [28]. The possibility that this is related to the dependence of the electron polarization capacity of oxygen on its dimensions in the lattice, as is the case in simple oxides [29], is not ruled out. The effect of electron polarization of oxygen on the electrostatic dipole-dipole interaction in antiferroelectrics was studied in [20-33]. Internal fields in lead zirconate, corresponding to displacements of ions determined in [8], were calculated in [34]. It must be pointed out that model theories explaining phase transitions between ferro- and antiferroelectric phases do not yet exist. In particular, nothing is known of the physical factors that can cause the electron polarization of oxygen to change, affecting the relative stability of the phases.

Schematic diagrams of typical phase transitions [35] are illustrated in Figure 17.3 and the second components of a number of investigated solid solutions of the perovskite class are listed in Table 23. References to the literature are also given there.

Table 23. Second Components of Several Investigated Solid Solutions of Antiferroelectrics of the Perovskite Class  $ABO_3-A'B'O_3$

Group I	Group II
	$PbZrO_3$
$BaZrO_3$ [16, 34, 36] $PbTiO_3$ [3, 27-40] $BaTiO_3$ [41, 42] $PbNb_2O_6$ [19, 46] $PbTa_2O_6$ [19] $NaNbO_3$ [42] $PbFe_{1/2}Ta_{1/2}O_3$ [44]	$SrZrO_3$ [18, 24, 33, 43] $CaZrO_3$ [25, 44] $\epsilon$ - $PbSnO_3$ [19, 44, 47] $\epsilon$ - $CdZrO_3$ [44] $\epsilon$ - $PbCeO_3$ [44] $Bi_{1/2}K_{1/2}ZrO_3$ [48] $Bi_{1/2}Na_{1/2}ZrO_3$ [48]
	$PbHfO_3$
$BaHfO_3$ [46] $PbTiO_3$ [44]	$SrHfO_3$ [46] $CaHfO_3$ [47]
	$NaNbO_3$
$KNbO_3$ [70, 72, 73, 85-87] $LiNbO_3$ [72] $PbNb_2O_6$ [46] $CdNb_2O_6$ [82] $BaNb_2O_6$ [78] $PbZrO_3$ [43, 88] $SrNb_2O_6$ [79, 81] $PbTiO_3$ [80]	$NaTaO_3$ [55, 84, 86, 83] $CaTiO_3$ [79] $CaNb_2O_6$ [79] $NaNb_2O_6$ [84] $FsNbO_3$ [84] $SrTiO_3$ [81]
	$PbMg_{1/2}W_{1/2}O_3$
$PbTiO_3$ [88, 89, 101] $PbMg_{1/2}Nb_{1/2}O_3$ [89, 101]	$CaMg_{1/2}W_{1/2}O_3$ [89] $BaMg_{1/2}W_{1/2}O_3$ [89]

In the second group of solid solutions, which are formed in a rather broad range of concentrations, a new antiferroelectric phase occurs and, in addition, there are often new nonpolar phases [10, 22, 45, 46]. The temperatures of the phase transitions between the nonpolar phases rise as the concentration of the second component is increased, despite the reduction

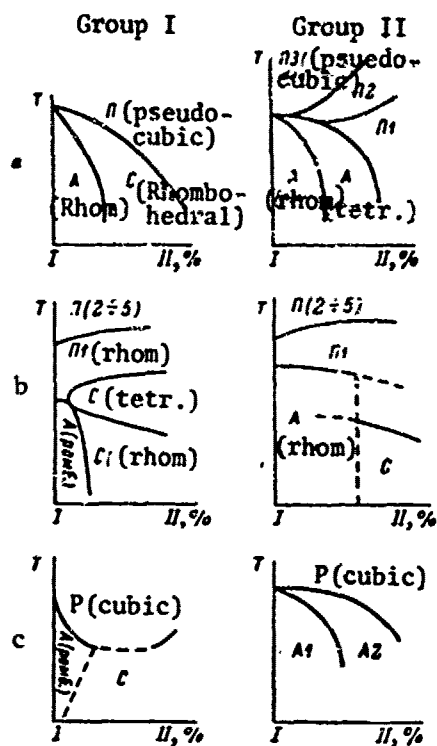


Figure 17.3. Schematic diagrams of typical phase transitions in antiferroelectrics of the perovskite class based on  $\text{PbZrO}_3$  and  $\text{PbHfO}_3$  (a),  $\text{NaNbO}_3$  (b) and  $\text{PbMg}_{1/2}\text{W}_{1/2}\text{O}_3$  (c) (according to Kraynik [35]). Phases: A -- antiferroelectric; C - ferroelectric; P -- paraelectric.

of the polarizability of the ions. It should also be recalled that the Curie points drop in other ferroelectric solid solutions after such substitution of ions. Therefore it can be assumed that these transitions are apparently different in nature from ferroelectric phase transitions.

Such transitions were detected in solid solutions of  $\text{CaTiO}_3$  [49-52], in several aluminates, orthoferrites, rare-earth hallates [53, 54],  $\text{NaNbO}_3$  [55-58], etc. These transitions are usually classified as "buckling" transitions [59-61]. The change in the temperatures of the buckling phase transitions agrees qualitatively with deviations of ion dimensions (in the case of solid solutions the average dimensions are used) from the dimensions required for the cubic structure. During buckling phase transition the structure is distorted in such a way that the requirements of tight packing of the ions and preservation of the angles of homeopolar bonds are satisfied. This type apparently also includes high-temperature transitions in  $\text{NaNbO}_3$  and its solid solutions (see below). Therefore it seems to us

natural to distinguish these transitions from antiferroelectric transitions in which long-range dipole-dipole interaction apparently plays an important role.

Such differentiation is easily done experimentally only if the free energy of the antiferroelectric state is sufficiently close to the free energy of the ferroelectric state, since in this case antiferroelectrics manifest strong anomalies in permittivity, field induced phase transitions are possible in the ferroelectric state, etc. In the case of buckling phase transitions, and also phase transitions into the antiferroelectric state with free energy very different from the free energy of the ferroelectric state, these phenomena do not occur.

We will now examine specific cases of solid solutions. As an example of solutions with a ferroelectric rhombohedral phase we will examine solid solutions of  $\text{PbZrO}_3$ - $\text{PbTiO}_3$  (the t factor increases as the concentration of the second component is increased).

The actual diagrams of the phase transitions may have a form more complex than shown for simplicity in Figure 17.3a. Figure 17.4 represents the diagram of phase transitions when the concentration of  $\text{PbTiO}_3$  is low [5, 39]. Anomalies appear in the region of the phase transitions on the curves of the temperature dependences of permittivity, thermal expansion and heat capacity [5]. Phase A1 (Figure 17.4) is a rhombic antiferroelectric phase, analogous to the antiferroelectric phase of pure lead zirconate; C1 is a ferroelectric rhombic phase, which occurs in lead zirconate and in all solid solutions of group I (Figure 17.3a); A2 is an antiferroelectric phase, observed in  $\text{PbZrO}_3$  with certain impurities, the superstructure of which differs from that of rhombic phase A1 of lead zirconate, but which is similar to a new pseudotetragonal antiferroelectric phase that usually occurs in solid solutions of group II, and also in lead hafnate (Figure 17.3a).

More recently new ferroelectric phase C2 was found. The detailed structure of this new phase is not known at this time. It turned out that the ferroelectric state occurs at lower temperatures in solid solutions of the system  $\text{PbZrO}_3$ - $\text{PbTiO}_3$ - $\text{PbSnO}_3$ - $\text{PbNb}_2\text{O}_6$  [62, 63] and  $\text{PbHfO}_3$ - $\text{PbTiO}_3$  [64] in some range of concentrations, than the antiferroelectric state (phase A2). The application of a strong field induces phase transition into the ferroelectric state in a rather wide range of temperatures of the antiferroelectric phase. The application of pressure to a specimen in the ferroelectric state causes transitions to the antiferroelectric state, which is explained by reduction of the volume of the elemental nucleus during transition from the ferro- into the antiferroelectric state, characteristic of solid solutions based on lead zirconate and lead hafnate.

As an example of solid solutions of group 'I' we will examine solutions of  $\text{PbZrO}_3$ - $\text{SrZrO}_3$ . These solid solutions were analyzed in [19, 24, 36, 45].

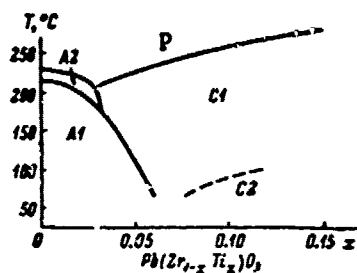


Figure 17.4. Diagram of phase transitions in solid solutions  $\text{PbZrO}_3$ - $\text{PbTiO}_3$  with a low concentration of  $\text{PbTiO}_3$  (according to Sawaguchi [5] and Dungan, et al [39]). Phases: A1 -- rhombic antiferroelectric; A2 -- pseudotetragonal antiferroelectric; C1 and C2 -- rhombohedral ferroelectric phases; P -- paraelectric phase.

As the concentration of the second component in these solutions increases a new antiferroelectric phase, isostructural phase A2 in solid solutions  $\text{PbZrO}_3$ - $\text{PbTiO}_3$

(Figure 17.4) appears. This phase has a pseudotetragonal structure, to which is applicable a simple model with a double lattice parameter and ion displacements, alternating in opposite directions; the configuration of the ion displacements is not known. The phase transition from one antiferroelectric phase to another is accompanied by anomalies in permittivity, thermal expansion and thermal capacity. The application of a strong biasing electric field increases permittivity and lowers the temperature of the phase transition.

In addition to these two transitions, two other transitions appear as the concentration of  $\text{SrZrO}_3$  is increased, the temperatures of which rise as the concentration of the second component is increased (Figure 17.3a). The third phase transition was described in [10, 45] and the fourth in [10]. These phase transitions are accompanied by slight anomalies in the temperature dependence of permittivity, relative elongation and elasticity coefficients. The results of extrapolation of the temperatures of these transitions to pure  $\text{SrZrO}_3$  agree satisfactorily with the temperatures of the phase transitions in  $\text{SrZrO}_3$ , recently observed in [65].

The two high-temperature phase transitions are more likely related to the "buckling" phase transitions than to antiferroelectric phase transitions. This is supported, in particular, by the rise of temperatures of these transitions with increasing  $\text{SrZrO}_3$  concentration, despite the associated reduction of electron polarizability of type A ions after substitution of  $\text{Pb}^{++}$  by  $\text{Sr}^{++}$ . We will also note that such substitution of ions in ferroelectrics of the perovskite class lowers the Curie point.

The properties of solid solutions based on lead hafnate are similar to those of solutions based on lead zirconate, although they differ in details. As structural factor  $t$  increases, the rhombohedral ferroelectric phase appears (for instance, after substitution of lead ions by barium ions [66], or after substitution of hafnium ions by titanium ions [64]), and when  $t$  decreases (for instance after substitution of  $\text{Pb}^{++}$  ions by  $\text{Ca}^{++}$  [27] or  $\text{Sr}^{++}$  [60]), at least two different antiferroelectric phases -- rhombic and pseudotetragonal, continue to exist in a certain range of

concentrations. Also, new nonpolar phases appear, the temperatures of which rise as the concentration of the second components is increased, despite the reduction of average polarization capacities.

See Table 23 for references to literature on certain other investigated solid solutions.

#### 4. Sodium Niobate

The anomalous dielectric properties of sodium niobate were first discovered by Matthias [67, 68], who classified it as a ferroelectric. Vousden [69], Shirane, et al [70] and Cross and Nicholson [71], however, demonstrated that sodium niobate is an antiferroelectric at room temperature and in the absence of a field sodium niobate displays under these conditions a perovskite type structure with rhombic distortion. The parameters of the rhombic elemental nucleus, according to [72, 73] are:  $a = a_0\sqrt{2} = 5.568$ ,  $b = 4a_0 = 15.518$ ,  $c = a_0\sqrt{2} = 5.505 \text{ \AA}$ , where  $a_0$  is the parameter of the cubic nucleus with the perovskite type structure.

The elemental nucleus consists of 8 formula units. The parameters of the nonprimitive monoclinic elemental nucleus, containing 16 units, often used for describing sodium niobate, are:  $a_m = c_m = 2 \cdot 5.914$ ;  $b_m = 4 \cdot 3.881 \text{ \AA}$ ,  $\beta = 90^\circ 39'$  [74]. The spatial group at room temperature, describing displacements of  $\text{Nb}^{5+}$ , according to [72, 73], is  $D_{2h}^9 - \text{Pbma}$ . The elemental nucleus consists of 4 layers with a thickness of  $a_0$ , located perpendicular to the  $b$  axis. The basic component of the displacements of  $\text{Nb}^{5+}$  ions lies on the  $a$  axis and is equal to  $0.15 \text{ \AA}$  [73]. All displacements of  $\text{Nb}^{5+}$  lie entirely in layers parallel to (010), i.e., the displacements of  $\text{Nb}^{5+}$  on the  $b$  axis are equal to zero. Here two layers with displacements of one symbol alternate with two layers with displacements of another. The structure of  $\text{NaNbO}_3$  according to [72, 73] is illustrated in Figure 17.5.

The application to a crystal of an electric field perpendicular to the  $b$  axis leads to the appearance of a rhombic ferroelectric phase whose  $b$  parameter is one-half that of the antiferroelectric phase, and consequently  $b = 2a_0$  [75, 76]. In certain cases this phase remains in the metastable state even after elimination of the field [75, 76]. As the temperature increases to  $\sim 360^\circ\text{C}$  its stability increases and in certain crystals, in the absence of an electric field, a phase transition occurred into this phase [77]. The induced ferroelectric phase is analogous to the rhombic ferroelectric phase occurring in solid solutions  $\text{NaNbO}_3\text{-KNbO}_3$ . Spontaneous polarization is  $\sim 10 \text{ \mu C/cm}^2$  [76].

The application of a strong field parallel to the  $b$  axis at room temperature in fields up to  $130 \text{ kV/cm}$  did not cause transition into the

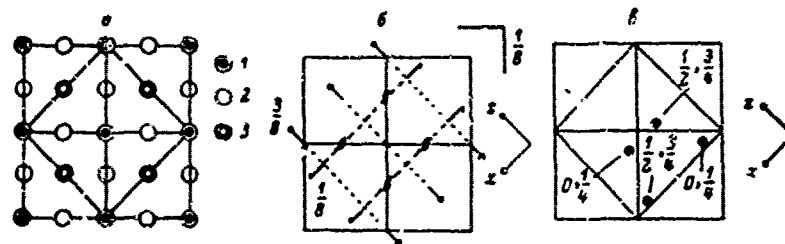


Figure 17.5. Schematic representation of sodium niobate structure according to Megaw and Wells [72, 73] in projection on plane (010). a -- position of atoms in perovskite structure; b -- elements of symmetry of spatial group  $P6_{3mc}$ ; c -- location of Nb atoms (displacements are exaggerated for clarity, displacement of Nb on x is  $-0.17$ , and on z,  $\sim 0.04$  Å).

Atom	Coordinate y of non-displaced ions in fractions of lattice constant	
1 -- Nb	0 1/4	1/2 3/4
2 -- O	1/8 3/8	5/8 7/8
3 -- Na	0 1/4	1/2 3/4
	1/8 3/8	5/8 7/8

ferroelectric phase, but when the temperature was lowered below  $-120^{\circ}\text{C}$  [71] normal hysteresis loops were observed in a strong field. According to [71] phase transition to the ferroelectric state in the absence of a field occurs at  $\sim -200^{\circ}\text{C}$ . Once forming, the normal loops were also observed at higher temperatures up to  $-50^{\circ}\text{C}$ . There is information (Shirane's report at the 1956 congress of the American crystallographic society) that the structure of this phase is monoclinic. It is theorized [65] that in addition to antiparallel displacements of ions, perpendicular to the b axis, parallel components of displacements on the b axis also occur, i.e., the phase is ferroelectric.

In ceramic specimens of  $\text{NaNbO}_3$  at temperatures below  $-80^{\circ}\text{C}$  [78, 79], there are also normal hysteresis loops which, having formed, last to  $0^{\circ}\text{C}$ , degenerating gradually. A metastable ferroelectric phase is induced in ceramic specimens at temperatures above  $50^{\circ}\text{C}$  in a strong electric field [80], which vanishes on heating above  $270^{\circ}\text{C}$ . Its structure was not investigated. Spontaneous polarization was  $\sim 50$   $\mu\text{C}/\text{cm}^2$ . Extremely complex twinning occurs in  $\text{NaNbO}_3$  crystals [75, 76].

The refractor coefficient of  $\text{NaNbO}_3$  is minimal in the direction of the a axis, i.e., in the direction of the basic displacement of  $\text{Nb}^{5+}$  ions [9]. This is quite analogous to the results of optical analysis of  $\text{BaTiO}_3$  and  $\text{PbZrO}_3$ . No proportionality could be established in  $\text{NaNbO}_3$  between birefringence and the corresponding deformation of the elemental nucleus.

As temperature changes a large number of phase transitions occur in  $\text{NaNbO}_3$ . These transitions have been investigated in a number of works [71, 74, 77, 81-83]. At approximately  $360^\circ\text{C}$  there is a phase transition from one rhombic phase to another, close to tetragonal, with nonprimitive elemental nucleus  $2a_0 \times 4b_0 \times 2c_0$  [76]. To this transition corresponds maximum  $\epsilon$ , change of birefringence and latent heat of transition equal to 50 cal/mole [70]. The application of a stationary field increases  $\epsilon$ , measured in a weak variable field. At temperatures above this transition  $\epsilon$  obeys the Curie-Weiss law. Also, at  $430^\circ$ , according to x-ray diffraction data [77, 82], a transition occurs, apparently into the tetragonal phase with nucleus  $2a_0 \times 2b_0 \times 2c_0$ , at  $470-480^\circ\text{C}$  into another tetragonal phase, which is verified by a jump in  $\epsilon$  and birefringence [70, 71, 81], and also by x-ray diffraction data [77, 82]; at  $\sim 520^\circ\text{C}$ , into a new tetragonal phase with nucleus  $a_0 \times a_0 \times c_0$ , substantiated by x-ray diffraction data [74, 77], and also by the presence of a jump of  $\epsilon$  and birefringence [75]; at  $580^\circ\text{C}$  [84] -- into another tetragonal phase and, finally, at  $650^\circ\text{C}$  -- into a cubic phase (verified optically and by x-ray diffraction data, and by the presence of a jump of the temperature coefficient  $\epsilon$  [70, 71, 74, 81, 82]). Here the transitions at  $\sim 360^\circ$ ,  $\sim 580^\circ$  and  $640^\circ\text{C}$  are first order transitions. The nature of these phase transitions is discussed below.

#### 5. Solid Solutions Based on Sodium Niobate

Solid solutions based on sodium niobate can be divided conditionally into the following two groups: a high-temperature ferroelectric tetragonal phase occurs in solutions of the first group, and such a phase does not occur in solutions of the second group (Figure 17.3b and Table 23). As already mentioned, sodium niobate in the low-temperature range has a ferro-ferroelectric, apparently monoclinic phase, but the effect of substitutions of ions on the temperature range of its existence has not been investigated. It follows from experimental data (Table 23) that the second components of most solutions of the first group are characterized by higher electron polarizability of type A ions compared to  $\text{Na}^+$ .

As an example of solutions of the second group we will examine solutions of  $(\text{Na}, \text{K})\text{NbO}_3$ . These solutions have been analyzed [70, 72, 73, 85, 86]. A detailed description of the monocrystals of these solutions with small concentrations of  $\text{KNbO}_3$  is given in [85]. A diagram of the phase transitions according to [85] is seen in Figure 17.6. A phase transition from rhombic antiferroelectric phase A1 with  $b \approx 4a_0$  into rhombic ferroelectric phase C1 with  $b \approx 2a_0$  can be seen in monocrystals. In region A1, with a  $\text{KNbO}_3$  concentration less than 0.6 mole %, the application of an electric field perpendicular to the b axis causes a phase transition into the rhombic ferroelectric phase, but after removal of the field the specimen returns to the antiferroelectric state. In region A1 + C1 these two phases coexist.

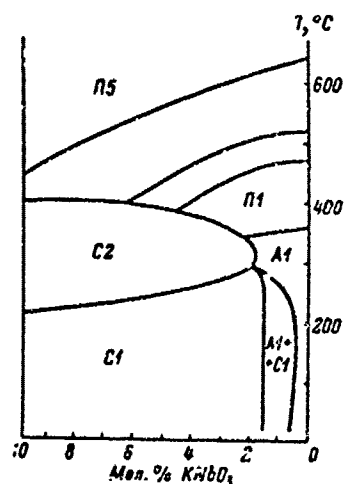


Figure 17.6. Diagram of phase transitions in system  $(\text{Na}, \text{K})\text{NbO}_3$  at low  $\text{KNbO}_3$  concentration (according to Cross [85]). Phases: A1 -- rhombic antiferroelectric; C1 -- rhombic ferroelectric; P1 -- pseudo-tetragonal paraelectric; P5 -- cubic paraelectric.

been shown [55, 56] that compounds containing less than 50% sodium tantalate display antiferroelectric properties and are analogous in terms of dielectric properties to pure sodium niobate. An interesting feature of these solid solutions is the veering of the phase transition line from the rhombic antiferroelectric phase to rhombic paraelectric phase (which occurs in pure sodium niobate at  $360^\circ\text{C}$ ). This breakaway occurs in the 50-60% sodium tantalate concentration range. These results were confirmed [92, 93], both on polycrystalline specimens and on monocrystals. The general form of the phase transition diagram in this system is seen in Figure 17.3b. Compounds containing more than 55% sodium tantalate display ferroelectric properties below the phase transition point [55, 56, 92]. In compounds close to the solution with 55 mole % sodium tantalate (region of breakaway of phase transition line to paraelectric phase), the two phases coexist in a certain range of concentrations.

References to certain works in which various solid solutions based on sodium niobate were analyzed are given in Table 23. There is a great similarity between sodium niobate and silver niobate, the antiferroelectric properties of which were discovered and investigated in [96].

Several high-temperature phase transitions occur in sodium niobate at temperatures above  $360^\circ\text{C}$ , and also in silver niobate. These phase transitions are usually classified as so-called "buckling" phase transitions

The structures of the ferroelectric phase occurring with the application of the field and of rhombic ferroelectric phase C1, occurring in solid solutions with potassium niobate, are identical in terms of displacements of  $\text{Nb}^{5+}$  ions, but apparently differ somewhat in terms of the positions of oxygen ions [73, 27]. Nb ions are displaced  $\sim 0.17 \text{ \AA}$  on the a axis. With a further increase in the concentration of potassium niobate tetragonal ferroelectric phase C2 appears. To the phase transition from the rhombic phase to tetragonal correspond anomalies of the curves of the temperature dependences of  $\epsilon$  and heat capacity [70]. It can be concluded on the basis of [70, 75, 86] that parameter b remains up to 30-35% duplicated in the rhombic ferroelectric phase.

As an example of solutions of the second group we will examine solutions of  $\text{Na}(\text{Nb}, \text{Ta})\text{O}_3$ . It has

[55, 56, 88, 96]. When nucleus parameters decrease the temperatures of these transitions rise in some of the solid solutions and when the parameters increase, the temperatures drop, so that phase transition from the cubic to tetragonal phase occurs when the nucleus parameter is the same for all investigated compositions of various solid solutions, equal to 3.94 Å [88, 91]. Buckling of the structure continues into the temperature range in which antiferro- and ferroelectric phases occur, and deformations due to ferro- and antiferroelectricity resemble buckling deformations.

The superstructure lines in the rhombic and tetragonal ferroelectric phases of sodium-cadmium niobates persist in the entire domain of the solid solutions [89]. The superstructure lines of solid solutions of sodium-lead niobates gradually vanish in the tetragonal ferroelectric phase as the concentration of lead niobate is increased, but this does not lead to any anomalies in ferroelectric properties [88]. In the case of  $\text{NaNbO}_3$  and solid solutions based on  $\text{NaNbO}_3$ , buckling deformations apparently coexist with ferro- and antiferroelectric deformations, which are the result of electrostriction, and they can be separated from each other. Generally speaking, however, buckling deformations may have a considerable effect on ferro- and antiferroelectric deformations, and such separation is not always possible.

#### 6. Lead Magnotungstate

Lead magnotungstate ( $\text{PbMg}_{1/2}\text{W}_{1/2}\text{O}_3$ ) was first synthesized and analyzed in [97]. X-ray diffraction analysis [89], done both on polycrystalline specimens and on monocrystals, revealed that the distribution of  $\text{Mg}^{2+}$  and  $\text{W}^{6+}$  ions in this compound is ordered in the octahedral positions of the crystal lattice and Mg, W, and Mg ions alternate on all three axes of the original cubic lattice. In addition to superstructural lines corresponding to the ordering of Mg and W ions, the x-ray diffraction patterns reveal superstructural lines due to antiparallel displacements of ions. It was found that the structure of  $\text{PbMg}_{1/2}\text{W}_{1/2}\text{O}_3$  is rhombic; the parameters of the elemental nucleus are:  $a = 22.73$ ;  $b = 22.78$ ;  $c = 15.89$  Å. The spatial group is  $D_2^5-C222_1$ . The elemental nucleus contains 128  $\text{PbMg}_{1/2}\text{W}_{1/2}\text{O}_3$  units. The elemental nucleus is depicted schematically in Figure 17.7. There are no dielectric hysteresis loops up to break-through field intensities.

The antiferroelectric Curie point of lead magnotungstate is 36°C. To this temperature correspond a sharp  $\epsilon$  peak and spontaneous reduction of volume [99] (Figure 17.8). Above the Curie point the law  $\epsilon = \epsilon_0 + C/(T - \theta)$  is valid, where  $\epsilon_0 = 58$ ,  $\theta = 167^\circ\text{K}$ ,  $C = 2.2 \cdot 10^5 \text{K}$  [97]. It is not surprising that there is no dispersion of  $\epsilon$  at frequencies up to  $10^{10}$  Hz in the region of the antiferroelectric phase transition [20, 21, 100]. Lead magnotungstate was the first antiferroelectric material in which  $\tan \delta$  was found to increase with increasing frequency in the  $10^{10}$  Hz range [20]. The

increase of  $\tan \delta$  with frequency continues even into the millimeter wavelength range [2]. This is evidence for the long wave mode of lattice vibrations. Measurements of  $\epsilon$  in a variable field with a simultaneous application of a weak stationary field showed a slight (up to 2%) increase in  $\epsilon$  [101].

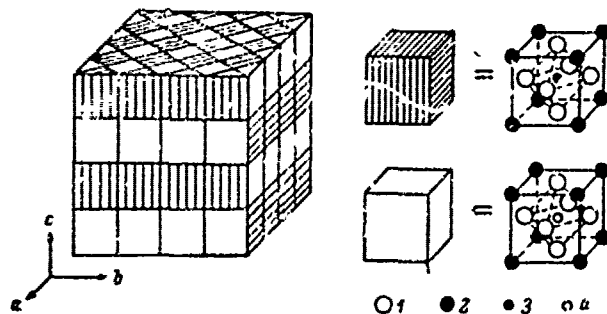


Figure 17.7. Schematic diagram of elemental nucleus of  $\text{PbMg}_{1/2}\text{W}_{1/2}\text{O}_5$  (according to Zaslavskiy and Bryzhina [98]): 1 --  $\text{O}^{2-}$ ; 2 --  $\text{Pb}^{2+}$ ; 3 --  $\text{W}^{6+}$ ; 4 --  $\text{Mg}^{2+}$ .

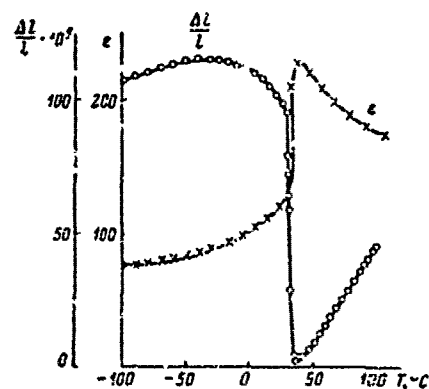


Figure 17.8. Temperature dependence of permittivity and thermal expansion of polycrystalline  $\text{PbMg}_{1/2}\text{W}_{1/2}\text{O}_5$  (according to Smolenskii, et al [99]).

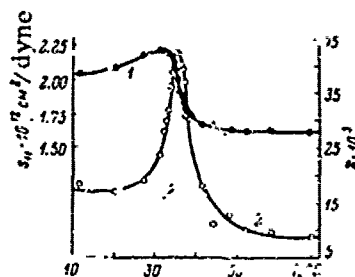


Figure 17.9. Temperature dependence of elastic pliancy  $s_{11}$  (1) and logarithmic attenuation decrement  $\delta$  (2) of polycrystalline  $\text{PbMg}_{1/2}\text{W}_{1/2}\text{O}_5$  (according to Shuvalov and Minayeva [104]).

An anomalous heat capacity corresponds to the antiferroelectric transition. The latent heat of transition is 275 cal/mole [102]. The Curie point drops with the application of hydrostatic pressure [103].  $dT_c/dp = -5.92 \cdot 10^{-3}$  deg/atm up to 2,000 atm, and saturation tends to occur with a further increase of pressure. Blurring of the phase transition is noted with increasing pressure [103]. Near the antiferroelectric Curie point mechanical losses peak and the pliancy coefficients display an anomaly [104, 105] (Figure 17.9). Internal friction is greater in the

antiferroelectric phase than in the paraelectric phase, obviously due to losses on twinned boundaries.

### 7. Solid Solutions Based on Lead Magnotungstate

These solid solutions can also be divided conditionally into two groups (Figure 17.3c and Table 23). A ferroelectric phase occurs in solid solutions of lead magnotungstate with lead titanate and lead magnoniobate [99, 100]. When lead ions are substituted by  $\text{Ca}^{2+}$  and  $\text{Ba}^{2+}$  ions, no ferroelectric phases occur in lead magnotungstate. The phase transitions in these solutions are illustrated schematically in Figure 17.3c [99].

The temperature of the transition to the paraelectric phase in solid solutions with lead titanate and lead magnoniobate, depending on the concentration of the solutions, passes through a minimum, which cannot be explained on the basis of the assumption of statistical distribution of ions in the octahedral positions. An interesting feature of many of these solutions is the appearance of a ferroelectric phase at temperatures lower than the antiferroelectric point. Double hysteresis loops appear in a certain temperature range, corresponding to phase transition from the antiferroelectric to the ferroelectric phase, and the critical field increases here with increasing temperature. At lower temperatures normal hysteresis loops are observed. The coercive field of these loops is weaker than the field in which they begin to appear, apparently evidence of the metastability of the ferroelectric phase in the absence of a field in the investigated temperature interval. The antiferroelectric Curie point drops as the strength of the stationary field increases. This is characteristic of antiferroelectric phase transitions with rather close free energies of the ferro- and antiferroelectric states (no such reduction in the fields applied could be detected in pure lead magnotungstate).

The Curie point drops in solid solutions of lead magnotungstate with barium and calcium magnotungstate as the concentration of the second component is increased to 20 and 5%, respectively [99]. These concentrations presumably correspond to the limits of solubility. The dependence of polarization on field strength is linear in the  $-196$  to  $+60^\circ\text{C}$  temperature range, all the way up to break-through fields.

Yet another anomaly is found in solid solutions with calcium magnotungstate, in addition to anomalies of  $\epsilon$  and thermal expansion, which correspond to the Curie point. The anomaly in question apparently corresponds to a phase transition to a new antiferroelectric phase.

### 8. $\text{PbCo}_{1/2}\text{W}_{1/2}\text{O}_3$

The compound  $\text{PbCo}_{1/2}\text{W}_{1/2}\text{O}_3$  was first synthesized in [106]. The phase transition was found [107, 103], accompanied by an anomaly of  $\epsilon$  at  $20^\circ\text{C}$ , and it was suggested that it is a ferro- or antiferroelectric phase transition. Monocrystals were grown [109-111] and x-ray diffraction analysis

and analysis of the dielectric and magnetic properties were conducted up to helium temperatures, indicating that  $\text{PbCo}_{1/2}\text{W}_{1/2}\text{O}_3$  is antiferroelectric and antiferromagnetic. The distribution of  $\text{Co}^{++}$  and  $\text{W}^{5+}$  cations in this compound is ordered. At  $26^\circ\text{C}$  symmetry is pseudomonoclinic with subnucleus parameters  $a_m = c_m = 4.009 \text{ \AA}$ ,  $b_m = 3.988 \text{ \AA}$  and  $\beta = 90^\circ 10'$ . At  $50^\circ\text{C}$  symmetry is cubic. The antiferroelectric Curie point is  $+32^\circ\text{C}$  according to dielectric measurements. The application of a stationary field displaces the Curie point toward lower temperatures.

According to Isupov's dilatometric data, transition from the para- to antiferroelectric state is accompanied by a reduction of volume, in contrast to the case of lead magnetungstate, in which volume increases. The sign of volume change contradicts other data [112]. Furthermore, according to Isupov, around  $-20^\circ\text{C}$  there is a phase transition, apparently between different antiferroelectric phases, accompanied by an increase in volume with falling temperature and also by a bend on the  $\epsilon$  curve. Further, according to Bokov's data [113], at  $-205^\circ\text{C}$  a phase transition occurs from the antiferro- to ferroelectric state, accompanied by a discontinuity on the  $\epsilon$  curve and by a  $\tan \delta$  peak. At temperatures below  $-100^\circ\text{C}$  in fields of  $150 \text{ kV/cm}^{-1}$  double hysteresis loops are seen, and here the critical field decreases as temperature falls. At temperatures below that of liquid nitrogen there are normal hysteresis loops with a coercive force weaker than the break-through field in which the loops appear.

Thus, the properties of this compound are very similar to those of solid solutions of lead magnetungstate with lead titanate and lead magnetobate [99], and the antiferroelectric phase occurring below  $-20^\circ\text{C}$  and the antiferroelectric phase in lead magnetungstate and its solutions can be assumed identical, and their ferroelectric phases can also be assumed identical. At  $-264^\circ\text{C}$  a transition occurs to the antiferromagnetic state [111].

#### 9. $\text{PbCd}_{1/2}\text{W}_{1/2}\text{O}_3$

The compound  $\text{PbCd}_{1/2}\text{W}_{1/2}\text{O}_3$  was first synthesized in [113], where it was also assumed that it is a ferro- or antiferroelectric material. In this compound, as in other analogous tungstates, there is ordering of ions occupying the octahedral positions in the lattice. At room temperature the structure is pseudomonoclinic, and in the  $400^\circ\text{C}$  region there is a phase transition to the cubic phase, accompanied by an increase in the volume of the nucleus [114, 115].

No dielectric hysteresis loops are seen at temperatures of  $-190$  to  $+160^\circ\text{C}$  [116]. The temperature dependence of  $\epsilon$  is characterized by a jump around  $410$ - $420^\circ\text{C}$  and a level maximum at  $190$ - $250^\circ\text{C}$  [115, 117]. The temperature dependence of  $\epsilon$  in a wide frequency range is illustrated in Figure 17.10. On the basis of high-frequency measurements of  $\epsilon$  it may be concluded that the phase transition at  $420^\circ\text{C}$  is a transition to a polarized, possibly antiferroelectric state. At temperatures below  $420^\circ\text{C}$  several

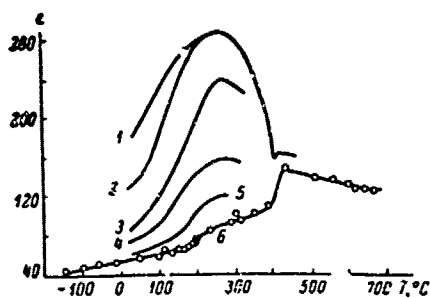


Figure 17.10. Temperature dependence of  $\epsilon$  of polycrystalline  $\text{PbCd}_{1/2}\text{W}_{1/2}\text{O}_3$  on various frequencies (Poplavko, et al [117]). 1 -- at frequency  $1.05 \cdot 10^5$ ; 2 -- at  $3.7 \cdot 10^6$ ; 3 --  $1.35 \cdot 10^8$ ; 4 --  $3 \cdot 10^8$ ; 5 --  $1.9 \cdot 10^9$ ; 6 --  $3.7 \cdot 10^{10}$  Hz.

and  $\text{PbLu}_{1/2}\text{Ta}_{1/2}\text{O}_3$  were also synthesized and analyzed [119].  $\text{PbHo}_{1/2}\text{Nb}_{1/2}\text{O}_3$  and  $\text{PbIn}_{1/2}\text{Nb}_{1/2}\text{O}_3$  were first synthesized in [120]. These compounds have a monoclinic structure at room temperature [112, 121].

At the antiferroelectric Curie points there are sharp  $\epsilon$  peaks ( $\epsilon_{\text{max}} < 300$ ). Transition to the antiferroelectric state is accompanied by a reduction of volume. Also, compounds containing Yb have low-temperature transitions [112, 119].

X-ray diffraction analysis of  $\text{PbYb}_{1/2}\text{Nb}_{1/2}\text{O}_3$  [112] in the antiferro- and paraelectric regions revealed superstructure lines due to ordering of niobium ytterbium ions. Furthermore, due to antiparallel displacements of ions there is superstructure in the antiferroelectric region, which vanishes in the paraelectric phase.

Presented below are data on the Curie points of antiferroelectrics of the perovskite type, containing rare-earth ions in the octahedral positions [119]:

Compound	$T, ^\circ\text{C}$
$\text{PbYb}_{1/2}\text{Nb}_{1/2}\text{O}_3$ .....	300
$\text{PbYb}_{1/2}\text{Ta}_{1/2}\text{O}_3$ .....	285
$\text{PbLu}_{1/2}\text{Nb}_{1/2}\text{O}_3$ .....	270
$\text{PbLu}_{1/2}\text{Ta}_{1/2}\text{O}_3$ .....	278

phase transitions apparently occur [116]. There is considerable dispersion of  $\epsilon$  and high value of  $\tan \delta$  at high temperatures in this temperature region, related [117] to the fact that these transitions possibly lead to the appearance of ferroelectric phases.

#### 10. Antiferroelectric Materials Containing Rare-Earth Ions in Octahedral Positions

The first of the antiferroelectrics with the formula  $\text{A}^{2+}(\text{B}^{3+}\text{B}^{5+})\text{O}_3$ , where  $\text{B}^{3+}$  is a rare-earth ion, to be discovered was  $\text{PbYb}_{1/2}\text{Nb}_{1/2}\text{O}_3$  [118]. Antiferroelectrics  $\text{PbYb}_{1/2}\text{Ta}_{1/2}\text{O}_3$ ,  $\text{PbLu}_{1/2}\text{Nb}_{1/2}\text{O}_3$

## 11. BiFeO<sub>3</sub>

This compound, in which electric and magnetic ordering are combined, is discussed in Chapter 18. We will point out here that the nature of the electric ordering in this compound is not conclusively established. The small  $\epsilon$  at the Curie point  $T_c = 850^\circ\text{C}$  [122] indicates that a phase transition occurs from the paraelectric phase to the antiferroelectric phase. Along with the phase transition to the paraelectric phase, BiFeO<sub>3</sub> has several phase transitions in the range of electric ordering [122-125]. Some of these are possibly transitions between antiferroelectric and ferroelectric phases, and some may be so-called isomorphic phase transitions that take place without alteration of the spatial group.

The superstructure lines seen in neutron radiography analyses [126-128] are evidence for a multiplet elemental nucleus. Electron diffraction [129] and x-ray diffraction [130] analyses, however, did not reveal any superstructure. It can be concluded, apparently, that antiparallel displacements of cations occur at the investigated temperatures, and the superstructures related to antiparallel displacements of oxygen, since displacement of such heavy ions as Bi<sup>5+</sup> and Fe<sup>3+</sup> would have been detected. The positions of the cations, according to [129, 130] are quite different.

The spatial group of BiFeO<sub>3</sub>, with consideration of the multiplicity of the nucleus, has not yet been determined. The absence of antiparallel displacements of cations, along with an indication of the generation of the second harmonic on BiFeO<sub>3</sub> powder [128] indicate that BiFeO<sub>3</sub> is polar at room temperature, which excludes antiferroelectricity at higher temperatures.

Investigation of solid solutions based on BiFeO<sub>3</sub> indicate the closeness of the free energies of the ferro- and antiferroelectric phases. In many solid solutions  $\epsilon$  increases with increasing structural factor  $t$  and the ferroelectric state occurs (for instance in solid solutions BiFeO<sub>3</sub> with PbFe<sub>1/2</sub>Nb<sub>1/2</sub>O<sub>3</sub> [123], PbTiO<sub>3</sub> [131, 128], BaFe<sub>1/2</sub>Nb<sub>1/2</sub>O<sub>3</sub> [132]), and when structural factor  $t$  decreases, the antiferroelectric state becomes more stable (for instance in solid solutions with LaFeO<sub>3</sub> [132, 133]). Different conclusions are reached in [132, 133] concerning the nature of the rhombohedral region of the solid solutions.

## §2. Other Displacement Type Antiferroelectric Compounds

### 1. Tungsten Trioxide

The anomalous dielectric properties of WO<sub>3</sub> were first discovered in [134] and [135]. Hysteresis loops and high permittivity were found in these

works, with the result that  $\text{WO}_3$  was classified as a ferroelectric. Subsequent works, however, showed that antiferroelectricity may exist in certain phases of  $\text{WO}_3$ .

The structure of  $\text{WO}_3$  is a deformed  $\text{ReO}_3$  type structure, which can be derived from the perovskite structure by removing a type A angle ion. It is constructed of octahedrons, connected to each other at the vertices and forming a three-dimensional structure. The structure of  $\text{WO}_3$  was investigated at room temperature in [136-139]. The spatial group is  $C_{2h}^5 - P2_1/n$ . The structure is monoclinic. The elemental nucleus has 8 units. The configuration of ion displacements concurs with the results of [136], but contradicts the results of [138]. According to [139] tungsten ions are displaced in antiparallel from the centers of the octahedrons in such a way that the crystal is nonpolar on all three axes. It is concluded that if the structure is antiferroelectric, polarization lies basically in plane ab. The lattice parameters at  $+30^\circ\text{C}$  are:  $a = 7.30$ ,  $b = 7.53$ ,  $c = 7.68 \text{ \AA}$ ,  $\beta = 90^\circ 54'$  [139].

When  $\text{WO}_3$  is cooled from room temperature to about  $17^\circ\text{C}$  a phase transition occurs from monoclinic to triclinic crystalline phase [140, 141]. With further cooling in the  $-50$  to  $-40^\circ\text{C}$  range there is a phase transition to a new phase (during heating this transition occurs at  $-20^\circ\text{C}$ ). It was previously assumed that its structure is trigonal [142, 143], but it is confirmed in [141] to be monoclinic. According to [144], permittivity drops sharply during the first cooling in the  $-40$  to  $50^\circ\text{C}$  range, but after repeated heating and cooling the temperature dependence levels off. There are data on the observation of dielectric hysteresis loops and concerning the motion of domain boundaries under the influence of an electric field [134, 143, 145], which suggests the properties in this phase to be ferroelectric.

As the temperature increases above room temperature a phase transition occurs at  $330^\circ\text{C}$  from monoclinic to rhombic [146-148]. The positions of the ions in this phase presumably do not differ much from the positions of the ions in the monoclinic phase, achieved at room temperature.

At  $740^\circ\text{C}$  a phase transition takes place to the tetragonal phase [147, 149]. It was shown [149] that a simple antiparallel configuration of ion displacements on the c axis exists in this phase, corresponding to the Kittel antiferroelectric structure. Chains of  $\text{W}^{6+}$  ions, displaced in the positive direction on the c axis, alternate with chains of ions displaced in the negative direction on the c axis. The elemental nucleus contains two  $\text{WO}_3$  units and has dimensions  $a = a_0\sqrt{2}$ ,  $c = a_0$ , where  $a_0$  is the cubic lattice constant. At  $910^\circ\text{C}$  a phase transition occurs, apparently to another tetragonal phase [142, 144, 150]. At  $1,230^\circ\text{C}$  there is a phase transition to a new, apparently also tetragonal phase [142, 144]. It is

not possible at this time to make a firm conclusion about the nature of the various phases of  $\text{WO}_3$ , due to the high conductivity, which interferes with reliable dielectric measurements, even at low temperatures.

## 2. Lead Orthovanadate

The dielectric properties of poly- and monocrystals of lead orthovanadate ( $\text{Pb}_3\text{V}_2\text{O}_8$ ) were studied in [151]. It was found that near  $100^\circ\text{C}$  a phase transition occurs, accompanied by anomalous permittivity (Figure 17.11) and thermal expansion, and also by the disappearance of twinning structure on heating. No hysteresis loops were observed. It may be assumed that the phase transition observed is antiferroelectric [151].

Lead orthovanadate has a rhombic structure [152] with  $a_k = 7.65 \text{ \AA}$ ,  $\alpha = 46^\circ 02'$ , has one unit in its elementary nucleus and belongs to spatial group  $\text{D}_{3d}^5 - \text{R}\bar{3}\text{m}$ . The crystalline structure of lead orthovanadate is illustrated in Figure 17.12. Its lattice is constructed of isolated  $\text{VO}_4$  tetrahedrons, surrounded by lead ions. The phase transition at  $100^\circ\text{C}$  is accompanied on heating by sharp compression on the c axis and relatively little expansion in the direction perpendicular to c, so that the volume here shrinks.

In addition to the phase transition at  $100^\circ\text{C}$  there is a phase transition near  $0^\circ\text{C}$ , accompanied by anomalous  $\epsilon$  and an increase in volume on heating.

## 3. Lead Silicate ( $\text{Pb}_4\text{SiO}_6$ )

A reversible phase transition takes place at  $155^\circ\text{C}$  in lead silicate,  $\text{Pb}_4\text{SiO}_6$ , which apparently corresponds to contraction during heating [153, 154]. It was shown [155] that this transition is accompanied by a sharp anomaly in permittivity. The peak value of  $\epsilon$  is a low  $< 40$ . No hysteresis loops were observed. On the basis of these data this phase transition is assumed to be of antiferroelectric character [155].

## 53. Antiferroelectric Compounds with Order-Disorder Type Phase Transition

The properties of long known antiferroelectrics with the order-disorder transition of the group  $\text{NH}_4\text{H}_2\text{PO}_4$  (ADP) and periodates ( $(\text{NH}_4)_2\text{H}_5\text{IO}_6$ , etc.) is given in [156]. Therefore we will simply point out here that new data were found recently concerning the ordering of protons in the hydrogen bonds during transition to the antiferroelectric state in ADP. According to nuclear magnetic resonance analyses [157, 158], the sharp increase in time between skips of deuterons along the bond  $\text{O}-\text{D}\dots\text{O}$  in deuterated ADP corresponds to transition to the antiferroelectric state. It is thought that the hydrogen bond, which play an active part in spontaneous

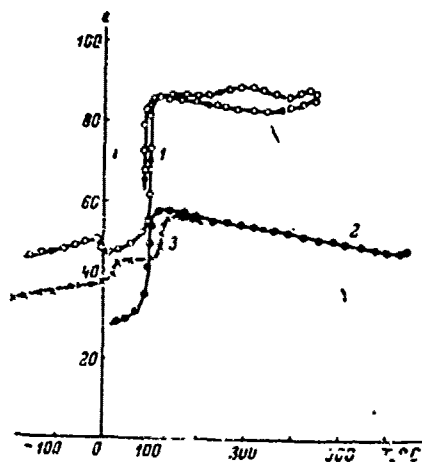


Figure 17.11. Temperature dependence of permittivity of  $\text{Pb}_3\text{V}_2\text{O}_8$  (Isupov, et al [151]): 1, 2 -- different polycrystalline specimens, frequencies 500 kHz and 58 MHz, respectively; 3 -- monocrystal, frequency 500 kHz, field parallel to c axis (perpendicular to planes of cleavage).

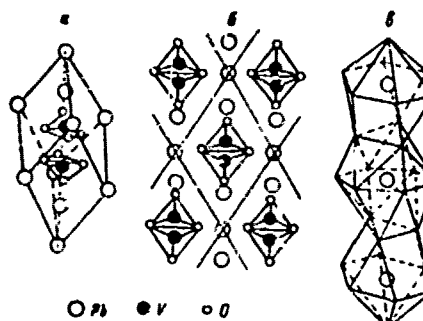


Figure 17.12. Crystalline structure of lead orthovanadate: a -- rhombohedral elementary nucleus  $\text{Pb}_3\text{V}_2\text{O}_8$  (Bachman [152]); b -- projection onto plane perpendicular to  $\langle 100 \rangle$ ; c -- background of lead ions.

polarization, induce dipole moments in groups  $\text{PO}_4$ ,  $\text{IO}_6$ , among others, and their ordering leads also to ordering of the dipole moments of these groups.

We will proceed now to description of the properties of comparatively recently discovered order-disorder type antiferroelectrics.

### 1. Cesium Trihydro-selenite

A report appeared in [159] concerning the discovery of antiferroelectricity in  $\text{CsH}_3(\text{SeO}_3)_2$ . More detailed data are found in [160]. The Curie point of this antiferroelectric is 145°K, the paraelectric and antiferroelectric phases have triclinic symmetry and belong to the same spatial group  $C_1^1$ -P1. In the antiferroelectric phase there is a superstructure on the c axis, so that  $c_{\text{anti}} \approx 2c_{\text{para}}$ .

Careful investigations of the pyroeffect did not detect spontaneous polarization. There is no piezoelectric effect. Near the Curie point were found double hysteresis loops, each loop with extremely narrow, possible zero "width." These loops apparently correspond to induced phase transition between the antiferro- and paraelectric phases (although it still cannot be ruled out that this transition is between the antiferro- and

ferroelectric phases). The critical field diminishes with increasing temperature and vanishes at the Curie point. Permittivity, perpendicular to plane (100), peaks at the Curie point. There is also a peak in direction [010]. No anomaly was found in  $\epsilon$  in direction [001].  $\Theta = 65^\circ\text{K}$ ,  $C = 1.4 \cdot 10^3 \text{K}$ . In the presence of a stationary field the Curie point drops (to  $-2.8^\circ\text{C}$  for 32 kV/cm),  $\epsilon_{\text{max}}$  first increases and then begins to fall as the critical field is reached. Below the Curie point there are no domains and it is concluded that the crystal remains single-domain, which agrees with triclinic symmetry. There is a slight change in birefringence at the Curie point. It can be concluded that the antiparallel dipole moments are near the plane perpendicular to the c axis. The anomalous heat capacity at the Curie point corresponds to  $\delta Q = 116 \text{ cal/mole}$ . The entropy change is  $\delta S = 0.81 \text{ cal/mole}\cdot\text{deg}$ . On the basis of data [160, 161], the phase transition should be classified as the order-disorder type.

## 2. Copper Forminate Tetrahydrate

A dielectric anomaly in copper forminate tetrahydrate  $(\text{Cu}(\text{HCOO})_2 \cdot 4\text{H}_2\text{O})$  is reported in [162, 165]. On the basis of the investigation of dielectric properties in [163] it is concluded that this compound is an antiferroelectric with the Curie point  $-39^\circ\text{C}$ . Also, at  $17^\circ\text{K}$  a transition occurs to the antiferromagnetic state [164].

The crystalline structure is determined [165, 166] through neutron radiography. At room temperature the crystal is monoclinic, and the spatial group is  $C_{2h}^5 - P2_1/a$ . The elemental nucleus contains two units, and some of the hydrogen atoms are disordered. The crystal consists of alternating layers, formed by water molecules and copper forminate groups. The layers are parallel to planes (01). There is superstructure in the antiferroelectric phase, corresponding to the doubling of parameter c with the elemental nucleus [167].

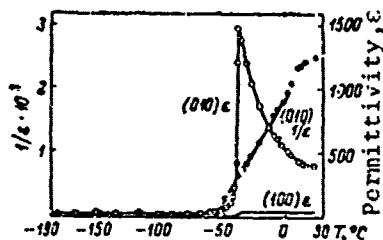


Figure 17.13. Temperature dependence of permittivity of copper forminate tetrahydrate in directions perpendicular to planes (010)-(010)  $\epsilon$  and (100)-(100)  $\epsilon$  (according to Okada [198]).

The permittivity in the direction perpendicular to the plane (010) displays at  $-39^\circ\text{C}$  a sharp peak (Figure 17.13),  $\epsilon_{\text{max}} \sim 1,500$  and the Curie-Weiss constant is  $3.2 \cdot 10^4 \text{K}$  [163]. At temperatures somewhat below the Curie point are double hysteresis loops. An external field occurs at the transition point [163]. Deuteration increases the Curie point to  $-27^\circ\text{C}$ . There is a  $\lambda$ -form heat capacity anomaly at the Curie point. The entropy change at the transition is  $0.78 \text{ cal/mole}\cdot\text{deg}$  in tetrahydrate and  $0.90 \text{ cal/mole}\cdot\text{deg}$

in deuterated tetrahydrate [168]. The first order antiferroelectric phase transition is of the order-disorder type and is related to ordering of hydrogen ions in the layers of water molecules.

### 3. Ammonium Halides

The opinion was offered in [169] that the tetragonal phase (phase III) of the ammonium halides  $\text{NH}_4\text{I}$  and  $\text{NH}_4\text{Br}$ , with the CsCl structure, is antiferroelectric. Antiparallel displacements of the ions  $\text{I}^-$  and  $\text{Br}^-$  are detected in this phase, resulting in the appearance of superstructure lines on x-ray diffraction patterns [170, 171]. At 235°K in  $\text{NH}_4\text{Br}$  and 231°K in  $\text{NH}_4\text{I}$  a phase transition occurs to phase II, which is cubic. The elemental nucleus of the tetragonal phase has the parameters  $a' = a\sqrt{2}$  and  $c' = a$ , where  $a$  is the parameter of the initial cubic nucleus, and contains two units [170-172]. The spatial group of phase III is  $D_{4h}^7$ -P4/nmm. Diagrams of the phase transitions in these compounds are presented in [173] as functions of temperature and pressure. When pressure is applied, the temperature of the phase transition between phases III and III drops. Deuteration also lowers the temperature of this transition.

Many attempts have been made at dielectric measurements of ammonium halides [174, 175], but the results of the various researchers differ with respect to both permittivity and the temperatures of dielectric anomalies related to phase transitions.

The nuclear magnetic resonance (NMR) of protons in ammonium halides was investigated in [176, 177] as a function of temperature. The NMR of the halogen ions was investigated in [178]. A small abrupt change in the second moment of the proton resonance line was observed [177] in the region of the phase transition between phases II and III in ammonium bromide. It was shown [178] that quadrupole expansion of the nuclear resonance line of  $\text{Br}^{81}$  occurs in phase III of ammonium bromide, and the magnitude of this expansion characterizes to some degree the ordering of the crystal. Nagamiya [179] proposed a theory of phase transitions in ammonium halides, in which the effect of polarization of halogen ions and the interaction of octupole moments of ammonium tetrahedra are taken into account.

### 4. Rubidium Nitrate

On the basis of investigation of the dielectric properties of rubidium nitrate ( $\text{RbNO}_3$ ) it is theorized in [180, 181] that this crystal is antiferroelectric. According to differential thermal analysis [182] there are four stable forms in rubidium nitrate between room temperature and the melting point, the temperatures of the phase transitions between which are:

IV  $\xrightarrow{181^\circ\text{C}}$  III  $\xrightarrow{215^\circ\text{C}}$  II  $\xrightarrow{371^\circ\text{C}}$  I. Two anomalies in  $\epsilon$  were found [180, 181], corresponding to phase transitions between phases IV and III and between phases III and II. The application of a field expands the region of phase III

and increases somewhat  $\epsilon$  in phases IV and II; also, double hysteresis loops were observed in phase IV, on the basis of which it is assumed [180] that phase II is antiferroelectric, and in [181] phase IV as well. The structures of the phases are described in [183-185].

### 5. Potassium Nitrate

A theory is advanced [186] that the phase of potassium nitrate ( $\text{KNO}_3$ ) existing at room temperature (usually called phase II) is antiferroelectric. Its structure is rhombic, of the aragonite type, the spatial group is  $D_{2h}^{16}$ - $P_{nma}$  and the antipolar direction is axis b. On heating, phase II changes at  $130^\circ\text{C}$  to phase I, having the calcite type structure with spatial group  $D_{3d}^6$ - $R\bar{3}c$ . On cooling, an intermediate phase III forms, possessing ferroelectric properties. Its structure is similar to that of phase I, the spatial group is  $C_{3v}^5$ - $R3m$  and its range of existence is  $\sim 10$ - $20^\circ\text{C}$  [186-188]. It is shown [188] that a stationary field lowers the temperature of transition between phases II and I. Also, double hysteresis loops were observed in phase II. These data support the assumption of the antiferroelectric nature of phase II.

### 6. Other Antiferroelectric Compounds of the Order-Disorder Type

There are data concerning the formation of a sinusoidal antiferroelectric phase in sodium nitrate between the ferroelectric and paraelectric phases [189, 190]. This phase is characterized by the appearance of a superstructure on axis a [189], corresponding to an eight-fold increase of period  $a_0$  on this axis [190]. A model of the new phase is proposed [190], which satisfactorily explains the x-ray diffraction data. This model incorporates sinusoidal modulation of the ordering parameter in each layer, with a thickness equal to the parameter  $a_0$ . In other words, this model has sinusoidal modulation of the summary dipole moment of each layer (Figure 17.14). (We will recall that the ordering parameter is  $S = \frac{N_+}{N} - \frac{N_-}{N}$ , where  $N$  is the number of elemental nuclei per unit of volume,  $N_+$  is the number of nuclei with positive polarity and  $N_-$  is the number of nuclei with negative polarity). The sinusoidal antiferroelectric phase exists in about a  $1^\circ\text{C}$  temperature range ( $\sim +163$  to  $\sim +164^\circ\text{C}$ ). Anomalies in the temperature dependence of the lattice constants [191], permittivity [192] and heat capacity [193] correspond to the phase transitions between the ferro- and antiferroelectric phases (temperature  $T_{fa}$ ) and between the antiferro- and paraelectric phases (temperature  $T_{ap}$ ).



Figure 17.14. Schematic diagram of sinusoidal modulation of summary dipole moments in anti-ferroelectric phase of  $\text{NaNO}_2$  (according to Yamada [190]). The arrows show the magnitude and direction of dipole moments of layers with thickness corresponding to parameter  $a_0$  of ferroelectric phase.

Electromechanical measures indicated the absence of the piezoelectric effect in the sinusoidal phase [194]. Studies of the quadrupole splitting of NMR lines on  $\text{Na}^{23}$  in the temperature range corresponding to the sinusoidal phase [195] revealed additional separation indicating the coexistence of two different gradients. How this result correlates with the eight-fold increase in the nucleus of this phase and presence of a certain relationship between the parameter  $S$  and quadrupole splitting, also observed in [195] in the ferroelectric phase, remains unclear. The application of hydrostatic pressure increases both  $T_{fa}$  and  $T_{ap}$ , and here the range of existence of the sinusoidal phase expands from  $-1^\circ\text{C}$  at 1 bar to  $-8^\circ$  at 10 kbar [196].

The number of antiferroelectrics, beyond the compounds which we have examined, is obviously unlimited. Several phases have been found in thiourea  $\text{SC}(\text{NH}_2)_2$  [197-201], in which the ordering of the dipole moments of thiourea molecules differs. Some of these phases are antiferro- or ferroelectric. Phase transitions have been observed in many alums, some of which are apparently antiferroelectric [202-204]. There have been reports that certain crystalline phases of ice are perhaps even antiferroelectric [205]. The list is almost infinite.

#### 54. Discussion of Concept of Antiferroelectricity

Most contemporary researchers have an opinion concerning the commonality of the nature of ferro- and antiferroelectrics. One may conclude from examination of experimental data that one antiparallel orientation or other more general form of orientation of dipole moments is not enough to permit the classification of a crystal as an antiferroelectric. It is necessary that a phase transition occur in the crystal, accompanied by the characteristic anomaly of dielectric properties.

From estimates of the electrostatic dipole-dipole interaction in the ferro- and antiferroelectric phases with the perovskite structure can be concluded that its magnitude differs little for all these phases. This agrees satisfactorily with experimental data on the nearness of the free energies of the ferro- and antiferroelectric phases, which governs the possibility of phase transitions between these phases. This is hardly a random coincidence. It is the basis on which many researchers conclude that electrostatic interaction plays a great part in the formation of antiferroelectricity and determination of relative stability of ferro- and antiferroelectric phases, even though short-range forces perhaps play a greater role in antiferroelectrics than in ferroelectrics.

It should be pointed out that along with theories that regard electrostatic dipole-dipole interaction as the cause of spontaneous polarization, there have been many attempts to explain it from the standpoint of the electron states of atoms. Such works include, in particular [206]. According to [206] the d-zones of transition elements and p-zones of oxygen are close in ferroelectrics of the perovskite class. The result of this proximity of zones (pseudodegeneration) is displacement of atomic nuclei from the initial positions in the lattice and formation of dipole moments. Thorough examination, apparently, can also be applied to antiferroelectrics. In any case, that the effects of pseudodegeneration may be the deciding factor in the phase transitions of certain antiferroelectrics cannot be ruled out.

If one proceeds from the assumption of generality of the nature of ferro- and antiferroelectricity, then one obviously should not classify transitions of the buckling type as antiferroelectric phase transitions. In accordance with Smolenskiy and Matthias [207, 208], Megaw [59] pointed out that ferro- and antiferroelectric phases in compounds of the perovskite class are characterized primarily by the presence of displacements of ions of the transition elements with an unfilled next to the last d-shell from their initial positions in the centers of the octahedrons. It has also been shown that displacements of lead ions also occur in lead-containing perovskites. The phases that occur after buckling transitions are characterized by displacements of oxygen ions as a result of the alternating slope of the octahedrons as a whole. The displacements of A type ions that usually occur in this case facilitate tighter packing of the ions. Displacements of B type ions relative to the oxygen shell are not characteristic of these phases. This apparently means that the phases that form after buckling transitions and after antiferroelectric phase transitions are different in nature.

It is noteworthy, on the other hand, that oxygen-octahedral titanates and niobates are known, in which type B ions are displaced from the centers of the octahedron, but in which there are, nevertheless, no phase transitions that are accompanied by anomalous dielectric properties. Such compounds include, for instance, barium tetratitanate  $\text{BaTi}_4\text{O}_9$  [209]. The configuration of the shortest distances B-O, which is usually tied to the distribution of homeopolar bonds, is analogous to tetragonal barium titanate. It may be assumed that there are no low-frequency long-wave optical modes of vibrations in such compounds, since their permittivity is low, and they should not be called antiferroelectrics.

Thus, it is now customary to classify as antiferroelectric phases only those phases with a free energy close to the free energy of ferroelectric phases. The antiferroelectrics, in addition to compensation of dipole moments, are characterized by considerable anomalies in dielectric properties on transition to the paraelectric state, reduction of the temperature of these transitions and increase of  $\epsilon$  when an electric field is applied, and also phase transitions into the ferroelectric state are possible (when some of the ions are substituted under the influence of temperature, electric field, pressure).

## BIBLIOGRAPHY

1. Kittel, C. Phys. Rev., Vol. 82, p. 729, 1951.
2. Shirane, G., E. Sawaguchi and Y. Takagi, Phys. Rev., Vol. 84, p. 476, 1951.
3. Frenkel, J., Acta Physicochim. U.R.S.S., Vol. 3, p. 23, 1935.
4. Frenkel, J. I., Statisticheskaya Fizika (Statistical Physics), USSR Academy of Sciences Publishing House, Moscow-Leningrad, 1948.
5. Sawaguchi, E., J. Phys. Soc. Japan, Vol. 3, p. 615, 1953.
6. Tennery, V. J., J. Am. Ceram. Soc., Vol. 49, p. 483, 1966.
7. Sawaguchi, E., H. Maniwa and S. Hoshino, Phys. Rev., Vol. 83, p. 1073, 1951.
8. Jona, F., G. Shirane, F. Mazzi and R. Pepinsky, Phys. Rev., Vol. 105, p. 849, 1957.
9. Jona, F., G. Shirane and R. Pepinsky, Phys. Rev., Vol. 97, p. 1584, 1955.
10. Kravnik, N. N., ZhTF [Zhurnal Tekhnicheskoy Fiziki; Journal of Technical Physics], Vol. 28, p. 525, 1958.
11. Gul'po, L., FTT [Fizika Tverdogo Tela: Solid State Physics], Vol. 8, p. 2469, 1966.
12. Tennery, V. J., J. Electrochem. Soc., Vol. 112, p. 1117, 1965.
13. Smolenskiy, G. A., DAN SSSR (Reports of USSR Academy of Science), Vol. 70, p. 405, 1950.
14. Smolenskiy, G. A., ZhTF, Vol. 20, p. 137, 1950.
15. Smolenskiy, G. A., ZhTF, Vol. 21, p. 1045, 1951.
16. Roberts, S., J. Am. Ceram. Soc., Vol. 33, p. 63, 1950.
17. Sawaguchi, E. and T. Kittaka, J. Phys. Soc. Japan, Vol. 7, p. 336, 1952.
18. Petrev, V. M., Izv. AN SSSR, ser. fiz. (News of USSR Academy of Sciences, Physics Series), Vol. 23, p. 953, 1965.
19. Khuchua, N. P., I. N. Shamileva and V. V. Mal'tseva, Izv. AN SSSR, ser. fiz., Vol. 31, p. 1891, 1967.
20. Khuchua, N. P. and V. A. Yevseyev, FTT, Vol. 8, p. 258, 1966.

21. Poplavko, Yu. M. and V. G. Tsykalov, FTT, Vol. 9, p. 3305, 1967.
22. Marutake, M. and T. Ikeda, J. Phys. Soc. Japan, Vol. 10, p. 424, 1955
23. Rapoport, E., Phys. Rev. Lett., Vol. 17, p. 1097, 1966.
24. Shirane, G., Phys. Rev., Vol. 86, p. 219, 1952.
25. Sawaguchi, E., G. Shirane and Y. Takagi, Phys. Rev., Vol. 6, p. 333, 1951.
26. Shirane, G. and R. Pepinsky, Phys. Rev., Vol. 71, p. 812, 1963.
27. Kraynik, N. N., ZhTF, Vol. 28, p. 536, 1958.
28. Venetsev, Yu. N. and G. S. Zhdanov, Izv. AN SSSR, ser. fiz., Vol. 21, p. 275, 1957.
29. Tessman, J. H., A. H. Kahn and W. Shockley, Phys. Rev., Vol. 92, p. 890, 1953.
30. Takagi, Y., Proc. Intern. Conf. Theor. Phys., Tokyo, p. 824, 1953.
31. Kinase, W., Progr. Theor. Phys., Vol. 13, p. 529, 1955.
32. Kraynik, N. N., FTT, Vol. 2, p. 993, 1960; Izv. AN SSSR, ser. fiz., Vol. 24, p. 1187, 1960.
33. Lawless, W. N., J. Phys. Soc. Japan, Vol. 23, p. 325, 1967.
34. Lyubimov, V. N., Yu. N. Venetsev, S. P. Solov'yev, G. S. Zhdanov and A. B. Bakushinskiy, FTT, Vol. 4, p. 3543, 1962.
35. Kraynik, N. N., Izv. AN SSSR, ser. fiz., Vol. 28, p. 643, 1964.
36. Shirane, G. and S. Hoshino, Acta Cryst., Vol. 7, p. 203, 1954.
37. Shirane, G. and S. Hoshino, Phys. Rev., Vol. 80, p. 248, 1952.
38. Shirane, G. and A. Takeda, J. Phys. Soc. Japan, Vol. 7, p. 5, 1952.
39. Dungan, R. H., H. M. Barnett and A. H. Stark, J. Am. Ceram. Soc., Vol. 45, p. 382, 1962.
40. Barnett, H. M., J. Appl. Phys., Vol. 33, p. 1606, 1962.
41. Smolenskiy, G. A., A. I. Agranovskaya and N. V. Kraynik, DAN SSSR, Vol. 91, p. 55, 1953.
42. Ikeda, T., J. Phys. Soc. Japan, Vol. 14, p. 1286, 1959.

43. Kraynik, N. N., FTT, Vol. 2, p. 685, 1960.
44. Nomura, S. and T. Kawakubo, *J. Phys. Soc. Japan*, Vol. 17, p. 573, 1962.
45. Ref. Zhurn. "Fizika" (Abstract Journal: Physics), No. 1, p. 171, abs. No. 1541, 1957.
46. Kraynik, N. N., Izv. AN SSSk, ser. fiz., Vol. 21, p. 411, 1957.
47. Venevtsev, Yu. N. and G. S. Zhdanov, Izv. AN SSSR, ser. fiz., Vol. 20, p. 178, 1956.
48. Buhner, C. F., *J. Chem. Phys.*, Vol. 36, p. 798, 1962.
49. Granicher, H. and O. Jakits, *Nuovo Cimento*, No. 3, p. 480, 1954.
50. McQuarrie, M., *J. Am. Ceram. Soc.*, Vol. 38, p. 444, 1955; Vol. 40, p. 35, 1957.
51. Smolenskiy, G. A., V. A. Isupov, A. I. Agranovskaya and Ye. D. Sholokhova, ZhTF, Vol. 27, p. 2528, 1957.
52. Mitsui, T. and W. B. Westphal, *Phys. Rev.*, Vol. 124, p. 1354, 1961.
53. Geller, S., *J. Chem. Phys.*, Vol. 24, p. 1236, 1956.
54. Geller, S., *Acta Cryst.*, Vol. 10, p. 248, 1957.
55. Isupov, V. A., Izv. AN SSSR, ser. fiz., Vol. 21, p. 402, 1957.
56. Isupov, V. A., Izv. AN SSSR, ser. fiz., Vol. 22, p. 1504, 1958.
57. Cross, L. E., *Phil. Mag.*, Vol. 1, p. 76, 1956.
58. Ismailzade, I. G., Kristallografiya (Crystallography), Vol. 7, p. 718, 1962.
59. Megaw, H. D., *Ferroelectricity in Crystals*, London, 1957.
60. Granicher, H., *Nuovo Cimento, Suppl.* 6, p. 1220, 1957.
61. Isupov, V. A., Kristallografiya, Vol. 4, p. 603, 1959.
62. Jaffe, B., *Proc. IRE*, Vol. 49, p. 1264, 1961.
63. Berlincourt, D., H. Jaffe, H. H. Krueger and B. Jaffe, *Appl. Phys. Lett.*, Vol. 3, p. 90, 1963.
64. Hall, C. A., R. H. Dungan and A. H. Stark, *J. Am. Ceram. Soc.*, Vol. 47, p. 259, 1964.

55. Carlsson, L., *Acta Cryst.*, Vol. 23, p. 901, 1967.
56. Wilcox, D. L. and R. L. Cook, *J. Am. Ceram. Soc.*, Vol. 46, p. 343, 1963.
57. Matthias, B. T., *Phys. Rev.*, Vol. 75, p. 1771, 1949.
58. Matthias, B. T. and J. P. Remeika, *Phys. Rev.*, Vol. 82, p. 727, 1951.
59. Vousden, P., *Acta Cryst.*, Vol. 4, p. 545, 1951.
70. Shirane, G., R. Newnham and R. Pepinsky, *Phys. Rev.*, Vol. 96, p. 581, 1954.
71. Cross, L. E. and B. J. Nicholson, *Phil. Mag.*, Vol. 46, p. 453, 1955.
72. Megaw, H. D. and M. Wells, *Acta Cryst.*, Vol. 11, p. 858, 1958.
73. Wells, M. and H. D. Megaw, *Proc. Phys. Soc.*, Vol. 78, p. 6 (i), No. 505, p. 1258, 1961.
74. Francombe, M. H., *Acta Cryst.*, Vol. 9, p. 256, 1956.
75. Wood, E. A., R. C. Miller and J. P. Remeika, *Acta Cryst.*, Vol. 15, p. 1273, 1962.
76. Miller, R. C., E. A. Wood, J. P. Remeika and A. Savage, *J. Appl. Phys.*, Vol. 33, p. 1623, 1962.
77. Lefkowitz, L. and H. D. Megaw, *Acta Cryst.*, Suppl., Vol. 16, A188, 1963.
78. Isupov, V. A. and V. I. Kosyakov, *FTT*, Vol. 1, p. 929, 1959.
79. Kraynik, N. N., *Izv. AN SSSR, ser. fiz.*, Vol. 22, p. 1492, 1958.
80. Dungan, R. H. and R. D. Golding, *J. Am. Ceram. Soc.*, Vol. 47, p. 73, 1964.
81. Wood, E. A., *Acta Cryst.*, Vol. 4, p. 353, 1951.
82. Solov'yev, S. P., Yu. N. Venevtsev and G. S. Zhdanov, *Kristallografiya*, Vol. 6, p. 218, 1961.
83. Ismailzade, I. G., *Kristallografiya*, Vol. 8, p. 363, 1963.
84. Tenney, V. J., *J. Am. Ceram. Soc.*, Vol. 48, p. 537, 1965.
85. Cross, L. E., *Nature*, Vol. 181, p. 178, 1958.
86. Reisman, A. and E. Banks, *J. Am. Ceram. Soc.*, Vol. 80, p. 1877, 1958.
87. Wells, M. and H. D. Megaw, *Acta Cryst.*, Vol. 13, p. 1072, 1960.

88. Francombe, M. H. and B. Lewis, *J. Electronics*, Vol. 2, p. 387, 1957.
89. Lewis, B. and E. A. D. White, *J. Electronics*, Vol. 1, p. 646, 1956.
90. Bratschun, W. R. and R. L. Cook, *J. Am. Ceram. Soc.*, Vol. 44, p. 136, 1961.
91. Tennery, V. J., *J. Am. Ceram. Soc.*, Vol. 49, p. 376, 1966.
92. Iwasaki, H. and T. Ikeda, *J. Phys. Soc. Japan*, Vol. 18, p. 157, 1963.
93. Ismailzade, I. G., *Izv. AN SSSR, ser. fiz.*, Vol. 28, p. 675, 1964.
94. Iwasaki, H., *Japan J. Appl. Phys.*, Vol. 2, p. 737, 1963.
95. Glaister, R. M., *J. Am. Ceram. Soc.*, Vol. 43, p. 348, 1960.
96. Francombe, M. H. and B. Lewis, *Acta Cryst.*, Vol. 11, p. 175, 1958.
97. Smolenskiy, G. A., A. I. Agranovskaya and V. A. Isupov, *FTT*, Vol. 1, p. 990, 1959.
98. Zaslavskiy, A. I. and M. F. Bryzhina, *Kristallografiya*, Vol. 7, p. 709, 1962.
99. Smolenskiy, G. A., N. N. Krainik and A. I. Agranovskaya, *FTT*, Vol. 2, p. 981, 1961.
100. Khuchua, N. P. and L. F. Lychkataya, *Izv. AN SSSR, ser. fiz.*, Vol. 28, p. 708, 1964.
101. Krainik, N. N. and A. I. Agranovskaya, *FTT*, Vol. 2, p. 70, 1960.
102. Strukov, B. A., K. A. Minayeva, T. L. Skomorokhova and V. A. Isupov, *FTT*, Vol. 8, p. 972, 1966.
103. Polandov, I. N., *FTT*, Vol. 5, p. 1147, 1963.
104. Shuvalov, L. A. and K. A. Minayeva, *DAN SSSR*, Vol. 146, p. 308, 1962.
105. Minayeva, K. A., B. A. Strukov and V. A. Koptsik, *FTT*, Vol. 8, p. 1631, 1966.
106. Filip'yev, V. S., M. F. Kapriyanov and V. G. Fesenko, *Kristallografiya*, Vol. 8, p. 790, 1963.
107. Belyayev, I. N., V. S. Filip'yev and Ye. G. Fesenko, *ZhSKh [Zhurnal strukturnoy khimii; Journal of Structural Chemistry]*, Vol. 5, p. 19, 1963.

108. Filip'yev, V. S. and Ye. G. Fesenko, Kristallografiya, Vol. 9, p. 293, 1964.
109. Bokov, V. A., S. A. Kizhayev, I. Ye. Myl'nikova and A. G. Tutov, FTT, Vol. 6, p. 3038, 1964.
110. Bokov, V. A., S. A. Kizhayev, I. Ye. Myl'nikova, A. G. Tutov and A. G. Ostroumov, Izv. AN SSSR, ser. fiz., Vol. 29, p. 929, 1965.
111. Kizhayev, S. A. and V. A. Bokov, FTT, Vol. 8, p. 1957, 1966.
112. Tomashpoi'skiy, Yu. Ya. and Yu. N. Venevtsev, FTT, Vol. 6, p. 2598, 1964.
113. Belyayev, I. N., V. S. Filip'yev and Ye. G. Fesenko, ZhSKh, Vol. 4, p. 719, 1963.
114. Filip'yev, V. S. and Ye. G. Fesenko, Izv. AN SSSR, ser. fiz., Vol. 29, p. 894, 1965.
115. Roginskaya, Yu. Ye. and Yu. N. Venevtsev, Kristallografiya, vol. 10, p. 341, 1965.
116. Isupov, V. A. and L. T. Yemel'yanova, Kristallografiya, Vol. 11, p. 776, 1966.
117. Poplavko, Yu. M., V. G. Tsykalov, V. I. Molchanov and V. A. Isupov, FTT, Vol. 10, p. 1542, 1968.
118. Smolenskiy, G. A., A. I. Agranovskaya, S. N. Popov and V. A. Isupov, ZhTF, Vol. 28, p. 2152, 1958.
119. Isupov, V. A. and N. N. Krainik, FTT, Vol. 6, p. 3713, 1964.
120. Kupriyanov, M. F. and Ye. G. Fesenko, Kristallografiya, Vol. 10, p. 246, 1965.
121. Kupriyanov, M. F. and Ye. G. Fesenko, Izv. AN SSSR, ser. fiz., Vol. 29, p. 925, 1965.
122. Krainik, N. N., N. P. Khuchua, V. V. Zhdanova and V. A. Yevseyev, FTT, Vol. 8, p. 816, 1965.
123. Krainik, N. N., N. P. Khuchua, V. V. Zhdanova, I. E. Mylnikova and N. N. Parfenova, Proc. Intern. Meet. Ferroelectr., Vol. i, Prague, p. 377, 1966.
124. Ismailzade, I. G., DAN SSSR, ser. mat. i fiz. (Reports of USSR Academy of Sciences, Mathematics and Physics Series), Vol. 170, p. 85, 1966.

125. Tomashpol'skiy, Yu. Ya., Yu. N. Venevtsev and G. S. Zhdanov, ZhETF [Zhurnal eksperimental'noy i teoreticheskoy fiziki; Journal of Experimental and Theoretical Physics], Vol. 46, p. 1921, 1964.
126. Plakhtiy, V. P., Ye. I. Mal'tsev and D. M. Kaminker, Izv. AN SSSR, ser. fiz., Vol. 28, p. 436, 1964.
127. Sosnowska, I., E. Sosnowsky, S. W. Kiselev and R. P. Oserow, Proc. Symp. Inelast. Scatt. Neutr., Bombay, p. 533, 1965.
128. Smith, R. I., G. D. Achenbach, R. Gerson and W. J. James, J. Appl. Phys., Vol. 39, p. 70, 1968.
129. Tomashpol'skiy, Yu. Ya., Yu. N. Venevtsev and G. S. Zhdanov, Kristallografiya, Vol. 9, p. 846, 1964.
130. Tomashpol'skiy, Yu. Ya., Yu. N. Venevtsev and G. S. Zhdanov, Kristallografiya, Vol. 12, p. 252, 1967.
131. Venevtsev, Yu. N., G. S. Zhdanov, S. P. Solov'yev, Ye. V. Bezus, V. V. Ivanova, S. A. Fedulov and A. G. Kapyshev, Kristallografiya, Vol. 5, p. 620, 1960.
132. Kraynik, N. N., N. P. Khuchua, A. A. Berezhnoy, A. G. Tutov and A. Yu. Cherkashchenko, Izv. AN SSSR, ser. fiz., Vol. 29, p. 1026, 1965.
133. Roginskaya, Yu. Ye., Yu. N. Venevtsev and G. S. Zhdanov, ZhETF, Vol. 44, p. 1418, 1963.
134. Matthias, B. T., Phys. Rev., Vol. 76, p. 430, 1949.
135. Nagasawa, S., Denki Kagaku, Vol. 16, p. 57, 1948; Vol. 17, p. 174, 1949.
136. Braekken, H., Z. Krist., Vol. 78, p. 484, 1931.
137. Andersson, G., Acta Chem. Scand., Vol. 7, p. 154, 1953.
138. Ueda, R. and J. Kobayashi, Phys. Rev., Vol. 91, p. 1565, 1952.
139. Tanisaki, S., J. Phys. Soc. Japan, Vol. 15, p. 573, 1960.
140. Tanisaki, S., J. Phys. Soc. Japan, Vol. 14, p. 680, 1959.
141. Tanisaki, S., J. Phys. Soc. Japan, Vol. 15, p. 566, 1960.
142. Sawada, S., J. Phys. Soc. Japan, Vol. 11, p. 1246, 1956.
143. Matthias, B. T. and A. Wood, Phys. Rev., Vol. 84, p. 1255, 1951.
144. Sawada, S., J. Phys. Soc. Japan, Vol. 11, p. 1237, 1956.

145. Hirakawa, K., *Busseiron Kenkyu*, Vol. 38, p. 82, 1951.
146. Rosen, C., E. Banks and B. Foster *Acta Cryst.*, Vol. 9, p. 475, 1956.
147. Wyart, J. and M. Foex, *Compt. Rend.*, Vol. 232, p. 2459, 1951.
148. Sawada, S. and G. C. Danielson, *Phys. Rev.*, Vol. 113, p. 1008, 1959.
149. Kehl, W. L., R. G. Hay and D. Wahl, *J. Appl. Phys.*, Vol. 23, p. 212, 1952.
150. Foex, M., *Compt. rend.*, Vol. 220, p. 917, 1945; Vol. 228, p. 1335, 1949.
151. Isupov, V. A., N. N. Kraynik, I. D. Fridberg and I. Ye. Zelenkova, *FTT*, Vol. 7, p. 1051, 1965.
152. Bachmann, H. G., *Naturwiss.*, Vol. 39, p. 570, 1952; *Fortschr. Miner.*, Vol. 31, p. 9, 1959; *Neues Jahrb. Miner., Abt. A., Kristallogr. Miner. Gesteinskunde*, Vol. 9/10, p. 209, 1953.
153. Geller, R. F., A. S. Creamer and E. N. Bunting, *J. Res. NBS*, Vol. 13, p. 237, 1934.
154. Arguly, J. F. and F. A. Hummel, *J. Am. Ceram. Soc.*, Vol. 43, p. 452, 1960.
155. Isupov, V. A., *FTT*, Vol. 7, p. 2221, 1965.
156. Kentsig, V., *Segnetoelektriki i Antisegetoelektriki (Ferroelectrics and Antiferroelectrics)*, IL [Foreign Literature] Publishing House, Moscow, 1960.
157. Soest, J. F. and E. A. Uehling, *Bull. Am. Phys. Soc.*, Vol. 12, p. 290, 1967.
158. Geni, V. J., D. E. O'Reilly and T. Tsang, *Phys. Rev.*, Vol. 167, p. 445, 1968.
159. Makita, Y. and R. Pepinsky, *Bull. Am. Phys. Soc.*, Vol. 7, p. 177, 1962.
160. Makita, Y., *J. Phys. Soc. Japan*, Vol. 20, p. 1567, 1965.
161. Khanna, R. K., M. Horak and E. R. Lippincott, *J. Chem. Phys.*, Vol. 45, p. 982, 1966.
162. Kirivama, R., *Bull. Chem. Soc. Japan*, Vol. 35, p. 1199, 1962.
163. Okada, K., *Phys. Rev. Lett.*, Vol. 15, p. 252, 1965.
164. Kobayashi, H. and T. Masada, *J. Phys. Soc. Japan*, Vol. 18, p. 511, 1963.

165. Kiriya, R., N. Ibamoto and K. Matsuo, *Acta Cryst.*, Vol. 7, p. 482, 1954.
166. Okada, K., M. J. Kay, D. T. Gromer and I. Almodovar, *J. Chem. Phys.*, Vol. 44, p. 1648, 1966.
167. Turberfield, K. C., *Sol. St. Comm.*, Vol. 5, p. 887, 1967.
168. Okada, K., *Phys. Rev.*, Vol. 164, p. 685, 1967.
169. Sonin, A. S., *Kristallografiya*, Vol. 6, p. 137, 1961.
170. Ketelaar, J. A., *Nature*, Vol. 134, p. 250, 1934.
171. Weigle, J. and H. Saini, *Helv. Phys. Acta*, Vol. 9, p. 515, 1936.
172. Smits, A. and D. Tollenaar, *Z. Phys. Chem.*, Vol. B52, p. 22, 1942.
173. Stevenson, R., *J. Chem. Phys.*, Vol. 34, p. 1757, 1961.
174. Kamiyoshi, K. J., *J. Chem. Phys.*, Vol. 24, p. 1265, 1956.
175. M. J. Meinel, and R. Clinet, *Arch. Sci. fasc. spec.*, Vol. 10, p. 15, 1957.
176. Gutowsky, H. S., G. E. Pake and R. Bersohn, *J. Chem. Phys.*, Vol. 22, p. 643, 1954.
177. Iton, J., K. Kusaka and Y. Saito, *J. Phys. Soc. Japan*, Vol. 17, p. 463, 1962.
178. Iton, J. and Y. Yamagata, *J. Phys. Soc. Japan*, Vol. 17, p. 481, 1962.
179. Nagamiya, T., *Proc. Phys.-Math. Soc. Japan*, Vol. 24, p. 137, 1942; Vol. 25, p. 540, 1943; *Changements de Phase Soc. Chim. Phys.*, Paris, 1952.
180. Dantsiger, A. Ya. and Ye. G. Fesenko, *Kristallografiya*, Vol. 8, p. 894, 1963.
181. Dantsiger, A. Ya. and Ye. G. Fesenko, *Kristallografiya*, Vol. 10, p. 338, 1965.
182. Plyushchev, V. Ye., T. B. Markina and L. P. Shklover, *DAN SSSR*, Vol. 108, p. 645, 1956.
183. Brown, R. N. and A. C. McLaren, *Acta Cryst.*, Vol. 15, p. 974, 1962.
184. Finbak, C. and O. Hassel, *Z. Phys. Chem.*, B35, p. 25, 1937.
185. Korhonen, *Ann. Acad. Sci. Fenni, Sec. A*, Vol. 1, p. 37, 1951.

186. Sawada, S., S. Nomura and S. Fujii, J. Phys. Soc. Japan, Vol. 13, p. 1549, 1958.
187. Sawada, S., S. Nomura and Y. Asao, J. Phys. Soc. Japan, Vol. 16, p. 2486, 1961.
188. Dantsiger, A. Ya., Izv. AN SSSR, ser. fiz., Vol. 29, p. 1042, 1965.
189. Tanisaki, S., J. Phys. Soc. Japan, Vol. 16, p. 579, 1961.
190. Yamada, Y., I. Shibuya and S. Hoshino, J. Phys. Soc. Japan, Vol. 18, p. 1594, 1963.
191. Hoshino, S. and I. Shibuya, J. Phys. Soc. Japan, Vol. 16, p. 1254, 1961.
192. Takagi, Y. and K. Gesi, J. Phys. Soc. Japan, Vol. 19, p. 143, 1964.
193. Hoshino, S., J. Phys. Soc. Japan, Vol. 19, p. 140, 1964.
194. Hamano, K., J. Phys. Soc. Japan, Vol. 19, p. 945, 1964.
195. Betsuyaku, V., J. Phys. Soc. Japan, Vol. 21, p. 187, 1966.
196. Gesi, K., K. Ozawa and Y. Takagi, J. Phys. Soc. Japan, Vol. 20, p. 773, 1965.
197. Solomon, A. L., Phys. Rev., Vol. 104, p. 1191, 1956.
198. Goldsmith, G. I. and J. G. White, J. Chem. Phys., Vol. 31, p. 1175, 1959.
199. Futuma, H., J. Phys. Soc. Japan, Vol. 17, p. 434, 1962.
200. Dvoryankin, V. F., Kristallografiya, Vol. 4, p. 925, 1959.
201. Dvoryankin, V. F. and B. K. Vaynshteyn, Kristallografiya, Vol. 5, p. 589, 1960.
202. Pepinsky, R., F. Jona, G. Shirane, Phys. Rev., Vol. 102, p. 1181, 1956.
203. Bowers, K. D. and J. Owen, Rep. Progr. Phys., Vol. 18, p. 504, 1955.
204. Burns, G., J. Chem. Phys., Vol. 32, p. 1585, 1960.
205. Whalley, E., J. B. R. Heath and D. W. Davidson, J. Chem. Phys., Vol. 48, p. 2362, 1968.
206. Bersuker, I. B. and B. G. Vekhter, FTT, Vol. 9, p. 2652, 1967; Izv. AN SSSR, ser. fiz., Vol. 33, p. 199, 1969.

207. Smolenskiy, G. A. and N. V. Kozhevnikova, DAN SSSR, Vol. 76, p. 519, 1951.
208. Matthias, B. T., Science, Vol. 113, p. 591, 1951.
209. Templeton, D. H. and C. H. Dauben, J. Chem. Phys., Vol. 32, p. 1515, 1960.

## CHAPTER 18. FERROELECTRICS WITH MAGNETIC ORDERING

The rapid development of the physics of ferroelectricity and magnetism during the last two decades has strengthened concepts concerning the nature of these phenomena and increased the number of known ferroelectric and ferromagnetic materials. The result has been the discovery of a number of ferroelectrics with magnetic ordering. These compounds were first synthesized by Smolenskiy, et al [1-5], who synthesized ferroelectric-antiferromagnetic compounds with the perovskite type structure. Eventually two other families of ferroelectrics with magnetic ordering were discovered -- hexagonal magnetites and boracites. Ferroelectrics with spontaneous magnetization are of tremendous importance, since these compounds possess several effects attributed to the mutual effect of electric and magnetic subsystems. The presence of these effects follows directly from thermodynamic theory, and before proceeding to review experimental works, we will briefly discuss the basic results of theoretical examination.

### §1. Elements of Thermodynamic Theory of Ferromagnetic Ferroelectrics

The first thermodynamic examination of a ferromagnetic ferroelectric material was conducted by Smolenskiy [6], who investigated the second order phase transition from the ferromagnetic (or ferroelectric) to the ferroferromagnetic state at a temperature close to the temperature of transition from the paramagnetic to ferromagnetic (or from the paraelectric to ferroelectric) state. In other words, he examined the case when the magnetic and ferroelectric Curie points are close. Later on Nedlin [7] showed that the results of this work are general and do not depend on the nearness of the temperatures of both transitions.

There is a magnetoelectric effect in the ferroferromagnetic phase, i.e., the electric and magnetic moments are linear functions (in weak fields) of the magnetic and electric field.

$$\left. \begin{aligned} P &= \chi^e E + \chi^{eH} H, \\ M &= \chi^m H + \chi^{mE} E. \end{aligned} \right\} \quad (1.1)$$

Here  $\chi^e$  is the tensor of the electric and  $\chi^m$  the tensor of the magnetic and

$$\chi_{ij} = \chi_{ji} = - \frac{\partial^2 \Phi}{\partial E_i \partial H_j} \quad (18.2)$$

is the tensor of composite magnetoelectric susceptibility. Near the transition point

$$\chi^{ee} = \frac{\partial P}{\partial E} = \chi^{ee} = \frac{\partial M}{\partial E} \approx (T - T_c)^{-1/2} \quad (18.3)$$

The case was examined [6, 7] when the axis of easy magnetization and the ferroelectric axis coincide and the magnetic and electric fields are parallel to this axis. Thus, the superposing of external fields alters only polarization and magnetization, but not their direction. With fields of arbitrary direction the thermodynamic theory should be formulated for each specific crystal with consideration of its symmetry.

During transition to the ferro-ferromagnetic phase from the ferro-magnetic (ferroelectric), magnetic (electric) susceptibility exhibits positive jump, i.e.,

$$\left[ \begin{array}{l} \chi_{ff} \\ \chi_{cf} \end{array} \right]_{T=T_c} > \left[ \chi_{ff} \right]_{T=T_c} \quad (\text{or } \left[ \chi_{cf} \right]_{T=T_c} > \left[ \chi_{cf} \right]_{T=T_c}).$$

Here the subscripts ff, f and c denote the ferro-ferromagnetic, ferro-magnetic and ferroelectric phases, respectively.

Nitsek and Smolenskiy [8] did a thermodynamic study of a ferro-ferromagnetic with consideration of anisotropy. They examined a crystal cubic in the paraelectric and paramagnetic phases. It was shown that electric (magnetic) ordering causes magnetic (electric) anisotropy to become uniaxial and the interaction of the magnetic and electric subsystems can be regarded, in particular, as the consequence of electro- and magnetostriction. Change in electric polarization deforms the crystal, which, in turn, by virtue of magnetostriction, alters magnetization and vice versa. The same conclusion can be reached by viewing the thermodynamic potential as the sum of elastic ( $\Phi_{el} = c_{ijkl} u_{ij} u_{kl}$ ), magnetoelastic ( $\Phi_{me} = A'_{ijkl} u_{ij} M_k M_l$ ) and electroelastic ( $\Phi_{eel} = A''_{ijkl} u_{ij} P_k P_l$ ) energies.

The equilibrium values of the deformation tensor components are determined from the condition of minimum thermodynamic potential in terms of variables  $u_{ij}$ . These equilibrium values have as terms a part that is quadratic in terms of polarization components ( $B'_{ijkl} P_k P_l$ ), i.e. a part that is quadratic in terms of magnetization components ( $B''_{ijkl} M_k M_l$ ). As a result of substitution of equilibrium values  $u_{ij}$  in the expression for the

thermodynamic potential terms of the type  $M_1 M_2 P_1 P_2$  appear in it, which indicates interaction of the electric and magnetic subsystems.

This is all valid for ferromagnetic-ferroelectrics. The formulation of thermodynamic theory of antiferromagnetic ferroelectrics requires the knowledge of their specific symmetry, position of magnetic ions in the nucleus, character of magnetic ordering, i.e., for each substance it is essential to conduct a special examination. Nedlin [9], however, showed that the second order phase transition from the ferroelectric to ferroelectric and magnetically ordered state can be examined in rather general form, whence can be made certain conclusions that are valid for a large class of antiferromagnetic ferroelectrics.

The possible symmetry of ferromagnetic ferroelectrics was examined theoretically in [10, 11]

## 52. Perovskites

The first ferroelectrics with magnetic ordering were  $\text{PbFe}_{1/2}\text{Nb}_{1/2}\text{O}_3$  and  $\text{PbFe}_{2/3}\text{W}_{1/3}\text{O}_3$  [1-5]. These compounds have a perovskite type structure.

Ions  $\text{Fe}^{3+}$ ,  $\text{Nb}^{5+}$  and  $\text{W}^{6+}$  occupy the octahedral positions and there is no ordering of these ions. The ferroelectric Curie point of  $\text{Pb}_{1/2}\text{Nb}_{1/2}\text{O}_3$  is  $357^\circ\text{K}$  and of  $\text{Pb}_{2/3}\text{W}_{1/3}\text{O}_3$   $178^\circ\text{K}$ . The temperature dependence of magnetic susceptibility of  $\text{PbFe}_{2/3}\text{W}_{1/3}\text{O}_3$  is illustrated in Fig. 18.1.

The temperature at which the dependences  $\epsilon(T)$  and  $1/\epsilon(T)$  have a discontinuity [5] was taken as the temperature of antiferromagnetic ordering (Neel temperature). Due to the unordered distribution of magnetic ( $\text{Fe}^{3+}$ ) and diamagnetic ( $\text{W}^{6+}$ ) ions, part of the  $\text{Fe}^{3+}$  ions have as next door neighbors in the octahedral sublattice only diamagnetic ions and therefore do not participate in magnetic ordering. In the first approximation such ions behave like paramagnetic ions and are responsible for the growth of magnetic susceptibility as the temperature falls below the Neel point. The presence of magnetic ordering in  $\text{PbFe}_{2/3}\text{W}_{1/3}\text{O}_3$  and  $\text{PbFe}_{1/2}\text{Nb}_{1/2}\text{O}_3$  was verified later by neutron radiographic analyses [12, 13] which showed that a magnetic structure of the so-called G-type forms, in which the magnetic moment of each ion is antiparallel to the magnetic moment of their nearest neighbors.

According to magnetic measurement data, the Neel temperature of  $\text{PbFe}_{2/3}\text{W}_{1/3}\text{O}_3$  is  $365^\circ\text{K}$  and of  $\text{PbFe}_{1/2}\text{Nb}_{1/2}\text{O}_3$ ,  $143^\circ\text{K}$  [5]. The analogous magnetic properties are displayed by  $\text{PbFe}_{1/2}\text{Ta}_{1/2}\text{O}_3$ , the Neel temperature of which is  $180^\circ\text{K}$  [14]. If in the examined compounds there is no ordering of the various ions occupying the octahedral positions, then in  $\text{PbCo}_{1/2}\text{W}_{1/2}\text{O}_3$ , also having a perovskite structure, the ions  $\text{Co}^{2+}$  and  $\text{W}^{6+}$  are ordered and the elemental nucleus is accordingly doubled [15-17]. According to the

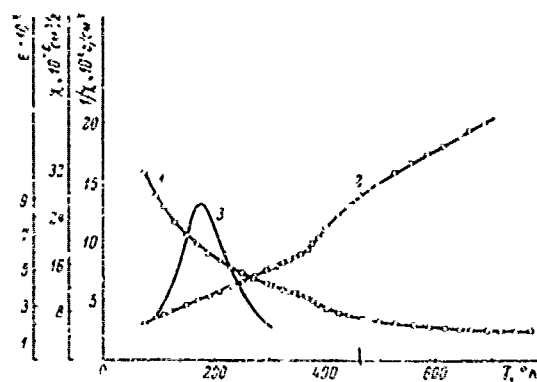


Figure 18.1. Temperature dependence of magnetic susceptibility  $\chi(1)$ ,  $\frac{1}{\chi}$  (2) and permittivity  $\epsilon$  (3)  $\text{PbFe}_{2/5}\text{W}_{1/3}\text{O}_3$ . Measurements were made on monocrystalline powder (according to Bokov, et al [5]).

data of Bokov, et al [17]  $\text{PbCo}_{1/2}\text{W}_{1/2}\text{O}_3$  transitions at 305°K from the paraelectric to the antiferroelectric state. As the temperature drops, starting at 170°K it becomes possible to observe electric field induced transition from the antiferroelectric to the ferroelectric state. As the temperature continues to drop, the transition field diminishes and at 63°K transition occurs spontaneously [18].

The volumetric interaction between magnetic ions  $\text{Co}^{2+}$  in  $\text{PbCo}_{1/2}\text{W}_{1/2}\text{O}_3$  proceeds in the chain  $\text{Co-O-W-O-Co}$ . Therefore the interaction is weak and magnetic ordering occurs only below 90°K [19]. In terms of its magnetic properties  $\text{PbCo}_{1/2}\text{W}_{1/2}\text{O}_3$  is a typical weak ferromagnetic with spontaneous magnetization of  $0.15 \text{ G}\cdot\text{cm}^3/\text{g}$  at 4.2°K [19]. Thus, at temperatures below 9°K  $\text{PbCo}_{1/2}\text{W}_{1/2}\text{O}_3$  is simultaneously a ferroelectric and a weak ferromagnetic. The temperature dependences of magnetic susceptibility and spontaneous magnetization are presented in Figure 18.2.

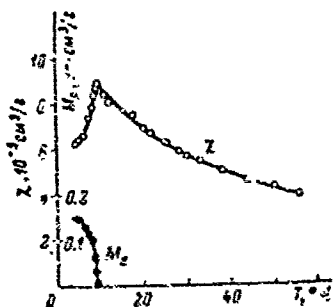


Figure 18.2. Temperature dependence of magnetic susceptibility ( $\chi$ ) and spontaneous magnetization ( $M_s$ ) of  $\text{PbCo}_{1/2}\text{W}_{1/2}\text{O}_3$ . Measurements were made on monocrystalline powder (according to Kizhaye and Bokov [19]).

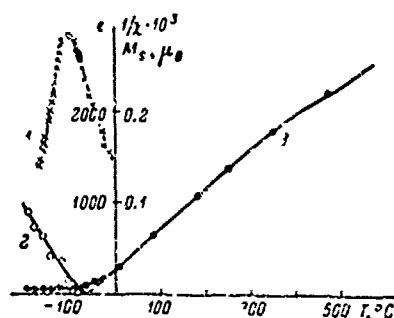
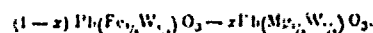
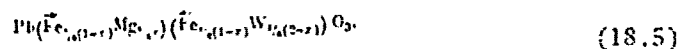


Figure 18.3. Temperature dependence of permittivity (1), spontaneous magnetization (2) in Bohr magnetons per  $\text{Fe}^{3+}$  ion and inverse magnetic susceptibility (3) of solid solution  $0.7 \text{PbFe}_{2/3}\text{W}_{1/3}\text{O}_3 - 0.3\text{PbMg}_{1/2}\text{W}_{1/2}\text{O}_3$  (according to Smolenskiy, et al [20]).

On the basis of complex perovskites Smolenskiy, et al [20] produced ferroelectric solid solutions that are simultaneously ferrimagnetics, i.e., uncompensated antiferromagnetics. Ferrimagnetism was obtained in the system



We will recall that  $\text{Pb}(\text{Mg}_{1/2}\text{W}_{1/2})\text{O}_3$  is an antiferroelectric. Ions  $\text{Mg}^{2+}$  and  $\text{W}^{6+}$ , occupying the octahedral positions, are ordered, i.e., there are two octahedral sublattices. The formation of solid solutions of this system can be regarded as the substitution of some of the  $\text{Mg}^{2+}$  and  $\text{W}^{6+}$  ions by  $\text{Fe}^{3+}$  ions. It is obvious that when stoichiometry is maintained the number of  $\text{Fe}^{3+}$  ions in the octahedral sublattices of Mg and W should differ and, by separating the sublattices the formula of the solid solution can be written in the form:



If now magnetic ordering occurs and a G-type antiferromagnetic structure is formed, which is characteristic of all perovskites with iron, then the magnetic sublattices will coincide with the sublattices in the parentheses in (18.5). The directions of the magnetic moments of  $\text{Fe}^{3+}$  ions in (18.5) are indicated by arrows. Since the number of  $\text{Fe}^{3+}$  ions in the sublattices differs, then the magnetic moments of the sublattices will not be compensated, i.e., ferrimagnetism should occur. Experimental investigations of this system have shown that the ordering of ions occupying the octahedral positions takes place when the concentration of  $\text{PbMg}_{1/2}\text{W}_{1/2}\text{O}_3$  exceeds 20%. Solid solutions with  $x < 0.88$  display ferroelectric properties, and in the range of concentrations  $0.2 < x < 0.4$  there is stable spontaneous magnetization. The temperature dependences of permittivity, spontaneous magnetization and inverse magnetic susceptibility are illustrated in Figure 18.3. The latter dependence is of the form characteristic of ferrimagnetics.

Also noteworthy among perovskites is  $\text{BiFeO}_3$ . According to x-ray diffraction analyses this compound has rhombohedral symmetry [21-23]. Although structural analyses have been quite numerous [13, 24-26], the question of its spatial group cannot be considered conclusively answered. As shown by magnetic measurements done by Smolenskiy [27],  $\text{BiFeO}_3$  is an antiferromagnetic with a Neel temperature of  $643^\circ\text{K}$ . According to neutron radiographic analysis, the magnetic structure is of the G-type [12, 24]. The question of whether or not  $\text{BiFeO}_3$  is a ferroelectric was solved for a long time chiefly by investigating solid solutions, the properties of which were extrapolated to pure  $\text{BiFeO}_3$ . The systems  $\text{BiFeO}_3\text{-PbTiO}_3$  [21, 28, 29] and  $\text{BiFeO}_3\text{-PbFe}_{1/2}\text{Nb}_{1/2}\text{O}_3$  [30-36] have been most thoroughly studied<sup>1</sup>. Later on Kravnik, et al [32] were able to measure the permittivity of polycrystalline  $\text{BiFeO}_3$  at high frequencies in a wide temperature range. The results of these measurements favor the antiferroelectric properties of  $\text{BiFeO}_3$ . Whether  $\text{BiFeO}_3$  is a ferro- or antiferroelectric is a question discussed in Chapter 17, §1.

Many ferroelectric perovskites of complex composition with magnetic ordering have been synthesized and analyzed by Zhdanov and Venovtsev and coworkers. The results of these works can be found in review [38]. Some information concerning these compounds is given in Chapter 19.

### §3. Hexagonal Manganites

Hexagonal manganites were first synthesized by Bertaut, et al [39]. The general formula of these compounds is  $\text{AMnO}_3$ , where A is any rare-earth ion from Ho to Lu, and also Sc and Y. Manganites are of a new, previously unknown type of structure (spatial group  $\text{P6}_3\text{cm}$  (Figure 18.4) [39, 40]).

The oxygen ions in this structure comprise triangular bipyramids, which, connected at the vertices, form layers perpendicular to the sixth order axis. The manganese ions are located inside the bipyramids and the rare-earth, yttrium or scandium ions are located between the layers of the bipyramids. Hexagonal manganites are uniaxial ferroelectrics, the polar axis of which is the sixth order axis. Spontaneous polarization is  $\sim 5 \cdot 10^{-6} \text{ C cm}^{-2}$  [41-44]. The ferroelectric Curie temperature of these compounds is very high and cannot be determined according to the disappearance of hysteresis loops due to high electrical conductivity. However, a set of experimental data, such as jump of elemental nucleus parameters, maximum pyroelectric current, maximum permittivity, observed at about the same temperature, makes it possible to establish quite reliably the temperature of the antiferroelectric phase transition. Such analyses have been conducted for  $\text{YMnO}_3$  [43] and  $\text{YbMnO}_3$  [43, 45]. For  $\text{HoMnO}_3$  and  $\text{ErMnO}_3$

<sup>1</sup>Analyses of solid solutions based on  $\text{BiFeO}_3$  are presented in the reviews [37, 38].

there are data only concerning the temperatures of maximum permittivity [43]. The information known at this time concerning the temperatures of the ferroelectric and antiferromagnetic phase transitions in hexagonal manganites is summarized in Table 24.

Table 24. Ferroelectric Curie Points ( $T_c$ ) and Temperatures of Antiferromagnetic Ordering ( $T_H$ ) of Hexagonal Manganites

Phase transition	Y <sub>2</sub> MnO <sub>5</sub>	HoMnO <sub>3</sub>	ErMnO <sub>3</sub>	TbMnO <sub>3</sub>	YbMnO <sub>3</sub>	LuMnO <sub>3</sub>	ScMnO <sub>3</sub>
$T_c$ , °C	660 [43] 630 [44] 640 [43]	600 [43]	560 [43]	—	710 [43] 720 [43]	—	—
$T_H$ , °K	77 [47]	76 [48]	79 [48]	86 [48]	—	91 [48]	120 [48]

A feature of these ferroelectrics is their low permittivity; thus, on the polar axis  $\epsilon \sim 23$ -25 at room temperature and  $\epsilon \sim 60$  at the Curie point [46]. The ferroelectric domains are indistinguishable in polarized light, but can be discerned by etching the surface perpendicular to the polar axis [49].

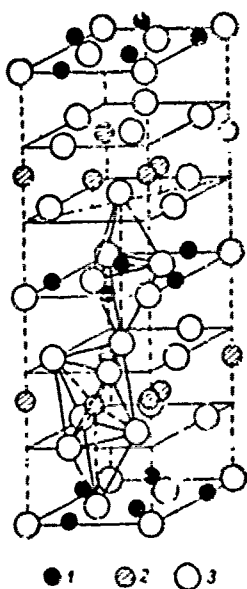


Figure 18.4. Elemental nucleus of  $YMnO_3$ : 1 --  $Mn^{3+}$ ; 2 --  $Y^{3+}$ ; 3 --  $O^{2-}$ .

In terms of their magnetic properties the manganites are antiferromagnetics. They feature the absence of anomalous magnetic susceptibility at the Neel point [50-52]. Data on Neel temperatures were also obtained from neutron radiography, and in the case of  $YMnO_3$ , from analysis of the Messbauer effect on  $Fe^{57}$  nuclei in specimens in which 10% of the  $Mn^{3+}$  ions were substituted by  $Fe^{3+}$  ions [47]. The results of all these measurements are presented in Table 24. The discussion here concerns ordering of the magnetic moments of  $Mn^{3+}$  ions. There is still no information concerning magnetic ordering in the sublattice of rare-earth ions. The magnetic structure of manganites was investigated chiefly on the example of  $YMnO_3$ , both theoretically

[53] and experimentally by the neutron diffraction method [54-56]. As a result of these investigations it was established that the magnetic moments of  $Mn^{3+}$  ions lie in the planes perpendicular to the sixth order axis, and form six magnetic sublattices.

#### §4. Boracites

Indications that the mineral boracite  $Mg_3B_7O_{13}Cl$  has ferroelectric properties were first uncovered by le Corre [57]. In subsequent works [58, 59], however, doubt was cast on the presence of ferroelectricity in this mineral, and only after the works of Ascher, Schmidt, et al [60-65] in which several compounds similar to natural boracite were synthesized and analyzed, did it become clear that they all are apparently ferroelectrics. The general formula of such compounds can be written in the form  $Me_3B_7O_{13}X$ , where  $Me = Mg, Cr, Mn, Fe, Co, Ni, Cu, Zn, Cd$  and  $X = Cl, Br, I$ . The structure of boracites, analyzed by Ito, et al [66], and also their dielectric properties will be discussed in Chapter 19. We will discuss here the domain structure and magnetic properties. The domain structure has been investigated only on boracites with nickel, for which the direction of spontaneous polarization has been established and detailed crystallo-optic analysis conducted [65]. Like other boracites, this compound belongs to the cubic acentrosymmetric spatial group  $F\bar{4}3c(T_d^2)$  in the paraelectric phase. The matrix of piezoelectric coefficients  $g$  in this case has the form

$$\begin{pmatrix} 0 & 0 & 0 & g_{11} & 0 & 0 \\ 0 & 0 & 0 & 0 & g_{11} & 0 \\ 0 & 0 & 0 & 0 & 0 & g_{11} \end{pmatrix} \quad (18.6)$$

Spontaneous polarization occurs on one of the edges of the cubic elemental nucleus, i.e., cubic directions of the type  $\{100\}$ . The spontaneous deformation that occurs here can be regarded as the result of the piezoelectric effect, and in accordance with (10.45) deformation consists in displacement in the plane perpendicular to the polar axis. The elemental nucleus becomes rhombic with polar axis  $z'$ , coinciding with the pseudocubic direction  $[001]$ , and with axes  $x'$  and  $y'$ , coinciding with pseudocubic directions  $[110]$  and  $[\bar{1}10]$  (Figure 18.5). The indicatrix axes of the  $180^\circ$  domains are rotated  $90^\circ$  relative to each other. Therefore such domains can be distinguished in polarized light. The configurations of the  $90^\circ$  domains of the boracites are quite varied and in many cases do not agree with the general rules discussed in Chapter 7. Often the polarization vectors are arranged "head to head," and "tail to tail." The domain walls differ in many cases from surfaces with rational indices and are often strongly curved, which apparently is a result of the smallness of rhombic distortions.

The magnetic properties of boracites with paramagnetic ions have not yet been analyzed sufficiently, but there are data concerning the behavior of magnetic susceptibility at temperatures above  $77^\circ K$  for most of the compounds [62]. All these compounds are apparently antiferromagnetics with rather low Neel points. Ni-I-boracite, the magnetic properties of which are most thoroughly investigated (Figure 18.6), displays very interesting properties. Antiferromagnetic ordering occurs in this compound at  $120^\circ K$  and then Ni-I-boracite becomes a ferroelectric at  $64^\circ K$ . The

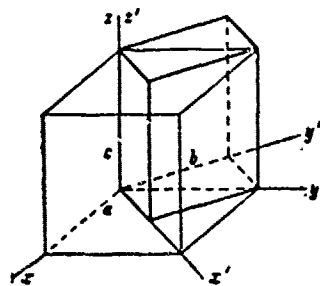


Figure 18.5. Relations between elemental nuclei of cubic and rhombic modifications of boracite (Schmidt [65]).

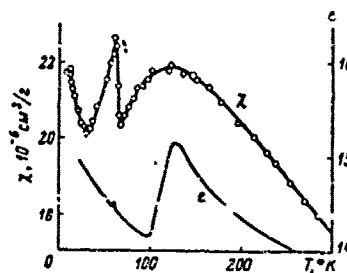


Figure 18.6. Temperature dependence of permittivity ( $\epsilon$ ) and magnetic susceptibility ( $\chi$ ) of  $\text{Ni}_3\text{B}_7\text{O}_{13}\text{I}$  (Ascher, et al [63]).

reduction of symmetry at the ferroelectric Curie point leads to the appearance of slight spontaneous magnetization and Ni-I-boracite becomes a weak ferromagnetic. Spontaneous magnetization is perpendicular to spontaneous polarization, which corresponds to magnetic point group  $m'm2'$ .

If spontaneous polarization  $P_s$  is parallel to cubic direction  $[001]$ , then magnetization  $M_s$  may be directed either on  $[110]$  or on  $[\bar{1}\bar{1}0]$ . Thus, in the ferroelectric domain there may be antiparallel ferromagnetic domains, but in the ferromagnetic domain  $P_s$  can have only one direction. Hence follow a number of purely domain effects, which were also detected experimentally [63, 65]. By changing the direction of  $P_s$  with an electric field, it is also possible to alter the direction of  $M_s$ , and conversely. Thus, if the direction of  $P_s$  is changed from  $[001]$  to  $[00\bar{1}]$ ,  $M_s$  rotates  $90^\circ$  from  $[110]$  or from  $[\bar{1}\bar{1}0]$  to  $[1\bar{1}0]$ , or to  $[\bar{1}10]$ . The opposite effect also occurs, i.e., if magnetization is first directed, for instance, on  $[110]$  and the crystal is remagnetized by applying a magnetic field on  $[1\bar{1}0]$ , then the direction of  $P_s$  should change from  $[001]$  to  $[00\bar{1}]$ .

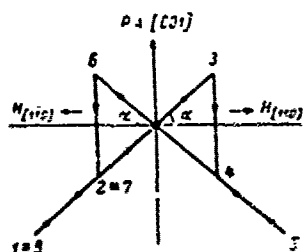


Figure 18.7. Quadratic magneto-electric hysteresis loop for  $\text{Ni}_3\text{B}_7\text{O}_{13}\text{I}$  with  $H$  on  $\pm[110]$  and  $P_s$  on  $[001]$  at  $46^\circ\text{K}$  (according to Ascher, et al [63]).

In accordance with theory Ni-I-boracite displays the linear magneto-electric effect. Taking the direction of  $P_s$  as the  $z$  axis and the direction of  $M_s$  as the  $y$  axis, in accordance with the symmetry of the crystal, we

have the following equations for linear magnetoelectric effects:

$$P_2 = \chi_{12}^{me} H_1, \quad (18.7a)$$

$$M_3 = \chi_{33}^{me} E_3, \quad (18.7b)$$

$$M_2 = \chi_{23}^{me} E_3, \quad (18.7c)$$

$$P_1 = \chi_{13}^{me} H_3, \quad (18.7d)$$

The effect described by equation (18.7a) has been investigated experimentally [63, 54]. The dependence of the change of electric polarization on magnetic field intensity is represented in Figure 18.7. It has the "butterfly" form. This is related to the fact that remagnetization occurs in a magnetic field of ~6 ke intensity. The transition 3 → 4 (Figure 18.7) is related to a change in the direction of  $M_s$  from  $M_s || [\bar{1}\bar{1}0]$  to  $M_s || [110]$ , and the transition 6 → 7 to the reverse rotation from  $M_s || [110]$  to  $M_s || [\bar{1}\bar{1}0]$ . Its absolute value  $\gamma^{me} \sim 3.3 \cdot 10^{-4}$  at 15°K.

#### BIBLIOGRAPHY

1. Smolenskiy, G. A. and W. A. Ioffe, Communications du Colloque international de magnetisme de Grenoble (France, 2-6 July 1958), Communication No. 71.
2. Smolenskiy, G. A. and A. I. Agranovskaya, ZhTF [Zhurnal tekhnicheskoy fiziki; Journal of Technical Physics], Vol. 28, p. 1494, 1958.
3. Smolenskiy, G. A., A. I. Agranovskaya, S. N. Popov and V. A. Isupov, ZhTF, Vol. 28, p. 2152, 1958.
4. Isupov, V. A., A. I. Agranovskaya and N. P. Khuchua, Izv. AN SSSR, ser. fiz. (News of USSR Academy of Sciences, Physics Series), Vol. 24, p. 1271, 1960.
5. Bokov, V. A., I. Ye. Myl'nikova and G. A. Smolenskiy, ZhETF [Zhurnal eksperimental'noy i teoreticheskoy fiziki; Journal of Experimental and Theoretical Physics], Vol. 42, p. 643, 1962.
6. Smolenskiy, G. A., FTT [Fizika tverdogo tela; Solid State Physics], Vol. 4, p. 1095, 1962.
7. Nedlin, G. M., FTT, Vol. 4, p. 3569, 1962.
8. Mitsek, A. I. and G. A. Smolenskiy, FTT, Vol. 4, p. 3581, 1962.
9. Nedlin, G. M., Izv. AN SSSR, ser. fiz., Vol. 29, p. 890, 1965.
10. Lyubimov, S. V., FTT, Vol. 5, p. 951, 1963.

11. Shuvalov, L. A. and N. V. Belov, Kristallografiya (Crystallography), Vol. 7, p. 192, 1963.
12. Kiselev, S. V., R. P. Ozerov and G. S. Zhdanov, DAN SSSR (Reports of USSR Academy of Sciences), Vol. 145, p. 1255, 1962.
13. Plakhtiy, V. P., Ye. I. Mal'tsev and D. M. Kaminker, Izv. AN SSSR, ser. fiz., Vol. 28, p. 436, 1964.
14. Nomura, S., H. Takabayashi and Nakagawa, Japan J. Appl. Phys., Vol. 7, p. 600, 1968.
15. Belyayev, I. N., V. S. Filip'yev and Ye. G. Fesenko, Zh. Strukt. Khim. (Journal of Structural Chemistry), Vol. 4, p. 719, 1963.
16. Filip'yev, V. S. and Ye. G. Fesenko, Kristallografiya, Vol. 9, p. 293, 1964.
17. Bokov, V. A., S. A. Kizhayev, I. Ye. Myl'nikova and A. G. Tutov, FTT, Vol. 6, p. 3058, 1964.
18. Bokov, V. A., S. A. Kizhayev, I. Ye. Myl'nikova, A. G. Tutov and A. G. Ostroumov, Izv. AN SSSR, ser. fiz., Vol. 28, p. 436, 1964.
19. Kizhayev, S. A. and V. A. Bokov, FTT, Vol. 8, p. 1957, 1966.
20. Smolenskiy, G. A., V. A. Isupov, N. N. Kraynik and A. I. Agranovskaya, Izv. AN SSSR, ser. fiz., Vol. 25, p. 1333, 1961.
21. Venetsev, Yu. N., G. S. Zhdanov, S. P. Solov'yev, Ye. V. Bezus, V. V. Ivanova, S. A. Fedulov and A. G. Kapyshev, Kristallografiya, Vol. 5, p. 620, 1960.
22. Filip'yev, V. S., N. P. Smolinov, Ye. G. Fesenko and I. N. Belyayev, Kristallografiya, Vol. 5, p. 958, 1960.
23. Zaslavskiy, A. I. and A. G. Tutov, DAN SSSR, Vol. 135, p. 815, 1960.
24. Kiselev, S. V., A. N. Kshnyakina, R. P. Ozerov and G. S. Zhdanov, FTT, Vol. 5, p. 3312, 1963.
25. Tomashpol'skiy, Yu. Ya., Yu. N. Venetsev and G. S. Zhdanov, DAN SSSR, Vol. 152, p. 1313, 1963.
26. Sosnovskaya, I., P. Sosnovski, S. V. Kiselev and R. O. Ozerov, Proc. a Symp. Inelast. Scatter. of Neutr. (Bombay, 15-19 December 1964), Vol. 11, IAEA, Vienna, p. 513, 1965.
27. Smolenskiy, A. G., V. M. Yudin, Ye. S. Sher and Yu. Ye. Stolypin, ZhETF, Vol. 43, p. 877, 1962.

28. Fedulov, S. A., Yu. N. Venevtsev, G. S. Zhdanov, Ye. G. Smazhevskaya and I. S. Rez, Kristallografiya, Vol. 7, p. 77, 1962.
29. Fedulov, S. A., F. B. Ladyzhinskiy, A. I. Pyatigerskaya and Yu. N. Venevtsev, FTT, Vol. 6, p. 475, 1964.
30. Kraynik, N. N., N. P. Khuchua, A. A. Berezhnoy and A. G. Tutov, FTT, Vol. 7, p. 132, 1965.
31. Zhdanova, V. V., FTT, Vol. 7, p. 143, 1965.
32. Kraynik, N. N., N. P. Khuchua, V. V. Zhdanova and V. A. Yeliseyev, FTT, Vol. 8, p. 816, 1966.
33. Ismailzade, I. G., DAN SSSR, Vol. 170, p. 85, 1966.
34. Smith, D. I., G. D. Achenbach, K. Gerson and W. J. James, J. Appl. Phys., Vol. 39, p. 70, 1968.
35. Ismailzade, I. G., Kristallografiya, Vol. 13, p. 431, 1968.
36. Buhner, C. F., J. Chem. Phys., Vol. 36, p. 798, 1962.
37. Smolenskiy, G. A., V. A. Bokov, V. A. Isupov, N. N. Kraynik and G. M. Nedlin, Segnetoelektriki (Ferroelectrics), Rostov University Publishing House, p. 129, 1968.
38. Venevtsev, Yu. N., G. S. Zhdanov, Yu. Ye. Roginskaya, Yu. Ya. Tomashpol'skiy, V. N. Lyubimov, L. I. Shvorneva, K. P. Mitrofanov and A. S. Viskov, Segnetoelektriki, Rostov University Publishing House, p. 155, 1968.
39. Bertaut, E. F., F. Forrat and P. Fang, Compt. rend., Vol. 256, p. 1958, 1963.
40. Yakei, I. L., W. C. Koehler, F. Bertaut and F. Forrat, Acta Cryst., Vol. 16 p. 947, 1963.
41. Bokov, V. A., G. A. Smolenskiy, S. A. Kichayev and I. Ye. Mylnikova, FTT, Vol. 5, p. 3607, 1963.
42. Tamuro, H., F. Sawaguchi and A. Kikuchi, Japan J. Appl. Phys., Vol. 4, p. 621, 1965.
43. Coeure, Ph., P. Guinet, I. C. Peuzin, G. Buisson and E. S. Bertaut, Proc. Intern. Meet. Ferroelectr., Vol. 1, 332, Prague, p. 33, 1966.
44. Penzin, J. C., Compt. rend., Vol. 261, p. 2195, 1965.
45. Ismailzade, I. G. and S. A. Kichayev, FTT, Vol. 7, p. 298, 1965.

46. Smolenskiy, G. A., V. A. Bokov, V. A. Isupov, N. N. Kraynik and G. M. Nedlin, *Helv. Phys. Acta*, Vol. 41, p. 1187, 1968.
47. Chappert, J., *Phys. Lett.*, Vol. 18, p. 229, 1965.
48. Koehler, W. C., H. L. Yakel, E. O. Wollan and J. W. Cable, *Phys. Lett.*, Vol. 9, p. 93, 1963.
49. Safrankova, M., H. Fousek and S. A. Kiznev, *Czechosl. J. Phys.*, B17, p. 559, 1967.
50. Kizhayev, S. A., V. A. Bokov and O. V. Kachalov, *FTT*, Vol. 8, p. 265, 1966.
51. Bertaut, E. F., R. Pauthenet and M. Mercier, *Phys. Lett.*, Vol. 18, p. 13, 1965.
52. Kohn, K. and A. Tasaki, *J. Phys. Soc. Japan*, Vol. 20, p. 1273, 1965.
53. Nedlin, G. M., *FTT*, Vol. 6, p. 2708, 1964; Vol. 7, p. 739, 1965.
54. Bertaut, E. F. and M. Mercier, *Phys. Lett.*, Vol. 5, p. 27, 1963.
55. Bertaut, E. F., R. Pauthenet and M. Mercier, *Phys. Lett.*, Vol. 7, p. 110, 1963.
56. Bertaut, E. F., M. Mercier and R. Pauthenet, *J. Phys.*, Vol. 25, p. 550, 1964.
57. le Corre, Y., *J. Phys. Radium*, Vol. 18, p. 629, 1957.
58. Sonin, A. S. and I. S. Zheludev, *Kristallografiya*, Vol. 8, p. 183, 1963.
59. Jona, F., *J. Phys. Chem.*, Vol. 63, p. 1750, 1959.
60. Ascher, E., H. Schmidt, D. Tar, *Sol. St. Comm.*, Vol. 2, p. 45, 1964.
61. Schmidt, H., *J. Phys. Chem. Sol.*, Vol. 26, p. 973, 1965.
62. Schmidt, H., H. Rieder, E. Ascher, *Sol. St. Comm.*, Vol. 3, p. 327, 1965.
63. Ascher, E., H. Rieder, H. Schmidt and H. Stossel, *J. Appl. Phys.*, Vol. 37, p. 1404, 1966.
64. Schmidt, H. and I. M. R. Trooster, *Sol. St. Comm.*, Vol. 5, p. 31, 1967.
65. Schmidt, H., *Rost Kristallov (Growth of Crystals)*, Vol. 7, "Nauka" Publishing House, Moscow, p. 32, 1967.
66. Ito, T., N. Morimoto and R. Sadanaga, *Acta Cryst.*, Vol. 4, p. 310, 1951.

## CHAPTER 19. REVIEW OF FERROELECTRIC COMPOUNDS

### §1. Ferroelectrics with the Perovskite Type Structure

#### 1. Strontium Titanate

Rushman and Strivens [1] discovered that the Curie temperature of solid solutions  $\text{BaTiO}_3\text{-SrTiO}_3$  falls linearly as the concentration of  $\text{SrTiO}_3$  increases. Extrapolation of this dependence made it possible to propose that  $\text{SrTiO}_3$ , at temperatures close to  $0^\circ\text{K}$ , will have maximum  $\epsilon$ , and that strontium titanate is therefore a ferroelectric.

Measurements of  $\epsilon$  in  $\text{SrTiO}_3$  at low temperatures were first done by Smolenskiy [2-4] on polycrystalline specimens. It was found that the  $\epsilon$  of  $\text{SrTiO}_3$  at low temperatures passes through a maximum. At temperatures below that of the maximum dielectric hysteresis loops were observed. This led to the conclusion that strontium titanate is actually a ferroelectric with a Curie point of  $15\text{-}35^\circ\text{K}$ .

Somewhat later Hulm [5] conducted analogous measurements and did not find the  $\epsilon$  peak. According to his data  $\epsilon$  of strontium titanate obeys the Curie-Weiss law from  $300$  to  $50^\circ\text{K}$ , and at temperatures below  $50^\circ\text{K}$  increases more smoothly than follows from the law  $\epsilon = C/(T - \theta)$ , and approaches a constant value of  $\sim 1,500$  as the temperature approaches  $0^\circ\text{K}$ . At  $4^\circ\text{K}$   $\epsilon$  was not found to be dependent on field intensity all the way up to  $25$   $\text{kV/cm}$ . Hence Hulm concludes that strontium titanate is not a ferroelectric.

Strontium titanate has been analyzed by many researchers in past years; the question of its ferroelectric properties has been discussed repeatedly, but even today the behavior of strontium titanate at low temperatures is not sufficiently clear.

Strontium titanate is practically cubic at  $20^\circ\text{C}$  with  $a = 3.904 \text{ \AA}$  [6]. Granicher and Jakits [7], extrapolating the dependence of the temperature of phase transitions in solid solutions  $\text{SrTiO}_3\text{-CaTiO}_3$  on the

$\text{CaTiO}_3$  concentration, concluded that strontium titanate changes to the tetragonal phase below  $-100^\circ\text{K}$ . Muller, as a result of analyzing the EPR of impurity ions  $\text{Fe}^{3+}$  in  $\text{SrTiO}_3$  crystals, verified that on cooling below  $-100^\circ\text{K}$  a phase transition occurs in strontium titanate to the tetragonal phase, whereupon the crystal breaks down into numerous twins [8, 9]. The existence of this phase transition is also substantiated by other works on EPR analysis in  $\text{SrTiO}_3$  [10-13]. Rimai and de Mars [13] determined the transition temperature as  $110 \pm 2.5^\circ\text{K}$  and noted that this transition occurs much more smoothly than the transition from the cubic phase to tetragonal in  $\text{BaTiO}_3$  and is not a first order transition. Cooling of the crystal below  $110^\circ\text{K}$  is accompanied by a sudden drop in the linear expansion coefficient [14], which at  $20^\circ\text{C}$  is  $(9.2 \pm 0.8) \cdot 10^{-6}/^\circ\text{K}$  [15].

X-ray diffraction analysis and analysis of birefringence of  $\text{SrTiO}_3$  at low temperatures are described in [16-18]. According to [16]  $\text{SrTiO}_3$  above  $110^\circ\text{K}$  has a cubic lattice and a linear expansion coefficient of  $9.4 \cdot 10^{-6}/^\circ\text{K}$ . At about  $110^\circ\text{K}$  the change of lattice parameters during cooling practically ceases, and separation of the x-ray lines, indicating tetragonal distortion, was noted only at temperatures close to  $65^\circ\text{K}$ . Then, during heating, this separation is clearly discernible in the  $65-120^\circ\text{K}$  temperature range. The magnitude of tetragonal distortion was found to be  $c/a = 1.00056$ . In the  $55-65^\circ\text{K}$  range no line separation was noted, but from  $35$  to  $55^\circ\text{K}$  separation of the lines (triplet) was clearly discernible. This separation is related to rhombic distortion ( $a:b:c = 0.9998:1:1.0002$ ). Below  $100^\circ\text{K}$  the specimen expands when cooled, and more strongly as the temperature approaches  $10^\circ\text{K}$ ; below  $10^\circ\text{K}$  the specimen contracts. The possibility of a phase transition to the rhombohedral phase at  $10^\circ\text{K}$  is pointed out in [16].

Birefringence was noted in the  $\text{SrTiO}_3$  crystal [16] at room temperature, which could indicate extremely low tetragonal distortion of the lattice with  $c/a = 1.00008$ . Slight birefringence was also noted [17, 18] at  $20^\circ\text{C}$  and it was also concluded that there is distortion of the lattice at room temperature. Rhombohedral distortion [17] and rhombic distortion [18] are proposed at  $20^\circ\text{C}$ . The possibility of birefringence due to mechanical stresses, however, is also admitted [17, 18].

Birefringence  $\Delta n$  on two axes coinciding with the fourth axes of the cubic lattice begins to change near  $110^\circ\text{K}$  [18], and on the third axis at  $-35^\circ\text{K}$ .  $\Delta n$  begins to increase below  $110^\circ\text{K}$  [17]; in the interval from  $60$  to  $20^\circ\text{K}$  there is a plateau in the temperature dependence of birefringence, and with further cooling  $\Delta n$  increases and peaks. Here the increase of birefringence below  $110^\circ\text{K}$  and change in the character of its dependence near  $60^\circ\text{K}$  are related to phase transitions. Yet another phase transition is presumed to occur in the  $20$  to  $4.2^\circ\text{K}$  region. The authors point out that at  $77^\circ\text{K}$  the character of blurring of the lines on the x-ray diffraction

patterns could not be attributed to tetragonal distortion of the lattice, although it is satisfactorily explained by pseudomonoclinic rhombic distortion with  $a = c = 3.8870 \text{ \AA}$ ,  $b = 3.8988 \text{ \AA}$ ,  $b/a = 1.0030$ ,  $\Delta\beta = 6'$ . Discrepancies among the various data are not surprising, since distortions of the lattice are extremely small.

Analysis of the heat capacity of strontium titanate, conducted in the 51 to 300°K interval [19], and from 20 to 80°K [20], revealed no anomalies on the  $c_p(T)$  curve. This may be regarded as an indication of low thermal effects during phase transitions.

Optic analysis of monocrystals revealed that at 20°C strontium titanate has the refraction index  $n = 2.37$  at  $\lambda = 7,000 \text{ \AA}$  and  $n = 2.67$  at  $\lambda = 4,000 \text{ \AA}$  [21];  $n = 2.380$  at  $\lambda = 6,563 \text{ \AA}$ ;  $n = 2.409$  at  $\lambda = 5,893 \text{ \AA}$  and  $n = 2.488$  at  $\lambda = 4,861 \text{ \AA}$  [22] and  $n = 2.39$  [23]. The refraction index decreases with heating:  $dn/dT = (-6.2 \pm 0.1) \cdot 10^{-5} \text{ 1/}^\circ\text{C}$  at  $\lambda = 5,460 \text{ \AA}$  [15].

Below 100°K [24, 25], during analysis of a strontium titanate plate, perpendicular to [100], in polarized light, a fine twinning structure was noted. The twins had a width of 10-50 micron and were parallel to the cubic axes [011], as in the case of 90° domains in tetragonal barium titanate. The direction of extinction agreed with tetragonal distortions. No changes in the twinning pattern (that could be related to phase transitions) were noted in the 80 to 4.2°K interval. The application of an electric field of 4-15 kV/cm [18, 25] did not alter the twinning configuration.

Numerous investigators [15, 20, 24, 38] have analyzed the dielectric properties of highly pure polycrystalline specimens and monocrystals of  $\text{SrTiO}_3$ . The results of these works confirm that the  $\epsilon$  of  $\text{SrTiO}_3$ , increasing with cooling, does not pass through a peak, but approaches some constant at temperatures close to 0°K. Apparently the peak in the temperature dependence of  $\epsilon$  described in previous works [2-4], is related to the low purity of materials used for the synthesis of the specimens.

The permittivity of  $\text{SrTiO}_3$ , approximately 270 at 20°C (for polycrystalline specimens) and 300-400 (for monocrystals), increases with cooling (Figure 19.1) according to the Curie-Weiss law:  $\epsilon = \epsilon_0 + \frac{C}{T - \theta}$ , where  $C$ , according to various authors, varies from  $7.83 \cdot 10^4 \text{ }^\circ\text{K}$  to  $8.64 \cdot 10^4 \text{ }^\circ\text{K}$ ,  $\theta$  from 17 to 38°K, and  $\epsilon_0 = 43$ . On cooling below 80-100°K a gradual deviation from the Curie-Weiss law begins, and the growth rate of  $\epsilon$  diminishes gradually, remaining practically constant below 10°K, reaching 5,300-6,300 in polycrystalline specimens and 18,000-20,000 in monocrystals.

To explain this temperature dependence Barrett [39] developed Slater's theory, conducting a quantum-mechanical examination of ionic polarization. Here Sr and O ions are regarded as fixed in the lattice nodes, and each Ti

ion as an independent anharmonic oscillator. It is proposed that titanium ions are weakly bonded and their interaction is achieved only through an electric field. The "anharmonic" part of the potential energy of the oscillator is regarded as excitation. This account of the effect of discreteness of the energy levels of oscillators on ionic polarization of Ti led to the dependence

$$\epsilon = \frac{C}{\frac{\theta_1}{2} \operatorname{cth}\left(\frac{\theta_1}{2T}\right) - \theta}$$

where  $\theta$  is the extrapolated Curie temperature and  $\theta_1 = \frac{h\nu}{k}$  is the characteristic temperature determined by the frequency  $\nu$  of the oscillator. This equation, with proper selection of constants  $C$ ,  $\theta_1$  and  $\theta$ , satisfactorily describes the experimental temperature dependence of  $\epsilon$ . When  $T \gg \theta_1$ ,

$\frac{\theta_1}{2} \operatorname{cth}\left(\frac{\theta_1}{2T}\right)$  asymptotically approaches  $T$  and the equation acquires the form:

$\epsilon = C/(T - \theta)$ , i.e., is converted to the Curie-Weiss law. When the temperature approaches  $0^\circ\text{K}$ ,  $\operatorname{cth}(\theta_1/2T) \approx 1$  and  $\epsilon \approx C/(\theta_1/2 - \theta)$ , i.e., when

$T \ll \theta_1$   $\epsilon$  is independent of temperature. Thus, roughly speaking,  $\theta_1$  separates the low-temperature region, where due to quantum effects the temperature dependence of  $\epsilon$  deviates from the Curie-Weiss law, from the high-temperature region, where the behavior of  $\epsilon$  is described in classical approximation by the Curie-Weiss law. Neavor [31] obtained satisfactory agreement with the experiment for  $\theta = 45^\circ\text{K}$  and  $\theta_1 \approx 100^\circ\text{K}$ , i.e., when  $\epsilon = 0.453\theta_1$ . Hegenbarth [20] obtained  $\theta = 27^\circ\text{K}$  and  $\theta_1 \approx 80^\circ\text{K}$ . The temperature  $\theta_1 = 100^\circ\text{K}$  corresponds to oscillator frequency  $2.1 \cdot 10^{12}$  Hz or  $70 \text{ cm}^{-1}$ , which just lies in the far infrared region.

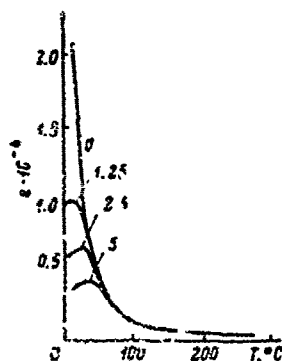


Figure 19.1. Temperature dependence of permittivity of  $\text{SrTiO}_3$  monocrystal in direction [110] in various stationary biasing fields. (According to Sawaguchi, et al [25]).

Measurement of  $\epsilon$  in pseudocubic directions [100], [110] and [111] [35] showed that the permittivities along these three axes take the same path and differ little from each other. The slight difference in the values of  $\epsilon$  on the various axes are related by the authors to the presence of internal residual mechanical stresses.

Contrary to Hulm's results [5], the  $\epsilon$  of  $\text{SrTiO}_3$  at low temperatures depends strongly on electric field strength [28, 29, 34, 38]. This dependence diminishes with increasing temperature, but is still quite noticeable at 70°K (Figure 19.1).

Hegenbarth [28] demonstrated that the dependence of  $\epsilon$  on temperature and the field naturally derived from Barrett's theory. On the basis of the expression for free energy

$$F - F_0 = A \left( \frac{\theta_1}{2} \coth \frac{\theta_1}{2T} - \theta \right) P^2 + \\ + BP^4 + \dots - EP$$

and assuming that  $E$  remains constant during the measurements and  $B$  is independent of temperature, the author arrives at the conclusion that the maximum in the temperature dependence of  $\epsilon$  will occur only in fields greater than

$$E_k = \left( \frac{\theta_1 - 2\theta}{3} \right)^{1/2} \left( \frac{4A^2}{B} \right)^{1/4}.$$

Here the following relation should be satisfied:

$$(1/\epsilon_{\text{max}})^{1/2} = (54B)^{1/4} E^{1/2}.$$

Experimental data agree satisfactorily with these dependences. It was found that  $E_k = 1.58$  kV/cm.

As shown by the measurements of Rupprecht, et al [40], at temperatures from 90 to 230°K and frequencies from 1 kHz to 36 GHz the dependence of  $\epsilon$  of  $\text{SrTiO}_3$  monocrystal on  $T$  and stationary field, parallel to the measured field, can be described by the expression

$$\epsilon(T, E) = \frac{\epsilon(T, 0)}{[1 + (A_{\text{hkz}}/C)^{1/2} (T, 0) E]^2}.$$

where  $\epsilon(T, 0) = C/(T - \theta)$ , and  $A_{\text{hkz}}$  is the anisotropic nonlinearity constant, depending on the direction of the field  $E$  relative to the crystallographic axes:  $A_{100} = 1.15 \cdot 10^{-18}$ ,  $A_{110} = 0.96 \cdot 10^{-18}$ ,  $A_{111} = 0.69 \cdot 10^{-18}$  °K·m<sup>2</sup>/V<sup>2</sup>.

Nonlinearity in the behavior of  $\epsilon$  is attributed to the anharmonic recurrent force acting on the titanium ion when it is displaced from its position of equilibrium.

The  $\tan \delta$  of  $\text{SrTiO}_3$  in the region of sonic frequencies is 0.00025 [28]. The curve of the temperature dependence of  $\tan \delta$  has two

maxima: one at 13-14°K and the other near 72°K (at 500 Hz) [20, 23, 32]. As the frequency on which the measurements are made increases, a displacement of the second maximum is noted toward the region of higher temperatures. Presumably the cause of this relaxation maximum of  $\tan \delta$  are impurities and annealing conditions [20]. According to [40],  $\tan \delta$  of strontium titanate monocrystal can be represented as the sum:  $\tan \delta_0$  and  $\tan \delta_F$ , where  $\tan \delta_0$  is the field-independent contribution and  $\tan \delta_F$  is the field-dependent contribution. It has been found that  $\tan \delta_F = \omega(B_{hkz}/C)\epsilon^5(T, 0)E^2$ , where  $B_{hkz}$  is the anisotropic constant (at frequencies of 2.3 to 6.5 kHz in the 90 to 230°K region  $B = 4.8 \cdot 10^{-3}$  m.sec°K/V<sup>2</sup>). The temperature dependence of  $\tan \delta$  is satisfactorily described in the 90-230°K range by the expression  $\tan \delta_0 = (A + DT^2)/(T - \theta)$ .

More recent investigations [41, 42] in the 3 to 36 GHz frequency range led for zero biasing field to the expression  $\tan \delta = (A + BT + DT^2)/(T - \theta)$ , where  $\theta = 37^\circ\text{K}$ , the parameter A is determined by attenuation on lattice defects, and the parameters B and D arise due to attenuation related to anharmonic interaction in the lattice. The magnitude of parameter A is determined by the number of lattice defects (including impurity ions) and vanishes in highly pure monocrystals, whereas the parameter B and D are practically independent of the production method, treatment and purity of the specimen.  $\tan \delta$  is proportional to frequency in the entire 3-36 GHz range.

At low temperatures in fields less than 130 V/cm the dependence  $P(E)$  is linear [15, 29]. The hysteresis loops appear only in the higher fields. On this basis Granicher [29] proposed that in the absence of an electric field  $\text{SrTiO}_3$  is in the paraelectric state, whereas the application of a field converts it to a state energetically close to ferroelectric, i.e., an electric field "induces" the ferroelectric state. It should be pointed out in this regard that the nonlinearity of the dependence  $P(E)$  of ferroelectrics in small fields is always relatively weak and the assumption of "induced ferroelectricity" would be more valid in the case of the detection of double hysteresis loops. According to Granicher [29], at 4.2°K ( $f = 50$  Hz,  $E = 8$  kV/cm)  $P_S \approx 3 \cdot 10^{-6}$  C/cm<sup>2</sup>,  $P_{res} \approx 1 \cdot 10^{-6}$  C/cm<sup>2</sup>,  $E_C = 300-500$  V/cm.

Weaver [31] analyzed the temperature dependence of spontaneous polarization of  $\text{SrTiO}_3$  monocrystals. This researcher obtained a smaller  $P_S$  than was obtained in [29]:  $\sim 1.5 \cdot 10^{-6}$  C/cm<sup>2</sup> at 1.4°K, and  $E_C = 670$  V/cm. Hegenbarth [20] points out that the dependence  $P(E)$  in fields up to 12.5 kV/cm is not strictly linear, even at temperatures above 80°K, whereas below 80°K weak dielectric hysteresis loops appear, which are quite pronounced at 20°K. The existence of hysteresis loops at relatively high temperatures ( $\sim 70^\circ\text{K}$ ) was also pointed out by Mitsui and Westphal [24]. The dependence  $P_{res}(T)$  of  $\text{SrTiO}_3$  monocrystals, determined according to the hysteresis loops, is illustrated in Figure 19.2. As seen in the figure,

the residual polarization exists in an extremely wide temperature range, gradually diminishing on heating. It is presumed [36] that the dielectric hysteresis loops in  $\text{SrTiO}_3$  are not related to the ferroelectric state of the substance and are explained by the influence of space charges. This assumption, however, has not been checked.

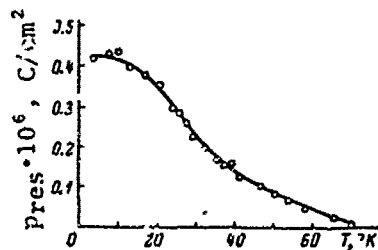


Figure 19.2. Temperature dependence of residual polarization of  $\text{SrTiO}_3$  monocrystal (according to Mitsui and Westphal [24]).

The effect of hydrostatic pressure on the  $\epsilon$  of strontium titanate was analyzed in [43, 44]. It was found that as pressure increases,  $\epsilon$  diminishes according to the expression  $\epsilon = C^*/(p - p_0)$ , where  $C^* = 12,600$  kbar and  $p_0 = -40$  kbar [44].

According to Granicher [29], at low temperatures piezoelectric oscillations can be excited in strontium titanate monocrystals polarized by a field of at least 600 V/cm.

The elastic constants of strontium titanate monocrystals were first analyzed by Poindexter and Giardini [45] at 20°C. The following elastic piezoelectric coefficients were obtained:  $s_{11} = 3.3 \cdot 10^{-13}$ ,  $s_{12} = 0.74 \cdot 10^{-13}$  and  $s_{44} = 2.1 \cdot 10^{-11}$  cm<sup>2</sup>/dyne. Bell and Rupprecht [46] measured the elastic modulus of  $\text{SrTiO}_3$  monocrystal in the 330 to 77°K temperature range. At 295°K  $c_{11} = 3.22 \cdot 10^{12}$  dyne/cm<sup>2</sup>,  $c_{12} = 1.20 \cdot 10^{12}$  dyne/cm<sup>2</sup> and  $c_{44} = 1.22 \cdot 10^{12}$  dyne/cm<sup>2</sup>. The elastic moduli increase gradually from 20°C to 112°K, where the velocity of ultrasound changes notably. For a transverse wave on axis [100] the velocity decreases 15% within the limits of 3°K. Measurements on axes [111] also indicate a change in the elastic modulus at 112°K. Here there was no temperature hysteresis, which indicates a second order transition. Below the transition temperature the velocity changes little all the way to 77°K. For a longitudinal wave on axis [100] attenuation becomes so great that measurements cannot be made below 112°K. The sharp increase in attenuation of shear and longitudinal waves and the great change in the velocity of ultrasound in monocrystalline  $\text{SrTiO}_3$  was also noted by Kregstad and Moss [47].

Rupprecht and Winter [33, 48] measured the elastic and electro-mechanical constants of crystalline  $\text{SrTiO}_3$  in the 300 to 4.2°K range. It was shown in this work that in addition to the piezoelectric effect, which is caused by the application of a biasing electric field, and which is proportional to this field, crystalline  $\text{SrTiO}_3$  displays a piezoelectric effect in the absence of an external field as well. Thus, the piezoelectric

modulus in a stationary electric field is described by the expression  $d_{31}^* = d_{31} + 2q_{31}E_3$ , where  $d_{31}^*$  is the measured and  $d_{31}$  the true piezoelectric modulus,  $q_{31}$  is the electrostriction coefficient and  $E_3$  is the field perpendicular to the length of a longitudinally vibrating bar, the facets of which correspond to the planes (100), (010) and (001). At 243.3°K  $q_{31} = (1.732 \pm 0.002) \cdot 10^{-19} \text{ m}^2/\text{V}^2$ , and  $d_{31} = (1.21 \pm 0.27) \cdot 10^{-14} \text{ m/V}$ . Here  $q_{31} = Q_{31}/(T - T_1)^2$  and  $d_{31} = D_{31}/(T - T_2)$ , where  $Q_{31} = (6.92 \pm 0.07) \cdot 10^{-15} \text{ m}^2 \cdot \text{deg}^2 \cdot \text{V}^{-2}$ ,  $D_{31} = (1.02 \pm 0.32) \cdot 10^{-12} \text{ m} \cdot \text{deg} \cdot \text{V}^{-1}$ ,  $T_1 = (41.48 \pm 0.01)^\circ\text{K}$ ,  $T_2 = (99.5 \pm 5.8)^\circ\text{K}$ .

At temperatures above the phase transition temperature  $T_t = 102.52 \pm 0.031^\circ\text{K}$  the elastic pliancy coefficients diminish slowly on cooling far from  $T_t$ , but near  $T_t$  they increase sharply. Below  $T_t$  they drop sharply and between 80 and 66°K are practically constant. Measurements at 22 and 17°K yielded: at 22°K  $s_{11} = (24.5 \pm 0.3) \cdot 10^{12} \text{ m}^1/\text{N}$ ; at 17°K  $s_{11} = (9.3 \pm 0.6) \cdot 10^{12} \text{ m}^2/\text{N}$ . Considering that at 66°K  $s_{11} = 5.36 \cdot 10^{12} \text{ m}^2/\text{N}$ , the authors conclude that the maximum elastic pliancy occurs in the interval from 66 to 22°K. The final true piezoelectric modulus  $d_{31}$  in the entire temperature range below 300°K verifies the deviation of symmetry of the  $\text{SrTiO}_3$  crystal from cubic at temperatures above  $T_t$ .

Schmidt and Hegenbarth [37] analyzed the electrostriction deformations and piezoelectric constants  $d_{33}$ ,  $g_{33}$ ,  $d_{31}$  and  $g_{31}$  of monocrystalline strontium titanate in a slowly changing biasing electric field. They found that at 80°K  $d_{33}$  and  $g_{33}$  are linear functions of  $E$  (for  $E$  up to 12 kV/cm), whereas at 20°K the rate of increase of  $g_{33}$  slows down somewhat as the field is increased, and  $d_{33}$  peaks and then drops off. The values of  $d_{31}$  and  $g_{31}$  at 80°K are negative and increase in absolute value as  $E$  increases, but at 20°K they increase in absolute value only to 1.5 kV/cm, after which they vanish and then become negative. These anomalies are tied to the slow establishment of the equilibrium state of the crystal. The authors indicate the presence of the piezoelectric effect in the crystals after the removal of the field, which vanishes only after a long period of shorting of the electrodes. The possibility is not ruled out that the existence of the piezoelectric effect after application of a field is related to an electric effect.

To explain the phase transition near 110°K Cowley [49] proposed that this phase transition is related to random degeneration of two branches of the dispersion curves: longitudinal acoustic branch and transverse optical branch of lowest frequency. This assumption, however, is taken to task [48]. The authors indicate that if such degeneration were the cause of the transition, then the transition temperature  $T_t$  would depend notably

on the strength of the biasing field, but in reality there is no such dependence.

Horner [50] considers that a new type of excitation can be viewed as the cause of this phase transition at 110°K: the bonded state of two ferroelectric soft phonons, the frequency of which becomes zero at  $T_t$ .

This excitation represents vibrations of ion quadrupole moments propagating in the crystal. Horner points out that this excitation could be detected experimentally near  $T_t$  according to the second order Raman scattering.

It is noteworthy that strontium titanate has been the object of numerous investigations of optical spectra, theoretical and experimental analysis of lattice vibrations and experimental checking of dynamic theory [51-77]. Many works have been devoted to analysis of EPR, NMR and the Messbauer effect in  $\text{SrTiO}_3$  [78-85], analysis of lattice defects, semiconductor properties, superconductivity and luminescence [86-110]. There are also measurements of thermal conductivity and the electrocaloric effect [111-114]. Certain works are devoted to discussion of the polarization of ions in strontium titanate [115, 117].

By way of summarizing the results discussed above, we point out that several phase transitions occur in strontium titanate during cooling, of which the one at 100-110°K is nonferroelectric, whereas the nature of the phase transitions at lower temperatures is not clear. The character of the dependence of  $\epsilon$  on  $T$  and  $E$  is satisfactorily explained in Barrett's theory by the paraelectric behavior of  $\text{SrTiO}_3$  and does not require assumptions concerning the presence of the ferroelectric phase transition. Nevertheless, low-temperature phase transitions do occur in  $\text{SrTiO}_3$  at temperatures of the order of 30°K, and there is little reason to deny their ferroelectric origin.

## 2. Lead Titanate

The x-ray diffraction analysis done by Megaw in 1946-1947 showed that lead titanate ( $\text{PbTiO}_3$ ) has a tetragonally distorted lattice at 20°C with a high degree of distortion:  $c/a = 4.141/3.891 = 1.0635$  [118, 119]. Jonker and van Santen [120], discovering that the temperature of the ferroelectric phase transition in solid solutions  $(\text{Ba}, \text{Pb})\text{TiO}_3$  and  $(\text{Sr}, \text{Pb})\text{TiO}_3$  increases as the concentration of lead titanate increases, proposed that  $\text{PbTiO}_3$  is a ferroelectric. However, the first experimental evidence for the existence of a ferroelectric phase transition in  $\text{PbTiO}_3$  near 500°C was obtained by Smolenskiy [2-4, 121] and Shirane, et al [122, 123] working independently.

X-ray diffraction analyses confirm Megaw's results on the tetragonal distortion of the  $\text{PbTiO}_3$  lattice at room temperature and yield close values

of the parameters  $c$  and  $a$  and the ratio  $c/a$  [122-126]. At a higher temperature, as seen in Figure 19.3, the constant  $a$  increases smoothly and  $c$  diminishes. Here the volume of the nucleus and the ratio  $c/a$  decrease. At temperatures close to  $-100^\circ\text{C}$  ( $490-510^\circ\text{C}$ )  $c$  and  $a$  change sharply and the lattice becomes cubic. The phase transition to the cubic phase is accompanied by a substantial reduction of volume. The sharp change of parameters in the region of the transition suggests a first order phase transition. It was established that conversion to the rhombic and rhombohedral phases, analogous to the low-temperature phase transitions in barium titanate [123], do not exist in  $\text{PbTiO}_3$ . At lower temperatures, however, phase conversions, apparently of a different nature, do occur [127, 129].

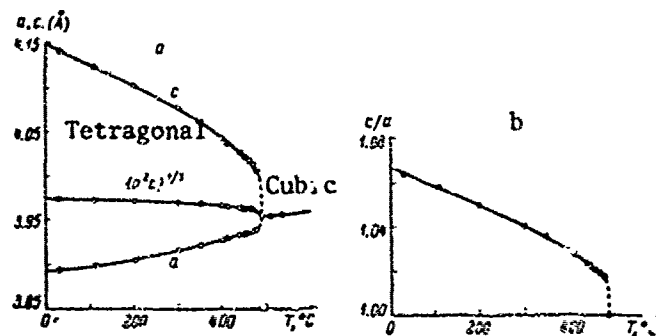


Figure 19.3. Temperature dependence of lattice parameters of  $\text{PbTiO}_3$  (according to Shirane, et al [123]):

a -- lattice periods and volume of nucleus; b -- ratio  $c/a$ .

X-ray diffraction analysis showed that when specimens are slowly cooled, a phase transition occurs near  $-100^\circ\text{C}$ , in which the values  $c$  and  $a$  change and superstructure lines appear, which could be identified on the assumption that  $a' = 4a$  and  $c' = 4c$ , where  $a$  and  $c$  are the former lattice parameters. During the transition there is a reduction in the volume of the elemental nucleus. Analysis of the temperature dependence of  $\epsilon$  of lead titanate during slow cooling ( $0.5^\circ\text{C}$  per minute) revealed two very small, but distinct jumps in  $\epsilon$  at  $-100$  and  $-150^\circ\text{C}$ . The jump of  $\epsilon$  at  $-100^\circ\text{C}$  agrees satisfactorily with the phase transition at  $-100^\circ\text{C}$ , revealed by x-ray diffraction analysis. The existence of the transition at  $-150^\circ\text{C}$  has not been checked by x-ray diffraction analysis. A change in the slope of the curve  $\epsilon(T)$  was also noted near  $-60^\circ\text{C}$ . The authors [127, 128] feel that the transitions in  $\text{PbTiO}_3$  at  $-100$  and  $-150^\circ\text{C}$  are similar to the phase transitions of buckling found by Cross and Nicholson in  $\text{NaNbO}_3$  at  $470$  and  $520^\circ\text{C}$ .

The great volumetric spontaneous deformation, determined by the change in  $(a^2c)^{1/3}$  (Figure 19.3a) causes the linear expansion coefficient  $\alpha$  of a polycrystalline specimen to become negative in the ferroelectric

state in a wide temperature range [121, 124]. At  $-30^{\circ}\text{C}$  there are discontinuity on the curve  $\Delta l/l(T)$  and maximum on the curve  $\alpha(T)$ . Smolenskiy [121] proposes that this anomaly in volumetric expansion is related to a low-temperature phase transition. This is apparently one of the low-temperature phase transitions described in [127-129]. The transition to the low-temperature modification, according to both dilatometric data [121] and the results of x-ray diffraction analyses [127], takes place with a reduction of volume. The difference in the transition temperatures may be related to the fact that the measurements in [127] were made during cooling and in [121] during heating. The relative elongation of  $\text{PbTiO}_3$  mono-crystals [132], in addition to the anomaly at the Curie point, also manifests an anomaly in the  $370\text{-}450^{\circ}\text{C}$  temperature range. This, however, does not agree with the results of measurements on polycrystalline specimens [121, 124], although it does find some confirmation in the results of measurements of the temperature dependence of  $\epsilon$  of polycrystalline  $\text{PbTiO}_3$  with mineralizers [4]. The anomalies in this temperature region are most likely not characteristic of pure lead titanate and are caused by contaminants.

Shirane, Pepinsky and Frazer [130, 131] conducted an x-ray diffraction analysis of monocrystals and neutron radiographic analysis of polycrystalline  $\text{PbTiO}_3$  specimens at room temperature and determined the displacement of ions from symmetric positions. For the case when the Pb ion is used as the origin of the coordinate system and the centers of the ions are placed at points with the coordinates: Pb: (000), Ti:  $(1/2, 1/2, 1/2 + \delta z_{\text{Ti}})$ ,  $\text{O}_I$   $(1/2, 1/2, \delta z_{\text{O}_I})$  and  $\text{O}_{II}$   $(1/2, 0, 1/2 + \delta z_{\text{O}_{II}})$ , the following values of  $\delta z$  were obtained:  $\delta z_{\text{Ti}} = +0.040$ ,  $\delta z_{\text{O}_I} = +0.112$ ,  $\delta z_{\text{O}_{II}} = +0.112$  or (in angstroms):  $\delta z_{\text{Ti}} = +0.17 \text{ \AA}$ ,  $\delta z_{\text{O}_I} = +0.47 \text{ \AA}$ ,  $\delta z_{\text{O}_{II}} = +0.47 \text{ \AA}$ . However, since  $\delta z_{\text{O}_I} = \delta z_{\text{O}_{II}}$ , it is more convenient to place the origin of the coordinate system at the center of the octahedron (Figure 19.4). Then  $\delta z_{\text{O}_I} = 0$ ,  $\delta z_{\text{Ti}} = +0.30 \text{ \AA}$ ,  $\delta z_{\text{Pb}} = +0.47 \text{ \AA}$ , i.e., the Ti and Pb ions are displaced in the same direction in relation to the oxygen octahedron. The authors point out that these displacements are much larger than those of Ba and Ti in barium titanate. Calculation on the basis of neutron radiographic data of the ionic part of spontaneous polarization, assuming a purely ionic crystal, yields  $54 \cdot 10^{-6} \text{ C/cm}^2$ , whereas the analogous calculation for  $\text{BaTiO}_3$  yields for its value  $17 \cdot 10^{-6} \text{ C/cm}^2$ .

Calorimetric analysis of lead titanate was undertaken in works [124, 133, 134]. The heat capacity passes through a sharp peak at the Curie point. The latent heat of transition is 1,150 cal/mole [124, 133]. The corresponding change in entropy is  $-0.80 R$ , where  $R$  is the universal gas constant. According to [134] the heat of transition is 900 cal/mole.

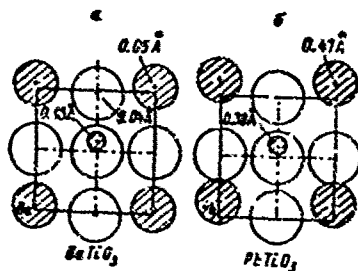


Figure 19.4. Elemental nucleus of  $\text{PbTiO}_3$  with origin of coordinate system at center of oxygen octahedron (b) compared to elemental nucleus of  $\text{BaTiO}_3$  (a) (according to Shirane, et al [131]).

More recent measurements verified this character of the temperature dependence, but showed that birefringence varies from crystal to crystal and can be much lower for twinned crystals than for single-domain crystals [137]. Despite the fact that spontaneous deformation is much greater in lead titanate than in barium titanate, its birefringence is only about one-third that of the latter [138]. This fact, like the nonmonotonic character of the temperature dependence of birefringence of  $\text{PbTiO}_3$ , is possibly related to overlapping of the electron shells of the ions in the presence of great spontaneous polarization [139]. It should be recalled that the spontaneous birefringence of  $\text{PbTiO}_3$  was calculated [140] and it was found that lead titanate should be optically positive, even though this disagrees with experimental data. The correct sign was obtained in the calculation conducted in [141].

The domain structure of  $\text{PbTiO}_3$  was first analyzed by Fesenko [126], who observed polysynthetic twinning on (101) and (011). Domain width was 0.1 to 10 micron. The angle between the domain walls and crystal facet ( $\alpha = 46^\circ 45'$ ) coincided satisfactorily with the calculated value. On heating above  $400^\circ\text{C}$  rearrangement of the domain structure begins and near  $500^\circ\text{C}$  the domains vanish. On cooling a simpler domain structure appears. In most cases the area of layers of the monocrystal filled with c-domains is small, and heating above the Curie point leads to disappearance of c-domains [128, 142]. Analysis of the temperature at which the domain structure vanishes and appears [137] showed that the temperature hysteresis of the phase transition reaches  $3\text{--}4^\circ\text{C}$ . In a crystal broken down into  $90^\circ$  domains reorientation of the domains begins at  $20^\circ\text{C}$  only when  $E \approx 14\text{--}17\text{ kV/cm}$  [127]. This process, however, does not proceed to completion due to rupture of the crystal with a further increase in the field. When a field of  $10.5\text{ kV/cm}$  is applied to a single-domain crystal, wedges are formed, comprising an angle of  $45^\circ$  with the direction of the field and cutting through the entire crystal in 1-1.5 sec. After 0.5-1 min the entire crystal consists of two

The refraction coefficient of  $\text{PbTiO}_3$  monocrystals was analyzed in [125, 126, 135]. The mean refraction index was investigated using a selenium-sulfur alloy. It was established that the refraction index differs for crystals grown by different methods, and at room temperature varies from 2.65 to 2.71.

The birefringence of  $\text{PbTiO}_3$  [131, 136] at room temperature for  $\lambda = 5,896\text{ \AA}$  is 0.01, gradually increases on heating, reaches a maximum value of 0.018 at  $400^\circ\text{C}$ , diminishes to 0.012 near the Curie point, and suddenly vanishes at the

domains. Strengthening of the field caused displacement of the boundary through the crystal, and elimination of the field caused motion in the opposite direction until the entire crystal became single-domain.

The dielectric and piezoelectric properties of lead titanate have been analyzed to a much lesser extent than those of many other ferroelectrics. The reason for this is that the production of well sintered polycrystalline specimens of lead titanate is impeded by the volatility of lead oxide at high temperatures. Losses of PbO during roasting lead to disruption of the stoichiometric ratio of the oxides. Until this day it has not been possible to produce well sintered lead titanate ceramics without using mineralizing additives. At room temperature, moreover, the coercive field of lead titanate is very strong and the domains can be completely reoriented only in extremely high fields, exceeding the presently attainable electric strength of the specimen. At the same time, the rapid increase in electrical conductivity and reduction of electric strength during heating prohibits reorientation of domains at high temperatures, close to the Curie point, where  $T_c$  is lower. Therefore spontaneous polarization and the piezoelectric properties of pure  $PbTiO_3$  have not yet been measured.

The permittivity of  $PbTiO_3$ , measured in weak fields, increases during heating and peaks in the region of 490-510°C. The permittivity of ceramics with considerable porosity [78] is 50 at room temperature. It was established during investigation of the ceramics that above the Curie temperature the Curie-Weiss law is obeyed, where  $C = 1.1 \cdot 10^5$ °C, and  $\theta = 420$ °C [124] and  $C = 1.54 \cdot 10^5$ °C,  $\theta = 490$ °C [126].

The dielectric properties of lead titanate monocrystals were first analyzed by Belyayev and Khodakov [143]. Permittivity at room temperature was found to be 170. It was found that at radio frequencies  $\epsilon$  depends little on frequency and increases notably only on transition to low frequencies. The electrical conductivity increases both with increasing temperature and with increasing field. The energy of activation was found to be 1.06 eV for the investigated crystals, grown from a mixture of PbO,  $V_2O_5$  and  $TiO_2$ .

More recent measurements [125] showed that  $\epsilon$  at room temperature depends strongly on the method of growing the crystals and varies from 75 to 150. The permittivity, measured in a weak variable field, does not depend on the strength of a simultaneously applied stationary field up to  $E = 50$  kV/cm. According to Bhide, et al [138], the permittivity of monocrystalline  $PbTiO_3$  is equal at 10 kHz to 30 at room temperature and ~10,000 at 495°C. Above the Curie temperature the Curie-Weiss law is valid, with  $C = 1.1 \cdot 10^5$  and  $\theta = 485$ °C (Figure 19.5).

Introducing various additives to lead titanate in the quantities 0.1, 0.5 and 1%, Tien and Carlson [144] were able to obtain relatively well sintered ceramics (with a porosity of up to 94-95.5% of the theoretical). For ceramics with a 1 mole % additive of  $CaF_2$  they obtained a piezoelectric

modulus  $d_{33} = 130 \cdot 10^{-12}$  C/N =  $3.9 \cdot 10^{-6}$  CGSE. The densest  $\text{PbTiO}_3$  ceramics were obtained by adding 1-2 mole %  $\text{MnO}_2$  [145]. Here  $\epsilon = 210-280$ ,  $\tan \delta = 0.0075-0.008$ ,  $k_p = 4-5\%$  at  $20^\circ\text{C}$  and the electric resistance is  $10^{12}-5 \cdot 10^{12}$  ohm $\cdot$ cm.

Last [63] and Yatsenko [56] analyzed the optic absorption spectra of lead titanate. Last found absorption bands  $\nu_1$  and  $\nu_2$  at  $590$  and  $405$   $\text{cm}^{-1}$ , and Yatsenko at  $575$  and  $420$   $\text{cm}^{-1}$ . It follows from these data that the force constant  $k$  for valent vibrations is  $(1.04-1.4) \cdot 10^5$  dyne/cm, the effective charge of the vibrating system is  $Q = (1.57-1.8)e$ , and for deformation vibrations  $k = (0.60-0.76) \cdot 10^5$  dyne/cm,  $Q = (1.3-1.5)e$ .

Blokhin [146, 147], on the basis of analysis of the x-ray  $\mu$ -spectrum of absorption, proposes that the bond of the atoms Ti and O in  $\text{PbTiO}_3$  are basically covalent, which the author attributes to the substantial polarizing action of Pb atoms on Ti and O atoms. The author concludes that lead titanate is an electron semiconductor, in which electrical conductivity, governed by the transition of electrons from the 3d- to the 4s, p-band, should increase sharply when the temperature is increased.

Kabalkina and Vereshchagin [148] analyzed the effect of hydrostatic pressure (up to  $18,000$  kg/cm) on crystal lattice parameters. They established that when the pressure is increased, parameter  $a$  increases linearly with pressure, and parameter  $c$  decreases linearly (at  $p = 18,000$  kg/cm  $\Delta c = -0.10$  Å,  $\Delta a = +0.01$  Å), in connection with which the ratio  $c/a$  decreases. The dependence of  $\Delta c$  on pressure can be represented in the form  $\Delta c/c = -14.3 \cdot 10^{-7} p$ . Extrapolating their data, the authors reached the conclusion that the phase transition to the nonferroelectric state at  $20^\circ\text{C}$  should occur at pressures of the order of  $27,000$  kg/cm $^2$ , and hence assume  $dT_c/dp \approx 18 \cdot 10^{-3}$  deg/atm.

Also noteworthy are several works on analysis of  $\text{PbTiO}_3$  with the aid of optic. spectra, EPR, diffusion of slow neutrons [55, 56, 63, 149-151].

The first attempt to explain the high Curie temperature of  $\text{PbTiO}_3$  was undertaken by Smolenskiy [3], who explained the properties of lead titanate by the features of the electron shell of the  $\text{Pb}^{2+}$  ion, which differs sharply from the electron shell of alkaline-earth ions and which is responsible for the considerably more pronounced covalent character of the chemical bond in lead titanate. Megaw [152], stressing the importance of the partially covalent character of bonds in  $\text{PbTiO}_3$ , notes that the homeopolar system of bonds in  $\text{PbO}$  plays an important role, and the Pb-O bonds in  $\text{PbO}$  form a shallow tetrahedron with the lead atom at the vertex. The displacement of the lead atom in  $\text{PbTiO}_3$  relative to the center of the oxygen polyhedron surrounding it causes the four oxygen atoms lying in the plane perpendicular to  $\Gamma_5$ , to form with the lead a tetrahedron similar to

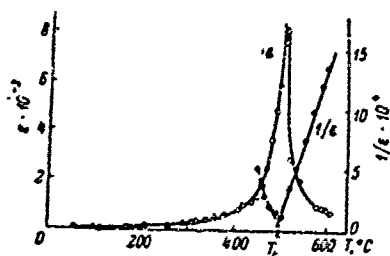


Figure 19.5. Temperature dependence of  $\epsilon$  and  $1/\epsilon$  of monocrystalline  $\text{PbTiO}_3$  at 10 kHz in weak fields (Bhide, et al [138]).

ionic crystal, i.e., the charge +2 is ascribed to the titanium ion, +1 to the lead ion and -1 to the oxygen ion. The origin of the coordinate system is placed at the center of the titanium ion. The calculation yielded the spontaneous polarization of  $\text{PbTiO}_3$  ( $90.5 \cdot 10^{-6} \text{ C/cm}^2$ ), numerical expression for the contribution of electronic and ionic polarization of individual ions to spontaneous polarization, and the internal field acting on the various ions:

Ion	$P_{\text{ion}} \cdot 10^{-6}, \text{ C/cm}^2$	$\frac{P_{\text{ion}}}{P_0} \cdot 100, \%$	$\frac{P_{\text{ion}}}{P_0} \cdot 100, \%$	$\frac{P_{\text{ion}}}{P_0} \cdot 100, \%$
Pb . . . . .	1.93	13.8	4.8	38.6
Ti . . . . .	0.62	3.0	0	3.0
O <sub>I</sub> . . . . .	7.12	32.6	8.4	41.0
O <sub>II}, O<sub>III</sub> . . . . .</sub>	2.23	2.10.3	2.8.4	2.18.7

Hence it is clear that the greatest contribution to spontaneous polarization comes from  $\text{O}_I$  ions, and the smallest from Ti ions. It should be pointed out, however, that since the contribution of the various ions to the ionic part of spontaneous polarization depends on the choice of the coordinate origin, the contribution of  $\text{O}_I$  ions to spontaneous polarization will also vary, depending on where the authors place the origin of the coordinate system. Approximately 70% of spontaneous polarization is ascribed to the electronic component. Despite the obvious usefulness of such calculations, a careful attitude should be taken toward the results, in view of the arbitrary choice of the effective charges of the ions, due to the lack of reliable information concerning the electro-polarizability of the various ions in the crystal lattice, and several other assumptions in the calculation.

The important role of the high electron polarizability of the  $\text{Pb}^{2+}$  ion, determined by the unshared pair of 6s-electrons, which in many compounds including, probably,  $\text{PbTiO}_3$ , displays stoichiometric activity, is stressed in [155]. Also noted is the possibility that in lead titanate, possessing a large share of covalent bonds, dipole moments may occur as a result of

the one seen in  $\text{PbO}$ . Thus the large ratio  $c/a$  and high Curie temperature, according to Megaw, are explained by the formation of directional bonds by the lead atom. Belyayev also shares this point of view [153].

Venevtsev, et al [154] calculated the internal field and spontaneous polarization of  $\text{PbTiO}_3$  in the tetragonal phase. The displacements of ions were taken from [131]. It was assumed that the charge of each ion is one-half the charge that would occur in a purely

these bonds. It is also stated that the partially covalent character of bonds in  $\text{PbTiO}_3$  may increase ion polarizability of the crystal lattice, decreasing the recurrent forces and giving the vibrations of the ions an anharmonic character [155]. It is further noted that odd hybrid states, in which participate the 6s- and 6p-orbits, as a result of antisymmetric excitations [157], can occur in  $\text{PbTiO}_3$ , and these can create a dipole moment, increasing the ion polarizability and, consequently, permittivity. Thus, electrostatic forces of dipole-dipole interaction, which are great due to the high electron and ion polarizabilities of the crystal lattice, are stated in [155] as the main cause of the high Curie temperature of lead titanate. The high magnitude of these polarizabilities, in turn, is related to the specific structure of the electron shell of the  $\text{Pb}^{2+}$  ion and partially covalent character of the bond.

### 3. Cadmium Titanate

The ferroelectric properties of cadmium titanate ( $\text{CdTiO}_3$ ) were discovered by Smolenskiy [2, 3], according to whose data transition to the ferroelectric state takes place at approximately  $50^\circ\text{K}$ . At room temperature, nevertheless,  $\text{CdTiO}_3$  has a rhombically distorted structure of the perovskite class rather than a cubic structure. According to Megaw [158], the nucleus is doubled on all three rhombic axes and the lattice parameters are:  $a = 10.695$ ,  $b = 7.615$ ,  $c = 10.834 \text{ \AA}$ .

More recent x-ray diffraction analyses of  $\text{CdTiO}_3$  [159], performed on monocrystals, showed that doubling occurs only on the b axis and the lattice parameters are:  $a = 5.438$ ,  $b = 7.615$ ,  $c = 5.417 \text{ \AA}$ . The rhombic elemental nucleus contains four "molecules" of  $\text{CdTiO}_3$ . Either  $\text{Pc}m$  or  $\text{Pc}2_1n$  are possible spatial groups. The authors relate the symmetry of  $\text{CdTiO}_3$  to the polar group  $\text{Pc}2_1n$ . Hence they find the displacements of ions in the elemental nucleus of  $\text{CdTiO}_3$  at  $20^\circ\text{C}$  (Table 25). According to [159], all displacements of  $\text{O}_{\text{II}}$  ion on the y axis are identical with respect to magnitude and sign, and the same applies to displacement of  $\text{O}_{\text{III}}$  ions. However,  $\Delta y_{\text{O}_{\text{II}}} = -0.03$  and  $\Delta y_{\text{O}_{\text{III}}} = +0.07$ . While the dipole moments created by the displacements of all other ions are mutually compensated, the components of dipole moments of ions  $\text{O}_{\text{II}}$  and  $\text{O}_{\text{III}}$  on the y axis are mutually uncompensated. It follows, therefore, from Table 25 that the elemental nucleus of  $\text{CdTiO}_3$  displays a dipole moment at room temperature. It should be borne in mind, however, that the choice of the polar group  $\text{Pc}2_1n$  was made only on the basis of x-ray diffraction data without checking for the presence of piezo- or pyroelectric properties.

Table 25. Coordinates of Ions in Cadmium Titanate

Ions	Position of Ions				Error	
Cd	x	0+0.006	0-0.006	1/2+0.006	1/2-0.006	±0.002
	y	3/4	1/4	1/4	3/4	-
	z	0+0.006	0-0.006	1/2-0.016	1/2+0.016	±0.002
Ti	x	1/2+0.005	1/2-0.005	0+0.005	0-0.005	±0.005
	y	0	1/2	1/2	0	-
	z	0-0.065	0+0.065	1/2+0.085	1/2-0.065	±0.011
O <sub>I</sub>	x	0-0.03	0+0.03	1/2+0.03	1/2-0.03	±0.015
	y	3/4	1/4	3/4	1/4	±0.025
	z	1/2+0.05	1/2-0.05	0+0.05	0-0.05	±0.015
O <sub>II</sub>	x	1/4+0.05	1/4-0.05	3/4-0.05	3/4+0.05	±0.005
	y	0-0.03	0-0.03	1/2-0.03	1/2-0.03	±0.015
	z	1/4+0.06	3/4+0.06	3/4-0.06	1/4-0.06	±0.015
O <sub>III</sub>	x	1/4+0.05	1/4-0.05	3/4-0.05	3/4+0.05	±0.005
	y	1/2+0.07	1/2+0.07	0+0.07	0+0.07	±0.015
	z	1/4+0.06	3/4+0.06	3/4-0.06	1/4-0.06	±0.015

According to Smolenskiy's data [2-4],  $\epsilon$  of polycrystalline cadmium titanate increases with cooling and peaks at a temperature of 50°K, below which CdTiO<sub>3</sub> displays ferroelectric properties. Hegenbarth conducted a more thorough analysis [34]. He measured the  $\epsilon$  (at 800 Hz and 50 V/cm) of polycrystalline CdTiO<sub>3</sub> specimens, sintered at 1,250°C, in various biasing fields (Figure 19.6). The permittivity, equal to ~900 at 80°K, increases to 2,300 at 50 ± 0.5°K, and then drops again. As seen in Figure 19.6, it

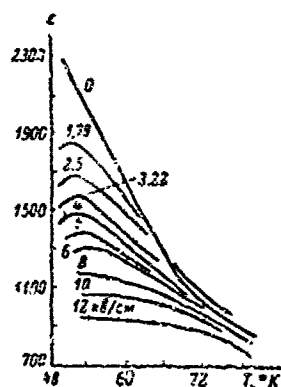


Figure 19.6. Temperature dependence of permittivity of polycrystalline cadmium titanate in various stationary biasing fields (according to Hegenbarth [34]).

is strongly dependent on the direction of the field. At 20.4°K  $\epsilon$  is 1,490, and at 10°K  $\epsilon = 1,200$ . Below the Curie point dielectric hysteresis loops are seen. Hegenbarth [160] also analyzed the electrocaloric effect of polycrystalline CdTiO<sub>3</sub> specimens at 59.7, 68.6 and 78.7°K. Its magnitude is low due to the sufficiently high entropy of the lattice at these rather high temperatures.

Rhombic distortion of the CdTiO<sub>3</sub> nucleus is regarded [161] as the result of buckling phase transition that occurs at high temperatures, and the phase transition at 50°K is regarded as a transition to the ferroelectric state. The opinion is

both ionic and electronic polarization at 20°C, were calculated in [118]. For this purpose data [159] on the positions of ions in the elemental nucleus and the structural coefficients calculated for non-displaced positions were used. The charge of the cadmium ion was set at +1, +1/2 was ascribed to titanium and -1 to oxygen. The spontaneous polarization calculated with the stated prerequisites is  $18 \cdot 10^{-6}$  C/cm<sup>2</sup>, and the contribution of electronic polarization is 52%.

Polycrystalline specimens of CdTiO<sub>3</sub> have a  $\epsilon$  peak [103] at 960°C. Solid solutions (Cd, Sr)TiO<sub>3</sub>, (Cd, Li)(Ti, Nb)O<sub>3</sub> and (Cd, Li)(Ti, Ta)O<sub>3</sub> have  $\epsilon$  peaks in the 750-1,000°C region. It is reported that dielectric hysteresis loops were observed in these specimens at around room temperature; these hysteresis loops vanished at 110°C. Hence it is concluded [163] that at 960°C an antiferroelectric transition occurs in CdTiO<sub>3</sub>, and at 100°C there is a transition from the antiferroelectric state to the ferroelectric state. However, Poplavko reported at the sixth All-Union Conference on Ferroelectricity the results of MHF measurements of CdTiO<sub>3</sub> specimens in a wide temperature range. According to his data  $\epsilon$  of cadmium titanate decreases monotonically between 20 and 1,000°C and, consequently, no  $\epsilon$  peaks were observed in this temperature region.

Thus, there are two points of view at this time: one consists in the fact that the distortion of the CdTiO<sub>3</sub> lattice at room temperature is a result of a buckling transition, and the other ascribes ferroelectricity and antiferroelectricity to CdTiO<sub>3</sub> in the temperature range up to 960°C. In this regard it is noteworthy first of all that the geometric criterion of CdTiO<sub>3</sub> ( $t = 0.88$ ) is much less than unity and about the same as that of calcium titanate, where the buckling phase transition occurs at temperatures of the order of 1,000°C. Thus, at more or less high temperatures a buckling phase transition may take place in cadmium titanate, similar to the phase transition that occurs in CaTiO<sub>3</sub>. Secondly, the character of the temperature dependence of  $\epsilon$  below room temperature (Figure 19.6) is more typical of the phase transitions from the paraelectric phase to the ferroelectric phase than of the transition from one ferroelectric phase to another. Third, since the measurement technique was not described [163] and interpretation of the results of dielectric measurements at temperatures of 900-1,000°C requires great care, and since Poplavko's results do not agree with other data [163], the validity of the conclusions [163] is doubtful. Therefore the viewpoint which regards rhombic distortion of the CdTiO<sub>3</sub> nucleus at room temperature as the result of a high-temperature buckling transition, caused by the nonconformity of the relatively small cadmium ion with the geometric requirements of the perfect perovskite type lattice, is preferable at this time.

#### 4. Sodium-Bismuth and Potassium-Bismuth Titanates

The ferroelectric properties of NaBi-titanate ( $\text{Na}_{0.5}\text{Bi}_{0.5}\text{TiO}_3$ ) and KBi-titanate ( $\text{K}_{0.5}\text{Bi}_{0.5}\text{TiO}_3$ ) were discovered by Smolenskiy, et al [155].

Preliminary x-ray diffraction analysis [155] indicated that  $\text{Na}_{0.5}\text{Bi}_{0.5}\text{TiO}_3$  crystallizes into a perovskite type structure, and at 20°C the lattice parameters, calculated in the assumption of a cubic lattice, were found to be  $a = 3.88 \text{ \AA}$ . Data concerning the phase transitions in sodium-bismuth titanate were obtained from the results of dielectric and dilatometric analyses (Figure 19.7). According to the temperatures of the peak and discontinuity on the curve  $\epsilon(T)$  and jumps of the linear expansion coefficient of polycrystalline specimens, it was found that the Curie temperature is  $\sim 320^\circ\text{C}$ , and a low-temperature phase transition occurs in the vicinity of  $200^\circ\text{C}$ .

The x-ray diffraction patterns of NaBi-titanate lack superstructure lines [164], indicating the unordered distribution of Na and Bi ions in the nodes with the coordinate number 12, which concurs with experimental results [155]. Slight separation of some of the lines was noted. Calculations showed that  $\text{Na}_{0.5}\text{Bi}_{0.5}\text{TiO}_3$  has a rhombohedrally distorted lattice at room temperature with the parameters  $a = 3.891 \pm 0.02 \text{ \AA}$ ,  $\alpha_{\text{rh}} = 89^\circ 36' \pm 3'$  and  $V = 58.7 \pm 0.1 \text{ \AA}^3$ .

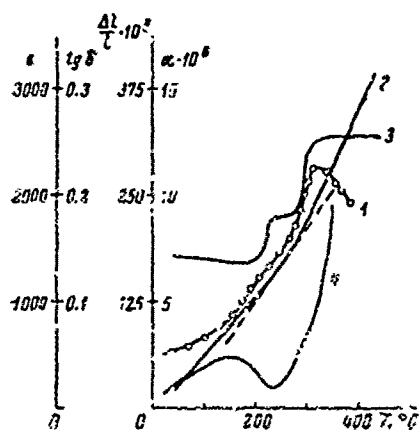


Figure 19.7. Temperature dependence of  $\epsilon$ ,  $\tan \delta$ , relative change of length and thermal expansion coefficient of polycrystalline  $\text{Na}_{0.5}\text{Bi}_{0.5}\text{TiO}_3$  (according to Smolenskiy, et al [155]): 1 --  $\epsilon$  at 500 kHz; 2 --  $\Delta L/L$ ; 3 --  $\alpha$ ; 4 --  $\tan \delta$  at 1 kHz.

A well formed and nearly rectangular hysteresis loop is seen during analysis of polycrystalline specimens of NaBi titanate in strong electric fields [155]. At  $116^\circ\text{C}$   $P_s = 8.0 \cdot 10^{-6} \text{ C/cm}^2$ ,  $E_c = 14 \text{ kV/cm}$ .

It is pointed out [155] that the use of the ion radii presented in [121] yields a structural factor  $t$  equal to 0.91 for NaBi-titanate, and since the antiferroelectric state is more characteristic of compounds with  $t$  much less than one, it could be expected that this compound will be an antiferroelectric. The fact that NaBi-titanate is a ferroelectric is

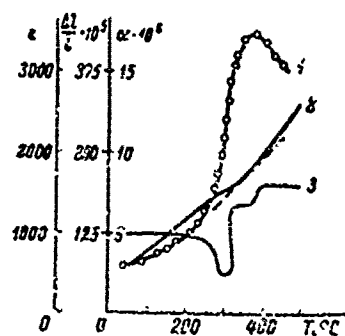


Figure 19.8. Temperature dependence of  $\epsilon$ , relative change of length and thermal expansion coefficient of polycrystalline  $K_{0.5}Bi_{0.5}TiO_3$

(according to Smolenskii, et al [155]): 1 --  $\epsilon$  at 500 kHz; 2 --  $\Delta L/L$ ; 3 --  $\alpha$ .

attributed to the large average dipole moment of A ions, which governs the high electron polarizability of  $Bi^{3+}$ . This is reasonable from the standpoint of the energy of electrostatic dipole-dipole interaction, since an increase in the dipole moment of A ions often facilitates the development of the ferroelectric state. Also indicated is the possibility that the presence of  $Bi^{3+}$  ions in the given compound, by increasing the degree of homeopolarity of the chemical bonds, increases the electron polarizability of oxygen ions. This also increases the relative stability of the ferroelectric state.

According to the results of preliminary x-ray diffraction analysis [155],  $K_{0.5}Bi_{0.5}TiO_3$  has a perovskite type structure, and the parameters of its nucleus, assuming a cubic lattice, are  $a = 3.94 \text{ \AA}$ . More recent analysis [164] verified that in the case of NaBi-titanate there are no superstructure lines on the x-ray diffraction patterns of  $K_{0.5}Bi_{0.5}TiO_3$  that would indicate ordering of the K and Bi ions. Some lines were separated, but as in the case of NaBi-titanate, expansion was slight, and the rear lines on the x-ray diffraction patterns were blurred. In contrast to NaBi-titanate, KBi-titanate is tetragonally distorted at room temperature and has the parameters:  $a = 3.913 \pm 0.003 \text{ \AA}$ ,  $c = 3.993 \pm 0.003 \text{ \AA}$ ,  $c/a = 1.02$  and the volume of the nucleus  $V = 61.1 \pm 0.15 \text{ \AA}^3$  [120].

The phase transition temperatures of KBi-titanate were first determined from dielectric and dilatometric analyses (Figure 19.8). The Curie temperature -- at  $\sim 380^\circ\text{C}$  and the low-temperature phase transition at  $\sim 300^\circ\text{C}$  [155]. As a result of high-temperature x-ray diffraction analysis [164] it was found that up to about  $270^\circ\text{C}$  the symmetry of  $K_{0.5}Bi_{0.5}TiO_3$  remains tetragonal, but near  $270^\circ\text{C}$  a phase transition occurs. The symmetry of the phase existing above this temperature could not be determined due to the smallness of the distortions and diffusion of the lines. At  $410^\circ\text{C}$  a transition occurs to the paraelectric cubic phase. The considerable divergence in the phase transition temperatures of [155] and [164] requires further investigation to refine the dielectric data and the structural changes of potassium-bismuth titanate during heating.

The high Curie temperature of  $K_{0.5}Bi_{0.5}TiO_3$  (like that of  $Na_{0.5}Bi_{0.5}TiO_3$ ) can be explained [155] by the fact that the  $Bi^{3+}$  ions have

the same electronic configuration as  $Pb^{2+}$  and apparently govern in the same manner the high electron and ion polarizabilities of the lattice. The level peaks on the curves  $\epsilon(T)$  of both KBi- and NaBi-titanates indicate ferroelectric phase transitions of blurred character in these compounds.

## 2. Potassium Niobate and Potassium Tantalate

The ferroelectric properties of potassium niobate  $KNbO_3$  and potassium tantalate  $KTaO_3$  were discovered by Matthias [166].

Potassium niobate, possessing a perovskite type cubic structure above  $435^\circ C$ , transitions below this temperature into the ferroelectric state and becomes tetragonal. With further cooling, transitions occur into the rhombic, and then into the rhombohedral phases [167-171]. According to Wood [168],  $KNbO_3$  has a rhombic nucleus at  $25^\circ C$ , containing two units with the parameters:  $a_0 = 5.702$ ,  $b_0 = 5.739$ ,  $c_0 = 3.984 \text{ \AA}$ . The lattice parameters at room temperature [169, 170] are somewhat lower than those determined by Wood:  $a_0 = 5.6946$ ,  $b_0 = 5.7203$ ,  $c_0 = 3.9714 \text{ \AA}$  [169] and  $a_0 = 5.695$ ,  $b_0 = 5.721$ ,  $c_0 = 3.973 \text{ \AA}$  [170].

When the long diagonal of the rhombic phase is taken as the z axis [172], the lattice parameters at room temperature are  $a = 5.697$ ,  $b = 3.971$ ,  $c = 5.720 \text{ \AA}$ , and the spatial group will be  $Bmm2$ . When the origin of the coordinate center is placed at the center of the niobium atom the coordi-

nates of the atom will be: Nb:  $(0, 0, 0)$ , K:  $(0, \frac{1}{2}, \frac{1}{2} + z_K)$ ,  $O_I: (0, \frac{1}{2}, z_{O_I})$ ,  $O_{II}: (\frac{1}{4} + x_{O_{II}}, 0, \frac{1}{4} + z_{O_{II}})$ . The value given in [172] is  $z_K = 0.017 \pm 0.001$ ,  $z_{O_I} = 0.021 \pm 0.002$ ,  $z_{O_{II}} = 0.035 \pm 0.002$ ,  $x_{O_{II}} = 0.004 \pm 0.002$ . Hence it follows that the oxygen octahedra remain nearly regular. Inside the octahedron Nb is displaced  $0.030c_0$  (i.e.,  $0.17 \text{ \AA}$ ) from the center of mass of the six oxygen atoms making up the octahedron, toward one of the edges of the octahedron. The analogous displacement of the Ti ion of barium titanate in the rhombic phase is  $0.022c_0$  ( $0.125 \text{ \AA}$ ).

The phase transition temperatures during heating and cooling according to various data are presented in Table 26.

For the lower transition temperature hysteresis was observed in certain cases at  $45^\circ C$  [170]. Data on the temperature hysteresis of phase transition: in  $KNbO_3$  [168, 170, 173] are convincing evidence of the presence here of first order phase transitions.

The temperature dependence of the lattice constant of  $KNbO_3$  in the tetragonal and rhombic phases was analyzed in [171]. The temperature

Table 26. Phase Transition Temperatures in Potassium Niobate (in °C)

1) Кубическая фаза - тетрагональная фаза		2) Тетрагональная фаза - ромбическая фаза		3) Ромбическая фаза - ромбоэдрическая фаза		6) Источник
4) Нагрев	5) Охлаждение	4) Нагрев	5) Охлаждение	4) Нагрев	5) Охлаждение	
435 ± 5	420 ± 5	225 ± 5	221 ± 5	—	—	[104]
430	410	221	211	-15	-55	[170]
131	425	222	207	-27	-52	[175]

- KEY: 1. Transition between cubic and tetragonal phases;  
 2. Transition between tetragonal and rhombic phases;  
 3. Transition between rhombic and rhomboedrical phases;  
 4. Heating  
 5. Cooling  
 6. Source

dependence of the parameters in the rhombohedral phase has not been investigated, but it is known that at  $-140^{\circ}\text{C}$ ,  $a = 4.016 \pm 0.02 \text{ \AA}$  and  $\sigma = 89^{\circ}50' \pm 1'$  [170].

Cotts and Knight [173], analyzing the NMR and NQR of  $\text{Nb}^{93}$  in monocrystalline  $\text{KNbO}_3$ , concluded that the phase transition from the rhombohedral phase to rhombic occurs over a considerable temperature interval ( $12\text{-}20^{\circ}\text{C}$ ). Structural change occurs much more rapidly in both high-temperature transitions. Since the intensity of the lines gradually changes during phase transitions, and the frequencies of the two phases coincide, it is obvious that transition occurs at different temperatures in different parts of the crystal. This may be caused by the difference in the concentration of defects in the lattice and the presence of internal stresses.

Shirane and his coworkers [169, 171], measuring the latent heat of transitions  $\Delta E$  in polycrystalline  $\text{KNbO}_3$  and calculating the corresponding entropy changes  $\Delta S$ , found the following data: for transition from cubic to tetragonal phase  $\Delta E = 190 \pm 15 \text{ cal/mole}$ ,  $\Delta S = 0.28 \text{ cal/mole}\cdot\text{deg}$ ; for transition from tetragonal to rhombic  $\Delta E = 85 \pm 10 \text{ cal/mole}$ ,  $\Delta S = 0.17 \text{ cal/mole}\cdot\text{deg}$ ; for transition from rhombic to rhombohedral  $\Delta E = 32.5 \text{ cal/mole}$ ,  $\Delta S = 0.12 \text{ cal/mole}\cdot\text{deg}$ . The latent heat of transition of polycrystalline  $\text{KNbO}_3$  from the ferroelectric state to the paraelectric state [174, 175] is  $134 \pm 5 \text{ cal/mole}$ , whereas more recent measurements [176] gave even smaller values: for ceramics  $110 \pm 10 \text{ cal/mole}$ ; for a small monocrystal  $115 \pm 15 \text{ cal/mole}$ .

The permittivity of  $\text{KNbO}_3$  peaks during all three phase transitions [170]. Its temperature dependence above the Curie point is satisfactorily

described by the Curie-Weiss law with  $C = 2.68 \cdot 10^5 \text{ }^\circ\text{C}$  and  $\theta = 350 \text{ }^\circ\text{C}$  [174, 175]. Spontaneous polarization of  $\sim 26 \text{ } \mu\text{C}/\text{cm}^2$  was found [174, 175] from the dielectric hysteresis loops obtained for monocrystals in the tetragonal state near the Curie point. Triebwasser [175] calculated the coefficients in the expression for free energy:  $F = F_0(T) + A(T - \theta)P^2 + BP^4 + DP^6$ , where  $F_0(T)$  is the free energy for zero polarization.  $A = 2.60 \cdot 10^{-5} \text{ } 1/^\circ\text{C}$ ,  $B = 5.0 \cdot 10^{-13} \text{ (erg/cm}^3\text{)}^{-1}$ ,  $D = 4.1 \cdot 10^{-23} \text{ (erg/cm}^3\text{)}^{-1}$ ,  $\theta = 360.4 \pm 5.9 \text{ }^\circ\text{C}$ . The temperature dependence of  $P_s$ , calculated with the same constants, shows satisfactory agreement with the experimental data. The electro-mechanical properties of polycrystalline  $\text{KNbO}_3$  were analyzed [177]. The radial coefficient of electromechanical coupling is 0.28-0.30. The frequency constant passes through sharp peaks at the points of low-temperature phase transitions, marked at 220 and  $-12 \text{ }^\circ\text{C}$ .

The results of NMR and IQR analyses of  $\text{Nb}^{93}$  in potassium niobate [173] indicate a considerable degree of covalence of the bonds. Also noteworthy is Hewitt's work [178], in which several characteristics pertaining to the nuclear quadrupole resonance of  $\text{Nb}^{93}$  in  $\text{KNbO}_3$  are determined and calculated. The optical spectra of  $\text{KNbO}_3$  were analyzed in [63, 179, 180]. The method of growing  $\text{KNbO}_3$  monocrystals is discussed in [181, 182], and the method of producing pure potassium niobate in [183].

The most interesting feature of potassium niobate is that it is the only ferroelectric in which there is the same alternation of phases as in barium titanate: cubic, tetragonal, rhombic and rhombohedral phases. Moreover, if the ratios of the transition temperature  $T_t$  to the Curie temperature  $T_c$  for  $\text{BaTiO}_3$  are 1, 0.69 and 0.49, then these ratios for  $\text{KNbO}_3$  are quite close to the values: 1, 0.71 and 0.38 [170]. The latent heats of transitions of  $\text{KNbO}_3$  are greater than those of barium titanate. This is explained by the great distortion of the potassium niobate lattice compared to that of  $\text{BaTiO}_3$ . Changes in entropy at the Curie point of these two compounds are approximately proportional to the values  $(c/a - 1)$  in the tetragonal phase.

At room temperature potassium tantalate  $\text{KTaO}_3$ , in contrast to potassium niobate, has a cubic lattice with  $a = 3.9885 \text{ } \text{Å}$  [169]. The Curie temperature of potassium tantalate [184], determined according to the  $\epsilon$  peak and the appearance of dielectric hysteresis loops, is  $13.2 \text{ }^\circ\text{K}$ . According to this work  $\epsilon$  of  $\text{KTaO}_3$  obeys the Curie-Weiss law in the  $52\text{-}85 \text{ }^\circ\text{K}$  temperature range with  $C = (6.1\text{-}8.3) \cdot 10^4 \text{ }^\circ\text{K}$  and  $\theta = 14\text{-}14.6 \text{ }^\circ\text{K}$ . Below  $52 \text{ }^\circ\text{K}$   $\epsilon$  is lower than predicted by the Curie-Weiss law, and below  $13.2 \text{ }^\circ\text{K}$  [184],  $\epsilon$  decreases almost linearly with cooling. Below  $13 \text{ }^\circ\text{K}$  dielectric hysteresis loops appear, but at  $5 \text{ kV/cm}$  they are again far from saturation. The Curie-Weiss

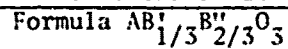
law is valid [26] in the 80 to 303°K temperature range, where  $\epsilon_0 = 39$ ,  $\theta = 2.8^\circ\text{K}$ ,  $C = 5.99 \cdot 10^4 \text{K}$ .

According to the data in [185], in which the nonlinear properties of monocrystalline  $\text{KTaO}_3$  were analyzed near the Curie point  $\theta = 1 \pm 0.5^\circ\text{K}$ .

Above the Curie temperature, as should be expected for a crystal with a center of symmetry,  $\text{KTaO}_3$  has no linear electrooptic effect, but there is a large quadratic electrooptic effect. At the same time the generation of the second and third harmonics in the microwave range at 4.2° and linear and quadratic dependences of permittivity on electric field strength were noted. The generation of the second harmonic and linear dependence of permittivity on the field, however, are possible only if the crystal does not have a center of symmetry. Another evidence for the acentrosymmetric character of the crystal at this temperature is the discovery of a measurable piezoelectric effect. It should be pointed out that the extrapolated Curie temperature [185] does not agree with that determined in [184], and the temperature of the ferroelectric phase transition was not determined at all. The possibility is not excluded that the discrepancy between the results of [184] and [185] is related to inadequate purity of the first monocrystals analyzed in [184], which may have contained some niobium impurity and could have had a somewhat higher Curie temperature. Then, however, it becomes uncertain how to explain the data [185] about the absence of a center of symmetry in  $\text{KTaO}_3$  at 4.2°K. In any case the situation with  $\text{KTaO}_3$  is quite reminiscent of  $\text{SrTiO}_3$ , in which the existence of a ferroelectric phase transition is still at issue.

The optical spectra and certain other optical properties were analyzed in [58, 179, 180, 186-192], NMR, EPR in [193-195], semiconductor properties of  $\text{KTaO}_3$  in [196-199].

#### 6. Ferroelectrics with the Perovskite Type Structure and General



As we have already stated, ferroelectrics with the perovskite type structure and formula of the type  $AB_{1/3}^I B_{2/3}^{II} O_3$  ( $\text{PbMg}_{1/3}^{2+} \text{Nb}_{2/3}^{5+} O_3$  and  $\text{PbNi}_{1/3}^{2+} \text{Nb}_{2/3}^{5+} O_3$ ) were discovered by Smolenskiy and Agranovskaya [200]. The discovery of these ferroelectrics stimulated work on the synthesis of other compounds of this type, in which Nb was substituted by Ta, and Mg by Ni, Co and Zn. As a result Bokov and Myl'nikova discovered several new ferroelectrics:  $\text{PbMg}_{1/3}^{2+} \text{Ta}_{2/3}^{5+} O_3$ ,  $\text{PbNi}_{1/3}^{2+} \text{Ta}_{2/3}^{5+} O_3$ ,  $\text{PbCo}_{1/3}^{2+} \text{Nb}_{2/3}^{5+} O_3$ ,  $\text{PbCo}_{1/3}^{2+} \text{Ta}_{2/3}^{5+} O_3$  and  $\text{PbZn}_{1/3}^{2+} \text{Nb}_{2/3}^{5+} O_3$  [201, 202]. Later Smolenskiy, Agranovskaya and Isupov discovered the first ferroelectric tungstate with the perovskite type structure:  $\text{PbFe}_{2/3}^{3+} \text{W}_{1/3}^{6+} O_3$  [203].

The properties of  $\text{PbMg}_{1/3}\text{Nb}_{2/3}\text{O}_3$  have already been discussed in Chapter 16. We will therefore examine only those properties not described in that chapter. At room temperature  $\text{PbMg}_{1/3}\text{Nb}_{2/3}\text{O}_3$  has a cubic lattice with  $a = 4.04 \text{ \AA}$  [204]. The absence of superstructure lines on x-ray diffraction patterns indicates the absence of ordering of ions Mg and Nb [205, 206]. The temperature of the ferroelectric phase transition (average Curie temperature), estimated from dilatometric and piezoelectric measurements, is  $-10$  to  $-20^\circ\text{C}$  [207]. According to Ismailzade's data  $\text{PbMg}_{1/3}\text{Nb}_{2/3}\text{O}_3$  at  $-15^\circ\text{C}$  has a tetragonal lattice with  $a = 4.020$ ,  $c = 4.044 \text{ \AA}$  [204]. However, the optical analyses of Bokov and Myl'nikova [208] showed that the symmetry of the ferroelectric phase of this compound is more likely rhombic. Spontaneous polarization, determined on a monocrystal, is  $24 \cdot 10^{-6} \text{ C/cm}^2$  at  $-170^\circ\text{C}$  [208].

The electrooptic properties of  $\text{PbMg}_{1/3}\text{Nb}_{2/3}\text{O}_3$  were analyzed by Berezhnoy [209]. The study was made at  $\lambda = 5,500 \text{ \AA}$  with a field on [100] and light beam on [010] in the temperature range from  $20$  to  $100^\circ\text{C}$ . It was found that the dependence of birefringence on the field is essentially quadratic in the range of fields employed (up to  $10$ - $20 \text{ kV/cm}$ ). Bonner, et al [210] determined the refraction coefficient  $n = 2.56$  at  $6,328 \text{ \AA}$  and electrooptic coefficients  $(M_{11} - M_{12}) = +0.015$ ,  $M_{44} = +0.008 \text{ m}^4/\text{C}^2$ .

Smolenskiy, et al studied the electrooptic effect of  $\text{PbMg}_{1/3}\text{Nb}_{2/3}\text{O}_3$  in the  $-30$  to  $+100^\circ\text{C}$  temperature range. They showed that in a weak field the dependence of  $\Delta n$  on  $E$  is quadratic in almost the entire temperature range, whereas with large  $E$  it becomes practically linear, although as  $E$  increases, the contribution of higher order effects usually increases. As the temperature rises the range of fields in which the dependence is quadratic expands and above  $80^\circ\text{C}$  in fields up to  $18 \text{ kV/cm}$  the effect is only quadratic. At room temperature and  $\lambda = 6,240 \text{ \AA}$  the quadratic electrooptic coefficients describing the dependence on the square of the field were:  $(R_{11} - R_{12}) = 13.0 \cdot 10^{-8} \text{ CGSE}$ ,  $R_{44} = 2.3 \cdot 10^{-8} \text{ CGSE}$ , and the coefficients describing the dependence on the square of polarization were:  $(M_{11} - M_{12}) = 18.3 \cdot 10^{-14} \text{ CGSE}$ ,  $M_{44} = 2.8 \cdot 10^{-14} \text{ CGSE}$ . An increase was observed in  $n_0^3(R_{11} - R_{12})$  with decreasing wavelength, related to the approach of the natural absorption band of the crystal to the edge.

The behavior of  $\text{PbMg}_{1/3}\text{Nb}_{2/3}\text{O}_3$  is discussed from the viewpoint of the concepts of blurred ferroelectric phase transitions (see Chapter 16). In the region of the blurred phase transition above the mean Curie temperature the quadratic effect in weak field is attributed to the effect in the paraelectric phase and orientation of polar regions. The sudden increase in  $R_{11} - R_{12}$  as the temperature drops is attributed to the increased contribution of orientation processes. The change to a linear dependence is presumably the result of the transition of apolar regions to

the ferroelectric state under the influence of a field, leading to the combining of polar regions. At higher temperatures, naturally, the change to a linear function takes place in stronger fields.

The compound  $\text{PbNi}_{1/3}\text{Nb}_{2/3}\text{O}_3$  at room temperature has a cubic lattice with  $a = 4.025 \text{ \AA}$  [204]. The Curie temperature lies in the region  $-110$  to  $-140^\circ\text{C}$ . The properties of this compound were also described in Chapter 16.

The compound  $\text{PbCo}_{1/3}\text{Nb}_{2/3}\text{O}_3$  at  $20^\circ\text{C}$  is cubic with  $a = 4.04 \text{ \AA}$  [201]. The permittivity of  $\text{PbCo}_{1/3}\text{Nb}_{2/3}\text{O}_3$  monocrystal at 1 kHz peaks at  $-70^\circ\text{C}$  (Figure 19.9). Since the phase transition of this compound is blurred and its properties resemble those of  $\text{PbMg}_{1/3}\text{Nb}_{2/3}\text{O}_3$  and  $\text{PbNi}_{1/3}\text{Nb}_{2/3}\text{O}_3$ , this temperature also gives only an approximate representation of some average Curie temperature. There is no saturation of hysteresis loops although there is a clearly discernible discontinuity on the principal polarization curve.

The compound  $\text{PbZn}_{1/3}\text{Nb}_{2/3}\text{O}_3$ , assuming a cubic lattice, has an elemental nucleus with  $a = 4.64 \text{ \AA}$  [201]. However, since the peak  $\epsilon$  at 1 kHz occurs in this compound at  $140^\circ\text{C}$  (Figure 19.10), and well saturated hysteresis loops are found below this temperature, it is clear that the crystal should not be cubic at room temperature.

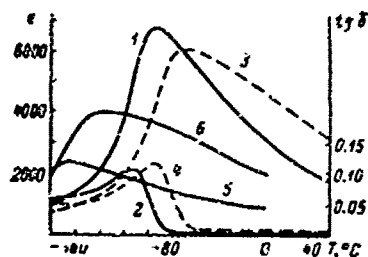


Figure 19.9. Temperature dependences of  $\epsilon$  and  $\tan \delta$  of the monocrystals of several perovskites at 1 kHz (for  $\text{PbNi}_{1/3}\text{Ta}_{2/3}\text{O}_3$  at 450 kHz) (according to Bokov and Myl'nikova [201]).

1 -  $\epsilon$ ; 2 -  $\tan \delta$   $\text{PbMg}_{1/3}\text{Ta}_{2/3}\text{O}_3$ ; 3 -  $\epsilon$ ; 4 -  $\tan \delta$   $\text{PbCo}_{1/3}\text{Nb}_{2/3}\text{O}_3$ ; 5 -  $\epsilon$   $\text{PbNi}_{1/3}\text{Nb}_{2/3}\text{O}_3$ ; 6 -  $\tan \delta$   $\text{PbNi}_{1/3}\text{Nb}_{2/3}\text{O}_3$

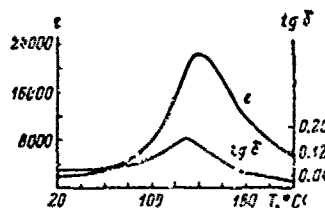


Figure 19.10. Temperature dependence of  $\epsilon$  and  $\tan \delta$  of  $\text{PbZn}_{1/3}\text{Nb}_{2/3}\text{O}_3$  monocrystal at 1 kHz (according to Bokov and Myl'nikova [201]).

The compound  $\text{PbMg}_{1/3}\text{Ta}_{2/3}\text{O}_3$  is cubic at  $20^\circ\text{C}$  with  $a = 4.02 \text{ \AA}$  [201]. At 1 kHz maximum  $\epsilon$  occurs near  $-98^\circ\text{C}$  (Figure 19.9). Below this temperature dielectric hysteresis loops are observed. The phase transition is blurred [201].

$\text{PbNi}_{1/3}\text{Ta}_{2/3}\text{O}_3$  also has a cubic lattice at  $20^\circ\text{C}$  with  $a = 4.01 \text{ \AA}$  [201]. Maximum  $\epsilon$  at 1 kHz lies between  $-160$  and  $180^\circ\text{C}$  (Figure 19.9). The dielectric hysteresis loops at  $-196^\circ\text{C}$  are far from saturated, even in fields with a strength of  $150 \text{ kV/cm}$ . The ferroelectric phase transition is blurred.

$\text{PbCo}_{1/3}\text{Ta}_{2/3}\text{O}_3$  is also cubic at room temperature ( $a = 4.01 \text{ \AA}$  [201]). At 1 kHz maximum  $\epsilon$  lies near  $-140^\circ\text{C}$  (Figure 19.9). The phase transition is blurred. The dielectric hysteresis loops are far from saturated, but are nevertheless quite distinct.

The ferroelectric properties of the compound  $\text{PbCd}_{1/3}\text{Nb}_{2/3}\text{O}_3$  are described in [212, 213]. Its permittivity passes through a level maximum in the region  $250$ - $300^\circ\text{C}$ , although the nucleus at room temperature is, according to the authors, cubic with  $a = 4.123 \text{ \AA}$ . The position of maximum  $\epsilon$  depends on frequency. It may be assumed that this compound is a ferroelectric with a strongly blurred transition.

At room temperature  $\text{PbFe}_{2/3}\text{W}_{1/3}\text{O}_3$  has a cubic lattice with  $a = 3.97 \text{ \AA}$ , and no superstructure lines indicating the ordering of Fe and W ions in the octahedral nodes are seen on its x-ray diffraction patterns [203, 206]. The permittivity of  $\text{PbFe}_{2/3}\text{W}_{1/3}\text{O}_3$  passes through a peak at  $-90$  to  $-70^\circ\text{C}$ ; at  $-196^\circ\text{C}$  there are dielectric hysteresis loops [203]. The phase transition is apparently quite blurred. The theory is advanced [203] that  $\text{PbFe}_{2/3}\text{W}_{1/3}\text{O}_3$ , in which 66.7% of the ions in the octahedral positions are  $\text{Fe}^{3+}$  ions, is simultaneously a ferroelectric and an antiferroelectric. This assumption was confirmed by the results of [202]. Its properties are described in greater detail in Chapter 18.

The synthesis of the perovskite  $\text{PbSc}_{2/3}\text{W}_{1/3}\text{O}_3$ , which at  $20^\circ\text{C}$  has a cubic lattice with  $a = 4.067 \text{ \AA}$ , is described in [212, 213]. According to [212]  $\epsilon$  of this compound passes through a maximum at  $-12^\circ\text{C}$ , where it reaches 2,500. On the basis of the low geometric criterion ( $t = 0.92$ ) this compound is an antiferroelectric. It is not indicated, however, whether the compound was checked for the presence of a dielectric hysteresis loop.

The perovskite  $\text{PbMn}_{2/3}\text{W}_{1/3}\text{O}_3$ , with a  $\epsilon$  peak temperature equal to  $200^\circ\text{C}$ , is also described in [212-215]. At  $20^\circ\text{C}$  its lattice is monoclinically distorted:  $a = c = 4.098 \text{ \AA}$ ,  $b = 4.014 \text{ \AA}$ ,  $\beta = 90^\circ 23'$ . On the basis that  $t = 0.96$  the compound is an antiferroelectric. It is not indicated [212-215] whether the valence of manganese was controlled. Meanwhile this is essential. If manganese is reduced to divalent, then the formation of  $\text{PbMn}_{0.5}^{2+}\text{W}_{0.5}^{6+}\text{O}_3$  cannot be ruled out.

The ferroelectric properties of the perovskite class compounds  $\text{BaBi}_{2/3}^{3+}\text{W}_{1/3}^{6+}\text{O}_3$  and  $\text{BaBi}_{2/3}^{3+}\text{Mo}_{1/3}^{6+}\text{O}_3$ , the former of which has a rhombic lattice

with  $a = 4.348 \text{ \AA}$ ,  $\gamma = 90^\circ 20'$ , are reported in [216, 217]. On the basis of these x-ray diffraction data the former compound is classified as a ferroelectric (the Curie point is stated as  $450^\circ\text{C}$ ). The latter is monoclinic with  $a = c = 4.360 \text{ \AA}$ ,  $b = 4.321 \text{ \AA}$ ,  $\beta = 90^\circ 30'$  and is classified as an antiferroelectric ( $T_c = 500^\circ\text{C}$ ). These conclusions are doubtful. The presence of pseudocubic distortion at room temperature is not in itself proof of the ferro- or antiferroelectric state. From the dependence  $\epsilon(T)$  presented in [216] it follows only that  $\epsilon$  increases as the temperature increases. This, however, may be related also to increased electrical conductivity with heating. Moreover, the  $\epsilon$  of  $\text{BaBi}_{2/3}\text{W}_{1/3}\text{O}_3$  at  $20^\circ\text{C}$  is very low (about 25) which is completely uncharacteristic of ferroelectrics of the perovskite class. It is also asserted [217] that the perovskites  $\text{BaCu}_{1/3}\text{Ta}_{2/3}\text{O}_3$  ( $T_c = 470^\circ\text{C}$ ),  $\text{BaCu}_{1/3}\text{Nb}_{2/3}\text{O}_3$  ( $T_c = 390^\circ\text{C}$ ),  $\text{SrCu}_{1/3}\text{Nb}_{2/3}\text{O}_3$  ( $T_c = 390^\circ\text{C}$ ),  $\text{SrCu}_{1/3}\text{Ta}_{2/3}\text{O}_3$  ( $T_c = 1,250^\circ\text{C}?$ ) also possess ferroelectric properties. At  $20^\circ\text{C}$  they all have tetragonal distortion with  $c/a$  from 1.031 to 1.049. At  $380^\circ\text{C}$   $\text{BaCu}_{1/3}\text{Nb}_{2/3}\text{O}_3$  displays in x-ray diffraction analysis a transition to the cubic phase and a maximum  $\epsilon$  is noted. The ferroelectric properties of these compounds, in our opinion, also need to be checked.

Examination of the experimental data on ferroelectrics of the type  $\text{PbB}_{1/3}^{2+}\text{B}_{2/3}^{5+}\text{O}_3$  reveals that all these compounds lack long-range ordering in the distribution of  $\text{B}^{2+}$  and  $\text{B}^{5+}$  ions in the octahedral positions. The phase transitions are more or less strongly blurred, dielectric polarization is of a clearly relaxation character. In this connection all these compounds may be excellent objects for investigation of the kinetics of blurred ferroelectric phase transitions and the effect of the blurring of transitions on dielectric polarization.

The Curie temperatures of these ferroelectrics are compared in Table 27 [158] (the Curie temperature is assumed equal to the temperature of the maximum at 1 kHz).

Table 27. Transition Temperatures in Niobates and Tantalates with the Formula  $\text{PbB}_{1/3}^{2+}\text{B}_{2/3}^{5+}\text{O}_3$

Compound	$T_c, ^\circ\text{C}$	Compound	$T_c, ^\circ\text{C}$	Diff. in Curie temps. of niobate and tantalate
$\text{PbCa}_{1/3}\text{Nb}_{2/3}\text{O}_3$	250-300	—	—	—
$\text{PbZn}_{1/3}\text{Nb}_{2/3}\text{O}_3$	140	—	—	—
$\text{PbMg}_{1/3}\text{Nb}_{2/3}\text{O}_3$	-17	$\text{PbNb}_{1/3}\text{Ta}_{2/3}\text{O}_3$	-98	86
$\text{PbCa}_{1/3}\text{Nb}_{2/3}\text{O}_3$	-70	$\text{PbCo}_{1/3}\text{Ta}_{2/3}\text{O}_3$	-140	70
$\text{PbNi}_{1/3}\text{Nb}_{2/3}\text{O}_3$	-120	$\text{PbNi}_{1/3}\text{Ta}_{2/3}\text{O}_3$	-180	60

$\text{PbCd}_{1/3}\text{Nb}_{2/3}\text{O}_3$  and  $\text{PbZn}_{1/3}\text{Nb}_{2/3}\text{O}_3$  have a maximum Curie temperature, apparently related to the high electron polarizability of  $\text{Cd}^{2+}$  and  $\text{Zn}^{2+}$ . As always, niobates have a higher Curie temperature than the corresponding tantalates.

### 7. Ferroelectric Compounds of the Type $\text{AB}'_{0.5}\text{B}''_{0.5}\text{O}_3$

The first ferroelectrics of the type  $\text{AB}'_{0.5}\text{B}''_{0.5}\text{O}_3$  ( $\text{PbSc}_{0.5}^{3+}\text{Nb}_{0.5}^{5+}\text{O}_3$  and  $\text{PbSc}_{0.5}^{3+}\text{Ta}_{0.5}^{5+}\text{O}_3$ ) were discovered by Smolenskiy, Isupov and Agranovskaya [218]. During the course of further research on complex perovskites of this class the investigators discovered the ferroelectric compounds  $\text{PbFe}_{0.5}^{3+}\text{Nb}_{0.5}^{5+}\text{O}_3$  and  $\text{PbFe}_{0.5}^{3+}\text{Ta}_{0.5}^{5+}\text{O}_3$  [219-221] and a considerable number of antiferroelectrics (see Chapter 17). Several works have been done on new compounds of this type under the supervision of Yu. N. Venetsev and Ye. G. Fesenko.

According to Ismailzade's data [222],  $\text{PbSc}_{0.5}\text{Nb}_{0.5}\text{O}_3$  has a tetragonally distorted lattice at 30-32°C with  $a = 4.083 \pm 0.001 \text{ \AA}$ ,  $c = 4.074 \pm 0.001 \text{ \AA}$ ,  $c/a = 1.002$ . We see in Figure 19.11 that the permittivity of polycrystalline specimens of  $\text{PbSc}_{0.5}\text{Nb}_{0.5}\text{O}_3$  pass through a peak near 100°C, whereas  $\tan \delta$  at the same temperature has a characteristic drop [218, 220]. Spontaneous polarization, determined on polycrystalline specimens from hysteresis loops, according to [218], is  $3.6 \cdot 10^{-6} \text{ C/cm}^2$  at 18°C, and the coercive field is  $E = 6 \text{ kV/cm}$ . At 25°C [223],  $P_s = 15 \cdot 10^{-6} \text{ C/cm}$ . The large  $P_s$  obtained in [223] is apparently the result of better sintering of the specimens.

According to Agranovskaya's data [206], the lattice of  $\text{PbSc}_{0.5}\text{Ta}_{0.5}\text{O}_3$  at room temperature is cubic with  $a = 4.07 \text{ \AA}$ . According to Ismailzade's data [222],  $a = 4.072 \pm 0.001 \text{ \AA}$  at 30-32°C. The permittivity peaks at 26°C (Figure 19.11) [218, 220]. Below this temperature there are dielectric hysteresis loops [218].

Calculation of the parameters of  $\text{PbFe}_{0.5}\text{Nb}_{0.5}\text{O}_3$  at room temperature in the assumption of a cubic lattice yielded  $a = 4.00 \text{ \AA}$  [206, 224]. More recent analyses [225] showed that this compound is rhombohedral at room temperature with  $a = 4.014 \text{ \AA}$  and  $\alpha = 89.92^\circ$ . It was found from dielectric measurements on the basis of the  $\epsilon$  peak temperature (Figure 19.12) that the temperature of the ferroelectric phase transition is 110-112°C [219, 224]. Measurement of the  $\epsilon$  of  $\text{PbFe}_{0.5}\text{Nb}_{0.5}\text{O}_3$  at frequencies of 450 and 4,500 kHz [224] showed that the temperature at which  $\epsilon$  peaks does not depend on the temperature on which the measurements were made. In this sense  $\text{PbFe}_{0.5}\text{Nb}_{0.5}\text{O}_3$  differs substantially from ferroelectrics of the  $\text{PbNb}_{1/3}\text{Nb}_{2/3}\text{O}_3$  type. There are distinct dielectric hysteresis loops below the Curie point. At -156°C spontaneous polarization is  $5.3 \cdot 10^{-6} \text{ C/cm}^2$  and

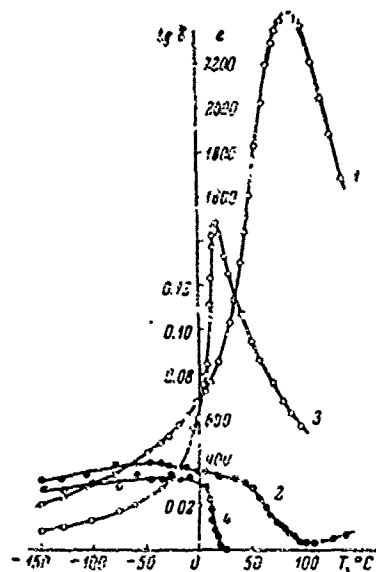


Figure 19.11. Temperature dependence of  $\epsilon$  and  $\tan \delta$  of polycrystalline specimens of  $\text{PbSc}_{0.5}\text{Nb}_{0.5}\text{O}_3$  (1 --  $\epsilon$ ; 2 --  $\tan \delta$ ) and  $\text{PbSc}_{0.5}\text{Ta}_{0.5}\text{O}_3$  (3 --  $\epsilon$ ; 4 --  $\tan \delta$ ) at frequency of 1 kHz in weak fields (according to Smolenskiy, et al [213]).

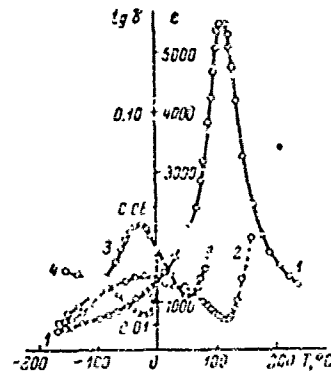


Figure 19.12. Temperature dependence of  $\epsilon$  and  $\tan \delta$  of polycrystalline specimens of  $\text{PbFe}_{0.5}\text{Nb}_{0.5}\text{O}_3$  (1 --  $\epsilon$ ; 2 --  $\tan \delta$ ) and  $\text{PbFe}_{0.5}\text{Ta}_{0.5}\text{O}_3$  (3 --  $\epsilon$ ; 4 --  $\tan \delta$ ) at frequency of 1 kHz in weak fields (according to Smolenskiy, et al [220]).

total polarization is  $6.2 \cdot 10^{-6} \text{ C/cm}^2$ , the coercive field  $F_c = 10 \text{ kV/cm}$  [224]. On the curve  $\Delta L/L(T)$  in the region of the phase transition there is a discontinuity, to which correspond linear expansion coefficient of polycrystalline specimen [224]. This indicates that spontaneous volumetric deformation and, accordingly, volumetric electrostriction are positive.

Investigation of the radial piezoelectric vibrations of specimens of  $\text{PbFe}_{0.5}\text{Nb}_{0.5}\text{O}_3$  polarized by a field of 27 kV/cm for 2.5 hours showed that the resonance and antiresonance frequencies decrease monotonically during heating and approach the Curie temperature, and at the Curie point pass through a sharp minimum. Piezoelectric modulus  $d_{31}$  is  $-1.7 \cdot 10^{-6} \text{ CGSE}$  at room temperature and passes through a minimum near the Curie point [224]. At room temperature the electrical conductivity of polycrystalline  $\text{PbFe}_{0.5}\text{Nb}_{0.5}\text{O}_3$  specimens is of the order of  $10^{-8} \text{ ohm}^{-1} \cdot \text{cm}^{-1}$ . At 212°C transition occurs from one linear segment of the dependence  $\log \rho = f(1/T)$  to another linear segment. The energy of activation in the 20-212°C temperature range is 0.76 eV, and 2.3 eV above 212°C. The sign of thermal emf was positive in the entire 20-350°C temperature range. Below 212°C, apparently, electrical conductivity is impurity, and at higher temperatures natural electrical conductivity prevails [224].

The UHF dispersion in  $\text{PbFe}_{0.5}\text{Nb}_{0.5}\text{O}_3$  was investigated in [226, 227]. It was shown that notable dispersion of  $\epsilon$  in the paraelectric phase occurs in the frequency range : low  $5 \cdot 10^8$  Hz. In the  $5 \cdot 10^8 - 2 \cdot 10^9$  Hz frequency range dispersion of  $\epsilon$  occurs only below the Curie temperature and is of the same character as the UHF dispersion of  $\epsilon$  in barium titanate. The "low-frequency" dispersion is related to a reduction of the influence of electrical conductivity on  $\epsilon$  and  $\tan \delta$  (due to relaxation of the space charge) as the frequency increases. A change in frequency does not cause displacement of the peak on the curve  $\epsilon(T)$ . Magnetic susceptibility of polycrystalline  $\text{PbFe}_{0.5}\text{Nb}_{0.5}\text{O}_3$  increases during cooling, and the dependence  $1/\chi = f(T)$  is characteristic of antiferromagnetics. In [224], however, it was not possible to completely exclude the presence of ferromagnetic impurity in the specimen and the presence of the antiferromagnetic state was convincingly proved only in [214], after the monocystals were grown (see Chapter 18).

At room temperature  $\text{PbFe}_{0.5}\text{Ta}_{0.5}\text{O}_3$  has the cubic lattice with  $a = 4.00 \text{ \AA}$  [206, 224]. The Curie temperature, determined on the basis of dielectric measurement results, is  $-30$  to  $-25^\circ\text{C}$  [220, 224]. At this temperature the  $\epsilon$  of  $\text{PbFe}_{0.5}\text{Ta}_{0.5}\text{O}_3$  peaks (Figure 19.12), and below this temperature dielectric hysteresis loops are found. At  $-136^\circ\text{C}$  spontaneous polarization, determined on polycrystalline specimens, is  $2.4 \cdot 10^{-6} \text{ C/cm}^2$ , total polarization is  $2.9 \cdot 10^{-6} \text{ C/cm}^2$ ,  $E_c = 17 \text{ kV/cm}$  [224]. The curve  $\Delta l/l(T)$  has a discontinuity in the vicinity of the phase transition, and the linear expansion coefficient of the polycrystalline passes through a minimum, which indicates positive volumetric electrostriction [224].

It is noteworthy with regard to examination of the investigated ferroelectrics of the  $\text{PbB}'_{0.5}\text{B}''_{0.5}\text{O}_3$  type, where  $B' = \text{Sc}$  and  $\text{Fe}^{3+}$  and  $B'' = \text{Nb}$  and  $\text{Ta}$ , that even though the x-ray diffraction patterns of these compounds show no superstructure lines, the blurring of phase transitions is relatively slight, and dielectric polarization is not clearly of a relaxation character. This is apparently explained by the presence of short-range order in the distribution of  $B'$  and  $B''$  ions in the octahedral positions of the lattice in the absence of long-range order. Investigation of this distribution is important, both for solving the problem of the properties of ferroelectrics with a blurred phase transition and for solving the problem of synthesizing ferro-ferrimagnetics. Preliminary evaluation of the short-range ordering in  $\text{PbFe}_{0.5}\text{Nb}_{0.5}\text{O}_3$  indicated that the  $\text{NbO}_6$  octahedron, on the average, surrounds approximately 3.9  $\text{FeO}_6$  octahedrons [228].

The synthesis of new ferro- and antiferroelectric perovskite type compounds  $\text{PbCo}_{0.5}^{3+}\text{Nb}_{0.5}\text{O}_3$ ,  $\text{PbMn}_{0.5}^{5+}\text{Nb}_{0.5}\text{O}_3$ ,  $\text{PbMn}_{0.5}^{2+}\text{W}_{0.5}^{5+}\text{O}_3$ ,  $\text{PbMn}_{0.5}^{2+}\text{W}_{0.5}^{6+}\text{O}_3$ ,  $\text{PbMn}_{0.5}^{2+}\text{Ta}_{0.5}^{6+}\text{O}_3$ ,  $\text{PbMn}_{0.5}^{3+}\text{Re}_{0.5}^{5+}\text{O}_3$ ,  $\text{BaBi}_{0.5}\text{Nb}_{0.5}\text{O}_3$ ,  $\text{BaBi}_{0.5}\text{Ta}_{0.5}\text{O}_3$ ,

$\text{BaBi}_{0.5}\text{V}_{0.5}\text{O}_3$ ,  $\text{BaCu}_{0.5}\text{W}_{0.5}\text{O}_3$  and  $\text{SrCu}_{0.5}\text{W}_{0.5}\text{O}_3$  is reported in [215, 215-217].

For  $\text{PbCo}_{0.5}^{3+}\text{Nb}_{0.5}\text{O}_3$  at 11°C there is an  $\epsilon$  peak (where  $\epsilon$  reaches ~600). Due to the presence of the  $\epsilon$  peak, and on the basis of the geometric criterion  $t = 0.93$ , the compound is a ferroelectric.  $\text{PbMn}_{0.5}^{3+}\text{Nb}_{0.5}\text{O}_3$  displays expansion of lines on x-ray diffraction patterns at 20°C. On this basis, in connection with the fact that its  $t = 0.97$ , this compound is an antiferroelectric. The lattices of  $\text{PbMn}_{0.5}^{2+}\text{W}_{0.5}^{6+}\text{O}_3$  and  $\text{PbMn}_{0.5}^{3+}\text{W}_{0.5}^{5+}\text{O}_3$  are monoclinically distorted, and at 150 and 165°C, respectively, there are  $\epsilon$  peaks (where  $\epsilon \approx 160-200$ ). Since both compounds have  $t < 1$ , they are antiferroelectrics. How the authors regulated and controlled the valence of Mn and W ions is not stated in the articles.

X-ray diffraction analysis of  $\text{PbMn}_{0.5}^{2+}\text{Re}_{0.5}^{6+}\text{O}_3$  at 120°C reveals a transition from monoclinic to cubic. By analogy with the compounds  $\text{PbCo}_{0.5}\text{W}_{0.5}\text{O}_3$  and  $\text{PbYb}_{0.5}\text{Nb}_{0.5}\text{O}_3$  the substance is an antiferroelectric.  $\text{PbMn}_{0.5}^{3+}\text{Re}_{0.5}^{5+}\text{O}_3$  is also an antiferroelectric ( $T_c = 95^\circ\text{C}$ ). The reasons for these conclusions are not given, nor are the methods of controlling the valence specified.

The compounds  $\text{BaBi}_{0.5}\text{Nb}_{0.5}\text{O}_3$  and  $\text{BaBi}_{0.5}\text{Ta}_{0.5}\text{O}_3$ , having rhombohedrally distorted lattices at 20°C, are related to ferroelectrics, and the monoclinically distorted compound  $\text{BaBi}_{0.5}\text{V}_{0.5}\text{O}_3$  is related to antiferroelectrics. As proof for  $\text{BaBi}_{0.5}\text{V}_{0.5}\text{O}_3$  the authors point to the reduction of  $\epsilon$  from ~85 to ~25 as the frequency increases from  $10^4$  to  $5 \cdot 10^7$  Hz, although it would be more natural to relate this reduction of  $\epsilon$  to the smaller contribution of the space charge relaxation to polarization.

The compounds  $\text{BaCu}_{0.5}\text{W}_{0.5}\text{O}_3$  and  $\text{SrCu}_{0.5}\text{W}_{0.5}\text{O}_3$  display tetragonal distortion with  $c/a = 1.095$  at 20°C. According to the results of electron micrographic analyses [229], the Cu ion in the  $\text{BaCu}_{0.5}\text{W}_{0.5}\text{O}_3$  lattice is displaced 0.20 Å relative to the barium ion on the z axis head on toward the oxygen ions, and the W ion is displaced 0.10 Å in the direction of displacement of the oxygen ions. In this connection both compounds are classified as ferroelectric.

The production of ferroelectrics of the perovskite type with vacancies in terms of oxygen, with the general formula  $\text{PbB}_{0.5}^{2+}\text{B}_{0.5}^{5+}\text{O}_{2.75}$ , is described in [230]. The synthesized compounds have a Curie temperature much different from the Curie point of compounds of the type  $\text{AB}_{1/3}^{2+}\text{B}_{2/3}^{5+}\text{O}_3$ . For example: in  $\text{PbCo}_{0.5}^{2+}\text{Nb}_{0.5}^{5+}\text{O}_{2.75}$   $T_c = -15^\circ\text{C}$  (in  $\text{PbCo}_{1/3}\text{Nb}_{2/3}\text{O}_3$   $T_c = -76^\circ\text{C}$ ), in

$\text{PbCo}_{0.5}^{2+}\text{Ta}_{0.5}^{5+}\text{O}_{2.75}$   $T_c = -60^\circ\text{C}$  (in  $\text{PbCo}_{1/3}\text{Ta}_{2/3}\text{O}_3$   $T_c = -140^\circ\text{C}$ ), in  
 $\text{PbNi}_{0.5}^{2+}\text{Nb}_{0.5}^{5+}\text{O}_{2.75}$   $T_c = -7.5^\circ\text{C}$  (in  $\text{PbNi}_{1/3}\text{Nb}_{2/3}\text{O}_3$   $T_c = -120^\circ\text{C}$ ). In connec-  
tion with the possibility of producing phases of the type  $\text{PbB}_{1/3}^{2+}\text{B}_{2/3}^{5+}\text{O}_3$   
and  $\text{PbB}_{0.5}^{3+}\text{B}_{0.5}^{5+}\text{O}_3$  during synthesis, the phase that was formed was checked  
in the work. It was shown by x-ray diffraction analysis that the  
synthesized compounds have a superstructure related to the doubling of  
the perovskite lattice parameters, absent in compounds of the type  
 $\text{PbNi}_{1/3}^{2+}\text{Nb}_{2/3}^{5+}\text{O}_3$ . A check of the valence of  $\text{B}^{2+}$  ions was done with the aid  
of magnetic measurements. The results of these measurements showed the  
presence of  $\text{Co}^{2+}$  in the compound  $\text{PbCo}_{0.5}^{2+}\text{Nb}_{0.5}^{5+}\text{O}_{2.75}$ . Quantitative deter-  
mination of the relative concentration of  $\text{Co}^{2+}$  and  $\text{Co}^{3+}$  ions obviously  
would have been desirable here.

Many of the compounds of the type  $\text{AB}'_{0.5}\text{B}''_{0.5}\text{O}_3$  listed in the review,  
to which are ascribed ferro- and antiferroelectric properties, required  
further investigation. In many cases more rigorous checking of the  
composition is required, and in other cases -- more careful analysis of  
the dielectric properties and explanation of the nature of phase transitions.

#### 8. Cesium Chlorogermanate ( $\text{CsGeCl}_3$ )

$\text{CsGeCl}_3$  was first prepared by Karantasis and Capatos [231]. The  
crystals were twinned and displayed birefringence, disappearing above  $155^\circ\text{C}$   
and reappearing on cooling. The crystals displayed piezoelectric and pyro-  
electric properties. Christensen and Rausen [232] reported that the  
substance is a ferroelectric.

Above  $155^\circ\text{C}$   $\text{CsGeCl}_3$  has a cubic structure of the perovskite type [232].  
At  $175^\circ\text{C}$   $a = 5.475 \text{ \AA}$ . Below  $155^\circ\text{C}$  the structure becomes rhombic (with  $a =$   
 $= 5.444 \text{ \AA}$ ,  $\alpha = 89.63^\circ$  at  $25^\circ\text{C}$ ). With rhombohedral distortion, as follows  
from x-ray diffraction data [232], the germanium ion is displaced on the  
tertiary axis. The chlorine ions are also displaced from the ideal  
perovskite positions. The Cs-Cl distance, however, changes little: from  
 $3.85$  to  $3.88 \text{ \AA}$ . The Ge-Cl distance differs considerably: three distances  
equal  $3.13 \text{ \AA}$ , three others  $2.74 \text{ \AA}$  (the Ge-Cl distances in the cubic phase  
are  $2.74 \text{ \AA}$ ).

The permittivity of the polycrystalline substance [232] peaked at  
 $155^\circ\text{C}$ . There are no data in the work concerning the presence of dielectric  
hysteresis loops. This is related, perhaps, to the difficulties involved  
in analyzing the given compound, which is very susceptible to the effects  
of the atmosphere, forcing physical measurements to be made in an atmosphere  
of nitrogen.

$\text{CsGeCl}_3$  is the only halide with the perovskite structure that is, apparently, a ferroelectric.

There are indications in the literature that the plumbohalides of cesium  $\text{CsPbX}_3$ , where  $X = \text{Cl, Br, I}$  [233-236], have ferroelectric properties, of which the compound  $\text{CsPbCl}_3$  has been investigated most thoroughly. At room temperature  $\text{CsPbCl}_3$  has a tetragonal structure of the perovskite class with  $c/a = 1.007$ . The phase transition to the cubic phase occurs at  $47^\circ\text{C}$ . Dielectric measurements were hampered by the photoconductivity of the crystal. Therefore, although permittivity also peaks at low temperatures (at  $-90^\circ\text{C}$  in light and at  $-150^\circ\text{C}$  in darkness), and the dependence  $P(E)$  resembles a hysteresis loop, additional study is required to determine conclusively the nature of the phase transition in this compound.

### 5? Lithium Niobate and Lithium Tantalate

Matthias and Remeika [237] reported on the ferroelectric properties of lithium niobate ( $\text{LiNbO}_3$ ) and lithium tantalate ( $\text{LiTaO}_3$ ). For a long time these crystals were not subjected to further analysis and they were described in the literature as ferroelectrics with an ilmenite structure. In the last few years these crystals attracted the attention of numerous investigators, principally because of their interesting electrooptic, piezoelectric and mechanical properties. Consequently both crystals are now quite well investigated.

The crystalline structure of  $\text{LiNbO}_3$  and  $\text{LiTaO}_3$ , though not of the ilmenite type, is nevertheless related to it. It is rhombohedral with  $a = 5.4920 \text{ \AA}$ ,  $\alpha = 55^\circ 53'$  for  $\text{LiNbO}_3$  and  $a = 5.470 \text{ \AA}$ ,  $\alpha = 55^\circ 12'$  for  $\text{LiTaO}_3$  [238, 239]. The elemental nucleus contains two formula units and at room temperature is described by the spatial group  $C_{3v}^6 - R3c$ .

The Curie temperature of  $\text{LiNbO}_3$  is  $1,140-1,210^\circ\text{C}$  [240, 241] (apparently that of the pure crystal is  $1,210^\circ\text{C}$ ) and the Curie temperature of  $\text{LiTaO}_3$  [238] is  $655^\circ\text{C}$ . Spontaneous polarization occurs on the tertiary axis.

The crystal lattice of these compounds (Figure 19.13) is constructed of oxygen octahedrons  $\text{NbO}_6$  and  $\text{TaO}_6$ , connected just as in perovskite. Therefore one can arrive at it from the perovskite structure by rotating the octahedrons in space. Here, of the 12 oxygens of the cubic octahedron, three atoms approach its center, three leave its center and as a result the space between the octahedrons in the niobate and tantalate of lithium can be imagined as two oxygen octahedrons with a common face (Figure 19.13). The question of the location of the lithium ion in this space has long remained unclear.

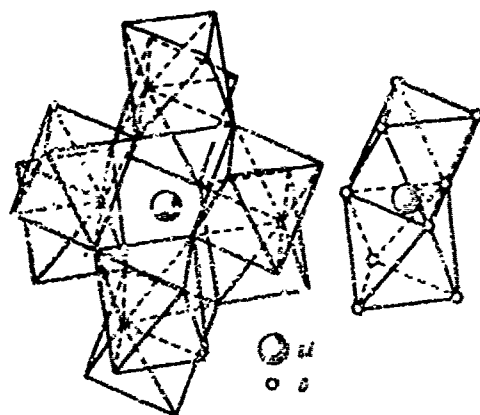


Figure 19.13. Crystal structure of  $\text{LiNbO}_3$  (paraelectric phase) and surroundings of Li ion by oxygen ions. (According to Isupov [240]).

According to the results of neutron radiographic analysis of Shiozaki and Mitsui [239], the average position of the lithium ion (discounting displacement on the tertiary axis in the ferroelectric phase) corresponds to the center of the common facet of both octahedrons, comprising the free space between the  $\text{NbO}_6$  and  $\text{TaO}_6$  octahedrons. Shiozaki and Mitsui theorize that the lithium ions are randomly distributed between these niobium- or tantalum-free octahedrons, so that their average position then corresponds to the center of the facet.

In 1964, at the 4th All-Union Conference on Ferroelectricity, Isupov [240] advanced the theory that the lithium ion actually is located in the center of the common facet of both octahedrons, as illustrated in Figure 19.13. Here it is stressed that the lithium ion is small enough (in contrast to its usual coordination) to occupy the center of the triangular oxygen ring, as is the case with boron in most of its oxygen compounds. Attention was also attracted by the fact that the interatomic distances [239] agree satisfactorily with the assumption that the lithium ion occupies the center of the common facet. Actually, the distance between the center of the oxygen triangle and its vertex was found to be 1.19 Å, and the sum of radii of the lithium ion and oxygen ion, according to Pauling, as noted in [239], is 1.25 Å.

The conclusions recently reached by Abrahams and his coworkers [241-243] from the results of x-ray diffraction and neutron radiographic analyses of  $\text{LiNbO}_3$ , completely verified the validity of this assumption. According to Abrahams, the Nb ion of  $\text{LiNbO}_3$  in the paraelectric phase lies between the oxygen planes, perpendicular to the tertiary axis (i.e., inside the octahedron) and the lithium ion -- in the oxygen plane (i.e., in the plane of the facet). With the onset of the ferroelectric state the

lithium ion leaves the plane of the common facet and the niobium ion is displaced from the center of the octahedron. Both ions move in the same direction.

The dielectric properties and thermal expansion of the  $\text{LiNbO}_3$  crystal was analyzed [244] in a wide range of temperatures. It was discovered that permittivity at 1,140°C, measured at 75 MHz on the tertiary axis, peaks sharply at 1,140°C (Figure 19.14, curve 1) and in about the same region sharp contraction of the crystal occurs on heating. Hence the authors conclude that the Curie point is 1,140°C. Analysis of  $\text{LiNbO}_3$  crystals grown by Chokhral'skiy's method, showed that the Curie temperature of these crystals is 1,210°C [241]. Apparently the discrepancy between the results [240] is related to differences in the methods of growing the crystals. (In [240] the crystals were grown from molten solution and could contain impurities).

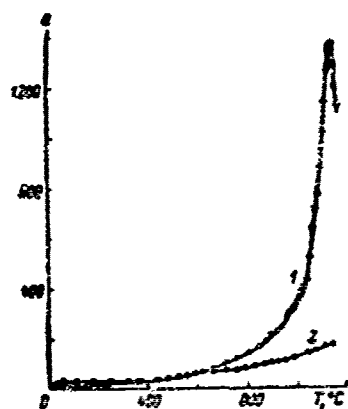


Figure 19.14. Temperature dependence of  $\epsilon$  of  $\text{LiNbO}_3$  (according to Smolenskii, et al [240]): 1 --  $\epsilon$  on tertiary axis; 2 -- perpendicular to tertiary axis.

replaced by contraction. In the paraelectric region the coefficients of linear expansion are: on the tertiary axis  $\alpha_3 = 5.7 \cdot 10^{-6} / ^\circ\text{C}$ , and perpendicular to it  $\alpha_1 = 21 \cdot 10^{-6} / ^\circ\text{C}$ .

At room temperature the clamped and free permittivities of  $\text{LiNbO}_3$  ( $\epsilon^T$  and  $\epsilon^S$ , respectively) are:  $\epsilon_{11}^T = 82-84.6$ ,  $\epsilon_{33}^T = 28.6-29$  [250, 251].

According to [252],  $\epsilon_{11}^T - \epsilon_{11}^S = 38.5$ ,  $\epsilon_{33}^T - \epsilon_{33}^S = 2.5$ . Spontaneous polarization was estimated on the basis of pyroelectric measurements. According to [253], for  $\text{LiNbO}_3$  at room temperature  $P_s > 50 \cdot 10^{-6} \text{ C/cm}^2$ .

There are indications [244-248] of the existence of low-temperature phase transitions in  $\text{LiNbO}_3$ . According to [245], the lattice parameters of  $\text{LiNbO}_3$  change abruptly at 600°C. These data were verified [246, 247], where dielectric anomalies were discovered at 600 and 950°C. A slight peak of electrooptic coefficient  $r_{22}$  was detected [248] at 150-170°C and it is indicated that there are also slight anomalies of  $\epsilon$  and thermal expansion at the same temperature.

$\text{LiTaO}_3$  has no such anomalies in thermal expansion below the Curie point [249]. On heating, as the Curie point is approached, elongation on the tertiary axis is

According to [254], for  $\text{LiTaO}_3$  at  $200^\circ\text{C}$   $P_s = 65 \cdot 10^{-6} \text{ C/cm}^2$ , and according to [255], at  $20^\circ\text{C}$   $P_s = (48-52) \cdot 10^{-6} \text{ C/cm}^2$ .

$\text{LiNbO}_3$  and  $\text{LiTaO}_3$  monocystals usually break up into  $180^\circ$  domains, observation of which is possible by etching the crystals [256-259]. It is stated [260, 261] that lithium niobate monocystals can be rather easily monodomained. One of the methods of monodomains is polarization of the polydomain crystals at temperatures of the order of  $1,200^\circ\text{C}$  with a weak electric field (a few  $\text{V/cm}$ ).

The elastic and piezoelectric properties of  $\text{LiNbO}_3$  and  $\text{LiTaO}_3$  are rather thoroughly investigated in [250, 251, 262, 263]. According to [250], the elastic constants of  $\text{LiNbO}_3$  at  $20^\circ\text{C}$  are  $s_{11}^E = 0.581 \cdot 10^{-12}$ ,  $s_{33}^E = 0.495 \times 10^{-12}$ ,  $s_{44}^E = 1.481 \cdot 10^{-12} \text{ cm}^2/\text{dyne}$ ,  $c_{11}^E = 1.925 \cdot 10^{12}$ ,  $c_{33}^E = 2.435 \cdot 10^{12}$ ,  $c_{44}^E = 0.565 \cdot 10^{12} \text{ dyne/cm}^2$ ; according to [251], in the  $20-200^\circ\text{C}$  temperature range  $s_{11}^E = 0.564[1 + (T - 20) \cdot 1.5 \cdot 10^{-4}] \cdot 10^{-12}$ ,  $2s_{13}^E + s_{44}^E = 1.39[1 + (T - 20) \cdot 2.0 \cdot 10^{-4}] \cdot 10^{-12}$ ,  $s_{14}^E = -0.084 \cdot 10^{-12}$ ,  $s_{33}^E = 0.494[1 + (T - 20) \times 1.5 \cdot 10^{-4}] \cdot 10^{-12} \text{ cm}^2/\text{dyne}$ , where  $T$  is temperature in  $^\circ\text{C}$ . According to [263] the elastic constants of  $\text{LiTaO}_3$  at  $20^\circ\text{C}$  are:  $c_{11} = 2.298 \cdot 10^{12}$ ,  $c_{12} = 0.441 \cdot 10^{12}$ ,  $c_{13} = 0.811 \cdot 10^{12}$ ,  $c_{14} = 0.104 \cdot 10^{12}$ ,  $c_{33} = 2.781 \cdot 10^{12}$ ,  $c_{44} = 0.968 \cdot 10^{12}$ ,  $c_{66} = 0.929 \cdot 10^{12} \text{ dyne/cm}^2$ . The piezoelectric constants and the electromechanical bond coefficients of  $\text{LiNbO}_3$  [250] are:  $d_{31} = 0.097 \cdot 10^{-6}$ ,  $d_{33} = 0.213 \cdot 10^{-6}$ ,  $d_{22} = 0.488 \cdot 10^{-6} \text{ CGSE}$ ,  $k_{31} = 8.7\%$ ,  $k_{33} = 32.7\%$ ,  $k_{22} = 24.6\%$ ,  $k_{15} = 44.6\%$ , and according to [251]:  $d_{15} = 222[1 + (T - 20) \cdot 2.8 \times 10^{-4}] \cdot 10^{-8}$ ,  $d_{22} = 62.3[1 + (T - 20) \cdot 2.4 \cdot 10^{-4}] \cdot 10^{-6}$ ,  $d_{31} = 2.59[1 + (T - 20) \cdot 11 \cdot 10^{-4}] \cdot 10^{-8}$ ,  $d_{33} = 48.7[1 + (T - 20) \cdot 2.9 \cdot 10^{-4}] \cdot 10^{-8} \text{ CGSE}$ ,  $k_{31} = 2\%$ ,  $k_{22} = 32\%$ ,  $k_{33} = 47\%$ . The piezoelectric elements of  $\text{LiNbO}_3$  were studied for the purpose of analyzing the elastic properties of other compounds at temperatures up to  $1,050^\circ\text{C}$  [262]. The piezoelectric constants and bond coefficients of  $\text{LiTaO}_3$  are:  $d_{33} = 0.248 \cdot 10^{-6} \text{ CGSE}$ ,  $k_{33} = 20\%$ ,  $k_{15} = 31.1\%$  [250],  $e_{15} = 2.58$ ,  $e_{22} = 1.59$ ,  $e_{31} = -0.24$ ,  $e_{33} = 1.40 \text{ C/m}^2$  [263]. The principles of propagation of acoustic waves in lithium niobate crystals were examined [264-269] and extremely small attenuation was found. The mechanical Q-factor of monodomain lithium niobate  $Q = 1.681 \cdot 10^5$  at  $500 \text{ MHz}$  for longitudinal waves on the tertiary axis [269], permitting lithium niobate to be employed in lag lines.

The refraction coefficients of  $\text{LiNbO}_3$  and  $\text{LiTaO}_3$ , birefringence and their temperature and frequency dependences were analyzed [248, 270-275].

At 25°C and  $\lambda = 4,200 \text{ \AA}$   $n^e = 2.3038$ ,  $n^0 = 2.4144$ ; for  $\lambda = 40,000 \text{ \AA}$ ,  $n^e = 2.0564$ ,  $n^0 = 2.1193$ . Measurements of birefringence as a function of temperature indicate that phase transitions to the paraelectric state in lithium niobate and lithium tantalate are second order transitions. The electrooptic effect of  $\text{LiNbO}_3$  and  $\text{LiTaO}_3$  was investigated [248, 276-279]. The electrooptic constants of  $\text{LiNbO}_3$  at 20°C are [279]:  $r_{33} = 32.2 \cdot 10^{-10}$ ,  $r_{13} = 10.0 \cdot 10^{-10}$ ,  $r_{22} = 6.81 \cdot 10^{-10}$ ,  $r_{51} = 32.6 \cdot 10^{-10} \text{ cm/V}$ . The piezoelectric coefficients of lithium niobate were studied [248] and it was found that the difference of piezoelectric coefficients  $\pi_{11} - \pi_{12}$  diminishes as wavelength diminishes.

Several problems related to the use of the optic properties of  $\text{LiNbO}_3$  for practical purposes, in particular the use of  $\text{LiNbO}_3$  for modulating laser emission and for generating optic harmonics, are studied in [280-291]. The dielectric dispersion and optic spectra of lithium niobate were investigated in [292-295], and NQR in  $\text{LiNbO}_3$  and  $\text{LiTaO}_3$  in [296]. The subject of crystal growth is discussed in [257, 261, 297-299]. Also noteworthy was an attempt to formulate a theory of ferroelectricity in  $\text{LiNbO}_3$  and  $\text{LiTaO}_3$  crystals, based on the theory that they are of the ilmenite type structure [300].

### 53. Ferroelectrics with Tetragonal Oxygen Structure of Potasso-Tungsten Bronze

Many compounds with the general formulas  $\text{AB}_2\text{O}_6$  and  $\text{A}_6\text{B}_{10}\text{O}_{30}$  crystallize in a structure of the tetragonal oxygen potasso-tungsten bronze type. The octahedrons in this structure, as in perovskite, are connected at their vertices in parallel rectilinear octahedron chains. These chains, however, are connected differently than in perovskite. Whereas in perovskite tetragonal channels are formed between the chains directed on the c axis, in the KW-bronze structure trigonal, tetragonal and pentagonal channels are formed (Figure 19.15). If here the same infinite rectilinear chains of octahedrons are formed in the perovskite in directions perpendicular to the connecting chains, these chains are finite in the KW-bronze structure in these directions and are not rectilinear. They consist of four octahedrons each and are connected through an octahedron, which uses as the bond with its neighbors sections of the chains adjacent to the vertex (Figure 19.15).

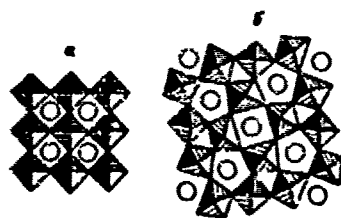


Figure 19.15. Comparison of tetragonal KW-bronze type structure (b) with perovskite type structure (a).

Table 28. Certain Properties of Compounds with KW-Bronze Structure

1) Состав	2) Симметрия	3) Параметры решетки, Å			4) ε в поликристаллическом образце при 20°С	5) Характер фазового перехода	6) Источники
		a	b	c			
PbNb <sub>2</sub> O <sub>6</sub>	P	17.65	17.91	7.36	280	570	Четкий 304, 305
PbTa <sub>2</sub> O <sub>6</sub>	P	17.695	17.72	7.749	~360	~250	303, 308, 309
BaTa <sub>2</sub> O <sub>6</sub>	T	17.88	—	7.810	132	—	307, 308, 310
Ba <sub>2</sub> Nb <sub>10</sub> O <sub>27</sub>	T	12.46	—	3.95	—	—	311
Sr <sub>2</sub> Nb <sub>10</sub> O <sub>27</sub>	T	12.34	—	3.94	—	—	311
K <sub>2</sub> Nb <sub>10</sub> O <sub>27</sub>	P	17.75	17.90	7.84	300	350	Сильно размыт 312, 313
K <sub>1.5</sub> Nb <sub>10</sub> O <sub>27</sub>	T	17.70	—	7.82	600	-110	Размыт 312, 313
K <sub>1.5</sub> Nb <sub>10</sub> O <sub>27</sub>	T	—	—	—	—	420	Четкий 303
K <sub>2</sub> Sr <sub>4</sub> Nb <sub>10</sub> O <sub>29</sub>	T	12.47	—	3.942	—	100	314
Nd <sub>2</sub> Nb <sub>10</sub> O <sub>27</sub>	P	—	—	—	—	550	315
K <sub>2</sub> Pb <sub>10</sub> O <sub>27</sub>	P	—	—	—	—	~460	316
Nd <sub>2</sub> Pb <sub>10</sub> O <sub>27</sub>	P	—	—	—	—	~500	316
K <sub>0.5</sub> Ce <sub>0.5</sub> Ta <sub>2</sub> O <sub>6</sub>	T	12.56	—	3.92	—	—	317
K <sub>0.5</sub> Pb <sub>0.5</sub> Ta <sub>2</sub> O <sub>6</sub>	T	12.55	—	3.91	—	—	317
K <sub>0.5</sub> Nd <sub>0.5</sub> Ta <sub>2</sub> O <sub>6</sub>	T	12.61	—	3.96	—	—	317
Ba <sub>2</sub> Nb <sub>10</sub> O <sub>27</sub>	T	18.00	—	8.02	1000	-25	Размыт 312, 313
Sr <sub>2</sub> Nb <sub>10</sub> O <sub>27</sub>	T	17.55	—	7.82	400	+10	312, 313
Ln <sub>2</sub> Nb <sub>10</sub> O <sub>27</sub>	T	—	—	—	~600	~45	318
Ba <sub>2</sub> FeNb <sub>10</sub> O <sub>29</sub>	T	17.95	—	7.98	~500	~100	312, 313, 319
Sr <sub>2</sub> FeNb <sub>10</sub> O <sub>29</sub>	T	17.50	—	7.72	~200	—	312, 313
Ba <sub>2</sub> Ti <sub>2</sub> Nb <sub>8</sub> O <sub>26</sub>	T	12.54	—	4.01	—	—	320
Ba <sub>2</sub> Zr <sub>2</sub> Nb <sub>8</sub> O <sub>26</sub>	T	12.67	—	4.117	—	—	321
Nd <sub>2</sub> Fe <sub>2</sub> Nb <sub>8</sub> O <sub>26</sub>	T	12.58	—	3.90	~70	—	312
Bi <sub>2</sub> Fe <sub>2</sub> W <sub>2</sub> O <sub>26</sub>	T	—	—	—	—	—	312
KTaWO <sub>6</sub>	T	12.36	—	3.90	—	—	310
Ba <sub>1.5</sub> Sm <sub>0.5</sub> Fe <sub>2</sub> Nb <sub>8</sub> O <sub>26</sub>	T	—	—	—	~200	+55	Четкий 312, 322
Ba <sub>1.5</sub> Sm <sub>0.5</sub> Fe <sub>2</sub> Nb <sub>8</sub> O <sub>26</sub>	T	12.46	—	3.926	~150	100	312, 322
Ba <sub>1.5</sub> Eu <sub>0.5</sub> Fe <sub>2</sub> Nb <sub>8</sub> O <sub>26</sub>	T	—	—	—	~300	~120	322
Ba <sub>1.5</sub> Gd <sub>0.5</sub> Fe <sub>2</sub> Nb <sub>8</sub> O <sub>26</sub>	T	—	—	—	~300	~100	312, 322
Ba <sub>1.5</sub> Y <sub>0.5</sub> Fe <sub>2</sub> Nb <sub>8</sub> O <sub>26</sub>	T	—	—	—	~300	0	Размыт 323
Ba <sub>1.5</sub> Th <sub>0.5</sub> Fe <sub>2</sub> Nb <sub>8</sub> O <sub>26</sub>	T	12.53	—	3.941	~400	0	312
Ba <sub>1.5</sub> Nd <sub>0.5</sub> Fe <sub>2</sub> Nb <sub>8</sub> O <sub>26</sub>	T	12.48	—	3.927	~100	+50	312
Ba <sub>1.5</sub> Sm <sub>0.5</sub> Fe <sub>2</sub> Nb <sub>8</sub> O <sub>26</sub>	T	12.46	—	3.91	50	+100?	312
Pb <sub>2</sub> Nd <sub>2</sub> Fe <sub>2</sub> Nb <sub>8</sub> O <sub>26</sub>	T	12.43	—	3.92	~200	—	312
Ba <sub>2</sub> Nd <sub>2</sub> Ni <sub>2</sub> Nb <sub>8</sub> O <sub>26</sub>	T	12.48	—	3.900	~60	~100?	312
Ba <sub>2</sub> Sm <sub>2</sub> Ni <sub>2</sub> Nb <sub>8</sub> O <sub>26</sub>	T	12.44	—	3.87	~60	0?	312
Bi <sub>2</sub> Nd <sub>2</sub> Fe <sub>2</sub> Nb <sub>8</sub> O <sub>26</sub>	T	12.54	—	3.86	~100	—	312
Ba <sub>2</sub> Ce <sub>2</sub> Ni <sub>2</sub> Nb <sub>8</sub> O <sub>26</sub>	T	12.53	—	3.942	~150	-50?	312
Bi <sub>2</sub> Sr <sub>2</sub> Ti <sub>2</sub> Nb <sub>8</sub> O <sub>26</sub>	T	12.33	—	3.869	—	5	324
K <sub>2</sub> BiTa <sub>2</sub> W <sub>2</sub> O <sub>26</sub>	T	12.41	—	3.92	—	—	310
Nd <sub>2</sub> SrTa <sub>2</sub> W <sub>2</sub> O <sub>26</sub>	T	12.33	—	3.87	—	—	310

- KEY: 1. Compound  
 2. Symmetry  
 3. Lattice parameters, Å  
 4. ε of polycrystalline specimens at 20°C  
 5. Character of phase transition  
 6. Source  
 7. Distinct  
 8. Quite blurred  
 9. Blurred  
 10. Comment: P -- rhombic symmetry; T -- tetragonal

In the KW-bronze lattice the A ions can theoretically occupy three spaces in the pentagonal, tetragonal and trigonal channels and thereby have the coordination numbers  $10 + 5 = 15$ ,  $8 + 4 = 12$  and  $5 + 6 = 9$ , respectively. The octahedrons in the elemental nucleus are also different. As seen in Figure 19.15, the KW-bronze structure has octahedrons of more regular and less regular form. Considering the ratio of the number of different channels and the difference between the octahedrons, the crystallochemical formula of compounds with this structure should be written in the form  $A'_4 A''_2 A'''_2 B'_8 B''_2 O_{30}$  or  $A'_2 A''_2 A'''_4 B'_4 B''_2 O_{15}$ . Here A' are ions occupying spaces in the pentagonal channels, A'' in tetragonal, A''' in trigonal, B' are ions occupying octahedrons of less regular form, B'', ions in more regular octahedrons (Figure 19.15).

Characteristically, nearly all compounds with the KW-bronze structure have in positions A a greater or lesser number of vacancies. In practically all these compounds the vacancies in the trigonal channels are unoccupied and the chemical formula often has the form  $A_6 B_{10} O_{30}$ . In compounds of the type  $AB_2 O_6$  (i.e.,  $A_5 B_{10} O_{30}$ ), there are only five atoms for every six vacancies in the tetragonal and pentagonal channels. Also known are compounds such as  $Sb_{0.67} Nb_2 O_6 = Sb_{3.33} Nb_{10} O_{30}$  [301] and  $Sr_2 Nb_{10} O_{27}$  [302] with the KW-bronze structure. These compounds are also known, however, with the structure in which the vacancies in all channels, including trigonal, can be assumed to be completely filled:  $K_6 Li_4 Nb_{10} O_{30}$  for example [303]. In any case, of course, the possibility cannot be ruled out that Li ions occupy the middle of the oxygen triangles in these channels (similar to the distribution of Li in  $LiNbO_3$ ) rather than vacancies with coordination number 9.

The lattice parameters of a number of compounds with the KW-bronze structure at  $20^\circ C$ , and some information concerning phase transitions in ferroelectrics with this structure, are listed in Table 28.

The geometric requirements of the KW-bronze type lattice on the ions that constitute it have not yet been sufficiently investigated. In particular, the distribution of atoms A' and A'' and vacancies in the spaces of the various channels, and of ions B' and B'' in the octahedral positions, has been studied little. Certain conclusions are made [324] about this distribution in several compounds with the KW-bronze structure.

The ferroelectric properties of lead metaniobate were discovered by Goodman [304].

$PbNb_2 O_6$  melts congruently at  $1,343^\circ C$  [325], and below this temperature exists in one of the two modifications: high-temperature modification with the KW-bronze type structure, stable above  $1,150-1,200^\circ C$ , and low-temperature rhombohedral form, stable below  $1,150-1,200^\circ C$  [326]. According to Francoise [326], the low-temperature modification belongs to

the rhombohedrally deformed perovskite class with elemental nucleus dimensions  $a = 6.206 \text{ \AA}$ ,  $\alpha = 58^\circ 18'$  or, if regarded as pseudocubic,  $a' = 8.664 \text{ \AA}$ ,  $\beta = 88^\circ 30'$ . This modification lacks ferroelectric properties.

The modification of lead metaniobate formed at high temperatures exists at room temperature in the metastable state and changes to the rhombohedral form when heated up to  $700^\circ\text{C}$ . The high-temperature modification is tetragonal above  $570^\circ\text{C}$  with  $a_T = 12.46$ ,  $c_T = 3.907 \text{ \AA}$ , and below  $570^\circ\text{C}$  has rhombic symmetry and ferroelectric properties. On cooling below  $570^\circ\text{C}$  the tetragonal elemental nucleus lengthens on one of the diagonals of the square base and contracts on the other diagonal. Here the period  $c$  becomes twice as large as  $c_T$ . Using as the new crystallographic axes the diagonals of the square face, we obtain a rhombic elemental nucleus, containing 20 units. According to [305],  $a = 17.65 \text{ \AA}$ ,  $b = 17.91 \text{ \AA}$ ,  $c = 7.73 \text{ \AA}$ . As the temperature rises,  $a$  increases and  $b$  decreases so that the rhombic distortion becomes less, and period  $c$  increases linearly. At the phase transition  $a$  and  $b$  decrease suddenly,  $c$  increases sharply and the volume of the nucleus decreases approximately 0.33% [305]. The coefficient of linear expansion of  $\text{PbNb}_2\text{O}_6$  is negative in a wide temperature range, and between  $570$  and  $1,000^\circ\text{C}$  averages  $8.8 \cdot 10^{-6} \text{ 1/}^\circ\text{C}$  [304].

The optic properties and domain structure were analyzed on flaky monocrystals perpendicular to the  $c$  axis [305]. The refraction coefficients for  $\lambda = 6,703 \text{ \AA}$  were:  $n_\alpha = 2.40 \pm 0.01$  parallel to the  $a$  axis,  $n_\beta = 2.43 \pm 0.01$  parallel to the  $b$  axis and  $n_\gamma = 2.60 \pm 0.01$  parallel to the  $c$  axis. Examination of the crystal on the  $c$  axis in polarized light in the extinction position revealed a set of light narrow orthogonal bands at an angle of  $45^\circ$  to the  $a$  and  $b$  axes. Hence it is concluded that planes (110) may be the planes of twinning. Assuming that  $P_s$  coincides with the  $b$  axis, the continuity of the normal component of  $P_s$  on transition through the domain wall is ensured when the boundaries make an angle of  $44^\circ 35'$  with the  $b$  axis. The  $180^\circ$  boundaries obviously should be parallel to the  $b$  axis. Above  $560^\circ\text{C}$  the domain pattern vanishes. With receding below the Curie point, the domains reappear, but the pattern is usually much different from the former. An attempt to change the domain structure by applying a field on the  $a$  and  $b$  axes failed to reveal any motion of the  $90^\circ$  boundaries in fields up to  $5 \text{ kV/cm}$  at temperatures up to  $300^\circ\text{C}$ .

The permittivity of polycrystalline  $\text{PbNb}_2\text{O}_6$  at  $20^\circ\text{C}$  is  $\sim 220$ , and peaks at about 7,000 [304]. Above the transition temperature the Curie-Weiss law, with  $C = 2.95 \cdot 10^5$  and  $T_0 = 488\text{--}530^\circ\text{C}$  [304], is valid. Investigation of the permittivity of monocrystalline  $\text{PbNb}_2\text{O}_6$  [305, 326] revealed strong anisotropy. As seen in Figure 19.16,  $\epsilon$  on the  $c$  axis is nearly independent of temperature, but on axes  $a$  and  $b$   $\epsilon$  peaks sharply at  $560^\circ\text{C}$ , where it reaches 24,000.  $\epsilon_a$  and  $\epsilon_b$  are lower than  $\epsilon_c$  at low temperatures, and  $\epsilon_a > \epsilon_b$ . It is concluded on the basis of dielectric measurements and

data on crystal structure that spontaneous polarization lies in the plane perpendicular to the c axis. By analogy with barium titanate, during whose transition to the ferroelectric state elongation of the nucleus and the greatest reduction of  $\epsilon$  correspond to the direction of spontaneous polarization, it is assumed that spontaneous polarization in  $\text{PbNb}_2\text{O}_6$  occurs on the b axis.

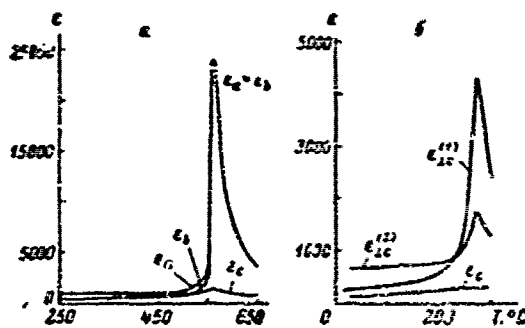


Figure 19.16. Temperature dependence of permittivity of monocrystalline  $\text{PbNb}_2\text{O}_6$  and  $\text{PbTa}_2\text{O}_6$ .  $\epsilon_c^{(1)}$  and  $\epsilon_c^{(2)}$  measured in mutually perpendicular directions.

(According to Francombe and Lewis [305] and Subbarao, et al [309]).

At 20°C in fields of ~60 kV/cm ceramic lead metaniobate has dielectric hysteresis loops, far from saturation [304]. It was found from these loops that  $P_{\text{res}} = 0.6 \cdot 10^{-6}$  C/cm<sup>2</sup> and  $E_c > 17$  kV/cm. The dependence of polarization of the monocrystals on field strength (up to 30 kV/cm) is slightly nonlinear. Residual polarization is slight. Using a stationary field of 20 kV/cm at 200-250°C it was possible to polarize ceramic  $\text{PbNb}_2\text{O}_6$  and observe piezoelectric properties [204]. The piezoelectric modulus of this ceramic  $d_{33} = 8.1 \cdot 10^{-12}$  C/kg, the electromechanical bond coefficient  $k_{33} = 26\%$  and Young's modulus  $c_{33} = 6.2 \cdot 10^{11}$  dyne/cm.

Orientation polarization of ceramic  $\text{PbNb}_2\text{O}_6$  was calculated in [327] as a function of the electric field applied to the specimen, proceeding from the properties of the monocrystal with consideration of 180° and 90° reorientations. As a result of the calculations the form of the basic polarization curves was found for various ratios of  $E_c'$  and  $E_c''$  (critical fields, determining reorientation of 180° and 90° domains).

The ferroelectric properties of lead metatantalate were discovered by Smolenskiy and Agronovskaya [306]. These authors did their study in the assumption of possible isostructuring of the metatantalate and metaniobate of lead. Subsequent x-ray diffraction analyses verified that the ferroelectric modification of  $\text{PbTa}_2\text{O}_6$  is isostructural to the ferroelectric

modification of  $\text{PbNb}_2\text{O}_6$  [309, 328]. The temperature of the phase transition to the ferroelectric state was initially determined from the results of dielectric measurements as 240-260°C [307, 309].

$\text{PbTa}_2\text{O}_6$ , like  $\text{PbNb}_2\text{O}_6$ , may exist in two modifications -- rhombohedral nonferroelectric, formed only below 1,150°C, and modification with the KW-bronze structure, stable at higher temperatures [309]. As pointed out in [309], once formed, rhombic  $\text{PbTa}_2\text{O}_6$  cannot be returned by heat treatment to the rhombohedral form. The lattice parameters of the rhombohedral modification are:  $a = 7.147 \text{ \AA}$ ,  $\alpha = 94^\circ 47'$ . The elemental nucleus contains two formula units.

At 26°C [308] the ferroelectric modification of  $\text{PbTa}_2\text{O}_6$  has a rhombic lattice with parameters  $a = 17.605 \text{ \AA}$ ,  $b = 17.720 \text{ \AA}$ ,  $c = 7.749 \text{ \AA}$ . According to [309],  $a = 17.68 \text{ \AA}$ ,  $b = 17.27 \text{ \AA}$ ,  $c = 7.754 \text{ \AA}$ . The ratio  $b/a$  [308] is 1.005; according to [309], approximately 1.002, and much smaller than that of  $\text{PbNb}_2\text{O}_6$  (1.016). As the temperature rises, period  $b$  decreases and periods  $a$  and  $c$  and the volume of the nucleus increase [308]. It follows from these data that at 280°C the lattice is tetragonal ( $a = b$ ).

According to [329], where the positions of the heavy atoms (Pb and Ta) in  $\text{PbTa}_2\text{O}_6$  are determined, the vacancies for lead correspond to voids in the tetragonal channels. Ta atoms were also observed to shift from the ideal positions for KW-bronze. It is suggested that the doubling of parameter  $c$  is the result of the slope of the oxygen octahedrons.

Dilatometric analysis of polycrystalline specimens [309, 330] showed that the phase transition to the paraelectric state is accompanied by a slight shrinkage of volume, by virtue of which the coefficient of linear expansion passes through a minimum. This indicates that three-dimensional spontaneous deformation and, consequently, three-dimensional electrostriction are positive.

Optical analysis of monocrystals of the ferroelectric modification of  $\text{PbTa}_2\text{O}_6$  [309] showed them to be biaxial rhombic crystals. The largest refraction coefficient lies on crystallographic axis [001]. Twinning is often observed in thin sections of the crystal, parallel to plane (001). The boundaries of the twin are oriented approximately along (110), but are always curved and irregular. Birefringence was measured with an accuracy of 10-15% and the following values were obtained:  $n_\beta - n_\alpha = 0.116$ ,  $n_\gamma - n_\beta = 0.043$ ,  $n_\gamma - n_\alpha = 0.059$ . Hence the crystals are optically positive.

Analysis of birefringence during heating [309] showed that  $\text{PbTa}_2\text{O}_6$ , in contrast to  $\text{PbNb}_2\text{O}_6$ , does not become tetragonal on transition to the paraelectric state, but retains slight rhombic distortion: at 360°C

$n_R - n_\alpha$  is still of the order of 0.03 and the crystals are still biaxial. Twin boundaries {110} do not disappear and the twins retain the same relative orientation in relation to each other. Thus, the temperature of the ferroelectric phase transition cannot be determined by visual observation of a heated crystal under the microscope. On the basis of the dependences of birefringence on temperature obtained in [309] it was assumed that the ferroelectric phase transition in  $\text{PbTa}_2\text{O}_6$  is a second order transition.

The permittivity of polycrystalline  $\text{PbTa}_2\text{O}_6$  is relatively low (~300) at 20°C, and the peak reaches 1,000. In the paraelectric region  $\epsilon$  changes according to the Curie-Weiss law with the constant  $C = 6.6 \cdot 10^4$  °K [330].

At room temperature  $\epsilon$  of the monocrystal is ~150 on the c axis. The permittivity perpendicular to this axis is usually 300-700, depending on the configuration of the twins in the crystal. The permittivity on the c axis depends little on temperature and experiences no sudden changes at the temperature of the phase transition (Figure 19.16). The  $\epsilon$  in two mutually perpendicular directions, perpendicular to the c axis, peaks at 265°C. The fact that  $\epsilon$  on these two axes is also different in the paraelectric phase substantiates that rhombic symmetry is retained even above the Curie point. The permittivity in the direction yielding the highest peak obeys the Curie-Weiss law with  $C = 1.5 \cdot 10^5$  °C and  $\theta = 257$ °C [309].

In the presence of variable fields up to 50 kV/cm at room temperature polycrystalline specimens of  $\text{PbTa}_2\text{O}_6$  have distinct, but nevertheless not completely saturated dielectric hysteresis loops. Spontaneous polarization of polycrystalline lead metatantalate has a value not less than  $4 \cdot 10^{-6}$  C/cm, and the coercive field -- not less than 12 kV/cm [330]. As the temperature rises, the coercive field drops rapidly, and total polarization diminishes slowly. Hysteresis loops are seen in monocrystals (not completely saturated) at  $E = 25$  kV/cm when the field is perpendicular to the c axis. At room temperature  $P_s = (8-10) \cdot 10^{-6}$  C/cm<sup>2</sup>. If the field is parallel to the c axis the relation between polarization and field strength is linear up to 15 kV/cm [309].

Coates and Kay [331] reported on the antiferroelectric properties of  $\text{PbTa}_2\text{O}_6$ , but this report is erroneous, apparently because of the sizable deviation from the stoichiometric composition during preparation of the specimens [332].

The fact that the phase transition in  $\text{PbTa}_2\text{O}_6$  is a second order phase transition or close to it, whereas in  $\text{PbNb}_2\text{O}_6$  it is clearly a first order phase transition, is extremely interesting. In solid solutions of  $\text{K}(\text{Pb}, \text{Ta})\text{O}_3$  the transition also approaches the second transitions by measure of substitution of niobium ions with tantalum ions. Thus, there is

reason to believe that the phase transitions in tantalates generally are closer to second order than in the corresponding niobates.

There is presently great interest in the compounds  $K_2Li_4Nb_{10}O_{30}$  [303],  $K_2Sr_4Nb_{10}O_{30}$  [314] and  $Na_2Ba_4Nb_{10}O_{30}$  [315]. Monocrystals of potassolithium niobate are transparent from  $\lambda = 4000$  to  $5000 \text{ \AA}$ . Its refraction coefficients are [303]:  $n^e = 2.197$ ,  $n^o = 2.326$  at  $5,320 \text{ \AA}$ ,  $n^e = 2.163$ ,  $n^o = 2.277$  at  $6,328 \text{ \AA}$ ,  $n^e = 2.112$ ,  $n^o = 2.208$  at  $10,640 \text{ \AA}$ . For the point group  $4mm$ , to which the given crystal belongs, optic polarization of the second harmonic is determined through the amplitude of electric field  $E$  and nonlinear coefficients:  $P_x = 2X_{15}E_xE_z$ ,  $P_y = 2X_{15}E_yE_z$ ,  $P_z = X_{31}(E_x^2 + E_y^2) + X_{33}E_z^2$ . It is found that  $X_{33}$  of potasso-lithium niobate is 18 times, and  $X_{31}$  14 times greater than  $X_{11}$  of quartz and is about the same as  $X_{31}$  of  $LiNbO_3$ . An advantage of the given crystal over  $LiNbO_3$ , however, is its much lower "optic fatigue" -- nonuniform refraction coefficient during long-term illumination by strong (laser) light. The linear electrooptic matrix is characterized by the coefficients  $r_{13}$ ,  $r_{51}$  and  $r_{33}$ . It was found that  $|(n^e)^3 r_{33}| = 7.9 \cdot 10^{-8} \text{ cm/V}$ , and  $|(n^o)^3 r_{13}| = 1.05 \cdot 10^{-8} \text{ cm/V}$ .

The electrooptic coefficient of the  $K_2Sr_4Nb_{10}O_{30}$ , tetragonal at  $20^\circ C$ , is 7 times greater than that of  $LiNbO_3$  [314]. The nonlinear coefficients of the rhombic  $Na_2Ba_4Nb_{10}O_{30}$  crystal are about double those of lithium niobate ( $X_{33}$  is 28,  $X_{32}$  20 and  $X_{31}$  23 times greater than  $X_{11}$  of quartz). Its linear electrooptic matrix is characterized by the coefficients  $r_{13}$ ,  $r_{23}$ ,  $r_{33}$ ,  $r_{51}$  and  $r_{42}$ . It was found that  $|n_z^3 r_{33}| = 6.2 \cdot 10^{-8}$ ,  $|n_x^3 r_{13}| = 2.3 \cdot 10^{-8}$ ,  $|n_y^3 r_{23}| = 1.7 \cdot 10^{-8} \text{ cm/V}$ .  $r_{13}$ ,  $r_{23}$  and  $r_{33}$  have the same sign.

Numerous studies have been done on solid solutions with the KW-bronze structure. Solid solutions based on  $PbNb_2O_6$  are described in [333-355]. Smolenskiy and coworkers showed that although the metaniobate, of barium, strontium and potassium do not have the KW-bronze structure, solid solutions  $(Ba, Sr)Nb_2O_6$  and  $(Ba, Ca)Nb_2O_6$  have this structure and are ferroelectrics [356]. The ferroelectric properties of the solid solutions  $(Ba, La_{2/3})Nb_2O_6$  and  $(Ba, Bi_{2/3})Nb_2O_6$  were also discovered there. These and other solid solutions based on  $BaNb_2O_6$  were later scrutinized in [348, 357-359].

#### 34. Cadmium Pyroniobate

Wainer and Wentworth [360] reported a high  $\epsilon$  for cadmium pyroniobate ( $Cd_2Nb_2O_7$ ), increasing rapidly on cooling from room temperature. The

same year Cook and Jaffe demonstrated that  $\text{Cd}_2\text{Nb}_2\text{O}_7$  is a ferroelectric [361].

Cadmium pyroniobate has a pyrochlore type structure [362, 363], in which many compounds with the general formula  $\text{A}_2\text{B}_2\text{O}_7$  crystallize. This structure is characterized by oxygen octahedrons  $\text{BO}_6$ , connected at their vertices in endless chains. Here rows of mutually parallel chains, connected at the vertices, alternate with rows of mutually parallel chains perpendicular to the chains of the first row (the chains are packed by the "polennitsa" principle). The octahedrons of the adjacent chains are also connected together at the vertices (Figure 19.17). Connected thusly the  $-\text{O}-\text{B}-\text{O}-$  chains are zig-zags. The framework formed out of octahedrons has the composition  $(\text{B}_2\text{O}_6)_\infty$ . In the spaces between the octahedrons are located ions A and one-seventh of the oxygen ions not included in the framework of octahedrons. Consequently a cubic lattice results, belonging to the spatial group  $\text{C}_h^7\text{-Fm}\bar{3}\text{m}$ . Compounds with a pyrochlore type structure can be formed if the geometric criterion  $t = 0.866 (R_A^{(8)} + R_O) / (R_B + R_O)$  (where  $R_A^{(2)} = 1.03 R_A^{(6)}$  is the radius of ion A for k. ch. 8) is from 0.94 to 1.16 [364].

The cadmium pyroniobate lattice is cubic at room temperature with  $a = 10.372 \pm 0.001 \text{ \AA}$  [365]. Several phase transitions take place in  $\text{Cd}_2\text{Nb}_2\text{O}_7$  as the temperature is lowered, of which the transition at  $-80$ - $90^\circ\text{C}$  is related to a peak on the curve  $\epsilon(T)$ , characteristic of ferroelectrics [365-369] (Figure 19.18). At temperatures a few degrees above the temperature of the main peak there is a step on the curve  $\epsilon(T)$ , which probably is also related to a phase transition [369-373]. Described also [371] are bends on the curve  $\epsilon(T)$  at  $-68$ ,  $-47$  and  $-12^\circ\text{C}$  and, corresponding to them, peaks in the temperature dependence of heat capacity. The existence of these high-temperature phase transitions, as will be seen below, cannot be considered proved. At  $-188$  to  $-193^\circ\text{C}$  there is a "hump" on the curve  $\epsilon(T)$ , which apparently is related to a low-temperature phase transition [366, 367].

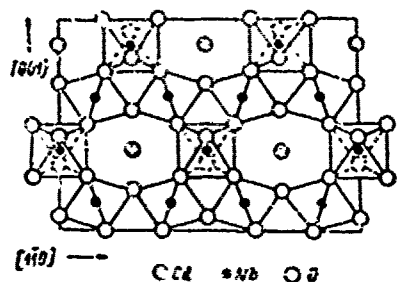


Figure 19.17. Projection of structure of pyrochlore type on plane (110).

X-ray diffraction analysis below the Curie temperature, which we will call the temperature of the peak on the curve  $\epsilon(T)$  at  $-80$  to  $-90^\circ\text{C}$ , was carried out in [365]. At  $-150^\circ\text{C}$  there was no separation of lines related to lattice distortion on the powder patterns of polycrystalline  $\text{Cd}_2\text{Nb}_2\text{O}_7$ . Analysis of monocrystals with the aid of the Weissenberg chamber showed very weak splitting of some diffraction maxima, but no conclusion could be reached concerning the structure

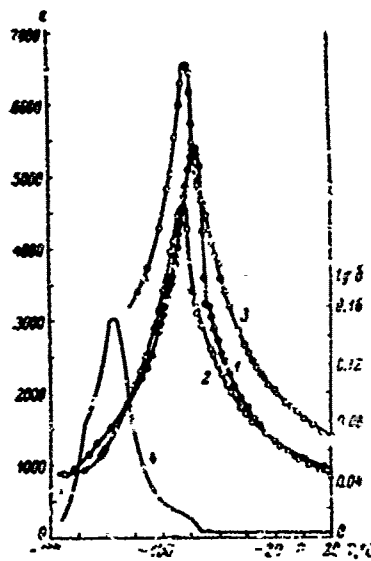


Figure 19.18. Temperature dependence of  $\epsilon$  and  $\tan \delta$  of hot pressed and ordinary polycrystalline specimens, and also monocrystal of  $\text{Cd}_2\text{Nb}_2\text{O}_7$  (in direction [110]) at 1 kHz in a field of 40 V/cm (according to de Bretteville [369]).

not be ruled out. The authors conclude that if the lattice of pure  $\text{CdNb}_2\text{O}_7$  is tetragonal at  $-150^\circ\text{C}$ , the lattice parameters will then be:  $a = 10.364 \text{ \AA}$ ,  $c/a = 1.000\%$ .

Analysis of  $\text{Cd}_2\text{Nb}_2\text{O}_7$  monocrystals, pure and with the impurity NaF, in polarized light [365] revealed that a transition occurs to a monocubic phase in pure monocrystals at  $91^\circ\text{K}$ , and in monocrystals with the impurity NaF at  $123^\circ\text{C}$ . This agrees satisfactorily with the results of dielectric measurements. Below the Curie temperature there were no positions of extinction or domain structure. At great magnifications many parallel wedges were visible near the edges of the crystal faces. They are parallel to direction [211] and are of the order of 1 micron wide. A very fine two-dimensional network is visible in the central part of the flake. The lines of the network are perhaps the walls of very tiny domains. That the wedges are parallel to [211] apparently indicates tetragonal or rhombic distortion of the lattice. Birefringence is apparently very weak, of the order of 0.004 [365].

The temperature dependence of the heat capacity  $c_p$  of cadmium pyroniobate was studied in [368]. The maximum heat capacity was noted

of the ferroelectric phase. The only conclusion reached is that there is displacement of cadmium ions in relation to niobium ions in the ferroelectric phase. Monocrystals grown from  $\text{Cd}_2\text{Nb}_2\text{O}_7$  melt in NaF, in which some of the CdO was substituted by NaF, were analyzed in the same work. The composition of these crystals could be described approximately by the formula  $\text{Cd}_{1.6}\text{Na}_{0.4}\text{Nb}_2\text{O}_{6.6}\text{F}_{0.4}$ .

These crystals had a lattice period  $a = 10.372 \pm 0.001 \text{ \AA}$  at  $20^\circ\text{C}$ , were also ferroelectric, but had a lower Curie temperature, equal to  $-120^\circ\text{C}$  on cooling and  $-112^\circ\text{C}$  on heating. Splitting of diffraction maxima was greater in these monocrystals than in a monocrystal of pure  $\text{Cd}_2\text{Nb}_2\text{O}_7$ . This precluded the possibility of a rhombohedral structure. The parameters  $a = 10.378 \text{ \AA}$  and  $c/a = 1.0011$  were obtained on the assumption of a tetragonal lattice, but the possibility of rhombic distortion could

at 193.2°K. The latent heat of transition was  $18 \pm 2$  cal/mole, and the corresponding entropy change was  $0.09 \pm 0.01$  cal/°K·mole. According to de Bretteville and Gnan [371], the phase transition at -80°C, corresponding to the Curie temperature, is related to a heat of transition of 18 cal/mole and the transitions at -76, -68, -47 and -12°C, to the heats: 5.2, 1.2, 0.75, 0.39 cal/mole, respectively. de Bretteville [372], by calculating the thermodynamic values according to the dielectric properties, obtained 5.1 cal/mole for the transition at -80°C, 3.2 and 0.73 cal/mole for the transitions at -74 and -60°C. The summary latent heat of these transitions is 9.0 cal/mole, i.e., one-half the experimental value found for the transition at -80°C. The discrepancy is attributed to the random orientation of the vector of polarization in polycrystalline specimens.

Above the Curie point  $\epsilon$  changes in accordance with the Curie-Weiss law [365, 367]. Here the constant C of polycrystalline specimens varies from  $4 \cdot 10^4$  to  $10 \cdot 10^4$ °K, and  $\theta$  from 145 to 175°K. The permittivity of the monocrystal with NaF impurity is 850 at 20°C and peaks at 20,000 at the Curie temperature. Constant C is  $1.1 \cdot 10^5$ °K,  $\theta = 177$ °K.

It was found [369] that the nonlinearity of dielectric polarization of cadmium pyroniobate, determined by the presence of the third harmonic in the current through the specimen, appears at temperatures above the Curie point. Since the temperature at which the third harmonic appears does not depend on field strength (from 10 to 200 V/cm) and is close to the temperature of the step on the curve  $\epsilon(T)$ , the authors feel that spontaneous polarization occurs with the phase transition corresponding to the step. At extremely low temperatures nonlinearity diminishes and the third harmonic vanishes. At  $21 \cdot 10^9$  Hz  $\epsilon$  of polycrystalline cadmium pyroniobate at 20°C is 150 and  $\tan \delta = 0.002$  [369].

The application of a stationary field of 5 kV/cm to monocrystalline  $\text{Cd}_2\text{Nb}_2\text{O}_7$  (grown from NaF) or to a polycrystalline specimen displaces the Curie point toward higher temperatures [365, 370]. Here it decreases, both below and above the Curie temperature. At 15 kV/cm, however, there is no further displacement of maximum  $\epsilon$  of the polycrystalline specimen. Only a further reduction of  $\epsilon$  below and above the Curie point is noted, and at the peak  $\epsilon$  was practically constant.

Dielectric hysteresis loops are seen below the Curie point down to 1.2°K. The residual polarization of a polycrystalline specimen [361] near -196°C is  $5.2 \cdot 10^{-6}$  C/cm<sup>2</sup>, and in a field of 25 kV/cm at 100°K [367]  $P_s = 1.8 \cdot 10^{-6}$  C/cm<sup>2</sup>. A value of  $-6 \cdot 10^{-6}$  C/cm<sup>2</sup> was obtained for spontaneous polarization at -185°C in a field applied along [111] from the loops obtained for a monocrystal grown from NaF. If, however, spontaneous polarization is directed along [100], it will be  $\sqrt{2}$  times greater, i.e., about  $10 \cdot 10^{-6}$  C/cm<sup>2</sup>. From the loops obtained for a monocrystal grown by Shrokbarger's method [369], it was found that in a field parallel to [110] at -140°C,  $P_s = 5.1 \cdot 10^{-6}$  C/cm<sup>2</sup>.

The dependence of dielectric polarization of polycrystalline

$\text{Cd}_2\text{Nb}_2\text{O}_7$  on a variable field was analyzed [376] for fields up to 60 kV/cm. It was thereby established that below the Curie temperature, and not very close to it in fields of the order of 20-25 kV/cm, dielectric hysteresis loops are seen, typifying ferroelectrics, with pronounced saturation (Figure 19.19a). As the field increases, a new strong increase in polarization occurs (Figure 19.19b), and then new (secondary) saturation (Figure 19.19c). Figure 19.19 illustrates the hysteresis loops at  $-118^\circ\text{C}$  ( $30^\circ\text{C}$  below the Curie temperature). The loops, as seen in the figure, are very narrow. Assuming that spontaneous polarization ( $P_s''$ ) can be calculated on the basis of secondary saturation, just as ( $P_s'$ ) is calculated on the basis of primary saturation, at  $-118^\circ\text{C}$  (assuming incomplete secondary saturation)  $P_s''/P_s' > 2.7$  [376]. As the Curie temperature is approached the secondary growth of polarization and secondary saturation are manifested in smaller fields. The function  $P(E)$  is also slightly nonlinear in some interval above the Curie temperature [376].

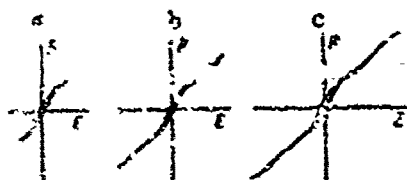


Figure 19.19. Form of dielectric hysteresis loops of polycrystalline cadmium pyroniobate for various variable field strengths at  $-118^\circ\text{C}$  (according to Isupov and Skubitskiy [375]): a -- 22.4; b -- 44.6, c -- 60 kV/cm.

The temperature dependences of total and spontaneous polarization and of the coercive field of cadmium pyroniobate, determined in fields  $E_{\text{max}} = 21.2$  and  $40.9$  kV/cm, indicate a difference in spontaneous polarization determined in various fields, apparently related to the fact that in the field  $E_{\text{max}} = 21.2$  kV/cm primary saturation is incomplete in the polycrystalline specimen, although this is difficult to see by the shape of the loop. It is noteworthy that the values of spontaneous polarization ( $\sim 3.5 \cdot 10^{-6}$  C/cm<sup>2</sup>) obtained in [370] are close to those obtained in [361]. In high fields near the Curie temperature there are peaks of total polarization and coercive field, attributed to the secondary growth of polarization in high fields and to some expansion of the loop.

The elastic and piezoelectric properties of polycrystalline specimens of cadmium pyroniobate were analyzed [373] by the dynamic method with the specimen placed simultaneously in a stationary biasing field in a wide temperature range. It was found that a sharp minimum of Young's modulus  $Y$  on the curve  $Y(T)$  corresponds to the peak on the curve  $\epsilon(T)$  (Figure 19.20). Piezoelectric vibrations were also detected at temperatures above the Curie point, and piezoelectric vibrations could be observed in large fields to nearly  $0^\circ\text{C}$ . Neither minima nor discontinuities were noted on the curves  $\epsilon(T)$  at temperatures above the Curie point. It was discovered that the depth of the minimum on the curve  $Y(T)$  diminishes when the stationary field is strengthened to 7-9 kV/cm and then increases, and at somewhat lower temperatures there is a level minimum, which is displaced toward

lower temperatures when the stationary field is increased. When  $E = 18.5$  kV/cm this displacement leads to a change in the sign of curvature of the low-temperature part of the curve. Piezoelectric modulus  $d_{31}$ , measured in biasing field  $E = 1$  kV/cm at  $-150^\circ\text{C}$  is  $-0.35 \cdot 10^{-6}$  CGSE and reaches  $-1.2 \cdot 10^{-6}$  CGSE at the peak near the Curie point [273].

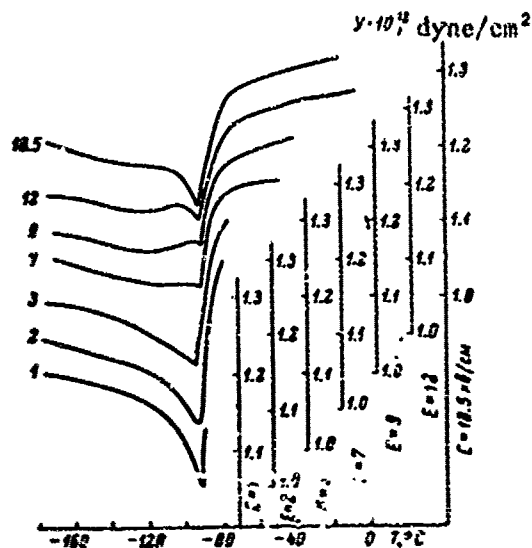


Figure 19.20. Temperature dependence of Young's modulus of polycrystalline specimens of  $\text{Cd}_2\text{Nb}_2\text{O}_7$  in various biasing stationary electric fields. The numbers to the left of the curves indicate the strength of the stationary field (in kV/cm). To avoid overlapping, the curves are displaced on the ordinate axis. To each field corresponds its zero point on the ordinate axis. (According to Isupov and Skubitskiy [373]).

Various possibilities are examined to explain the anomalous dependence of dielectric polarization of  $\text{Cd}_2\text{Nb}_2\text{O}_7$  on electric field strength [370, 373].

It may be assumed first of all that cadmium pyroniobate has two types of domains with different energies of fixation. The low-energy domains rotate in relatively weak fields, forming a saturated hysteresis loop. The high-energy domains are oriented only by a strong field. As the field weakens, elastic stresses or any other forces should return the domains to the initial position.

The ratio  $P''_s/P'_s$ , however, is too large to explain the secondary growth of polarization of reorientations of the  $90^\circ$ ,  $60^\circ$ ,  $70^\circ$  or  $110^\circ$  domains. It follows from x-ray diffraction data, moreover, that spontaneous deformation of the  $\text{Cd}_2\text{Nb}_2\text{O}_7$  lattice is extremely low in the

ferroelectric region ( $c/a = 1.0005$ ). That the reorientation of the domains was related to high internal stresses with such little deformation is improbable. To this can be added the fact that the perfect matching of the forward and reverse paths on the hysteresis loop in the region of high fields requires the complete exclusion of any hysteresis whatsoever during reorientation of domains with a high energy of fixation, which is hardly acceptable, regardless of the domain structure. This explanation, therefore, should probably be rejected.

It may be assumed, secondly, that cadmium pyroniobate is a ferroelectric or ferrielectric with spontaneous polarization  $P'_S$  below the Curie point, and changes in a strong electric field to another ferro- or ferrielectric state with spontaneous polarization  $P''_S$ . As we have already indicated, at  $-118^\circ\text{C}$  the ratio  $P''_S/P'_S > 2.7$ . Since the higher the temperature is and the closer it is to the Curie point the smaller the fields are in which secondary growth and saturation of polarization appear on the hysteresis loops, the difference of the free energies of the state with  $P'_S$  and that with  $P''_S$  should also diminish as the Curie point is approached. Consequently, two phase transitions should occur in a rather strong electric field as the specimen is cooled from high temperatures: one from the paraelectric state to the state with  $P''_S$  and one from the state with  $P''_S$  to the state with  $P'_S$ .

The results of analysis of the elastic properties of cadmium pyroniobate [373] concur with the given hypothesis. In weak stationary fields there is only one minimum on the curve  $Y(T)$ , which corresponds to transition from the paraelectric phase to the  $P'_S$  phase. When the field is increased, two minima appear (Figure 19.20): a sharp at higher temperatures, which may be related to transition from the paraelectric phase to the  $P''_S$  phase, and a level minimum at lower temperatures, which apparently corresponds to transition from the  $P''_S$  state to the  $P'_S$  state. The blurred character of the latter is probably caused by the fact that the specimen is polycrystalline, the grains are oriented variously in relation to the field and the transition from one state to the other occurs in the different grains at different field strengths. The reduction and subsequent increase of the depth of the minimum on the curve  $Y(T)$  (Figure 19.20) with increasing biasing field strength cannot yet be explained.

As regards the phase transitions in cadmium pyroniobate, three low-temperature transitions can be considered certain: near  $-190^\circ\text{C}$ , the Curie temperature at  $80-90^\circ\text{C}$  and the transition a few degrees above. A report [371] of phase conversions at higher temperatures requires further checking.

It is noteworthy that Megaw [374], on the basis of examination of chains of oxygen octahedrons in a structure of the pyrochlore type, also concluded that cadmium pyroniobate possibly has ferroelectric properties.

It is clear from the examined properties of  $\text{Cd}_2\text{Nb}_2\text{O}_7$  that they are extremely unusual and interesting. In future analysis of this compound, however, it will be necessary to analyze monocrystals, primarily by microscopic investigation in polarized light with the crystal subjected to strong electric fields. It is desirable here to use variable fields and stroboscopic illumination. Other properties of the monocrystal, of course, must also be scrutinized by means of low-temperature x-ray diffraction and neutron radiographic analyses.

Some reports appeared relatively recently concerning new ferroelectrics with the pyrochlore type structure [216]. The published data on these compounds are presented in Table 29.

Table 29. Some Properties of Compounds with the Pyrochlore Type Structure, Described in [216]

1) Формула	2) Симметрия	3) Параметры решетки, Å	4) Температура Кюри, °C	5) Электропроводность при 20°C, $\text{ohm}^{-1}\text{cm}^{-1}$
$\text{Pb}_2\text{BiNbO}_6$	6) Моноклинная	$a = c = 10.777, b = 19.143, \beta = 90.29^\circ$	475	$3 \cdot 10^{-13}$
$\text{Pb}_2\text{BiTaO}_6$	7) Тетрагональная	$a = 10.686, c = 10.811$	420	$4 \cdot 10^{-13}$
$\text{Pb}_2\text{Bi}_x\text{W}_y\text{Ce}_z$	8) То же	$a = 10.637, c = 10.797$	410	$2 \cdot 10^{-13}$
$\text{Pb}_2\text{Bi}_x\text{Mo}_y\text{Ta}_z$	8) То же	$a = 11.262, c = 11.551$	500	$2 \cdot 10^{-13}$

- KEY: 1. Formula  
 2. Symmetry  
 3. Lattice parameters, Å  
 4. Curie temperature, °C  
 5. Electrical conductivity at 20°C,  $\text{ohm}^{-1}\text{cm}^{-1}$   
 6. Monoclinic  
 7. Tetragonal  
 8. Same

The permittivity of these compounds at 20°C varies from 75 to 95. These compounds have  $\epsilon$  maxima at 400-500°C [216], where  $\epsilon$  reaches 120-145. No information was given concerning dielectric hysteresis loops or the piezoelectric effect of polarized ceramics. A conclusion concerning ferroelectric properties was reached on the basis of the above-mentioned  $\epsilon$  maxima and lattice distortions. These results and the conclusions require checking.

#### §5. Strontium Pyrotantalate

The ferroelectric properties of strontium pyrotantalate ( $\text{Sr}_2\text{Ta}_2\text{O}_7$ ) were discovered by Smolenskiy and his coworkers [375]. The permittivity of polycrystalline specimens at 1 kHz was 100-120 at 20°C and increased on cooling. It was found that at temperatures from -84 to -55°C it peaks to approximately 170. At a temperature, which, for various specimens lies

in the range from  $-190$  to  $-150^{\circ}\text{C}$  there is a second  $\epsilon$  peak [307]. At  $1\text{ kHz}$  and  $20^{\circ}\text{C}$   $\tan \delta$  is  $0.0007$ , and with cooling it increases, reaching  $0.007$  at  $-180^{\circ}\text{C}$  [375]. Below the temperature of maximum  $\epsilon$  are dielectric hysteresis loops. At  $-170^{\circ}\text{C}$  the polycrystalline specimen has  $P_s = 0.14 \cdot 10^{-6}\text{ C/cm}^2$

[376]. Thus, strontium pyrotantalate is a ferroelectric with Curie temperature of approximately  $-84$  to  $-55^{\circ}\text{C}$ . The low-temperature peak is apparently related to a low-temperature phase transition. Near  $170^{\circ}\text{C}$  there is a slight bend in the curve  $\epsilon(T)$ . It is probably related to yet another phase transition. The linear expansion coefficient of the polycrystalline specimen is  $7.4 \cdot 10^{-6}\text{ 1/}^{\circ}\text{C}$  in the temperature range of  $-100$  to  $0^{\circ}\text{C}$  [376].

The crystal structure of  $\text{Sr}_2\text{Ta}_2\text{O}_7$  was analyzed [328]. It was found that strontium pyrotantalate has a tetragonal lattice with  $a = 10.628\text{ \AA}$ ,  $c = 10.908\text{ \AA}$ . The lattice parameters of  $\text{Sr}_2\text{Ta}_2\text{O}_7$  are close to the lattice periods of compounds with the pyrochlore type structure. However, some of the x-ray diffraction patterns are radically different. This nearness of parameters to the parameters of pyrochlore compounds is very likely random only, and the structure of strontium pyrotantalate has nothing in common with the pyrochlore structure.

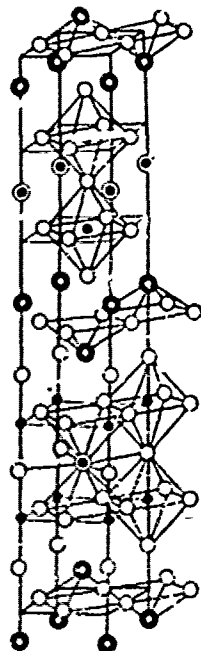
The dielectric properties of several solid solutions based on strontium pyrotantalate were analyzed in [307, 375, 377]. The phase transition temperatures of these solutions jump sharply when tantalum ions are substituted by niobium ions: the Curie temperature rises approximately  $32^{\circ}$  per mole % of  $\text{Sr}_2\text{Nb}_2\text{O}_7$ . This rise in the Curie temperature with identical  $\text{Nb}^{5+}$  and  $\text{Ta}^{5+}$  ion radii can be attributed to a change in the character of chemical bond and great polarizability of the  $\text{Nb}^{5+}$  ion compared to the  $\text{Ta}^{5+}$  ion. The Curie temperature of  $(\text{Sr}, \text{Ba})_2\text{Ta}_2\text{O}_7$  solid solutions rises by measure of substitution of strontium ions by barium ions. The low-temperature phase transition apparently shifts in the same direction as the Curie temperature. A slight discontinuity on the curve  $\epsilon(T)$ , seen in strontium pyrotantalate near  $165^{\circ}\text{C}$ , is transformed here into a small peak, the height of which increases, and the temperature at which it occurs decreases linearly. In the  $(\text{Sr}, \text{Ca})_2\text{Ta}_2\text{O}_7$  system the Curie temperature rises rapidly by measure of substitution of Sr ions by Ca ions.

Thus, in solid solutions based on strontium pyrotantalate, as strontium ions are substituted by the larger barium ions with higher electron polarizability and by smaller calcium ions with lower electron polarizability the transition temperatures change quite differently than in ferroelectric solid solutions  $(\text{Sr}, \text{Ba})\text{TiO}_3$  and  $(\text{Sr}, \text{Ca})\text{TiO}_3$  with the perovskite type structure, where the substitution of Sr ions by Ba ions raises the Curie temperature, and by Ca ions -- raises the Curie temperature somewhat at first and then lowers it. An attempt is made [376] to explain this dependence of the Curie temperature on the concentration of solid solutions by the assumption that the phase transition in strontium

pyrotantalate to the state possessing spontaneous polarization is of a character intermediate between the ferroelectric phase transition and the buckling transition. This assumption enables one to understand the dependence of the transition temperature on the average dimension of A ions, which is more characteristic of the buckling transition.

#### 56. Ferroelectrics with Lamellar Perovskite-Like Structure

Smolenskiy, Ispup, Agranovskaya, analyzing the properties of lamellar compounds described by Aurivillius [378], discovered the ferroelectric properties of  $\text{PbBi}_2\text{Nb}_2\text{O}_9$  [379]. The discovery of the ferroelectric properties of one representative of a large family of lamellar



● Ca ○ Bi ● Ta ○ O

Figure 19.21. Crystal structure of lamellar perovskite-like compound  $\text{CaBi}_2\text{Ta}_2\text{O}_9$ .

The thickness of the perovskite-like layers is determined by the value  $n$  entering the chemical formula: these layers, in terms of their thickness, contain  $n$  oxygen octahedra. By virtue of the fact that the bismuth-oxygen layers are parallel to planes (001) of the cubic perovskite lattice, the structure of these compounds above the Curie point is tetragonal. As follows from [382], the structure of  $\text{ABi}_2\text{B}_2\text{O}_9$  compounds in the paraelectric

compounds, which include compounds of the types  $\text{ABi}_2\text{B}_2\text{O}_9$ ,  $\text{A}_2\text{Bi}_2\text{B}_3\text{O}_{12}$ , etc. stimulated interest in the properties of other compounds of this class. The dielectric properties and crystal structure of numerous compounds with a lamellar structure were analyzed concurrently by Smolenskiy, Ispupov and Agranovskaya [380, 381] and Ismailzade [382-384]. Thus, a vast new class of ferroelectrics was discovered. The discovery of the ferroelectric properties of  $\text{PbBi}_2\text{Nb}_2\text{O}_9$  also prompted a number of foreign investigators (Subbarao [385-390], Fang [391-394], Van Uitert [395], among others) to start investigating lamellar compounds.

Compounds belonging to the examined structural types have a common formula  $\text{A}_{n-1}\text{Bi}_2\text{B}_n\text{O}_{5n+3}$ . They are all built on the same principle: perovskite-like layers, which are formed by cutting the cubic perovskite lattice with parallel planes (001), alternating with bismuth-oxygen layers (Figure 19.21) [378].

state is apparently described by the spatial group  $D_{4h}^{17} - I4/mmm$ .

Adjacent perovskite-like layers are displaced relative to each other by  $a/\sqrt{2}$  in the direction [110]. The result is that in directions [001] segments of the chains from octahedrons in terms of  $n$  octahedrons, connected at the vertices, alternate with segments of chains from  $BiO_{12}$  and  $AO_{12}$  cubic octahedrons, connected to each other by their faces. (It should be pointed out that the surrounding of the Bi ion in the bismuth-oxygen layer can also be regarded as a polyhedron with 13 vertices, rather than as a cubic octahedron, with the result that above one of the square faces of the cubic octahedron there is yet another oxygen ion. Naturally, it is not any farther from the examined bismuth ion than the ion at the vertices of the cubic octahedron).

From a number of works it follows convincingly that the total substitution of  $Bi^{3+}$  by the trivalent ions of the rare-earth elements is impossible in these compounds [388, 396]. As regards the dimensions of ions A and B, since they form a perovskite-like layer the same requirement must be imposed on them as in the case of the perovskite structure, but somewhat more rigid. As stated in [381], changes in the dimensions of perovskite nuclei, which can be distinguished in perovskite-like layers, will lead to expansion or contraction of the bismuth-oxygen layers. Naturally, the possibilities of this expansion or contraction are unlimited.

The geometric criterion (tolerance-factor)  $t$  of the perovskite type structure is used [397] for determining the possibility of the formation of lamellar perovskite-like compounds. It is shown that in such evaluation the formation of the series  $A_{n-3}Bi_4B_nO_{3n+3}$  with  $A = Ba, Ca, Pb$  and  $Bi, B = Ti$  and  $Fe$ , where  $n$  increases from compound to compound, is correctly predicted. It was established, in particular, that in the series  $Ba_{n-3}Bi_4Ti_nO_{3n+3}$ , where the criterion  $t$  increases with the value  $n$ , compounds are formed only to  $n = 6$ . When  $n = 6$ ,  $t = 0.99$ . Hence it is concluded that  $t = 0.99$  is the upper bound of the values of  $t$  at which compounds with a lamellar perovskite-like structure are formed. The lower bound is found to be 0.87. Such an evaluation nevertheless does not explain why there are no zirconates with a lamellar structure. When Ti is substituted by Zr the geometric criterion of the perovskite structure obviously would decrease considerably, indicating the possibility of the formation of the compounds  $Ba_{n-3}Bi_4Zr_nO_{3n+3}$  with a rather large  $n$ . Such compounds, however, do not form. Apparently it would be correct to add to the estimate proposed in [397] another estimate that compares the dimensions of perovskite nuclei with the optimal distances between the bismuth and oxygen ions in bismuth-oxygen layers, for instance with the aid of the geometric criteria:

$$t' = \frac{R_{Bi} + R_O}{R_A + R_O} \quad t'' = \frac{R_{Bi} + R_O}{\sqrt{2}(R_B + R_O)}$$

The condition that  $t'$  and  $t''$  must be close to one limits the sizes of ions A and B, and by the same token the tension or compression of the bismuth-oxygen layers.

Ferroelectrics with a lamellar perovskite-like structure have a rhombically (or more complexly) distorted pseudotetragonal structure below the Curie temperature. Elongation occurs on one of the diagonals of the square base of the tetragonal nucleus, and compression on the other. On this basis Smolenskiy and coworkers [379] proposed that spontaneous polarization in this type of compounds is directed parallel to the plane of the layers (perpendicular to the c axis). Subbarao [389], who found the dielectric hysteresis loop of bismuth titanate monocrystal on the c axis, concluded that the c axis is the ferroelectric axis. Subsequent studies have shown that the spontaneous polarization of bismuth titanate lies nearly in the plane of the layers. We will examine this subject in greater detail below.

The characteristics of ferroelectrics with a lamellar perovskite-like structure are listed in Table 30. It is seen there that when going from Ba compounds to Sr compounds, and then Ca, i.e., with diminishing radius of the A ion, the Curie temperature increases. We will examine in detail only a few of the ferroelectrics listed in Table 30.

Table 30. Ferroelectrics with Lamellar Perovskite-Like Structure

Compound	z	Lattice parameters at 20°C (in Å)			Curie temp., °C	Source
		a	b	c		
PbBi <sub>2</sub> Nb <sub>2</sub> O <sub>9</sub>	2	5.492	5.503	25.53	526-560	379, 386
BaBi <sub>2</sub> Nb <sub>2</sub> O <sub>9</sub>	2	5.552	5.564	25.645	100-200	351, 383
SeBi <sub>2</sub> Nb <sub>2</sub> O <sub>9</sub>	2	5.497	5.505	25.080	430	381, 383
CaBi <sub>2</sub> Nb <sub>2</sub> O <sub>9</sub>	2	5.435	5.455	24.87	575-650	378, 381, 382
Na <sub>0.5</sub> Bi <sub>1.5</sub> Nb <sub>2</sub> O <sub>9</sub>	2	5.47	5.47	26.94	—	378
K <sub>0.5</sub> Bi <sub>1.5</sub> Nb <sub>2</sub> O <sub>9</sub>	2	5.508	5.508	25.28	530	378, 401
Bi <sub>2</sub> TiNbO <sub>9</sub>	2	5.4094	5.453	25.180	600-650, 630	382, 389
PbBi <sub>2</sub> Ta <sub>2</sub> O <sub>9</sub>	2	5.498	5.496	25.41	430	381, 388
SeBi <sub>2</sub> Ta <sub>2</sub> O <sub>9</sub>	2	5.506	5.576	25.680	70-110	381, 384, 388
SrBi <sub>2</sub> Ta <sub>2</sub> O <sub>9</sub>	2	5.515	5.520	25.015	310-335	381, 383, 388
CaBi <sub>2</sub> Ta <sub>2</sub> O <sub>9</sub>	2	5.435	5.4685	24.970	550-600	381, 382
Bi <sub>2</sub> TiTaO <sub>9</sub>	2	5.402	5.436	25.15	870	378, 389
Bi <sub>2</sub> Ti <sub>2</sub> O <sub>12</sub>	3	5.4883	5.4442	32.840	675	383, 387, 385
BaBi <sub>2</sub> Ti <sub>2</sub> O <sub>12</sub>	4	5.447	5.456	41.78	375-400	383, 387, 388
SrBi <sub>2</sub> Ti <sub>2</sub> O <sub>12</sub>	4	5.430	5.428	41.070	530-540	388, 390, 390
CaBi <sub>2</sub> Ti <sub>2</sub> O <sub>12</sub>	4	5.405	5.420	40.900	780	388, 399
PbBi <sub>2</sub> Ti <sub>2</sub> O <sub>12</sub>	4	5.440	5.550	41.360	570	383, 389
Na <sub>0.5</sub> Bi <sub>1.5</sub> Ti <sub>2</sub> O <sub>12</sub>	4	5.427	5.460	40.85	655	388, 389
K <sub>0.5</sub> Bi <sub>1.5</sub> Ti <sub>2</sub> O <sub>12</sub>	4	5.449	5.482	41.15	550	388, 389
Bi <sub>2</sub> SrTi <sub>2</sub> O <sub>12</sub>	4	5.408	5.441	41.05	670	388, 389
Bi <sub>2</sub> FeTi <sub>2</sub> O <sub>12</sub>	4	5.445	5.455	41.31	750	387, 400
Ba <sub>2</sub> Bi <sub>2</sub> Ti <sub>2</sub> O <sub>12</sub>	5	3.88	3.83	56.3	379	393
Sr <sub>2</sub> Bi <sub>2</sub> Ti <sub>2</sub> O <sub>12</sub>	5	3.867	3.861	48.80	285	388, 389
Pb <sub>2</sub> Bi <sub>2</sub> Ti <sub>2</sub> O <sub>12</sub>	5	3.861	3.851	49.70	310	388, 389
Bi <sub>2</sub> Fe <sub>2</sub> Ti <sub>2</sub> O <sub>12</sub>	5	3.890	3.885	55.85	—	387, 400
Bi <sub>2</sub> Fe <sub>2</sub> Ti <sub>2</sub> O <sub>12</sub>	8	5.491	5.502	76.20	—	387, 400

The permittivity of polycrystalline BaBi<sub>2</sub>Nb<sub>2</sub>O<sub>9</sub>, measured at 500 kHz, is 220-280 at room temperature and passes through a smooth maximum near 260°C (Figure 19.22). At 1 kHz, however, the maximum is seen near 100°C.

The curve  $\tan \delta(T)$  has a maximum, the location of which also depends on frequency. Thus, dielectric polarization is of distinctly relaxation character. No dielectric hysteresis loops were evidenced in the 20-150°C temperature range in fields up to 60 kV/cm [381].

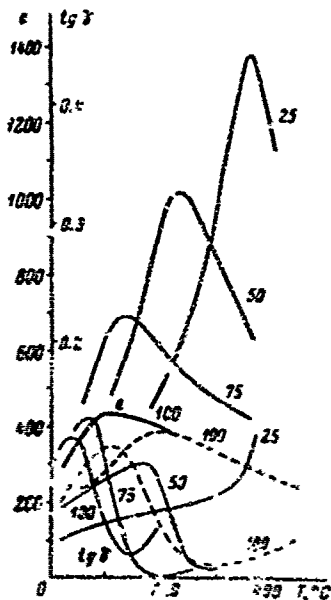


Figure 19.22. Temperature dependence of  $\epsilon$  and  $\tan \delta$  of solid solutions  $(Pb_{1-x}Ba_x)Bi_2Nb_2O_9$  in weak fields at 1 kHz and of compound  $BaBi_2Nb_2O_9$  at 1 kHz (continuous curves) and 450 kHz (broken curves). The numbers near the curves indicate the value of  $x$  in mole % (according to Smolenskiy, et al [381]).

ions get into the bismuth-oxygen layers, substituting Bi ions, whereas some of the Bi ions substitute Ba ions in the perovskite-like layers [381]. Actually, as we have already pointed out, if all Ba ions ( $R = 1.38 \text{ \AA}$ ) are located in a perovskite-like layer, and all Bi ions ( $R = 1.29 \text{ \AA}$ ) are in a bismuth-oxygen layer, the lattice should have large deformations: elongation of the bismuth-oxygen layers and compression of the perovskite-like layers perpendicular to the  $c$  axis. This is clearly seen by comparing the dimensions of the elemental nucleus of  $BaTiO_3$  ( $a = 3.986 \text{ \AA}$ ;  $c = 4.026 \text{ \AA}$ ) and the period  $a_T = 3.912 \text{ \AA}$  of the compound  $BaBi_2Nb_2O_9$ . The migration of some of the Ba ions to the bismuth-oxygen layers and of some of the Bi ions to the perovskite-like layers should reduce, but not completely eliminate,

Solid solutions of  $(Ba, Pb)Bi_2Nb_2O_9$  and  $(Ba, Sr)Bi_2Nb_2O_9$  [381] were analyzed to prove the existence of ferroelectric properties in  $BaBi_2Nb_2O_9$ . The temperature of peak  $\epsilon$  in  $(Ba, Pb)Bi_2Nb_2O_9$  rises by measure of substitution of Ba ions by Pb ion, and the peak itself becomes more distinct, whereupon the dependence of the temperature of the peak on frequency decreases. (Figure 19.22). Dielectric hysteresis loops were found in the investigated solid solutions with a concentration of 25 and 50 mole %  $PbBi_2Nb_2O_9$ . The analogous phenomena are also found in the second system. Hence it may be concluded that solid solutions of these systems are ferroelectric and that  $BaBi_2Nb_2O_9$  is therefore also a ferroelectric. The relaxation character of its dielectric polarization, however, compels the assumption that this compound is a ferroelectric with a blurred phase transition.

The blurring of the phase transition in  $BaBi_2Nb_2O_9$  can be

explained by assuming some of the Ba

compression of the perovskite-like layers. The random distribution of Ba ions migrating into the bismuth-oxygen layers and of Bi ions crossing over into the perovskite-like layers leads to blurring of the phase transition in the nodes of these layers and to dielectric polarization of relaxation character [381].

The gradual substitution of Ba ion in solid solutions by Pb ions causes the average radius of the divalent ion to decrease (for  $Pb^{2+}$   $R = 1.26\text{\AA}$ ); the cause of the redistribution of ions is apparently eliminated little by little and the concentration of divalent ions in bismuth-oxygen layers and of Bi ions in the perovskite-like layers decreases [381]. Here the blurring of the phase transition decreases correspondingly and dielectric polarization gradually loses its relaxation character.

The high permittivity of bismuth titanates has long been known [396, 402]. The ferroelectric properties of  $Bi_4Ti_3O_{12}$  were discovered independently and almost simultaneously by various researchers: in the USSR Smolenskiy and coworkers [381] discovered dielectric hysteresis loops in polycrystalline  $Bi_4Ti_3O_{12}$ , and Ismailzade [383] -- phase transition from the rhombic to tetragonal phase. Abroad Subbarao [387] and Van Uitert and Egerton [395] discovered and quite thoroughly analyzed the ferroelectric properties of this compound.

$Bi_4Ti_3O_{12}$  monocrystals are thin flakes, like mica, readily separating. The c axis is perpendicular to the plane of the flakes. The permittivity in the direction of the c axis is 110-220 at 20°C [395, 403]. Investigations in polarized light [389, 395, 402] showed that the crystals have twinned regions and the twins are shaped like thin strips parallel or perpendicular to each other. Often the twins are spindle-shaped, starting or ending at the middle of the crystal. Twin boundaries like at an angle of 45° to extinction and are parallel to the a axes of the paraelectric phase [389]. The optical illuminance of adjacent regions differs and changes (dark regions become light and conversely) when the crystal is rotated 4° with crossed nicols. The application of a stationary field to the crystal on the c axis did not cause any notable motion of twin boundaries [395, 403]. In a variable field and in stroboscopic light, however, there was notable motion of some of them [395]. Birefringence vanishes at 643°C [395].

In a field parallel to the c axis the hysteresis loop is well expressed, but is, as a rule, asymmetric. After "conditioning" of the crystal in a variable field the loop becomes symmetric and nearly rectangular. Spontaneous polarization, determined on the basis of these loops, varies from  $(1.5-2) \cdot 10^{-6}$  C/cm<sup>2</sup> [402] to  $(3-3.5) \cdot 10^{-6}$  C/cm<sup>2</sup> [389, 395]. As pointed out in [404-406],  $Bi_4Ti_3O_{12}$  has some threshold field, below which dielectric hysteresis loops do not appear. Double loops may occur in higher fields and ordinary loops in even higher fields. In this connection the authors consider the question of the existence of

ferroelectric and antiferroelectric phases, and in many cases speak of ferroelectricity in bismuth titanate.

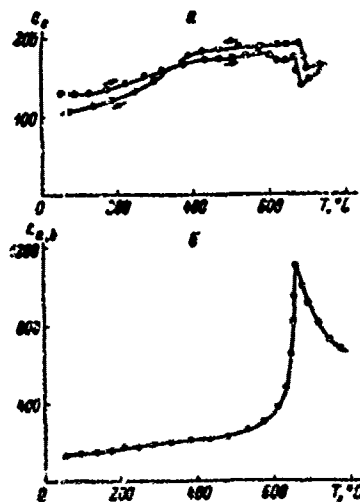


Figure 19.23. Temperature dependence of  $\epsilon_c$  (a) and  $\epsilon_{ab}$  (b) of  $\text{Bi}_4\text{Ti}_3\text{O}_{12}$  monocrystal (according to Kraynik, et al [407]).

An analysis of  $\epsilon$  on the  $c$  axis of monocrystalline  $\text{Bi}_4\text{Ti}_3\text{O}_{12}$  and perpendicular to it was conducted in [407]. It was disclosed here that a sharp  $\epsilon$  peak occurs at the Curie point only perpendicular to the  $c$  axis (Figure 19.23). Processes of repolarization of  $\text{Bi}_4\text{Ti}_3\text{O}_{12}$  and the effect of a stationary field on the hysteresis loops were studied in [408, 409].

Very noteworthy in terms of understanding the phenomena that occur in bismuth titanate, are the works of Cummins and Cross [410, 411]. It is shown in these works that when the plane of the crystal is rotated 10-15° in relation to the plane of the microscope stage it becomes possible to see ferroelectric domains. These domain walls are seen together with the

twin network observed in preceding works. The walls of the domains are displaced by an electric field applied along the  $b$  axis. Hysteresis loops were found in direction  $b$  with a coercive field of 50 kV/cm and

$P_s^{(b)} \approx 30 \cdot 10^{-6}$  C/cm<sup>2</sup>. Spontaneous polarization on the  $c$  axis was  $P_s^{(c)} \approx 4 \cdot 10^{-6}$  C/cm<sup>2</sup>. Hence Cummins and Cross conclude that  $\text{Bi}_4\text{Ti}_3\text{O}_{12}$  has monoclinic symmetry (point group  $m$ ), that spontaneous polarization exceeds  $30 \cdot 10^{-6}$  C/cm<sup>2</sup> and lies at an angle of  $\sim 90^\circ$  to the plane of the crystal, and that reversal of the direction of the component  $P_s^{(c)}$  on the  $c$  axis is not accompanied by a change in the sign of  $P_s^{(b)}$ .

#### §7. Barium Aluminate ( $\text{BaAl}_2\text{O}_4$ )

The ferroelectric properties of  $\text{BaLi}_{2x}\text{Al}_{7-2x}\text{F}_{4x}\text{O}_{4-4x}$  monocrystals with  $x$  from 0.15 to 0.30, the Curie temperature of which lies in the range from 127 to 153°C, and which have a hexagonal lattice with  $a = 10.44$ ,  $c = 8.77$  Å, were described in [412]. Spontaneous polarization was found on the hexagonal axis  $c$ . Hysteresis loops were far from rectangular. Spontaneous polarization varied from  $0.08 \cdot 10^{-5}$  to  $0.15 \cdot 10^{-6}$  C/cm<sup>2</sup>, the coercive field from 4.7 to 20.1 kV/cm.  $P_s$  and  $\bar{\epsilon}_c$  decrease on heating and vanish at the transition point. Permittivity  $\epsilon_c$  varies from 10 to 14 at

room temperature. The ratio of  $\epsilon$  at the peak to  $\epsilon$  at 20°C varies from 1.27 to 1.68.

It is presumed [412] that these crystals have the  $\text{BaAl}_2\text{O}_4$  structure with doubled parameter  $a$  (for  $\text{BaAl}_2\text{O}_4$   $a = 5.209$ ,  $c = 8.761 \text{ \AA}$  [413]). It follows from [414], however, that the parameter  $a$  of  $\text{BaAl}_2\text{O}_4$  is doubled, so that we may assume that the structure of the ferroelectric crystals produced in [412] is the same as that of barium aluminate. According to [413] the symmetry of  $\text{BaAl}_2\text{O}_4$  is described by the centrosymmetric spatial group  $D_6^h-C6_32$ . Apparently, if  $\text{BaAl}_2\text{O}_4$  is also a ferroelectric its paraelectric phase will be characterized by this spatial group.

In contrast to the ferroelectrics examined above, the lattice of  $\text{BaAl}_2\text{O}_4$  is built up of  $\text{AlO}_4$  tetrahedrons connected at the vertices and forming an endless three-dimensional framework. Barium ions are located in the spaces of the framework [413], and they have the coordination number nine: six oxygen ions form the top and bottom faces of the polyhedron, three -- the relatively large equatorial triangle.

The existence of ferroelectric properties in barium aluminate has not yet been proved conclusively.

#### 58. Molybdates of Rare-Earth Elements

The ferroelectric properties of gadolinium molybdate  $\text{Gd}_2(\text{MoO}_4)_3$  were reported in [415]. Gadolinium molybdate, doped with neodymium ( $\text{Gd}_{0.97}\text{Nd}_{0.03}$ ) $_2(\text{MoO}_4)_3$ , with the Curie point 159°C, operated as a laser crystal at -138 and 25°C. A light beam can also be modulated by an electric field with the aid of ferroelectrics containing paramagnetic ions. So far, however, such modulation has not been achieved.

The compound  $\text{Gd}_2(\text{MoO}_4)_3$  has a pseudotetragonal (rhombic) nucleus, belonging to the spatial group  $C$  [sub- and superscripts illegible]-Pba2,  $a$  [illegible sign]  $b = 10.40$  and  $c = 10.66 \text{ \AA}$  [415]. Examination of the crystal in polarized light on the  $c$  axis reveals two families of mutually perpendicular domain boundaries. The boundaries lie at an angle 45° to the  $a$  and  $b$  axes. On heating to 159°C they disappear, and on cooling reappear. The permittivity is  $\epsilon_c \approx 10$  and peaks at the Curie point. Spontaneous polarization, determined according to the hysteresis loops in a field parallel to the  $c$  axis, drops on heating and vanishes at 159°C. Data are listed in Table 31 on the molybdates of certain rare-earth elements according to [416, 417]. The growth of monocrystals of these molybdates (by Chokhrai'skiy's method) is described in [418].

Table 31. Characteristics of Certain Rare-Earth Molybdates

1) Соединение	2) Параметры псевдо-тетрагонального ядра [417], Å		3) $T_{dep}$ (по [410]), °C	4) Диэлектрические характеристики [410]			5) Температура измерения диэлектрических свойств, °C
	a	c		5) $\epsilon_r \cdot 10^6$ , кул./см <sup>2</sup>	6) $F_c$ , кВ/см	7) $\epsilon_r$ , кВ/см	
Pr <sub>2</sub> (MoO <sub>4</sub> ) <sub>3</sub>	7.49	10.87	—	—	—	—	—
Nd <sub>2</sub> (MoO <sub>4</sub> ) <sub>3</sub>	7.40	10.82	—	—	—	—	—
Zn <sub>2</sub> (MoO <sub>4</sub> ) <sub>3</sub>	7.35	10.88	130	0.24	9.5	12	50
Er <sub>2</sub> (MoO <sub>4</sub> ) <sub>3</sub>	7.35	10.87	161	0.14	12.4	9.5	25
Gd <sub>2</sub> (MoO <sub>4</sub> ) <sub>3</sub>	7.31	10.63	159	0.17	5.0	10	25
Th <sub>2</sub> (MoO <sub>4</sub> ) <sub>3</sub>	7.29	10.57	157	0.18	6.3	11	25
Dy <sub>2</sub> (MoO <sub>4</sub> ) <sub>3</sub>	7.29	10.80	—	—	—	—	—
Hf <sub>2</sub> (MoO <sub>4</sub> ) <sub>3</sub>	7.28	10.53	—	—	—	—	—

- KEY: 1. Compound  
 2. Parameters of pseudotetragonal nucleus [417], Å  
 3. Dielectric characteristics [410]  
 4. Temperature at which dielectric properties were measured  
 5.  $\epsilon_r \cdot 10^6$  C/cm<sup>2</sup>  
 6.  $F_c^S$ , kV/cm

### 59. Ferroelectrics of the Type YMnO<sub>3</sub>

Ferroelectrics of the YMnO<sub>3</sub> type crystallize in a hexagonal structure [419-428]. Spontaneous polarization of the order of  $(4-5) \cdot 10^{-6}$  C/cm<sup>2</sup> occurs on the c axis. These ferroelectrics have antiferromagnetic properties at low temperatures. These properties were already discussed in Chapter 18. Therefore we will not examine them in this section. We will point out simply that the low-temperature modifications of the aluminates of yttrium and certain rare-earth elements also have a hexagonal structure with  $a \approx 3.7$  Å and  $c = 10.5$  Å (the high-temperature modifications of these compounds have a structure of the perovskite type) [429]. It is presumed that at temperatures above the Curie point ferroelectrics of the type YMnO<sub>3</sub> have the lattice of the low-temperature modification of YAlO<sub>3</sub>. The lattice of YAlO<sub>3</sub>, as that of YMnO<sub>3</sub> (Figure 18.4), is constructed of trigonal bipyramids of BO<sub>5</sub>, connected together by the vertices of the equatorial triangular section of the bipyramid in flat networks perpendicular to the c axis. These layers of bipyramids are separated from each other by the planes of yttrium ions. The ions of the rare-earth elements or of yttrium are surrounded by eight oxygen ions. This environment can be represented as an octahedron, near which are two oxygen atoms, one above the top face and one below the bottom face. In contrast to the perovskite type structure, the lattice of hexagonal YAlO<sub>3</sub> and YMnO<sub>3</sub> does not have the chains -O-Al-O-Al-O or -O-Mn-O-Mn-O- on the c axis. There are, however, -O-Y-O-Y-O- chains on the c axis.

## 510. Compounds with Boracite Type Structure

Compounds with the general formula  $Me_3^{2+}B_7O_{13}X^-$ , where  $Me^{2+} = Mg, Ni, Co, Fe, Zn, Cd, Cu$  and  $Cr$ , and  $X^- = Cl, Br$  and  $I$ , possess a boracite type structure. This structural type derived its name from the mineral boracite  $Mg_3B_7O_{13}$ . The phase transition from the low-temperature modification to the cubic high-temperature modification occurs in this compound at  $255^\circ C$  [430]. For the cubic modification  $a = 12.1 \text{ \AA}$ , the nucleus contains 8 units and the spatial group is  $T_d^5-F\bar{4}3c$ . The low-temperature modification, the result of weak distortion of the cubic lattice, has rhombic symmetry with  $a \approx 8.54, c = 12.0 \text{ \AA}$ . The nucleus contains 4 units. The spatial group is  $C_{2v}^5-Pca$ .

An idea of the distribution of atoms in the lattice of the high-temperature modification of boracite can be gained from Figure 19.24, which illustrates one-eighth of the cubic elemental nucleus, constructed according to the data in [430]. The vertices of the cube are occupied by chlorine ions, which are surrounded octahedrally by magnesium ions. The magnesium ions, occupying the middle of the edges, form a cubic octahedron. The boron ions, located at the center of the faces of the cube, form an octahedron. On the edges of this octahedron are oxygen ions, which divide the distance from one vertex of the octahedron to the other as 1/3:2/3. Thus, the oxygen ions form 8 oxygen triangles. Four of these triangles are centered by boron ions (in the figure -- the left front and right rear top faces of the octahedron, and also the right front and left rear bottom faces). The four boron ions located in these triangles form a tetrahedron around the oxygen ion located at the center of the cube. These boron ions are displaced somewhat from the plane of the triangle in the direction of the central oxygen ion (this enabled the authors [430] to talk about trigonal  $BO_3$  pyramids). However, the approach to examination of the structure through  $BO_3$  triangles is more convenient and no less correct, if the displacement of the boron ion from the plane of the triangular ring is borne in mind. The elemental nucleus is obtained from the cubes shown in Figure 19.24 by translating them  $a/2$  in directions [100], [010] and [001] and rotating them  $\pi/2$  around these axes. The Mg ions are located in the elongated  $ClO_4Cl$  octahedrons, where the O ions form a nearly square rectangle, the plane of which is perpendicular to the direction Cl-Cl. Four boron ions are located in the oxygen triangles and three in the oxygen tetrahedrons.

It is useful to consider the boracite type structure as  $ClMg_6$  octahedrons connected at the vertices in the same manner as  $TiO_6$  octahedrons are connected in the perovskite structure. All other atoms are located in the spaces between the  $ClMg_6$  octahedrons and perhaps in the initial examination of ferroelectric phenomena they can be viewed temporarily as complex

$(B_7O_{13})^{5-}$  ions. Then the formula of boracite can be written the same as for perovskites in the form  $ABC_3$ , where  $A = (B_7O_{13})^{5-}$ ,  $B = Cl^-$ ,  $C = Mg^{2+}$ .

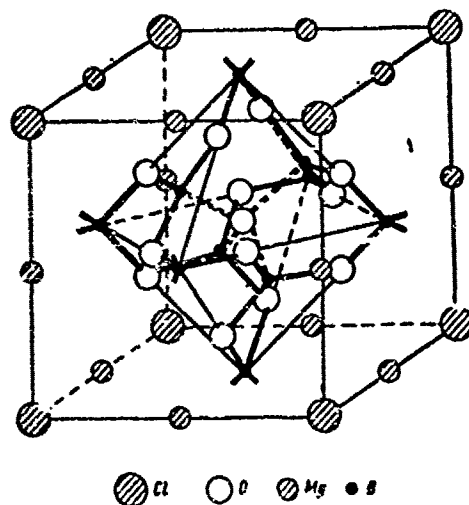


Figure 19.24. Boracite type crystal structure (one-eighth of elemental nucleus).

The distance Mg-Cl in the octahedron is  $a/4 = 3.02 \text{ \AA}$ . The sum of the ionic radii of  $Mg^{2+}$  and  $Cl^-$  is  $0.74 + 1.81 = 2.55 \text{ \AA}$ . Thus, ionic polarizability of  $Cl^-$  should be exceptionally high. After substitution of chlorine by bromine the sum of radii becomes  $0.74 + 1.96 = 2.70 \text{ \AA}$ , and after substitution by iodine --  $0.74 + 2.20 = 2.94 \text{ \AA}$ . Here the ionic polarizability of the halogen decreases sharply, which should lead to a lowering of the phase transition temperature. It is clear from Table 32, where the characteristics of several compounds of the boracite type structure are listed, that the substitution of chlorine by bromine and iodine is actually associated with a substantial reduction of the phase transition temperatures. The only exception is ZnI-boracite. Boracites with Cd, Zn and  $Mn^{2+}$  ions and high electron polarizability, have the maximum  $T_c$ .

The temperature dependence of  $\epsilon$  and  $\tan \delta$  of certain compounds with the boracite structure is illustrated in Figure 19.25 [434]. Here we see that the permittivity is low (of the order of 10). The temperatures of  $\epsilon$  peaks correspond to the phase transition temperatures. In electric fields  $Ni_3B_7O_{13}Cl$ , at temperatures  $10^\circ C$  below the transition point, display motion of domain walls [434]. Thus, the phase transitions are transitions from the nonpolar phase to the polar phase. According to [435] several boracites (FeCl-, FeBr-, FeI-, ClCl-, ZnCl-boracites) have a low-temperature phase transition from the rhombic phase to rhombohedral. The various properties of boracites are also examined in [436-440].

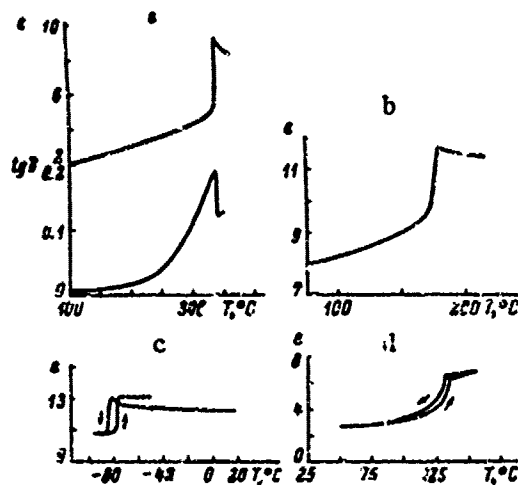


Figure 19.25. Temperature dependence of permittivity and  $\tan \delta$  of various boracite monocrystals (Ascher [434]). a --  $\text{Ni}_3\text{B}_7\text{O}_{13}\text{Cl}$  in direction [100] at 48 MHz; b --  $\text{Co}_3\text{B}_7\text{O}_{13}\text{Br}$  in direction [111] at 100 kHz; c --  $\text{Co}_3\text{B}_7\text{O}_{13}\text{I}$  in direction [111] at 50 kHz, in relative units.

Table 32. Parameters of Pseudocubic Lattice and Phase Transition Temperatures of Compounds with Boracite Structure

Me <sup>2+</sup> ions	X <sup>-</sup> ions					
	Cl		Br			
	a, Å	T <sub>c</sub> , °K	a, Å	T <sub>c</sub> , °K	a, Å	T <sub>c</sub> , °K
Mg	12.070	538	12.079	292	—	—
Ce	12.121	254	12.153	<10(?)	12.171	<10(?)
Mn	12.248	680	12.301	566	12.32	412
Fe	12.177	605	12.190	492	12.225	345
Co	12.123	623	12.108	456	12.119	197
Ni	12.019	610	12.035	398	12.046	61
Cu	11.935	365	11.955	224	—	—
Zn	12.10	723	12.104	586	12.091	687
Cd	12.48	788	12.501	735	12.58	617

### §11. Ferroelectric Chalcogenides of Antimony and Bismuth

The ferroelectric properties of the crystals of compounds of the type  $\text{SbSi}$ , where instead of antimony bismuth may also be used, instead of sulfur-selenium, instead of iodine -- other halogens, were described in [441, 442]. The crystal lattice has rhombic symmetry, both in the paraelectric and in the ferroelectric phases. The lattice parameters at room temperature and at the Curie temperature [441, 443] are presented in Table 33. The c axis is the ferroelectric axis.

Table 33. Lattice Parameters and Curie Temperatures of Ferroelectric Chalcogenides

Compound	Lattice para., Å			$T_c$ , °C
	a	b	c	
SbSBr	8.20	8.70	3.95	-180
SbSI	8.48	10.10	4.16	22
BiSBr	8.02	8.70	4.01	-170
BiSI	8.46	10.15	4.14	-180

The elemental nucleus, described according to Donges [443] by the spatial group  $D_{2h}^{16}$ -Pnam and characteristic of the paraelectric phase, is illustrated in Figure 19.26. The lattice is constructed of  $SbS_4I_4$  polyhedrons. Sulfur ions are located at the vertices of the triangular pyramid, inside which lies the  $Sb^{3+}$  ion. The iodine ions form a rectangle, the plane of which lies between the antimony ions and the more distant sulfur ions. In this way irregular polyhedrons with 8 vertices are formed. They are connected by their vertices, faces and edges so that on the c axis are formed channels with walls constructed of negatively charged iodine and sulfur ions, and positive antimony or bismuth ions are located in the channels.

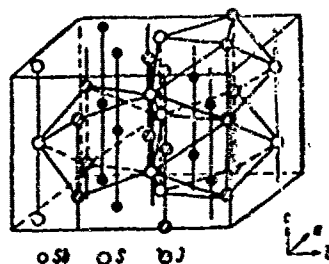


Figure 19.26. Crystal structure of SbSI.

The permittivity of SbSI on the c axis passes through a sharp peak at the transition point:  $\epsilon_{max} = (1-5) \cdot 10^4$ . There are small discontinuities on the curve  $\epsilon_c(T)$  in the 210-230°K region, and also near 160°K [444].

Perpendicular to the c axis  $\epsilon$  is  $\sim 25$  [445]. Spontaneous polarization at 0°C is  $25 \cdot 10^{-6}$  C/cm<sup>2</sup>, the coercive field is  $\sim 100$  V/cm [445]. The piezoelectric properties of SbSI are analyzed in [446, 447]. The piezoelectric modulus  $d_{33}$  in the peak near the Curie point, i.e., near room temperature, reaches  $127 \cdot 10^{-6}$  CGSE. The coefficient of the electromechanical bond  $k_{33}$  reaches 90% near the transition temperature, and near 0°C is equal to 75-85% and changes little on cooling [447]. SbSI is characterized by a large hydrostatic piezoelectric modulus  $d_h$ , reaching  $\sim 45 \cdot 10^{-6}$  CGSE at the peak [446].

The very interesting phenomena in SbSI and isomorphic crystals were discovered and thoroughly analyzed by Fridkin and his coworkers, and also by a number of other Soviet researchers [448-466]. It was shown [448] that the presence of a relatively high concentration of nonequilibrium carriers in ferroelectric semiconductors makes it essential to take into

account the free energy of the electron subsystem in the expansion of the free energy of the crystal in terms of P:

$$F = F_0 + aP^2 + \frac{b}{2}P^4 + \dots + nE_g(P),$$

where  $n$  is the concentration of nonequilibrium carriers, determined by photoconductivity, and  $E_g$  is the width of the forbidden zone. The conclusion is drawn from thermodynamic examination that the width of the forbidden zone should depend on the temperature and pressure in the vicinity of the phase transition in SbSI. This conclusion was confirmed experimentally in [465], where the change in the width of the forbidden zone associated with changing pressure and temperature was recorded on the basis of the displacement of maximum photocurrent, which in SbSI fits on the edge of natural absorption. The width of the forbidden zone remains constant in the ferroelectric phase up to 250 atm. It decreases as hydrostatic pressure is further increased, and  $(\frac{\partial E_g}{\partial p})_T = -(1.3 \pm 0.3) \cdot 10^{-4}$  eV/atm, but at pressures above 1,000 atm it again changes little. The dependence on pressure is slight in the paraelectric state. The width of the forbidden zone decreases as the temperature rises, and rapidly in the phase transition region, where  $(\frac{\partial E_g}{\partial p})_p = -(20 \pm 4) \cdot 10^{-4}$  eV/deg.

The displacement of the Curie temperature of SbSI during illumination of the crystal, predicted by Fridkin, is experimentally proved [450, 453]:

$$\Delta T_c = \frac{\Delta E_g}{\pi (\Delta P_s)^2} C.$$

where  $\Delta P_s$  is the jump of spontaneous polarization,  $C$  is the Curie-Weiss constant. The direction of displacement of  $T_c$  is determined by the sign of  $\Delta E_g$ . It turned out that during illumination, which causes  $n$  to grow two orders of magnitude, the Curie temperature drops 1°C. The displacement is noninertial in relation to the turning on and off of the light.

The character of the temperature dependence of permittivity, the presence of a jump in spontaneous polarization, the existence of sharp phase boundaries between the paraelectric and ferroelectric phases in the vicinity of the phase transition indicate that the ferroelectric phase transition in SbSI is a first order transition.

Many works have been published pertaining to analysis of the optical and semiconductor properties of SbSI and isomorphic ferroelectrics [449, 451-453, 457-460, 462-472], analysis of changes in the crystal

structure during phase transition [473, 475], microscopic observation of domain structure and lattice distortions of SbSI crystals under the influence of various factors [464, 476-478], analysis and discussion of other properties [444, 453-455, 479-485], preparation of crystals [467, 486, 487].

#### BIBLIOGRAPHY

1. Rushman, P. F. and M. A. Strivens, *Trans. Farad. Soc.*, Vol. 42A, p. 231, 1946.
2. Smolenskiy, G. A., DAN SSSR (Reports of USSR Academy of Sciences, Vol. 70, p. 405, 1950.
3. Smolenskiy, G. A., ZhTF [Zhurnal tekhnicheskoy fiziki; Journal of Technical Physics], Vol. 20, p. 137, 1950.
4. Smolenskiy, G. A., DAN SSSR, Vol. 85, p. 985, 1952.
5. Hulm, J. K., *Proc. Phys. Soc.*, Vol. 65A, p. 1184, 1950.
6. Roth, R. S., *J. Res. Nat. Bur. Stand.*, Vol. 58, p. 75, 1957.
7. Granicher, H. and O. Jakits, *Suppl. Nuovo Cim.*, Vol. 11, No. 3, p. 480, 1954.
8. Muller, K. A., *Arch. des Sciences*, Vol. 10, fasc. spec., p. 150, 1957.
9. Muller, K. A., *Helv. Phys. Acta*, Vol. 51, p. 175, 1958.
10. Muller, K. A., *Phys. Rev. Lett.*, Vol. 2, p. 531, 1959.
11. Debroy, W. J., R. F. Vieth and M. I. Browne, *Phys. Rev.*, Vol. 115, p. 79, 1959.
12. deMars, G. A. and L. Rinali, *Bull. Am. Phys. Soc.*, ser. 11, 7, No. 1, Pt. 1, 7, 1962.
13. Rinali, L. and G. A. deMars, *Phys. Rev.*, Vol. 127, p. 762, 1962.
14. Gubin, A. N., A. M. Kashtanova, Ye. A. Potapov and A. A. Shibaev, Fizika tverdogo tela [Solid State Physics], Vol. 4, p. 3223, 1962.
15. Granicher, H., *Arch. des Sciences*, Vol. 11, fasc. spec., p. 28, 1958.
16. Little, E. W., *J. Appl. Phys.*, Vol. 35, p. 2212, 1964.
17. Bogdanov, S. A., A. M. Kashtanova and L. A. Fisekova, Izv. V. SSSR, ser. fiz. (News of USSR Academy of Sciences, Physics Series), Vol. 12, p. 396, 1965.

18. Cross, L. E. and D. Chakravorthy, Proc. Intern. Meet. Ferroelectr., Vol. 1, Prague, p. 394, 1966.
19. Todd, S. S. and R. E. Lorenson, J. Am. Chem. Soc., Vol. 74, p. 2043, 1952.
20. Hegenbarth, E., Phys. St. Sol., Vol. 2, p. 1544, 1962.
21. Levin, S. B., N. J. Field, F. M. Plock and L. Merker, J. Opt. Soc. Am., Vol. 45, p. 737, 1955.
22. Merker, L., Mining Engng., Vol. 7, p. 645, 1955.
23. Gorina, Yu. I., A. M. Kashtanova, G. V. Maksimova and G. I. Skanavi, Kristallografiya (Crystallography), Vol. 6, p. 473, 1961.
24. Mitsui, T. and W. B. Westphal, Phys. Rev., Vol. 124, p. 1354, 1961.
25. Sawaguchi, E., A. Kikuchi and J. Kadera, J. Phys. Soc. Japan, vol. 18, p. 459, 1963.
26. Rupprecht, G. and R. O. Bell, Phys. Rev., Vol. 135, 1748, 1964.
27. Linz, A., Phys. Rev., Vol. 91, p. 753, 1953.
28. Youngblood, J. F., Phys. Rev., Vol. 95, p. 1291, 1955.
29. Granicher, H., Helv. Phys. Acta, Vol. 29, p. 210, 1956.
30. Novosiltsev, N. S., A. L. Khodakov, M. I. Sholokhevich, Ye. G. Fesenko and O. P. Kramarov, Izv. AN SSSR, ser. fiz., Vol. 21, p. 293, 1957.
31. Weaver, H. E., J. Phys. Chem. Sol., Vol. 11, p. 274, 1959.
32. Gubkin, A. V., A. M. Kashtanova and G. I. Skanavi, ITF, Vol. 3, p. 1110, 1961.
33. Winter, W. H. and G. Rupprecht, Bull. Am. Phys. Soc., ser. II, Vol. 7, No. 7, p. 133, 1962.
34. Hegenbarth, E., Monatsber. Deutsch. Akad. Wiss., Berlin, Vol. 1, p. 411, 1959.
35. Sawaguchi, E., A. Kikuchi and J. Kadera, J. Phys. Soc. Japan, Vol. 17, p. 106, 1962.
36. Itchner, D. and H. Granicher, Helv. Phys. Acta, Vol. 37, p. 624, 1964.
37. Schmidt, G. and E. Hegenbarth, Phys. St. Sol., Vol. 5, p. 529, 1963.
38. Hegenbarth, E., Phys. St. Sol., Vol. 6, p. 353, 1964.

39. Barrett, J. H., Phys. Rev., Vol. 86, p. 118, 1952.
40. Rupprecht, G., R. O. Bell and B. D. Silverman, Phys. Rev., Vol. 123, p. 97, 1961.
41. Rupprecht, G. and R. O. Bell, Phys. Rev., Vol. 125, p. 1915, 1962.
42. Silverman, B. D., Phys. Rev., Vol. 125, p. 1921, 1962.
43. Moreno, M. and H. Granicher, Helv. Phys. Acta, Vol. 37, p. 624, 1964.
44. Samara, G. A. and A. A. Giardini, Phys. Rev., Vol. 140, A954, 1965.
45. Poindexter, E. and A. A. Giardini, Phys. Rev., Vol. 110, p. 1069, 1958.
46. Bell, R. O. and G. Rupprecht, Bull. Am. Phys. Soc., Vol. 7, No. 1, pt. 1, p. 7, 1962.
47. Krogstad, B. S. and R. W. Moss, Bull. Am. Phys. Soc., ser. II Vol. 7, No. 3, p. 192, 1962.
48. Rupprecht, G. and W. H. Winter, Phys. Rev., Vol. 155, p. 1019, 1967.
49. Cowley, R. A., Phys. Rev., Vol. 134, A981, 1964.
50. Horner, H., Phys. Lett., Vol. 25A, p. 464, 1967.
51. Murzin, V. N. and A. I. Demeshina, FTT, Vol. 5, p. 2359, 1963.
52. Murzin, V. N. and A. I. Demeshina, Izv. AN SSSR, ser. fiz., Vol. 28, p. 695, 1964.
53. Murzin, V. N., A. I. Demeshina and S. V. Bogdanov, Izv. AN SSSR, ser. fiz., Vol. 29, p. 920, 1965.
54. Solov'yev, S. P., O. L. Kukhto, N. A. Chernoplekov and M. G. Zemlyakov, FTT, Vol. 8, p. 2699, 1966.
55. Stekhanov, A. I. and A. A. Karamyan, FTT, Vol. 8, p. 448, 1966; Izv. AN SSSR, ser. fiz., Vol. 31, p. 1104, 1967.
56. Yatsenko, A. F., Izv. AN SSSR, ser. fiz., Vol. 22, p. 1456, 1958; Vol. 24, p. 1308, 1960.
57. Barker, A. S., Phys. Rev., Vol. 145, p. 391, 1966.
58. Barker, A. S. and J. J. Hopfield, Phys. Rev., Vol. 135A, p. 1732, 1964.
59. Barker, A. S. and M. Tinkham, Phys. Rev., Vol. 125, p. 1527, 1962.
60. Cowley, R., Phys. Rev. Lett., Vol. 9, p. 159, 1962.

61. Fraitova, D. and A. Zentkova, Czechosl. Fiz. Zh. (Czechoslovakian Physics Journal), Vol. 13, p. 670, 1963.
62. Gandy, H. F., Phys. Rev., Vol. 113, p. 795, 1959.
63. Last, J. T., Phys. Rev., Vol. 105, p. 1740, 1957.
64. Narayanan, R. S. and K. Vedam, Zs. Phys., Vol. 163, p. 158, 1961.
65. Noland, J. A., Phys. Rev., Vol. 94, p. 724, 1954.
66. O'Shea, D. C., R. V. Kolluri and H. Z. Cummins, Sol. St. Comm., Vol. 5, p. 241, 1967.
67. Perry, C. H., B. N. Khanna and G. Rupprecht, Phys. Rev., Vol. 135, A408, 1964.
68. Rajagopal, A. K. and R. Srinivasan, Phys. Chem. Sol., Vol. 23, p. 633, 1962.
69. Rimai, L. and J. L. Parsons, Sol. St. Comm., Vol. 5, p. 387, 1967.
70. Rupprecht, G., Bull. Am. Phys. Soc., ser. II, Vol. 7, No. 7, p. 7, 1962.
71. Rupprecht, G., Phys. Rev. Lett., Vol. 12, p. 580, 1964.
72. Sabzberg, C. D., J. Opt. Soc. Am., Vol. 51, p. 1149, 1961.
73. Schaufele, R. F. and M. J. Weber, J. Chem. Phys., Vol. 46, p. 2859, 1967.
74. Schaufele, R. F., M. J. Weber and B. D. Silverman, Phys. Lett., Vol. 25A, p. 47, 1967.
75. Silverman, B. D. and G. F. Koster, Zs. Phys., Vol. 165, p. 334, 1961.
76. Spitzer, W. G., R. C. Miller, D. A. Kleinman and L. E. Howarth, Phys. Rev., Vol. 126, p. 1710, 1962.
77. Turlier, P., L. Eyraud and C. Eyraud, Compt. rend., Vol. 243, p. 659, 1956.
78. Aisenberg, S., H. Statz and G. F. Koster, Phys. Rev., Vol. 116, p. 811, 1959.
79. Bhide, V. G. and H. C. Bhasin, Phys. Rev., Vol. 159, p. 586, 1967.
80. Bhide, V. G., H. C. Bhasin and G. K. Shenov, Phys. Lett., Vol. 24A, p. 109, 1967.
81. Muller, K. A., Proc. Intern. Meet. Ferroelectr., Vol. 2, Prague, p. 369, 1966.

82. Rimai, L., T. Deutsch and R. D. Silverman, Phys. Rev., Vol. 133, A1123, 1964.
83. Sakudo, T., H. Unoki and J. Fujii, J. Phys. Soc. Japan, Vol. 21, p. 2739, 1966.
84. Unoki, H. and T. Sakudo, J. Phys. Soc. Japan, Vol. 23, p. 546, 1967.
85. Weber, M. J. and R. R. Allen, J. Chem. Phys., Vol. 38, p. 720, 1963.
86. Ambler, E., J. H. Colwell, W. R. Hosler and J. F. Schooley, Phys. Rev., Vol. 148, p. 280, 1966.
87. Brews, J. S., Phys. Rev. Lett., Vol. 18, p. 662, 1967.
88. Cardona, M., Phys. Rev., Vol. 140, A631, 1965.
89. Cox, G. A. and R. H. Treder, J. Brit. J. Appl. Phys., Vol. 16, p. 117, 1965.
90. Eagles, D. M., J. Phys. Chem. Sol., Vol. 26, p. 472, 1965.
91. Frederikse, H. P. R. and W. R. Hosler, Phys. Rev., Vol. 161, p. 822, 1967.
92. Frederikse, H. P. R., W. R. Hosler, W. K. Thurber, J. Rabenstein and R. Siebenmann, Phys. Rev., Vol. 158, p. 775, 1967.
93. Frederikse, H. P. R., W. R. Thurber and W. R. Hosler, Phys. Rev., Vol. 154, p. A142, 1964.
94. Kahn, A. H. and A. J. Leyendecker, Phys. Rev., Vol. 123, A1321, 1961.
95. Kaiser, W. and R. Zurek, Phys. Lett., Vol. 23, p. 608, 1966.
96. Koonce, C. S., M. L. Cohen, J. F. Schooley, W. R. Hosler and E. C. Pfeiffer, Phys. Rev., Vol. 165, p. 380, 1961.
97. Paladino, A. E., J. Am. Ceram. Soc., Vol. 48, p. 476, 1965.
98. Paladino, A. E., J. F. Pugh and E. S. Rigsby, J. Phys. Chem. Sol., Vol. 26, p. 501, 1965.
99. Pfeiffer, E. C. and J. F. Pugh, J. Phys. Chem. Lett., Vol. 12, p. 783, 1967.
100. Rados, W. H. and J. F. Pugh, J. Am. Ceram. Soc., Vol. 49, p. 511, 1966.
101. Schooley, J. F., W. R. Hosler and M. J. Allen, Phys. Rev. Lett., Vol. 12, p. 474, 1964.

102. Schooley, J. F., W. R. Hosler, E. Ambler, J. H. Becker, M. L. Cohen and C. S. Koonce, *Phys. Rev. Lett.*, Vol. 14, p. 305, 1965.
103. Sihvonen, Y. T., *J. Appl. Phys.*, Vol. 38, p. 4431, 1967.
104. Simanek, E. and Z. Sroubek, *Phys. St. Sol.*, Vol. 8, K47, 1965.
105. Walters, L. C. and R. E. Grace, *J. Phys. Chem. Sol.*, Vol. 28, pp. 239 and 245, 1967.
106. Waugh, J. S., A. E. Paladino, B. di Benedetto and R. Wantman, *J. Amer. Ceram. Soc.*, Vol. 46, p. 60, 1963.
107. Weber, M. J. and R. F. Schaufele, *J. Chem. Phys.*, Vol. 43, p. 1702, 1965.
108. Weber, M. J. and R. F. Schaufele, *Phys. Rev.*, Vol. 138, p. 1544, 1965.
109. Yamamoto, H., S. Makishima and S. Shionoya, *J. Phys. Soc. Japan*, Vol. 23, p. 1321, 1967.
110. Yasunaga, H. and I. Nakada, *J. Phys. Soc. Japan*, Vol. 22, p. 388, 1967.
111. Hegenbarth, E., *Phys. St. Sol.*, Vol. 8, p. 59, 1965.
112. Hegenbarth, E., *Proc. Intern. Meet. Ferroelectr.*, Vol. 1, Prague, p. 104, 1966.
113. Kikuchi, A. and F. Sawaguchi, *J. Phys. Soc. Japan*, Vol. 19, p. 1497, 1964.
114. Sueneno, Y., *J. Phys. Soc. Japan*, Vol. 20, p. 174, 1965.
115. Granicher, H. and W. N. Lawless, *Helv. Phys. Acta*, Vol. 38, p. 362, 1965.
116. Lawless, W. N. and H. Granicher, *Proc. Intern. Meet. Ferroelectr.*, Vol. 1, Prague, p. 69, 1966.
117. Lawless, W. N. and H. Granicher, *Phys. Rev.*, Vol. 157, p. 440, 1967.
118. Megaw, H. D., *Trans. Farad. Soc.*, Vol. 42A, p. 224, 1946.
119. Megaw, H. D., *Proc. Roy. Soc.*, Vol. A189, p. 261, 1947.
120. Jonker, G. H. and J. van Santen, *Chem. Weekblad*, Vol. 43, p. 672, 1947.
121. Smolenskiy, G. A., *ZhTE*, Vol. 21, p. 1045, 1951.
122. Shirane, G., S. Hoshino and K. Suzuki, *J. Phys. Soc. Japan*, Vol. 5, p. 453, 1950.

123. Shirane, G., S. Hoshino and K. Suzuki, *Phys. Rev.*, Vol. 80, p. 1105, 1950.
124. Shirane, G. and S. Hoshino, *J. Phys. Soc. Japan*, Vol. 6, p. 265, 1951.
125. Fesenko, Ye. G., O. P. Kramarov, A. L. Khodakov and M. L. Sholokhovich, *Izv. AN SSSR, ser. fiz.*, Vol. 21, p. 305, 1957.
126. Fesenko, Ye. G., *DAN SSSR*, Vol. 88, p. 785, 1953.
127. Kobayashi, J. and R. Ueda, *Phys. Rev.*, Vol. 99, p. 1900, 1955.
128. Kobayashi, J., S. Okamoto and R. Ueda, *Phys. Rev.*, Vol. 103, p. 830, 1956.
129. Nomura, S. and J. Kobayashi, *J. Phys. Soc. Japan*, Vol. 13, p. 114, 1958.
130. Shirane, G., R. Pepinsky and B. C. Frazer, *Phys. Rev.*, Vol. 97, p. 1178, 1955.
131. Shirane, G., R. Pepinsky and B. C. Frazer, *Acta Cryst.*, Vol. 9, p. 111, 1956.
132. Kramarov, O. P., A. L. Khodakov, M. L. Sholokhovich and Ye. G. Fesenko, *Segnetoelektriki (Ferroelectrics)*, Rostov State University Publishing House, 1961.
133. Shirane, G. and E. Sawaguchi, *Phys. Rev.*, Vol. 81, p. 458, 1951.
134. Nomura, S. and S. Sawada, *J. Phys. Soc. Japan*, Vol. 10, p. 108, 1955.
135. Sholokhovich, M. L., Ye. G. Fesenko, O. P. Kramarov and A. L. Khodakov, *DAN SSSR*, Vol. 111, p. 1025, 1956.
136. Shirane, G. and R. Pepinsky, *Phys. Rev.*, Vol. 98, p. 1201, 1955.
137. Fesenko, Ye. G. and R. V. Kolesova, *Kristallografiya*, Vol. 4, p. 62, 1959.
138. Bhide, V. G., K. G. Desmuth and M. S. Hedge, *Physica*, Vol. 28, p. 871, 1962.
139. Kanzig, W., *Segnetoelektriki i Antisegnetoelektriki (Ferroelectrics and Antiferroelectrics)*, IL [Foreign Literature] Publishing House, Moscow, 1960.
140. Kinase, W., J. Kobayashi and N. Yamada, *Phys. Rev.*, Vol. 116, p. 348, 1959.
141. Mayssner, L. B. and A. S. Sonin, *FTT*, Vol. 7, p. 3657, 1965.

142. Kobayashi, J., *J. Appl. Phys.*, Vol. 29, p. 866, 1958.
143. Belyayev, I. N. and A. L. Khodakov, *ZhETF* [Zhurnal eksperimental'noy i teoreticheskoy fiziki; Journal of Experimental and Theoretical Physics], Vol. 22, p. 376, 1952.
144. Tien, T. Y. and W. G. Carlson, *J. Am. Ceram. Soc.*, Vol. 45, p. 576, 1962.
145. Matsuo, Y., M. Fujimura and H. Sasaki, *J. Am. Ceram. Soc.*, Vol. 48, p. 111, 1965.
146. Blokhin, M. A., *DAN SSSR*, Vol. 95, p. 965, 1954.
147. Blokhin, M. A., *DAN SSSR*, Vol. 95, p. 1165, 1954.
148. Kabalkina, S. S. and D. F. Vereshchagin, *DAN SSSR*, Vol. 143, p. 818, 1962.
149. Stekhanov, A. I., A. A. Karamyan and N. I. Astaf'yev, *FTT*, Vol. 7, p. 157, 1965.
150. Gainon, D. J. A., *Phys. Rev.*, Vol. 134, A 1300, 1964.
151. Perry, C. H., B. N. Khanna and G. Rupprecht, *Phys. Rev.*, Vol. 135, A 408, 1964.
152. Megaw, H. D., *Acta Cryst.*, Vol. 7, p. 187, 1954.
153. Belyayev, I. N., *Izv. AN SSSR, ser. fiz.*, Vol. 22, p. 1436, 1958.
154. Venevtsev, Yu. N., G. S. Zhdanov, S. P. Solov'yev and Yu. A. Zubov, *Kristallografiya*, Vol. 3, p. 473, 1968.
155. Smolenskiy, G. A., V. A. Isupov, A. I. Agranovskaya and N. N. Kraynik, *FTT*, Vol. 2, p. 2982, 1960.
156. Smolenskiy, G. A., *ZhTF*, Vol. 27, p. 1778, 1957.
157. Orgel, L. E., *J. Chem. Soc.*, No. 12, p. 3315, 1959.
158. Megaw, H. D., *Proc. Phys. Soc.*, Vol. 58, p. 133, 1946.
159. Kay, H. F. and J. L. Miles, *Acta Cryst.*, Vol. 10, p. 213, 1957.
160. Hezenbarth, E., *Cryogenics*, Vol. 1, p. 242, 1961.
161. Isupov, V. A., *Kristallografiya*, Vol. 4, p. 603, 1959.
162. Lyubimov, V. N., Yu. N. Venevtsev and G. S. Zhdanov, *Kristallografiya*, Vol. 7, p. 12, 1962.

163. Rodicheva, E. N., V. M. Lebedev, Z. I. Shapiro, S. A. Fedulov and Yu. N. Venevtsev, Proc. Intern. Meet. Ferroelectr., Vol. 1, Prague, p. 370, 1966.
164. Ivanova, V. V., A. G. Kapyshev, Yu. N. Venevtsev and G. S. Zhdanov, Izv. AN SSSR, ser. fiz., Vol. 24, p. 354, 1962.
165. Bckiy, G. B., Vvedeniye v Kristallokhimiyu (Introduction to Crystallo-Chemistry), MGU [Moscow State University] Publishing House, 1960.
166. Matthias, B. T., Phys. Rev., Vol. 75, p. 1771, 1949.
167. Matthias, B. T. and J. P. Remeika, Phys. Rev., Vol. 82, p. 727, 1951.
168. Wood, E. A., Acta Cryst., Vol. 4, p. 353, 1951.
169. Vousden, P., Acta Cryst., Vol. 4, p. 375, 1951.
170. Shirane, G., H. Danner, A. Pavlovic and R. Pepinsky, Phys. Rev., Vol. 95, p. 672, 1954.
171. Shirane, G., R. Newnham and R. Pepinsky, Phys. Rev., Vol. 96, p. 581, 1954.
172. Katz, L. and H. D. Megaw, Acta Cryst., Vol. 22, p. 639, 1967.
173. Cotts, R. M. and W. D. Knight, Phys. Rev., Vol. 96, p. 1285, 1954.
174. Triebwasser, S. and J. Halpern, Phys. Rev., Vol. 98, p. 1562, 1955.
175. Triebwasser, S., Phys. Rev., Vol. 101, p. 995, 1956.
176. Hall, J. J. and S. Triebwasser, J. Am. Chem. Soc., Vol. 81, p. 6395, 1959.
177. Egerton, L. and D. M. Dillon, J. Am. Ceram. Soc., Vol. 42, p. 458, 1959.
178. Hewitt, R. R., Phys. Rev., Vol. 121, p. 45, 1961.
179. Kurtz, S. K., Proc. Intern. Meet. Ferroelectr., Vol. 1, Prague, p. 415, 1966.
180. Frova, A. and P. J. Boddy, Phys. Rev., Vol. 153, p. 606, 1967.
181. Timofeyeva, V. A. and V. Z. Bychkov, Rost Kristalloy (Growth of Crystals), No. 4, "Nauka" Publishing House, Moscow, p. 140, 1964.
182. Miller, C. E., J. Appl. Phys., Vol. 29, p. 255, 1958.
183. Reisman, A., F. Holtberg, S. Triebwasser and M. Berkenblit, J. Am. Chem. Soc., Vol. 78, p. 719, 1956.

184. Hulm, J. K., B. T. Matthias and E. A. Long, *Phys. Rev.*, Vol. 79, p. 885, 1950.
185. Geusic, J. C., S. K. Kurtz, T. J. Nelson and S. H. Wemple, *Appl. Phys. Lett.*, Vol. 2, p. 185, 1963.
186. Miller, R. C. and W. G. Spitzer, *Phys. Rev.*, Vol. 129, p. 94, 1963.
187. Baer, W. C., *Phys. Rev. Lett.*, Vol. 16, p. 729, 1966.
188. Fleury, P. A. and J. M. Worlock, *Phys. Rev. Lett.*, Vol. 18, p. 665, 1967.
189. Joseph, R. J. and B. D. Silverman, *J. Phys. Chem. Sol.*, Vol. 25, p. 1125, 1964.
190. Perry, C. H. and T. F. McNelly, *Phys. Rev.*, Vol. 154, p. 456, 1967.
191. Schaufele, R. F., M. J. Weber and J. C. Waugh, *Phys. Rev.*, Vol. 140, A872, 1965.
192. Shirane, G., R. Nathans and V. J. Minkiewicz, *Phys. Rev.*, Vol. 157, p. 396, 1967.
193. Wemple, S. H., *Bull. Am. Phys. Soc.*, ser. II, Vol. 8, No. 1, p. 62, 1963.
194. Benneth, L. N. and J. I. Budnik, *Phys. Rev.*, Vol. 120, p. 1812, 1960.
195. Unoki, H. and T. Sakudo, *J. Phys. Soc. Japan*, Vol. 21, p. 1730, 1966.
196. Kahng, D. and S. H. Wemple, *J. Appl. Phys.*, Vol. 36, p. 2925, 1965.
197. Seuhouso, L. S., G. E. Smith and M. V. De Paolis, *Phys. Rev. Lett.*, Vol. 15, p. 776, 1965.
198. Wemple, S. H., *Phys. Rev.*, Vol. 157, A1575, 1965.
199. Wemple, S. H., D. Kahng and H. J. Braun, *J. Appl. Phys.*, Vol. 38, p. 353, 1967.
200. Smolenskiy, G. A. and A. I. Agranovskaya, *ZhTF*, Vol. 28, p. 1491, 1958.
201. Bokov, V. A. and I. Ye. Myl'nikova, *FTT*, Vol. 2, p. 2728, 1960.
202. Myl'nikova, I. Ye. and V. A. Bokov, *Rost Monokristallov* (Growth of Monocrystals), No. 3 USSR Academy of Sciences Publishing House, Moscow, p. 438, 1961.
203. Smolenskiy, G. A., A. I. Agranovskaya and V. A. Isupov, *IJT*, Vol. 1, p. 990, 1959.

204. Ismailzade, I. G., Kristallografiya, Vol. 5, p. 316, 1960.
205. Smolenskiy, G. A. and A. I. Agranovskaya, FTT, Vol. 1, p. 1562, 1959.
206. Agranovskaya, A. I., Izv. AN SSSR, ser. fiz., Vol. 24, p. 1275, 1960.
207. Smolenskiy, G. A., V. A. Isupov, A. I. Agranovskaya and S. N. Popov, FTT, Vol. 2, p. 2906, 1960.
208. Bokov, V. A. and I. Ye. Myl'nikova, FTT, Vol. 3, p. 841, 1961.
209. Berezhnov, A. A., Izv. AN SSSR, ser. fiz., Vol. 81, p. 1154, 1967.
210. Bonner, W. A., E. F. Dearborn, J. E. Geusik, H. M. Marcos and L. G. Van Uitert, Appl. Phys. Lett., Vol. 10, p. 163, 1967.
211. Smolenskiy, G. A., N. N. Kraynik, A. A. Berezhnoy and I. Ye. Myl'nikova, FTT, Vol. 10, p. 467, 1968.
212. Venevtsev, Yu. N. et al, DAN SSSR, Vol. 158, p. 86, 1964.
213. Tomashpoi'skiy, Yu. Ya. and Yu. N. Venevtsev, FTT, Vol. 7, p. 517, 1965.
214. Bokov, V. A., I. Ye. Myl'nikova and G. A. Smolenskiy, ZhETF, Vol. 42, p. 643, 1962.
215. Roginskaya, Yu. Ye., Yu. N. Venevtsev and G. S. Zhdanov, ZhETF, Vol. 48, p. 1224, 1965.
216. Viskov, A. S., Yu. N. Venevtsev and G. S. Zhdanov, DAN SSSR, Vol. 162, p. 325, 1963.
217. Venevtsev, Yu. N., A. G. Kapyshev, A. S. Viskov, V. M. Levedev, V. M. Petrov and G. S. Zhdanov, Proc. Int. Meet. Ferroelectr., Vol. 1, Prague, p. 261, 1966.
218. Smolenskiy, G. A., V. A. Isupov and A. I. Agranovskaya, FTT, Vol. 1, p. 170, 1959.
219. Smolenskiy, G. A., A. I. Agranovskaya, S. N. Popov and V. A. Isupov, ZhTF, Vol. 28, p. 2152, 1958.
220. Smolenskiy, G. A., A. I. Agranovskaya, V. A. Isupov and S. N. Popov, Fizika Dielektrikov (Physics of Dielectrics), USSR Academy of Sciences Publishing House, Moscow, p. 339, 1960.
221. Smolenskiy, G. A., A. I. Agranovskaya and V. A. Isupov, FTT, Vol. 1, p. 977, 1959.
222. Ismailzade, I. G., Kristallografiya, Vol. 4, p. 417, 1959.

223. Johnson, V. J., M. W. Valenta, J. E. Dougherty, R. M. Douglas and J. W. Meadows, *J. Phys. Chem. Sol.*, Vol. 24, p. 85, 1963.
224. Isupov, V. A., A. I. Agranovskaya and N. P. Khuchua, *Izv. AN SSSR, ser. fiz.*, Vol. 24, p. 1271, 1960.
225. Buhner, C. F., *J. Chem. Phys.*, Vol. 36, p. 798, 1962.
226. Khuchua, N. P., Candidate Dissertation, Institute of Semiconductors, USSR Academy of Sciences, Leningrad, 1967.
227. Khuchua, N. P., *Proc. Int. Meet. Ferroelectr.*, Vol. 2, Prague, p. 161, 1966.
228. Yudin, V. M., A. G. Tutov, A. B. Sherman and V. A. Isupov, *Izv. AN SSSR, ser. fiz.*, Vol. 31, p. 1798, 1967.
229. Platonov, G. L., Yu. Ya. Tomashpol'skiy, Yu. N. Venevtsev and G. G. Zhdanov, *Izv. AN SSSR, ser. fiz.*, Vol. 31, p. 90, 1967.
230. Kupriyanov, M. F. and Ye. G. Fesenko, *Izv. AN SSSR, ser. fiz.*, Vol. 31, p. 1086, 1967.
231. Karantaesis, T. and L. Capatos, *Compt. rend.*, Vol. 291, p. 74, 1935.
232. Christensen, A. N. and S. E. Rasmussen, *Acta Chem. Scand.*, Vol. 19, p. 421, 1965.
233. Møller, C. K., *Nature*, Vol. 182, p. 1436, 1958.
234. Møller, C. K., *Mat.-Fys. Medd. Dan. Vid. Selsk.*, Vol. 32, No. 2, 1959.
235. Møller, C. K., *Kgl. Dan. Vid. Selsk. Mat.-Fys. Medd.*, Vol. 32, No. 1, pp. 1-18; No. 2, pp. 1-27, 1959.
236. Ainger, F. W., C. C. Clark, A. Marsh and P. Waterworth, *Proc. Int. Meet. on Ferroelectr.*, Vol. 1, Prague, p. 295, 1966.
237. Matthias, B. T. and J. P. Remeika, *Phys. Rev.*, Vol. 76, p. 1886, 1949.
238. Shapiro, Z. I., S. A. Fedulov and Yu. N. Venevtsev, *FTI*, Vol. 6, p. 316, 1964.
239. Shiozaki, Y. and T. Mitsui, *J. Phys. Chem. Sol.*, Vol. 24, p. 1057, 1961.
240. Isupov, V. A., *Segnetoelektriki (Ferroelectrics)*, Rostov State University Publishing House, p. 109, 1968.
241. Abrahams, S. C., J. M. Reddy and J. L. Bernstein, *J. Phys. Chem. Sol.*, Vol. 27, pp. 59 and 997, 1966.

242. Abrahams, S. C., W. C. Hamilton and J. M. Reddy, *J. Phys. Chem. Sol.*, Vol. 27, p. 1013, 1966.
243. Abrahams, S. C., H. J. Levinstein and J. M. Reddy, *J. Phys. Chem. Sol.*, Vol. 27, p. 119, 1966.
244. Smolenskiy, G. A., N. N. Kraynik, N. P. Khuchua, V. V. Zhdanova and I. E. Mylnikova, *Phys. St. Sol.*, Vol. 13, p. 309, 1966.
245. Ismailzade, I. G., *Kristallografiya*, Vol. 10, p. 287, 1965.
246. Shapiro, Z. I., S. A. Fedulov, Yu. N. Venevtsev and L. G. Rigerman, *Kristallografiya*, Vol. 10, p. 869, 1965.
247. Shapiro, Z. I., S. A. Fedulov, L. G. Rigerman and Yu. N. Venevtsev, *Proc. Int. Meet. Ferroelectr.*, Vol. 1, Prague, p. 277, 1966.
248. Vasilevskaya, A. S., A. S. Sonin, I. S. Rez and T. A. Plotinskaya, *Izv. AN SSSR, ser. fiz.*, Vol. 31, p. 1159, 1967.
249. Iwasaki, H., H. Toyoda and H. Kubota, *J. Appl. Phys.*, Vol. 6, p. 1533, 1967.
250. Chkalova, V. V., V. S. Bondarenko, and Z. I. Shapiro, *Izv. AN SSSR, Neorgan. Materialy* (News of USSR Academy of Sciences, *Inorganic Materials*), Vol. 3, p. 1715, 1967.
251. Yamada, T., N. Niizeki and H. Toyoda, *Japan J. Appl. Phys.*, Vol. 6, p. 151, 1967.
252. Shimada, Y., K. Sawamoto and H. Toyoda, *Japan J. Appl. Phys.*, Vol. 6, p. 1467, 1967.
253. Savage, A., *J. Appl. Phys.*, Vol. 7, p. 5071, 1966.
254. Roytberg, M. B., Z. I. Shapiro and A. Z. Rabinovich, *FIZ*, Vol. 9, p. 3613, 1967.
255. Iwasaki, H., N. Uchida and T. Yamada, *Japan J. Appl. Phys.*, Vol. 6, p. 1336, 1967.
256. Nassau, K., H. J. Levinstein and G. M. Loiacono, *Appl. Phys. Lett.*, Vol. 6, p. 228, 1965.
257. Nassau, K., H. J. Levinstein and G. M. Loiacono, *J. Phys. Chem. Sol.*, Vol. 27, p. 983, 1966.
258. Levinstein, H. J., A. A. Ballman and C. D. Capio, *J. Appl. Phys.*, Vol. 37, p. 4585, 1966.

259. Niizeki, N., T. Yamada and H. Toyoda, Japan J. Appl. Phys., Vol. 6, p. 318, 1967.
260. Nassau, K. and H. J. Levinstein, Appl. Phys. Lett., Vol. 7, p. 69, 1965.
261. Nassau, K., H. J. Levinstein and G. M. Loiacono, J. Phys. Chem. Sol., Vol. 27, p. 989, 1966.
262. Frazer, D. B. and A. W. Warner, J. Appl. Phys., Vol. 37, p. 3853, 1966.
263. Smith, R. T., Appl. Phys. Lett., Vol. 11, p. 146, 1967.
264. Smolyakov, B. P., L. M. Meyl'man, V. P. Klyuyev, I. A. Shpil'ko and U. Kh. Kopvillem, FTT, Vol. 9, p. 3002, 1967.
265. Grace, M. J., R. W. Kedzie, M. Kestigian and A. B. Smith, Appl. Phys. Lett., Vol. 9, p. 155, 1966.
266. Smith, A. B., M. Kestigian, R. W. Kedzie and M. J. Grace, J. Appl. Phys., Vol. 38, p. 4928, 1967.
267. Spencer, E. G. and P. V. Lenzo, J. Appl. Phys., Vol. 38, p. 423, 1967.
268. Spencer, E. G., P. V. Lenzo and K. Nassau, Appl. Phys. Lett., Vol. 7, p. 67, 1965.
269. Wen, C. P. and R. F. Mayo, Appl. Phys. Lett., Vol. 9, p. 135, 1966.
270. Sonin, A. S. and L. G. Lomova, FTT, Vol. 9, p. 3315, 1967.
271. Boyd, G. D., W. L. Bond and H. L. Carter, J. Appl. Phys., Vol. 38, p. 1941, 1967.
272. Iwasaki, H., H. Toyoda, N. Niizeki and H. Kubota, Japan J. Appl. Phys., Vol. 6, p. 1101, 1967.
273. Miller, R. C., G. D. Boyd and A. Savage, Appl. Phys. Lett., Vol. 6, p. 77, 1965.
274. Miller, R. C. and A. Savage, Proc. Int. Meet. Ferroelectr., Vol. 1, Prague, p. 405, 1966.
275. Miller, R. C. and A. Savage, Phys. Lett., Vol. 9, p. 169, 1966.
276. Iwasaki, H., H. Toyoda, N. Niizeki and H. Kubota, Japan J. Appl. Phys., Vol. 6, p. 1419, 1967.
277. Kaminow, I. P. and W. D. Johnston, Phys. Rev., Vol. 160, p. 519, 1967.

278. Peterson, G. E., A. A. Ballman, P. V. Lenzo and B. M. Bridgenbaugh, *Appl. Phys. Lett.*, Vol. 5, p. 62, 1964.
279. Zook, J. D., D. Chen and N. Otto, *Appl. Phys. Lett.*, Vol. 11, p. 159, 1967.
280. Mustel', Ye. R., V. N. Parygin and V. S. Solomatin, *Vestn. Mosk. Univ., Fizika, Astronomiya* (Herald of Moscow University, Physics, Astronomy), Vol. 1, p. 109, 1968.
281. Ashkin, A., G. D. Boyd, J. M. Dziedzic, R. G. Smith, A. A. Ballman, H. J. Levinstein and K. Nassau, *Appl. Phys. Lett.*, Vol. 9, p. 72, 1966.
282. Levinstein, H. J., A. A. Ballman, R. T. Denton, A. Ashkin and J. M. Dziedzic, *J. Appl. Phys.*, Vol. 38, p. 3101, 1967.
283. Osterlink, L. M. and R. Targ, *Appl. Phys. Lett.*, Vol. 10, p. 115, 1967.
284. Yevlapova, N. F., A. S. Kovalev, V. A. Koptsik, L. S. Korriyenko, A. M. Prokhorov and L. N. Rashkovich, *ZhETF, Letters*, Vol. 5, p. 351, 1967.
285. Colles, M. J. and R. S. Smith, *Appl. Phys. Lett.*, Vol. 10, p. 309, 1967.
286. Dugnay, M. A., L. E. Hargrove and K. B. Jefferts, *Appl. Phys. Lett.*, Vol. 9, p. 287, 1966.
287. Giordmaine, J. A. and R. C. Miller, *Phys. Rev. Lett.*, Vol. 14, p. 973, 1965.
288. Giordmaine, J. A. and R. C. Miller, *Appl. Phys. Lett.*, Vol. 9, p. 298, 1966.
289. Midwinter, J. E. and J. Warner, *J. Appl. Phys.*, Vol. 38, p. 519, 1967.
290. Smith, R. C., K. Nassau and M. Galvin, *Appl. Phys. Lett.*, Vol. 7, p. 256, 1965.
291. Soffer, B. H. and I. M. Winer, *Phys. Lett.*, Vol. 24A, p. 282, 1967.
292. Guseva, L. M., V. F. Kluyev, I. S. Rez, S. A. Fedulov, A. P. Lyubimov and Z. I. Tatarov, *Izv. AN SSSR, ser. fiz.*, Vol. 31, p. 1161, 1967.
293. Axe, J. D. and D. F. O'Kane, *Appl. Phys. Lett.*, Vol. 9, p. 58, 1966.
294. Barker, A. S. and R. Loudon, *Phys. Rev.*, Vol. 158, p. 433, 1967.
295. Bosomworth, D. R., *Appl. Phys. Lett.*, Vol. 9, p. 330, 1966.
296. Burns, G., *Phys. Rev.*, Vol. 127, p. 1193, 1962.

297. Fedulov, S. A., Z. I. Shapiro and P. B. Ladyshevskiy, Kristallografiya, Vol. 10, p. 268, 1965.
298. Eallman, A. A., J. Am. Ceram. Soc., Vol. 48, p. 112, 1965.
299. Nassau, K., Proc. Int. Meet. Ferroelectr., Vol. 1, Prague, p. 270, 1966.
300. Shveyntler, G., Probl. Sovz. Fiz. (Problems of Contemporary Physics), No. 6, Segneto- i Antisegetoelektricheskiye Yavleniya (Ferro- and Antiferroelectric Phenomena), p. 93, 1953.
301. Scapski, A. C., Acta Chem. Scand., Vol. 20, p. 580, 1966.
302. Masuno, K., J. Phys. Soc. Japan, Vol. 19, p. 323, 1964.
303. Van Uitert, L. G., S. Singh, H. J. Levinstein, J. E. Geusic and W. A. Bonner, Appl. Phys. Lett., Vol. 11, p. 161, 1967.
304. Goodman, G., J. Am. Ceram. Soc., Vol. 36, p. 368, 1953.
305. Francombe, M. H. and B. Lewis, Acta Cryst., Vol. 11, p. 696, 1958.
306. Smolenskiy, G. A. and A. I. Agranovskaya, DAN SSSR, Vol. 97, p. 237, 1954.
307. Isupov, V. A., Izv. AN SSSR, ser. fiz., Vol. 21, p. 402, 1957.
308. Ismailzade, I. G., Kristallografiya, Vol. 4, p. 658, 1959.
309. Subbarao, E. C., G. Shirane and F. Jona, Acta Cryst., Vol. 13, p. 226, 1960.
310. Galasso, F., L. Katz and R. Ward, J. Am. Chem. Soc., Vol. 81, p. 5898, 1959.
311. Francombe, M. H., Acta Cryst., Vol. 13, p. 131, 1960.
312. Kraynik, N. N., V. A. Isupov, M. F. Bryzhina and A. I. Agranovskaya, Kristallografiya, Vol. 9, p. 352, 1964.
313. Ismailzade, I. G., Kristallografiya, Vol. 8, p. 351, 1963.
314. Giess, E. A., G. Burns, D. F. O'Kane and A. W. Smith, Appl. Phys. Lett., Vol. 11, p. 233, 1967.
315. Geusic, J. E., H. J. Levinstein, J. J. Rubin, S. Singh and L. G. Van Uitert, Appl. Phys. Lett., Vol. 11, p. 269, 1967.
316. Subbarao, E. C. and G. Shirane, J. Chem. Phys., Vol. 32, p. 1846, 1960.

317. Wolten, G. M. and A. B. Chase, *Inorg. Chem.*, Vol. 5, p. 484, 1966.
318. Fang, P. H., R. S. Roth and F. Forrat, *Compt. rend.*, Vol. 253, p. 1039, 1961.
319. Fang, P. N., R. S. Roth and H. Johnston, *J. Am. Ceram. Soc.*, Vol. 43, p. 169, 1960.
320. Stephenson, N. C., *Acta Cryst.*, Vol. 18, p. 496, 1965.
321. Goodman, G., *J. Am. Ceram. Soc.*, Vol. 43, p. 105, 1960.
322. Fang, P. H., R. S. Roth and H. S. Schofer, *Bull. Am. Phys. Soc.*, Ser. II, Vol. 5, No. 1, Pt I, pp. 57-58, 1960; P. M. Pan, P. H. Fang, R. S. Roth, *Ibid.*; R. S. Roth and P. H. Fang, *Ibid.*
323. Sinyakov, Ye. V. and Ye. F. Dudnik, *FTT*, Vol. 4, p. 2971, 1962.
324. Kruchan, Ya. Ya., *Izv. AN SSSR, ser. fiz.*, Vol. 31, p. 1094, 1967.
325. Roth, R. S., *J. Res. Nat. Bur. Stand.*, Vol. 62, p. 27, 1959.
326. Francoabe, M. H., *Acta Cryst.*, Vol. 9, p. 683, 1956.
327. Isupov, V. A., *FTT*, Vol. 9, p. 1417, 1967
328. Ismailzade, I. G., *Izv. AN SSSR, ser. fiz.*, Vol. 22, p. 1485, 1958.
329. Gasperin, M., *Bull. Soc. Franc. Miner. Crist.*, Vol. 87, p. 50, 1964.
330. Isupov, V. A., *FTT*, Vol. 1, p. 242, 1959.
331. Coates, R. V. and H. F. Kay, *Phil. Mag.*, Vol. 3, p. 1449, 1958.
332. Coates, R. V., *Acta Cryst.*, Vol. 14, p. 84, 1961.
333. Anan'yeva, A. A., G. I. Gusakova and M. A. Ugryumova, *Kristallografiya*, Vol. 10, p. 430, 1965.
334. Anan'yeva, A. A. and M. A. Ugryumova, *Akustich. Zh.* (Acoustics Journal), Vol. 10, p. 265, 1964.
335. Anan'yeva, A. A. and M. A. Ugryumova, *Akustich. Zh.*, Vol. 11, p. 24, 1965.
336. Bindar, Ye. J., Ya. Ya. Kruchan and R. Zh. Freyndenfel'd, *Izv. AN LatvSSR, ser. khim.* (News of Academy of Sciences LatvSSR, Chemistry Series), No. 1, p. 9, 1963.
337. Ismailzade, I. G., *Kristallografiya*, Vol. 4, p. 658, 1959.

338. Isupov, V. A. and V. I. Kosyakov, ZhTF, Vol. 28, p. 2175, 1958.
339. Kruchan, Ya. Ya., Izv. AN LatvSSR, ser. fiz. i tekhn. (News of Academy of Sciences LatvSSR, Physics and Technology Series), No. 2, p. 8, 1964.
340. Kruchan, Ya. Ya., Ye. I. Bindar and E. Zh. Freyndenfel'd, Izv. LatvSSR, ser. Khim., No. 3, p. 265, 1967.
341. Kruchan, Ya. Ya. and E. Zh. Freyndenfel'd, Izv. AN LatvSSR, ser. Khim., No. 6, p. 637, 1963.
342. Mikhaylov, P. S. and B. A. Rotenberg, Izv. AN SSSR, ser. fiz., Vol. 21, p. 1287, 1960.
343. Smazhevskaya, Ye. G. and N. A. Podel'ner, Izv. AN SSSR, ser. fiz., Vol. 24, p. 1394, 1960.
344. Smazhevskaya, Ye. G. and V. I. Rivkin, Izv. AN SSSR, ser. fiz., Vol. 24, p. 1398, 1960.
345. Smolenskiy, G. A., V. A. Isupov and A. I. Agranovskaya, FTI, Vol. 1, p. 442, 1959.
346. Freyndenfel'd, E. Zh., Ya. Ya. Kruchan and Ye. I. Bindar, Izv. AN LatvSSR, ser. Khim., No. 2, p. 18, 1962.
347. Baxter, P. and N. J. Hellicar, J. Am. Ceram. Soc., Vol. 43, p. 578, 1960.
348. Francombe, M., Acta Cryst., Vol. 13, p. 151, 1960.
349. Goodman, G., Trans. Brit. Ceram. Soc., Vol. 56, 12A, 1958.
350. Goodman, G., U. S. Patent No. 2895165, 3 September 1957.
351. Nelson, K. E. and R. I. Cook, J. Am. Ceram. Soc., Vol. 42, p. 138, 1959.
352. Srikanta, S., V. E. Tare, A. P. B. Sinha and A. B. Pissas, Acta Cryst., Vol. 15, p. 255, 1962.
353. Subbarao, E. C., J. Am. Ceram. Soc., Vol. 42, p. 448, 1959.
354. Subbarao, E. C., J. Am. Ceram. Soc., Vol. 45, p. 523, 1962.
355. Subbarao, E. C. and G. Shirane, J. Chem. Phys., Vol. 32, p. 1846, 1960.
356. Smolenskiy, G. A., Ya. M. Ksendzov, A. I. Agranovskaya and S. Ya. Popov, Fizika Dielektrikov, Vol. II, USSR Academy of Sciences Publishing House, Moscow-Leningrad, p. 244, 1959.

357. Smolenskiy, G. A., V. A. Isupov and A. I. Agranovskaya, FTT, Vol. 1, p. 992, 1959.
358. Lenzo, P. V., E. G. Spencer and A. A. Ballman, Appl. Phys. Lett., Vol. 11, p. 23, 1967.
359. Masuno, K., J. Phys. Soc. Japan, Vol. 19, p. 323, 1964.
360. Wainer, E. and Ch. Wentworth, J. Am. Ceram. Soc., Vol. 55, p. 207, 1952.
361. Cook, W. R. and H. Jaffe, Phys. Rev., Vol. 88, p. 1426, 1952.
362. Cook, W. R. and H. Jaffe, Phys. Rev., Vol. 89, p. 1297, 1953.
363. Bystroem, A., Arkiv Kemi, Miner., Geol., Vol. 18A, No. 21, 1944.
364. Isupov, V. A., Kristallografiya, Vol. 3, p. 99, 1958.
365. Jona, F., G. Shirane and R. Pepinsky, Phys. Rev., Vol. 99, p. 1215, 1953.
366. Haim, J. K., Phys. Rev., Vol. 92, p. 504, 1953.
367. Shirane, G. and R. Pepinsky, Phys. Rev., Vol. 92, p. 504, 1953.
368. Danner, H. R. and R. Pepinsky, Phys. Rev., Vol. 99, p. 1215, 1953.
369. de Bretteville, A., F. A. Holden, T. Vasilos and L. Reed, J. Am. Ceram. Soc., Vol. 40, p. 86, 1957.
370. Isupov, V. A. and O. K. Khomutetskiy, ZhTF, Vol. 27, p. 2704, 1957.
371. de Bretteville, A. and R. M. Oman, Bull. Am. Phys. Soc., Series II, Vol. 5, p. 62, 1959.
372. de Bretteville, A., Bull. Am. Phys. Soc., Series II, Vol. 7, p. 280, 1962.
373. Isupov, V. A. and V. N. Skubitskiy, FTT, Vol. 5, p. 957, 1963.
374. Negaw, H. D., Ferroelectricity in Crystals, London, 1957.
375. Smolenskiy, G. A., V. A. Isupov and A. I. Agranovskaya, DAN SSSR, Vol. 108, p. 232, 1956.
376. Isupov, V. A., Kristallografiya, Vol. 4, p. 603, 1959.
377. Smolenskiy, G. A., V. A. Isupov and A. I. Agranovskaya, DAN SSSR, Vol. 113, p. 803, 1957.
378. Aurivillius, B., Arkiv. f. Kemi, Vol. 1, p. 449, 1950; Vol. 2, p. 510, 1951.

379. Smolenskiy, G. A., V. A. Isupov and A. I. Agranovskaya, FTT, Vol. 1, p. 158, 1959.
380. Smolenskiy, G. A., V. A. Isupov and A. I. Agranovskaya, Tez. Dokl. III Soveshch. po Segnetoelektrichestvu (Thesis of Report at Third Conference on Ferroelectricity), USSR Academy of Sciences Publishing House, Moscow, p. 40, 1960.
381. Smolenskiy, G. A., V. A. Isupov and A. I. Agranovskaya, FTT, Vol. 3, p. 895, 1961.
382. Ismailzade, I. G., Izv. AN SSSR, ser. fiz., Vol. 24, p. 1198, 1960.
383. Ismailzade, I. G., Azerb. Khim. Zh. (Azerbaijani Chemical Journal), No. 5, p. 91, 1961.
384. Ismailzade, I. G., Kristallografiya, Vol. 8, p. 852, 1963.
385. Subbarao, E. C., Bull. Am. Phys. Soc., Series II, Vol. 5, p. 423, 1960.
386. Subbarao, E. C., J. Chem. Phys., Vol. 34, p. 695, 1961.
387. Subbarao, E. C., Phys. Rev., Vol. 122, p. 804, 1961.
388. Subbarao, E. C., J. Am. Ceram. Soc., Vol. 45, p. 166, 1962.
389. Subbarao, E. C., J. Phys. Chem. Sol., Vol. 23, p. 6, 1962.
390. Hrizo, J. and E. C. Subbarao, Rev. Sci. Instr., Vol. 34, p. 8, 1963.
391. Fang, P. H., C. Robbins and F. Forrat, Compt. rend., Vol. 252, p. 683, 1961.
392. Fang, P. H., C. Robbins and B. Aurivillius, Phys. Rev., Vol. 126, p. 892, 1962.
393. Aurivillius, B. and P. H. Fang, Phys. Rev., Vol. 126, p. 893, 1962.
394. Fang, P. H. and E. Fatuzzo, J. Phys. Soc. Japan, Vol. 17, p. 238, 1962.
395. Van Uitert, L. G. and L. Egerton, J. Appl. Phys., Vol. 32, p. 959, 1961.
396. Popper, P., S. N. Ruddlesden and T. A. Ingles, Trans. Brit. Ceram. Soc., Vol. 5, p. 356, 1957.
397. Ismailzade, I. G., V. I. Nesterenko, F. A. Mirishvili and I. G. Rustamov, Kristallografiya, Vol. 12, p. 468, 1967.
398. Ismailzade, I. G. and V. I. Nesterenko, Kristallografiya, Vol. 12, p. 717, 1967.

399. Ismailzade, I. G., Izv. AN SSSR, Neorg. Materialy (News of USSR Academy of Sciences, Inorganic Materials), Vol. 3, p. 1295, 1967.
400. Ismailzade, I. G. and F. A. Mirishli, Izv. AN SSSR, Neorg. Mater., Vol. 3, p. 2121, 1967.
401. Smolenskiy, G. A., N. N. Kraynik, V. A. Isupov, Ye. I. Myl'nikova, I. V. Plotnikova and Chan Van T'yau, Tezisy Dokl. VI Vsesoyuzn. Soveshch. po Segnetoelektrichestvu (Theses of Reports at Sixth All-Union Conference on Ferroelectricity), Riga, 1968.
402. Skanavi, G. I. and A. I. Demeshina, ZhETF, Vol. 31, p. 303, 1956.
403. Tambovtsev, D. A., V. M. Skorikov and I. S. Zheludev, Kristallografiya, Vol. 8, p. 889, 1963.
404. Pulvary, Ch. F., Proc. Int. Meet. on Ferroelectr., Vol. 1, Prague, p. 347, 1966.
405. Pulvary, Ch. F. and A. S. De la Paz, J. Appl. Phys., Vol. 37, p. 1754, 1966.
406. Hamilton, D. L., J. Appl. Phys., Vol. 38, p. 10, 1967.
407. Kraynik, N. N., I. Ye. Myl'nikova and S. F. Kolesnichenko, FTT, Vol. 10, p. 260, 1968.
408. Cummins, S. E., J. Appl. Phys., Vol. 35, p. 3015, 1964.
409. Cummins, S. E., J. Appl. Phys., Vol. 36, p. 1958, 1965.
410. Cummins, S. E., J. Appl. Phys., Vol. 37, p. 2510, 1966.
411. Cummins, S. E. and L. E. Cross, Appl. Phys. Lett., Vol. 10, p. 14, 1967.
412. Dunne, T. G. and N. R. Stemple, Phys. Rev., Vol. 120, p. 149, 1958.
413. Wallmark, S. and A. Westgreen. Arkiv Kemi. Min., Geol., Vol. 126, No. 55, 1938.
414. Hoppe, R. and B. Schepers, Naturwiss., Vol. 47, p. 376, 1960.
415. Borchardt, H. J. and P. E. Bierstedt, Appl. Phys. Lett., Vol. 8, p. 50, 1966.
416. Borchardt, H. J. and P. E. Bierstedt, J. Appl. Phys., Vol. 38, p. 2057, 1967.
417. Nassau, K., H. J. Levinstein and G. M. Loiacono, J. Phys. Chem. Sol., Vol. 26, p. 1805, 1965.

418. Kestigian, M., *J. Am. Ceram. Soc.*, Vol. 48, p. 544, 1965.
419. Yakel, H. L., W. C. Koehler, F. Bertaut and E. F. Forrat, *Acta Cryst.*, Vol. 16, p. 957, 1963.
420. Ismailzade, I. G. and S. A. Kizhayev, *FTT*, Vol. 7, p. 298, 1965..
421. Bokov, V. A., G. A. Smolenskiy, S. A. Kizhayev and I. Ye. Myl'nikova, *FTT*, Vol. 5, p. 3607, 1963.
422. Bertaut, E. F., F. Forrat and P. U. Fang, *Compt rend.*, Vol. 256, p. 1953, 1963.
423. Bertaut, E. F. and F. Lissalde, *Sol. St. Comm.*, Vol. 5, p. 173, 1967.
424. Coeure, P., *Compt. rend.*, Vol. 261, p. 4369, 1965.
425. Coeure, P., P. Guinet, J. C. Peuzin, G. Buisson and E. F. Bertaut, *Proc. Int. Meet. on Ferroelectr.*, Vol. 1, Prague, p. 332, 1966.
426. Jimenez Biaz, D., *Proc. Int. Meet. on Ferroelectr.*, Vol. 2, Prague, p. 127, 1966.
427. Peuzin, J. C., *Sol. St. Comm.*, Vol. 5, p. 13, 1967.
428. Tamura, H., E. Sawaguchi and A. Kikuchi, *Japan J. Appl Phys.*, Vol. 4, p. 621, 1965.
429. Bertaut, F. and J. Mareschal, *Compt. rend.*, Vol. 257, p. 867, 1963.
430. Ito, T., N. Morimoto and R. Sadanaya, *Acta Cryst.*, Vol. 4, p. 310, 1951.
431. Heide, F., *J. Phys. Chem.*, Vol. 63, p. 1750, 1959.
432. Heide, F., G. Walter and R. Urlau, *Naturwiss.*, Vol. 48, p. 97, 1961.
433. Schmid, H., *J. Phys. Chem. Sol.*, Vol. 26, p. 973, 1965.
434. Asher, E., H. Schmid and D. Tar, *Sol. St. Comm.*, Vol. 2, p. 45, 1964.
435. Schmid, H. and J. M. Trooster, *Sol. St. Comm.*, Vol. 5, p. 31, 1967.
436. Beyrikh, G., *Zap. Vsesoyuzn. Mineralogich. Obshch.* (Transactions of All-Union Mineralogical Society), Vol. 94, p. 448, 1965.
437. Zheludev, I. S. and L. A. Shuvaiov, *Kristallografiya*, Vol. 1, p. 681, 1956.
438. LeCorre, Y., *J. Phys. et Radium*, Vol. 18, p. 629, 1957.
439. Tar, D., *Helv. Phys. Acta*, Vol. 37, p. 165, 1964.

440. Asher, E., H. Rieder, H. Schmid and H. Stoszel, *J. Appl. Phys.*, Vol. 37, p. 1404, 1966.
441. Fatuzzo, E., G. Hurbecke, W. J. Merz, R. Nitsche, H. Roetschi and W. Ruppel, *Phys. Rev.*, Vol. 127, p. 2036, 1962.
442. Nitsche, R., H. Roetschi and F. Wild, *Appl. Phys. Lett.*, Vol. 4, p. 210, 1964.
443. Donges, E., *Zs. anorg. allg. Chemie*, Vol. 263, p. 112, 1950.
444. Krayvik, N. N., S. N. Popov and I. Ye. Myl'nikova, *FTT*, Vol. 8, p. 3664, 1966.
445. Merz, W. J. and R. Nitsche, *Izv. AN SSSR, ser. fiz.*, Vol. 28, p. 681, 1964.
446. Berlincourt, D., H. Jaffe, W. J. Merz and R. Nitsche, *Appl. Phys. Lett.*, Vol. 4, p. 61, 1964.
447. Hamano, K., T. Nakamura, Y. Ishibashi and T. Ooyane, *J. Phys. Soc. Japan*, Vol. 20, p. 1886, 1965.
448. Fridkin, V. M., *ZhETF, Letters*, Vol. 3, p. 252, 1966.
449. Alekseyeva, V. G. and Ye. G. Landsberg, *FTT*, Vol. 6, p. 3138, 1966.
450. Belyayev, L. M., I. I. Groshik, V. A. Lyakhovitskaya, V. N. Nosov and V. M. Fridkin, *ZhETF, Letters*, Vol. 6, p. 481, 1967.
451. Gerzanich, Ye. I., *FTT*, Vol. 9, p. 2995, 1967.
452. Grekov, A. A., V. A. Lyakhovitskaya, A. I. Rodin and V. M. Fridkin, *FTT*, Vol. 8, p. 3092, 1966.
453. Grigas, B. P., I. P. Grigas and R. I. Belyatskas, *FTT*, Vol. 9, p. 1532, 1967.
454. Grigas, B. P., *FTT*, Vol. 9, p. 2998, 1967.
455. Grigas, I. P. and A. S. Karpus, *FTT*, Vol. 9, p. 2887, 1967.
456. Gulyanov, K., V. A. Lyakhovitskaya, I. A. Tikhomirova and V. M. Fridkin, *DAN SSSR*, Vol. 161, p. 1060, 1965.
457. Nosev, V. N., *Kristallografiya*, Vol. 12, p. 359, 1967.
458. Nosov, V. N. and V. A. Lyakhovitskaya, *Kristallografiya*, Vol. 11, p. 322, 1966.
459. Nosov, V. N. and V. M. Fridkin, *FTT*, Vol. 8, p. 148, 1966.

460. Pikka, T. A., Kristallografiya, Vol. 12, p. 1075, 1967.
461. Rudyak, V. M. and A. A. Bogomolov, FTT, Vol. 9, p. 3336, 1967.
462. Travina, T. S., et al, FTT, Vol. 9, p. 3664, 1967.
463. Fridkin, F. M., Ye. I. Gerzanich, I. I. Groshik and V. A. Lyakhovitskaya, ZhETF, Letters, Vol. 4, p. 201, 1966.
464. Fridkin, V. M., I. M. Gorelov, A. A. Grekov, V. A. Lyakhovitskaya and A. I. Rodin, ZhETF, Vol. 4, p. 461, 1966.
465. Fridkin, V. M., K. Gulyamov, V. A. Lyakhovitskaya, V. N. Nosov and N. A. Tikhomirova, FTT, Vol. 8, p. 1907, 1966.
466. Shaldin, Yu. V. and V. A. Lyakhovitskaya, FTT, Vol. 9, p. 1541, 1967.
467. Horak, J. and K. Cermak, Chekhoslov, Fiz. Zh., Vol. 15, p. 536, 1965.
468. Mori, T. and E. Sawaguchi, Japan J. Appl. Phys., Vol. 6, p. 269, 1967.
469. Ohi, K. and O. Ariizumi, J. Phys. Soc. Japan, Vol. 22, p. 1307, 1967.
470. Sasaki, Y., Japan J. Appl. Phys., Vol. 3, p. 558, 1964; Vol. 4, p. 228, 1965; Vol. 4, p. 614, 1965.
471. Ueda, S., S. Tatsuzaki and Y. Shindo, Phys. Rev. Lett., Vol. 18, p. 453, 1967.
472. Yamada, Y., J. Phys. Soc. Japan, Vol. 21, p. 2085, 1966.
473. Iwata, Y., S. Fukui, N. Koyano and I. Shibuya, J. Phys. Soc. Japan, Vol. 21, p. 1846, 1966.
474. Iwata, Y., N. Koyano and I. Shibuya, J. Phys. Soc. Japan, Vol. 20, p. 875, 1965.
475. Kikuchi, A., J. Oka and E. Sawaguchi, J. Phys. Soc. Japan, Vol. 23, p. 337, 1967.
476. Kawada, S. and M. Ida, J. Phys. Soc. Japan, Vol. 20, p. 1287, 1965.
477. Mori, T. and E. Sawaguchi, Japan J. Appl. Phys., Vol. 6, p. 792, 1967.
478. Sawaguchi, E. and T. Mori, J. Phys. Soc. Japan, Vol. 21, p. 2077, 1966.
479. Rudyak, V. M. and A. A. Bogomolov, FTT, Vol. 9, p. 3336, 1967.
480. Imai, K., S. Kawada and M. Ida, J. Phys. Soc. Japan, Vol. 21, p. 1855, 1966.

481. Masaki, H., J. Phys. Soc. Japan, Vol. 22, p. 1510, 1966.
482. Mali, M. and A. Levstik, Sol. St. Electronics, Vol. 10, p. 1225, 1967.
483. Mori, T., H. Tamura and E. Sawaguchi, J. Phys. Soc. Japan, Vol. 20, p. 281, 1965.
484. Mori, T., H. Tamura and E. Sawaguchi, J. Phys. Soc. Japan, Vol. 20, p. 1294, 1965.
485. Takama, T. and T. Mitsui, J. Phys. Soc. Japan, Vol. 23, p. 331, 1967.
486. Mokhosoyev, M. V., S. M. Aleykina and A. M. Gamol'skiy, Khal'kogenidy (Chalcogenides), "Naukova Dumka" Publishing House, Kiev, 1967.
487. Mori, T. and H. Tamura, J. Phys. Soc. Japan, Vol. 19, p. 1247, 1964.